Copyright is owned by the Author of the thesis. Permission is given for a copy to be downloaded by an individual for the purpose of research and private study only. The thesis may not be reproduced elsewhere without the permission of the Author.

Development of a Community-Engaged, Low-Cost Earthquake Early Warning System Using MEMS-Based Sensors: Enhancing and Adapting the PLUM Algorithm with Decentralised Processing and P-Wave Integration

A thesis presented in partial fulfilment of the requirements for the degree of
Doctor of Philosophy in Emergency Management
at
Massey University, Wellington,
New Zealand

Chanthujan Chandrakumar

2024

எல்லாம் வெல்லலாம்

(All Can Be Won)

Abstract

Earthquakes pose a significant threat to people and infrastructure, particularly in regions near active faults or offshore subduction zones, which are more frequently exposed to moderate to strong shaking. Earthquake Early Warning Systems (EEWS) provide crucial alerts immediately following an earthquake, offering a warning window ranging from a few seconds to tens of seconds. These systems have effectively reduced damage and allowed individuals to take protective actions. However, the high cost of establishing high-end EEWSs makes them unaffordable for many countries.

To address this, there is growing interest in using low-cost technologies such as Micro-Electromechanical Systems (MEMS)-based ground motion sensors to implement EEWSs. However, despite their potential, several knowledge gaps must be addressed to enhance their efficiency and effectiveness. Firstly, further investigation into decentralised processing for earthquake detection and alert generation is required. Traditional high-end EEWSs often rely on centralised processing units, which have proven vulnerable to critical delays and communication failures during major seismic events. Secondly, adapting and improving ground-motion-based or wave-field-based EEW algorithms is crucial for enhancing their performance, ensuring that EEWSs can provide timely and effective warnings in all regions during an earthquake, as opposed to the limitations posed by traditional source-based methods.

This doctoral research addresses these gaps by developing and evaluating a community-engaged, low-cost MEMS-based EEWS. The system utilises a ground-motion-based EEW algorithm adapted for decentralised processing, enabling rapid earthquake detection. It also integrates a P-wave detection algorithm to enhance the performance of the ground-motion-based approach. Guided by the Design Science Research methodology, this study seeks to answer three key research questions: (1) How can the Propagation of Local Undamped Motion (PLUM) ground-motion-based EEW algorithm be adapted and implemented for New Zealand's seismic conditions using decentralised processing? (2) How can high-accuracy P-wave detection be achieved in a community-engaged EEW network with high ambient noise? (3) How can the P-wave detection algorithm be integrated into the adapted PLUM algorithm to extend the warning window?

The study begins with a comprehensive literature review to identify research gaps in low-cost MEMS-based EEWSs, leading to the formulation of the research questions addressed in this thesis. To answer these questions, an experimental community-engaged EEW network was implemented in Greater Wellington, NZ, using low-cost MEMS-based sensors. This implementation was followed by adapting the PLUM algorithm to NZ-PLUM, making it compatible with New Zealand's seismic intensity by

employing region-specific Ground Motion Intensity Conversion Equations. The NZ-PLUM algorithm was then integrated into a sensor network operating under a decentralised processing architecture using a two-tier communication model, ensuring rapid and reliable data transmission and processing.

Building upon the implementation of the NZ-PLUM algorithm, integrating a P-wave detection algorithm into the NZ-PLUM approach was explored to extend the warning window. A performance analysis is conducted to identify the most effective P-wave detection algorithm for integration into the community-engaged EEWS. Subsequently, an empirical relationship between P-wave and S-wave amplitudes is established, leading to the development of a P-wave-based PLUM algorithm (NZ-PLUM-P), which provides an extended warning window before the onset of seismic shaking.

The outcomes of this doctoral research make significant advancements in community-engaged, low-cost EEWSs. A key contribution is developing a real-life experimental EEW network using two distinct algorithms, NZ-PLUM and NZ-PLUM-P, tailored to NZ's seismic context within a decentralised processing architecture. This study offers a versatile framework applicable to implementing community-engaged EEW networks at a low cost, making a substantial contribution to theory and practice. The methods developed for P-wave detection, constructing P-S wave amplitude relationships, executing EEW algorithms using decentralised processing and evaluating EEW network performance provide valuable tools for future research and implementation. Further, this cost-effective, community-driven model not only offers a viable solution for seismically active nations with limited resources but also has the potential to enhance the performance of existing high-end EEWS by increasing sensor density and extending warning capabilities. Providing earthquake early warnings can potentially be crucial in saving lives, protecting critical infrastructure, and enhancing public preparedness.

Acknowledgements

Completing this PhD journey has been challenging yet deeply rewarding, and it would not have been possible without the unwavering support and love of so many people.

First and foremost, I am profoundly grateful to the people of Sri Lanka for providing me with a free education up to my undergraduate degree. This foundation enabled me to pursue this PhD.

To my soulmate Abilashini, my everything, I am eternally thankful. Without you, I would not have been able to complete this PhD. You sacrificed so much—your well-established career, your family, and so much more—all for the sake of my degree. You have been my pillar of support through every mood and every challenge. Thank you for being my guardian angel. I could not have submitted this thesis without your unwavering love and encouragement.

I extend my deepest thanks to my parents, who worked tirelessly to provide me with a comfortable life and taught me the values of discipline and integrity. Despite numerous challenges, you have always encouraged me to stay positive. To my brother and friend, Chanjief, thank you for your constant support throughout my PhD journey, especially when progress felt distant. I am also grateful to my sister-in-law Bharatha and mother-in-law for their care and love.

I would also like to express my gratitude to my physics teacher, Mr Santharuban, whom I used to call my godfather, for recognising my potential in high school and motivating me to pursue a PhD before I even understood what it entailed. My heartfelt thanks go to my high school teachers, Mr Kesavan, Mr Sambasivam, and Mr Ganeshan, for their incredible support in helping me qualify for an engineering degree in highly competitive Sri Lanka.

I am incredibly privileged to have had the opportunity to study at Massey University, New Zealand. I am deeply thankful to Resilience to Nature's Challenges for funding my PhD. This journey would not have been possible without their generous financial support.

I owe immense gratitude to my primary supervisor, A/Prof. Raj Prasanna supported me in every possible way throughout my studies and constantly pushed me to reach the next level. He has been more than a supervisor—he has been a father figure, guiding me to become a better person and researcher. I am equally grateful to Dr. Marion Tan, my co-supervisor and a great friend in New Zealand, who supported me even before officially becoming my supervisor. I owe you a lifetime of gratitude. Without these two remarkable individuals, I would not be the researcher I am today.

During my PhD, I was fortunate to have four excellent supervisors: A/Prof. Raj Prasanna, Dr. Max Stephens, Dr. Marion Tan, and Dr. Caroline Holden. I am privileged to have had a caring and dedicated supervision team that gave me their time, energy, and enthusiasm. Each provided unique guidance, making my work more holistic and well-rounded. They stood by me through all the tough times during my PhD. I have never seen a supervisory team like mine—quick, efficient, and always working at my pace. The support you all provided, especially the knowledge shared by Dr. Caroline Holden regarding seismology, was invaluable to my research, as I had no prior knowledge in that area before starting my PhD. Dr. Max Stephens's precise comments have always helped me refine my publications, and I have always enjoyed discussing his ideas for presenting my work.

A special thanks goes to the Joint Centre for Disaster Research (JCDR) community. I would not have enjoyed this experience nearly as much without the company of my fellow PhD students, who shared the ups and downs of this journey with me. I am deeply thankful to my PhD buddy, Mr Annal Dhungana, who was always there to encourage me in the PhD room, and to fellow PhD students Mrs Manomita Das, Mr Sarjan Neupane, Mr Alfredo Jaramillo Velez, Mr Kianoush Rostami, Mr Richard Mowll, Mrs Kasuni Adikari and Mr Malintha Ranasinghe. I was fortunate to have my best friend, Mr Danuka Ravishan, at JCDR, where we shared much to fine-tune my PhD's technical aspects. My life at JCDR was further enriched by the presence of staff, post-docs, interns, and visiting scholars. I want to acknowledge Miss Alicia Cui, my dear friend, for her continuous support in promoting and sharing my research and guiding me in presenting my work to all audiences. I also want to thank my gym friend, Mr. Vinay Kumar, who has been a great source of motivation and has shown me how to maintain discipline.

To everyone who has been part of this journey—thank you. Your support, encouragement, and love have made all the difference.

Table of Contents

List of Tables

List of Figures

This illustration will be provided at the beginning of each chapter to position the reader in the thesis.

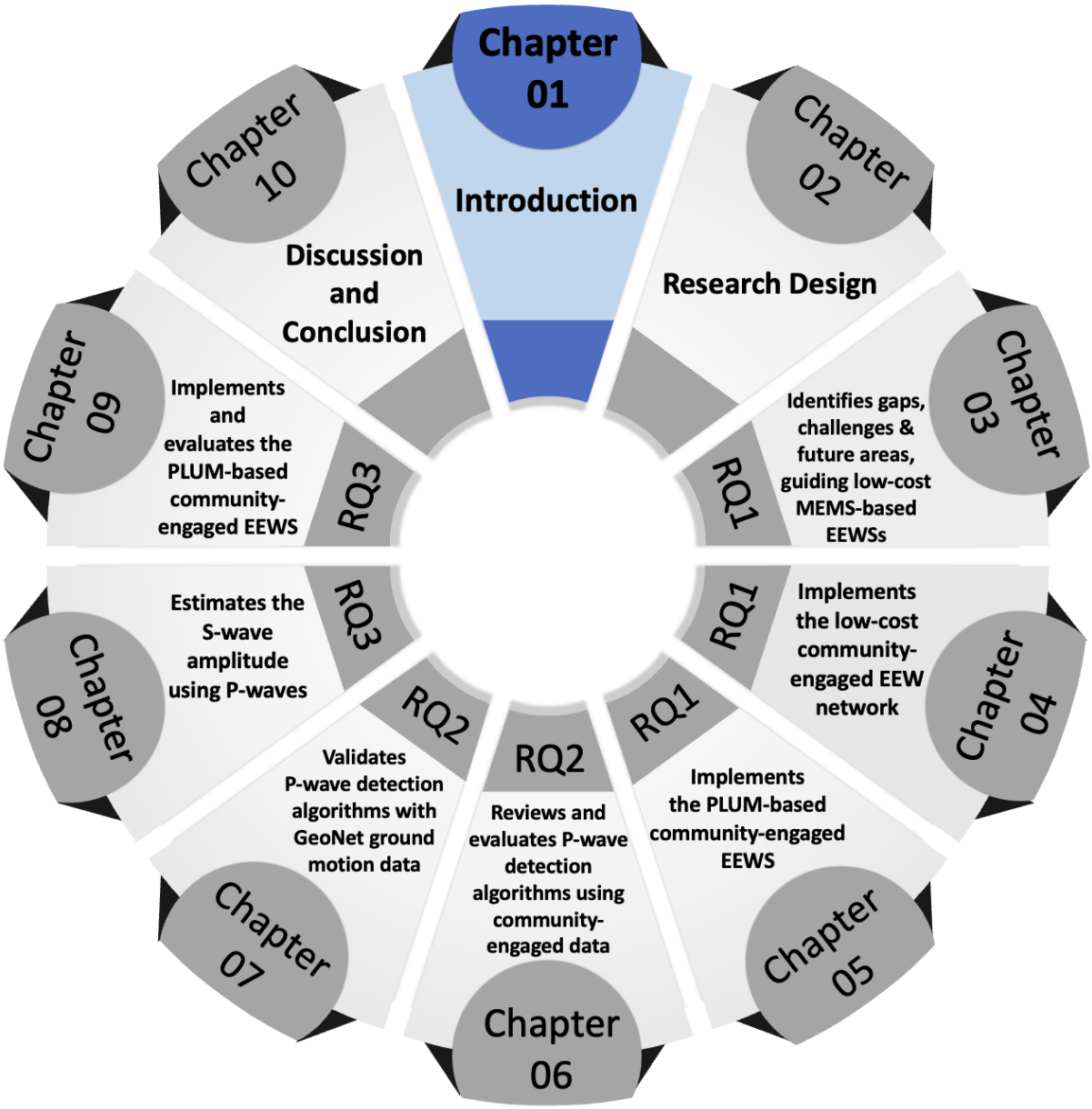

1 Introduction

Disasters have caused devastating consequences to humanity and infrastructure since the beginning of human history, with earthquakes presenting a significant and frequent threat to areas near active faults on land or offshore subduction zones (Adhikari et al., 2018; Strauss & Allen, 2016). Unlike other hazards, such as cyclones and tsunamis, earthquakes cannot be predicted in advance and can only be detected as they occur. This makes timely detection and warnings crucial but highly challenging (Fischer et al., 2012).

Given this challenge, Earthquake Early Warning System (EEWS) plays a critical role in providing the few precious seconds of warning that can potentially mitigate the impact of an earthquake (R. M. Allen & Stogaitis, 2022; Strauss & Allen, 2016). An EEWS comprises a network of seismic sensors, communication systems, computers, and alerting devices designed to notify areas during significant earthquakes just before they strike (R. M. Allen & Melgar, 2019; Fischer et al., 2012). These systems detect seismic activity and send real-time alerts, with the potential warning time ranging from a few seconds to tens of seconds, depending on the earthquake's geometry and the sensor network's configuration (Y. M. Wu & Zhao, 2006). Even within this short window, EEWS allows for crucial protective actions, such as "drop, cover, and hold," and enables automated systems to initiate precautionary measures like stopping trains to minimise derailment risks, shutting off gas distribution valves to reduce fire hazards, and switching off large machinery to prevent potential losses (Becker, Potter, Prasanna, et al., 2020; Becker, Potter, Vinnell, et al., 2020; Nakayachi et al., 2019; Strauss & Allen, 2016)

Despite this potential, the primary challenge in developing an EEWS lies in the necessity for immediate detection and alert generation during an earthquake event, a demanding task given the brief interval between detecting seismic activity and the onset of its potentially devastating shaking. However, the feasibility of EEWS is supported by two critical factors: the faster speed of information travel over communication networks compared to seismic waves and the fact that the most destructive seismic waves, the S-waves, follow the quicker, less harmful P-waves, providing a crucial, albeit brief, window for issuing warnings (Fischer et al., 2012).

Building on this foundation, the development of EEWS has historically faced challenges due to the complexities of earthquake-related data processing (Kanamori et al., 1997). However, significant advancements in seismic instrumentation, digital communication, and data processing technologies over the last three decades have enhanced the functionality and reliability of these systems (R. M. Allen & Melgar, 2019; Suárez et al., 2018). Today, many countries have implemented national EEWS that

offer warnings before severe ground shaking occurs, demonstrating their effectiveness in reducing damage and helping individuals physically and mentally prepare for earthquakes (R. M. Allen & Melgar, 2019; Chandrakumar, Prasanna, Stephens, & Tan, 2022; Cremen & Galasso, 2020; McBride et al., 2022). These systems are now integral to disaster preparedness strategies in earthquake-prone areas, reflecting substantial progress from their initial challenges to their current state of technological advancement.

Despite the increased implementations of national level EEWSs to enhance seismic resilience, the financial burden of establishing a high-end EEWS is substantial, often reaching hundreds of millions of dollars (Brooks et al., 2021; Given et al., 2018; Minson et al., 2015; Prasanna et al., 2022; Strauss & Allen, 2016). For instance, the ShakeAlert EEWS in the USA, which is operational in California, Oregon, and Washington, has incurred deployment costs of nearly 100 million USD and demands 30 million dollars annually for maintenance (Brooks et al., 2021). Such significant expenses make these systems unaffordable for economically disadvantaged countries and even some developed nations like New Zealand (NZ), which are at seismic risk (Becker, Potter, Prasanna, et al., 2020; Prasanna et al., 2022). Consequently, the high financial costs, combined with recent advancements in sensor technology, have prompted researchers to explore the feasibility of low-cost alternatives for earthquake detection, aiming to make EEWS more accessible and cost-effective for broader implementation (Lin et al., 2012).

In response to the high budgets associated with high-end EEWSs, there is a growing global initiative to develop low-cost alternative technologies. One promising approach is using Micro-Electromechanical Systems (MEMS)-based ground motion sensors, which have been utilised since the early 1990s and are effective for recording strong ground motions (Holland, 2003). Regions like Taiwan (Y. M. Wu et al., 2013) and the Sichuan-Yunnan border in China (Peng et al., 2019) have already incorporated MEMS-based sensors into their public alert systems. Experimental applications in California (Clayton et al., 2015), Iceland (TurnKey Earthquake Early Warning, 2020), and Costa Rica (Brooks et al., 2021) have also been explored using these cost-effective sensors within EEWSs. Notably, in 2021, Google launched an Earthquake Early Warning (EEW) service using MEMS-based sensors embedded in Android smartphones to detect seismic activities (R. M. Allen & Stogaitis, 2022). In NZ, the Crisis Response and Integrated Simulation Science Laboratory (CRISiSLab) at Massey University, has initiated an experimental community-engaged network deploying low-cost MEMS-based EEWS (Prasanna et al., 2022).

Despite these developments, research on low-cost EEWS still needs to be improved (Chandrakumar, Prasanna, Stephens, & Tan, 2022). An extensive literature review, presented in Chapter 3, identifies significant gaps in the current understanding and application of these systems, underscoring the need for

ongoing research and development in this field. These gaps are summarised in Section 1.1 for convenience. This doctoral project aims to contribute to the academic discourse and practice by addressing these gaps by exploring and enhancing low-cost MEMS-based EEWSs globally.

1.1 Research Gaps

The literature review (presented in detail in Chapter 3) has revealed several notable knowledge gaps in developing and implementing EEWSs. Specifically, there is a need for further exploration in decentralised processing for earthquake detection and alert generation. Additionally, enhancements to ground-motion-based or wave-field-based EEW algorithms are necessary to improve their performance. These gaps underscore the necessity for advanced research in this domain, highlighting areas that could significantly enhance the effectiveness and efficiency of EEWS. The identified gaps are summarised as follows:

Decentralised Processing in EEWS: Decentralised processing in EEWS involves performing all processing tasks at edge-layer devices, such as sensor nodes equipped with computational capabilities, rather than depending on a centralised system or remote cloud server for data processing. This approach reduces the time to issue alerts by eliminating the need for data to travel to a central server, thus providing a longer warning window for end users. It also enhances the resilience of EEWS against central system failures caused by earthquakes. Additionally, processing at the node level can decrease operational costs associated with maintaining sophisticated central processing systems (Fleming et al., 2009; Prasanna et al., 2022). Additionally, decentralised processing is particularly beneficial for community-engaged EEW networks, as it ensures that only critical intensity information is shared among sensors for alert generation, thus protecting the privacy of sensor hosts by preventing the exposure of potentially sensitive information (Bassetti & Panizzi, 2022).

Despite these advantages, most existing low-cost MEMS-based EEWSs predominantly rely on centralised data processing, with only a few systems, such as those introduced by Prasanna et al. (2022), Fleming et al. (2009) and Bassetti and Panizzi (2022), have implemented decentralised processing. This limited adoption highlights a significant gap in the research and development of decentralised processing for EEWS, indicating a critical area for further exploration and advancement (Chandrakumar, Prasanna, Stephens, & Tan, 2022).

Adaptation of Ground Motion-based or Wave-field-based Algorithms for Low-cost Earthquake Early Warning Systems: The research identifies a crucial gap in EEWS, highlighting the need for a greater focus on ground motion-based approaches like the Propagation of Local Undamped Motion

(PLUM) algorithm over the predominantly used source-based algorithms. The PLUM algorithm, known for its robustness, ease of implementation, and rapid alert generation, has proven successful in Japan's EEWS (Kodera et al., 2018). Unlike source-based algorithms, which estimate an earthquake's source parameters to predict shaking intensity and issue detailed alerts, PLUM employs a simple intensity threshold-based approach for generating alerts. Although this simplicity enhances its reliability, it does not provide the detailed earthquake characteristics typically offered by source-based methods. However, due to the complexities in estimating source characteristics, source-based algorithms face significant limitations, including creating larger blind zones and inaccuracies in predicting earthquake magnitude (Hoshiba & Iwakiri, 2011). These limitations undermine the reliability of source-based approaches, particularly in providing timely and accurate warnings. This highlights the potential advantages of adopting the PLUM algorithm for low-cost EEWS, which warrants further exploration and development.

Enhancing Ground Motion-based Algorithms for Low-cost Earthquake Early Warning Systems: The PLUM algorithm excels in complex seismic events, including detecting and generating alerts for multiple simultaneous earthquakes. However, it tends to provide shorter warning durations for areas far from the epicentre than source-based methods due to its reliance on S-waves, or Secondary waves, for earthquake detection and the limited prediction radius (R) for intensity prediction. Since S-waves are slower and more destructive than P-waves, or Primary waves, which are faster but less harmful, Kodera et al., (2018) proposed that integrating a P-wave detection algorithm into PLUM can enhance the warning time since P-waves arrive before S-waves. The integration of P-wave detection, particularly in decentralised processing architecture in a community-engaged EEW network, still needs to be explored in the current literature.

The above-described gaps in the literature have led the researcher to propose the following research questions and related research objectives. Through addressing these research questions and achieving the aligned objectives, the study aims to contribute significantly to the advancement of EEWS technology, offering more reliable, accurate, and timely EEW alerts.

1.2 Research Questions and Objectives

The research intends to bridge the identified gaps by exploring decentralised processing techniques, applying ground motion-based algorithms in the low-cost MEMS-based community-engaged EEWS initiated by Prasanna et al. (2022), and integrating P-wave detection into the PLUM algorithm for enhanced early warning capabilities. The ultimate objective of this work is to create **a community-engaged, low-cost MEMS-based EEWS that uses decentralised processing for the PLUM**

algorithm and integrates P-wave detection capability. This can be achieved by addressing the following research questions and accomplishing the related objectives.

1. **Research Question 1 (RQ1)**: How can a community-engaged, low-cost MEMS-based EEW network run the PLUM algorithm using decentralised processing be implemented?
    - Objective 1.1: Review the literature on existing EEW approaches globally and analyse their methodologies towards EEW (Chapter 3).
    - Objective 1.2: Implement an experimental community-engaged EEW network by installing low-cost MEMS-based ground motion sensors in households in the greater Wellington region of NZ (Chapter 4).
    - Objective 1.3: Implement the PLUM algorithm with decentralised processing in the experimental EEW network (Chapter 5).
2. **Research Question 2 (RQ2)**: How can P-waves be optimally detected in a community-engaged EEW network?
    - Objective 2.1: Review the literature on P-wave detection algorithms implemented globally (Chapter 6).
    - Objective 2.2: Compare the performance of various existing P-wave detection algorithms suitable for decentralised processing using ground motion data captured from the experimental community-engaged EEW network in the Greater Wellington Region (Chapter 6).
    - Objective 2.3: Validate the results obtained from objective 2.2 using a more extensive ground motion dataset (Chapter 7).
3. **Research Question 3 (RQ3)**: How can a P-wave detection algorithm be integrated into the PLUM algorithm to extend the warning window?
    - Objective 3.1: Establish a relationship between the amplitude of P-waves and S-waves in the context of NZ (Chapter 8).
    - Objective 3.2: Implement the P-wave-based PLUM algorithm with decentralised processing in the experimental EEW network (Chapter 9).
    - Objective 3.3: Evaluate the performance of both the PLUM and P-wave-based PLUM algorithms in the implemented EEWS (Chapter 9).

1.3 Research contribution

This PhD research significantly contributes to the knowledge and practice of EEWSs through several innovative developments:

1. **Development of a Community-Engaged PLUM-based EEWS:** The research introduces a PLUM-based EEWS that operates using low-cost MEMS-based seismographs with decentralised processing, eliminating the need for centralised processing units. This decentralised PLUM approach not only reduces system latency in issuing alerts but also addresses common issues in source-based algorithms, such as the overestimation or underestimation of earthquake magnitudes.
2. **Establishment of a P-wave detection enabled PLUM algorithm:** The research successfully develops a P-wave detection integrated PLUM algorithm for community-engaged EEW network. During the construction, a specific P-wave detection algorithm was selected, designed to detect P-waves in noisy environments effectively. This is critical for enhancing the warning window by utilising P-waves, which arrive earlier than the destructive S-waves mainly used for earthquake detection in PLUM-based systems.
3. **Documentation and Open Access to Research Outputs:** The research provides a valuable knowledge base by documenting the entire algorithm development process and maintaining an open-access public GitHub repository. This resource enables the broader research community to access, review, and extend the findings, fostering further innovations in earthquake early warning systems.

1.4 Research Outline

This research study adheres to Massey University's thesis by publication model. It comprises five peer-reviewed journal articles addressing the research questions presented in Chapters 3, 5, 7, 8, and 9. Two conference publications that further support exploring the research questions are included in Chapters 5 and 6. Table 1.1 depicts the alignment of the research questions, objectives, publications, chapters, and their respective publication status.

Table 1-1. Alignment of research questions, objectives, publications, chapters, and publication status.

Research Question	Research Objective	Manuscript	Chapter	Status
How can a community-engaged, low-cost MEMS-based EEW network run the PLUM algorithm using decentralised processing be implemented?	Review the literature on existing EEW approaches globally and analyse their methodologies towards EEW.	1st Manuscript: "Earthquake early warning systems based on low-cost ground motion sensors: A systematic literature review"	3	Published[1]
	Implement the PLUM algorithm with decentralised processing in the experimental EEW network.	2nd Manuscript: "Adapting PLUM: Earthquake early warning with node-level processing in New Zealand"	5	Published[2]
How can P-waves be optimally detected in a community-engaged EEW network?	Review the literature on P-wave detection algorithms implemented globally	3rd Manuscript: "Algorithms for detecting P-waves and earthquake magnitude estimation: Initial literature review findings"	6	Published[3]

[1] Journal: Frontiers in Sensors

[2] Conference: ISCRAM 2024

[3] Conference: Information Systems for Crisis Response and Management (ISCRAM) 2022

Research Question	Research Objective	Manuscript	Chapter	Status
	Compare the performance of various existing P-wave detection algorithms suitable for decentralised processing using ground motion data captured from the experimental community-engaged EEW network in the Greater Wellington Region.	4th Manuscript: "Performance analysis of P-wave detection algorithms for a community-engaged earthquake early warning system–a case study of the 2022 M5.8 Cook Strait earthquake"	6	Published[4]
	Validate the results obtained from objective 2.2 using a more extensive ground motion dataset	5th Manuscript: "Performance evaluation of P-wave detection algorithms for earthquake early warning using GeoNet sensor data in the Canterbury region"	7	Published[5]

[4] Journal: New Zealand Journal of Geology and Geophysics 2023

Research Question	Research Objective	Manuscript	Chapter	Status
How can a P-wave detection algorithm be integrated into the PLUM algorithm to extend the warning window?	Establish a relationship between the intensity of P-waves and S-waves in the context of New Zealand	6th Manuscript: "Estimating S-Wave intensity for early earthquake warning in New Zealand: Leveraging the first 3 seconds of P-wave intensity"	8	Published[5]
	Evaluate the performance of both the PLUM and P-wave-based PLUM algorithms in the implemented EEWS	7th Manuscript: "Performance Evaluation of a Community Engaged Low-Cost Earthquake Early Warning System for Aotearoa New Zealand"	9	Under Review[6]

1.5 The Structure of the Thesis

This thesis comprises ten chapters, each serving a distinct purpose within the scope of the research. As outlined in Section 1.4, the thesis includes seven manuscripts, each presented as individual chapters, except Chapter 6, which combines two manuscripts. Additionally, the thesis features an introductory chapter, a chapter on research philosophy and methodology, and a chapter detailing the implementation of the community-engaged EEW network (Chapter 4). The final chapter provides an overall discussion. Since six chapters are based on published manuscripts, some repetition across chapters is expected. The organisation of the thesis is visually represented in Figure 1.1, which outlines each chapter's placement and focus.

[5] Journal: Earth Science Informatics, Springer

[6] Journal: Seismological Research Letters

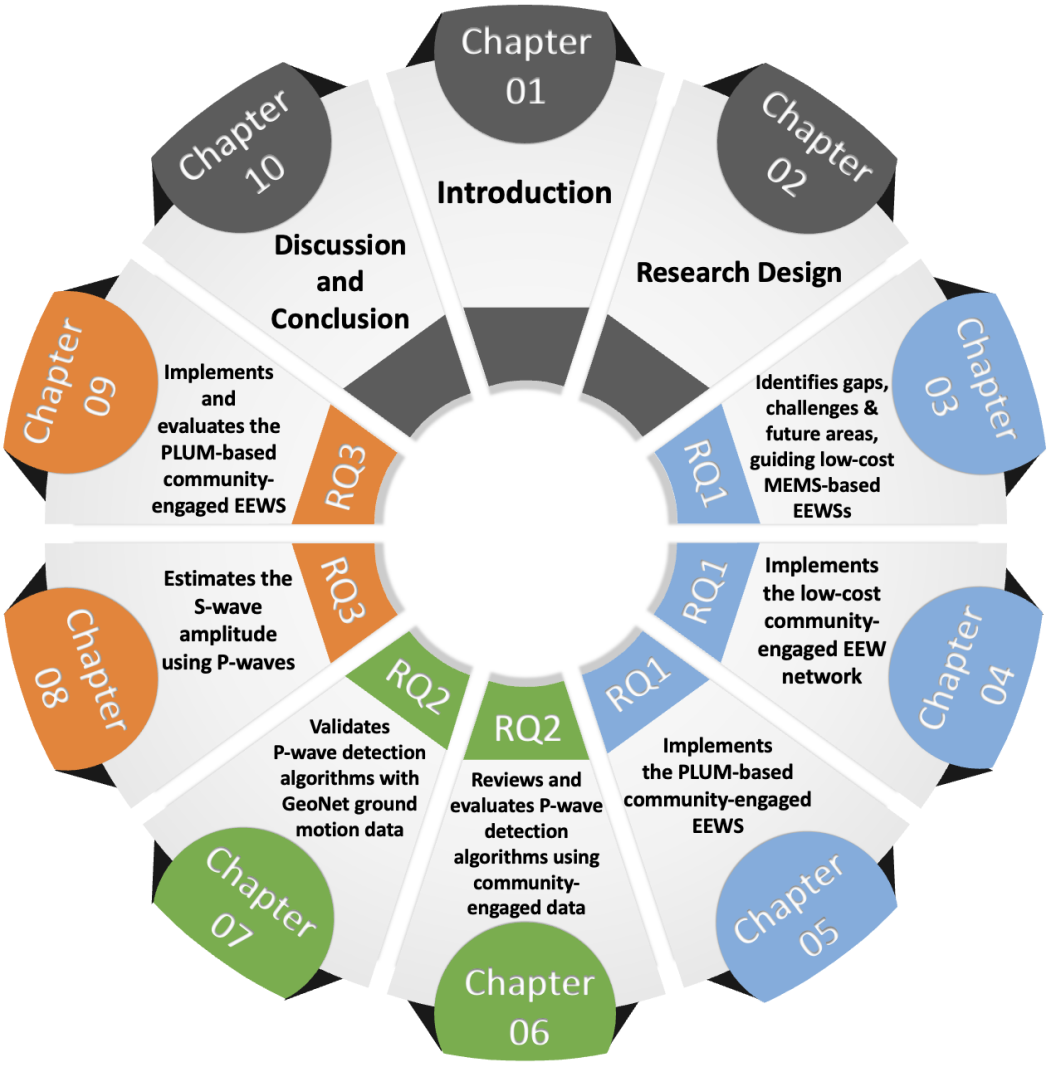

Figure 1-1. Thesis chapter outline.

Chapter 2

Chapter 2 delineates the research philosophy and methodology adopted throughout this doctoral study, explaining the rationale behind selecting Design Science Research (DSR) as the guiding methodology. It elaborates on how DSR is effectively utilised to address the research questions posed by the study, providing a structured approach to developing and testing the proposed solutions. Additionally, the chapter outlines the research methods employed to achieve the specific objectives of the thesis.

Chapter 3: Manuscript 1

Chapter 3 details the systematic literature review conducted to explore low-cost MEMS-based EEWSs implemented worldwide. The chapter addresses the first research question, "How can a community-engaged, low-cost MEMS-based EEW network run the PLUM algorithm using decentralised processing be implemented?" It analyses and synthesises findings from 59 articles, examining existing EEW

approaches and their methodologies. The findings are presented through a flowchart summarising the identified limitations, challenges, and future research directions within low-cost MEMS-based EEWS. Moreover, this chapter highlights the research gaps in the literature, which this study aims to address, providing a clear context for the subsequent research phases documented in this thesis.

Chapter 4

Chapter 4 details installing ground motion sensors within community members' households to establish a community-engaged EEW network in the Greater Wellington region. The chapter explains the method used for selecting 25 sensor locations from 80 willing-to-install responses received from the public. It also summarises the two comprehensive questionnaires conducted with the sensor hosts and presents a detailed installation guide. A technical note is also presented, which analyses the performance of ground motion sensors in different installation methods for a typical household floor type. This chapter fulfils Objective 1.2 of the thesis: Implement an experimental community-engaged EEW network by installing low-cost MEMS-based ground motion sensors in households within the greater Wellington region.

Chapter 5: Manuscript 2

Chapter 5 presents a work-in-progress paper published as a peer-reviewed conference article detailing the implementation of the PLUM EEW algorithm within a community-engaged, low-cost EEW network. The section discusses the method adopted to operate the PLUM EEW algorithm in NZ's seismic context, using decentralised processing to eliminate the need for centralised processing units.

Chapter 6: Manuscript 3 and 4

Chapter 6 comprises two peer-reviewed manuscripts focusing on reviewing and evaluating P-wave detection algorithms used in EEWSs. The first manuscript, presented as a work-in-progress paper published in a peer-reviewed conference, reviews the P-wave detection algorithms in EEWSs globally. This section addresses the research question, "How can P-waves be detected in a community-engaged EEW network?" by reviewing 144 research articles on various P-wave detection methods. The insights from this literature review guide the selection of an appropriate P-wave detection algorithm for the community-engaged EEWS. The second manuscript evaluates the four chosen algorithms' effectiveness in detecting earthquakes through community-based sensors. It identifies the most effective one for noisy environments, using a single earthquake as a case study with the community-engaged ground motion data. This evaluation supports Objective 2.2, which aims to compare the performance of different P-wave detection algorithms suitable for decentralised processing in a community-engaged setting.

Chapter 7: Manuscript 5

Chapter 7 expands on the research conducted in Chapter 6 by analysing the performance of four P-wave detection algorithms with a comprehensive dataset encompassing 46 earthquakes recorded by the GeoNet network between 2010 and 2011. This chapter addresses limitations in the earlier analysis by offering a broader scope of data to examine the frequency and accuracy of missed and late detections. It employs statistical methods to validate the effectiveness of the selected algorithms, further enhancing the robustness of the findings presented in Chapter 6.

Chapter 8: Manuscript 6

Chapter 8 features a published journal article that estimates S-wave amplitude by analysing the first three seconds of P-wave data. This research is pivotal in integrating the P-wave detection algorithm, as identified in Chapters 6 and 7, with the PLUM-based EEW network discussed in Chapters 4 and 5. This chapter examines ground motion recordings from the GeoNet network from 2010 to 2023, employing a linear regression model to estimate S-wave amplitude based on P-wave characteristics.

Chapter 9: Manuscript 7

Chapter 9 focuses on implementing and evaluating the P-wave-based PLUM algorithm in the experimental EEWS. It first describes integrating the P-wave detection algorithm into the PLUM-based system, enabling it to operate using decentralised processing. This implementation addresses Objective 3.2 of the thesis: Implement the P-wave-based PLUM algorithm with decentralised processing in the experimental EEW network. The chapter then evaluates and compares the real-life performance of the PLUM algorithm implemented in Chapter 5 and the enhanced P-wave-based PLUM algorithm within the implemented system. The findings contribute to understanding how P-wave integration can improve the warning time and overall efficiency of low-cost EEWS.

Chapter 10

Chapter 10 concludes the doctoral thesis by summarising the principal findings. It revisits the research questions and objectives set out at the beginning of the study, evaluating how these have been addressed throughout the research. The chapter highlights the significant contributions of the research to both academic knowledge and practical application in EEWS. Additionally, it discusses some limitations encountered during the study and suggests directions for future research.

Position of the reader

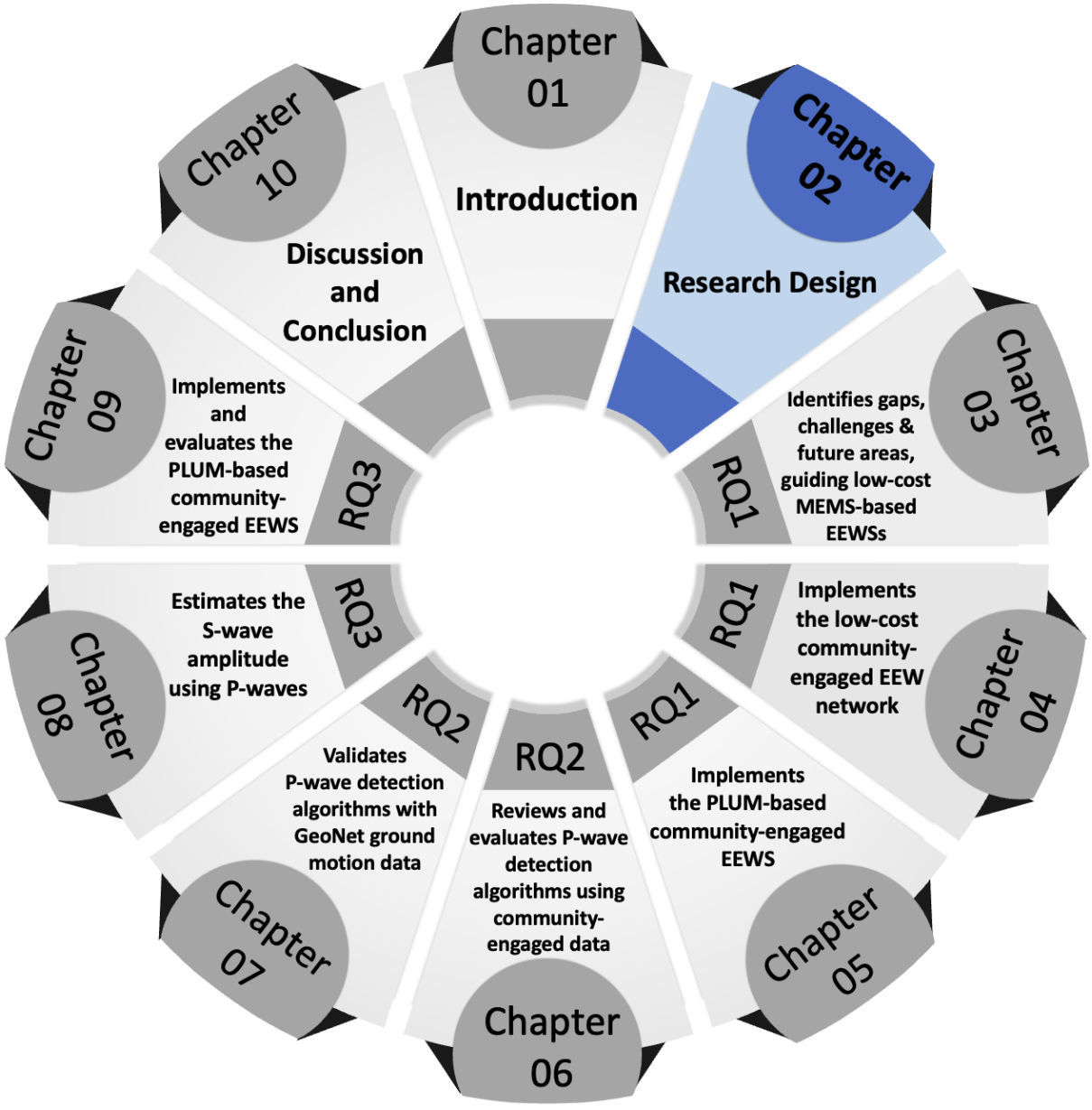

2 Research Design

This research positions itself within the Information Systems (IS) field because it focuses on enhancing the development, management, and effective use of technology systems, particularly in the context of EEWSs. IS are concerned with the technical and analytical aspects of how data is collected, managed, processed, and utilised to support decision-making and operational effectiveness (Information Systems (IS), 2023). In the context of EEWS, IS play a crucial role in developing and implementing systems that can process seismic data in real-time, enabling the timely detection of earthquakes and disseminating alerts to the public and authorities.

Applying IS principles to EEWS, this research integrates seismology, social science, and information technology to create a robust system that efficiently manages and uses data for critical applications such as disaster management and public safety. Therefore, this study contributes to advancing IS theory and practice, particularly in the design and implementation of EEWS.

Adopting IS as the conceptual framework; the research design of this doctoral study unfolds into two main segments: the research paradigm and the research methodology. The research paradigm explores the dominant philosophical viewpoints in IS and the rationale for their philosophical underpinnings (Morgan, 2007; Nogeste, 2007; Scotland, 2012). The research methodology comprises the chosen Design Science Research methodology and the specific research methods relevant to each research objective (Kilani & Kobziev, 2016). These components and sub-components are defined in the following sections, and the overall design of the research is provided.

This chapter presents the chosen design for this doctoral research, consisting of the research paradigm (Section 2.1), the methodology (Section 2.2), the Design Science Research (Section 2.2.1), the research methods (Section 2.3), and the ethical considerations (Section 2.4). The chapter then concludes with a chapter summary (Section 2.5).

2.1 Research Paradigms

A research paradigm provides a fundamental framework that guides a researcher's methodology and approach towards knowledge development (Morgan, 2007; Nogeste, 2007). Within the IS field, research paradigms such as positivism and interpretivism, offer distinct perspectives on conducting research and interpreting knowledge (Orlikowski & Baroudi, 1991). Understanding the strengths and weaknesses of these paradigms is crucial to aligning the chosen paradigm with the research objectives and questions. By examining the spectrum of positivism and interpretivism, researchers can select the paradigm that best supports the methodology and epistemological stance.

Positivism emphasises validating predefined hypotheses through empirical observation and logical reasoning, assuming reality is stable and objectively observable (Creswell, 2014a; Orlikowski & Baroudi, 1991; Scotland, 2012). It focuses on quantifiable measurements to understand phenomena (Flick, 2018). Conversely, interpretivism, often associated with social constructivism, views reality as subjective, shaped by individual experiences and social contexts (Klein & Myers, 1999; Scotland, 2012). Rather than seeking objective truth, interpretivism explores the complexity of human thought and culture through individuals' meanings and interpretations (Scotland, 2012).

The dichotomy between positivism and interpretivism has traditionally guided researchers in aligning their investigations with one of these paradigms. However, Orlikowski & Baroudi (1991) argue that no single paradigm is superior, as each has unique strengths and limitations. The nature of the research aims and objectives often dictates the choice of paradigm or even the integration of multiple paradigms. Researchers may blend positivism and interpretivism to address research questions needing objective and subjective insights, leading to a pragmatic approach (Orlikowski & Baroudi, 1991). "Pragmatism", as a philosophy, recognises multiple realities and the limitation of a singular viewpoint (Goldkuhl, 2004; Kelemen & Rumens, 2008), advocating for diverse methods, worldviews, assumptions, and techniques to tackle to complex research questions (Creswell, 2014b; Johnson & Onwuegbuzie, 2004; Mertens, 2015).

Pragmatism is the most fitting paradigm for this research, given the nature and multidisciplinary demands. This proposed research aims to develop a community-engaged, low-cost MEMS-based EEWS using decentralised processing to execute EEW algorithms. The PhD project requires a multidisciplinary approach as it intersects computer science, seismology, and the Internet of Things (IoT), necessitating objective algorithm and theorem development. However, the project also involves subjective human and social components as the system is embedded in community and expert engagements. These various technical and social interactions highlight the importance of an approach

accommodating objective and subjective perspectives. By embracing pragmatism, the research can effectively address the technical challenges and social considerations for implementing an EEWS.

2.2 Methodology

The methodology for this research follows a pragmatist approach, selecting methods that best address the research questions and objectives (Kaushik & Walsh, 2019; Mertens, 2015). Design Science Research (DSR) is particularly well-suited for this PhD project, which requires a multidisciplinary approach integrating both technological and social elements. DSR's iterative cycles support the development and refinement of research artefacts within real-world contexts, aligning with the study's goal of developing a community-engaged low-cost EEWS.

As a pivotal methodology for conducting IS research, DSR is especially effective for studies that bridge technology and social sciences (Brocke et al., 2020; Hevner et al., 2004). DSR's three iterative cycles, encompassing the environment, design elements, and knowledge base, are conducive to transdisciplinary efforts. A significant advantage of DSR is its capacity for artefact testing within the originating environment, enabling real-world application and feedback (Brocke et al., 2020).

This ability to test within the environmental aligns with the study's requirements, which aim to develop a theoretical framework while delivering tangible practical solutions on EEWS for the community. The iterative nature of DSR provides a robust framework for engaging with both qualitative and quantitative data, supporting the continuous development, testing, and refining research artefacts in a process that mirrors the dynamic and iterative nature of community engagement (Brocke et al., 2020).

2.2.1 Design Science Research (DSR)

This subsection delves into the specifics of the DSR framework as applied to this PhD research project. It starts with briefly discussing the artefact centre to the research: a community engaged, low-cost MEMS-based EEWS. Following this, three key cycles of DSR, as defined by Hevner (2007) as the relevance, design, and rigour cycles, will be discussed, illustrating how the cycles collectively contribute to the systematic development and refinement of the artefact within this multidisciplinary context.

2.2.1.1 Artefact and the Specific Components

The doctoral study focuses on developing an artefact: **a community-engaged, low-cost MEMS-based EEWS, operating on decentralised processing, that utilises both the PLUM algorithm adapted for NZ's seismic context, and a P-wave detection enabled PLUM algorithm**. The development of this artefact relies on three pivotal components:

1. **Implementation of the Community-Engaged EEW Network:** This foundational step involves deploying low-cost MEMS-based ground motion sensors across the community, laying the groundwork for an earthquake early warning system.
2. **Selection of a P-Wave Detection Algorithm for the Community-Engaged EEWS:** Critical to the artefact's functionality, this component entails choosing an effective P-wave detection algorithm that is compatible with the community-engaged network's capabilities and can operate efficiently at the node level.
3. **Implementation of the PLUM and P-wave Detection Enabled PLUM Algorithms:** This final component focuses on adapting the PLUM algorithm for NZ and integrating the P-wave detection capability, enabling the EEW network to execute using decentralised processing.

Figure 2-1 shows the main three stages of this doctoral study in accomplishing the proposed artefact.

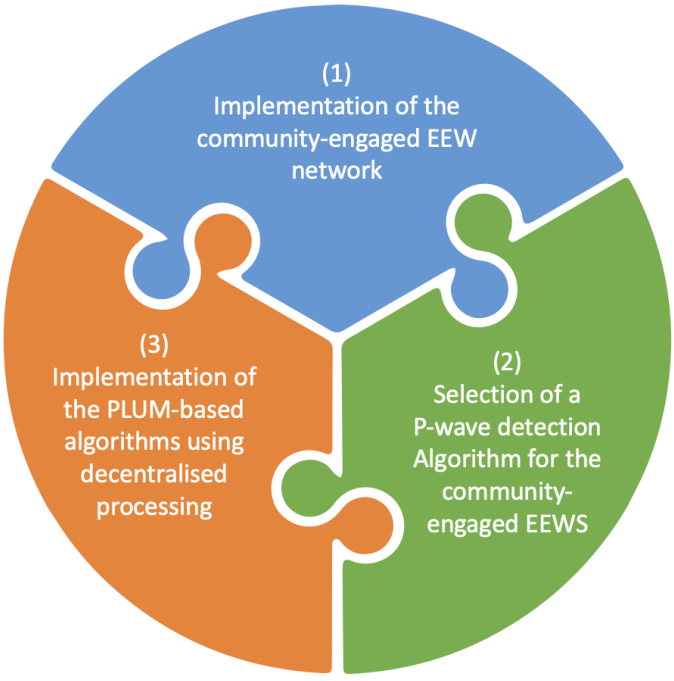

Figure 2-1. Three components towards developing the research artefact

2.2.1.2 Iterative Cycles of DSR

The interplay and development of these artefact components are guided by the iterative cycles of the DSR framework. In the following sections, the contributions of each component to the artefacts' construction will be detailed, highlighting how the DSR framework's facilitates a systematic approach to overcoming the complex challenges inherent in developing an effective community-engaged EEW network.

The DSR methodology positions the researcher in dual roles: an initiator actively designing the artefact and a collaborator engaging with stakeholders to refine and validate the artefacts. Central to this methodology are the three interrelated research cycles: the Relevance Cycle, the Design Cycle, and the Rigour Cycle (Figure 2-2). These cycles facilitate a continuous, iterative dialogue between the problem context, the artefact design and evaluation, and the knowledge base, ensuring a comprehensive and grounded approach.

- The **Relevance Cycle** connects the practical challenges in the research environment with the design science activities, ensuring that the research remains grounded in real-world problems.
- The **Design Cycle** involves the iterative development, assessment, and refinement of artefacts, allowing for the practical testing and enhancement of the proposed solutions.
- The **Rigour Cycle** strengthens the research with a solid theoretical foundation, drawing from scientific theories, empirical experiences, and expert insights to inform the design science activities.

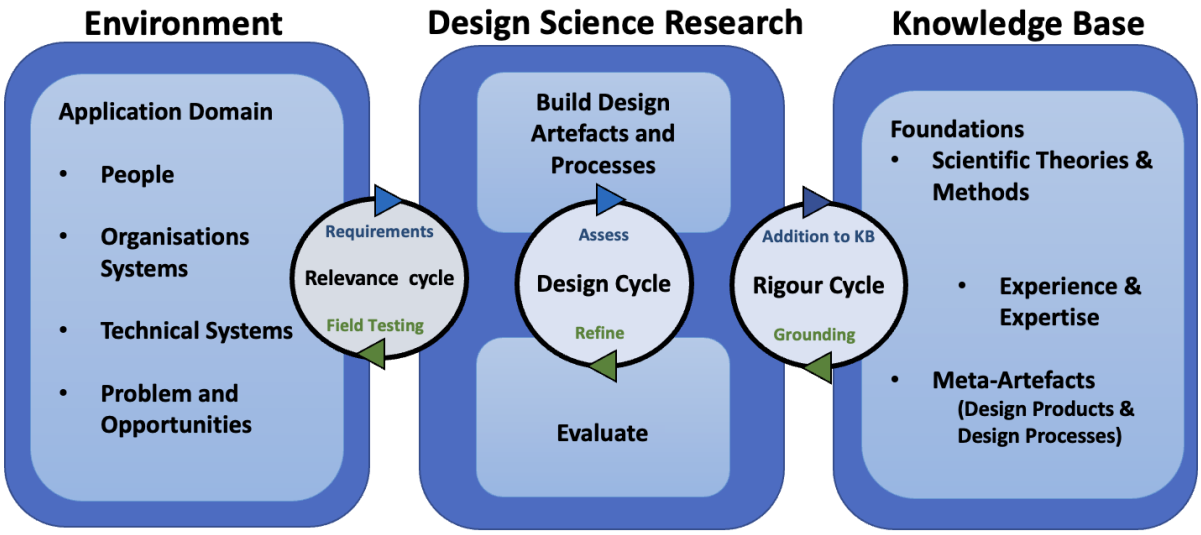

Figure 2-2. Design Science Research Cycles (Adapted from Hevner, 2007)

2.2.1.3 Relevance Cycle

The Relevance Cycle is crucial in bridging the gap between the research project's real-world environment and the design science activities (Brocke et al., 2020). It connects the environment—comprising people, organisational systems, and technical systems—to extract research requirements. These requirements underpin the construction of the artefact, which is then reintroduced into the environment for a thorough evaluation.

Beyond requirements gathering, the Relevance Cycle critically assesses the artefact against these initial requirements, identifying any functional deficits or inaccuracies. This evaluation is vital for refining the artefact, ensuring it evolves into a fully functional product that meets or exceeds expectations. The iterative nature of this Cycle, supported by feedback from field testing, facilitates the continuous development and adjustments based on real-world performance and user feedback.

The Relevance Cycle (see Figure 2-3) for this research begins with the requirements gathering through expert knowledge shared during webinar sessions and community workshops conducted by the CRISiSLab team (Prasanna et al., 2022; Tan et al., 2021), as well as insights from relevant literature on community-engaged EEW networks. The next step involves the initial installation and field testing of the sensor network to evaluate its effectiveness in recording seismic activity. Following this, a questionnaire is distributed to sensor hosts to collect further requirements, focusing on installation methods, sensor placement preferences, neighbourhood noise levels, maintenance practices, and any encountered challenges. The feedback informs the refinement of the initial sensor installation phase, leading the subsequent installation of additional sensors. In the second phase, the EEW network undergoes further field testing.

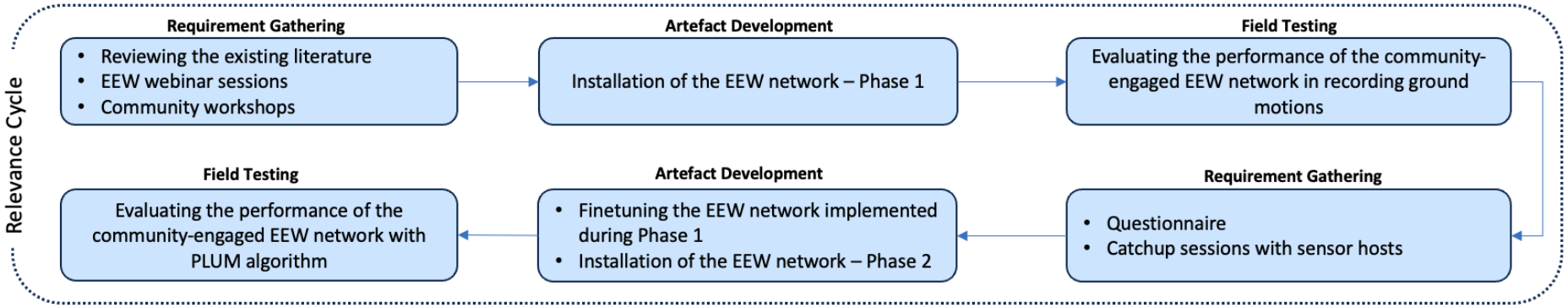

Figure 2-3. The iterative process taken during the Relevance Cycle for implementing the community-engaged EEW network with PLUM algorithm using decentralised processing

2.2.1.4 Rigour Cycle

The Rigour Cycle in DSR ensures the research is innovative and theoretically grounded. It draws from an extensive knowledge base encompassing scientific theories, methodologies, and cutting-edge techniques (Brocke et al., 2020). This Cycle provides researchers with an understanding of the existing landscape of their field, offering insights into current artefacts and methodologies and guiding the development of novel solutions. An extensive literature review within the Rigour Cycle helps identify the most appropriate methods and techniques for creating and evaluating artefacts. By grounding their work in the established body of knowledge, researchers ensure that their contributions—new algorithms, enhancements to existing models, or innovative design processes—advance academic discourse and offer practical applications. Thus, the Rigour Cycle enhances both academic integrity and practical significance.

In this doctoral study, the Rigour Cycle plays a continuous role across all three main components of the proposed artefact, emphasising the importance of a solid literature foundation in developing the proposed research outcome. Initially, a Systematic Literature Review identifies challenges and gaps in implementing a community-engaged low-cost MEMS-based EEW network, contributing to the knowledge base through journal publication. This groundwork informs further reviews on the PLUM algorithm and decentralised processing, enriching the knowledge base. For the second component, the literature review facilitates selecting an appropriate P-wave detection algorithm for the network, with findings from testing various algorithms using community-engaged data and an extensive earthquake database from GeoNet shared with the community. Finally, the third component involves a literature review of various methods for estimating S-wave amplitude using P-waves. This review lays the groundwork for establishing a relationship between P-wave and S-wave amplitudes, which is essential for integrating the P-wave detection algorithm with the PLUM algorithm. This is followed by a performance evaluation of the implemented EEWS using the PLUM-based algorithms. The findings from this research are subsequently disseminated through publication. Figure 2-4 illustrates the role of the Rigour Cycle in these developments.

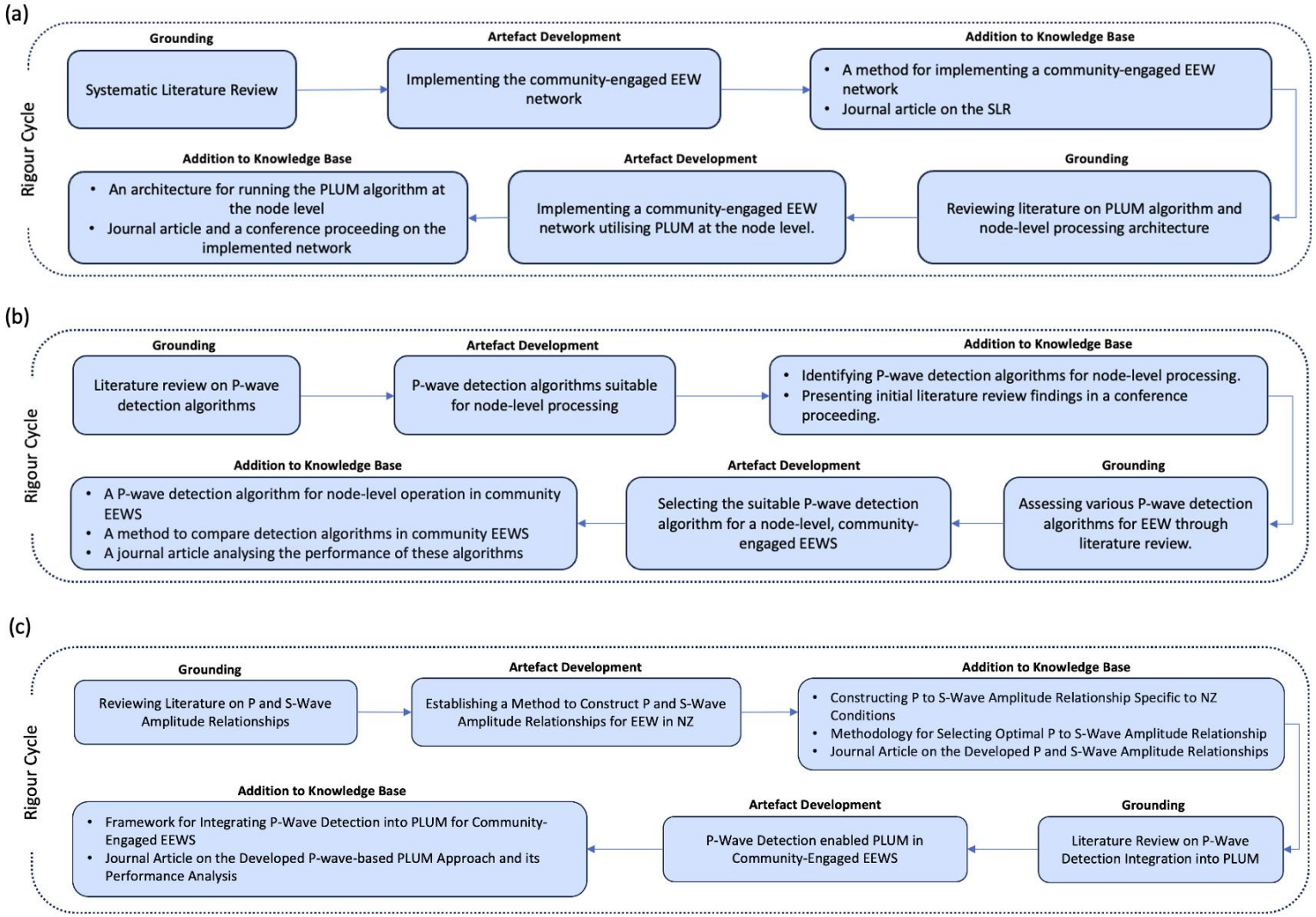

Figure 2-4. Panels (a), (b), and (c) depict the iterative progression of the Rigour Cycle in developing components 1, 2 and 3, respectively

2.2.1.5 Design Cycle

The Design Cycle is central to DSR, driving the iterative process of artefact creation, evaluation, and refinement (Hevner, 2007; Brocke et al., 2020). It integrates the theoretical insights from the Rigour Cycle and the practical demands of the Relevance Cycle, leading to enhancing the artefact that meets or exceeds the research objectives' expectations. While the Design Cycle is intrinsically linked to the Relevance and Rigour Cycles, it also operates with a degree of independence crucial for the creative and practical execution of the research (Hevner, 2007). This independence allows for a flexible yet focused approach to artefact development, enabling researchers to explore innovative solutions without being overly constrained by existing paradigms or user expectations.

The Design Cycle activities for this doctoral research are instrumental in constructing and refining the community-engaged and low-cost MEMS-based EEWS. The Cycle starts with the requirements identified through the Relevance Cycle and the acquiring knowledge from the Rigour Cycle. The artefact components are then prototyped within a laboratory environment, allowing for iterative refinement based on evaluation outcomes before field deployment:

- For the first component—implementing a community-engaged EEW network—undergoes a series of tests to determine the most effective sensor installation methods and refine the PLUM algorithm for decentralised processing.
- For the second component—selecting a P-wave detection algorithm—laboratory comparisons and statistical evaluations guide the choice and optimisation of algorithms for the network.
- For the third component—implementing a P-wave detection algorithm with PLUM—involves testing to establish a relationship between P and S-wave amplitudes, which is formulated and assessed using ground motion data.

Figure 2-5 encapsulates the Design Cycle's iterative process across the artefact's three components, illustrating the Cycle's pivotal role in guiding the artefact from conception to refinement and readiness for real-world application. This demonstrates the Cycle's crucial contribution to translating theoretical knowledge and practical needs into a functional and effective artefact for community-engaged EEWS.

Further, Figure 2-6 illustrates the proposed research methodology and how the research artefact maps onto the three different Cycles of the DSR model.

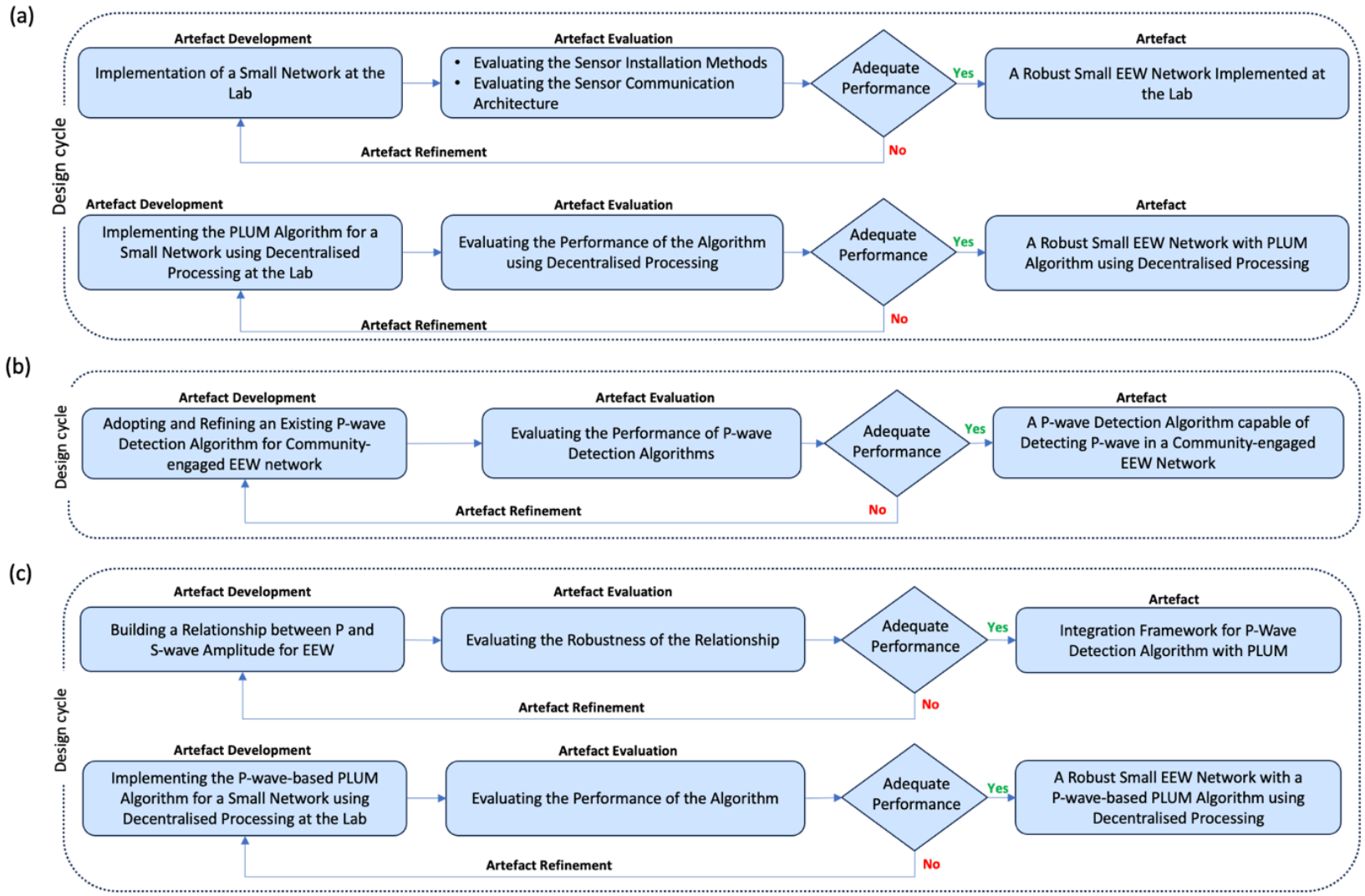

Figure 2-5. The Design Cycle's iterative process for artefact development: (a), (b), and (c) depict the Design Cycle stages of components 1, 2, and 3, respectively.

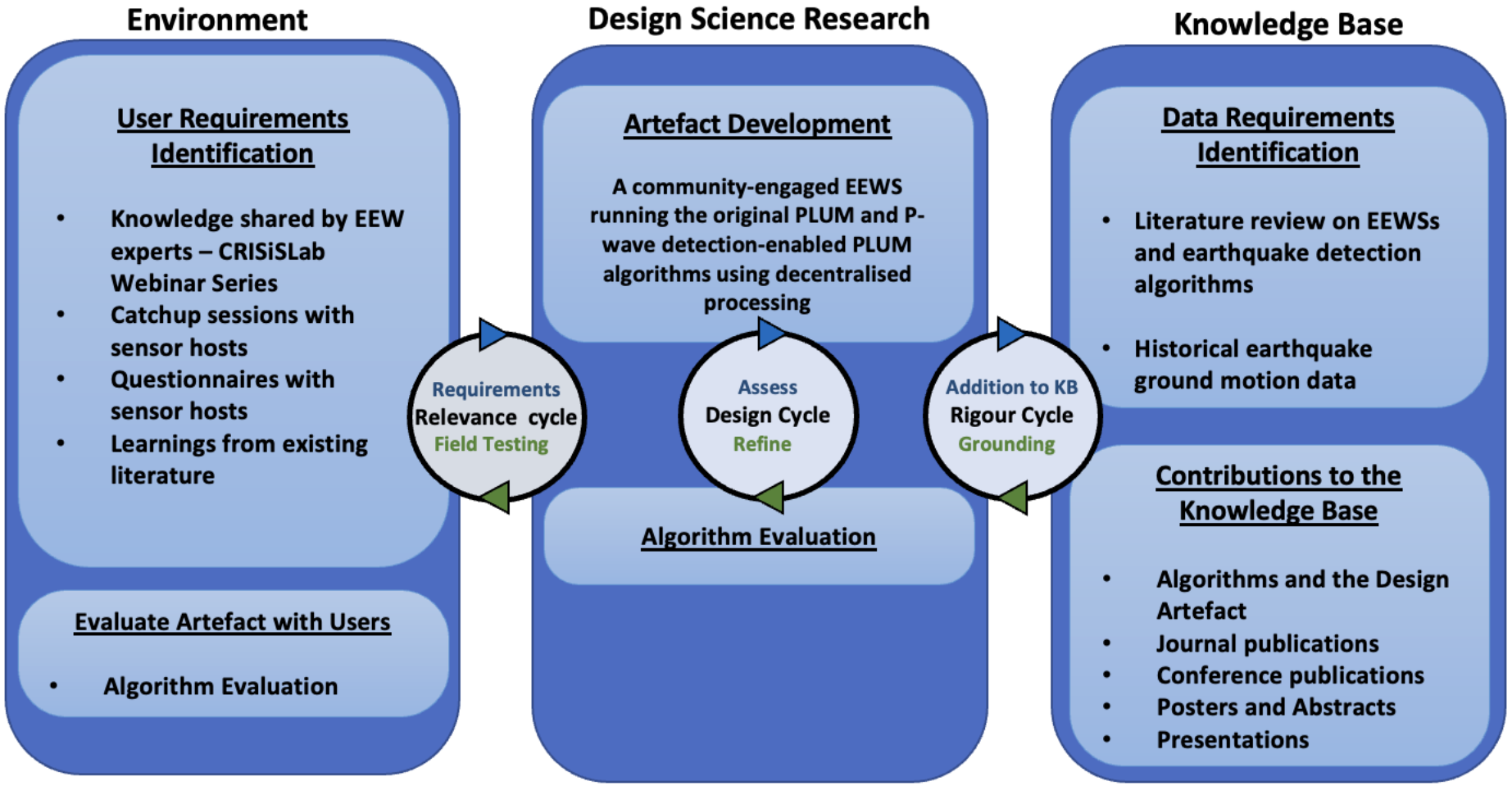

Figure 2-6. Graphical illustration of the proposed research framework driven by the DSR

2.3 Manuscripts and Methods

This thesis focuses on developing a "community-engaged, low-cost MEMS-based EEWS utilising decentralised processing for both the PLUM and P-wave detection enabled PLUM algorithms". The research addresses three primary questions (as outlined in Section 1.2) in building the proposed artefact. These questions are explored and answered by formulating three components, as elaborated in the methodology section (Section 2.2). The succeeding chapters of this thesis contribute to developing these components, leading to the design, creation, and evaluation of the artefact. Figure 2-7, presented in Chapter 1 and below, will appear at the beginning of each chapter, anchoring each manuscript's position within the broader thesis narrative.

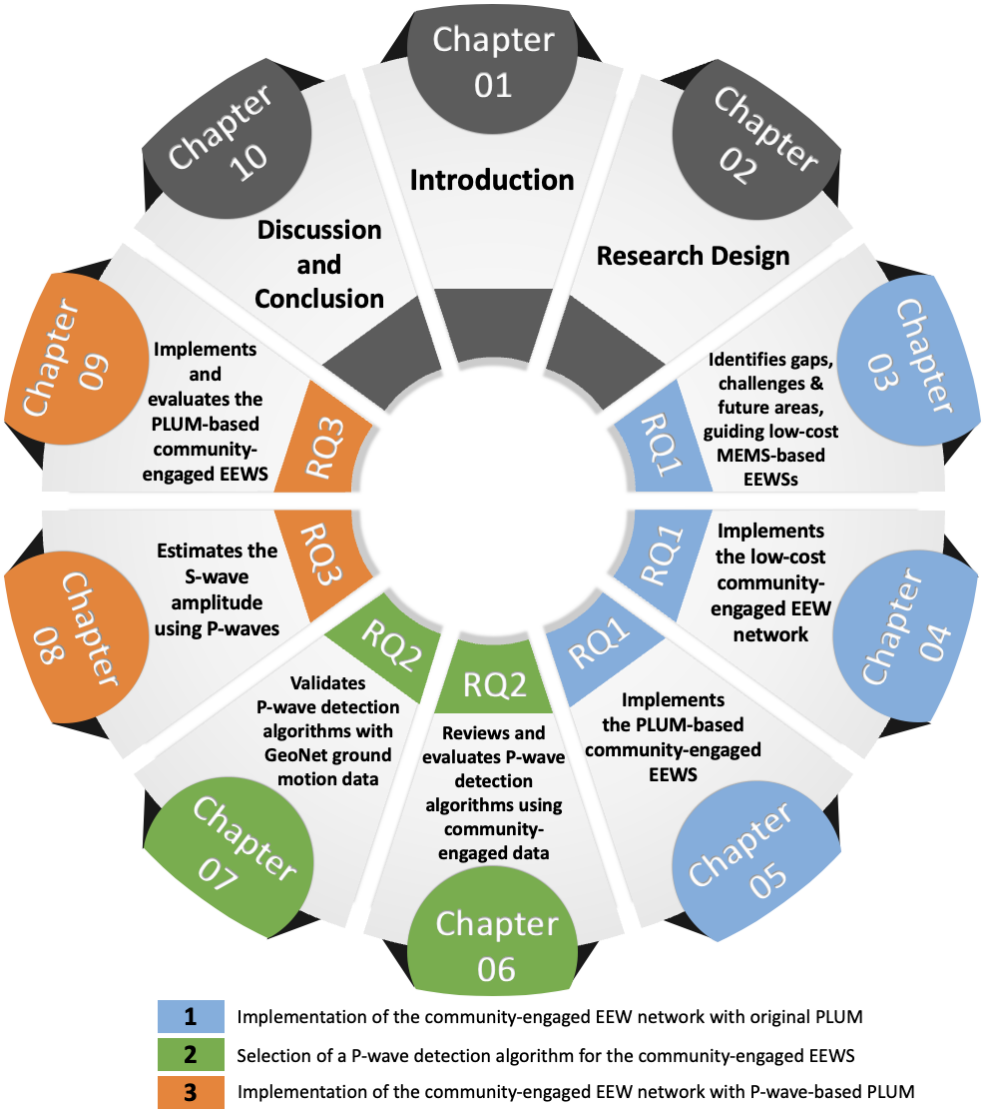

Figure 2-7. The chapters discussed in this doctoral study and their interconnectivity towards achieving the objectives of the study

Table 2-1 summarises the manuscripts, methods, and data sources employed throughout the study. However, each chapter delves into the specific methods employed to accomplish its stated objective for a comprehensive understanding.

Table 2-1. Research method and data sources used for the study is summarised chapter wise with their manuscript, key objective and overall objective for this doctoral study

Overall Objective	Chapter Number	Key Objective	Method	Data Source	Manuscript
Implementation of the Community-Engaged EEW Network with Original PLUM	3	To Identify gaps, challenges & future areas, guiding low-cost MEMS-based EEWSs.	Systematic literature review	Peer-reviewed academic papers identified through Scopus and Web of Science databases.	Manuscript 1
	4	To Implement a low-cost community-engaged EEW network	• A systematic approach that combined visualising existing sensor placements, a social media campaign to solicit community interest and strategic considerations like seismic activity and fault line proximity. • Laboratory test	• Online questionnaire • Data related to seismic activity, and fault line locations from GeoNet. • Ground motion recordings obtained from the laboratory experiments. • Academic articles on ground motion sensor comparisons.	

Overall Objective	Chapter Number	Key Objective	Method	Data Source	Manuscript
	5	To implement and evaluate the PLUM-based community-engaged EEWS.	• Laboratory test • Field testing with implemented EEW network	• Ground motion recordings captured from the implemented network. • Academic articles on PLUM algorithm and decentralised processing architecture.	Manuscript 2
Selection of a P-Wave Detection Algorithm for the Community-Engaged EEWS	6	To review the existing literature on P-wave detection algorithms implemented globally	Literature review	Peer-reviewed academic articles found in Scopus and Web of Science databases.	Manuscript 3
	6	To evaluate four P-wave detection algorithms using community-engaged ground motion data, aiding selection for community-engaged EEWS.	Statistical method	Ground motion data from the Raspberry Shake official database.	Manuscript 4

Overall Objective	Chapter Number	Key Objective	Method	Data Source	Manuscript
	7	To validate the P-wave detection algorithms with a larger GeoNet data to select the optimal P-wave detection algorithm.	Statistical method	Earthquakes captured from NZ's GeoNet network.	Manuscript 5
Implementation of the Community-Engaged EEW Network with P-wave-based PLUM	8	To establish a relationship between the amplitude of P-waves and S-waves for NZ	Statistical method - Linear regression	Earthquakes collected from the Canterbury Network (CanNet).	Manuscript 6
	9	To implement the P-wave-based PLUM algorithm with decentralised processing in the experimental EEW network	• Laboratory test • Field testing with implemented EEW network	Ground motion recordings captured from the community-engaged network.	Manuscript 7

Overall Objective	Chapter Number	Key Objective	Method	Data Source	Manuscript
	9	To evaluate the performance of the original and the P-wave-based PLUM algorithms in the implemented EEWS	• Laboratory test • Field testing with implemented EEW network	Ground motion recordings captured from the community-engaged network.	Manuscript 7

2.4 Ethics

This doctoral research project incorporates various data sets and methods, some involving community members who have installed ground motion sensors in their households. This study obtained peer-reviewed ethical approval as mandated by the Massey University code of ethical conduct for research, teaching, and evaluations involving human participants to ensure adherence to ethical standards (Massey University, 2024). Two 'low-risk' ethics notifications, with application IDs 4000027269 and 4000028144, were submitted to the Massey University Human Ethics Committee. These relate to the implementation of the first component of the study, which is the implementation of a community-engaged EEW network, for which two online questionnaires require ethical approval. The documentation of these ethics' notifications and the peer-reviewed approvals are available in Appendix A. The second and third components of this study does not necessitate the ethical approval process for human participation, as these phases solely utilise information derived from the literature and ground motion recordings.

2.5 Chapter Summary

This chapter covers the research design for this doctoral study. The research lies in the field of IS, aligns with the philosophy of pragmatism, and applies the DSR methodology for constructing a community-engaged, low-cost MEMS-based EEWS. The DSR methodology highlights the iterative engagement process, theoretical exploration, and artefact creation. The chapter also briefly outlines the manuscripts and methods to address the study's objectives. Finally, the chapter provides the ethical considerations for the PhD research.

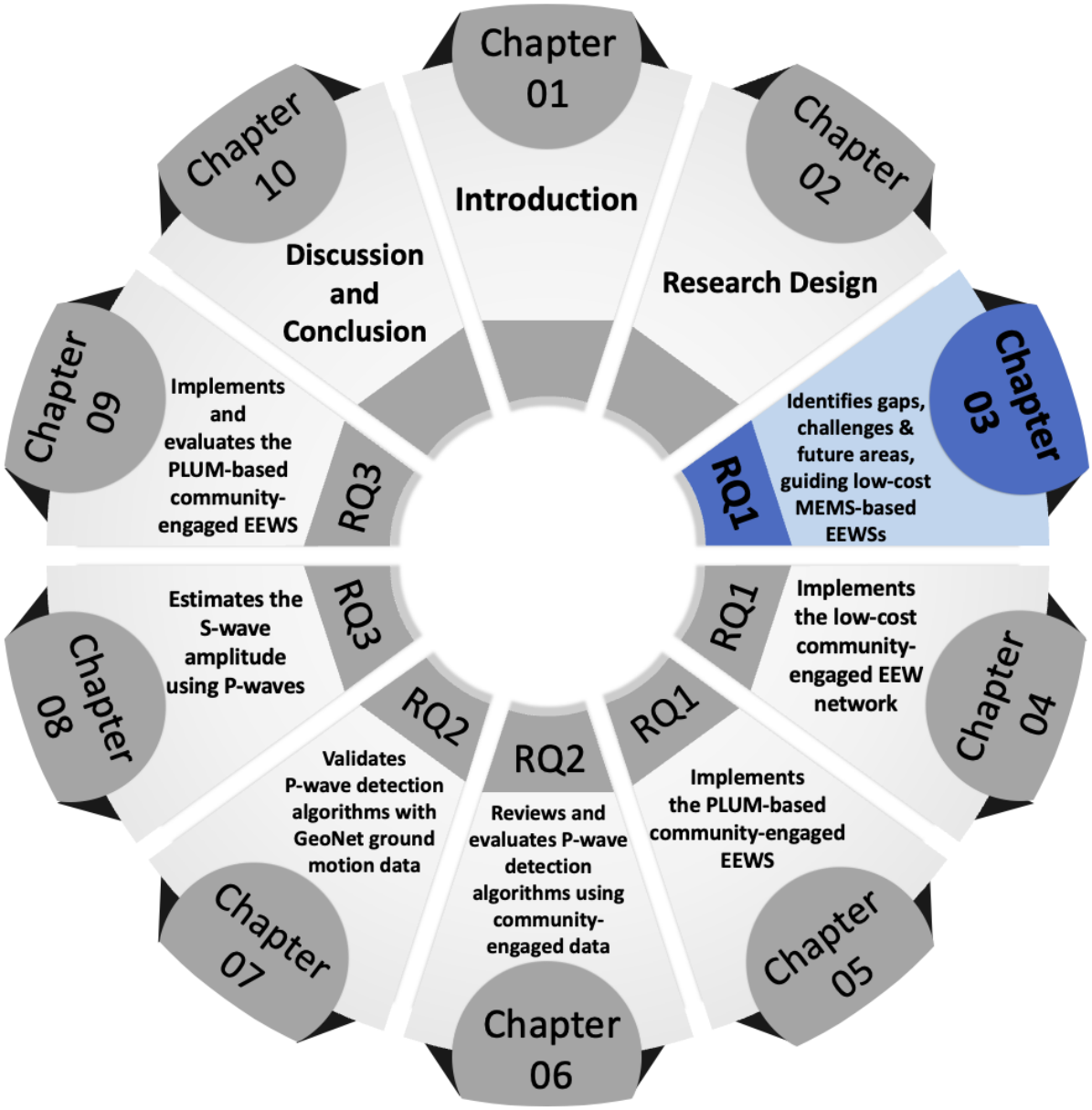
Chapter 01
Introduction
Chapter 02
Research Design
Chapter 03
RQ1
Identifies gaps, challenges & future areas, guiding low-cost MEMS-based EEWs
Chapter 04
RQ1
Implements the low-cost community-engaged EEW network
Chapter 05
RQ1
Implements the PLUM-based community-engaged EEWS
Chapter 06
RQ2
Reviews and evaluates P-wave detection algorithms using community-engaged data
Chapter 07
RQ2
Validates P-wave detection algorithms with GeoNet ground motion data
Chapter 08
RQ3
Estimates the S-wave amplitude using P-waves
Chapter 09
RQ3
Implements and evaluates the PLUM-based community-engaged EEWS
Chapter 10
Discussion and Conclusion

MASSEY UNIVERSITY
TE KUNENGA KI PŪREHUROA
UNIVERSITY OF NEW ZEALAND

GRADUATE RESEARCH SCHOOL

STATEMENT OF CONTRIBUTION
DOCTORATE WITH PUBLICATIONS/MANUSCRIPTS

We, the candidate and the candidate's Primary Supervisor, certify that all co-authors have consented to their work being included in the thesis and they have accepted the candidate's contribution as indicated below in the *Statement of Originality*.

Name of candidate:	CHANTHUJAN CHANDRAKUMAR
Name/title of Primary Supervisor:	Aprof. Raj Prasanna
In which chapter is the manuscript /published work:	3

Please select one of the following three options:

(●) The manuscript/published work is published or in press

- Please provide the full reference of the Research Output:

Chandrakumar C, Prasanna R, Stephens M, Tan ML. 2022. Earthquake early warning systems based on low-cost ground motion sensors: A systematic literature review. Frontiers in Sensors. 3. https://doi.org/10.3389/fsens.2022.1020202

( ) The manuscript is currently under review for publication – please indicate:

- The name of the journal:

Frontiers in Sensors

- The percentage of the manuscript/published work that was contributed by the candidate: 80.00

- Describe the contribution that the candidate has made to the manuscript/published work:

Chanthujan Chandrakumar led the conceptualisation and idea development of the study, co-constructed the methodology, conducted the formal analysis and investigation, and written the draft.

( ) It is intended that the manuscript will be published, but it has not yet been submitted to a journal

Candidate's Signature:	Chandrakumar Chanthujan — Digitally signed by Chandrakumar Chanthujan Date: 2024.08.14 12:14:34 +12'00'
Date:	14-Aug-2024
Primary Supervisor's Signature:	Raj Prasanna — Digitally signed by Raj Prasanna Date: 2024.08.21 11:10:38 +12'00'
Date:	21-Aug-2024

This form should appear at the end of each thesis chapter/section/appendix submitted as a manuscript/ publication or collected as an appendix at the end of the thesis.

3 Systematic Literature Review

This chapter presents the first manuscript for publication, titled "**Earthquake Early Warning Systems Based on Low-cost Ground Motion Sensors: A Systematic Literature Review**". This review comprehensively explores the current landscape of EEWSs that utilise low-cost MEMS-based sensors. Employing a rigorous research methodology, this review establishes research questions, conducts relevant article searches, applies exclusion criteria, extracts data, and performs analyses to identify three critical research gaps in these systems and future research areas. The literature review is conducted between September 2009 and 30th of March 2022.

The literature review addresses Objective 1.1 of this thesis: To review the literature on existing EEW approaches globally and analyse their methodologies towards EEW.

The article presented in this chapter has been published in 2022 in the journal *Frontiers in Sensors* as:

***Chandrakumar C**, Prasanna R, Stephens M, Tan ML. 2022. Earthquake early warning systems based on low-cost ground motion sensors: A systematic literature review. Frontiers in Sensors. 3. https://doi.org/10.3389/fsens.2022.1020202*

3.1 Abstract

Earthquake Early Warning System (EEWS) plays an important role in detecting ground shaking during an earthquake and alerting the public and authorities to take appropriate safety measures, reducing possible damages to lives and property. However, the cost of high-end ground motion sensors makes most earthquake-prone countries unable to afford an EEWS. Low-cost MEMS-based ground motion sensors are becoming a promising solution for constructing an affordable yet reliable and robust EEWS. This paper contributes to advancing Earthquake Early Warning (EEW) research by conducting a literature review investigating different methods and approaches to building a low-cost EEWS using MEMS-based sensors in different territories. The review of 59 articles found that low-cost MEMS-based EEWSs can become a feasible solution for generating reliable and accurate EEW, especially for developing countries and can serve as a support system for high-end EEWS in terms of increasing the density of the sensors. Also, this paper proposes a classification for EEWSs based on the warning type and the EEW algorithm adopted. Further, with the support of the proposed EEWS classification, it summarises the different approaches researchers attempted in developing an EEWS. Following that, this paper discusses the challenges and complexities in implementing and maintaining a low-cost MEMS-based EEWS and proposes future research areas to improve the performance of EEWSs mainly in (1) exploring node-level or decentralised processing, (2) introducing multi-sensor support capability, and (3) adopting ground motion-based EEW algorithms for generating EEW.

3.2 Introduction

Disasters have historically had severe effects on people and infrastructure (Coppola, 2007). Earthquakes are one of them, and they pose a substantial risk to areas near major active faults on land or in offshore subduction zones (Adhikari et al., 2018). Unlike other natural dangers such as cyclones and tsunamis, earthquakes cannot be predicted hours in advance, and when they are identified, earthquake detection and alerts occur in seconds. As a result of the short time between detecting an earthquake event and its imminent impact, developing an Earthquake Early Warning System (EEWS) is difficult (Fischer et al., 2012).

Despite having a short warning window, EEWS can be a valuable tool in increasing safety in regions prone to significant ground shaking (R. M. Allen & Melgar, 2019). The warning period may be long enough for pre-programmed systems to implement emergency actions, such as stopping trains to lessen the likelihood of a derailment, turning off heavy machinery to reduce the possibility of losses, and closing gas distribution valves (Strauss & Allen, 2016). In addition, a brief public alert could also enable

individuals to perform basic safety precautions like drop-cover-hold and mentally prepare for an impending earthquake (Becker, Potter, Prasanna, et al., 2020; Becker, Potter, Vinnell, et al., 2020; Nakayachi et al., 2019).

EEWS involves complex earthquake-related processing, which makes generating reliable alerts challenging (Kanamori et al., 1997). Technological advances in seismic instrumentation, digital communication, algorithms, and processing permit the implementation of a robust EEWS. Moreover, to identify earthquakes and send alerts in real-time, EEWSs require a network of geographically dispersed ground motion sensors to create alerts. As such, EEWS can be expensive to implement and maintain. In recent years multiple innovations, such as low-cost sensors (Y. M. Wu & Mittal, 2021) and new networking architecture (Prasanna et al., 2022), have made it possible to have more affordable systems.

According to their strong-motion data acquisition system (DAS) class, the four types of ground motion sensors employed in EEWSs are A, B, C, and D (Myers, 2008). Class A type sensors are high-performance near state-of-the-art sensors that can record ground motion in a high DAS resolution and DAS dynamic range. In contrast, for classes B, C and D, the DAS resolution and DAS dynamic range tend to decrease accordingly, and the cost related to each type of sensor will increase with the performance (with class A being the most expensive) (Myers, 2008). For example, implementing EEWS with class A sensors will cost millions of dollars, while the EEWS with class C and D sensors need thousands of dollars for implementation (Brooks et al., 2021). Therefore, EEWSs can be classified into two groups according to their implementation cost: conventional high-end EEWSs and low-cost EEWSs. The conventional high-end EEWSs are high-cost networks constructed using high-performing class A seismic sensors. The low-cost EEWSs are constructed using lower-classed sensors, mainly class C MEMS-based seismic sensors.

Low-cost alternative technology solutions are emerging to create cost-effective EEWSs instead of expensive high-end EEWSs. Internet of Things (IoT) technologies powered by microelectromechanical systems (MEMS)-based sensors are a part of low-cost solutions (R. M. Allen & Melgar, 2019). Past research has been conducted in developing EEWSs using low-cost Micro-electromechanical systems (MEMS) based sensors. Examples of systems that use low-cost MEMS sensors include those in Taiwan (Y. M. Wu et al., 2013), California (Clayton et al., 2015), Iceland (*TurnKey Earthquake Early Warning*, 2020), China (Peng et al., 2019) and New Zealand (Prasanna et al., 2022). These affordable EEWS deployments have shown the practicality and capacity of MEMS-based sensor networks to deliver EEW. They could become a solution for earthquake-prone countries that may not have the sufficient economic capability to afford high-end EEWSs (Prasanna et al., 2022).

In addition, low-cost MEMS-based networks can be helpful, as complementary systems, for territories that have already implemented conventional EEWSs. There are several examples (e.g., Taiwan, the West Coast of the USA, and parts of mainland China) where a low-cost EEWS work as a secondary system supporting their main high-end EEWS (Peng et al., 2020; B. R. Wu et al., 2017). Having a dense low-cost sensor network as a complementary system to the conventional EEWS could create a more robust solution to generate alerts with an acceptable level of warning time for the areas near the epicentre (Y. M. Wu et al., 2013).

Low-cost EEWSs have started showing promising results in detecting and providing warnings for ground shaking. In parallel, the affordability of low-cost ground motion sensors has created an opportunity to build crowdsourced EEWSs supported by community participation and engagement (Faulkner et al., 2011; Minson et al., 2015). Along with the inexpensive MEMS-based ground motion sensors that are easily accessible on the market, smartphones and laptops with MEMS-based accelerometers built into their hardware have also emerged as possible sensing tools that could serve as detection tools in an EEWS. Such ubiquity in consumer devices raises the possibility that these devices could be used to achieve operational EEWS via crowdsourcing (Minson et al., 2015). Therefore, there is a potential for low-cost MEMS-based sensors to open new avenues and opportunities supported by crowdsourced open EEWSs.

Recently, a few papers have reviewed EEW research (Cremen & Galasso, 2020; Tan et al., 2022; Velazquez et al., 2020), they cover the seismological, engineering, social, and organisational aspects and general state-of-the-art approaches to EEW. None of them is a comprehensive review of literature on existing low-cost EEWSs implemented worldwide focusing on the technical aspects. Such a technical review can be considered timely as it is invaluable to identify the strengths and weaknesses of the different approaches to inform opportunities and directions for future research in the area of low-cost EEW. In such a context, this article systematically reviews the existing low-cost EEWSs worldwide.

The remainder of this article is organised as follows. Section 3.3 outlines the methodology used in this study, followed by the findings from the systematic literature review (SLR) presented in Section 3.4. Discussion and future research areas are presented in Section 3.5. Finally, Section 3.6 concludes the paper by summarising the answers to the research questions raised.

3.3 Methodology

The steps outlined by Algiriyage et al. (2022) are adopted in this SLR to help with the reviewing process, including establishing research questions, finding relevant articles, applying exclusion criteria, extracting relevant data, and analysing the literature.

3.3.1 Research Questions

This review asks three research questions to ensure that the essential components related to low-cost EEWSs are covered:

1. **How to classify low-cost MEMS-based EEWSs?**
2. **What are the existing low-cost MEMS-based EEWSs implemented globally?**
3. **What are the limitations, challenges, and future research areas in the low-cost MEMS-based EEWSs domain?**

By searching the literature to answer Question 1, a classification structure can be drawn for classifying existing low-cost EEWSs. A classification structure will help the researchers have a consistent understanding of different types of EEWS, thus will help in the analysis and comparisons of implemented EEWSs. With Question 2, the SLR explores and finds details about existing low-cost MEMS-based EEWSs, their processing, warning type, and EEW algorithm used. However, details on how EEWSs deliver early warning is not discussed in this study since most articles do not discuss their alert distribution method. The third question explores the limitations and challenges of the current low-cost MEMS-based EEWSs. Answers to the question provide future research areas which will enable researchers to design low-cost EEWS that could overcome the identified challenges and difficulties.

3.3.2 Search for Relevant Articles

The search for the relevant articles in the literature was conducted using a keyword search in the Scopus and Web of Science databases on 30 March 2022. A review of the body of literature revealed little relevant material about low-cost EEWSs before September 2009; hence only articles published after that date were considered. To answer the research questions, “earthquake early warning” and “low-cost” were the primary keywords in the search. In addition, “earthquake warning” and “earthquake detection” were used as alternatives to “Earthquake Early Warning”. Alternatives to the phrase “low-cost” include “low cost”, “MEMS”, “cost”, “mobile”, “phone”, “smartphone”, “community-engaged”, “economical”, and “crowdsourced”. Peer-reviewed academic papers accessible online in full-text format and pertinent to the research aims are the only sources included in the initial literature search. Publications written in

languages other than English, grey literature like government or corporate reports and non-academic research were all excluded. The initial keyword search produced 354 relevant articles. Duplicates were removed, resulting in 218 unique papers.

3.3.3 Exclusion Criteria

The scope was narrowed to papers that only discussed low-cost MEMS-based implementations related to earthquake detection. The abstracts were manually examined, and those that contained the following information were discarded:

- low-cost EEW that uses different types of sensors other than MEMS-based accelerometers (e.g., optical fibre cables, satellite-based, resonant switches, etc.),
- low-cost implementations related to different disaster detections or structural monitoring,
- surveys or perceptions related to implementing low-cost EEWSs,
- EEWSs that use smartphones solely to notify the stakeholders (as notification tools rather than detecting sensors),
- articles lacking sufficient details related to the EEWS implementation, and
- articles that only broadly discuss earthquake detection algorithms without focusing on EEWS implementation were excluded.

After filtering and applying the inclusion-exclusion criteria, 59 articles were selected for this study. The methodology for the literature search, the selection criteria, and the number of papers returned at each stage are shown in Figure 3-1.

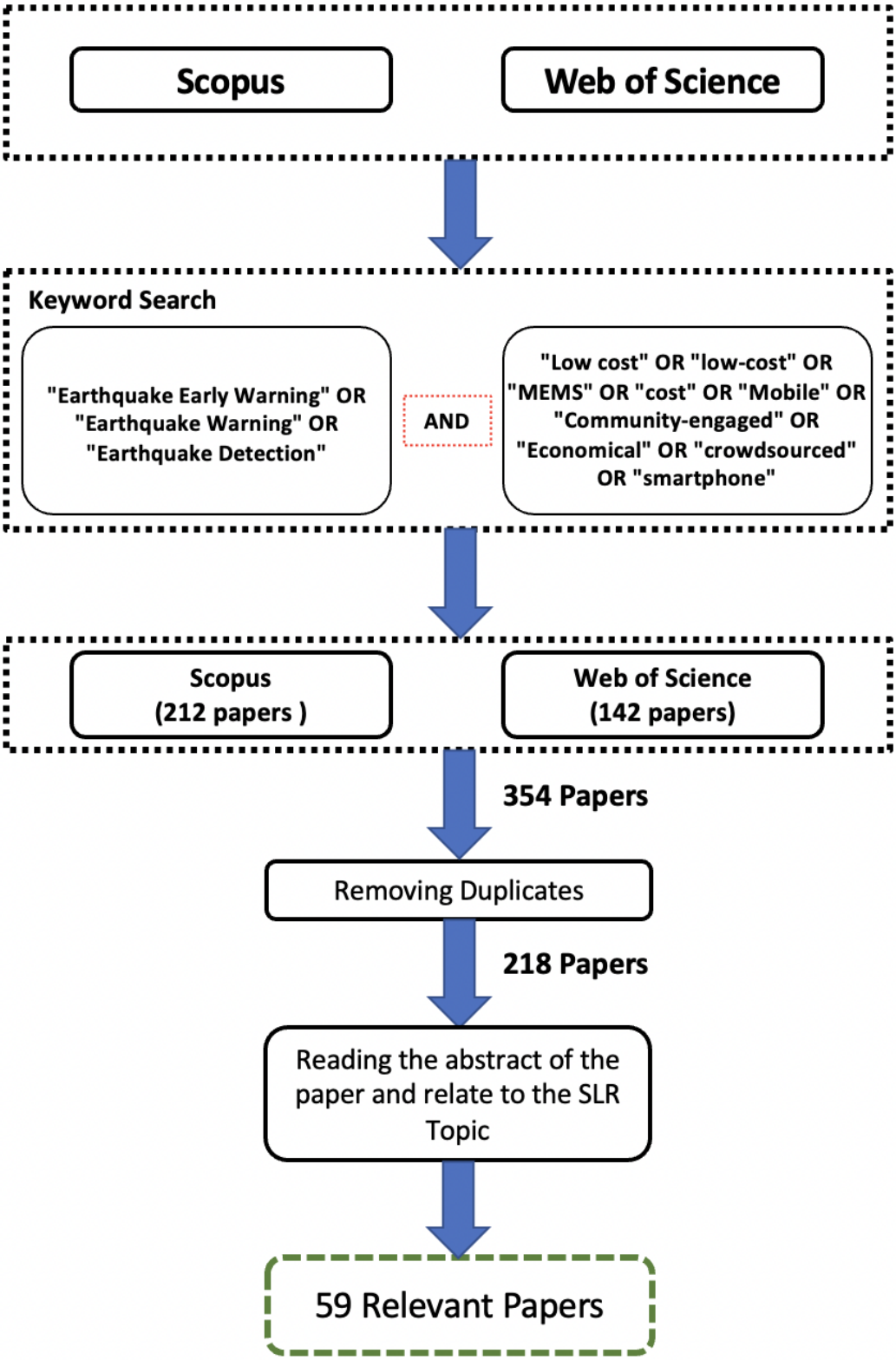

Figure 3-1. Systematic Literature Review process flow diagram.

3.3.4 Extract Relevant Data and Analyse the Literature

After identifying relevant articles, the next step of the methodology is to extract relevant information and analyse them to find answers to the research questions. The main activity to analyse qualitative data is to compare them through naming and classifying (Flick, 2007). As a result of this procedure, a structure for the data is created using Microsoft Excel, paving the way for a thorough comprehension of the problem, the field, and the data themselves. Constant comparison is conducted to analyse the articles to understand the different approaches implemented toward EEW and to develop a classification structure (Hernon, 2004). After extracting the relevant data using the literature, this SLR process is presented to answer the research questions.

3.4 Findings

This section shows the findings from the SLR of 59 articles. It shows the classifications for EEWS, which can help navigate the varying combinations of different characteristics of EEWSs that exist worldwide. Discussion follows on low-cost EEWSs that have already been implemented worldwide and the contexts and technologies used in the different systems.

3.4.1 Classification of EEWSs

The filtered articles revealed that there are different approaches to implementing EEWSs. However, to the authors' understanding, no existing framework classifies such approaches to implementing EEWSs according to their characteristics. EEWSs are complex systems, and a comprehensive classification of such systems can help better organise the study of EEWS. This will particularly be helpful for those researching, designing, or implementing EEWSs.

3.4.1.1 Classification of the EEWSs Based on the Warning Type

Findings show that EEWSs can be classified based on the number of sensors used to detect an earthquake (i.e. on-site networks use a single sensor and regional-based networks use an array of sensors) (Bindi et al., 2015; D. Y. Chen, Wu, et al., 2015; Picozzi, Emolo, et al., 2015).

On-site-based EEWS use only one sensor to detect an earthquake. To be more precise, it takes information from a sensor at a location to detect earthquakes and generate alerts at the same location using a single sensor, with all algorithm processing taking place at that station (R. M. Allen & Melgar, 2019; Bindi et al., 2015; Picozzi, Emolo, et al., 2015). In general, on-site EEWS serves a significant role in bridging the gap of the blind zone, which frequently experiences the worst ground shaking and

where an EEWS cannot issue an alarm close to the epicentre (D. Y. Chen, Wu, et al., 2015; C. Y. Wang et al., 2022). The basic form of an on-site EEWS can be a ground motion threshold-based method that sounds an alarm or warning as soon as unusual or harmful ground motion is discovered. However, few more advanced systems can identify P-waves and send out an alarm when the matching S-wave's intensity is expected to be damaging (R. M. Allen & Melgar, 2019).

On the other hand, regional EEWS use a network of sensors deployed in several parts of a particular earthquake-prone geographical area. Earthquake detection happens by processing the earthquake data collected by the network of sensors. The number of earthquake detection sensors can vary according to the sensor distribution and considered geographical area (Bindi et al., 2015; Picozzi, Emolo, et al., 2015). Generally, regional EEWSs can benefit areas far from the epicentre (D. Y. Chen, Wu, et al., 2015).

3.4.1.2 Classification of Regional EEWSs Based on the Implemented EEW Algorithm

Regional EEWSs can be further classified according to the type of algorithm used. Regional EEWSs are primarily implemented using two different kinds of EEW algorithms, namely: source-based and ground motion-based algorithms (R. M. Allen & Melgar, 2019). Figure 3-2 illustrates the classification based on EEW algorithms.

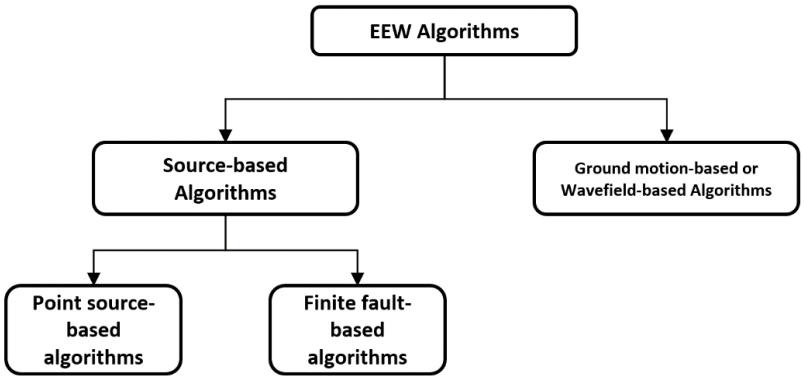

Figure 3-2. The proposed classification for the adopted EEW algorithm in regional EEWSs

3.4.1.2.1 Source-based Methods

Source-based approaches detect the earthquake and disseminate the alert to EEW stakeholders with detailed information about the detected earthquake. These methods typically identify an earthquake and characterise the position, origin time, and magnitude by using a suitable ground motion prediction equation plus a few seconds of P-wave data (0.5–4 s) from two to six sensors around the epicentre (GMPE) (R. M. Allen & Melgar, 2019).

Generally, source-based approaches could be implemented using two different types of algorithms: point source-based and finite fault-based (Figure 3-2). Even though both types of algorithms detect the earthquake characteristics using the P-waves, point source algorithms typically saturate for earthquake ~ M>6. The main causes of saturation are two: (1) it is difficult to distinguish earthquakes with a magnitude greater than six from those that occur in the first few seconds of the P-wave window, and (2) the lateral extent of the fault rupture is necessary for large earthquakes to determine the earthquake's magnitude (R. M. Allen & Melgar, 2019). On the other hand, finite fault algorithms tend to estimate the earthquake's ground motion without any saturation limitation by determining the fault rupture's finite extent.

3.4.1.2.2 Ground Motion or Wavefield-based Methods

Ground motion or wavefield-based algorithms became popular due to their robustness and fast processing time. They do not estimate the source parameters of an earthquake (Hoshiba, 2013; Hoshiba & Aoki, 2015; Kodera, 2018). Thus, they avoid vulnerabilities of the source-based algorithms (Hoshiba, 2021). The main idea behind these algorithms is to forecast the likely evolution of ground motion intensity in the future using the current state of ground shaking and knowledge of propagation physics in a short period of time. These algorithms assume that the observation sites are closer to the hypocentre than the prediction sites, meaning that the seismic sensor network plays a major role (Hoshiba, 2021). Table 3-1 summarises the number of EEWSs implemented according to the proposed classification.

Table 3-1. Number of approaches presented in the reviewed articles based on the proposed classification

	Regional approaches		On-site
	Source-based	Ground motion-based	
Number of Approaches	18	1	9

3.4.2 Low-Cost EEWSs Implemented Around the World

MEMS-based technologies have inspired researchers to implement low-cost EEWS in several countries worldwide over the last ten years, demonstrating promising results and robustness during an earthquake event. Even though many countries are prone to seismic hazards, only a few have successfully implemented any form of EEWS (Bindi et al., 2015). However, several countries are currently in the process of implementing more affordable low-cost EEWSs. This section summarises existing low-cost MEMS-based EEWSs into types: the experimental or initial stage and the public alert generation stage according to the classification proposed in Section 3.4.1. In general, experimental or initial stage EEWSs deliver EEWs only to a selected set of people primarily for testing, whereas EEWSs in the public alert generation stage, deliver EEWs to the general public in a seismic-prone area that can be a

region or an entire nation. Table 3-2 summarises the low-cost MEMS-based EEWSs identified from the selected articles.

Table 3-2. Summary of articles reviewed according to their warning type and EEW algorithm

Implementation Level	Regional EEWSs		On-site EEWSs
	Source-based Methods	Ground-motion-based Methods	
Experimental / Initial stage	Istanbul (Fischer et al., 2012) Japan (Uga et al., 2012) Italy (D'Alessandro et al., 2018) USA (Minson et al., 2015; Nof et al., 2019) Taiwan (B. M. Yang et al., 2018) Costa-Rica (Brooks et al., 2021) Northern India (Mittal et al., 2019) Canada (Taale et al., 2021) China (Zou et al., 2019)	New Zealand (Prasanna et al., 2022)	Kyrgyzstan (Bindi et al., 2015) BLESeis (Won et al., 2020) Taiwan (Hsu & Nieh, 2020) China (Hu et al., 2021) Italy (D'Alessandro et al., 2020; Picozzi, Emolo, et al., 2015) Northern India (Mittal et al., 2019)
Public alert generation	Taiwan (D. Y. Chen, Wu, et al., 2015) China (Peng et al., 2021) Quake Catcher Network[7](Cochran et al., 2009) MyShake[7] (Kong et al., 2020; Strauss et al., 2020) Community Seismic Network[8] (Clayton et al., 2015; Faulkner et al., 2011)		Taiwan (Y. M. Wu et al., 2013) China (Peng et al., 2013)

[7] EEWS that is operating in more than one country.

[8] EEWS that is operating in more than one country.

	Earthquake Network[8] (Bossu et al., 2021; Finazzi, 2020) Google[8] (R. M. Allen & Stogaitis, 2022) South Korea (Huang et al., 2020; Y. W. Kwon et al., 2020; Lee, Kim, et al., 2019; A. Wu et al., 2021)		

3.4.2.1 Regional Earthquake Early Warning Systems

As identified in the classification section above, regional EEWSs are implemented using two different algorithms for earthquake detection, namely source-based and ground motion or wavefield algorithms. Here, the source-based (point source and finite fault) and ground motion-based approaches are analysed separately.

3.4.2.1.1 Source-based Regional Earthquake Early Warning Systems

Source-based algorithms can be divided into two different algorithms: point-source-based and finite-fault-based. However, minimal information is available on the low-cost EEWSs that use a finite-fault algorithm for earthquake detection. Therefore, unless otherwise stated, all the implementations discussed here use point-source-based algorithms. Here, EEWSs were reviewed according to the type of sensor used.

EEWSs Using Dedicated MEMS-based Sensors

The first ever low-cost EEWS was developed by Fleming et al. (2009) from Germany. They used their in-house built low-cost sensors SOSEWIN 1 and SOSEWIN 2 to implement an experimental self-organizing seismic early warning network in Istanbul and Berlin (Fischer et al., 2012). The system consisted of a decentralised, self-organizing wireless mesh sensor network, with sensors connected via WLAN (Wireless Local Area Network 2.4 GHz or 5 GHz). This system detects the P-waves using the short-term-average (STA)/long-term-average (LTA) method and captures the details of the P-waves to determine the source characteristics of the earthquake.

In contrast to the above approach, most regional low-cost EEWSs are implemented using a centralised processing unit. A low-cost EEWS implemented by Y. M. Wu et al. (2013) in Taiwan is a prime example of that approach. They designed a low-cost ground motion sensor known as P-alert, which uses MEMS-based accelerometers where the processing of the EEW algorithm takes place at a centralised server.

The P-alert system uses the STA/LTA ratio (R. V. Allen, 1978) to detect the P-waves and continuously monitors the peak ground acceleration (PGA) using MEMS-based accelerometers. Following the detection of P-wave characteristics for the first three seconds of P-waves, they are sent to the central station via TCP/IP connections. During the alert generation, an event is declared once eight P-alert stations are triggered, and an alert will be disseminated to the public. A traditional earthquake location algorithm with a half-space linear increasing-velocity model is used to determine the hypocentre location. Peak displacement (Pd) and peak velocity attenuation (MPv) or peak displacement attenuation (MPd), and hypocentre distance are used to calculate magnitude. The system takes from 9s to 28s to generate a warning and an average of less than < 20s compared to the conventional high-end EEW in Taiwan, which generates warnings in 20s.

Also, the P-alert EEWS has been used to detect the earthquake's rupture directivity, building a real-time shake map for ongoing earthquakes and damage localisation in buildings after an earthquake (Hsu, Wu, et al., 2018; Hsu, Yin, et al., 2018; Jan et al., 2018; K. S. Wang et al., 2018; B. M. Yang et al., 2021; Yin et al., 2016) The P-alert system's performance was evaluated using Taiwan's 2018 Mw 6.4 Hualien earthquake (Hsu, Yin, et al., 2018). Using the same P-alert sensor network, Yang et al. (2018) implemented a regional EEWS called ShakeAlarm. ShakeAlarm can provide a wider lead time than their national-level regional EEWS operated by Central Weather Bureau (CWB) by bypassing the location estimation by employing the relationship between the shake contour area and earthquake magnitude (B. M. Yang et al., 2018). Similarly, a team of researchers from India implemented an EEWS at the Himalayan Belt using 100 P-alert sensors (Chamoli et al., 2021; Mittal et al., 2019).

Several researchers from China have also implemented EEWS in seismically active regions using low-cost MEMS-based sensors. As an initial step, Peng et al. (2017) constructed a sensor called GL-P2B using MEMS-based accelerometers (Peng et al., 2017). They demonstrated that their sensor could detect smaller earthquakes M < 1.5 and a high signal-to-noise ratio (SNR) at distances greater than 50 km for earthquakes of M > 3. To detect the earthquake, they used the same detection algorithms adopted by Y. M. Wu et al. (2007) and tested their network by deploying approximately 170 stations in Sichuan, China (Peng et al., 2017, 2019). Following that, another group of researchers implemented a low-cost EEWS by building a new low-cost MEMS-based ground motion sensor known as the SIT-S Model in addition to the GL-P2B sensors in the Zhejiang province (Finazzi, 2020; Zou et al., 2019). Afterwards, a hybrid EEWS was introduced in the Sichuan region by integrating the GL-P2B sensors with P-alert sensors and local broadband seismic stations. There are around 270 MEMS-based sensors (170 GL-P2B sensors and 100 P-alert sensors) and 13 local broadband seismic stations where the hybrid EEWS processing takes place at a centralised server (Peng et al., 2020). Currently, around 1631 MEMS-based stations contribute to the regional EEWS in the Sichuan Area operated by the Sichuan Earthquake

Administration (Peng et al., 2021). Processing of the EEW algorithm takes place at a centralised server adopting the peak displacement (Pd) scaling approach proposed by Kuyuk and Allen (2013) for estimating the earthquake magnitude and calculating seismic intensities at various target sites, a point source algorithm based on the conventional ground motion prediction equation (GMPE) is used (Peng et al., 2021).

The USA also plays a significant role in contributing to low-cost EEW. Areas near the San Andreas fault in California, USA, are prone to frequent seismic events. Such a context has motivated US researchers to investigate implementing EEWSs in this region. Two primary regional networks deliver alerts to the public in the USA using dedicated MEMS-based sensors: Quake Catcher Network (QCN). Clayton et al. (2015) from California constructed the CSN by building their in-house sensor. In their system, event detection is carried out at the centralised server (Google App Engine). In contrast, the sensor systems themselves generate measurements of characteristics like pick times, maximum amplitude, apparent frequency, and signal-to-noise levels in close to real-time (Clayton et al., 2015). The CSN's primary functions include monitoring the health and safety of structures, producing zonation maps of populated regions, and giving maps of maximum shaking soon after a significant earthquake to assist first responders (Hong et al., 2021).

On the other hand, the QCN distributed/volunteer computing initiative enables any internet-connected computer with an internal or external MEMS accelerometer to function as a strong-motion seismic station (Cochran et al., 2009). The QCN offers a dense, wide-scale seismic network by utilising the primary benefit of distributed computing, which is the ability to use a large number of processors at a cheap infrastructure cost. Data is analysed on an individual's laptop or desktop during idle computer cycles, and only a little amount of data is forwarded to a central server for additional analysis. The QCN servers go through the data, including detection time, signal amplitudes, Internet protocol (IP) addresses, and other relevant information, to ascertain which data corresponds to earthquakes. This system can detect moderate to large earthquakes (magnitude > 5). Over 2000 volunteers had signed up by 2014, mainly from California and Mexico (Hong et al., 2021). Currently, sensors called "Joy-Warrior" and "O-NAVI" are used as external MEMS accelerometers in computers. Following that, another team from the University of California Berkeley and the Humboldt State University implemented a small experimental MEMS-based EEWS called ElarmS to support the conventional high-end EEWS (Nof et al., 2019). They proved that a MEMS-based sensor array with a finite-fault model could estimate earthquake magnitude and shaking intensity distribution faster and more reliable compared to using Global Navigation Satellite Systems (GNSS) (Nof et al., 2019).

In addition to the above efforts, researchers in several other countries attempted to implement low-cost EEWSs. A group of researchers from Italy implemented an experimental MEMS-based low-cost EEWS

using Adel ASX1000 type accelerometers to detect small local magnitude earthquakes between 2.0 < M_L < 3.0 in two seismically active areas of Italy: the inner part of the Umbria Valley and the southern-eastern Alpne Front (Cascone et al., 2021). They used 15 ASX1000 prototype sensors and a centralised server where communication between the server and the sensors occurred via LAN connection (Cascone et al., 2021). In addition, several approaches were attempted by researchers in Italy toward low-cost EEWS (D'Alessandro et al., 2014, 2018). Also, Taale et al. (2021) from Canada explored the feasibility of implementing an experimental regional EEWS using the MEMS-based accelerometers embedded in the smart meters (SM). They have tested SM's capability in detecting an earthquake by doing different tests such as statics tests, noise floor tests, dynamic tests, etc. and declared that SM infrastructure as an EEWS is technically feasible.

EEWSs Implemented Using Smartphones

Off-the-shelf sensors like those found in smartphones are also offered as scalable opportunistic sensor nodes as an alternative to in-house-built low-cost MEMS-based sensors (Brooks et al., 2021). The nearly universal availability of MEMS-based class C accelerometers in cell phones makes phone-based sensing possible. These motion sensors can be configured to function as seismometers, identifying the shaking caused by earthquakes. Several countries have tried implementing low-cost EEWS using smartphones. Almost all the smartphone-based EEWSs are regional networks, and the processing of the earthquake detection algorithm takes place partially or entirely at a centralised location. Brooks et al. (2021) found that for an EEW generation, it is necessary to have at least four stationary smartphones to mitigate the effect of unwanted accelerations.

According to the EEW literature, Japan has implemented a low-cost EEWS using smartphones (Uga et al., 2012). This system is one of the earliest EEWS in the literature that uses smartphones as ground motion sensors. This EEWS has been integrated as a support system to Japan's conventional JMA EEWS. Like Japan's approach, Zambrano et al. (2014, 2015, 2017) developed an EEWS using smartphones, demonstrating robust results compared to Japan's approach. They constructed their EEW network using three different layers: smartphones, intermediate servers, and a control centre, where different tasks are assigned to these layers. They have also analysed different wave propagation techniques according to the geographical areas. At the time of the implementation, their method detected an earthquake 12 seconds before the peak acceleration, which was a notable achievement compared to other smartphone implementations.

Similar to Japan, a team of researchers from the USA implemented an EEWS with consumer smartphones via crowdsourcing. In their approach, in addition to MEMS-based accelerometer data, they incorporated data from GNSS (Global Navigation Satellite Systems) and GPS (Global Positioning

System) to overcome the saturation issue for predicting large earthquakes (M_w>7) (Minson et al., 2015). They tested their EEWS using simulated data from the Mw 7.0 Hayward fault earthquake in California and actual data from the Mw 9.1 Tohoku-Oki earthquake, and the results were promising. Similar to their approach, researchers from the University of California implemented a smartphone-based EEWS called "MyShake" (R. M. Allen et al., 2020; Kong et al., 2015) where they proved that a robust EEWS could be implemented using a smartphone-based network with artificial intelligence to distinguish an earthquake from human activities. The network delivers alerts to the phones if the estimated magnitude of an earthquake is 4.5 or greater or Modified Mercalli Intensity (MMI) 3.0 or greater zone (Strauss et al., 2020). MyShake can detect an earthquake and its characteristics within ~ 5 - 7 seconds after the origin time, and the alert can be disseminated to smartphones within ~ 1 - 5 seconds (R. M. Allen et al., 2020; Kong, Lv, et al., 2019).

Similar to MyShake, researchers from Italy implemented an EEWS called the EQN (Earthquake Network) using an android application installed on smartphones from the community. Like the other mobile phone-based approaches, this system uses a centralised server to process the EEW algorithm to detect an earthquake and its source parameters (Finazzi, 2016, 2020; Finazzi & Fassò, 2017). A statistical approach has been used to define the threshold based on the number of active smartphones using a fixed and dynamic sub-network-based detection algorithm to detect an earthquake with minimal false alerts (1 false alert per year). Also, during this approach, two ways for detecting earthquake epicentre were introduced, which are suitable for smartphone-based EEWSs. Currently, they have selected only phones stationed for charging as sensors. An earthquake is detected when concurrent triggers within 30 kilometres of each other surpass a dynamic threshold determined by the number of active smartphones and the intended false alarm probability, which is currently set at one per year per country (Bossu et al., 2021; Peng et al., 2017; B. M. Yang et al., 2021).

Following that, researchers from South Korea have also implemented a low-cost EEWS known as CrowdQuake that uses around eight thousand smartphones (Samsung Galaxy S7) securely embedded into enclosures and deployed at different locations (Huang et al., 2020; Y. W. Kwon et al., 2020; A. Wu et al., 2021). They have used a deep convolutional-recurrent neural network (CRNN) model to detect earthquakes using a centralised server (Y. W. Kwon et al., 2020). They demonstrated that their EEWS could detect earthquakes with MMI > 3.0 using two examples of detected earthquakes (Huang et al., 2020). Similarly, a team of researchers from Costa Rica built a smartphone-based EEWS using a mobile app (Brooks et al., 2021). They fixed the mobile phones using enclosures in different areas in the country where station spacing is ∼30 km and increases to 30–50 km away from the Middle America Trench. Also, due to the noisy nature of smartphone accelerometers, they use a quadrilateral mesh configuration of adjoining stations to trigger an alert (Brooks et al., 2021).

In 2020, Google launched the Android Earthquake Alerts system by forming a public-private partnership with the USGS (United States Geological Survey) using the already constructed MyShake EEW model (R. M. Allen & Stogaitis, 2022). Initially, it delivered ShakeAlert (Kohler et al., 2018) messages to all Android phones in California. Then in 2021, Google's EEWS was constructed using the already existing MyShake EEW model and started delivering alerts to New Zealand and Greece using the android phones in those regions (R. M. Allen & Stogaitis, 2022; Kong et al., 2016). Following that, Turkey, the Philippines, and some central Asia countries were added to Google's android EEWS (R. M. Allen & Stogaitis, 2022). Since Google's android Earthquake Alerts system is relatively new, there is not enough published literature to evaluate its performance.

The following figure (Figure 3-3) illustrates the timeline of smartphone-based EEWSs according to the literature.

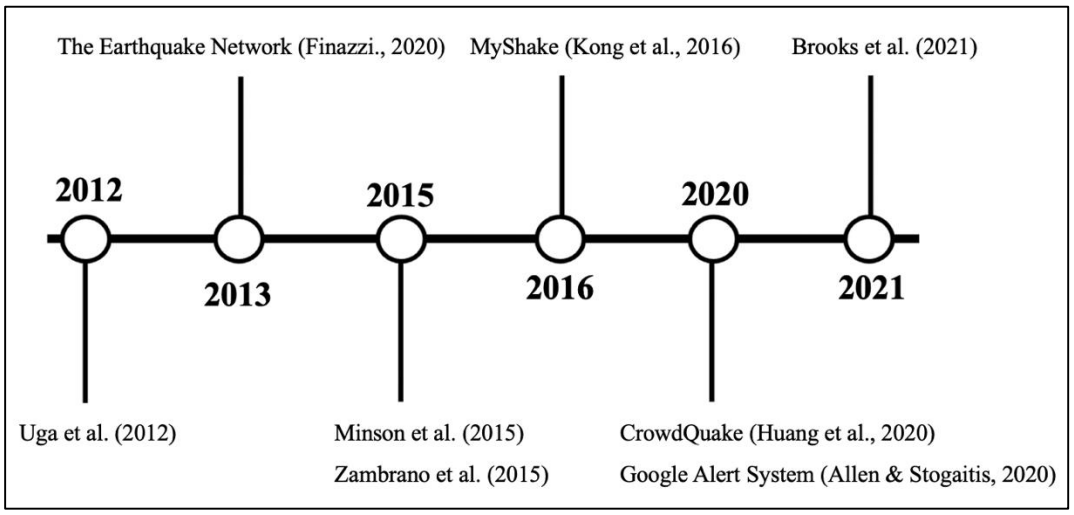

Figure 3-3. Timeline of smartphone-based EEWSs according to their year of publication

3.4.2.1.2 EEWSs Implemented Using Ground Motion or Wavefield-based Algorithms

There is no information on any systems that use smartphones as their ground motion sensors for ground motion or wave field-based algorithms. Thus, only implementations that use MEMS-based sensors are discussed here.

EEWSs with In-House Built MEMS-based Sensors

The usage of ground motion or wavefield algorithms in low-cost MEMS-based sensors is difficult to find in the literature. To the authors' knowledge, there is only one implementation from researchers at Massey University, New Zealand, which discusses a ground motion-based detection algorithm in a low-cost environment (Prasanna et al., 2022). In particular, they implemented an EEWS using Raspberry Shake 4D, a MEMS-based low-cost ground motion sensor manufactured by Raspberry Shake. Unlike

other EEWSs, the researchers processed their EEW algorithm at the node level rather than centrally. They employed PLUM as their EEW algorithm - a robust and well-known ground motion-driven method in EEWS (Kodera et al., 2018). Their results claim that decentralised processing can outperform traditional centralised processing in terms of system latency, redundancy, and implementation cost.

3.4.2.2 On-Site-based EEWSs Implemented Globally

There is minimal information in the literature on any systems that use smartphones as their ground motion sensors for on-site approaches except the one implemented by Hsu & Nieh (2020). Thus, we have mainly discussed implementations that use MEMS-based sensors.

EEWSs with In-House Built MEMS-based Sensors

On-site techniques, as described in Section 3.4.1, are primarily used to detect earthquakes and provide alerts at the sensor level. Even though it can detect an earthquake as soon as the seismic waves initially reach the sensor, there is a high probability of false alerts since the detection and generation of an alert depend only on one sensor. However, several countries have implemented the on-site approach as one of their EEWS due to its important benefit of minimal detection time, which can be useful in alerting the areas near the epicentre and rupturing fault during an earthquake (D. Y. Chen, Wu, et al., 2015). Even though the basic idea of the on-site approach is to generate an alert by using just a ground motion threshold, a few sophisticated approaches went beyond that scope by predicting the destructing S-wave's intensity using the detected P-waves – these will be discussed below.

Initial efforts to build a sophisticated on-site EEWS were conducted by Y.M. Wu et al. (2013) from Taiwan. They constructed an on-site EEWS using P-alert seismic sensors, the same sensor used for the regional EEWS. The P-alert sensor has a display showing the severity of the shaking and a sound warning mechanism with a touch screen. The earthquake's severity is determined using the first 3-second window of the P-wave, and an integrated alarm system is used to generate the alert. The time taken to detect the earthquake using the on-site approach is around 8 seconds. The P-alert system can provide 2-8 seconds warning time for sites in the Central Weather Bureau regional warning system's blind zone. Following that, by adopting the same detection mechanism and algorithms by Y. M. Wu et al. (2013), researchers from China implemented an on-site approach in the Zhaotong region by building their own low-cost sensor with three different alarms such as sound, text and screen flickering. Their approach took around 3.2 seconds to generate the warning; however, the system registered many false alarms that cannot be neglected (Peng et al., 2013). Likewise, another research team from China has implemented an on-site approach by building their own sensor called REMOS SIT (Ding et al., 2017).

Further, Hu et al. (2021) proposed another advanced low-cost seismic station for an on-site EEWS by embedding eight MEMS-based accelerometers into one system known as parallel acquisition. They proved that parallel acquisition would reduce the Root Mean Square value of the MEMS-based sensor's noise compared to using a single sensor. Also, they implemented their network in the Sichuan region, China using 45 proposed seismic stations and demonstrated that the proposed on-site EEWS could detect earthquakes accurately. Likewise, a multi-parameter wireless sensing system called MPwise was introduced by Boxberger et al. (2017) to detect an earthquake which can be used as an on-site or regional EEWS. However, they tested their EEWS using the on-site approach in Kyrgystan with the SeisComP seismic software for earthquake-related processing in terms of detecting earthquake source parameters. Unlike other approaches, this device is embedded with multi-sensor capability, which can be connected with different sensors for various applications.

In addition to the above approaches, using SOESWIN sensors, Bindi et al. (2015) constructed an on-site EEWS for one of the highest earthquake hazard regions in Kyrgyzstan which works as a support system for their regional warning network. Similarly, a group of South Korean researchers built a standalone earthquake detection and alerting device for residences that can send notifications to nearby devices. In their approach, they tried to disseminate the earthquake intensity by calculating the PGA (peak ground acceleration) values from the ground motion data (Lee, Khan, et al., 2019; Lee, Kim, et al., 2019). Further, there are also different on-site approaches that have been implemented by Won et al. (2020) and D'Alessandro et al. (2020) in detecting earthquakes.

3.5 Discussion

Complications towards developing high-end conventional EEWSs have motivated researchers to pursue other feasible options in implementing an EEWS, and low-cost MEMS-based EEWSs have come to the fore as one of the solutions. Low-cost EEWSs have become a solution for earthquake-prone countries which are not economically able to afford high-end EEWS. Also, low-cost EEWSs serve as a support system for countries with high-end conventional EEWSs. As discussed previously, low-cost EEWSs can be divided into two types: on-site approaches and regional approaches. Regional-based low-cost EEWSs are more robust and accurate in disseminating alerts, and on-site approaches generate rapid alerts. Still, it uses a single station to detect an earthquake which can compromise the reliability and accuracy of generating alerts (R. M. Allen & Melgar, 2019). However, this SLR process identified several limitations and challenges related to these low-cost regional EEWSs. This section discusses the future research opportunities for regional EEWSs arising from the limitations and challenges identified during the SLR process.

3.5.1 Limitations

According to the literature review, the first limitation identified is that most regional EEWSs process their earthquake-related data centrally. A central data processing site offers several benefits, including improved control for locating, gathering, and processing data both during and shortly after a disaster (Aizu, 2011). Centralised data processing does, however, bring up several technological constraints and bottlenecks. One of the critical restrictions is the potential for data collecting to be disrupted at a central site because of effects on telecommunications infrastructures after a significant earthquake(Kobayashi, 2014). After an earthquake, facilities for data processing, intermediate data gathering, and data transportation may be significantly disrupted or destroyed (Prasanna et al., 2017). Giving time-sensitive warnings to end users may be difficult if the central processing capability is unavailable due to a loss of connectivity.

Further, the SLR process indicated that almost all low-cost EEWSs are limited to a single type of ground motion sensor. For example, the EEWS developed by Y. M. Wu et al. (2013) uses only the P-alert sensors (Taiwan), and Peng et al. (2020) from China uses its in-house-built sensors for EEWS. Even though the MPwise device implemented by Boxberger et al. (2017) can support multiple MEMS-based sensors, they did not discuss the implementation of their system using multiple MEMS-based sensors. EEWSs without multi-sensor capability can be identified as one of the major limitations in almost all the low-cost MEMS-based EEWSs worldwide.

Another limitation is that most regional EEWSs globally are constructed using point source or finite fault source-based algorithms. Even though source-based algorithms generate reliable warnings, a significantly longer processing time is required for estimating earthquake source characteristics, making them less beneficial for the areas near the epicentre and effective only for areas far from the epicentre (Y. M. Wu et al., 2013). Areas affected during a large earthquake can be geographically large. On the other hand, significant earthquake damage will almost always occur at shorter epicentral distances and near the rupturing fault. Thus, it is crucial for any EEWS to generate an initial alert to the areas near the epicentre within a few seconds. To overcome this limitation, several countries have implemented on-site approaches that are fast but not reliable in generating alerts (Kodera et al., 2018).

3.5.2 Challenges

Network security is a major challenge for community-engaged EEWSs, especially as community involvement becomes an increasingly important factor in developing low-cost systems. In these networks, the public contributes by installing or maintaining sensors, making security a critical concern (Kong et al., 2016; Minson et al., 2015; Prasanna et al., 2022). For example, installing P-alert sensors

at houses or installing an EEW application on their smartphone sends data to the data processing centre. Although community participation is a promising alternative, network security becomes an issue that needs to be addressed and researched (Prasanna et al., 2022). Because sensors are spread over several geographic regions and are connected to various home-based private networks, security is essential to prevent unintentional or purposeful attacks. One specific component of system security is connected to spoof earthquake triggers, such as how simple it is to spoof earthquake triggers and how resistant the system is to spoof earthquake triggers from individual phones, ad hoc or coordinated groups of phones in a certain location and time period (Kong, Inbal, et al., 2019; Kong, Lv, et al., 2019).

Following that, the sensor density of MEMS-based sensors in an EEWS is picked out as another significant challenge. Even though implementing a regional EEWS ensures a robust system compared to an on-site-based EEWS, a significant amount of time such systems in detecting earthquakes needs to be addressed. Regional low-cost EEWSs generate an alert for ground shaking by analysing the ground motion data from more than one sensor. Generally, regional EEWS disseminate an alert if and only if at least more than one station is triggered, which is also called multi-station triggering (Bossu et al., 2021; Brooks et al., 2021; Cochran et al., 2019; Prasanna et al., 2022; Y. M. Wu & Mittal, 2021). This feature ensures a minimal number of false alerts generated by an EEWS. However, the multi-station triggering mechanism will cost a significant amount of time since it needs to wait for the data from multiple sensors. Therefore, to reduce the detection time of a low-cost regional EEWS, the sensor density should be significantly increased compared to conventional high-end EEWSs, where the high-end sensors are less prone to false alerts (Prasanna et al., 2022).

In addition to the challenges discussed above, detecting ground motions in smartphones while they are in motion is recognised as another challenge for smartphone-based EEWSs. When it comes to smartphone-based EEWSs, most EEWSs either work with smartphones that are fixed or while charging (Bossu et al., 2021; Brooks et al., 2021). This reduces the number of active sensors in the network. The number of sensors in the network tends to vary according to the time of the day (peak hours and non-peak hours), limiting the sensing capability of the EEWS. Even though few initiatives were carried out on machine learning techniques to detect an earthquake and other daily activities when smartphones are in mobility, they are still not integrated into most smartphone-based EEWSs.

3.5.3 Future Research

According to the identified limitations and challenges, the following are the future research areas proposed by this study.

Usage of Decentralised or Node-Level Processing

The ability to use sensors to decrease the amount of central processing and raise the level of processing at the node level has been made possible by advancements in sensor technology (edge computing) (Fischer et al., 2012; Prasanna et al., 2022). This will make it possible to process ground motion data and create warnings that may be shared across the sensor nodes and other connected devices at the node level (Prasanna et al., 2022). Decentralised or node-level processing has also been recognised as a new paradigm for real-time IoT tasks. It has become popular to handle issues with response time, requirement, saving bandwidth, costs, and data security and privacy (Franchi et al., 2019; Khan, 2020; Zhao et al., 2021). Furthermore, it makes systems more resilient by allowing end users to be warned at the local and regional levels, even when infrastructure failures affect parts of the system. To extract maximum benefits associated with sensor nodes' capabilities and capacities, only a few attempts have been made to implement EEWSs with decentralised processing (Fischer et al., 2012; Prasanna et al., 2022). However, EEWSs that process earthquake-related data at the node level are still in their infancy, creating more room for further investigations and exploration.

EEWSs with Multi-sensor Capability

The SLR process demonstrates the need for additional research to evaluate EEWSs that can integrate multiple MEMS-type sensors. These systems can be a promising approach toward having a denser sensor distribution in an EEWS. They can also generate benefits by having a large community-engaged EEW network where people can plug and play with their available ground motion sensor rather than limiting it only to a single type of sensor. However, EEWSs with multi-sensor capability need to be explored further. Therefore, there is a need for future research to investigate the possibilities of constructing a low-cost EEWS that can support different types of MEMS-based ground motion detection sensors.

Adaptation of Ground Motion or Wavefield-based EEW Algorithms

Ground motion or wavefield-based algorithms have shown promising results in overcoming the issues related to the source-based regional EEWSs (Hoshiba, 2021). Therefore, adopting ground motion-based algorithms into a regional-based EEWS can generate more robust and reliable alerts in a short period, making them a better alternative to on-site-based approaches for the earthquake-prone areas near the epicentre while keeping the source-based algorithms to generate warnings for the areas far from the epicentre. However, low-cost MEMS-based EEWSs constructed using ground motion algorithms have not been a subject of significant research. Even though the EEWS implemented by Prasanna et al.

(2022) adopted the PLUM-based ground motion approach, there is a significant opportunity for further research and improvement.

In addition to the above key research areas, network security of community-engaged EEWSs, and detecting ground motions using smartphones that are in motion are two areas that need further research.

Figure 3-4 illustrates the discussion flow, highlighting the limitations and challenges of regional low-cost EEWSs that attributes to the future research areas identified during this study.

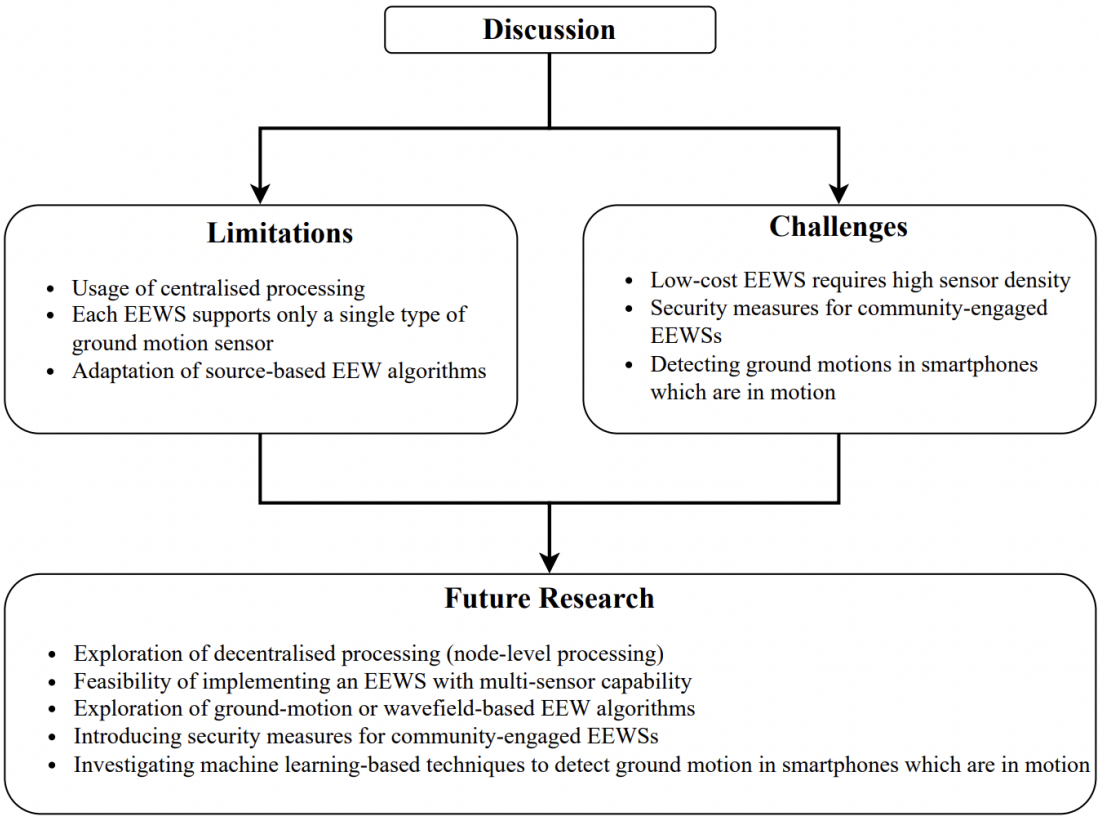

Figure 3-4. Discussion flowchart that summarises the limitations, challenges, and future research identified during this study

3.6 Conclusion

EEWSs already exist worldwide, and more countries are exploring the feasibility of designing and deploying EEWS for earthquake resilience. EEWSs are shifting from conventional high-end EEWSs towards a new concept of low-cost MEMS-based EEWSs that integrates and engages with the community. The development made in modern-day's IoT creates a path to implement an EEWS using low-cost MEMS-based ground motion detection sensors. Also, it has enabled the implementation of more sophisticated and robust low-cost MEMS-based EEWSs to generate reliable and accurate alerts.

This paper addresses the future research areas in the low-cost MEMS-based EEWSs by reviewing the literature and presenting an SLR on the low-cost EEWSs by generating three main systematic review questions. The findings from this review answered the following research questions:

1. How to classify low-cost MEMS-based EEWSs?

The reviewed articles revealed that networks can be classified into two categories according to the warning type and adopted EEW algorithm. Warning types can be on-site and regional, whereas the regional EEW algorithms can be classified as source-based and ground motion-based.

2. What are the existing low-cost EEWSs implemented around the world?

Low-cost EEWSs were classified according to research question 1 and analysed in terms of the type of low-cost sensor used, whether smartphones or in-house build.

3. What are the limitations and challenges in implementing a low-cost EEWS?

It was identified that: (1) most of the low-cost EEWSs were centralised, (2) EEWSs support only a single type of low-cost ground motion detection sensor, and (3) most of the regional EEWSs adopted the source-based algorithms which consume a significant amount of time in detecting and estimating earthquake parameters. Also, the main challenges in implementing a low-cost EEWS were identified as: (1) security measure which needs to be analysed further in terms of constructing a community-engaged EEWS, and (2) detecting human activities related motions from the earthquake's ground motion in smartphone-based EEWSs.

After answering these questions, opportunities, directions and research areas for further investigation were identified. Exploring the feasibility of decentralised processing, introducing multi-sensor support capability, and adopting ground motion-based EEW algorithms for regional EEWSs are areas for future research. Investigation into these identified research areas and opportunities for low-cost EEWSs will be beneficial for building robust, low-cost MEMS-based EEWS, significantly benefiting regions of high seismicity.

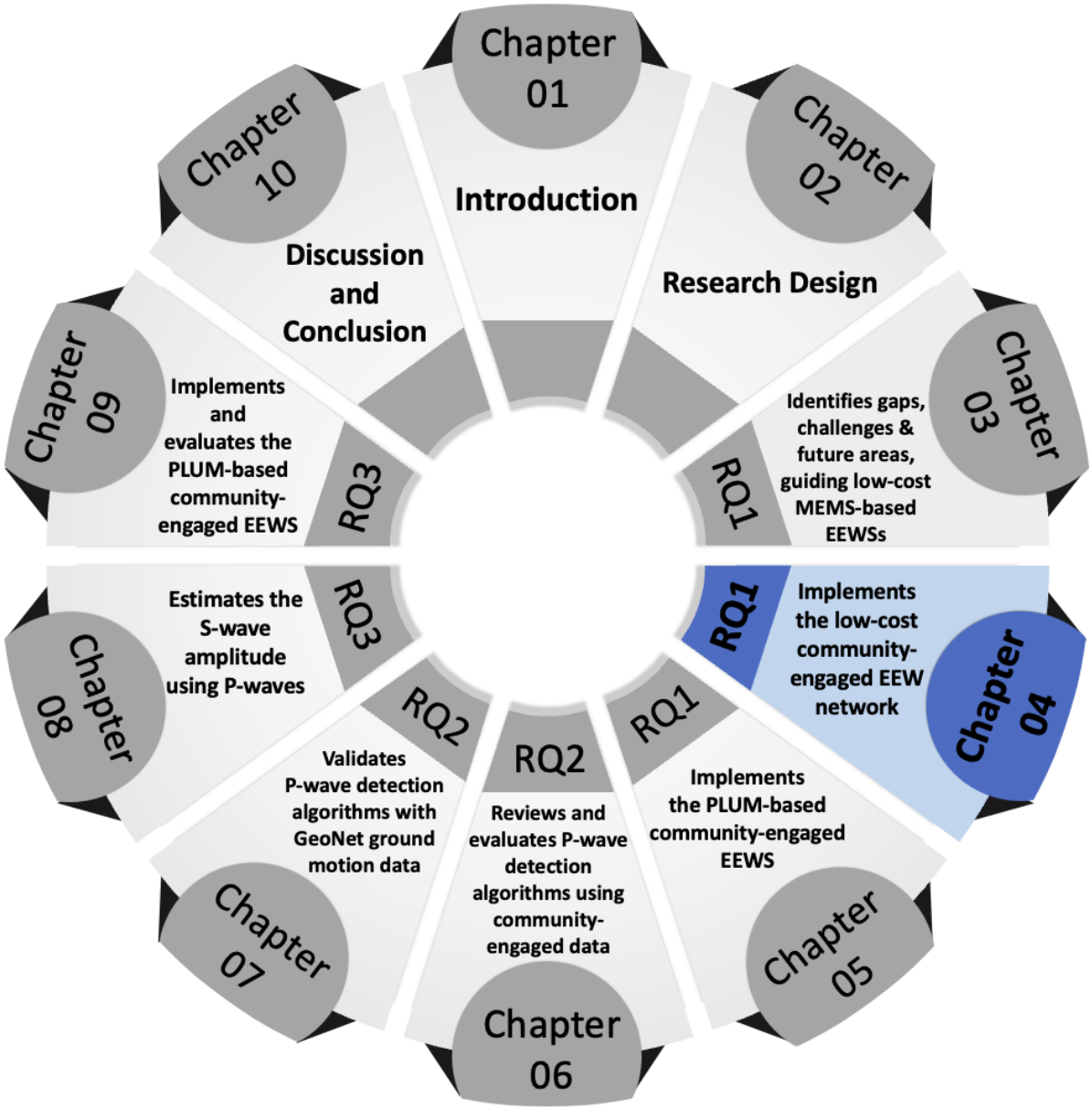
Chapter 01
Introduction
Chapter 02
Research Design
Chapter 03
RQ1
Identifies gaps, challenges & future areas, guiding low-cost MEMS-based EEWSs
RQ1
Implements the low-cost community-engaged EEW network
Chapter 04
RQ1
Implements the PLUM-based community-engaged EEWS
Chapter 05
RQ2
Reviews and evaluates P-wave detection algorithms using community-engaged data
Chapter 06
RQ2
Validates P-wave detection algorithms with GeoNet ground motion data
Chapter 07
RQ3
Estimates the S-wave amplitude using P-waves
Chapter 08
RQ3
Implements and evaluates the PLUM-based community-engaged EEWS
Chapter 09
Discussion and Conclusion
Chapter 10

MASSEY UNIVERSITY
TE KUNENGA KI PŪREHUROA
UNIVERSITY OF NEW ZEALAND

GRADUATE RESEARCH SCHOOL

STATEMENT OF CONTRIBUTION
DOCTORATE WITH PUBLICATIONS/MANUSCRIPTS

We, the candidate and the candidate's Primary Supervisor, certify that all co-authors have consented to their work being included in the thesis and they have accepted the candidate's contribution as indicated below in the *Statement of Originality*.

Name of candidate:	CHANTHUJAN CHANDRAKUMAR
Name/title of Primary Supervisor:	Aprof. Raj Prasanna
In which chapter is the manuscript /published work:	4

Please select one of the following three options:

○ The manuscript/published work is published or in press

- Please provide the full reference of the Research Output:

◉ The manuscript is currently under review for publication – please indicate:

- The name of the journal:

Bulletin of the New Zealand Society for Earthquake Engineering

- The percentage of the manuscript/published work that was contributed by the candidate: 80.00

- Describe the contribution that the candidate has made to the manuscript/published work:

Chanthujan Chandrakumar conceptualised the technical note, co-constructed the methodology, and conducted the formal analysis and investigation. He was also responsible for writing the first draft.

○ It is intended that the manuscript will be published, but it has not yet been submitted to a journal

Candidate's Signature:	Chandrakumar Chanthujan Digitally signed by Chandrakumar Chanthujan Date: 2024.08.14 12:35:34 +12'00'
Date:	14-Aug-2024
Primary Supervisor's Signature:	Raj Prasanna Digitally signed by Raj Prasanna Date: 2024.08.21 11:11:38 +12'00'
Date:	21-Aug-2024

This form should appear at the end of each thesis chapter/section/appendix submitted as a manuscript/ publication or collected as an appendix at the end of the thesis.

4 Implementation of the Low-cost Community-Engaged EEW Network

This chapter presents the process of implementing the community-engaged EEW network discussed in this PhD study. It covers the two installation phases, focusing on the factors considered for the network's implementation with sensor hosts from the community, particularly on selecting sensor locations. This chapter summarises findings from two questionnaire studies conducted with the sensor hosts, a technical note comparing different installation methods for wool carpet flooring, and a comprehensive installation guide for RS4D sensor installation in households.

This chapter addresses Objective 1.2 of this thesis: to implement an experimental community-engaged EEW network by installing low-cost MEMS-based ground motion sensors in households within the greater Wellington region.

The technical note discussed in this chapter has been submitted to the 2024 Bulletin of the New Zealand Society for Earthquake Engineering:

Chandrakumar C, *Stephens M, Prasanna R. (2024 - forthcoming) Installation methods for ground motion sensors in community-engaged earthquake early warning systems. Submitted to the 2024 Bulletin of the New Zealand Society for Earthquake Engineering*

The submitted form of the technical note and the sensor installation guide are provided in Appendix B.

4.1 Installation of Low-Cost MEMS-based Sensors in the Greater Wellington Region – Phase 1

As detailed in Chapter 2, installing sensors in the community aligns with the Relevance Cycle of the DSR methodology, where requirements are gathered to develop the artefact and then field-tested.

The initial deployment of the sensor network in the Greater Wellington region, carried out by the CRISiSLab research team, marks the first phase of network implementation. The phase commenced in 2020, prior to the initiation of this PhD study. During this stage, community-of-practice sessions, workshops, and EEW webinar sessions were conducted to gather requirements for implementing a community-engaged EEW network (Prasanna et al., 2022; Tan et al., 2021). After these sessions, sensors were distributed to hosts primarily engaged in these activities. Most of these initial hosts were researchers at Massey University, provided with sensors alongside a basic installation guide. The primary aim of this phase was to establish a foundational infrastructure for the EEW network and to evaluate its capability to record ground motion under real-world conditions. Figure 4-1 shows the station locations installed in the first phase of the community-engaged EEW system.

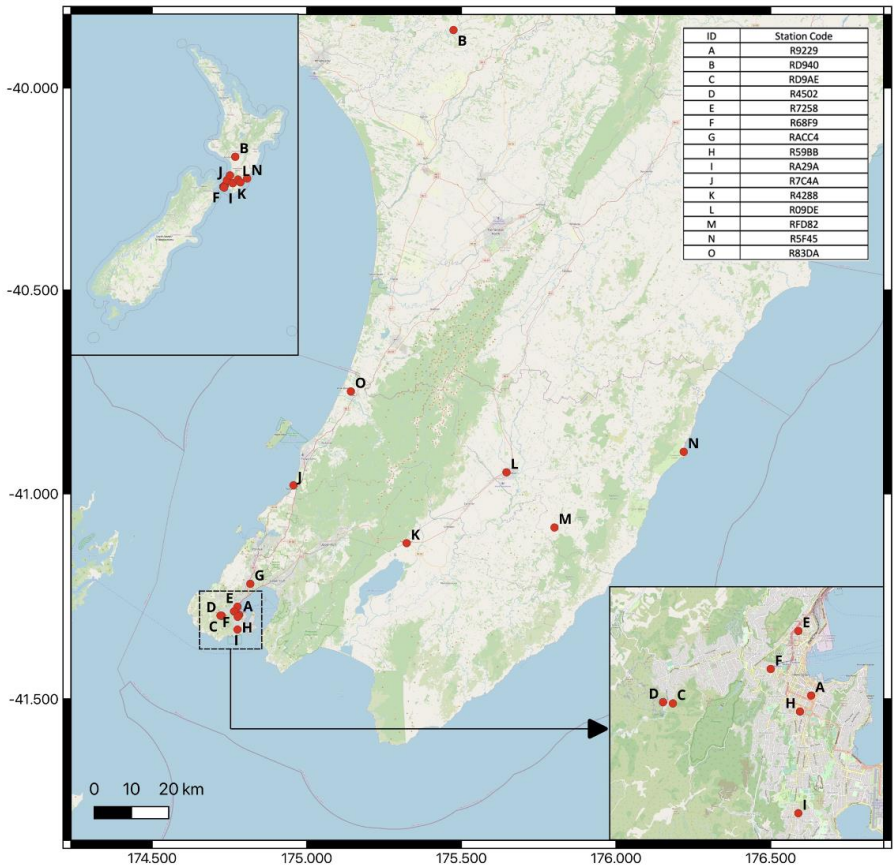

Figure 4-1. Station locations installed in the first phase of the community-engaged EEWS in the North Island of NZ.

This phase revealed significant challenges related to ambient noise within the network. This noise often resulted in false and missed detections at various stations, leading to unreliable alerts from the EEWS. Addressing the system's reliability is crucial, as the effectiveness of an EEW system hinges on its ability to minimise false and missed alerts (Minson et al., 2019). Hence, during this PhD study, a questionnaire was disseminated among the Phase 1 sensor hosts to gather more information regarding ambient noise and improve installation practices. The information sheet and the questionnaire used for this purpose are provided in Appendix C and D.

The survey contained 16 questions requesting information on sensor locations, such as the type of house (apartment or separate building), geography (e.g., on a hillside, flat surface, dune), sensor installation location within the house, floor type (e.g., concrete, wooden, stone), and ground type (e.g., solid rock, soft soil, sand). It also collected information on environmental noise, asking about the busyness of the neighbourhood and activities around the sensor location that might cause noise. Lastly, it inquired about internet connectivity and the hosts' maintenance measures for the sensors.

The survey responses from 14 sensor hosts resulted in the following summary:

- Most sensors (13 out of 14) were installed in separate houses, with only one in an apartment. Eight sensors were installed on the ground floor, four on the first and one on the second.
- Four sensors were installed in the living area, prone to foot traffic.
- The most common ground types were soft soil and solid rock. Most houses were situated on flat surfaces, while four were on hillsides.
- Ten houses were in quiet neighbourhoods, while four were in busy areas near heavy traffic.
- Six hosts installed sensors on the floor, and the remaining placed sensors on various surfaces, such as TV cabinets, windowsills, benches, and even a piano.
- Of the six floor-installed sensors, four were on wool carpet, one on a wooden floor, and one on a concrete floor.
- Only two hosts fixed their sensors to the installation surfaces, with the rest left loosely placed.
- Most hosts occasionally checked the sensor status more than once a month, with two checking daily.

Key findings from the questionnaire included:

1. Most sensors were not installed on the floor, which is not recommended for optimal RS4D performance.
2. Most sensors were installed in quiet locations ideal for ground motion recordings and were in separate houses.
3. Most sensors were loosely placed, making them easily dislodged.

4. The most common floor type was wool carpet.

Appendix E illustrates several installations conducted by the sensor hosts based on images received through the questionnaire. The insights gained from this questionnaire guided adjustments and improvements in sensor installation methods, ultimately enhancing the overall reliability and efficiency of the EEW network.

Further, the questionnaire revealed the improper installation of the sensors which contributed to the high ambient noise observed in the network. Identifying these noise sources and their potential from the Phase 1 installations led to the creation of a comprehensive installation guide for RS4D sensors in a community-engaged EEW network (Appendix F). This guide was circulated to Phase 1 sensor hosts to finetune the sensor installation methods and improve data quality.

As the next step during this study, a second phase of sensor installation was initiated to increase sensor density in the Greater Wellington region. By adopting a more systematic approach during Phase 2, the research aimed to mitigate the challenges identified in Phase 1. This PhD study focused on two main areas for Phase 2: (1) creating a questionnaire for potential Phase 2 sensor hosts to gather information about sensor installation locations before finalising them, and (2) conducting a study to analyse the sensor ground motion recording performance with different installation methods on wool carpet flooring, the most common carpet type in NZ. This study aimed to understand the impact of different installation methods in a community-engaged EEW network before delivering the second phase of sensors to enhance sensor installation techniques for optimal performance. Improved installation methods and careful selection of installation locations aimed to minimise ambient noise, thereby reducing false and missed detections in the sensor network.

4.2 Installation of Low-Cost MEMS-based Sensors in the Greater Wellington Region – Phase 2

As a part of this PhD study, a second phase of installation was initiated for 2023, with target of inviting a broader community from the general public to join the network by hosting sensors. To recruit participants, a banner (See Figure 4-2) was designed and circulated on social media to garner community interest in installing RS4D seismographs at their households. This campaign ran from 2 July to 31 July 2023. During this period, the community responded enthusiastically, resulting in 80 Expression Of Interests (EOI) from various individuals and households from the Greater Wellington Region.

Figure 4-2. Banner circulated on social media to encourage community participation in installing RS4D seismographs, running from 2 July to 31 July 2023.

The selection of optimal sensor locations was decided through the pool of 80 responses. The distribution of interested participants across the Wellington region were mapped by utilising the respondents' geospatial information. The location points were then visualised and analysed in a geographic context using a Python script. Figure 4-3 displays the geographical distribution of the 80 responses received from the EOI campaign for hosting RS4D seismographs in the Wellington region, highlighting a notable concentration of responses in Wellington City, followed by significant interest from Hutt Valley, Tawa, and Porirua suburbs. This geographic visualisation identified clusters of interest, areas with a higher concentration of willing participants, and potential gaps in coverage that required further attention.

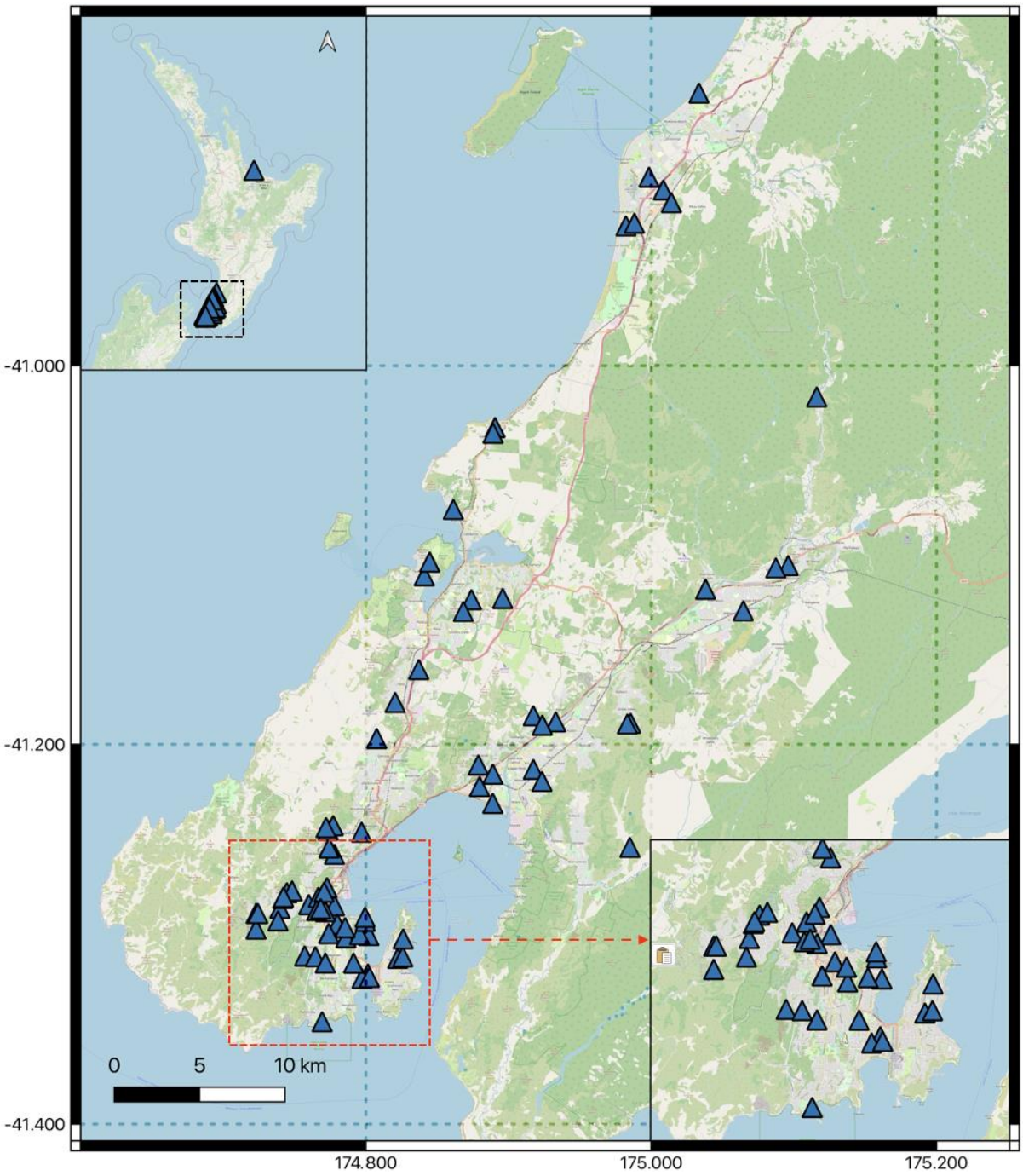

Figure 4-3. Geographical distribution of the 80 responses received from the EOI campaign for installing seismographs in the Wellington region, marked with blue triangles.

This geographically oriented analysis aided in identifying the selection of 25 participants for Phase-2 of the installation. The primary objective for selection was to choose locations that would maximise the earthquake monitoring capabilities by increasing the sensor density of the community-engaged network and, consequently, increase the EEWS warning time. To achieve this, a multi-faceted approach was implemented, considering several key factors including (1) EEW algorithm coverage requirement, (2)

seismic activity, (3) site and installation considerations, and (4) population density. These are explained in detail below:

1. EEW Algorithm Coverage Requirement

The PLUM algorithm (Kodera et al., 2018) is intended for adoption in the community-engaged EEW network. The PLUM algorithm predicts seismic intensities at designated prediction points by determining the maximum observed real-time seismic intensity from all stations within a specific radius of 30 km from each prediction point. At least two stations within this radius must exceed the alerting threshold to trigger a warning for that prediction point. For example, when a sensor's observed intensity exceeds a predefined threshold, the algorithm checks if any nearby sensors within the 30 km range exceed the threshold within a specified waiting period. An alert is generated and issued for the particular prediction point only when these conditions are met.

Given the need for two nearby sensors to confirm ground shaking, strategically placing sensor locations within the network is essential. When placing a sensor in a new area, another sensor location is chosen nearby (within a 5 km radius) to ensure two sensors are placed close together. This strategic placement reduces the detection delay between the sensors, as an increased detection delay would reduce the warning time.

2. Seismic Activity:

Figure 4-4 illustrates the epicentre locations of earthquakes greater than magnitude four in the Wellington and Marlborough region over the past 20 years, based on data from the GeoNet catalogue (GNS Science, 2022). The figure highlights that the entire region is subject to high levels of seismic activity, underscoring the necessity for strategic sensor placements along the Wellington region's perimeter to facilitate early earthquake detection.

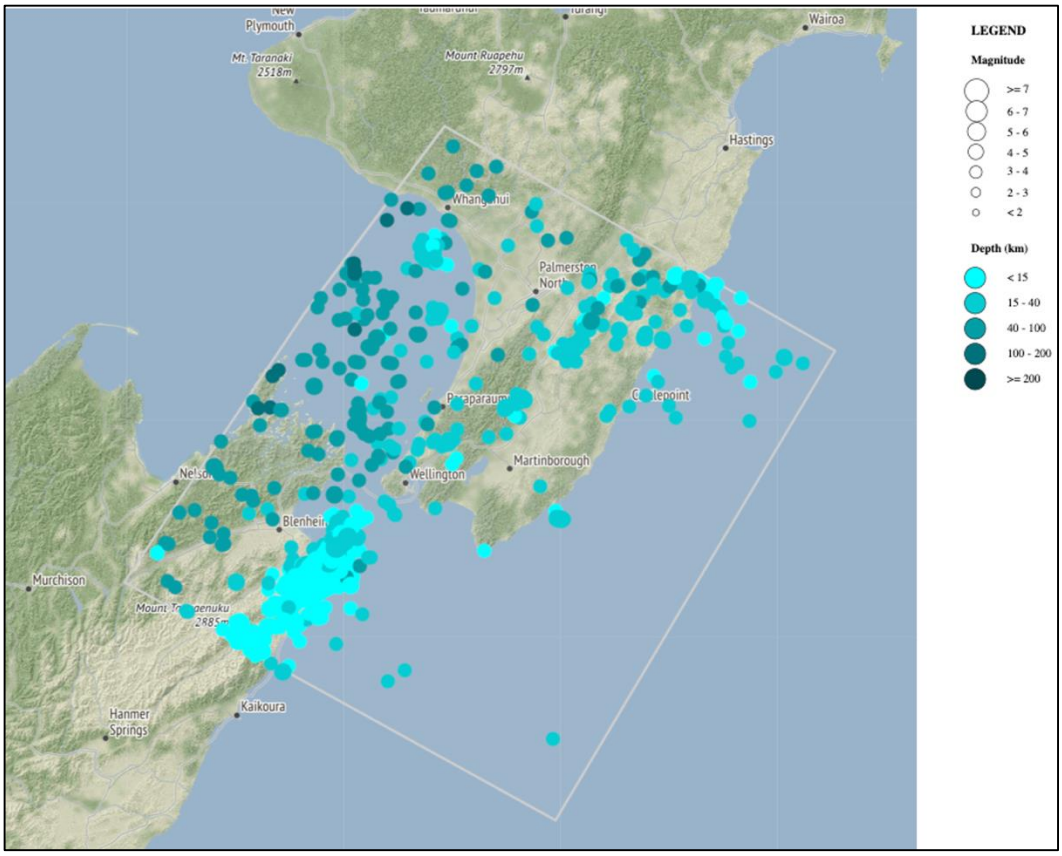

Figure 4-4. Seismic activity (earthquakes with a magnitude larger than four) in the Wellington region over the past 20 year: earthquake epicentres and depth (GNS Science, 2022)

Consequently, sensors were initially deployed in the lower part of the North Island, specifically targeting the Lyall Bay and Miramar suburbs of Wellington city, to detect the initial shaking from earthquakes originating in the northern part of the South Island (southern part of the Wellington region). Additionally, sensors were strategically placed in Otaki, Paraparaumu, Porirua, Johnsonville, and Newlands to cover the western and northern sides of the Wellington region. To further enhance coverage, sensors were installed in Upper Hutt, Stokes Valley, and Wainuiomata to monitor the eastern part of the Wellington region. This approach was designed to capture seismic activity from all directions, thereby improving the system's ability to provide timely and accurate earthquake warnings using the PLUM algorithm. Further, this ensures that the sensors were strategically placed around the perimeter of the Wellington region. In addition, when placing sensors in these areas, the algorithm coverage requirement also considered by placing another sensor close enough for rapid earthquake detection.

3. Site Constraints

After analysing coverage requirement and seismic activity, the following criteria focused on site characteristics and installation locations.

Weak deposits such as soils and other unconsolidated sediments can amplify earthquake ground motions. Seismic microzonation aims to identify these amplification effects by classifying subsoil classes or local ground-shaking properties for appropriate engineering design. In New Zealand, the current building code NZ1170.5 (Standards New Zealand, 2004) specifies five discrete subsoil classes ranging from A (Strong Rock), B (Rock), C (Shallow Soil), D (Deep or Soft Soil), and E (Very Soft Sediment) (Semmens et al., 2011).

The study examined the site classes of the houses from EOI, ranging from Class A to Class E. Soft sediments, although acceptable for ground motion recording, require soil amplification correction due to their propensity to amplify ground motion during earthquakes. Therefore, locations with site classes closer to A were prioritised for their stable ground conditions, essential for accurate sensor readings. However, most of the Wellington region is covered with Site Class B (Wellington City Council, 2022), while the Lower Hutt region, adjacent to Wellington, is mainly covered with Site Class D (Boon et al., 2011). Out of the 25 locations selected, 16 were in Site Class B, three in Site Class D, and one in Site Class C. The site classes for Paraparaumu, Otaki, and Upper Hutt stations remain unknown, accounting for five stations with undetermined site conditions.

Despite some stations being in Site Classes C and D and a few locations with unknown site conditions, these selections were made with discretion. Priority was given to areas with higher demand or necessity for sensors, ensuring a balanced and effective network coverage.

4. <u>Population Density</u>

The primary focus of a community-engaged EEW network is the ability to alert and protect the residents of the Wellington region during seismic events, particularly Wellington City, Hutt City, Upper Hutt City, and Porirua City. Covering all cities and their adjacent or distant suburbs with sensors to detect seismic events from any direction was challenging due to the limited number of sensors. Therefore, priority was given first to Wellington City, followed by Hutt City, Porirua City, and then Upper Hutt City. To effectively serve the Wellington City, the algorithm required a layer of sensors outside the city circumference to detect external events and sensors within the city to detect internal events, thereby ensuring timely alerts to the population.

Initially, the northern side of Wellington City was targeted, with sensor locations chosen in Thorndon, Johnsonville, Newlands, Porirua, Lower Hutt, and Upper Hutt to act as a "seismic shaking shield" for Wellington City. However, responses from the EOI showed a concentration in Wellington Central, with limited responses from outer Wellington City. Therefore, priority was given to placing sensors in these mentioned areas to create the seismic shield. A balance was struck between catering to the population density in Wellington City and providing adequate coverage for the outer Wellington region. Ultimately,

15 sensor locations were chosen in the outer layer to enhance earthquake monitoring and early warning capabilities for Wellington City.

Sensors were then placed along the coastal area of Wellington City (south of Wellington), focusing on EOIs received from Island Bay, Lyall Bay, and Miramar to capture earthquakes from the Cook Strait region. Since the west side of Wellington City is mostly forest (Makara Hill), no EOIs were received from that area, leaving only Karori as the west border for sensor installation to capture earthquakes from that direction. Similarly, except for one EOI from Wainuiomata, no EOIs were received beyond that region, as it is part of the Remutaka Forest Park. This created gaps in sensor coverage in the east and west parts of Wellington City.

The sensors installed in Wellington City act as a shield for areas such as Johnsonville, Newlands, Porirua, Lower Hutt, and Upper Hutt in the southern direction. Additionally, sensor locations chosen in Paraparaumu and Otaki served as a shield for Upper Hutt and Lower Hutt cities in the northern direction.

4.2.1 Final Sensor Locations

As a result of the comprehensive analysis and careful consideration of the four factors, 25 new sensor locations were selected for Phase 2 installation. These locations include:

- 15 sensors in Lower Hutt, Upper Hutt, Johnsonville, Newlands, Porirua, Paraparaumu, and Otaki
- Three sensors in Karori
- Four sensors in Wellington Central
- One each for Island Bay, Miramar, and Lyall Bay

These 25 sensors complement the existing sensors from Phase 1 in the community-engaged network. Figure 4-5 illustrates the sensor locations, with red markers denoting sensors installed during Phase 1 and blue markers indicating the proposed 25 new sensor locations for Phase 2.

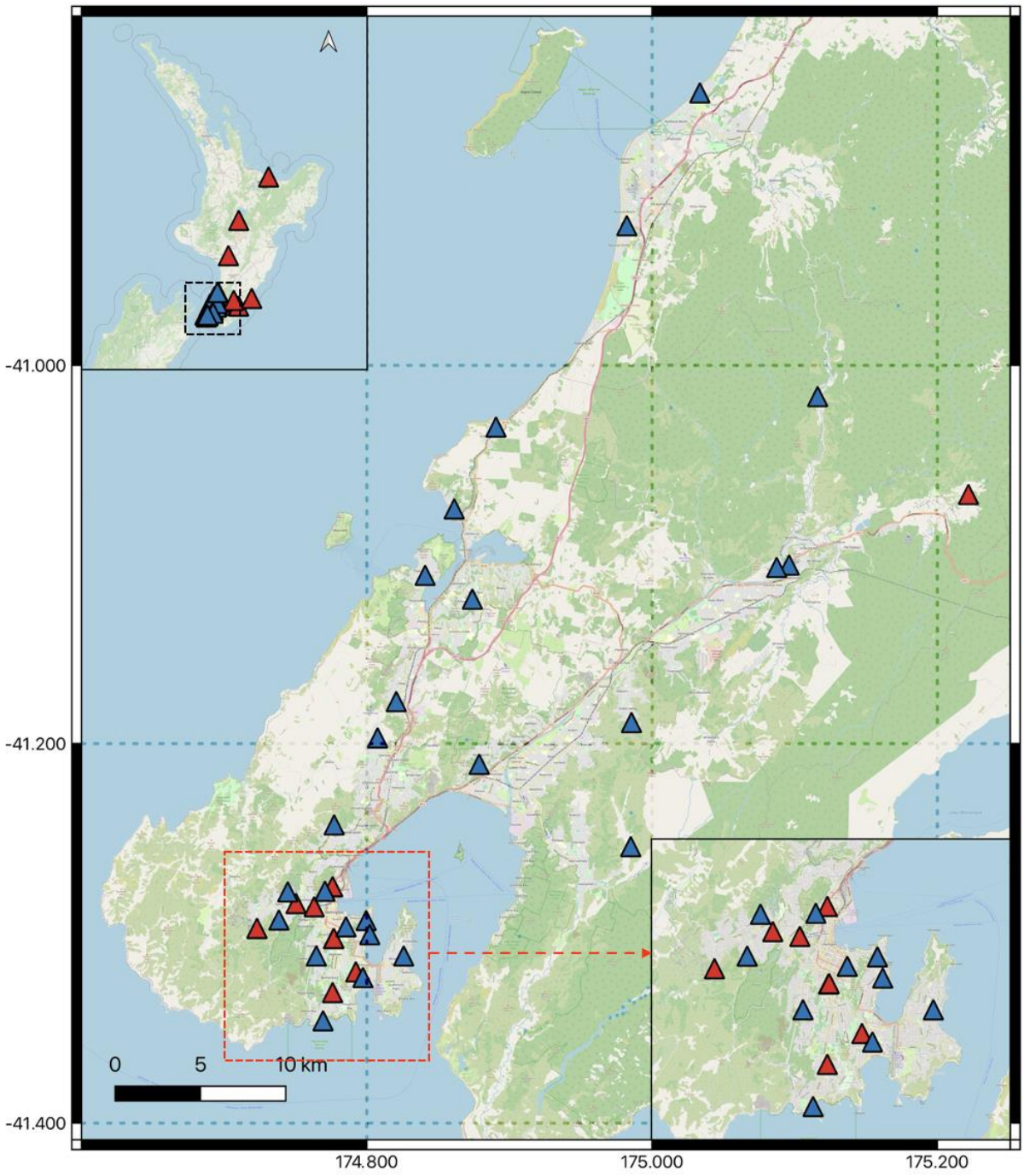

Figure 4-5. Map showcasing the sensor locations of the community-engaged EEW network in the Wellington region. The red markers represent the existing sensors, while the blue markers indicate the 25 selected sensor locations for second phase of installation.

After selecting the sensor locations, emails were sent to all respondents who expressed EOIs, informing them of their status. The status included whether they were selected as prioritised hosts, placed on a waiting list in case of non-response or declination from the initial choices, or not selected. Detailed instructions were sent to the chosen sensor hosts through email including an invitation to meet online to discuss next steps via Zoom. These online sessions aimed to explain the project and its focus and address any concerns and questions regarding sensor installation.

Following this initial communication, another questionnaire was shared with the selected sensor hosts to gather information on the planned sensor installation locations and their environmental conditions.

The main themes addressed in the questionnaire is summarised in the following table (Table 4-1), detailed questionnaire in Appendix G:

Table 4-1. Summary of Main Themes Addressed in the Phase 2 Sensor Installation Questionnaire

Theme	Requested information
Location Details	• Address of the planned sensor installation. • Specific installation site within the property (e.g., backyard, garage, living room). • The type of flooring used at the sensor installation site.
Environmental Factors	• Proximity to equipment or machinery that may generate vibrations. • Specification of such equipment and distance from the sensor if applicable
Installation Preferences	• Willingness to adhere or affix the sensor for optimal performance. • Additional materials needed for installation (e.g., longer ethernet or power cables).
Logistics	• Preferred installation dates. • Preferred method for receiving the sensor (collect from Massey University or delivery).
Site Assessment	• A photo of the planned installation location will be provided to assess suitability.

4.2.2 Evaluation of Sensor Installation Methods

Similar to Phase 1, the results from the installation survey of the chosen hosts indicated that most participants planned to install the sensors on wool carpet flooring. Given this finding, the researcher conducted an investigation into various installation methods for the RS4D seismograph on wool carpet made of synthetic material using a shake table, including the following methods:

1) Loosely placed sensor on carpet
2) Loosely placed sensor with an anti-slip sticker
3) Sensor with a heavy steel base placed on the carpet
4) Sensor fixed with double-sided tape on the carpet

A fifth sensor was installed directly on the shake table as a control reference. These methods were tested using simulations on a two-axis horizontal shake table to determine which yielded the best sensor performance and data quality. This study is published separately as a technical note and attached in B.

The shake table testing employed controlled experimentation in two tests: (1) sinusoidal waveforms at varying frequencies of 0.5, 1, 5, 10, and 15 Hz, and (2) ground motion data from three historically significant earthquakes: the 1992 Cape Mendocino earthquake, the 1940 El Centro earthquake, and the 1994 Northridge earthquake. For the sinusoidal wave testing, Fourier Spectral Analysis was performed on the recorded ground motion data from the sensors and compared to the reference sensor using the Root Mean Square Error (RMSE) metric for accuracy. For the earthquake ground motion testing, the RMSE from the recorded ground motion data from the sensors was compared to the reference sensor's RMSE. Further, the Acceleration Response Spectrum and Peak Ground Acceleration were also evaluated.

Since the shake table used in this study was limited to horizontal movements (X and Y directions), the vertical acceleration of the earthquakes could not be simulated. Therefore, to test the stability of the different sensor installation methods in three-dimensional space, the researcher conducted a stability test using vertical ground motion data downloaded from the PEER Ground Motion Database (Berkeley University, 2022). The potential for slip was evaluated by comparing the horizontal shear force applied by the earthquake to the static frictional force at the sensor installation interface, with a frictional force greater than the seismic shear force indicating that no slip would occur. The vertical acceleration data were used to calculate the vertical ground reaction force on the sensors during three different earthquake scenarios, evaluating each installation method.

The key findings from the technical note are as follows,

- The loosely placed sensor consistently yielded the lowest RMSE values across a broad frequency range for the sinusoidal wave testing, demonstrating the highest accuracy and superior performance in the ground motion testing. The anti-slip sticker method showed the second-best performance, closely aligning with the results of the loosely placed sensor. In contrast, other methods exhibited more significant deviations from the reference sensor data.
- Results from the stability tests indicated that installations with anti-slip stickers had the least potential for slip, followed by steel-plated installations. The loosely placed sensor exhibited the highest probability of slip among the methods tested.

Despite the lower stability of the loosely placed sensor, it demonstrated the highest accuracy in seismic signal replication. This accuracy, combined with the simplicity of the installation process and the

absence of a need for additional securing mechanisms, highlighted the effectiveness of the loosely placed method for RS4D sensor installation on wool carpeting. The anti-slip sticker method also showed strong performance, with minimal deviations compared to the loosely placed sensor and greater stability against slip. Given these findings, the study recommended both the loosely placed and anti-slip sticker installation methods for wool carpeting, providing sensor hosts with an option.

No further testing on different types of flooring was conducted since most respondents indicated that installation would be on wool carpet. For other types of flooring, double-sided tape was recommended to affix the sensor to the floor for added stability. However, additional research using a three-dimensional shake table is required to explore further installation methods and floor types, enhancing applicability and accuracy in different settings. This will enable a more comprehensive sensor performance evaluation under realistic seismic conditions, providing deeper insights into optimal installation techniques.

The sensors were delivered in person, along with the necessary materials for installation, such as power sockets and ethernet cables. A comprehensive installation guide, attached in Appendix F, was also provided to ensure proper setup and functionality. Appendix H illustrates several proper sensor installations completed by the sensor hosts during Phase 2.

Finally, according to DSR's Relevance Cycle, the performance of the fine-tuned sensor installations in Phase 1 and the newly installed Phase 2 sensor network is field tested during the performance analysis of the implemented EEWS presented in Chapter 9.

4.1 Chapter Summary

This chapter details the process of implementing a community-engaged EEW network in the Greater Wellington region, focusing on installing low-cost MEMS-based sensors across two phases. The first phase involved initial deployments and identified significant ambient noise issues, leading to the second phase's refinement of sensor installation techniques. The second phase utilised a systematic approach to select sensor locations, guided by four key factors, including EEW algorithm coverage, seismic activity, and site-specific considerations. Community interest was fostered through a social media campaign, resulting in 80 responses for expression-of-interest, from which 25 sensor locations were strategically chosen.

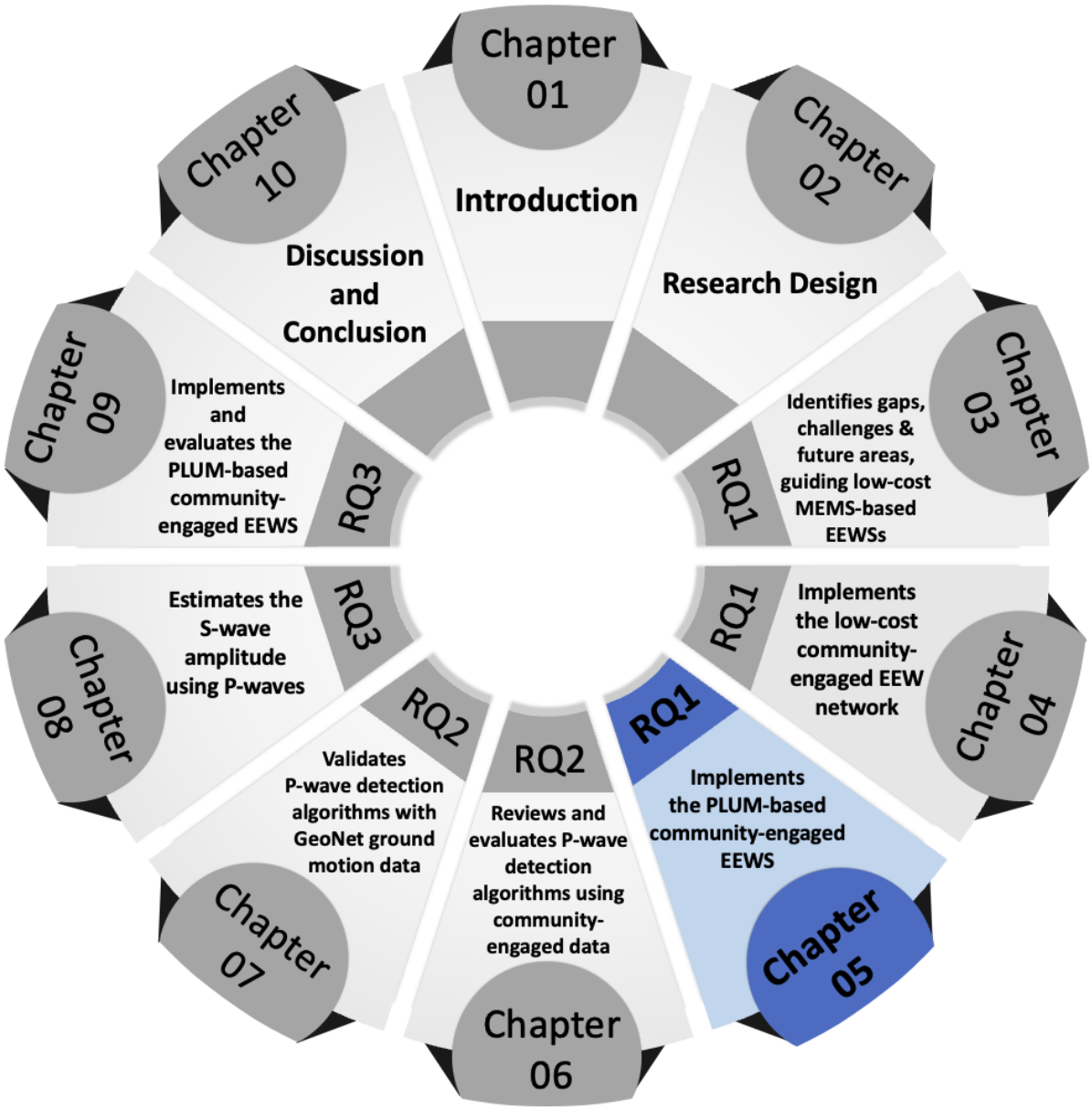
Chapter 01
Introduction
Chapter 02
Research Design
Chapter 03
Identifies gaps, challenges & future areas, guiding low-cost MEMS-based EEWSs
RQ1
Chapter 04
Implements the low-cost community-engaged EEW network
RQ1
Chapter 05
RQ1
Implements the PLUM-based community-engaged EEWS
Chapter 06
RQ2
Reviews and evaluates P-wave detection algorithms using community-engaged data
Chapter 07
RQ2
Validates P-wave detection algorithms with GeoNet ground motion data
Chapter 08
RQ3
Estimates the S-wave amplitude using P-waves
Chapter 09
RQ3
Implements and evaluates the PLUM-based community-engaged EEWS
Chapter 10
Discussion and Conclusion

MASSEY UNIVERSITY
TE KUNENGA KI PŪREHUROA
UNIVERSITY OF NEW ZEALAND

GRADUATE RESEARCH SCHOOL

STATEMENT OF CONTRIBUTION
DOCTORATE WITH PUBLICATIONS/MANUSCRIPTS

We, the candidate and the candidate's Primary Supervisor, certify that all co-authors have consented to their work being included in the thesis and they have accepted the candidate's contribution as indicated below in the *Statement of Originality*.

Name of candidate:	CHANTHUJAN CHANDRAKUMAR
Name/title of Primary Supervisor:	Aprof. Raj Prasanna
In which chapter is the manuscript /published work:	5

Please select one of the following three options:

(●) The manuscript/published work is published or in press

- Please provide the full reference of the Research Output:

Chandrakumar C, Tan ML, Holden C, Stephens M, Prasanna R. Adapting PLUM: Earthquake early warning with node-level processing in New Zealand. Proceedings of the 21st ISCRAM Conference. Münster, Germany, May 2024.

( ) The manuscript is currently under review for publication – please indicate:

- The name of the journal:

Proceedings of the 21st Information Systems in Crisis Response and Management (ISCRAM) Conference 2024

- The percentage of the manuscript/published work that was contributed by the candidate: 80.00

- Describe the contribution that the candidate has made to the manuscript/published work:

Chanthujan Chandrakumar conceptualised the article, co-constructed the methodology, and conducted the formal analysis and investigation. He has written first draft of the manuscript.

( ) It is intended that the manuscript will be published, but it has not yet been submitted to a journal

Candidate's Signature:	Chandrakumar Chanthujan Digitally signed by Chandrakumar Chanthujan Date: 2024.08.14 13:38:20 +12'00'
Date:	14-Aug-2024
Primary Supervisor's Signature:	Raj Prasanna Digitally signed by Raj Prasanna Date: 2024.08.21 11:16:15 +12'00'
Date:	21-Aug-2024

This form should appear at the end of each thesis chapter/section/appendix submitted as a manuscript/ publication or collected as an appendix at the end of the thesis.

5 Implementation of the PLUM-based Community-Engaged EEWS

This chapter presents the revised version of the manuscript titled “Adapting PLUM: Earthquake Early Warning with Node-Level Processing in New Zealand.” It focuses on adapting the PLUM algorithm for the community-engaged EEW network implemented in Chapter 4. The primary revisions in this chapter, compared to the published work-in-progress paper, include modifications to the PLUM algorithm to better suit NZ’s seismic context. Additionally, the discussion has been updated to reflect these adaptations, and the Future Work section has been revised for improved continuity with the next chapter. This study is conducted to achieve Objective 1.3 of this thesis: Implementing the ground motion-based EEW algorithm at the experimental EEW network to operate at the node level.

The article presented in this chapter was published as a work-in-progress paper in 2024 in the Proceedings of the 21st Information Systems for Crisis Response and Management (ISCRAM) Conference in Münster, Germany, as:

Chandrakumar C, Tan ML, Holden C, Stephens M, Prasanna R. Adapting PLUM: Earthquake early warning with node-level processing in New Zealand. Proceedings of the 21st ISCRAM Conference. Münster, Germany, May 2024.

5.1 Abstract

Is running the Propagation of Local Undamped Motion (PLUM) algorithm in a community-engaged earthquake early warning (EEW) network feasible, and can it function effectively at the node level without centralised processing units? This study investigates the practicality of deploying the PLUM algorithm for New Zealand within a decentralised architecture, shifting away from traditional centralised seismic data processing methods. The study uses cost-effective MEMS-based seismographs to decentralise EEW. The preliminary phase of the research included deploying sensors, adapting the PLUM for New Zealand's seismic context and establishing a two-tiered Primary-Secondary node structure for node-level intensity prediction and alert generation, with the sensors functioning as independent prediction points. Future work includes integration of P-wave detection into PLUM, threshold calibration for optimal alert issuance, and network expansion to reduce blind spots. This work-in-progress paper discusses progress towards a scalable, efficient EEW system that could serve as a replicable model for earthquake-prone regions globally, aiming for operational readiness that empowers communities against the threat of earthquakes.

5.2 Introduction

Earthquake Early Warning System (EEWS) has been recognised as a vital advancement towards mitigating the impacts of seismic events (R. M. Allen & Melgar, 2019; Chandrakumar, Prasanna, Stephens, & Tan, 2022). The evolution of EEWS has been propelled by technological advancements and research breakthroughs, resulting in the implementation of systems across various regions and countries (Chandrakumar, Prasanna, Stephens, & Tan, 2022; Cremen & Galasso, 2020; McBride et al., 2022). These systems are designed to provide advanced alerts, enabling individuals and authorities to take preventive measures to safeguard lives and infrastructure. The effectiveness of EEWS in reducing damages and injuries associated with seismic activities has been well documented globally (e.g., Fujinawa & Noda, 2013; Nakayachi et al., 2019; Suárez et al., 2009).

Despite the pronounced seismic hazard in Aotearoa New Zealand (NZ), the country lacks an official national EEWS, a critical gap in preparedness underscored by Becker et al. in their 2020 study. The country relies predominantly on the GeoNet programme, managed by GNS Science, for rapid earthquake information. GeoNet provides earthquake source parameters and ground-shaking data through a website and mobile app but lacks dedicated Earthquake Early Warning (EEW) capabilities (GeoNet, 2017; GNS Science, 2023).

The absence of an official EEWS in NZ is primarily due to various technical and non-technical challenges, with the high cost of advanced systems representing a considerable obstacle (Brooks et al., 2021; Prasanna et al., 2022). For cost-effective earthquake preparedness solutions, there has been a marked global trend towards adopting low-cost alternatives. Micro-electromechanical systems (MEMS) based ground motion sensors have gained prominence among these. Demonstrating a successful track record in seismic applications since the early 1990s, MEMS-based ground motion sensors have been effectively integrated into EEWS in various regions, facilitating real-time public alerting systems (Anthony et al., 2019; Holland, 2003).

In pursuing a cost-effective EEWS in NZ, Prasanna et al. (2022) have initiated and deployed an experimental, community-engaged network in the Greater Wellington region. As depicted in Figure 5-1, this innovative system leverages Raspberry Shake 4D (RS4D) seismographs equipped with MEMS-based accelerometers, signifying a pivotal development in earthquake detection and alert technology. This network adopts a decentralised processing approach to analyse and process ground motion data, diverging from the centralised processing approaches predominant in established EEWS globally. The network employs the Propagation of Local Undamped Motion (PLUM) algorithm (Kodera et al., 2018) for its earthquake early warning capabilities. However, Kodera's PLUM algorithm has been modified to suit NZ's specific seismic context and align with the country's intensity scale. This adapted version is referred to as "NZ-PLUM" in this study. Then, the NZ-PLUM has been optimised to operate on RS4D sensors with limited computational resources, enabling efficient node-level processing. Unless specified otherwise, the term NZ-PLUM will refer to the adapted PLUM algorithm, while "PLUM" will refer to Kodera's PLUM algorithm throughout this paper.

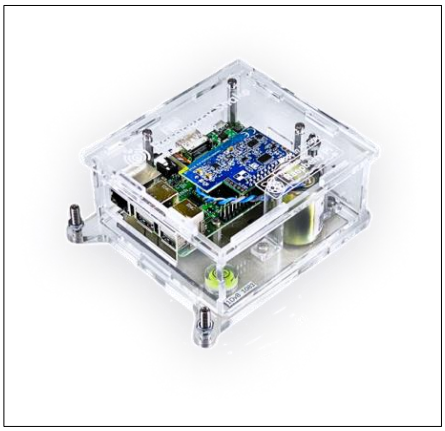

Figure 5-1. The Raspberry Shake 4D (RS4D) seismograph.

A previous study with the same network has proven the effectiveness of decentralised processing compared to conventional centralised approaches by applying the original PLUM algorithm to a selected array of sensors within a simulated environment (Prasanna et al., 2022). This work-in-progress

paper builds on past research and addresses the ongoing progression and practical application of the PLUM algorithm within a real-life operational context, including modification of the PLUM algorithm for NZ's context (NZ-PLUM) and adaptation for decentralised processing.

The article is structured as follows: Section 5.3 overviews the decentralised processing architecture and the PLUM algorithm. Section 5.4 describes the implementation of the EEWS, detailing the adaptation of the PLUM algorithm to the NZ-PLUM and its integration into a decentralised processing architecture within the community-engaged EEWS. Finally, Section 5.5 discusses the insights gained from the preliminary findings and outlines directions for future research. Section 5.6 concludes by emphasising the significance and potential impact of this research.

5.3 Background

5.3.1 Decentralised Processing Architecture

Two principal methodologies dominate the data processing landscape: centralised and decentralised processing (Xi, 2020). Centralised processing gathers data from diverse sources into a unified, centralised facility for analysis and processing. Conversely, in decentralised processing, individual nodes or sensors independently execute data analysis and processing tasks (Santamaria et al., 2019). This distinction primarily revolves around allocating computational responsibilities; centralised systems centralise data processing in a singular hub, whereas decentralised systems distribute these tasks across each node within the network, potentially augmenting the system's responsiveness and robustness against widespread failures.

Most EEWS operates on a centralised model, where a central facility receives and processes seismic data. While this centralised approach offers superior control and consistency in data handling, it is susceptible to critical delays and communication failures, particularly when major seismic events compromise infrastructure (Prasanna et al., 2022).

Recent technological advances have led to the enhancement of low-cost, MEMS-based sensors with in-built processing capabilities. These advancements enable data processing directly at the sensor nodes, allowing a transition from centralised to decentralised processing (Chandrakumar, Prasanna, Stephens, & Tan, 2022). Decentralised processing empowers the system to analyse seismic information and issue alerts where the data is collected, utilising the built-in computational power of the sensors. Aside from the decentralised approaches taken by Prasanna et al. (2022), Fleming et al. (2009) and Bassetti and Panizzi (2022), there is minimal documentation of decentralised processing for EEW.

The shift toward decentralised processing is motivated by multiple benefits. It reduces the time to issue alerts by removing the necessity for data to travel to a central server, allowing the system to provide a longer warning window for the end users. It also strengthens the resilience of the EEWS against central system failures caused by earthquakes. Furthermore, processing at the decentralised approach can decrease the operational costs associated with the upkeep of sophisticated central processing systems (Fischer et al., 2012; Prasanna et al., 2022).

5.3.2 The PLUM Algorithm.

Over the past three decades, significant advancements have been made in EEWSs (D. Y. Chen, Hsiao, et al., 2015; Clinton et al., 2016). These advancements have primarily focused on network-based[9] approaches, utilising source-based[10] models to estimate earthquake parameters like hypocentre locations and magnitudes (Kuyuk et al., 2014; Satriano et al., 2011). Traditional EEW systems analyse seismic data, including P-wave onsets and maximum displacement amplitudes (Meier et al., 2015; Noda et al., 2016). However, the accuracy of these predictions heavily depends on the precision of the estimated parameters, which poses challenges, particularly during complex seismic events like large magnitude earthquakes and simultaneous aftershocks (Hoshiba, 2013; Hoshiba et al., 2011).

Recognising these limitations, (Kodera et al., 2018) introduced an alternative approach known as the PLUM method. Based on Hoshiba (2013) work, this method offers a more direct ground motion estimation approach, emphasising cost-effectiveness and ease of implementation.

The PLUM algorithm predicts seismic intensities at designated prediction points, distributed across various areas based on seismic risk. For each area, the predicted seismic intensity is computed as the highest forecasted value among all its observation points. This computation involves selecting the maximum observed real-time seismic intensity within a radius R from each prediction point, incorporating site effect corrections with a continuous one-second update interval (Kodera et al., 2018).

Real-time ground motion data processing in PLUM is centralised; observation stations transmit their data to a central unit, which issues intensity predictions to the target sites. This system has pre-programmed prediction points and corresponding observation stations for streamlined processing

[9] A network-based approach in EEWS involves deploying a network of sensors across various locations within a geographical area. Earthquake detection is achieved by collectively processing the data gathered from this interconnected sensor network.

[10] Source-based EEWS models are designed to detect earthquakes and alert stakeholders, providing detailed information about the seismic event.

(Kodera et al., 2018). This method assumes that ground motion, responsible for significant seismic intensity, travels within the specified radius without notable attenuation. Figure 5-2 illustrates the PLUM algorithm's operation, demonstrating the intensity prediction at a prediction point using intensity data from surrounding observation stations.

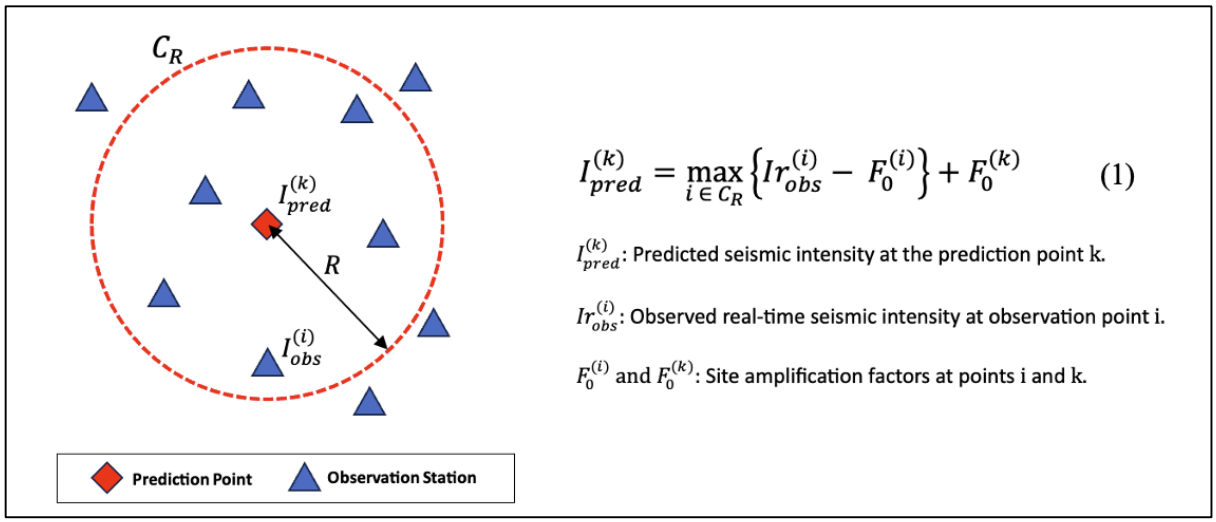

Figure 5-2. Overview of the PLUM: The illustration of the PLUM algorithm's operation demonstrating intensity prediction equation (1) for a prediction point based on observations from peripheral stations (Adapted from Kodera, 2018).

A key component in the operation of the PLUM method is monitoring the observed intensity at each observation station. The PLUM method triggers an EEW alert when the real-time ground motion predictions from two or more monitoring stations exceed a specified threshold. This alert is generated explicitly for the region surrounding the target station, ensuring timely warning dissemination.

The PLUM method's distinct advantage lies in its ability to continuously monitor ground motion distribution in real-time, addressing the overprediction issues and false alerts prevalent in traditional ground-motion-based systems. This was particularly evident following the Mw 9.0 Tohoku earthquake, where PLUM issued more reliable early warnings (Hoshiba, 2021). Further validation with the 2016 Kumamoto earthquake data reinforced PLUM's superiority, consistently providing earlier warnings and effectively reducing blind zones (Kodera et al., 2016).

Moreover, the PLUM method has shown resilience in handling multiple simultaneous earthquakes and predicting strong motion by monitoring real-time seismic intensities. This capability sidesteps technical issues associated with source-based models and suggests a potential for further improvements with denser seismic networks, including low-cost sensors (Kodera et al., 2016).

Despite its advantages, the PLUM method has limitations. Its effectiveness is contingent upon a dense observational network, as it is limited by the short prediction radius and site amplification factors that significantly influence seismic ground motion (Kodera et al., 2016). Additionally, the PLUM algorithm

tends to provide shorter warning durations than source-based methods. While it excels in predicting ground motion in complex seismic scenarios, the maximum warning time it offers is limited by the radius of observation.

5.4 Implementation of the EEWS

This section highlights the study's implementation of an EEWS with decentralised processing for the PLUM algorithm.

5.4.1 Implementation of the Network

The initial phase of seismic sensor installation was carried out in 2020 and 2021, utilising MEMS-based RS4D sensors for their affordability, accuracy, and processing power, aligning with the objectives of a community-engaged EEWS (Prasanna et al., 2022). Community participants were recruited to host these ground motion sensors within their households. A workshop was conducted to gain insights into user perspectives and to develop strategies for distributing sensors to the general public, promoting a citizen seismology approach (Tan et al., 2021).

Following that, the network expansion in 2023 aimed to increase sensor density, leveraging social media campaigns to gather community interest in hosting additional RS4D sensors. The campaign resulted in 80 expressions of interest, informing the strategic selection of sensor locations through geographical data analysis. By mapping the geographical spread of these responses, 25 locations were identified from the pool to install additional sensors. This expansion strategy aligns with insights from a recent study, which explores the necessity of a comprehensive approach to developing a community-engaged EEWS for NZ, addressing the technological, societal, and cultural challenges (Tan et al., 2023). The criteria for site selection encompassed algorithm coverage, seismic activity, and population density. This careful selection has contributed to a network comprising approximately 60 ground motion sensors across NZ, with a significant concentration of around 45 sensors within the Greater Wellington area.

5.4.2 Reason for Choosing PLUM for Decentralised Processing

In developing the decentralised architecture for EEWS, the crucial task was to select an algorithm that conforms to the computational limits of the RS4D sensor nodes. These nodes are limited by their processing capabilities, necessitating an EEW algorithm that is both lightweight and effective. Through benchmarking existing EEW algorithms, the PLUM algorithm stood out as the optimal solution with its robustness, lightweight design, and ease of implementation (Prasanna et al., 2022). Its successful

deployment in Japan's EEWS and validation across various global contexts affirm its appropriateness (Kodera et al., 2018). With its proven effectiveness with EEWSs worldwide, the PLUM algorithm was chosen for decentralised operation for this study.

5.4.3 Adaptation of PLUM to NZ-PLUM

In adapting the PLUM algorithm to the NZ context, the NZ-PLUM algorithm maintains the core principles of its predecessor but incorporates modifications appropriate to NZ. Kodera et al.'s (2018) PLUM algorithm aligns with the Japan Meteorological Agency's (JMA) instrumental seismic intensity (I_{inst}). It defines real-time pseudo-seismic intensity using an I_r parameter calculated from three-dimensional acceleration data. However, the JMA Scale differs from the Modified Mercalli Intensity[11] (MMI) scales used in NZ and the United States (Cochran et al., 2019; Dowrick et al., 2008).

In NZ, the relationship between MMI and Peak Ground Motion is defined using two sets of Ground Motion Intensity Conversion Equations (GMICEs): one based on Peak Ground Acceleration (PGA) and the other on Peak Ground Velocity (PGV) of the horizontal ground motion data (Moratalla et al., 2020). The NZ-PLUM algorithm has been specifically designed to utilise PGA using the conversion equation from Moratalla et al. (2020) (See Equation 2). This enables the NZ-PLUM algorithm to map PGA values to the NZ MMI scale, ensuring that intensity predictions are consistent with NZ seismic intensity measurement practices.

$$\log(PGA) = \begin{cases} \dfrac{(MMI - 1.7601)}{1.992} & if\ MMI < 5.5277 \\ \dfrac{MMI + 1.9095}{3.9322} & if\ MMI \geq 5.5277 \end{cases} \qquad (2)$$

For the experimental network, our goal is to issue alerts for shaking that would be felt by people. Therefore, we have set an MMI threshold of five (MMI 5.0) for triggering EEWs for the experimental system. The MMI 5.0 level typically corresponds to shaking that is felt outdoors, awakens most sleepers, and may cause some alarm indoors (Dowrick et al., 2008). Based on this MMI 5.0 threshold and the corresponding GMICE (Equation 2), the equivalent PGA threshold (T_H) for NZ-PLUM in this study is 42.3 cms^{-2}. However, establishing an ideal alert activation threshold requires carefully evaluating societal impacts and technical capabilities. Determining such a threshold is part of a broader, ongoing

[11] The Modified Mercalli Intensity scale is a qualitative tool used to describe the intensity and effects of an earthquake on the Earth's surface, structures, and inhabitants. It ranges from I (imperceptible) to XII (destruction), describing the impact on structures, the environment, and human perception and response.

conversation to formulate a comprehensive set of guidelines specific to NZ's unique needs and circumstances.

Another modification for the NZ-PLUM involves extending the real-time intensity calculation window from the typical one second—used in Kodera et al.'s (2018) approach and other EEW implementations—to three seconds. This extension improves the estimation of MMI intensity by reducing the impact of high ambient noise in the community-hosted network. The extended three-second window slides every 250 milliseconds, which has minimal effects on system latency. It also aligns with the output frequency of the RS4D sensors, which provide real-time ground motion acceleration data in 25-sample segments every 250 milliseconds.

5.4.4 Adaptation of NZ-PLUM for Decentralised Architecture

The adaptation to decentralised processing necessitates a fundamental reconfiguration. In this architecture, each sensor node assumes the role of processing, effectively rejecting the need for a centralised processing unit. This shift ensures that the NZ-PLUM algorithm's calculations are conducted within the individual sensor nodes, thus fully embracing the decentralised nature.

5.4.4.1 Defining Prediction Points for Decentralised Architecture

The next objective focused on enabling the functionality of the PLUM algorithm at the node level. Defining prediction points is a foundational step in the methodology for adapting the NZ-PLUM algorithm to decentralised architecture. The current implemented EEW network is depicted in Figure 5-3. In the original implementation of the PLUM algorithm, authorities selected prediction points based on regional seismic activity to disseminate alerts to those areas (Kodera et al., 2018). These regions had various prediction points, reflecting the seismic activities observed.

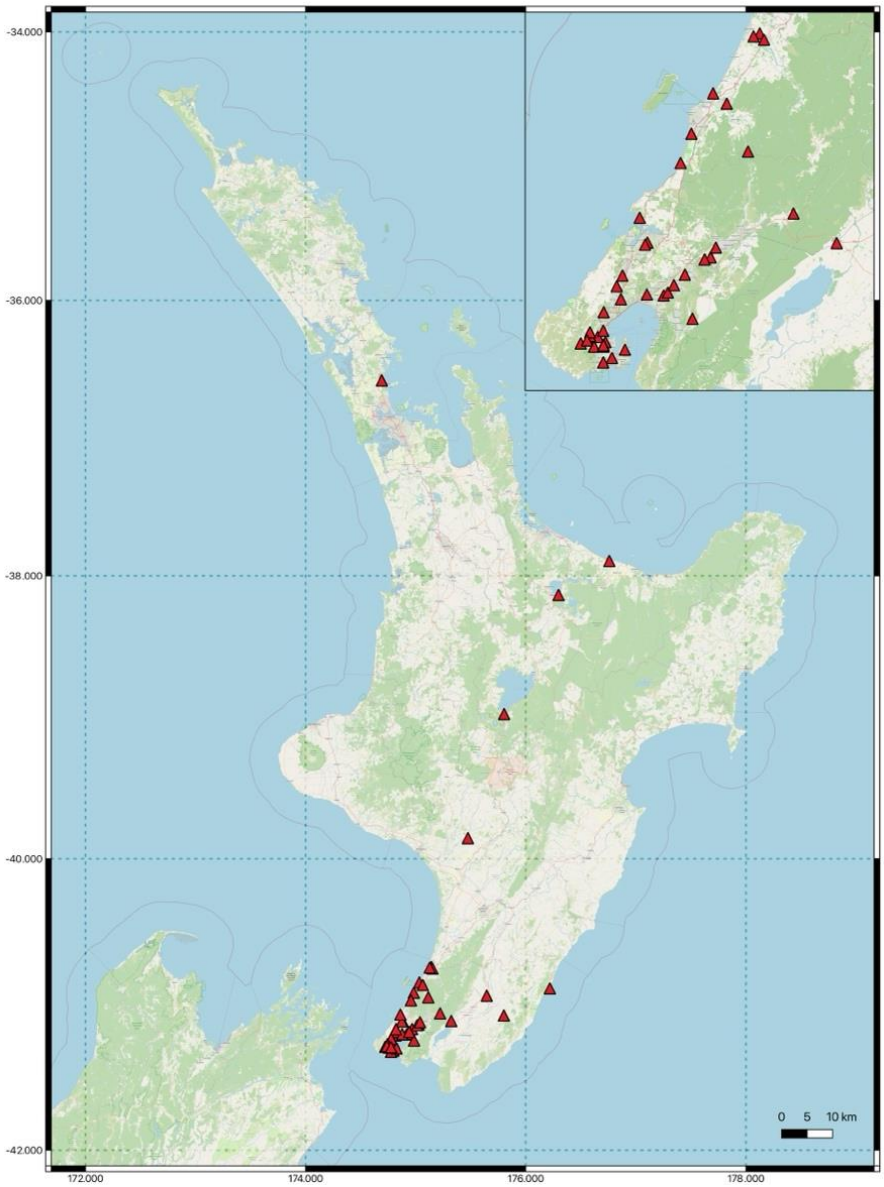

Figure 5-3. Overview of the EEW network, with red triangles indicating the RS4D stations deployed in North Island, NZ. The inset highlights the stations installed in the Greater Wellington region.

In this study, prediction points are designated as the RS4D sensors themselves which differs from Kodera et al.'s (2018) PLUM approach. Figure 5-4 presents four different prediction points as an example; each sensor marked in red represents a prediction point with a 30 km prediction radius (R) consistent with the PLUM. Sensors within this radius serve as observation stations around the prediction point and are responsible for predicting the seismic intensity at the prediction point. Currently, our focus is not on issuing EEW alerts for broader regions but on generating alerts specifically for the prediction point - the RS4D sensor. This strategy is rooted in the concept of a community-engaged EEW network, ensuring that each sensor host receives EEW alerts directly through their installed RS4D sensor. However, it is essential to note that, in future, the network has the potential to be augmented with

additional passive nodes. These nodes would also function as prediction points but receive alerts without estimating the intensity, enhancing the system's reach and effectiveness.

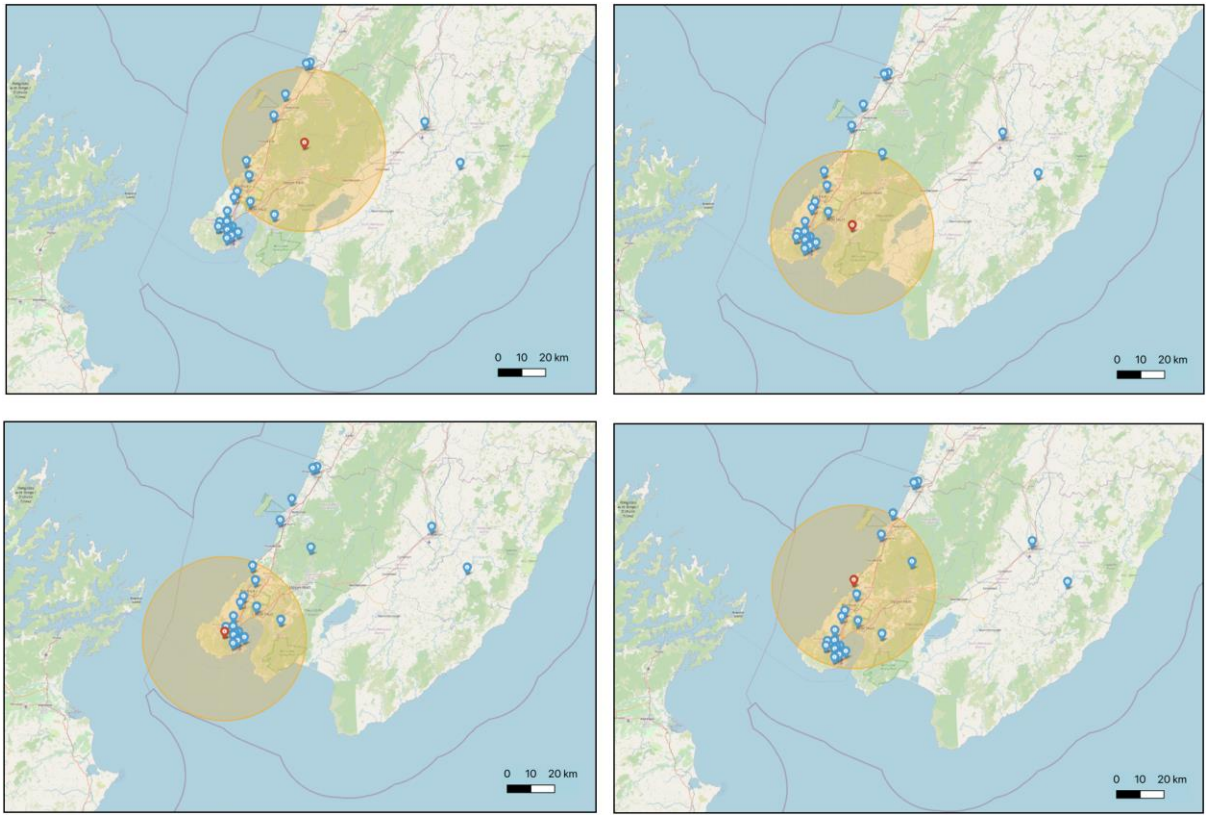

Figure 5-4. Illustration of four Prediction points with 30 km Prediction radii, highlighting sensors in red as designated Prediction points.

5.4.4.2 Implementing Decentralised Processing in the EEWS

Upon designating prediction points within the EEWS, the decentralised processing implementation of the NZ-PLUM algorithm was initiated, establishing a dual-tiered structure of RS4D sensors: Primary and Secondary. Each prediction point, with a 30 km radius, is approached as a distinct scenario where one RS4D sensor is appointed as the Primary sensor, entrusted with two key functionalities: **intensity prediction** and **alert generation** for its specific prediction site. Concurrently, the surrounding sensors, classified as Secondary sensors within the same radius, are tasked with transmitting real-time intensity data to the Primary sensor for analysis. A single sensor, therefore, may function as a Primary sensor for one prediction point and as a Secondary sensor for another; particularly in areas where prediction radii overlap. The selection of a Primary sensor is strategically based on its processing load, favouring sensors with minimal existing commitments to other prediction points. Figure 5-5 illustrates how decentralised processing utilises the NZ-PLUM algorithm, showcasing a prediction radius (Orange circle) scenario and the prediction point (Red icon), Primary (Purple icon) and Secondary stations (Blue icons).

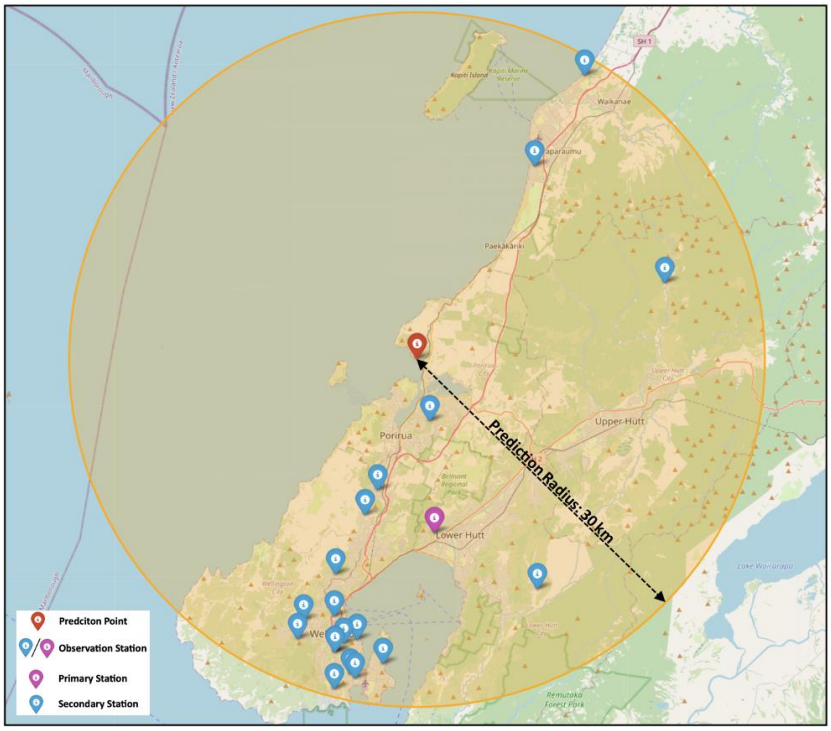

Figure 5-5. An Illustration of the NZ-PLUM algorithm adapted for decentralised processing, featuring a Prediction point, Primary station, and Secondary stations within a specified Prediction radius.

To address the potential failure of a Primary sensor, the system allocates at least three sensors to the Primary sensor role - one serves as the active Primary sensor, while the other two are on standby as backups. These backups also function as Secondary sensors, springing into action as the Primary sensor should the main one fail. This redundancy is crucial for maintaining continuous and uninterrupted seismic intensity predictions at each prediction point.

In contrast to the PLUM, which requires that all observation stations within the prediction radius update their real-time intensity to a centralised processing unit each second, the NZ-PLUM approach modifies the interaction between Secondary and Primary sensors. In the NZ-PLUM, Secondary sensors forward intensity updates (PGA) to the Primary sensor only when the observed intensity exceeds an internal threshold. This internal threshold helps maintain optimal performance of the Primary sensor by minimising the influx of data packets during PLUM operation.

The Primary sensor undertakes the task of predicting the intensity at the prediction point solely under two conditions: if its internal threshold is exceeded or if it receives an intensity update from any Secondary sensor within the prediction radius that has surpassed the internal threshold. The specifics of determining the internal threshold are detailed in a separate subsection.

Figures 5-6 illustrates the overall working flow of Primary sensor in terms of predicting the intensity to a given prediction point according to NZ-PLUM approach adapted for decentralised processing. The comprehensive operation of the Primary sensor's alert generation is detailed in the next section.

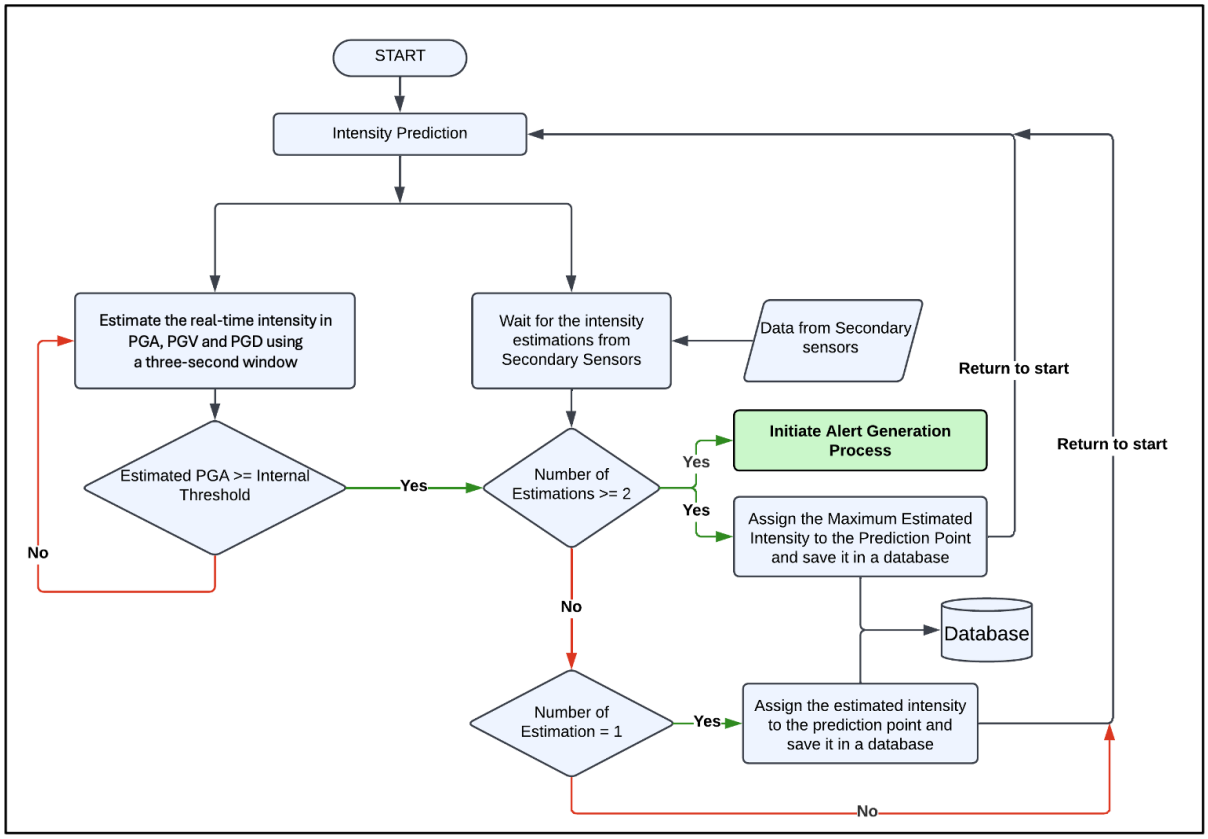

Figure 5-6. Flow chart explains the intensity prediction flow of the Primary sensor for the assigned prediction point.

5.4.4.3 Defining the Internal Threshold for Secondary-Primary Communication

The formulation of the internal threshold began with establishing a specific MMI range that effectively signals the necessity for an update without indicating considerable ground shaking.

The selection of an appropriate MMI range was based on the descriptions provided by Dowrick et al. (2008). This choice ensures that the system's criteria for triggering intensity updates are well-tuned to the regional seismic activity profiles, thereby maintaining the system's accuracy and relevance. After careful consideration, MMI 3.0 was selected as the internal threshold. MMI 3.0 is characterised by indoor light vibrations, where hanging objects might sway slightly. This level of intensity serves as a pragmatic threshold, allowing Secondary sensors to initiate communication with the Primary sensor early in the event of significant seismic activity or at the onset of a large earthquake, thereby optimising the timing of alert dissemination.

Following the selection of MMI 3.0 as the internal threshold, the challenge was addressed by translating this MMI value into measurable parameters for the sensors, specifically PGA, PGV, and PGD. Given that the sensors estimate intensity through these physical measures within a three-second sliding window updated every 250 milliseconds, it was crucial to determine an equivalent PGA value corresponding to MMI 3.0. To accomplish this, GMICEs (equation 2), as outlined by Moratalla et al. (2020), were utilised. Figure 5-7 visually illustrates the correlation between MMI levels and PGA values, as defined by the GMICEs. In the figure, the MMI threshold of 3.0 or above is marked with a green vertical line, setting a clear benchmark for triggering communication from Secondary to Primary sensors based on real-time seismic data.

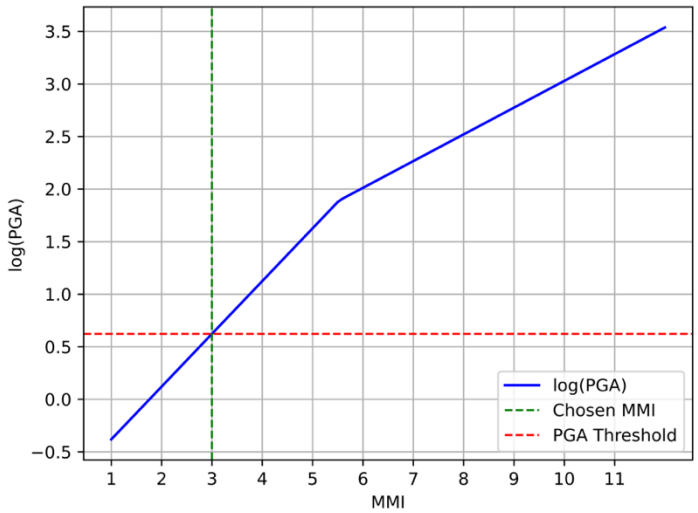

Figure 5-7. Correlation between MMI levels and PGA values in cms^{-2} as defined by GMICEs, featuring a green vertical line to indicate the MMI threshold of 3.0 and a horizontal red dotted line representing the log(PGA) threshold in cms^{-2} for transferring intensity estimations from Secondary to Primary sensor

Subsequently, the log(PGA) threshold was identified by analysing the intersection point depicted in Figure 5-7. The chosen log(PGA) value, serving as the internal threshold for Secondary sensors, was identified as 0.62, as represented by a red dashed horizontal line within the figure. After converting the logarithmic value to its original scale, the PGA internal threshold was determined to be approximately 4 cms^{-2}.

5.4.4.4 Alert Generation

Upon receiving the intensity estimation from a Secondary sensor, the Primary sensor predicts the intensity at the prediction points by taking the maximum observed intensity, including its own estimation. If a station's observed intensity exceeds the alerting threshold (T_H,), the system opens a 5-second time window to await confirmation for another threshold exceedance from any Secondary sensor within a 30-km radius. If the predicted intensity at the prediction point is greater than MMI 5.0 (PGA >

42.3 cms^{-2}) from two or more observational stations, then the Primary station generates an alert to the prediction point; otherwise, the event is dismissed.

In contrast to similar studies using PLUM (Cochran et al., 2019; Kilb et al., 2021; Saunders et al., 2022), which employ two levels of thresholds for the first and second stations to maximise warning time and reduce system latency, our study employs the same threshold value (T_H) for both stations' predicted intensity. This approach adheres to the Kodera et al.'s (2018) PLUM method.

5.5 Discussion

Table 5-1. summarises the key differences between the PLUM methodology and this research's NZ-PLUM decentralised approach. This proposed approach has optimised the processing capability of RS4D sensors for real-time seismic intensity prediction and alert dissemination. Transitioning to a decentralised architecture enhances the resilience of the EEWS by minimising the risks associated with a single point of failure, a potential issue in centralised systems.

Table 5-1. Comparative overview of traditional plum approach versus decentralised plum adaptation proposed in this study.

Characteristics	Traditional PLUM implementation	Experimental decentralised PLUM adaptation
Processing Approach	Centralised processing	Decentralised processing with a two-tiered Primary-Secondary structure
Prediction Point Determination	Selected based on areas of interest reflecting observed seismic activities	Sensors themselves are used as prediction points
Data Handling Method	All observations within a prediction radius are sent to a centralised unit in real time.	Secondary sensors process data independently, sending updates to a Primary sensor only if internal threshold is surpassed.
Intensity Predicting Method	Observations are collected and processed at a central location to predict the intensity at prediction points.	The Primary sensor is responsible for predicting the intensity when its threshold is exceeded or upon receiving data from Secondary sensors.
Alert Generation	Centralised system issues alert to the region.	The Primary sensor issues an alert for its prediction point.

Adapting and modifying the PLUM algorithm (NZ-PLUM) for NZ's seismic context is significant. Firstly, the adaptation to the NZ MMI scale, using GMICEs, enables the accurate prediction of ground shaking intensities tailored to local geological conditions. This localisation ensures that the system provides relevant and actionable alerts to residents and authorities in NZ, where the seismic environment and infrastructure differ from those in other regions where PLUM has been previously implemented (Cochran et al., 2019; Kodera, 2018).

Adapting the PLUM algorithm for decentralised application showcases the system's adaptability and the algorithm's suitability for environments with limited resources, particularly with the constraints of RS4D sensors. Identifying sensors as prediction points facilitates a community-centric warning system, ensuring swift alert delivery directly where needed. The classification of sensors into Primary and Secondary roles optimises task distribution, streamlining the network's operation.

A key focus for this proposed architecture was to minimise network traffic coming from the frequent intensity updates from Secondary sensors. Implementing an internal threshold curtails unnecessary data transfers, minimising the processing burden on Primary sensors.

The MMI scale was utilised for alert generation, with MMI 5.0 selected as an illustrative threshold to demonstrate the alerting process. However, establishing a definitive threshold needs further research for both societal impacts and technical capabilities, underscoring the need for a comprehensive discussion on this topic.

5.5.1 Future Work

In the next phase of our research, we will concentrate on a sequence of strategic undertakings designed to strengthen the capabilities of an operational decentralised processing EEWS:

1. **Pilot Implementation and Performance Assessment:** The proposed concept will be piloted by integrating it into several RS4D sensors. We will focus on investigating the PLUM algorithm's performance at the node level, with particular attention to the accuracy of intensity estimations. Data collected from these sensors will be stored in a dedicated database for subsequent analysis to evaluate the system's performance metrics thoroughly.
2. **Integrating P-wave Detection Into NZ-PLUM** – The NZ-PLUM approach primarily relies on detecting thresholds for horizontal shaking based on GMICEs, focusing on S-waves. However, this reliance on S-wave detection inherently limits the warning times that can be achieved. To address this limitation, integrating a P-wave detection algorithm into the NZ-PLUM approach presents a promising solution, as suggested by Kodera (2018) and Kodera et al. (2018).

3. **Network-Wide Implementation:** Upon completing the initial tests and refinements, the algorithm will be rolled out across the entirety of the operational network (45 sensors in the Wellington Region). This crucial step will mark the transition from a controlled testing environment to a real-world application, setting the stage for comprehensive system evaluation.
4. **Alert Generation and Threshold Calibration:** Research efforts will be directed toward fine-tuning the parameters that trigger alert generation. This task will entail a deep dive into alerts' societal impact and the technical nuances associated with threshold calibration, tailored to NZ's unique seismic profile.
5. **Communication Technology Exploration:** Pursuing alternative communication methodologies, such as Long Range (LoRa) wireless technologies, is essential, particularly as an alternative strategy to ensure network operability during traditional communication infrastructure failures.

The conceptual framework detailed in this work-in-progress paper will undergo operational testing, refinement, and expansion. Future results from the experimental network are planned for journal publication to validate the system's effectiveness and provide guidance for similar deployments in seismically active areas.

5.6 Conclusion

This work represents a notable contribution to EEWSs by adapting the PLUM algorithm for NZ seismic context and decentralised processing. The system's design, emphasising redundancy, cost-efficiency, and reduced latency, addresses the critical need for resilient seismic warning capabilities. Furthermore, the decentralised approach emerges as a viable solution following major earthquakes, where standard communication networks may fail. Future research will focus on integrating a P-wave detection algorithm to further enhance the warning time, calibrating thresholds specific to New Zealand's seismic environment, and exploring alternative communication technologies like LoRa to maintain system functionality during network disruptions. Overall, this study marks a significant step in developing a community-engaged, decentralised EEWS in New Zealand through integrating the NZ-PLUM algorithm.

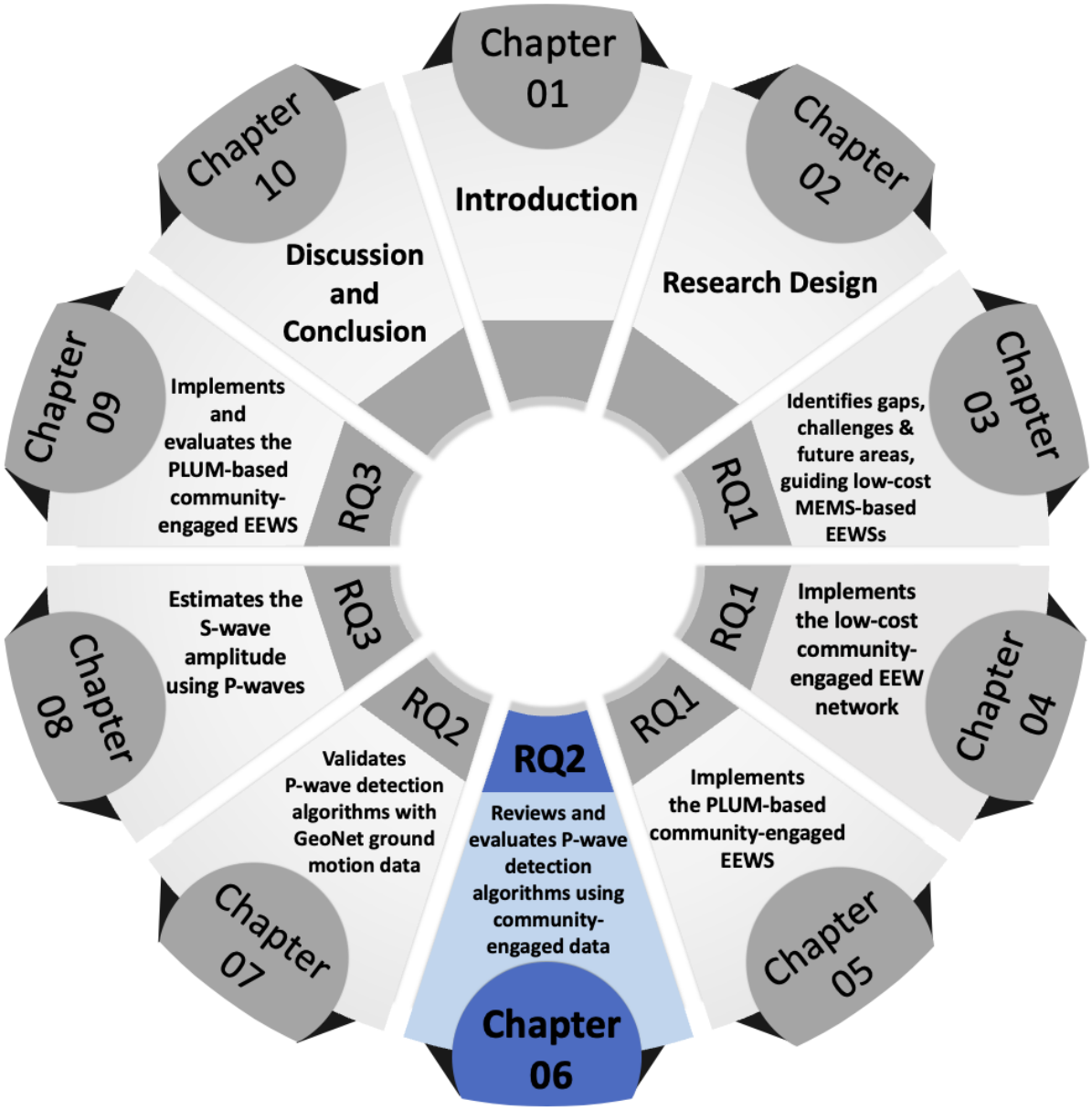
Chapter 01
Introduction
Chapter 02
Research Design
Chapter 03
Identifies gaps, challenges & future areas, guiding low-cost MEMS-based EEWs
RQ1
Chapter 04
Implements the low-cost community-engaged EEW network
RQ1
Chapter 05
Implements the PLUM-based community-engaged EEWS
RQ1
RQ2
Chapter 06
Reviews and evaluates P-wave detection algorithms using community-engaged data
Chapter 07
Validates P-wave detection algorithms with GeoNet ground motion data
RQ2
Chapter 08
Estimates the S-wave amplitude using P-waves
RQ3
Chapter 09
Implements and evaluates the PLUM-based community-engaged EEWS
RQ3
Chapter 10
Discussion and Conclusion

MASSEY UNIVERSITY
TE KUNENGA KI PŪREHUROA
UNIVERSITY OF NEW ZEALAND

GRADUATE RESEARCH SCHOOL

STATEMENT OF CONTRIBUTION
DOCTORATE WITH PUBLICATIONS/MANUSCRIPTS

We, the candidate and the candidate's Primary Supervisor, certify that all co-authors have consented to their work being included in the thesis and they have accepted the candidate's contribution as indicated below in the *Statement of Originality*.

Name of candidate:	CHANTHUJAN CHANDRAKUMAR
Name/title of Primary Supervisor:	Aprof. Raj Prasanna
In which chapter is the manuscript /published work:	6

Please select one of the following three options:

(●) The manuscript/published work is published or in press

- Please provide the full reference of the Research Output:

Chandrakumar C, Prasanna R, Stephens M, Tan ML, Holden C, Punchihewa A, Becker JS, Jeong S, Ravishan D. 2022. Literature review on earthquake early warning algorithms for detecting P-waves and earthquake magnitude estimation: Initial literature review findings. In: Thomas H, Vincent L, editors. Building disaster resilience. ISCRAM Asia Pacific Conference. Melbourne: ISCRAM ASIA

( ) The manuscript is currently under review for publication – please indicate:

- The name of the journal:

Information Systems in Crisis Response and Management (ISCRAM) Asia Pacific Conference 2022

- The percentage of the manuscript/published work that was contributed by the candidate: 80.00

- Describe the contribution that the candidate has made to the manuscript/published work:

Chanthujan Chandrakumar conceptualised the article, co-constructed the methodology, and conducted the formal analysis and investigation. He also wrote the first draft of the manuscript.

( ) It is intended that the manuscript will be published, but it has not yet been submitted to a journal

Candidate's Signature:	Chandrakumar Chanthujan — Digitally signed by Chandrakumar Chanthujan Date: 2024.08.14 13:41:38 +12'00'
Date:	14-Aug-2024
Primary Supervisor's Signature:	Raj Prasanna — Digitally signed by Raj Prasanna Date: 2024.08.21 11:12:16 +12'00'
Date:	21-Aug-2024

This form should appear at the end of each thesis chapter/section/appendix submitted as a manuscript/ publication or collected as an appendix at the end of the thesis.

MASSEY UNIVERSITY
TE KUNENGA KI PŪREHUROA
UNIVERSITY OF NEW ZEALAND

GRADUATE RESEARCH SCHOOL

STATEMENT OF CONTRIBUTION
DOCTORATE WITH PUBLICATIONS/MANUSCRIPTS

We, the candidate and the candidate's Primary Supervisor, certify that all co-authors have consented to their work being included in the thesis and they have accepted the candidate's contribution as indicated below in the *Statement of Originality*.

Name of candidate:	CHANTHUJAN CHANDRAKUMAR
Name/title of Primary Supervisor:	Aprof. Raj Prasanna
In which chapter is the manuscript /published work:	6

Please select one of the following three options:

(●) The manuscript/published work is published or in press

- Please provide the full reference of the Research Output:

Chandrakumar C, Tan ML, Holden C, Stephens MT, Prasanna R. 2023. Performance analysis of P-wave detection algorithms for a community-engaged earthquake early warning system—a case study of the 2022 M5.8 Cook Strait earthquake. New Zealand Journal of Geology and Geophysics. https://doi.org/10.1080/00288306.2023.2284276

( ) The manuscript is currently under review for publication – please indicate:

- The name of the journal:

New Zealand Journal of Geology and Geophysics

- The percentage of the manuscript/published work that was contributed by the candidate: 80.00

- Describe the contribution that the candidate has made to the manuscript/published work:

Chanthujan Chandrakumar conceptualised the article, co-constructed the methodology, and conducted the formal analysis and investigation. He also wrote the first draft of the manuscript.

( ) It is intended that the manuscript will be published, but it has not yet been submitted to a journal

Candidate's Signature:	Chandrakumar Chanthujan Digitally signed by Chandrakumar Chanthujan Date: 2024.08.14 13:42:56 +12'00'
Date:	14-Aug-2024
Primary Supervisor's Signature:	Raj Prasanna Digitally signed by Raj Prasanna Date: 2024.08.21 11:12:45 +12'00'
Date:	21-Aug-2024

This form should appear at the end of each thesis chapter/section/appendix submitted as a manuscript/ publication or collected as an appendix at the end of the thesis.

6 Review and Evaluation of P-Wave Detection Algorithms with Community-Engaged Data

This chapter presents the third and fourth manuscripts for publication from this study. The first manuscript is a Work in Progress paper (WiPe) titled "Algorithms for Detecting P-waves and Earthquake Magnitude Estimation: Initial Literature Review Findings." The version presented here has been revised from its published form, with updates made to the introduction and future work sections to ensure a smoother transition between the preceding and subsequent chapters of the thesis. Additionally, revisions have been made to eliminate redundancies that were previously addressed in earlier chapters. This systematic literature review examines P-wave detection and earthquake magnitude estimation algorithms employed in various EEWS. It focused on literature published between 2000 and 17 May 2022 and was conducted to fulfil Objective 2.1 of this thesis: to review the literature on P-wave detection algorithms implemented globally.

The WiPe was published in 2022 in the Proceedings of the Information Systems for Crisis Response and Management (ISCRAM) Asia Pacific Conference in Melbourne:

Chandrakumar C, Prasanna R, Stephens M, Tan ML, Holden C, Punchihewa A, Becker JS, Jeong S, Ravishan D. 2022. Literature review on earthquake early warning algorithms for detecting P-waves and earthquake magnitude estimation: Initial literature review findings. In: Thomas H, Vincent L, editors. Building disaster resilience, ISCRAM Asia Pacific Conference. Melbourne: ISCRAM ASIA PACIFIC; p. 138–155.

The second manuscript is a journal article titled "Performance Analysis of P-Wave Detection Algorithms for a Community-Engaged Earthquake Early Warning System – A Case Study of the 2022 M5.8 Cook Strait Earthquake." This study investigates the performance of four P-wave detection algorithms chosen from WiPe's literature review. It focuses mainly on their false detection rates and missed detections, using the ground motion data captured from the community-engaged EEW network during a single earthquake event, fulfilling Objective 2.2 of this thesis

The journal article was published in 2023 in the New Zealand Journal of Geology and Geophysics:

Chandrakumar C, Tan ML, Holden C, Stephens MT, Prasanna R. 2023. Performance analysis of P-wave detection algorithms for a community-engaged earthquake early warning system—a case study of the 2022 M5.8 Cook Strait earthquake. New Zealand Journal of Geology and Geophysics. https://doi.org/10.1080/00288306.2023.2284276

6.1 Algorithms for Detecting P-waves and Earthquake Magnitude Estimation: Initial Literature Review Findings

6.1.1 Abstract

Earthquake Early Warning System (EEWS) is crucial in alerting the public and authorities to take appropriate safety measures during an earthquake. Generally, EEWSs use three types of algorithms to generate alerts during an earthquake: source-based, ground motion or wavefield-based, and on-site-based approaches. However, source-based algorithms are commonly used in most EEWSs worldwide. A source-based EEWS uses a particular time frame of the P-wave of an earthquake to estimate the source parameters, such as magnitude and the location of that earthquake, with the support of P-wave detection and earthquake magnitude and location estimation algorithms. As the initial step of a research project to explore the best use of P-waves to generate earthquake alerts, this Work in Progress paper (WiPe) presents the initial findings from an ongoing literature review on exploring the algorithms used for P-wave detection and earthquake magnitude estimation.

6.1.2 Introduction

Earthquake Early Warning (EEW) algorithms adopted by the various systems globally can be categorised into three main types: source-based, ground motion or wavefield-based and on-site-based algorithms (R. M. Allen & Melgar, 2019). Each of these has its strengths and weaknesses. To overcome the weaknesses and utilise the strengths of these different types of systems, researchers have explored developing hybrid systems – systems that use more than one type of algorithm for generating EEW (Kodera, 2018; Peng et al., 2020).

An ongoing work In New Zealand, a research project led by the Crisis Response and Integrated Simulation Science Laboratory (CRISiSLab) of the Joint Centre for Disaster Research (JCDR), Massey University, is currently studying innovative approaches to Earthquake Early Warning System (EEWS) including using low-cost sensors and decentralised approach. They have implemented a novel EEW network architecture using the PLUM (Propagation of Local Undamped Motion) based algorithm at the sensor nodes to detect earthquakes (Prasanna et al., 2022). However, the PLUM algorithm has limitations, as the algorithm is mostly limited to a 30-kilometre radius which only can give a 10-second warning time upon S-wave detection during an earthquake (Prasanna et al., 2022). Having a 10-second warning time can be beneficial to the areas near the epicentre but providing 10 seconds of warning time for the areas far from the epicentre is not sufficient since a longer warning window can be provided to those areas at the moment of detecting an earthquake (Kodera et al., 2018).

A P-wave-based PLUM approach is proposed for the community-engaged EEWS implemented by the CRISiSLab team to address the key limitation of the original PLUM algorithm, which relies on S-waves for earthquake detection, thereby limiting warning times (Kodera et al., 2018). By integrating a P-wave detection algorithm into the PLUM approach, warning times can be increased. However, this integration requires constructing an empirical relationship between the amplitudes of P-waves and S-waves, which serves as a critical link between the P-wave detection algorithm and the PLUM algorithm. While the literature lacks extensive discussions on building such relationships specifically for the PLUM algorithm, many studies have established similar relationships for estimating earthquake magnitudes in other EEWS contexts.

A literature search on EEWSs reveals various approaches for detecting P-waves and establishing relationships between P and S-wave amplitudes to estimate earthquake magnitudes. Although numerous algorithms exist for P-wave detection and magnitude estimation, limited literature systematically reviews these approaches. To address this gap, this Work in Progress paper (WiPe) presents the initial findings of a review of current and past literature on P-wave detection algorithms and methods for estimating earthquake magnitude. These findings aim to assist researchers in developing or choosing more effective and robust algorithms for their EEWS.

The paper is structured as follows: Section 6.1.3 provides a background on EEWSs. Section 6.1.4 details the methodology used for conducting the proposed literature review. This is followed by Section 6.1.5, which presents the initial findings of the literature review. Finally, Section 6.1.6 concludes the paper by outlining the next steps of the research.

6.1.3 Background

Throughout history, disasters have created devastating consequences to people and infrastructures (Coppola, 2007). Earthquake is one that poses a serious threat to areas near major active faults on land or offshore subduction zones (Adhikari et al., 2018). Compared to other hazards such as cyclones and tsunamis, earthquakes cannot be predicted hours in advance where they can only be detected in the event of an earthquake: earthquake detection and warnings happen within seconds. This makes building an EEWS challenging due to the short period between the detection of an earthquake event and its forthcoming destructive impact (Fischer et al., 2012). Two facts enable the operation of EEWSs (i) the information travelling over communication networks moves faster than seismic waves - P-waves

(primary or pressure waves) and S-waves[12] (secondary or shear waves), and (ii) the most damage during an earthquake occur with S-waves which arrive later than P-waves (Fischer et al., 2012). To generate alerts, EEWSs use a network of sensors distributed in a geographical area to detect earthquakes and transmit alerts in real-time. Generally, the early warning window can be a few seconds to tens of seconds depending on the specific geometry of the earthquake and the stations used in EEWS (Y. M. Wu & Zhao, 2006).

During the last three decades, many high-end EEWSs have evolved and being operated in several countries or regions worldwide including Japan, Taiwan, Mexico, South Korea, China and USA (Y. Wang et al., 2020). Even though these systems have improved significantly, become more robust, and have shown better results in detecting earthquakes, exorbitant costs associated with building modern-day high-end EEWS can make it impractical and less affordable not only for developing countries but even for developed countries (Prasanna et al., 2022). For example, the ShakeAlert EEWS in the USA is currently implemented only in three states namely California, Oregon, and Washington and the implementation costs approximately 100 million USD (Brooks et al., 2021). The high financial costs associated with current EEWSs and the latest technical advances in sensor technology have steered researchers to investigate low-cost EEWSs to detect earthquakes (Lin et al., 2012). There have been several studies conducted in developing EEWSs using low-cost Micro-electromechanical systems (MEMS) based sensors. Examples of systems that use low-cost MEMS-based sensors include those in Taiwan (Lin et al., 2012), California (Clayton et al., 2015), China (Peng et al., 2013), Iceland (*TurnKey Earthquake Early Warning*, 2020) and New Zealand (R. M. Allen & Stogaitis, 2022; Prasanna et al., 2022).

Regarding EEW algorithms, source-based approaches detect earthquakes and provide detailed information, such as location, origin time, and magnitude, using a few seconds of P-wave data from nearby sensors (R. M. Allen & Melgar, 2019). However, these algorithms are often slower due to the time required to estimate source parameters, making them less effective for areas near the epicentre. To address this, on-site algorithms have been adopted, which detect earthquakes using a single station based on simple ground motion thresholds (R. M. Allen & Melgar, 2019; Bindi et al., 2015; Picozzi, Emolo, et al., 2015). These on-site algorithms are faster but tend to produce more false alerts. Some improved versions can detect P-waves and generate alerts if the following S-wave is predicted to be destructive (R. M. Allen & Melgar, 2019).

[12] Secondary or shear waves arrive following the P-waves during the earthquake and these are more destructive compared to P-waves.

In contrast, ground motion-based or wavefield-based algorithms have gained popularity for their robustness and speed. They do not estimate source parameters, thereby avoiding the vulnerabilities associated with source-based algorithms (Hoshiba, 2013; Hoshiba & Aoki, 2015; Kodera, 2018). Instead, they use real-time ground shaking data and propagation physics to forecast future ground motion intensity. Ground motion-based algorithms, such as the PLUM approach, are particularly suitable for regions near the epicentre, where rapid detection is crucial. However, they are limited to a defined alerting distance—such as 30 km for PLUM—which can result in limited warning time (Kodera et al., 2018).

6.1.4 Method

To explore the different algorithms used for EEW, relevant articles were collected from the databases Scopus and Web of Science using a keyword search on 17 May 2022. Articles published since 2000 were considered for the search because a scan of existing literature showed that there was not much literature related to EEW before then. To review the different algorithms used for P-wave detection and earthquake magnitude estimation, “earthquake early warning” and “p-detector” were used as the primary keyword to answer the questions. In addition to that, “earthquake warning” and “earthquake detection” were used as alternatives to “earthquake early warning”. Similarly, "p-wave", "s-wave", "p-phase", "s-phase" were used as alternatives to “p-detector”. Peer-reviewed academic publications available online in a full-text format and relevant to the research aims are only included in the search, and publications in languages other than English; grey literature, such as government or industry reports; and non-academic research are excluded from the search. The initial search produced 491 relevant articles. Duplicates from the Initial results were removed and filtered further if they had the following content.

- Algorithms which are not related to generating EEW.
- Evaluating and assessing the performance of the EEW algorithms.
- Algorithms related to structural monitoring and civil engineering.
- Algorithms not related to ground motion sensors, such as Optical fibres, Distributed Acoustic Sensing, GPS sensors, Gravity strain meters, GNSS sensors, and Transoceanic smart cables.
- Algorithms are only related to earthquake location estimations, calculating site factors, and reducing power consumption.
- Articles only discuss the EEW implementation and not the detection algorithm.

After filtering the articles, 144 articles were selected for review. Figure 6-1 illustrates the number of papers returned at each step following the filtering process.

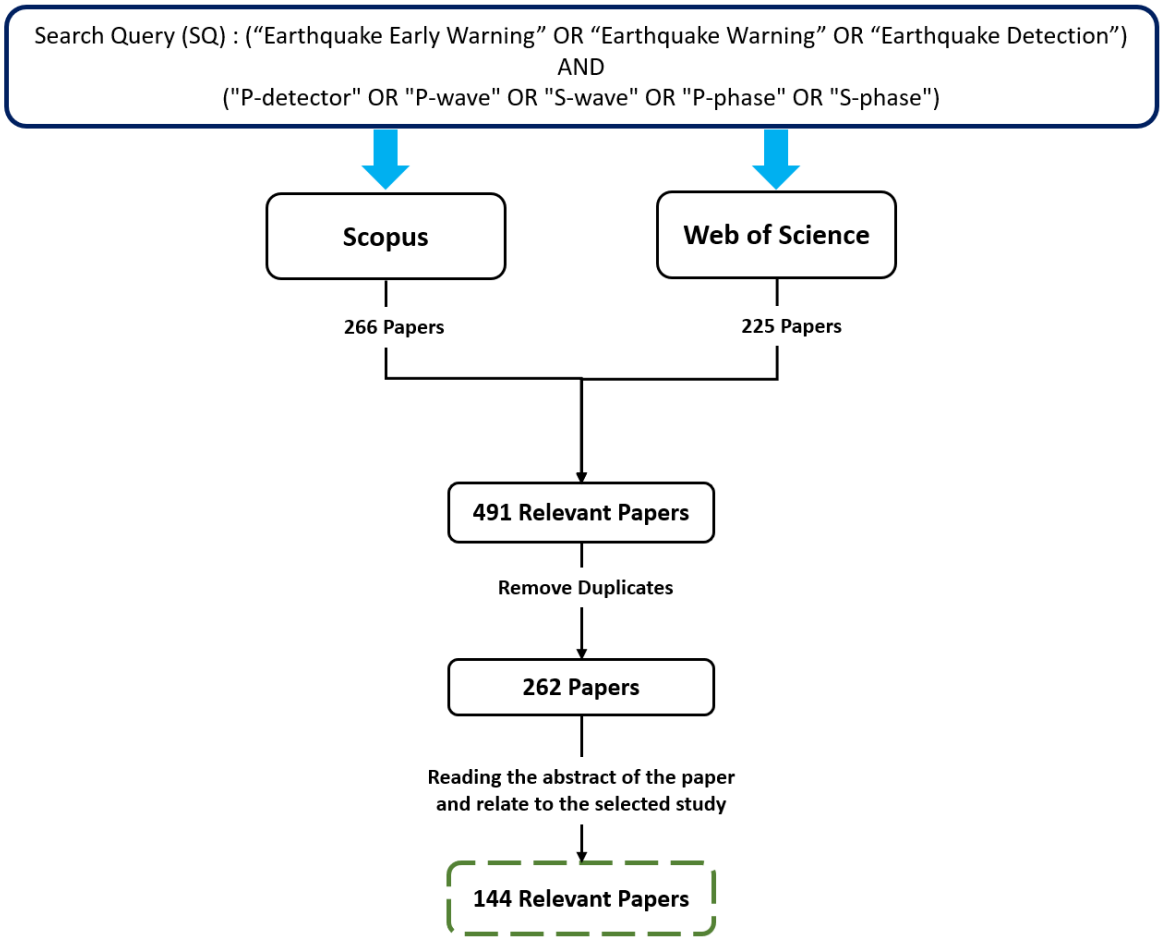

Figure 6-1. Flow diagram for the article filtration.

The relevant data from the selected articles are extracted by introducing a qualitative systematic review process where the research evidence is searched systematically from the primary qualitative studies and the findings are merged. Analysed information added to a Microsoft excel sheet by creating a table in an organised manner.

6.1.5 Findings

Analysis of the 144 articles reveals the different P-wave detection approaches, earthquake magnitude prediction techniques implemented worldwide, and the contextual differences between using such algorithms and the technologies used. The first sub-section discusses the various P-wave detection techniques adopted by different EEWSs. This will be followed by a discussion on the earthquake magnitude estimation algorithms.

6.1.5.1 P-Wave Detection Algorithms

Firstly, the literature on P-wave detectors was explored where different algorithms are proposed for the automatic detection of real-time P-wave arrivals. From the literature, the most commonly used method for detecting the P-waves is the Short-Term Average/Long-Term Average (STA/LTA) method (Ding et al., 2017; Peng et al., 2017; Qingkai & Ming, 2012; Y. M. Wu & Mittal, 2021). STA/LTA was introduced by R.V. Allen (1978) for automatically detecting the P-waves in seismology. The STA/LTA is the most used algorithm in weak motion. It has two moving windows namely: the STA window and the LTA window. It calculates the sum of the absolute value of STA and LTA amplitudes. The STA/LTA ratio is then calculated, and when it exceeds a predefined threshold, the phase of the P-wave is identified (Khalqillah et al., 2018). Even though STA/LTA algorithm has been adopted by several EEW implementations, STA/LTA algorithm is prone to result in false alerts due to the high background noise of the seismic instruments (Bose et al., 2020). This led researchers to implement different algorithms to detect P-waves with a minimal number of errors. The following table (Table 6-1) summarises different P-wave detection approaches attempted by researchers to detect P-waves during an earthquake.

Table 6-1. Summary of the approaches for EEW to detect P-waves during an earthquake.

Authors	Title of the Article	Approach in detecting P-waves
Küperkoch et al. (2010)	Automated determination of P-phase arrival times at regional and local distances using higher order statistics.	Identification of the P-phase is done by applying Akaike Information Criterion to the characteristic function. The accurate P-wave arrival time is determined using a pragmatic picking algorithm on the recalculated characteristic function. Also, a Jackknife procedure and an envelope function analysis are applied to the characteristic function to reduce the false P-phase picks.
Hafez et al. (2010)	Clear P-wave arrival of weak events and automatic onset determination using wavelet filter banks.	Automatic P-wave arrival detection of local events using wavelet transformation. The proposed algorithm is independent of the nature of the noise at the site and the type of seismometer used.

Authors	Title of the Article	Approach in detecting P-waves
Qingkai & Ming (2012)	Evaluation of earthquake signal characteristics for early warning.	This approach uses a modified STA/LTA method to detect P-waves. This approach eliminates the impacts of spike-type noise and small pulse-type noise prior to the commencement of the P-wave from the usual STA/LTA approach by adding two new parameters.
Bhardwaj et al. (2013)	Root sum of squares cumulative velocity: An attribute for earthquake early warning.	P-wave is detected by computing two parameters namely: Root Sum of Squares Cumulative Velocity (RSSCV) and Cumulative Absolute Velocity (CAV), and compared with predetermined threshold values.
Baillard et al. (2014)	An Automatic Kurtosis-Based P - and S -Phase Picker Designed for Local Seismic Networks.	A new kurtosis-based technique for automatically selecting P-phase and S-phase arrivals and easy to implement with high picking accuracy.
Bogiatzis & Ishii (2015)	Continuous wavelet decomposition algorithms for automatic detection of compressional- and shear-wave arrival times.	This method uses the continuous wavelet transformation of the waveform where P-waves are identified by calculating the wavelet coefficients using the vertical component of the ground motion recording.
Z. Wang & Zhao (2017)	Automatic event detection and picking of P, S seismic phases for earthquake early warning and application for the 2008 Wenchuan earthquake.	This approach uses combination of high-precision algorithms to detect phases of P and S-waves. First, an amplification coefficient is introduced to the STA/LTA characteristic function for a better detection of the P and S-phases. Along with that, higher order statistics and the Akaike information criterion function have been utilised to narrow the signal and lock more accurately on the arrival time of the P and S-phases.

Authors	Title of the Article	Approach in detecting P-waves
Kwon et al. (2018)	A new P-Wave detector via moving empirical cumulative distribution function.	This method is based on the shape of the absolute-valued signal's moving empirical cumulative distribution function (MECDF) in a moving window. It uses one fewer window than the STA/LTA approach, which removes the load of window length optimisation while maintaining a comparable level of performance.
Z. Li et al. (2018)	Machine Learning Seismic Wave Discrimination: Application to Earthquake Early Warning.	A machine learning based method It uses Trained Generative Adversarial Network (GAN) to detect P-waves.
Kodera (2018)	Real-Time Detection of Rupture Development: Earthquake Early Warning Using P Waves from Growing Ruptures.	This approach uses Kurtosis-based technique to detect P and S-waves.
Dokht et al. (2019	Seismic event and phase detection using time-frequency representation and convolutional neural networks.	A machine learning based method. Using a deep convolutional network (ConvNet), a generalised model has been created to enhance the ability to distinguish between earthquake and noise recordings. P and S waves are separated from one another, and their approximate arrival times are calculated using a secondary network that employs the main seismic arrivals' wavelet transform.
Mousavi et al. (2020)	Earthquake transformer—an attentive deep-learning model for simultaneous earthquake detection and phase picking.	A machine learning based method. It uses a global deep learning model for detecting earthquakes and picking the phases of P and S waves at the same time.

Authors	Title of the Article	Approach in detecting P-waves
Walter et al. (2020)	easyQuake: Putting machine learning to work for your regional seismic network or local earthquake study.	A machine learning based method. This approach uses an associator and a phase picker driven by machine learning to detect the arrival of P-waves.
Tous et al. (2020)	Deep neural networks for earthquake detection and source region estimation in north-central Venezuela.	A machine learning based method. P-wave earthquake detection and source region estimate using a deep convolutional neural network called UPC-UCV (Universitat Politecnica de Catalunya-Universidad Central de Venezuela), using single-station three-channel signal windows.
Bose et al. (2020)	Framework for Automated Earthquake Event Detection Based on Denoising by Adaptive Filter.	An Enhanced Variable Step-Size Least Mean Square (EVSSLMS) technique for P-wave detection. The EVSSLMS algorithm is used in the proposed event detection strategy to denoise the seismic data before the usual STA/LTA technique is used to detect the arrival of the P-wave.
Sugondo & Machbub (2021)	P-Wave detection using deep learning in time and frequency domain for imbalanced dataset.	A machine learning based method. The Synthetic Minority Oversampling Technique (SMOTE) approach to detect P-waves is proposed using deep learning with time domain and frequency domain as inputs.
Lapins et al. (2021)	A Little Data Goes a Long Way: Automating Seismic Phase Arrival Picking at Nabro Volcano with Transfer Learning.	A machine learning based method. Using the data from the Nabro volcano, a technique known as transfer learning was used to create a deep learning model for automating phase arrival detection for P-waves using a limited amount of training data.
Saad & Chen (2021)	Earthquake Detection and P-Wave Arrival Time Picking Using Capsule Neural Network.	A machine learning based method It uses a capsule neural network (CapsNet) to identify and detect P-waves during an earthquake automatically.

Authors	Title of the Article	Approach in detecting P-waves
Yanwei et al. (2021)	Deep learning for P-wave arrival picking in earthquake early warning.	A machine learning based method Convolution neural network-based automatic algorithm (DPick) was created and trained to detect P-waves.
Liu, Li, et al. (2022)	Discrimination between Earthquake P Waves and Microtremors via a Generative Adversarial Network.	A machine learning based method Generative adversarial network (GAN) for detecting P -waves and microtremors from the training set obtained from JAPAN.
W. Zhu et al. (2022)	An End-To-End Earthquake Detection Method for Joint Phase Picking and Association Using Deep Learning.	A machine learning based method A neural network design for processing seismic waveforms from several stations that were captured using a seismic network which proves that the end-to-end method can successfully detect P- and S-wave arrivals and accomplish precise earthquake detection.
Liu, Song, et al. (2022)	Seismic Event Identification Based on a Generative Adversarial Network and Support Vector Machine.	A machine learning based method A hybrid model based on a generative adversarial network (GAN) and a support vector machine (SVM) is introduced for the purpose of detecting P-waves and differentiating between earthquakes and microtremors.
D'Angelo et al. (2022)	A new picking algorithm based on the variance piecewise constant models.	It uses the variance piecewise constant models of the earthquake waveform to detect P and S-wave automatically.
Khan & Kwon (2022)	P-Detector: Real-Time P-Wave Detection in a Seismic Waveform Recorded on a Low-Cost MEMS Accelerometer Using Deep Learning.	A machine learning based method It uses a deep learning model that can detect P-waves in noisy environments.
Yamada & Mori (2022)	P-wave picking for earthquake early warning: Refinement of a Tpd method.	A refinement algorithm called Tpd method is used to determine the P-wave arrival time accurately.

Authors	Title of the Article	Approach in detecting P-waves
Wibowo et al. (2022)	Earthquake Early Warning System Using Ncheck and Hard-Shared Orthogonal Multitarget Regression on Deep Learning.	A machine learning based method. It uses an algorithm called Ncheck for picking the p-arrival on a multi-station waveform by handling the noise.

The number of approaches in detecting P-wave have increased over the past years. There are several approaches in detecting P-waves based on the mathematical equations (statistics) where the skewness, kurtosis and frequency changes of moving seismic windows were analysed for detecting P-waves (Baillard et al., 2014; Kodera, 2018; Küperkoch et al., 2010; J. Kwon et al., 2018; Yamada & Mori, 2022). Some researchers have tried wavelet transformation to detect P-waves. Usage of wavelet transformation shows that P-waves can be detected clearly even in a weak seismic event (Bogiatzis & Ishii, 2015; Hafez et al., 2010). As discussed, STA/LTA has shown issues in detecting P-waves in noisy environments. To overcome this issue, some researchers have tried improving the method by modifying or adding new parameters to the algorithm to eliminate the effects of noise (Qingkai & Ming, 2012; Z. Wang & Zhao, 2017). However, with the increased processing power of computers, machine learning has become one of the main tools in detecting P-waves. There are a significant number of articles showing that researchers are more focussing on machine learning techniques to detect P-waves where every year, the number of papers published on machine learning-based P-wave detection is increasing.

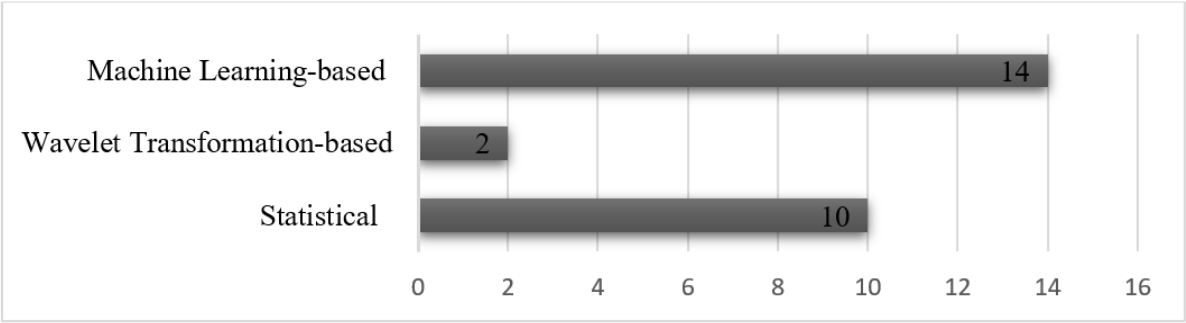

Figure 6-2. Number of articles published in P-wave detection according to the type of approach.

Analysis of different algorithms used for P-wave detection and the number of articles published in three different approaches (Figure 6-2) shows that the evolution of the algorithms started from statistical equations related to the skewness, kurtosis and frequency change of the seismic wave and moved towards machine learning-based techniques over the years. The following section discusses the algorithms used to estimate an earthquake's magnitude using a time window of a detected P-wave.

6.1.5.2 Algorithms for Estimating an Earthquake's Magnitude

Estimating an earthquake's magnitude using the detected P-wave window could assist the EEWS to provide alerts to end users with the earthquake's magnitude and it will help in dynamically changing the alerting zones according to the expected shaking. The literature on techniques used to predict the magnitude of an earthquake has been explored. Generally, in most of the algorithms, an earthquake's magnitude is predicted by analysing a 0.5-4 second time window of the detected P-waves (R. M. Allen & Melgar, 2019). The common technique used in many EEWS implementations is to determine the earthquake's magnitude from the time parameter (τ_c) and Peak displacement Amplitude (P_d) (Linear regression model) (D. Y. Chen et al., 2017; Peng et al., 2014; Tusa et al., 2017; Vallianatos et al., 2021; Y. M. Wu & Zhao, 2006). Several studies indicate that magnitude estimation of S-wave tends to saturate when using such a short time window of P-wave where earthquakes are significantly large and have long rupture durations (M > 6) (Hoshiba et al., 2011; Rydelek & Horiuchi, 2006). To overcome the saturation issues related to the linear regression model, different approaches were implemented by researchers to predict an earthquake's magnitude. The following table (Table 6-2) summarises the different earthquake magnitude prediction algorithms attempted by researchers.

Table 6-2. Summary of the approaches for EEW to estimate an earthquake's magnitude.

Authors	Title of the Article	Approach in Estimating Earthquake Magnitude
R. M. Allen & Kanamori (2003)	The potential for earthquake early warning in Southern California.	It uses the frequency content of the P-waves to determine earthquake's magnitude before any damaging ground motion occurs.
Odaka et al. (2003)	A new method of quickly estimating epicentral distance and magnitude from a single seismic record.	It calculates the magnitude of an earthquake from the maximum amplitude measured during a specified short time window following the arrival of the P-wave using an empirical magnitude-amplitude relationship.
Simons et al. (2006)	Automatic detection and rapid determination of earthquake magnitude by wavelet multiscale analysis of the primary arrival.	It uses the discrete wavelet transform-based method to analyse the waveform and calculate the final magnitude of an earthquake from the first few seconds of the P wave.

Authors	Title of the Article	Approach in Estimating Earthquake Magnitude
Y. M. Wu & Zhao (2006)	Magnitude estimation using the first three seconds P-wave amplitude in earthquake early warning.	Peak amplitude of displacement (Pd) in the first three seconds after the arrival of the P wave is used for the estimation of the earthquake's magnitude.
Lancieri & Zollo (2008)	A Bayesian approach to the real-time estimation of magnitude from the early P and S wave displacement peaks.	It uses the early P and S wave displacement peaks along with the Bayesian probabilistic approach for the real-time estimation of earthquake's magnitude.
Qingkai & Ming (2012)	Evaluation of earthquake signal characteristics for early warning.	It uses stepwise regression analysis of 12 kinds of parameters from the first 3 seconds of the P-wave to estimate the epicentral distance and magnitude of the earthquake.
Kuyuk & Allen (2013)	A global approach to provide magnitude estimates for earthquake early warning alerts.	It determines the earthquake's magnitude using the global scaling relation between Pd (Peak amplitude of displacement) of the P-wave window and magnitude of an earthquake.
Reddy & Nair (2013)	The efficacy of support vector machines (SVM) in robust determination of earthquake early warning magnitudes in central Japan.	This method uses an improved wavelet transformation-based earthquake magnitude prediction approach to estimate an earthquake's magnitude accurately.
J. Li et al. (2013)	Continuous estimates on the earthquake early warning magnitude by use of the near-field acceleration records.	It uses the statistical analysis method to determine the earthquake's magnitude by measuring the acceleration, displacement, and effective peak acceleration in each seismic record within a certain time after P wave arrival.
Hloupis & Vallianatos (2013)	Wavelet-based rapid estimation of earthquake magnitude oriented to early warning.	It uses a wavelet-based algorithm for estimating the earthquake magnitude.

Authors	Title of the Article	Approach in Estimating Earthquake Magnitude
Heidari et al. (2013)	Magnitude-scaling relations using period parameters τc and τpmax, for tehran region, Iran.	It determines the magnitude of an earthquake by combining and using the period parameters τpmax and τc from the vertical and horizontal components of a P wave's first three seconds.
Meier et al. (2015)	The Gutenberg algorithm: Evolutionary Bayesian magnitude estimates for earthquake early warning with a filter bank.	It uses the broadband frequency information of seismic signals in a probabilistic algorithm to estimate the earthquake magnitude.
Picozzi, Colombelli, et al. (2015)	A Threshold-based Earthquake Early-Warning System for Offshore Events in Southern Iberia.	It calculates the Pd (Peak amplitude of displacement) of the P-wave window and uses log Pd vs PGV (Peak Ground Velocity) empirical relationship to predict the earthquake's magnitude.
Hloupis & Vallianatos (2015)	Wavelet-based Methods for Rapid Calculations of Magnitude and Epicentral Distance: An Application to Earthquake Early Warning System.	It determines an earthquake's magnitude and estimate its epicentre using wavelet transform (WT) as a processing method. Wavelet coefficients used to characterize the seismogram of the P-wave portion are used for earthquake's magnitude and location estimation.
Yang & Motosaka (2015)	Ground motion estimation using front site wave form data based on RVM for earthquake early warning.	A machine learning-based method. It uses five input variables observed in the P-wave (earthquake PGA, PGD, pulse rise time, average period and the Vp max/Ap max ratio) in a relevant vector machine (RVM) to estimate the magnitude of an earthquake.
Atefi et al. (2017)	Rapid estimation of earthquake magnitude by a new wavelet-based proxy.	It uses a wavelet-based scale regression of log (λlog) value extracted from the P-wave window for predicting earthquake's magnitude.

Authors	Title of the Article	Approach in Estimating Earthquake Magnitude
Noda & Ellsworth (2017)	Determination of earthquake magnitude for early warning from the time dependence of P-wave amplitudes.	It calculates the displacement of the P-wave before the arrival of the peak amplitude and uses the built relationship between the earthquake magnitude (M) and P-wave displacement to estimate the earthquake's magnitude.
Lizurek et al. (2017)	Fast Moment Magnitude Determination from P-wave Trains for Bucharest Rapid Early Warning System (BREWS).	It uses P-wave spectral levels to determine the earthquake's magnitude.
Cuéllar et al. (2018)	An earthquake early warning algorithm based on the P-wave energy released in the ts–tp interval.	To estimate the magnitude threshold, the P-wave coda's energy on the vertical component during the tS - tP period is measured.
Z. Wang & Zhao (2018)	A new Mw estimation parameter for use in earthquake early warning systems.	It calculates the initial P-wave window's squared displacement integral (ID2) to estimate earthquake's magnitude.
Ochoa et al. (2018)	Fast magnitude determination using a single seismological station record implementing machine learning techniques.	A machine learning-based approach. It uses only five seconds of signal from a single three component seismic station's P wave to derive the earthquake's magnitude (Ml) using the Support Vector Machine Regression (SVMR) algorithm.
J. Zhu et al. (2021)	Magnitude Estimation for Earthquake Early Warning Using a Deep Convolutional Neural Network.	A machine learning-based approach. An advanced model for magnitude prediction that employs the 3-seconds of P-wave data into a deep convolutional neural network for earthquake magnitude estimation.

Authors	Title of the Article	Approach in Estimating Earthquake Magnitude
Zhang et al. (2021)	Real-Time Earthquake Early Warning with Deep Learning: Application to the 2016 M 6.0 Central Apennines, Italy Earthquake.	A machine learning-based approach. A deep learning technique that analyses continuous seismic waveform streams to simultaneously detect earthquakes and estimate their source properties such as earthquake's magnitude and location using fully convolutional networks.
Abdalzaher et al. (2022)	A Deep Learning Model for Earthquake parameters Observation in IoT System-based Earthquake Early Warning.	A machine learning-based approach. A deep learning model based on integrating autoencoder (AE) and convolutional neural network (CNN) is presented (3S-AE-CNN) for a rapid determination of an earthquake's magnitude and location after three seconds from the beginning of the P-wave.
J. Zhu et al. (2022b)	Magnitude Estimation for Earthquake Early Warning with Multiple Parameter Inputs and a Support Vector Machine.	A machine learning-based approach. To estimate earthquake magnitudes, it uses a variety of parameter inputs, including the support vector machine magnitude estimation (SVM-M) model.

Similar to P-wave detection algorithms, the methods for predicting the magnitude of an earthquake have increased over the years. As mentioned, almost all the algorithms analyse the characteristics of a P-wave in a particular time window to predict the magnitude of an earthquake. However, similar to the P-wave detection algorithms, the evolution of the magnitude estimation algorithms started from linear regression models where the magnitude of an earthquake is estimated by forming a correlation between the parameters of the detected P-wave time window and historical earthquakes' magnitude and moved towards machine learning-based techniques over the years. Further, analysis of different earthquake magnitude estimation approaches showed the different approaches to estimating the S-waves using the P-waves.

6.1.6 Next Steps and Future Work

The above analysis demonstrates that implementing the P-wave-based PLUM algorithm for EEW is achievable. From the identified P-wave detection algorithms in this study, selecting an appropriate P-wave detector will involve conducting experiments to identify a lightweight and easy-to-implement detection algorithm. This selection is particularly important because CRISiSLab's EEWS relies on decentralised processing with low-cost MEMS-based sensors with limited processing power and memory. Future experiments will be designed to rank P-wave detectors based on their processing time and accuracy, focusing on minimal processing time to ensure real-time operation.

To ensure the chosen algorithm's reliability, future work will thoroughly compare detection errors, specifically in terms of missed and false detections. Additionally, the algorithm's performance in noisy environments will be critically evaluated, as existing literature suggests that P-wave detectors often produce inaccurate results under such conditions. The algorithms will also be tested within the specific sensor environment of the CRISiSLab EEW network, which comprises surface-based stations installed in homes. This testing is essential, as algorithms effective only in low-noise or borehole environments may not be suitable for this network. Therefore, future work will focus on selecting a P-wave detector that excels in accuracy, noise resilience, and compatibility with surface-based sensor installations.

Following selecting an appropriate P-wave detection algorithm, the next phase of the research will focus on identifying the most suitable empirical relationship between the detected P-waves and the subsequent destructive S-waves. This phase will involve leveraging existing approaches used for estimating S-wave amplitudes based on P-waves, identified from the earthquake magnitude estimation methods. A detailed comparison and analysis of these approaches will be conducted to determine the most accurate and reliable empirical relationship between P and S-waves. The chosen relationship will be validated by examining its correlation strength and estimation accuracy.

Once the appropriate P-wave detection algorithm and empirical P-to-S-wave relationship are identified, the final step will be to integrate these components into the PLUM-based approach. This integration will enhance the PLUM algorithm's warning time by enabling earlier earthquake detection through P-waves.

6.1.7 Section Summary

This section presents the findings of a literature review that explored P-wave detection and earthquake magnitude estimation algorithms used in EEWSs worldwide, addressing Objective 2.1 of this study. The review systematically analyses 144 research articles, focusing on various approaches to detecting

P-waves and estimating earthquake magnitude. It categorises P-wave detection algorithms, ranging from traditional methods like the Short-Term Average/Long-Term Average (STA/LTA) approach to more sophisticated machine learning techniques. The review highlights the evolution of these algorithms, noting a growing shift towards machine learning due to its enhanced robustness and accuracy in noisy environments. Additionally, the chapter examines earthquake magnitude estimation algorithms, detailing how P-wave characteristics are used to predict magnitude and discussing the transition from linear regression models to more advanced machine learning techniques. By systematically categorising these algorithms, this chapter lays the groundwork for selecting suitable P-wave detection and S-wave amplitude estimation methods for community-engaged EEWSs, particularly in challenging, noisy environments. The insights gained from this review guides the subsequent phases of the study.

6.2 Evaluation of Four P-Wave Detection Algorithms Using Community-Engaged Ground Motion Data, Aiding Selection for Community-Engaged EEWS.

6.2.1 Abstract

Can a P-wave detection algorithm enhance the performance of an Earthquake Early Warning System (EEWS), particularly in community-engaged networks of low-cost ground motion sensors susceptible to noise? If so, what P-wave detection algorithm would perform the best? This study analyses the performance of four different P-wave detection algorithms using a community-engaged Earthquake Early Warning (EEW) network. The ground motion data from a 48-hour time window around a M5.8 earthquake on 22 September 2022 were used as the basis for this case study, where false and missed detections were analysed for each P-wave detection algorithm. The results indicate that a wavelet transformation-based P-wave picker is the most suitable algorithm for detecting an earthquake with minimal missed and false detections for a community-engaged EEWS. Our results show that a citizen seismology-based EEWS is capable of detecting events of interest to EEW when selecting an appropriate earthquake detection algorithm. The study also suggests future research areas for community-engaged EEWSs, including dynamically changing P-wave detection thresholds and improving citizen seismologists' user experience and involvement.

6.2.2 Introduction

Straddling the Australian and Pacific tectonic plates, Aotearoa New Zealand (NZ) is one of the most seismically active regions in the world. Every year, more than a hundred earthquakes of magnitude four or higher strike NZ (GeoNet, 2023). Earthquakes in the 2010 and 2011 Canterbury sequence and the 2016 Kaikōura earthquake have resulted in significant casualties, injuries, and property damage (Potter et al., 2015; Stevenson et al., 2011, 2017).

Several countries and territories have implemented a national Earthquake Early Warning System (EEWS) to alert the public up to tens of seconds before the incoming ground shaking following an earthquake (R. M. Allen & Melgar, 2019; R. M. Allen & Stogaitis, 2022; Chandrakumar, Prasanna, Stephens, & Tan, 2022; Cremen & Galasso, 2020; McBride et al., 2022). These systems have shown promising benefits in decreasing earthquake damage and assisting individuals in physically and mentally bracing for imminent ground shaking (Fujinawa & Noda, 2013; Nakayachi et al., 2019; Suárez et al., 2009).

Although NZ has a significantly high level of seismic hazard, there is no official national EEWS (Becker, Potter, Prasanna, et al., 2020). The GeoNet programme, operated by GNS Science—NZ's geological survey—is the only official source of earthquake information for NZ (GeoNet, 2017). Earthquake source parameters and ground-shaking information are disseminated after the earthquake through a website and a mobile phone app. Despite there being no official EEWS, a survey of 3084 participants in 2019 found that over 90% of the participants approve of implementing an EEWS in NZ (Becker, Potter, Vinnell, et al., 2020). However, several technical and non-technical challenges exist in developing an official EEWS in NZ. High costs related to implementing high-end EEWS are one of the primary challenges (Brooks et al., 2021; Given et al., 2018; Minson et al., 2015; Prasanna et al., 2022; Strauss & Allen, 2016). Further, the high installation and operating costs of implementing a country-wide EEW system raise the question of its economic sustainability in a country like NZ, which has around 5 million people (Becker, Potter, Prasanna, et al., 2020; Prasanna et al., 2022). However, having recognised the need for EEW, various other parties have started providing EEW services in NZ. For example, in April 2021, Google announced an EEW service for Android smartphone users in NZ (R. M. Allen & Stogaitis, 2022). Other commercial providers offer private in-house local EEW services to clients, but these services are not available to the general public (Becker, Potter, Prasanna, et al., 2020).

Low-cost alternative technologies are being developed worldwide to address the expensive implementation and maintenance costs associated with conventional high-end EEWSs. Such initiatives provide opportunities for researchers to develop economical solutions such as using micro-electromechanical systems (MEMS)-based ground motion sensors. MEMS-based accelerometers were introduced in seismic applications in the early 1990s (Holland, 2003) and have proven effective for recording strong ground motions. EEWSs operating in Taiwan (Y. M. Wu et al., 2013) and the Sichuan-Yunnan border region of China (Peng et al., 2019) have incorporated low-cost MEMS-based sensors for public alerting. California (Clayton et al., 2015), Iceland (*TurnKey Earthquake Early Warning*, 2020), Costa Rica (Brooks et al., 2021) and NZ (Prasanna et al., 2022) have also incorporated low-cost MEMS-based sensors into EEWSs, but only in experimental applications.

The recent proliferation of low-cost ground motion sensors has created opportunities for the broader public to participate in gathering ground motion data for EEW and other purposes (Finazzi, 2020; Subedi et al., 2020). Research partnerships between seismologists and non-scientist volunteers are known as citizen seismology, one of the emerging fields in EEW (K. H. Chen et al., 2020). Citizen seismology refers to the involvement of the general public in collecting seismic data through the use of seismic sensors installed in their homes or communities. Citizen seismology has various advantages, including increased sensor distribution, improved public engagement and awareness, and cost-effectiveness. Several initiatives have explored community-engaged seismic monitoring supported by

MEMS-based ground motion sensors in dedicated units, smartphones or laptops (R. M. Allen et al., 2020; Cochran et al., 2009; Faulkner et al., 2011; Mehrazarin et al., 2016; Minson et al., 2015). Furthermore, some low-cost citizen seismology-based EEWSs have demonstrated the feasibility and capability of MEMS-based sensor networks for delivering EEW.

False and missed alerts can have significant implications for the effectiveness of an EEWS, regardless of whether it relies on high-end or low-cost ground motion detection sensors (Minson et al., 2019). In this study, we use the following definitions of EEWS false and missed alerts. False alerts occur when the system generates an alert when there is no earthquake, while missed alerts happen when no alert is generated despite the occurrence of an earthquake (Brooks et al., 2021). Several studies in the literature have tested false and missed alerts generated by their EEWSs (Brooks et al., 2021; Kohler et al., 2020; Suárez et al., 2009; Xu et al., 2017). However, to the best of our knowledge, there is limited research conducted in analysing the false and missed alerts generated by a community-engaged EEWS. Although community-engaged EEWSs offer advantages, the network often experiences considerable levels of noise. This is expected because the sensors in the network are installed at individual households within the community, subject to environmental and man-made noise. The community-engaged EEWS network, therefore, is more susceptible to false and missed alerts compared to high-end EEWSs

In literature, the integration of multi-station data has been identified as a potential solution to address the issue of false and missed alerts in any EEWSs (Brooks et al., 2021; Kilb et al., 2021; Kohler et al., 2020; Y. M. Wu et al., 2013). By analysing data from multiple stations, the impact of false and missed detections at individual stations can be minimised, resulting in a reduction of false and missed alerts within the system. In this context, a false detection is considered when an algorithm erroneously identifies noise rather than a seismic wave using a single ground motion sensor. A missed detection occurs when an algorithm fails to detect the seismic wave in the single-station earthquake ground motion data. In addition to analysing multi-station data for alert generation, we hypothesise that integrating a robust P-wave detection algorithm for detecting P-waves during an earthquake could further contribute to the reduction of false and missed alerts in a community-engaged EEWS.

While there are several P-wave detection algorithms that could be implemented for EEWS (Chandrakumar, Prasanna, Stephens, Tan, et al., 2022), limited research has been conducted to evaluate the frequency of missed and false detections associated with each algorithm, particularly in the context of community-engaged ground motion network data. Therefore, there is a need to analyse different P-wave detection algorithms and assess their performance in terms of the number of missed and false detections for a community-engaged EEWS. This evaluation will assist researchers in selecting an appropriate earthquake detection algorithm that can enhance the overall performance of an EEWS. To that end, this study investigates the most appropriate algorithm for detecting P-waves in a community-

engaged EEWS. To evaluate the algorithm's performance in terms of false and missed detections, we have used an experimental community engaged EEWS with an emphasis on a case study involving a M5.8 earthquake.

The remainder of this article is organised as follows. Section 6.2.3 provides an overview of the community-engaged EEW network used for this study. The method adopted for the performance analysis of the P-wave detection algorithms is addressed in Section 6.2.4. Section 6.2.5 outlines the materials used for the specific case study. In Section 6.2.6, the results and the discussion are presented, followed by the conclusion in Section 6.2.7.

6.2.3 The Community-Engaged EEW Network

Planning for the implementation of the experimental EEWS started in 2020, and low-risk ethics approval was obtained to recruit participants from the community to host the ground motion sensors in their households. Low-cost MEMS-based Raspberry Shake (RS) 4D ground motion sensors were selected as suitable for the community-engaged EEWS due to their accessibility, accuracy and processing power (Prasanna et al., 2022). Our research team and community members discussed ideal geographical locations to host the sensors (Tan et al., 2021). Before distributing the sensors to the participants, we conducted an introduction session to increase awareness regarding earthquakes and techniques for handling and installing seismometers. As part of citizen seismology, the sensor hosts were given control over their instruments; we did not interfere with their installation method (whether fixed to the ground or just placed loosely) or their selection of installation site for the sensor within their house premises. The study made use of a total of 15 sensors, which were primarily installed in the lower North Island of NZ as illustrated in Figure 6-3. The sensors were connected to a peer-to-peer network using decentralised processing without any centralised servers to process data (Prasanna et al., 2022).

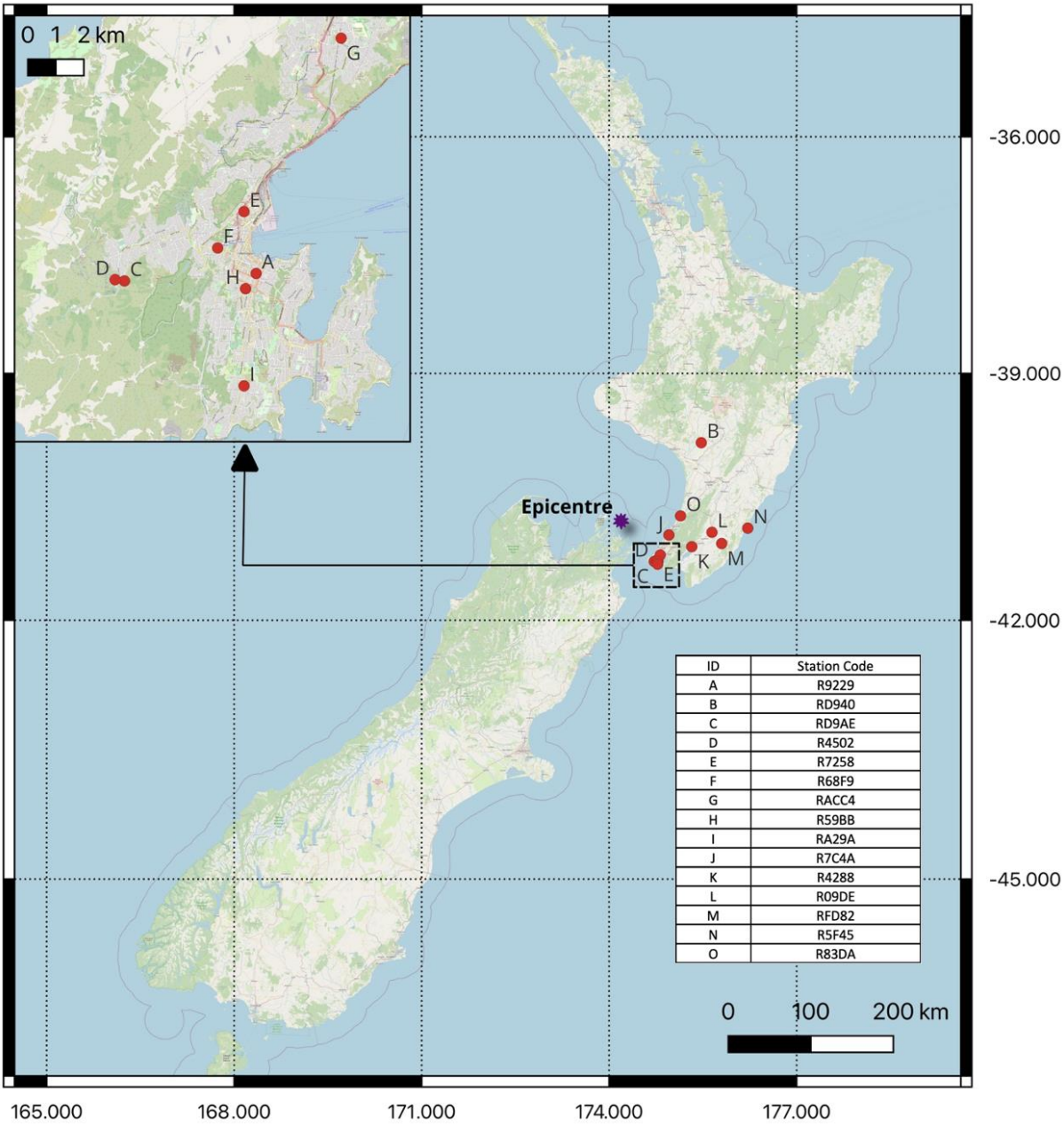

Figure 6-3. Figure 1. Map illustrating the location of the 15 RS 4D sensors installed for the experimental EEWS and the epicentre for the 22 September 2022 earthquake. The inset shows the locations of sensors installed in Wellington city; identified by station IDs A, C, D, E, F, G, H and I.

As of the current status of our network, our approach heavily relies on decentralised processing. In this context, we have identified the Propagation of Local Undamped Motion (PLUM) algorithm as the most suitable for our network. We have demonstrated the network's performance using simulated data in a study we published (Prasanna et al., 2022). The focus of this paper is primarily on network performance including system latency and warning window, thus real-time alert delivery to the end-user is outside the current scope. We plan to delve into this aspect in our future work as we explore and optimise the mechanisms for alert dissemination. The study presented in this paper is motivated by the ongoing

research efforts aimed at mitigating false detections caused by noise in individual stations of EEWSs, especially in the context of community-engaged networks where noise is inevitable.

6.2.4 Method for Testing Algorithms

Using a M5.8 22 September 2022 earthquake event as a case study (details provided in next section), this paper analyses the false and missed detections of the implemented experimental community-engaged EEWS during a 48-hour time window around the earthquake event using four different P-wave detection algorithms.

The approach taken in this study to explore false detections with community-engaged ground motion data using different P-wave detection algorithms differs from past studies on false alerts (e.g., Brooks et al., 2021; Kohler et al., 2020; Suárez et al., 2009; Xu et al., 2017). Those studies focused on EEWSs that do not involve the use of community-engaged sensors where the ground motion sensors are installed and maintained by the community members. We believe analysing false detections is crucial for assessing the appropriateness of the captured data for a community-engaged sensor network, given that the sensor network is hosted entirely by community members and the sensor installation may not always be optimal. Therefore, there is a possibility for some of the sensors to record noisy data. Along with the false detection analysis, this study also calculated the number of missed detections reported with each algorithm for the chosen earthquake.

The first step of the analysis was to validate the data for the earthquake event, which involved examining the data for the earthquake event from the 15 sensors. The data captured by the sensors were checked to see whether they were able to detect and record the ground motion caused by the 22 September 2022 earthquake. The data were also analysed for completeness, e.g. whether there were any missing data, and if so, mitigation measures (e.g. interpolation technique) were adopted to address them. Then the recorded ground motion data were filtered using a Butterworth-Bandpass filter from 0.1 to 20Hz to retain the earthquake signal's frequency content of interest and remove the low-frequency and high-frequency ambient noise (Claerbout, 1964; Virtanen et al., 2020).

After the data check, the performance of the P-wave detection algorithms was analysed by inspecting each sensor's frequency of missed and false detections using the chosen data. Vertical acceleration data were used as the input data since the P-waves are predominantly stronger in the vertical direction (Y. M. Wu, 2019; H. Zhang et al., 2003). The validity of the missed and false detections was then cross-checked by comparing them with the earthquake data reported on the GeoNet website (GeoNet, 2022a).

The results from the performance analysis will provide crucial insight into identifying the most appropriate P-wave algorithm that can be integrated into our experimental community-engaged EEWS with MEMS-based sensors.

6.2.5 Case Study Materials

6.2.5.1 Data for the Case Study

On 22 September 2022, a moderate M5.8 earthquake with a hypocentre depth of 52.7 km struck the Marlborough region of NZ (GeoNet, 2022a) (epicentre location shown in Figure 1). Despite the earthquake's epicentre being located 30 km away from population centres in the lower North Island, it caused moderate levels of shaking, particularly in the greater Wellington region, where the reported peak ground acceleration (PGA) was 1.63% g, and the peak ground velocity (PGV) was 1.04 cms^{-1} (GeoNet, 2022b). The experimental EEWS was operating during the earthquake, and ground motion data from the 15 community sensors were captured during this earthquake.

The testing timeframe considered for this study spans 48 hours around the earthquake: the earthquake took place on 22 September 2022, at 21:07:06 local time (UTC time: 2022-09-22T09:07:06Z). The data collection period encompassed the duration from 22 September 2022, 12:00:00 to 24 September 2022, 12:00:00, all recorded in the local time zone. We also searched for other earthquakes that could have potentially been recorded by our network during this timeframe. The initial quake search for this particular timeframe using the GeoNet database resulted in 78 earthquakes ranging from M0.8 to M5.8, covering the entire NZ region. Following that, we filtered the minimum magnitude of the quake search to M3, reducing the number of earthquakes to 19. Focussing on our recorded ground motion data, each earthquake from the filtered 19 earthquakes was investigated to determine whether it had made any moderate levels of shaking in the Wellington region. Of the 19 quakes, only the M5.8 earthquake (GeoNet public id: 2022p714540) caused moderate to significant shaking in the Wellington region. The remaining 18 earthquakes were mostly unnoticeable or weak shaking in the Wellington region, making them less relevant for the focus of this study. As a result, these earthquakes did not produce any recorded ground motion data indicating shaking at our stations.

Ground motion data were retrieved from the RS official database (Raspberry Shake, 2017) in miniSEED format (Ringler & Evans, 2015). RS has a database that archives ground motion data from all the RS ground motion sensors installed globally. We developed a Python script to download three-dimensional ground motion data from the RS database using the International Federation of Digital Seismograph Networks (FDSN) web service (DzIewonski, 2021). The downloaded data have a sampling rate of 100 Hz and have had the instrument response removed. To reduce processing time and simplify the analysis

process to identify missed and false detections correctly, the data for the 48-hour timeframe were broken into 10-minute small manageable data frames, yielding 288 data frames for each sensor.

6.2.5.2 P-wave Detection Algorithms Considered for This Study

In a previous study (Chandrakumar, Prasanna, Stephens, Tan, et al., 2022), we reviewed different P-wave detection algorithms in the literature and explained the evolution of earthquake detection algorithms, which began with statistical equations related to the skewness, kurtosis, and frequency change of the seismic wave and more recently progressed towards machine learning-based techniques. Among the 27 P-wave detection algorithms reviewed, ten were based on statistical techniques, two were based on wavelet transformation techniques, and the remaining 14 were based on machine learning techniques.

Among the P-wave detection algorithms mentioned above, four non-machine learning-based algorithms were chosen for this study and are summarised in Table 6-3: two traditional and frequently used algorithms (R. M. Allen & Melgar, 2019) and two newer algorithms which have been increasing in popularity due to their accuracy and reliability (Baillard et al., 2014; Hafez et al., 2013). Machine learning-based approaches were not selected because the community-engaged EEWS in this study is relatively new, and these approaches require a large database of earthquakes for training (W. Zhu et al., 2022) and the earthquake data must include labelled phase picks (W. Zhu & Beroza, 2019). In addition, since the experimental EEWS used for this study executes all the earthquake related algorithms at the node-level, we decided to consider only light-weight (low computational power) algorithms in this comparison. This consideration is important as our low-cost ground motion sensors come with limited processing power and memory capacity (Prasanna et al., 2022).

Table 6-3. Description of the P-wave detection algorithms selected for this study

Selected Algorithms	Description and Reference
The standard Short-Term Average/Long-Term Average (STA/LTA)	This algorithm has two moving windows: the STA window and the LTA window. It calculates the sum of the absolute value of STA and LTA amplitudes. Here, the energy of a short window is compared to that of a longer window. The STA/LTA ratio is then calculated, and when it exceeds a predefined threshold, the phase of the P-wave is identified (R. V. Allen, 1978).

Selected Algorithms	Description and Reference
Recursive STA/LTA – Decaying constant	Recursive STA/LTA is developed to avoid keeping a long data vector in memory for the STA window. This is more efficient and produces a decaying exponential impulse response, which will recover more quickly from large energy transients, rather than a rectangular impulse response of the standard STA/LTA algorithm (Withers et al., 1998).
Adapted Kurtosis-based P-wave picker	This algorithm employs kurtosis-derived characteristic functions (CF) and eigenvalue decompositions for P and S-wave detection (Baillard et al., 2014).
Adapted Wavelet-based P-wave picker	This algorithm uses maximum overlap wavelet transformation, where the "Daubechies-1 (db1)" wavelet function is used for the transformation. Squared complete first-stage detail from the wavelet transformation is used for the earthquake detection (Hafez et al., 2013).

Standard Short-Term Average/Long-Term Average (STA/LTA) (R. V. Allen, 1978) and recursive STA/LTA (Withers et al., 1998) were chosen as they are commonly used algorithms to identify P and S waves using amplitude changes in the seismic wave (Castilla et al., 2023). Furthermore, these two are openly available in the ObsPy library (Krischer et al., 2015). The two recently developed P-wave detection algorithms that are precise in terms of detecting P-wave onsets comprise the Kurtosis-based P-wave picker (Baillard et al., 2014), which is based on the kurtosis value of a seismic wave and can be thought of as a statistical measure that describes the shape of a distribution. The other algorithm, the maximum overlap discrete wavelet transformation-based P-wave picker (Hafez et al., 2013) uses time-frequency domain analysis for P-wave detection. Detailed instructions on implementing these two algorithms can be found in the original references, where the methods have been thoroughly documented.

6.2.5.3 Adapting and Fine-Tuning of Chosen Algorithms

The Standard STA/LTA and Recursive STA/LTA

For standard STA/LTA and Recursive STA/LTA algorithms, selecting the appropriate STA/LTA ratio and window lengths is crucial in processing ground motion data for EEW. The STA/LTA ratio determines whether a particular ground motion measurement represents an earthquake event or is simply a result of noise or other non-seismic signals. We considered the noise level of the sensor signal and the required detection sensitivity when selecting the appropriate STA/LTA ratio. The desired

sensitivity of earthquake detection is important; a highly sensitive system may lead to more false detections, while a less sensitive system will result in the opposite. The goal is to select a ratio that results in a high level of sensitivity while keeping the number of false detections to a minimum. The process of selecting the STA/LTA ratio may involve some trial and error, and the optimal ratio will likely be different for different EEWSs and datasets (Trnkoczy, 2012). The STA and LTA windows and ratio values were selected for our experiments based on historical data retrieved from the community-engaged ground motion sensors from June to August 2022. This selection aimed to minimise false detections caused by sudden spikes generated by environmental noise. Therefore, having considered the implementation of our community-engaged network, we have chosen the STA and LTA window lengths as 3 and 10 seconds, respectively. Both the STA and LTA window move along the time series and are updated every 0.5 seconds. Longer windows were adopted for more reliable and accurate detection, but the optimum values of 3 and 10 seconds were selected to balance accuracy and warning time. While shorter window lengths result in more warning time, they can also lead to more false detections. On the other hand, longer window lengths reduce false detections but offer less warning time. Further, by analysing the waveforms manually, the STA/LTA ratio for detecting a seismic event has been selected as 2.5, showing a higher sensitivity level for detection while maintaining a minimal number of false detections. To detect P-waves, both the standard STA/LTA and the recursive STA/LTA require a length of 0.5 to 3 seconds of data after the P-wave, depending on the noise level at the station.

Adopted Kurtosis-based P-wave Picker

The Kurtosis-based P-wave detector is a method for detecting the arrival of P-waves in seismic data by looking for the maximum kurtosis value in the seismic signal. Kurtosis is a statistical measure of a distribution's "peakedness" or "flatness". In seismic data, a P-wave typically has a higher kurtosis value than other seismic waves because it is characterised by a sharp and distinct arrival. To implement a kurtosis-based P-wave detector, the seismic signal is first divided into small windows or segments, each having 3 seconds in length, and the kurtosis of each segment is calculated. The segment with the maximum kurtosis value is then considered to be the P-wave arrival. Since this algorithm depends on the kurtosis value of the seismic wave, it needs only a fraction of second of data (< 1 sec) after the P-wave to detect it. The precise time of the P-wave arrival can be determined by interpolating the maximum kurtosis value. Along with calculating the kurtosis value, the additional steps mentioned in Baillard et al. (2014) were implemented to ensure the accurate detection of the P-wave in a seismic wave.

Wavelet-based P-wave Picker

The wavelet transform provides both time and frequency resolution, but the trade-off between the two can be adjusted by choosing different wavelet functions. Some wavelets provide high-frequency resolution at the expense of poor time resolution. Others, such as the Daubechies wavelets and Haar wavelets, provide good time resolution with less frequency resolution. For our study, the "Daubechies-1 (db1)" wavelet function has been used as recommended by Hafez et al. (2013). After manually analysing the data and checking the "db1" wavelet coefficients, first-order squared coefficients were chosen to detect the P-waves. The maximum value of the "db1" coefficient reported during the first eight seconds of the waveform has been selected as the threshold and checked for a consistent threshold exceedance in the upcoming data (0.3 second of time interval) to detect the P-waves, as stated by Hafez et al. (2013). For the threshold exceedance interval calculation, we used the same historical ground motion data used in the standard and recursive STA/LTA algorithm. This algorithm needs less than 1 second of data after the P-wave detection (Hafez et al., 2013).

It is essential to note that the tuning of algorithms, as discussed, is based on the data used in this study. The performance and behaviour of these algorithms may vary when tested with a larger earthquake dataset, particularly considering differences in earthquake magnitude and hypocentre depth. Therefore, the fine-tuning and adaptation of the selected algorithms are subject to further refinement and adjustment when applied to a broader range of earthquake scenarios in future testing. This adaptability will ensure the algorithms' effectiveness across seismic events.

6.2.6 Results and Discussion

This section summarises the results from analysing the 288 data frames for each sensor in the community-engaged EEWS. First, the ground motion recording obtained from the sensor network is briefly discussed. Performance analysis of selected P-wave algorithms with earthquake data is then presented, calculating the missed and false detections.

6.2.6.1 Validating the Data for the Earthquake Event

The first step of the validation was to evaluate whether the 15 sensors recorded quality data for the M5.8 earthquake. The recorded data are presented, followed by the data completeness check.

Sensor data capture: Figure 6-4 shows a summary of data from the 15 sensors, indicating that the community stations in the Lower North Island recorded the earthquake. It specifically shows the filtered vertical ground motion recorded over a duration of 85 seconds from 22-09-2022:21:07:15, including PGA values calculated for the initial three seconds following P-wave detection (PGA_3), overall PGA

for the earthquake event, and station distances from the epicentre; PGA values were determined based on the absolute maximum vertical acceleration recorded.

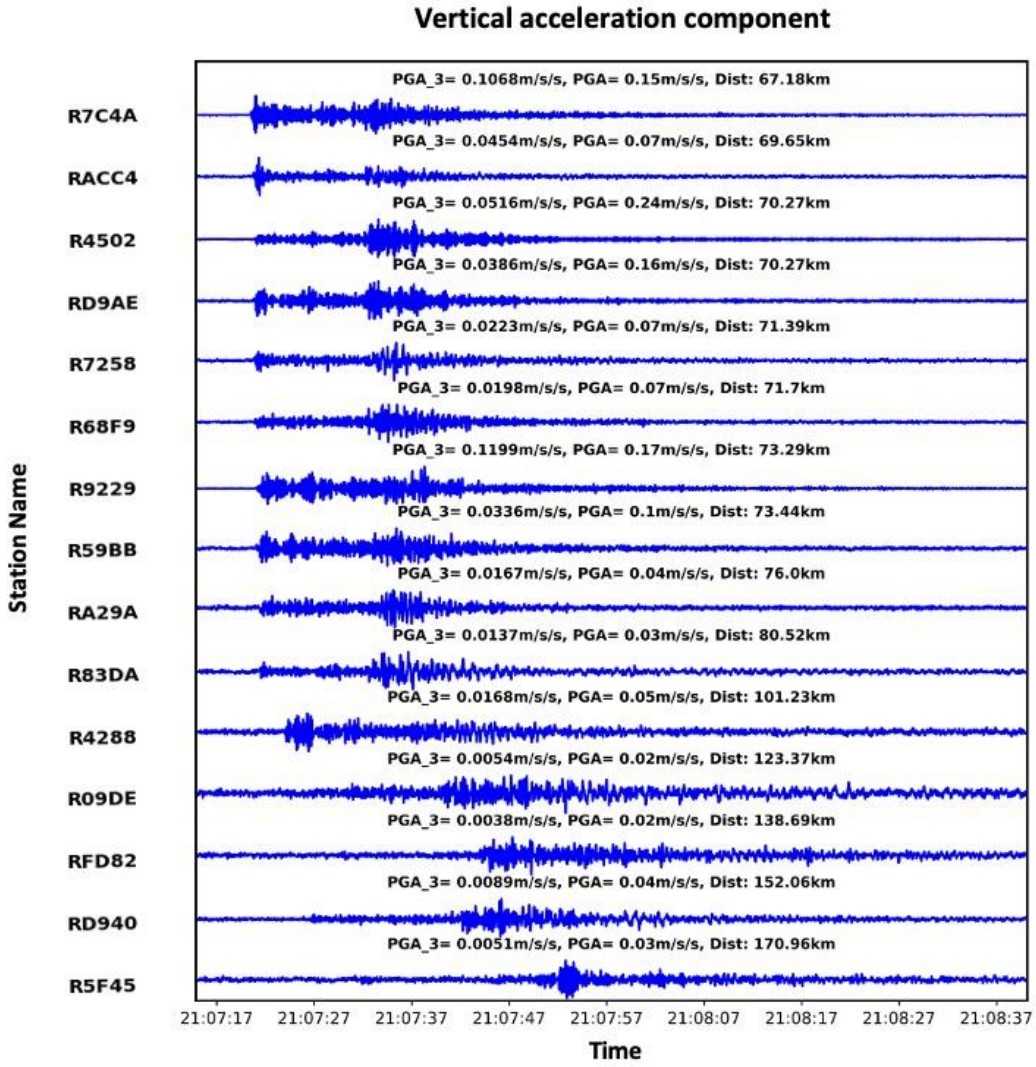

Figure 6-4. The figure displays the vertical ground motion acceleration data recorded for the M5.8 earthquake which is used for testing the performance of the chosen P-wave detection algorithms. Also, provided the PGA measured during the first three seconds after the detection of the P-wave (PGA_3), followed by the overall PGA reported for the earthquake (PGA), along with the corresponding epicentral distances. The following scaling ranges (in m/s/s) are used for the waveform shown: stations R7C4A, R9229, and R59BB from -0.2 to 0.2; stations RACC4, R7258, and R68F9 from -0.1 to 0.1; stations RA29A, R83DA, R4288, R09DE, RFD82, RD940, and R5F45 from -0.05 to 0.05; station R4502 from -0.5 to 0.5; station RD9AE from -0.25 to 0.25.

Data completeness: Due to unknown technical issues with the RS server where the data are collected, some data packets were dropped while the RS sensors sent their data to the database. Through appropriate communication, this issue was brought up and validated with the RS technical team. To overcome the issue of missing data, we used the obspy miniSEED stream merge feature along with the linear interpolation option to interpolate the data for the missing packets (Krischer et al., 2015). The method allowed us to interpolate data for the absent packets and mitigate the impact of missing data by

constructing continuous trends within the 10-minute data blocks. Interpolation can influence phase-picking algorithms, and we considered this during our analysis. We manually examined each false and missed detection and did not count those instances caused by data gaps. Despite these efforts, around 170 blocks were still missing from all 15 stations. This was less than 4% of the total data downloaded for this study. Despite the limitation, most of the data were still usable to evaluate the EEWS.

The data captured from the 15 sensors show promise, with preliminary results indicating that the implemented community-engaged EEW network can record earthquakes of interest to EEW. However, there is a need of analysing the systems' performance by evaluating the potential number of missed and false detections generated by this system.

6.2.6.2 Performance of the Selected Algorithms

Before analysing the missed and false detections using the recorded ground motion data, the processing time (i.e., computational delay) of the selected P-wave detection algorithms in detecting the P-waves was calculated. This was to see whether the algorithms will perform effectively in the context of EEW. One-hundred simulations were performed on a 15-second data frame. The average data processing time to detect P-waves for all four algorithms was less than 50 milliseconds, which is exceptionally efficient for EEWSs.

At first, the performance of the four P-wave detection algorithms was investigated by analysing the number of missed detections. Since all 15 sensors in the network captured the earthquake ground motion data, we had fifteen recordings (one from each sensor) for the particular earthquake, as shown in Figure 6-4. For each algorithm, a maximum of 15 missed detections can be reported since the number of sensors used for this study is 15. Table 6-4 presents the total missed detections per algorithm, cross-tabulated with the six stations furthest away from the centre (greater than 80 km from the epicentre).

Table 6-4. Missed detections reported along with their stations, epicentral distance, PGA values reported within the 3 seconds of P-wave detection, and the selected algorithms.

Station Name	Distance from the Epicentre (km)	Reported PGA Values (ms^{-2})	Missed Detections			
			STA/LTA	Recursive STA/LTA	Kurtosis-based P-wave Picker	Wavelet-based P-wave Picker
R83DA	80.52	0.0137	0	1	0	1
R4288	101.23	0.0168	0	0	0	0
R09DE	123.37	0.0054	1	1	1	1
RFD82	138.69	0.0038	1	1	1	1
RD940	152.06	0.0089	1	1	1	0
R5F45	170.96	0.0051	1	1	1	1

Station Name	Distance from the Epicentre (km)	Reported PGA Values (ms^{-2})	Missed Detections			
			STA/LTA	Recursive STA/LTA	Kurtosis-based P-wave Picker	Wavelet-based P-wave Picker
Total missed detections			4	5	4	4

Table 6-4 shows that the four algorithms performed similarly in terms of missed detections, with four or five out of the fifteen stations reporting missed detections. The recursive STA/LTA resulted in the highest number of missed detections, while the STA/LTA, wavelet-based P-wave picker and Kurtosis-based P-wave picker had the lowest number of missed detections.

Notably, only stations with a distance greater than 80 km from the epicentre recorded missed detections. Table 6-4 does not include the first nine stations within the 80 km radius from the epicentre as the data from those stations did not report any missed detections (i.e. each algorithm detected the P-waves correctly in the stations located 80 km or less from the epicentre). For stations R09DE, RFD82, and R5F45, all the detection algorithms missed detecting the P-waves from the earthquake data. This was due to the low PGA values reported that make the P-waves difficult to detect compared to other stations' data. Even though station R4288 is located more than 100 km from the epicentre, all algorithms detected the P-waves without any failure due to its higher PGA value compared to other stations in Table 6-4.

The table demonstrates that among the tested fifteen stations for all four algorithms, five stations (R83DA, R09DE, RFD82, RD940, R5F45) exhibited missed detections, with distances from the epicentre exceeding 80 km. Since the earthquake in this study only had moderate intensity, the shaking recorded by the stations further away from the epicentre (> 80kms) was comparatively low due to seismic wave attenuation. However, station R4288 is an exception for this scenario due to its larger-than-expected PGA value. This can be due to various causes such as wave path, local shallow site conditions, and building design and construction (Sokolov et al., 2012). With these observations, detecting P-waves becomes challenging if the wave is small in amplitude, to begin with, or if it has travelled a large distance from the source.

6.2.6.3 Evaluation of Algorithms Through Analysis of False Detections

After analysing the missed detections, we next tested the performance of the four algorithms by analysing the false detections. Table 6-5 summarises the false detections generated by each of the selected algorithms from the ground motion data captured by the 15 stations. The results show that the wavelet-based P-wave picker produces the least false detections (21), followed by the recursive STA/ LTA Algorithm (58), the standard STA/ LTA Algorithm (133), and the Kurtosis-based P-wave picker (184).

Table 6-5. False detections reported with the selected algorithms

Station Name	Standard STA/ LTA Algorithm	Recursive STA/ LTA Algorithm	Kurtosis-based P-wave Picker	The Wavelet-based P-wave Picker
R7C4A	1	0	7	0
RACC4	0	0	5	0
RD9AE	0	0	19	0
R4502 - noisy	46	16	7	9
R7258	0	0	1	0
R68F9	0	0	59	0
R9229	2	1	0	1
R59BB	1	1	1	0
RA29A - noisy	53	34	4	8
R83DA	1	0	1	0
R4288 - noisy	19	3	55	0
R09DE	3	0	11	0
RFD82	5	3	11	2
RD940	0	0	2	1
R5F45	2	0	1	0
Total False Detections	**133**	**58**	**184**	**21**

Most (86%) of the false detections from the standard STA/LTA algorithm were generated from three stations (mentioned noisy in Table 6-5). R4502, RA29A, and R4288 caused most of the false detections (46, 53, and 19, respectively), while the rest of the stations performed relatively well by generating five or fewer false detections. It is possible that the installation methods and sites of the three sensors could have affected their performance.

The same length of STA, LTA windows and ratio were applied for the recursive STA/LTA algorithm. The total number of false detections reported with this algorithm was 58, which is less than half of those reported with the standard STA/LTA algorithm. Further, the three stations (R4502, RA29A, R4288) show a significant reduction in the number of false detections compared to the standard STA/LTA algorithm, from 46 to 16, 53 to 34, and 19 to 3 false detections, respectively. This shows that the recursive STA/LTA significantly reduces false detections even with problematic stations. The reduction in false detections is due to its dynamic adaptation of STA value according to the changes in the seismic signals. In Figure 6-5, we present 60 seconds of vertical ground motion recordings captured by the noisy station R4502, along with the corresponding characteristic functions recorded for the STA/LTA ratio using both the standard STA/LTA (Figure 6-5-b) and the recursive STA/LTA (Figure 6-5-c) algorithms.

The comparison clearly demonstrates the superior noise-handling capabilities of the recursive STA/LTA algorithm over the standard STA/LTA. The characteristic function generated by the recursive STA/LTA algorithm exhibits smaller and smoother fluctuations compared to the standard STA/LTA algorithm. This smoother behaviour can be attributed to the decaying exponential impulse response employed by the recursive method. Unlike the rectangular impulse response used in the standard STA/LTA, the decaying exponential response ensures that the recursive algorithm recovers faster from large energy transients or transient noise spikes (Withers et al., 1998). Consequently, as observed in our results, this may result in the standard STA/LTA triggering false detection due to noise exceeding the set threshold whereas no false detections were reported by the recursive STA/LTA algorithm.

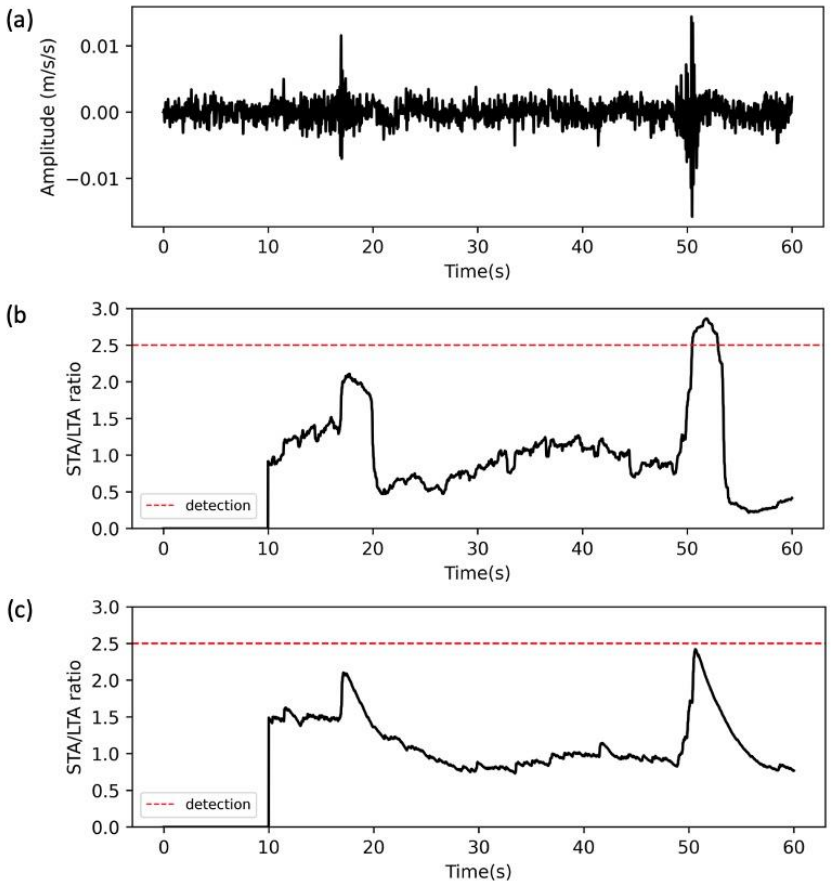

Figure 6-5. (a) Vertical ground motion recordings captured by station R4502 for a 60-second time frame starting at 6.56 am on September 22, 2022. (b) Characteristic function of the STA/LTA ratio recorded using the standard STA/LTA method. (c) Characteristic function of the STA/LTA ratio recorded using the recursive STA/LTA method.

Figure 6-6 shows the ground motion data and their respective STA/LTA ratio characteristic function for the standard and recursive STA/LTA algorithms for 10mins (600 seconds) ground motion data from the stations R4502, RA29A and R4288. It can be seen that the number of false detections reported with the standard STA/LTA algorithm for each of the three stations' data decreased considerably with the recursive STA/LTA algorithm. Station R4502 data with standard STA/LTA reported three false detections (Figure 6-6-a), whereas it only reported one with the recursive STA/LTA algorithm (Figure

6-6-b). Similarly, for the stations RA29A and R4288, the recursive STA/LTA performed better, from generating seven false detections (Figure 6-6-c) to four false detections (Figure 6-6-d) for RA29A, and from generating one false detection (Figure 6-6-e) to zero false detections (Figure 6-6-f) for R4288.

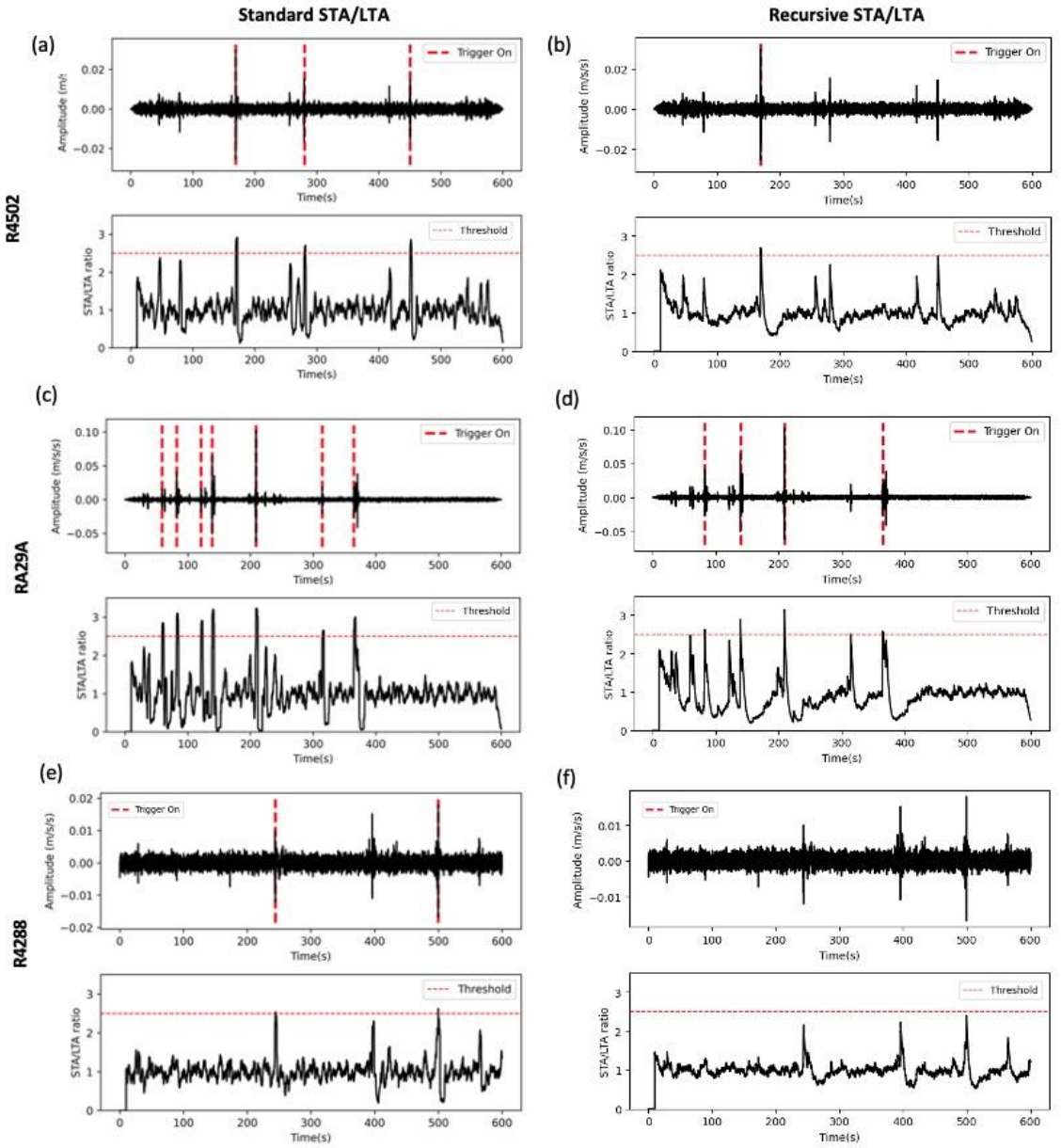

Figure 6-6. (a), (c) and (e) shows the false detections recorded with the standard STA/LTA algorithms for the stations R4502, RA29A and R4288, over a 10-minute data frame, respectively, whereas (b), (d) and (f) shows the false detections with the recursive STA/LTA algorithm.

The kurtosis-based P-wave picker algorithm performed the worst among the four algorithms tested. It reported 184 false detections during the evaluation. All stations except R9229 generated at least one false detection (See Table 6-5). Station R68F9 generated as many as 59 false detections within the testing period; in comparison, it performed well with the STA/LTA algorithms generating no false detections. The kurtosis-based P-wave picker produced the greatest number of false detections in this

study. Even though this algorithm has shown greater accuracy in detecting earthquakes and P-waves in other studies, no study has tested this algorithm's performance in a noisy environment (Baillard et al., 2014). Noise and data quality can be a concern arising from community-based EEW systems where researchers do not fully control the installation of the sensors.

The wavelet-based P-wave picker algorithm performed best, reporting only 21 false detections, a notable reduction compared to the other three algorithms. The wavelet-based P-wave picker algorithm reduces the number of false detections even more than the recursive STA/LTA algorithm. Figure 6-7 shows the number of false detections reported with the ground motion data from the noisy stations R4502, RA29A and R4288 within the same 10-minute timeframe as Figure 6-6. In Figure 6-7, the three noisy stations generated only one or no false detections. The frequency of false detections was significantly reduced compared to other chosen algorithms.

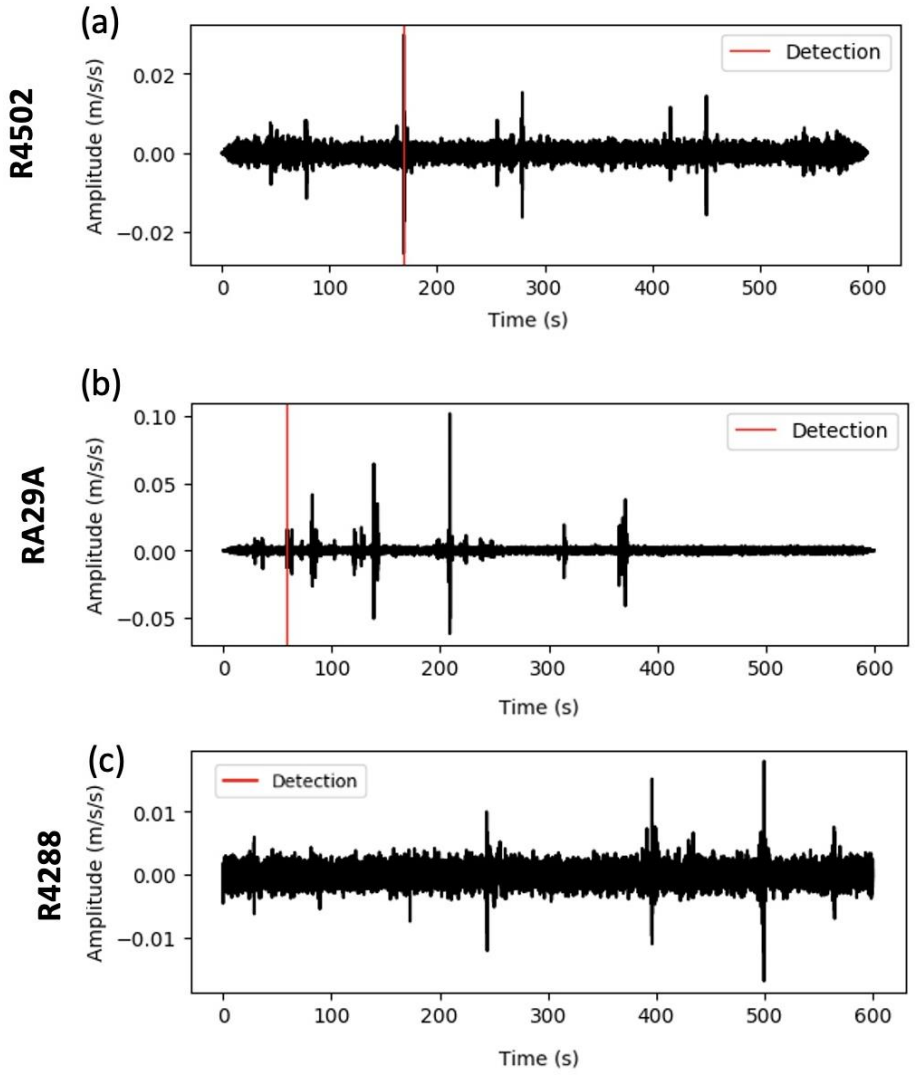

Figure 6-7. (a), (b) and (c) shows the false detections recorded with the wavelet-based P-wave picker for the noisy stations R4502, RA29A and R4288 over a 10-minute data frame, respectively.

The analysis of false detections showed that the wavelet transformation-based P-wave picker is the most suitable among the four P-wave detection algorithms as it produced the smallest number of false detections.

Following that, we conducted an initial study on noise within the community-engaged network to identify the frequency range and duration of spikes observed in the recorded data. The initial noise analysis revealed that the spikes noticed in the sensor data had durations varying from 1 second to 4 seconds, and their frequency content, as indicated by the spectrogram of the signal and power spectral density estimation, mainly fell within the range of 0 to 40 Hz. A significant concentration of frequencies was observed in the band between 10 to 30 Hz.

The literature shows that low-cost MEMS-based sensors, particularly Raspberry Shake 4D sensors, exhibit higher internal noise levels than high-end seismometers (Anthony et al., 2019). Given these limitations, implementing a community-engaged network using MEMS sensors poses challenges, especially when information regarding installation methods and site specifics is limited. Inadequate installation practices may increase noise in the EEWS. These elevated noise levels in the network can impact the suitability of P-wave detection algorithms commonly used in the literature, such as the standard STA/LTA, recursive STA/LTA, and kurtosis-based P-wave pickers. These algorithms might not provide optimal performance for our community-engaged network due to the specific noise characteristics observed.

Therefore, based on the results of the case study here, it is clear that the wavelet-based P-wave picker is the most appropriate P-wave detection algorithm for the experimental community-engaged EEWS, where the community members install the ground motion sensors without any influence or guidance from the researcher. This outcome aligns with the literature, showing that utilising a wavelet transformation-based P-wave picker can effectively detect P-waves in the presence of noisy data with fast processing capabilities (Hafez et al., 2010, 2013, 2020). The study's findings suggest that implementing a community-engaged low-cost EEWS can become a promising option by selecting an appropriate P-wave detection algorithm which is capable of reducing the occurrence of false and missed detections, even when dealing with noisy stations installed in unknown environmental and installation contexts.

Limitations and Future Work

The contribution of the work presented in this paper is to evaluate which P-wave detection algorithm would minimise missed and false detections in EEWs with instruments in potentially noisy environments. While the current investigation determined a wavelet-based P-wave picker to be the most

effective P-wave detection algorithm for the community-engaged EEWS, 21 false detections within 48 hours remain noteworthy. This quantity, equivalent to an average of one false detection every 2 hours, is potentially concerning in maintaining users' confidence in the system. A possible solution to be investigated is to include multiple stations in detecting an earthquake (Brooks et al., 2021; Cochran et al., 2009). In addition, another promising avenue for investigation involves implementing a filter-bank method to distinguish seismic signals from noise, building on the work of Chung et al. (2019) and Meier et al. (2015). In our approach, we intend to conduct an in-depth noise analysis to define specific frequency bands that can effectively identify seismic signals. Once the P-wave is detected, we are planning to employ a trigger filter and perform essential checks to confirm whether the received signal corresponds to a genuine seismic event or a non-seismic signal. This process may involve converting the signal into velocity or displacement for further assessment. Also, we are planning to analyse false alerts triggered by the community-engaged network as a system rather than a single station. We hypothesise that introducing multi-station triggering along with the proposed algorithm can reduce the number of false detections even further, making a citizen-seismology-based EEWS more feasible.

The results obtained from this performance analysis hold a pivotal role in guiding the selection of the most suitable P-wave detection algorithm for our forthcoming work. In this next phase, we plan to integrate the chosen P-wave detection algorithm with the PLUM algorithm in our experimental community-engaged EEWS setup. Currently, our network utilises the PLUM EEW algorithm (Prasanna et al., 2022), which has become popular due to its robustness, lightweight design and easy-to-implement nature, to detect ground shaking (Kodera et al., 2018). This integration can potentially extend the warning time beyond PLUM's threshold-based approach for detecting shakings. This proposed future integration could potentially be achieved by establishing an empirical relationship between P-wave and S-wave intensities tailored to the context of NZ. Future studies on this integration can help define a threshold for PLUM to issue earthquake alerts. The integration of PLUM and P-wave detection algorithm has been undertaken by Kodera (2018) in the Japan EEW context, where a P-wave detection algorithm was coupled with the PLUM framework, demonstrating that such an approach can effectively enhance the warning time for seismic events. Future studies applied in the context of NZ and in community-engaged networks could further support Kodera's (2018) approach.

In addition, the work here only evaluated four P-wave detection algorithms. However, the performance analysis method used in this study can also be applied to other P-wave algorithms identified by Chandrakumar, Prasanna, Stephens, Tan, et al. (2022). Unfortunately, most P-wave detection algorithms in the literature are not openly accessible nor available for implementation other than the ObsPy trigger algorithms. Making the algorithms open source will be helpful for the research community to understand and analyse their performance more easily. The proposed performance analysis method can

also be used to measure the performance of location-based dynamic threshold calculations for wavelet-based P-wave pickers. Another future research area should investigate dynamically changing the earthquake detection thresholds, as it could be a feasible solution to reduce false detections due to environmental noise in the sensor locations.

Another limiting factor in the outcomes of this work is the uncertainty surrounding the actual noise level in our community-hosted sensor network. While we have conducted a preliminary noise analysis to identify the frequency range and duration of spikes in the data, a comprehensive study on noise is warranted for a more thorough understanding. This future study will consider various factors, including sensor location, orientation, data quality, environmental influences, and the time of day, to gain deeper insights into the specific noise characteristics present in our network. By doing so, we aim to tailor the chosen P-wave detection algorithm according to the noise profile of our network, thereby improving the accuracy and reliability of our EEWS.

In addition to the noise analysis, future research should focus on investigating the usability, application, and utilisation of the sensors by citizen seismologists. Addressing potential false detections will involve examining the sensor installation methods and site locations chosen by the community hosts. Engaging with citizen seismologists will prove instrumental in designing a best-practice installation and user guide for the sensor hosts within our community-engaged EEWS.

Finally, even though this study discussed the missed detections reported by the four algorithms using a single earthquake data set, a comprehensive study on missed detections would need more data using a large database of earthquakes. A future study will evaluate the chosen P-wave detection algorithms using a larger dataset, such as the GeoNet earthquake database (GNS Science, 2022), and the fine-tuning and adaptation of the selected algorithms will undergo further refinement and adjustment to suit a more comprehensive range of earthquake scenarios in future testing.

6.2.7 Conclusion

This study analysed four P-wave detection algorithms using data from an experimental citizen seismology-based low-cost EEWS. The citizen seismology-based EEWS used for this study was entirely hosted by volunteers; the research team did not know the sensor location and installation method. This study used data from the experimental network, particularly looking at a 48-hour time window around a M5.8 earthquake. The results show that selecting an appropriate P-wave detection algorithm can reduce the number of missed and false detections, even with noisy sensors. The study findings have shown the wavelet-picker algorithm as the more suitable option for detecting P-waves in community-engaged EEWS. However, it is important to note that the limitations identified in the study

need to be addressed before confidently generalising that an algorithm as the most appropriate. More importantly, the obtained results here suggest that citizen-seismology-based EEW is capable of detecting events of interest to EEW, and selecting an appropriate algorithm can potentially reduce false and missed alerts generated by the system. In addition, further research and testing are needed to evaluate the feasibility and effectiveness of citizen-seismology EEWSs fully. Future studies should research further on how to improve citizen seismology-based EEW systems by investigating multi-station triggering, dynamically changing thresholds, and enhancing citizen seismologists' user experience and engagement. Further studies can also extend this work by applying the methods used in this study to different use cases and larger datasets.

6.3 Chapter Summary

Chapter 6 focused on identifying the most suitable P-wave detection algorithm for integration with the NZ-PLUM algorithm to enhance the warning time within the community-engaged EEW network. The first section provided a literature review detailing various approaches to P-wave detection and methods for estimating S-wave amplitude using initial P-waves in different EEWSs for earthquake magnitude estimation. Building on the insights gained from this review, the second section selected four P-wave detection algorithms appropriate for decentralised processing. These algorithms were evaluated based on their performance regarding false and missed detections, using 48 hours of data from the community-engaged network, including an earthquake case study. The evaluation concluded with the recommendation of the wavelet-based P-wave picker as the most effective algorithm for detecting P-waves within the implemented network.

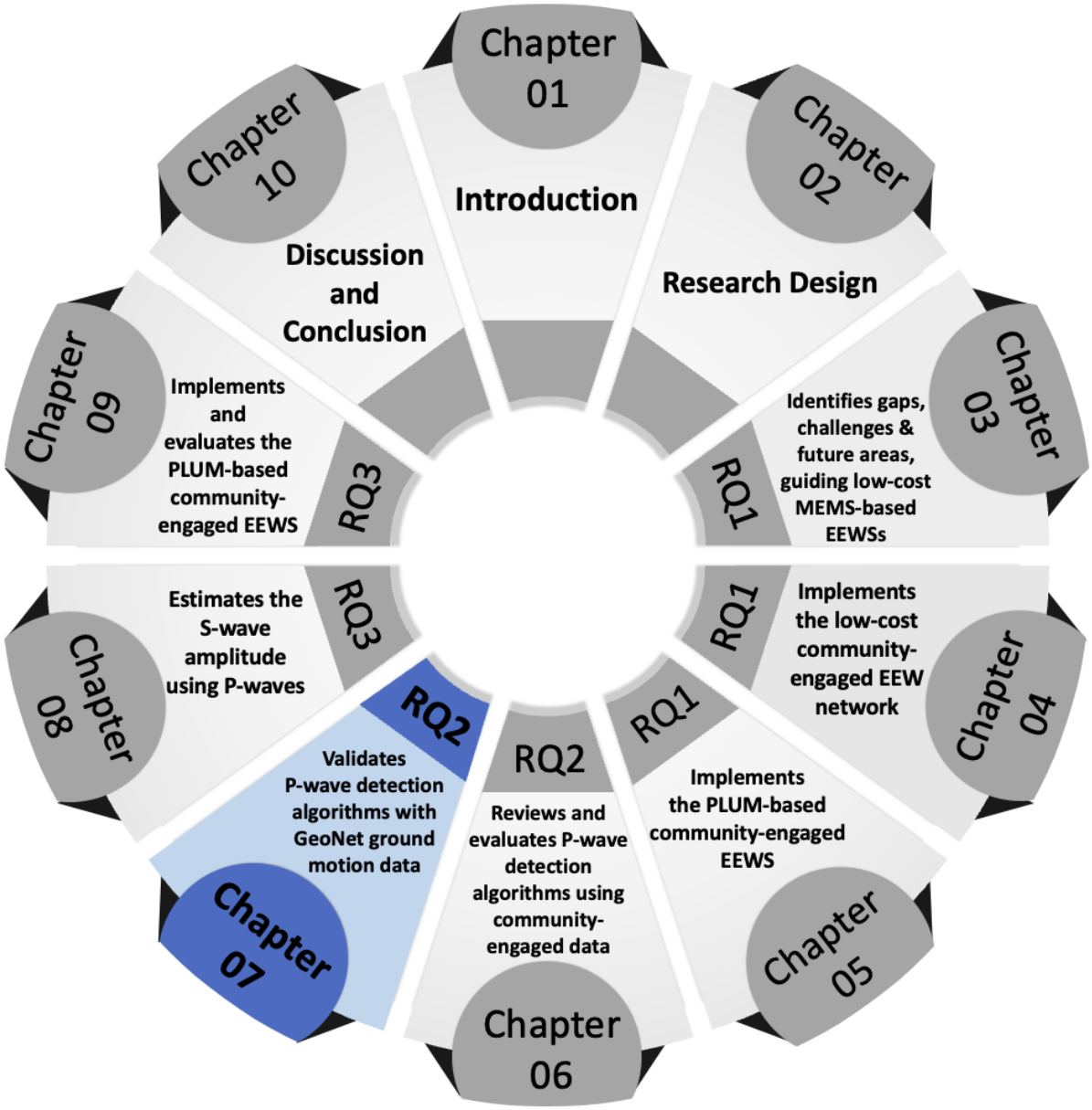
Chapter 01
Introduction
Chapter 02
Research Design
Chapter 03
Identifies gaps, challenges & future areas, guiding low-cost MEMS-based EEWSs
RQ1
Chapter 04
Implements the low-cost community-engaged EEW network
RQ1
Chapter 05
Implements the PLUM-based community-engaged EEWS
RQ1
Chapter 06
RQ2
Reviews and evaluates P-wave detection algorithms using community-engaged data
Chapter 07
RQ2
Validates P-wave detection algorithms with GeoNet ground motion data
Chapter 08
RQ3
Estimates the S-wave amplitude using P-waves
Chapter 09
RQ3
Implements and evaluates the PLUM-based community-engaged EEWS
Chapter 10
Discussion and Conclusion

MASSEY UNIVERSITY
TE KUNENGA KI PŪREHUROA
UNIVERSITY OF NEW ZEALAND

GRADUATE RESEARCH SCHOOL

STATEMENT OF CONTRIBUTION
DOCTORATE WITH PUBLICATIONS/MANUSCRIPTS

We, the candidate and the candidate's Primary Supervisor, certify that all co-authors have consented to their work being included in the thesis and they have accepted the candidate's contribution as indicated below in the *Statement of Originality*.

Name of candidate:	CHANTHUJAN CHANDRAKUMAR
Name/title of Primary Supervisor:	Aprof. Raj Prasanna
In which chapter is the manuscript /published work:	7

Please select one of the following three options:

(●) The manuscript/published work is published or in press

- Please provide the full reference of the Research Output:

Chandrakumar, C., Tan, M. L., Holden, C., Stephens, M. T., & Prasanna, R. (2025). Evaluating P-Wave detection algorithms for earthquake early warning: insights from GeoNet data in Canterbury, Aotearoa New Zealand. Earth Science Informatics, 18(1). https://doi.org/10.1007/s12145-024-01519-9

( ) The manuscript is currently under review for publication – please indicate:

- The name of the journal:

Springer Earth Science Informatics

- The percentage of the manuscript/published work that was contributed by the candidate: 80.00

- Describe the contribution that the candidate has made to the manuscript/published work:

Chanthujan Chandrakumar conceptualised the article, co-constructed the methodology, and conducted the formal analysis and investigation. He also wrote the first draft of the manuscript.

( ) It is intended that the manuscript will be published, but it has not yet been submitted to a journal

Candidate's Signature:	Chandrakumar Chanthujan — Digitally signed by Chandrakumar Chanthujan Date: 2024.08.14 13:45:27 +12'00'
Date:	14-Aug-2024
Primary Supervisor's Signature:	Raj Prasanna — Digitally signed by Raj Prasanna Date: 2025.03.03 11:00:31 +13'00'
Date:	3-Mar-2025

This form should appear at the end of each thesis chapter/section/appendix submitted as a manuscript/ publication or collected as an appendix at the end of the thesis.

7 Validation of the P-wave Detection Algorithms with GeoNet Ground Motion Data

This chapter presents the fifth manuscript for publication titled, "Evaluating P-Wave Detection Algorithms for Earthquake Early Warning: Insights from GeoNet Data in Canterbury, Aotearoa New Zealand". This study delves into the performance of four P-wave detection algorithms, explicitly focusing on their late and missed detections by evaluating the frequency and accuracy of P-wave detections across a broader range of earthquake scenarios using GeoNet's MEMS-based sensor network installed in the Canterbury region.

The research was conducted to meet Objective 2.3 of this thesis: To validate the results obtained from Objective 2.2 using a more comprehensive ground motion dataset.

The article presented in this chapter was published in 2024 in the Springer Earth Science Informatics Journal:

Chandrakumar C, Tan ML, Holden C, Stephens MT, Prasanna R. 2024. Evaluating P-Wave Detection Algorithms for Earthquake Early Warning: Insights from GeoNet Data in Canterbury, Aotearoa New Zealand. Submitted to the Springer Earth Science Informatics Journal.

7.1 Abstract

What is the most effective P-wave detection algorithm for an Earthquake Early Warning (EEW) system that minimises false, late and missed detections? This study evaluates the performance of four distinct P-wave detection algorithms in terms of their detection accuracy. Utilising a MEMS-based ground motion dataset from the GeoNet network, this study analyses the algorithms' performances by introducing four distinct pick deviation categories. Among the evaluated algorithms, the wavelet-based P-wave picker is identified as the most suitable and accurate for EEW systems, achieving a 98.3% success rate with a mean deviation of 0.12 s and a standard deviation of 0.63 s compared to the manual pick. This algorithm proves effective for both community-engaged and traditional EEWSs. The methodology used for performance comparison in this research is applicable to other regions and datasets, aiding in selecting more accurate and reliable P-wave detection algorithms. The study suggests extending this performance analysis to encompass a broader spectrum of traditional and modern algorithms in future research.

7.2 Introduction

Regions at tectonic plate boundaries experience significant seismic activity globally, posing substantial risks to populations and infrastructure. Aotearoa New Zealand (NZ), situated at the convergence of the Australian and Pacific tectonic plates, is characterised by significant seismic activity. The nation experiences over one hundred earthquakes of magnitude four or greater annually (GeoNet, 2023). Despite this heightened seismic risk, NZ lacks a comprehensive National Earthquake Early Warning System (EEWS) to provide timely alerts to the public and emergency responders (Becker, Potter, Prasanna, et al., 2020).

Globally, there is a growing trend towards developing economically viable EEWSs, often using low-cost micro-electromechanical systems (MEMS)-based ground motion sensors. These systems have seen successful implementations in regions such as Taiwan (Y. M. Wu et al., 2013) and the Sichuan-Yunnan border in China (Peng et al., 2019), with experimental applications in California (Clayton et al., 2015) and Costa Rica (Brooks et al., 2021). Additionally, low-cost sensors have facilitated citizen seismology, engaging communities in seismic monitoring and enhancing public engagement and sensor distribution at reduced costs (Finazzi, 2020; Subedi et al., 2020).

To enhance earthquake preparedness in NZ, the CRISiSLab team at Massey University has developed an innovative, community-engaged EEWS (Prasanna et al., 2022). This experimental system is distinctive in its use of decentralised processing for earthquake detection and alert generation, operating

on low-cost MEMS-based Raspberry Shake 4D (RS4D) seismographs. By opting for decentralised processing over a centralised approach, the system reduces the time required to issue alerts, thereby providing a longer warning window for end users. This approach enhances the system's resilience against central system failures during earthquakes and lowers operational costs associated with maintaining sophisticated central processing systems. Despite these sensors' limited processing power and memory, the system effectively processes seismic data within a network hosted by community members' homes, primarily across the Greater Wellington region.

However, community-engaged EEWS, while offering cost benefits, are challenged by high noise levels due to sensor placement in diverse domestic environments (Chandrakumar et al., 2023). These noise levels can increase false, late, and missed detections. A false alert occurs when noise is incorrectly identified as an earthquake at a single station, a late detection refers to picking up P-waves later in their arrival, and a missed alert happens when an actual P-wave is not detected by the algorithm (Brooks et al., 2021). These challenges significantly impact the reliability and effectiveness of EEWS (Brooks et al., 2021; Kohler et al., 2020; Minson et al., 2019; Suárez et al., 2009).

Integrating a robust P-wave detection algorithm into the system could be a feasible solution to mitigate these issues. This would help reduce false, late, and missed detections at individual stations, ultimately improving the overall performance of the EEWS. In a previous study, Chandrakumar et al. (2023) compared four different P-wave detection algorithms—two traditional, widely used methods and two newer algorithms gaining popularity for their accuracy and reliability. Despite the availability of machine learning-based P-wave pickers in the literature (Chandrakumar, Prasanna, Stephens, Tan, et al., 2022), this study did not select them due to the decentralised processing approach employed in the CRISiSLab EEWS, which relies on low-cost sensors with limited processing power and memory. Machine learning algorithms, while powerful, often require substantial computational resources and memory, making them unsuitable for this specific application. Thus, only lightweight (low computational power) algorithms were chosen for this comparison.

The previous study (Chandrakumar et al., 2023) introduced a lightweight P-wave detection algorithm to minimise false and missed detections at individual stations, leading to fewer false and missed alerts in the overall EEWS. The study evaluated these four algorithms using 48 hours of community-engaged ground motion data and a single earthquake scenario. However, the limited dataset restricted a comprehensive assessment of the algorithms' performance, particularly regarding late and missed detections.

To address this limitation, this study statistically investigates the performance of the same four P-wave detection algorithms across a broader range of earthquake scenarios, utilising GeoNet's MEMS-based

sensor network in the Canterbury region, focusing primarily on detection accuracy. This research identifies a robust P-wave detection algorithm that effectively minimises late and missed detections at individual stations. This contributes to any EEWSs implemented globally and developing reliable and robust community-engaged EEWS in NZ. Furthermore, this study establishes a methodology for statistically evaluating the performance of different P-wave detection algorithms.

The structure of this article is organised as follows: Section 7.3 provides a detailed explanation of the methodology used in this study, outlining the approach taken to analyse the performance of the algorithms. Section 7.4 presents the results obtained from the analysis of the P-wave detection algorithms. Section 7.5 discusses the key findings derived from the study, along with any identified limitations, and highlights potential areas for future research and improvement. Finally, Section 7.6 serves as the conclusion, summarising the primary outcomes and implications of the research.

7.3 Method

This study evaluates the performance of P-wave detection algorithms using GeoNet's Canterbury sensor network data (Berrill et al., 2011). The method includes selecting the sensor network and the data collection process, choosing and fine-tuning algorithms, describing the manual pick tool, and the performance analysis metrics used for evaluation.

7.3.1 Ground Motion Sensors Selected for This Study

This study utilised data from the Canterbury region, NZ, a location selected due to its significant seismic history and the impact of past earthquakes (Stevenson et al., 2011, 2017). The research employed data from the Canterbury Network (CanNet), a cost-effective strong motion network established by GeoNet before the 2010-2011 Canterbury earthquake sequence. CanNet features MEMS-based accelerometers, which are adept at recording ground motions (Berrill et al., 2011). Figure 7-1 illustrates the seismic stations and epicentre locations of the chosen earthquakes within the Canterbury region that are analysed for this study.

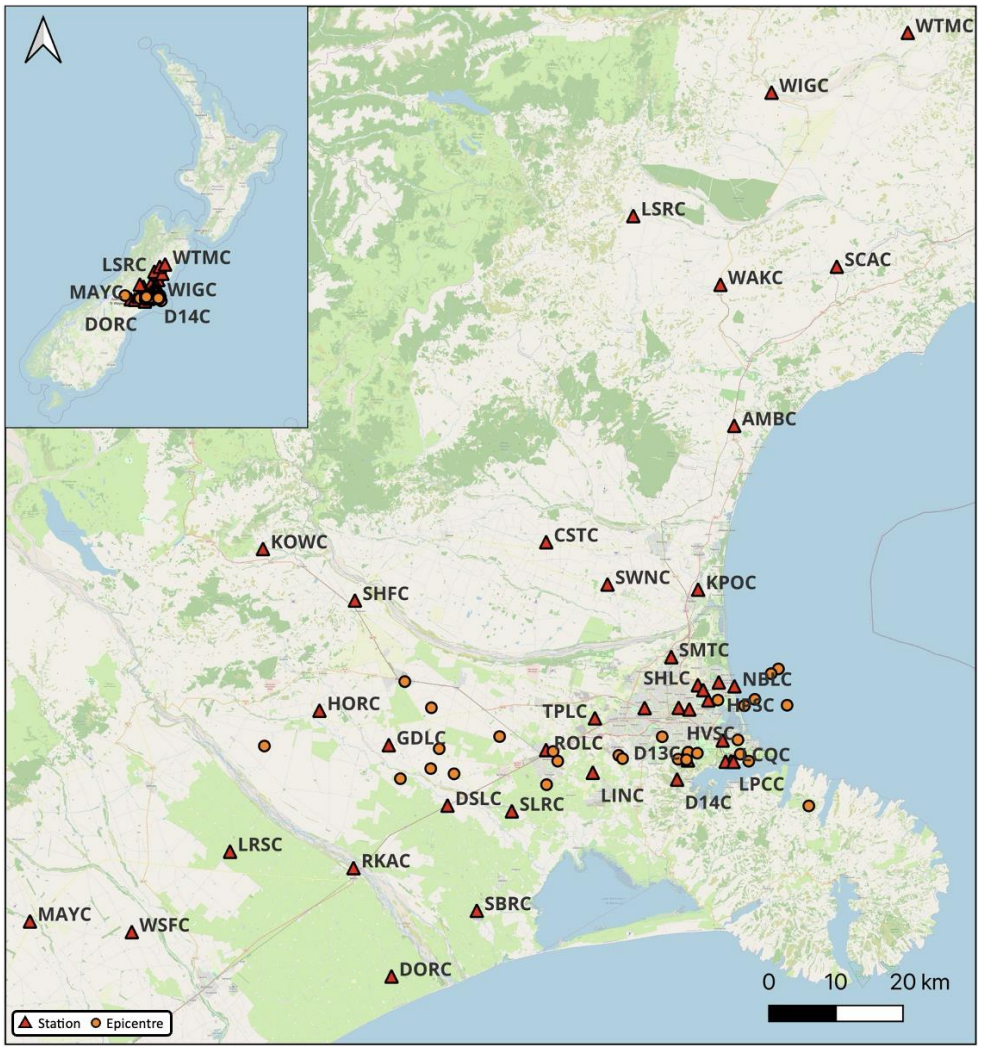

Figure 7-1. CanNet seismic stations and epicentre locations for this study.

7.3.2 Data Collection Process and Data Pre-processing

The Canterbury region of NZ experiences significant seismic activity, with 26 magnitude 5 (M5) or higher events recorded during 2010 and 2011. This study compiles a dataset of 46 earthquakes from January 1, 2010, to December 31, 2011, with magnitudes ranging from M3 to M7.2. Twenty events between M3 and M5 are selected, along with all occurrences of ground shaking above M5. Depending on the shaking caused by the earthquake, the number of stations capturing data ranges from 1 to 35.

Ground motion data is sourced directly from the GeoNet database in miniseed format. A primary limitation of this data is its focus exclusively on seismic events, capturing ground motion data immediately before and after an earthquake.

7.3.3 Description of the P-wave Detection Algorithms Compared in the Study

This study revisits and fine-tunes four P-wave detection algorithms previously analysed by Chandrakumar et al. (2023), encompassing traditional and advanced approaches. The traditional algorithms include the Standard Short-Term Average/Long-Term Average (STA/LTA) and Recursive STA/LTA, which are widely acknowledged for their ability to discern P and S waves through amplitude variations. Additionally, two more recent algorithms are explored: the Kurtosis-based P-wave picker and the Maximum Overlap Discrete Wavelet Transformation-based P-wave picker, representing advancements in statistical and time-frequency domain analysis for P-wave detection.

To ensure analysis consistency and comparison integrity, the P-wave detection algorithms were adapted and fine-tuned according to the methodology outlined in Chandrakumar et al. (2023). Below is a summary table (Table 7-1) offering an overview of the selected algorithms for this research, along with their adaptations and fine-tuning details.

Table 7-1: P-wave detection algorithms overview, as discussed in Chandrakumar et al. (2023).

Selected Algorithms	Description and Reference	Adaptation and Fine-tuning Details
The standard STA/LTA	Employs two moving windows (STA and LTA) to compare short-term energy to long-term seismic wave energy, triggering P-wave identification when the ratio exceeds a certain threshold (R. V. Allen, 1978).	The STA and LTA window lengths are set to three and ten seconds, respectively, with a chosen STA/LTA ratio of 2.5 to optimise detection accuracy while limiting false detections.
Recursive STA/LTA – Decaying constant	Builds on the STA/LTA method by using a decaying exponential impulse response for quicker recovery from energy changes, avoiding the need for extensive data storage in memory (Withers et al., 1998).	
Adopted Kurtosis-based P-wave picker	Automates P- and S-wave detection using kurtosis-derived characteristic functions and eigenvalue decompositions, relying on three-dimensional acceleration data (Baillard et al., 2014).	The seismic signal is segmented into 3-second windows for kurtosis calculation, identifying the P-wave based on maximum kurtosis.

Selected Algorithms	Description and Reference	Adaptation and Fine-tuning Details
Adopted maximum overlap wavelet-based P-wave picker	Implements maximum overlap wavelet transformation with "Daubechies-1 (db1)" wavelet function, utilising squared first-stage detail from the transformation for earthquake detection (Hafez et al., 2013).	The maximum value of the "db1" coefficient reported during the first eight seconds of the waveform has been selected as the threshold and checked for a consistent threshold exceedance in the upcoming data to detect the P-waves.

For an in-depth understanding of these algorithms, their comprehensive descriptions and technical details are provided in the previous study by (Chandrakumar et al., 2023).

7.3.4 Manual Pick Tool

In this study, the Manual P-wave Pick tool, developed by the author, plays a crucial role in assessing the performance of various P-wave detection algorithms. The tool is designed with three primary functions essential for effective P-wave analysis:

1. **Picking P-wave Arrival Time:** Users manually inspect each waveform to identify the start of the P-wave, focusing on the vertical acceleration component due to its prominence in P-wave detection (Y. M. Wu, 2019).

2. **Calculation of PGA for P-waves:** After identifying the start of the P-wave, the tool allows users to set a time window—using preset or custom durations—to calculate the Peak Ground Acceleration (PGA) based on the maximum vertical acceleration recorded within the chosen window.

3. **Padding Noise Data for Processing:** The tool addresses the challenge of the GeoNet data's focus on earthquake events by enabling users to extend the noise data through an artificial padding function. Users can specify a noise segment duration to be replicated and combined with the existing data, creating a dataset exceeding the 10-second noise requirement. This padding process only applies to earthquake data with sufficient noise before or after the seismic event.

These functionalities are integral to accurately detecting and analysing P-waves, ensuring that the data used in comparing algorithms is reliable and sufficient. For a more detailed walkthrough of the tool,

including step-by-step instructions and screenshots, please refer to the dedicated GitHub page: Manual P-wave Pick Tool GitHub.

7.3.5 Evaluation Metrics Used to Compare the Algorithms

The first step of the analysis is to filter the recorded ground motion data using a Butterworth-Bandpass filter from 0.1 to 20Hz to retain the earthquake signal's high-frequency content of interest and remove the low-frequency and high-frequency ambient noise (Claerbout, 1964; Virtanen et al., 2020). Then, the P-wave arrival times detected by each algorithm are then compared to those from the manual tool. Then, the deviations are calculated by subtracting the algorithm-detected time from the manually picked time. Negative deviations, indicating that the algorithm detected the P-wave earlier than the manual method, are considered efficient. However, it is essential to note that such early detections by algorithms might occasionally reflect human error in manual picking (W. Zhu et al., 2023; W. Zhu & Beroza, 2019). Conversely, positive deviations, which suggest a delay in detection, are seen as less desirable, and their significance diminishes as the deviation increases.

Deviations are categorised into four intervals for analysis, as outlined below:

1. **Accurate Picks:** Deviations within -0.5 to +0.5 seconds are exact, indicating the algorithm's effective detection timing compared to manual picks.
2. **Acceptable Picks:** Picks falling within a 0.5 to 1-second deviation are deemed acceptable, showing reasonable accuracy.
3. **Delayed Picks:** These are defined by a deviation of 1 to 3 seconds, indicating a significant delay in detection.
4. **Missed Detections:** Any pick beyond a 3-second deviation or undetected by the algorithm is classified as missing.

Figure 7-2 visually illustrates the type of deviations considered in this study by defining the picks reported by the manual picking tool as reference.

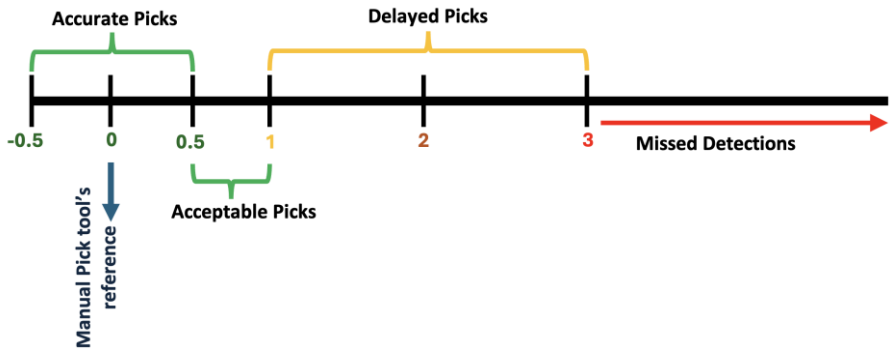

Figure 7-2. The categories of deviations considered in this study compared to the manual pick tool.

7.3.6 Statistical Analysis of Deviations Using Mean, Standard Deviation, and Test of Independence

To evaluate the deviations between the P-wave detection algorithms and the manual picks, the study calculates each algorithm's mean and standard deviation, using the manual picks as the benchmark. A lower mean deviation indicates higher accuracy, while a lower standard deviation signifies consistent performance.

A chi-square test of independence is also employed to assess the relationship between the type of algorithm used and the categorisation of its P-wave picks into Accurate, Acceptable, Delayed, and Missed detections. This statistical method evaluates whether the differences in pick classifications are significantly associated with the specific algorithms used.

7.4 Results

Initially, data from stations recording the chosen 46 earthquakes are input into the manual pick tool to select P-wave details such as arrival time and PGA, as outlined in Subsection 7.3.4. Waveforms lacking noise data or clear earthquake signals are excluded during the tool's inspection. This filtering yields 478 ground motion records.

The first subsection (Section 7.4.1) presents the results obtained with the chosen algorithms, explicitly focusing on the picking deviations introduced in Section 7.3.5. This is followed by Section 7.4.2, which discusses the statistical analysis conducted.

7.4.1 Performance Analysis of P-wave Detection Algorithms

The standard STA/LTA algorithm results in 398 accurate and 55 acceptable picks, with five missed detections and 20 delayed picks out of 478 potential detections. Similarly, the recursive STA/LTA algorithm performs strongly, identifying 412 accurate picks, 45 acceptable picks, 14 delayed picks, and seven missed detections.

The Kurtosis-based P-wave picker achieves 430 accurate picks and 16 acceptable picks, but it also reports ten late picks and 23 missed detections.

The wavelet-based P-wave picker, the fourth algorithm in the analysis, demonstrates the highest number of accurate picks at 444 and reports 26 acceptable picks, two delayed picks, and six missed detections, indicating strong potential for operational use.

Figure 7-3 provides a bar chart summarising the pick deviations for each algorithm, visually representing the frequency and types of deviations encountered.

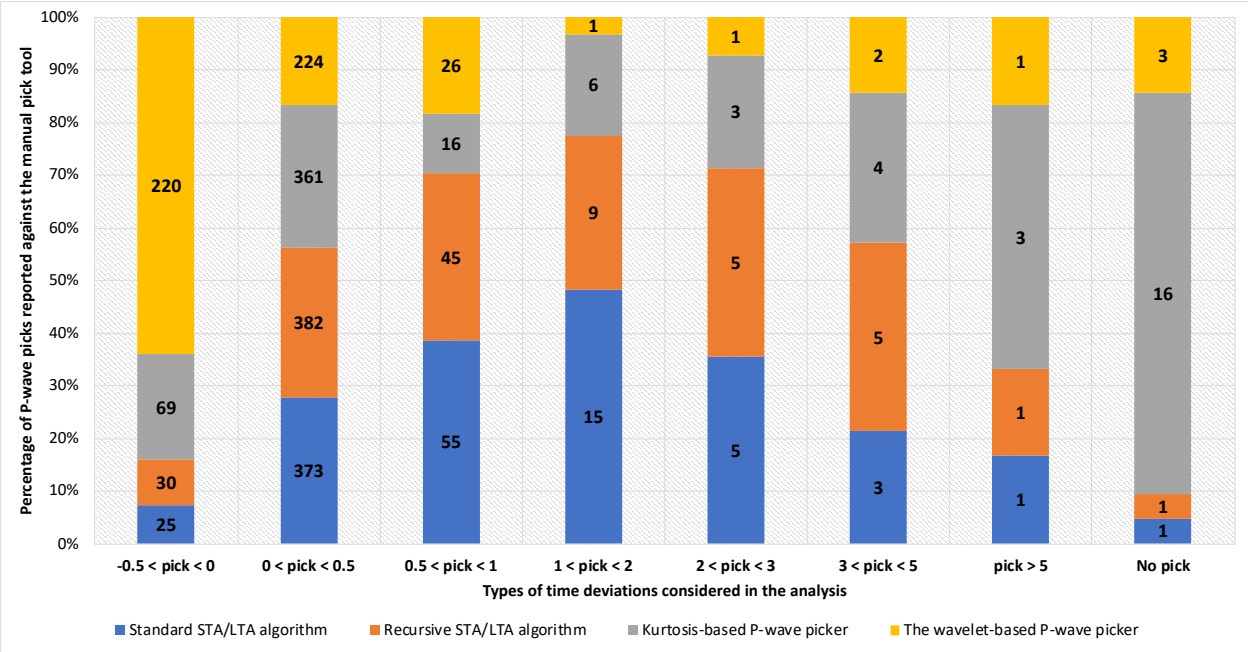

Figure 7-3. This chart illustrates the performance of four P-wave detection algorithms against the manual picking tool, showcasing the number of accurate, acceptable, delayed, and missed detections for each algorithm.

The comparative summary of Accurate, Acceptable, Delayed, and Missed picks is depicted in the bar chart provided in Figure 7-4. Upon analysing the efficacy of four distinct P-wave detection algorithms, a clear trend emerges: the standard STA/LTA algorithm reported the fewest Accurate picks, capturing about 83% of the total P-wave recordings. In contrast, the Wavelet-based P-wave picker demonstrated more promising performance, correctly identifying approximately 93% of the P-waves. The other two algorithms, the recursive STA/LTA and the Kurtosis-based P-wave picker fell between these extremes, reporting 86% and 90% Accurate picks, respectively.

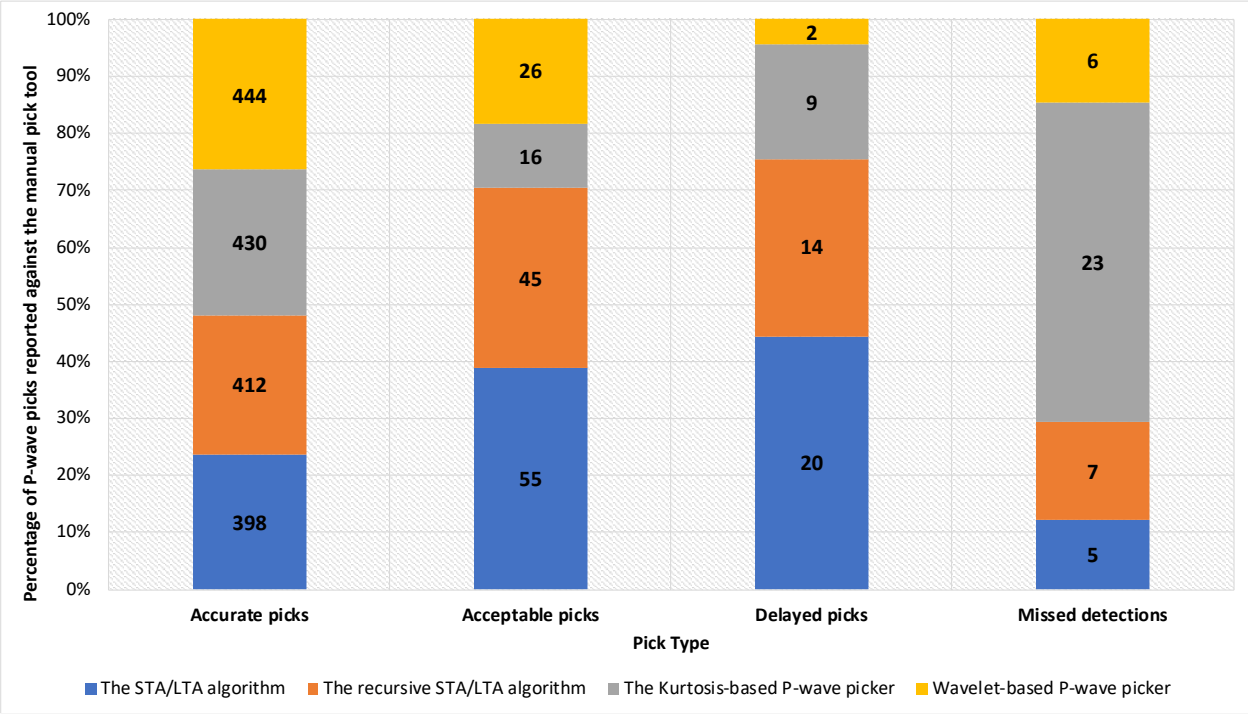

Figure 7-4. This chart visualises the proportion of Accurate, Acceptable, Delayed, and Missed picks for four different P-wave detection algorithms.

7.4.2 Mean and Standard Deviation Analysis of Picking Deviations

The performance of the chosen algorithms is evaluated through an analysis of the mean and standard deviation of each algorithm's picking deviations. Initially, 478 cases were considered, but cases with no P-wave detection were excluded from the analysis for each algorithm, and the remaining cases are used for evaluation (refer to Table 7-2 for each algorithm's sample size). The metrics from the manual pick tool serve as the benchmark, setting its mean and standard deviation values at zero, thus providing a baseline for deviation measurements.

Upon examining the standard deviation of the deviations across the algorithms, the wavelet-based P-wave picker exhibits the lowest value (0.63 s), indicating minimal variability in its deviation outcomes compared to the other three algorithms. However, more than relying solely on the standard deviation for comparison is required, especially since the evaluation is against the manual pick tool. The mean of the deviations is crucial, as it directly reflects each algorithm's proximity to the manual pick values, making it a more critical measure for determining algorithmic accuracy. Table 7-2 presents the mean and standard deviation for the four algorithms along with the manual pick tool.

Table 7-2. The sample size, the mean and the standard deviation of the deviations for the manual pick, the Standard STA/LTA, the Recursive STA/LTA, Kurtosis-based P-wave picker and the Wavelet-based P-wave picker algorithms

Algorithm	Sample size	Mean (s)	Standard deviation (s)
The manual pick tool	478	0	0
The standard STA/LTA	477	0.36	0.64
Recursive STA/LTA	477	0.34	0.69
Kurtosis-based P-wave picker	462	0.26	0.90
Wavelet-based P-wave picker	475	0.12	0.63

The analysis of mean deviations indicates that the wavelet-based P-wave picker algorithm exhibits the closest mean deviation to the manual pick, recorded at 0.12 s. In contrast, the standard STA/LTA, Recursive STA/LTA, and Kurtosis-based P-wave picker algorithms show higher mean deviations of 0.36 s, 0.34 s, and 0.26 s, respectively. These results suggest that the wavelet-based P-wave picker consistently aligns P-wave detection times most closely with the manual picks. Figure 7-5 presents the kernel density estimates for the deviations, illustrating each algorithm's comparative precision and reliability in detecting P-wave arrival times.

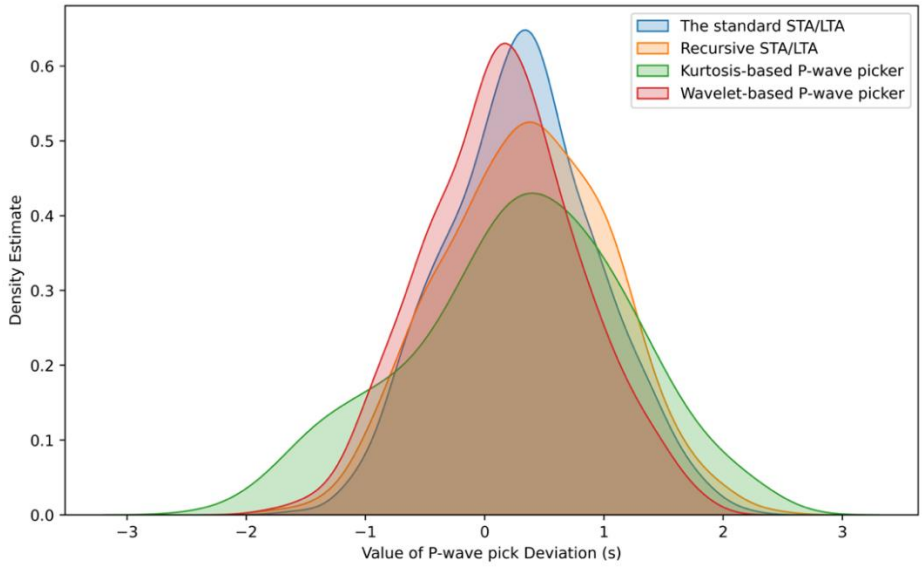

Figure 7-5. Kernel Density Estimates for P-wave detection algorithms displaying the deviation distributions for each algorithm, colour-coded for clarity: Standard STA/LTA (blue), Recursive STA/LTA (orange), Kurtosis-based P-wave Picker (green), and Wavelet-based P-wave picker (Red)

7.4.3 Test of Independence

A chi-square test is employed to investigate the association between the four algorithms and categorising P-wave picks into Accurate, Acceptable, Delayed, and Missed detections.

The chi-square results indicate a significant relationship between these variables, x^2 (df = 9, N = 1912) = 66.28, p = 8.13E-11. This minimal p-value signifies a statistically significant association between the algorithms and the types of picks. This suggests that the observed performance differences among the algorithms are unlikely to have occurred by chance alone. Therefore, there is a substantial relationship between the algorithms and the various types of picks.

Overall, the comparative analysis of the picking accuracy of four different P-wave detection algorithms recommends the wavelet-based P-wave picker as the most accurate algorithm for P-wave detection. It demonstrates the highest average accuracy relative to manual picks and exhibits the least variability in its deviation from those picks.

7.5 Discussion

This study has significant implications for EEWS within NZ and globally. By systematically evaluating the performance of four P-wave detection algorithms using a dataset from the GeoNet sensor network in the Canterbury region, this research provides critical insights into improving the accuracy and reliability of EEWS.

One of this study's key findings is the identification of the wavelet-based P-wave picker as the most effective algorithm for detecting P-waves. This algorithm demonstrates the highest average accuracy and minimal variability in its deviation from manual picks, making it a robust choice for implementation in EEWS. With a high success rate of 93% and 444 accurate picks (98.3% for both accurate and acceptable picks), compared to the commonly used standard STA/LTA algorithm (Chandrakumar, Prasanna, Stephens, Tan, et al., 2022), which showed a success rate of 83.3% (94.8% for both accurate and acceptable picks), its potential for operational use is evident. This algorithm can be applied to any EEWS to reduce late and missed detections.

Building on findings from a previous study (Chandrakumar et al., 2023), which identified the wavelet-based P-wave picker as the optimal choice for P-wave detection in community-engaged EEWS due to its ability to minimise false detections using limited community-engaged ground motion data, this study further confirms its effectiveness. The current analysis, focusing on picking accuracy using GeoNet data, also endorses the wavelet-based P-wave picker for its notable accuracy. Synthesising outcomes

from both studies, the wavelet-based P-wave picker emerges as the preferred algorithm for P-wave detection in EEWS. This consistency in performance across various detection aspects highlights the algorithm's robustness and adaptability in picking P-waves well in both community-engaged and traditional EEWSs.

The study's focus on late and missed detections are crucial, as these directly impact the reliability and effectiveness of EEWS (Minson et al., 2019). Late detections may not provide adequate time for individuals and automated systems to take protective actions, potentially compromising safety (Nadin, 2020) whereas Missed detections leaves people and systems unprepared for the impending shaking which can lead to increased injuries, fatalities, and property damage and undermine end users' trust and diminish the overall efficacy of the warning system (Minson et al., 2019). By providing an analysis of picking deviations and employing robust statistical methods, such as mean and standard deviation analysis and the chi-square test of independence, this research offers a solid framework for comparing the performance of different P-wave detection algorithms. The results indicate that the wavelet-based P-wave picker aligns closely with manual picks and maintains consistency across various seismic scenarios.

Furthermore, this study addresses a gap in the existing literature by comparing different P-wave detection algorithms within the context of EEWS rather than primarily comparing newly proposed algorithms with the traditional and widely used STA/LTA algorithm (Baillard et al., 2014; Hafez et al., 2013; J. Kwon et al., 2018; Yanwei et al., 2021). The methodology used for performance comparison in this research can be applied to other regions and datasets, facilitating the selection of more accurate and reliable P-wave detection algorithms.

Overall, identifying the wavelet-based P-wave picker as the most accurate and reliable algorithm underscores its potential for enhancing the effectiveness of EEWS globally, particularly in decentralised processing approaches. Focusing on reducing false, late and missed detections is vital for maintaining the trust and reliability of warning systems. This research provides a robust framework for comparing P-wave detection algorithms, which can be applied to other regions and datasets, thereby advancing the development of more accurate and reliable EEWS worldwide.

7.5.1 Limitations and Future Works

While this study discusses the detection accuracy of P-wave detection algorithms for EEWS, several limitations must be acknowledged.

First, the evaluation focused on four specific P-wave detection algorithms, balancing traditional and contemporary approaches. Despite their relevance, numerous other detection methodologies exist, suggesting a scope for broader comparative research. Further, the analysis is based on 46 earthquake events from the Canterbury region of NZ, primarily limited to shallow crustal earthquakes. Future research should extend this evaluation to include offshore, subduction-related, and deep earthquakes, both within NZ and globally, to provide a more comprehensive assessment of P-wave detection algorithm performance.

Rigorous manual picking is conducted to aim for consistency. However, this approach introduces a degree of subjectivity, as manual picking depends on individual interpretation (W. Zhu et al., 2023; W. Zhu & Beroza, 2019), which could influence the benchmark used for algorithm comparison.

Furthermore, although false detections were analysed in the previous study using community-engaged EEW network data (Chandrakumar et al., 2023), this investigation did not extensively explore false detections where it focused on the picking accuracy. The decision was informed by the GeoNet network's proper sensor installation in low-noise sites and the limitation of having only triggered data, which primarily captures data around earthquake events within the chosen timeframe.

7.6 Conclusion

This study evaluates the performance of four P-wave detection algorithms using a dataset from the GeoNet sensor network in the Canterbury region of NZ. To ensure a robust evaluation, the study introduces a manual pick tool. The wavelet-based P-wave picker emerged as the most effective algorithm, achieving a 98.3% success rate with a mean deviation of 0.12 seconds and a standard deviation of 0.63 seconds, compared to the widely used STA/LTA algorithm, which showed a 94.8% success rate with a mean deviation of 0.36 seconds and a standard deviation of 0.64 seconds. This research is crucial as it addresses the critical issue of late and missed detections, which directly impact the reliability and user trust in EEWS. Further, this study provides a detailed comparative evaluation by employing mean and standard deviation analysis and the chi-square independence test. The comparative method offers a versatile framework for assessing a broader range of P-wave detection algorithms, enhancing the potential for future research. Identified limitations include the potential for human error during manual P-wave picking. Future research should leverage a more comprehensive array of traditional and contemporary algorithms, thereby advancing the development of reliable and precise EEWS globally.

Position of the reader

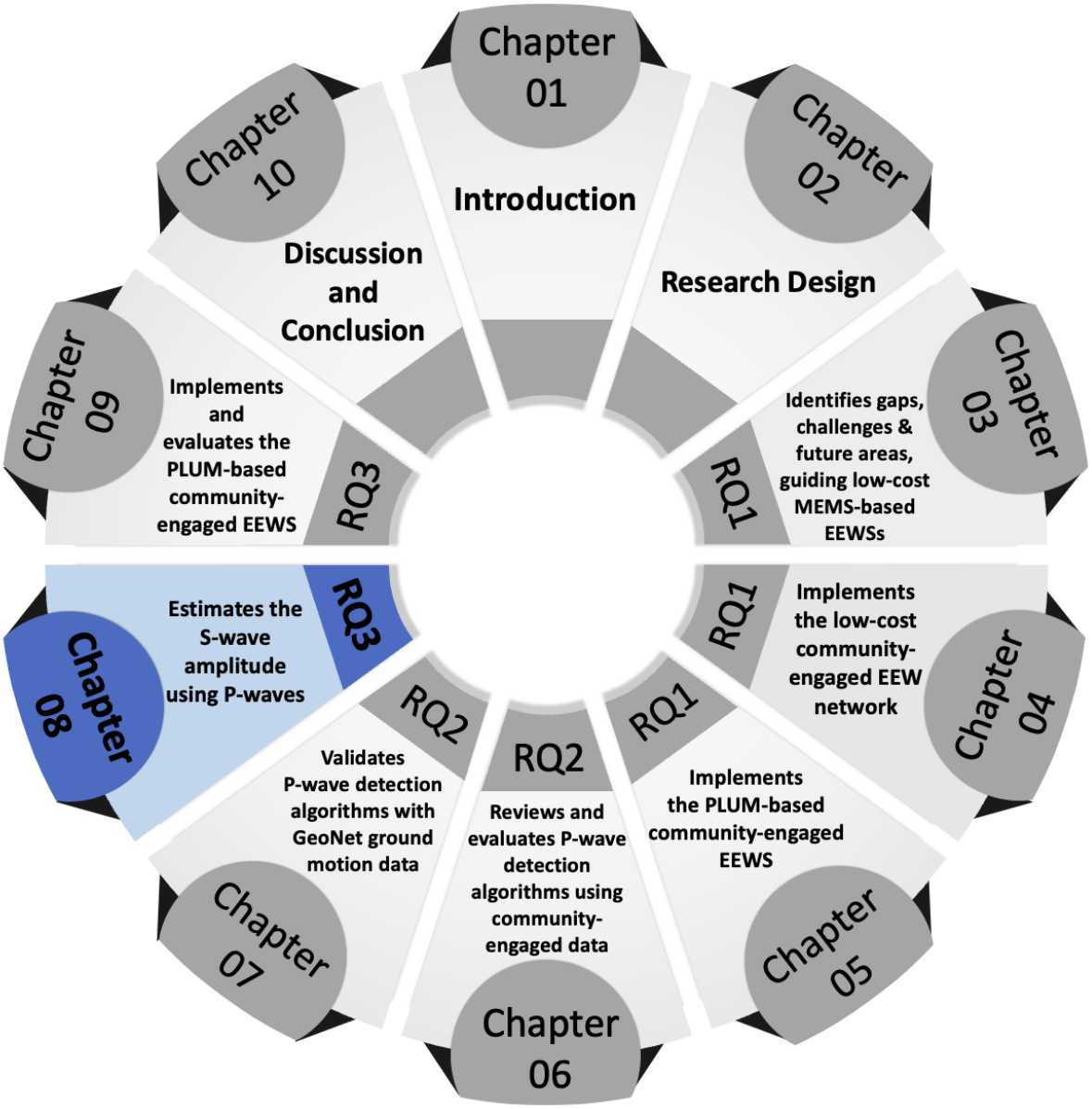

MASSEY UNIVERSITY
TE KUNENGA KI PŪREHUROA
UNIVERSITY OF NEW ZEALAND

GRADUATE RESEARCH SCHOOL

STATEMENT OF CONTRIBUTION
DOCTORATE WITH PUBLICATIONS/MANUSCRIPTS

We, the candidate and the candidate's Primary Supervisor, certify that all co-authors have consented to their work being included in the thesis and they have accepted the candidate's contribution as indicated below in the *Statement of Originality*.

Name of candidate:	CHANTHUJAN CHANDRAKUMAR
Name/title of Primary Supervisor:	Aprof. Raj Prasanna
In which chapter is the manuscript /published work:	8

Please select one of the following three options:

(●) The manuscript/published work is published or in press

- Please provide the full reference of the Research Output:

Chandrakumar C, Tan ML, Holden C, Stephens M, Punchihewa A, Prasanna R. 2024. Estimating S-wave amplitude for early earthquake warning in New Zealand: Leveraging the first 3 seconds of P-wave intensity. Springer Earth Science Informatics Journal.

( ) The manuscript is currently under review for publication – please indicate:

- The name of the journal:

Springer Earth Science Informatics Journal

- The percentage of the manuscript/published work that was contributed by the candidate: 80.00

- Describe the contribution that the candidate has made to the manuscript/published work:

Chanthujan Chandrakumar conceptualised the article, co-constructed the methodology, and conducted the formal analysis and investigation. He also wrote the first draft of the manuscript.

( ) It is intended that the manuscript will be published, but it has not yet been submitted to a journal

Candidate's Signature:	Chandrakumar Chanthujan Digitally signed by Chandrakumar Chanthujan Date: 2024.08.14 13:47:01 +12'00'
Date:	14-Aug-2024
Primary Supervisor's Signature:	Raj Prasanna Digitally signed by Raj Prasanna Date: 2024.08.21 11:14:13 +12'00'
Date:	21-Aug-2024

This form should appear at the end of each thesis chapter/section/appendix submitted as a manuscript/ publication or collected as an appendix at the end of the thesis.

8 Estimation of S-wave Amplitude Leveraging the Initial P-waves

This chapter presents the sixth manuscript of this study: "Estimating S-Wave Amplitude for Earthquake Early Warning in New Zealand: Leveraging the First 3 Seconds of P-Wave Intensity". This study explores the estimation of S-wave amplitude using the initial three seconds of the P-wave window for EEW, employing ground motion data from the GeoNet network in the Canterbury region. This investigation is conducted to fulfil Objective 3.1 of this thesis: Establish a relationship between the intensity of P-waves and S-waves in the context of New Zealand.

The article presented in this chapter was published in 2024 in the Springer Earth Science Informatics Journal as:

Chandrakumar C, Tan ML, Holden C, Stephens M, Punchihewa A, Prasanna R. 2024. Estimating S-wave amplitude for early earthquake warning in New Zealand: Leveraging the first 3 seconds of P-wave intensity. Springer Earth Science Informatics Journal.

8.1 Abstract:

This study addresses the critical question of predicting the amplitude of S-waves during earthquakes in Aotearoa New Zealand (NZ), a highly earthquake-prone region, for implementing an Earthquake Early Warning System (EEWS). This research uses ground motion parameters from a dataset comprising historical earthquakes in the Canterbury region of NZ. It explores the potential to estimate the damaging S-wave amplitude before it arrives, primarily focusing on the initial P-wave signals. The study establishes nine linear regression relationships between P-wave and S-wave amplitudes, employing three parameters: peak ground acceleration, peak ground velocity, and peak ground displacement. Each relationship's performance is evaluated through correlation coefficient (R), coefficient of determination (R^2), root mean square error (RMSE), and 5-fold Cross-validation RMSE, aiming to identify the most predictive empirical model for the Canterbury context. Results using a weighted scoring approach indicate that the relationship involving P-wave Peak Ground Velocity (Pv) within a 3-second window strongly correlates with S-wave Peak Ground Acceleration (PGA), highlighting its potential for EEWS. The selected empirical relationship is subsequently applied to establish a P-wave amplitude (Pv) threshold for the Canterbury region as a case study from which an EEWS could benefit. The study also suggests future research exploring complex machine learning models for predicting S-wave amplitude and expanding the analysis with more datasets from different regions of NZ.

8.2 Introduction

Earthquakes pose a significant hazard in Aotearoa New Zealand (NZ), one of the most seismically active regions globally (Anderson & Webb, 1994). Annually, over a hundred earthquakes of magnitude four or higher are recorded(GeoNet, 2023). The devastating impacts of significant seismic events, such as the 2010/2011 Canterbury sequence and the 2016 Kaikōura earthquake, underscore the urgent need for effective mitigation strategies (Potter et al., 2015; Stevenson et al., 2011, 2017). Earthquake Early Warning System (EEWS) emerges as a vital technology to reduce earthquake-related damages by providing advance alerts, yet NZ lacks an official national EEWS (Becker, Potter, Prasanna, et al., 2020). The GeoNet program, while serving as the official source of seismic information, does not provide early warnings (GeoNet, 2017; GNS Science, 2023). The absence of a formal EEWS is primarily attributed to the high costs associated with developing and maintaining such advanced systems, presenting a substantial challenge for their implementation in NZ (Brooks et al., 2021; Prasanna et al., 2022).

The increasing global interest in cost-effective EEWSs has led to the adoption of low-cost micro-electromechanical systems (MEMS)-based sensors. Since their introduction in the early 1990s (Holland, 2003), these sensors have been effectively utilised in seismic applications for real-time public alerting across various regions, including Taiwan (Y. M. Wu et al., 2013), China (Peng et al., 2019), California (Clayton et al., 2015), and Costa Rica (Brooks et al., 2021), albeit mostly in experimental setups. In NZ, the CRISiSLab team at Massey University has developed an experimental, community-engaged EEWS utilising Raspberry Shake 4D seismographs equipped with MEMS-based accelerometers (Prasanna et al., 2022). The system employs the Propagation of the Local Undamped Motion (PLUM) algorithm, known for its robustness and straightforward approach to detecting seismic activities and issuing alerts without the need to estimate seismic event characteristics (Chandrakumar et al., 2023).

A significant limitation of the PLUM algorithm is its maximum warning time of 10 seconds, primarily due to its reliance solely on S-wave detection. This study proposes addressing this limitation by leveraging the earlier arrival of P-waves (Kodera, 2018). A suitable P-wave detection algorithm has already been identified in a previous study (Chandrakumar et al., 2023), paving the way for this advancement. The system can capitalise on P-wave detection to extend warning times within the PLUM framework by establishing a reliable empirical relationship between P-wave and S-wave amplitudes (Kodera, 2018). This relationship offers two significant advantages. First, it enhances the effectiveness of the PLUM algorithm by providing more lead time for preparedness. Second, it enables the determination of P-wave thresholds for the early detection of significant shaking.

In this context, this research addresses a critical gap in NZ's EEWS capabilities by establishing robust empirical relationships between P-wave and S-wave amplitude parameters specific to the country's unique seismic landscape using linear regression models. Subsequently, the study identifies the most suitable empirical relationship for application in NZ's highly seismic Canterbury region. A case study utilising the chosen relationship is presented to define effective EEW alert thresholds for P-waves in the Canterbury region, demonstrating a practical application of the research findings.

The structure of this article is organised as follows: Section 8.3 provides a brief overview of the global literature on P-wave to S-wave amplitude relationships. Section 8.4 outlines the methodology employed in this research. Section 8.5 presents the results, which are discussed in Section 8.6 with respect to the established empirical relationships. Based on these findings, Section 8.7 introduces a case study that applies the selected empirical relationship to determine thresholds for felt earthquakes in New Zealand. Section 8.8 addresses the limitations of the study and suggests directions for future research, followed by Section 8.9, which offers a conclusive summary and highlights the key contributions of this research.

8.3 Background on P-wave and S-wave Amplitude Relationships

Researchers worldwide have explored various methods utilising P-wave measurements to estimate ground shaking, either by determining earthquake magnitude or predicting the amplitude of S-waves. One notable approach originated in Japan during the 1990s with the UrEDAS system, which pioneered the use of P-wave arrival to estimate earthquake magnitude and location (Nakamura, 2004). Following this, R. M. Allen & Kanamori (2003) introduced a method that estimates earthquake magnitude from the frequency content of P-wave arrivals.

In the Japanese seismic landscape, Yamamoto et al. (2008) introduced a new intensity parameter called M_I, showcasing that, for Japanese seismic data, P-wave intensity is consistently lower than S-wave intensity by approximately an M_I value of 1. Meanwhile, in Taiwan, researchers conducted an analysis of the relationship between P-wave and S-wave amplitude. They used various measurements from P and S waves, including Peak Ground Acceleration (Pa), Peak Ground Velocity (Pv), Peak Ground Displacement (Pd) and Period parameter (τ_c) from the 3 seconds following the P-wave detection, as well as Peak Ground Velocity (PGV) and Peak Ground Displacement (PGD) of S-waves for 26 damaging earthquakes (Y. M. Wu & Kanamori, 2005a, 2005b). Out of these parameters, they were able to select the most suitable relationship for their system, ultimately establishing Pd and τ_C thresholds for EEW. Further work investigated the relationship between Pd and PGV using records from Japan, Taiwan, and southern California (Y. M. Wu & Kanamori, 2008; Y. M. Wu & Mittal, 2021).

Researchers from USA, China and Italy contributed to advancing approaches by utilising Pd (measured within 3 s after P-wave detection) as a proxy for predicting PGV (Böse, Hauksson, Solanki, Kanamori, & Heaton, 2009; Caruso et al., 2017; Y. Wang et al., 2020; Zollo et al., 2014). In contrast, Colombelli et al. (2015) established an empirical relationship between three peak amplitude parameters of the P-wave window (Pa, Pv and Pd) and PGV.

While some studies suggest that predicting the ground shaking of an earthquake using just a few seconds of initial P-wave data is achievable (Olson & Allen, 2005; Zollo et al., 2006), others indicate that the estimation of ground shaking tends to saturate for larger events with longer rupture durations (Hoshiba et al., 2011; Rydelek & Horiuchi, 2006). Predicting the ground shaking of significant seismic events with limited real-time seismic data has become increasingly challenging due to the complexities involved. Larger crustal earthquakes with magnitudes (M) of 6, 7, and 8 are associated with fault lengths of about 10 km, 30 km, and 100 km, respectively, with rupture velocities close to of 3 km/s. Consequently, assuming a unilateral rupture, it could take up to 3, 10, and 30 seconds to rupture these faults completely (Wells & Coppersmith, 1994; Yamamoto et al., 2008). Also, it has become quite

challenging to determine the ground shakings of significant seismic events with limited real-time seismic data (Yamamoto et al., 2008). However, it is essential to note that these methods are still valuable for estimating lower bounds of expected ground shakings, aiding in the early assessment of earthquake strength (Kanamori, 2005).

These studies on P-wave and S-wave relationships worldwide have contributed significantly to improving EEW research. However, most of these findings are predominantly rooted in research outside NZ's unique geological and tectonic context. Therefore, researching and constructing a relationship between P and S-wave amplitude is crucial to successfully developing an EEWS tailored to NZ's unique geological and tectonic conditions. Findings in NZ also adds to the discourse in global research.

8.4 Method

8.4.1 Data Collection

The data for this study are strategically sourced from the Canterbury Region, NZ, chosen for its history of significant seismic activity and the notable impact of past earthquakes (Stevenson et al., 2011, 2017). This research utilises the Canterbury Network (CanNet), a low-cost strong motion network established by GeoNet before the 2010-2011 Canterbury earthquake sequence. CanNet is equipped with MEMS-based accelerometers designed to effectively record ground motions (Avery et al., 2004; Berrill et al., 2011). The selection of CanNet is deliberate, as its accelerometers closely match the response characteristics of the sensors used in the CRISiSLab EEWS. This ensures that the seismic data collected are reliable and relevant from a network mirroring the CRISiSLab EEWS.

The timeframe from 2010 to 2023 is chosen for data collection because it corresponds to the period during which GeoNet actively catalogued and recorded P-wave and S-wave picks for most of the CanNet recordings. This pre-existing identification of arrival times is critical. It significantly reduces the need for manual pickings across the numerous earthquake ground motion recordings.

The dataset compiled from this collection phase comprises 5254 earthquake waveforms captured from MEMS-based accelerometers, corresponding to 3245 earthquakes with a magnitude exceeding 3 ($M > 3$). Even though the data are limited, they serve the need to make a baseline for implementing a relationship between P and S-waves as an initial foundation. This focused dataset provides a strong foundation for investigating these relationships and advancing the operational capabilities of low-cost EEWSs.

8.4.2 Data Analysis

8.4.2.1 Data Inspection and Selection

The initial phase of the research involves an assessment of data quality to ensure the reliability of subsequent analyses. Each waveform from the 5254 records in the dataset is visually inspected during this phase. A specialised tool is developed to facilitate this inspection that allows for the individual review of waveforms (Figure 8-1). This tool generates four plots for each record, each serving a specific role in the inspection process. The first plot displays the vertical acceleration record, highlighting P and S-wave picks reported by GeoNet with distinctive red and blue vertical lines, facilitating precise waveform analysis (Figure 8-1-a). For a closer examination, the second plot provides an enlarged view of the absolute vertical acceleration record, focusing on a 5-second window around the P-wave pick to inspect the P-wave arrival (Figure 8-1-b). The third and fourth plots show horizontal acceleration records in the HNE: east component and HNN: north component directions, with the S-wave pick marked by a blue vertical line (Figure 8-1-c and 8-1-d).

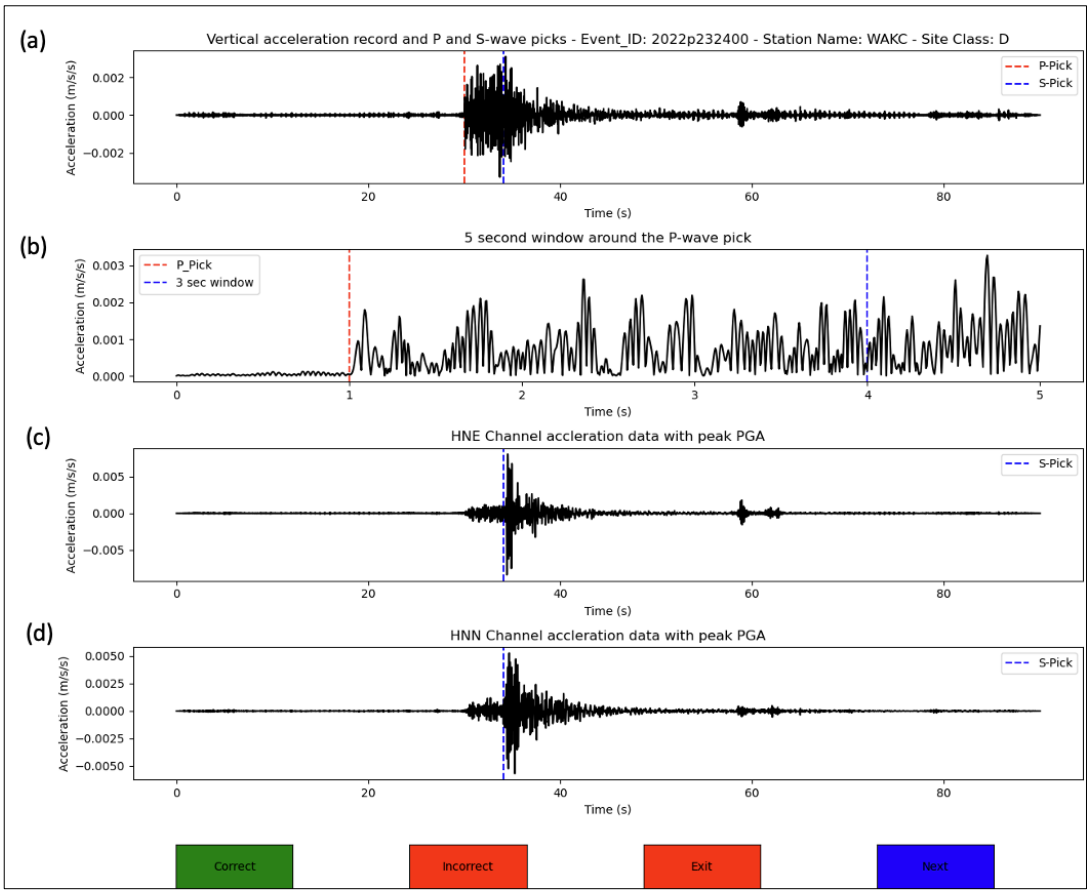

Figure 8-1. Interface of a seismic waveform inspection tool. (a) shows a vertical acceleration record with P and S-wave picks marked by red and blue lines, respectively. (b) displays an enlarged view of the absolute vertical record around the P-wave pick for detailed analysis. Panels (c) and (d) present horizontal acceleration records in the east (HNE) and north (HNN) directions, with S-wave picks indicated by blue lines.

During this phase, the focus is on verifying the accuracy of the P and S-wave picks recorded by GeoNet. Records with accurately identified picks are selected for further analysis, while those with erroneous picks are excluded. This process resulted in 4330 valid waveforms. Subsequently, these recordings are classified according to Site Classes defined for NZ based on soil characteristics (Dobry et al., 2000). The majority of the data belonged to Site Class D, and to maintain consistency in soil characteristics, only records from this class are retained, refined dataset of 3542 waveforms.

To ensure the relevancy and suitability of the data for the study, ground motion records are exclusively retained from stations situated within a 30-kilometre epicentral distance from each earthquake event, a selection criterion supported by previous research (Böse, Hauksson, Solanki, Kanamori, Wu, et al., 2009; Tsuno, 2021; Zollo et al., 2010). Two key considerations drove this strategy. First, it guarantees data relevancy, as P and S waves are less likely to be contaminated by other waves in the coda. Proximity to the epicentre enables the accurate detection of both P and S-waves. Second, data quality is enhanced closer to the epicentre due to a reduced noise-to-signal ratio, improving the precision of empirical relationships.

Additionally, a condition is imposed to include a maximum of four station records for each earthquake event. This filtering process results in the final selection of 763 earthquake events, with magnitudes ranging from 3 to 6.6, yielding 1,251 earthquake ground motion records suitable for further analysis. Figure 8-2 illustrates the Canterbury region chosen for this study, highlighting the seismic station locations and the epicentral locations of the earthquakes. Further, Table 8-1 summarises the earthquake magnitudes and the corresponding number of events.

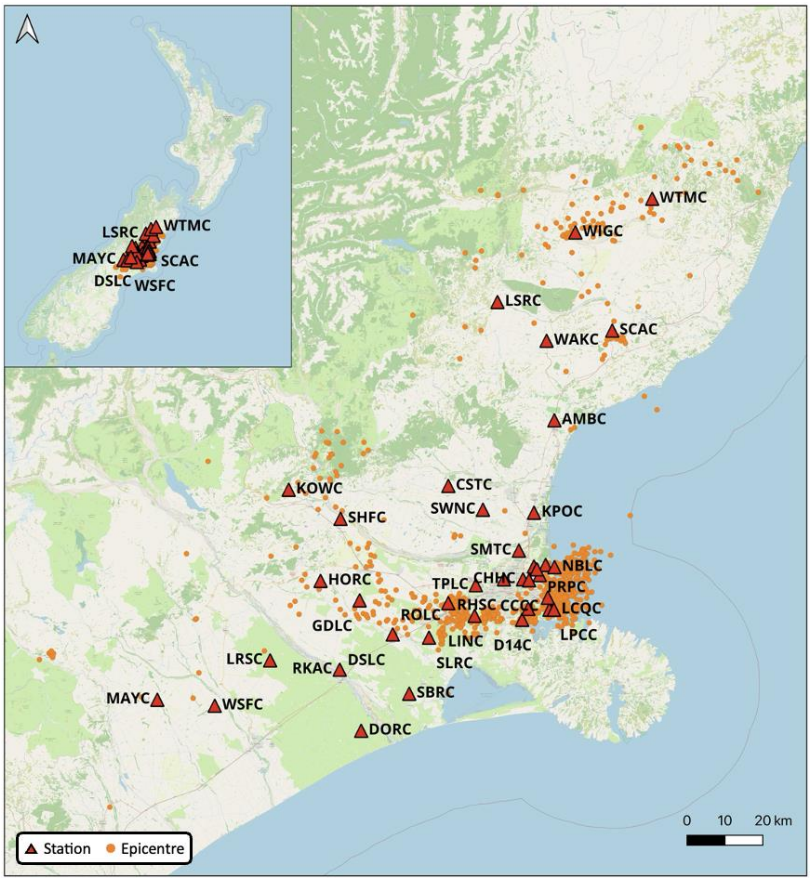

Figure 8-2. Map of the Canterbury region in NZ, showing the locations of seismic stations and the epicentres of selected earthquake events used in this study.

Table 8-1: Overview of Earthquake Magnitudes and Event Counts in the Dataset

Magnitude (M) range	Number of events
3 to 4	596
4 to 5	150
5 and above	17
Total	763

8.4.2.2 Data Allocation for Model Training and Evaluation

After filtering, the dataset is subjected to time-based splitting, where training and testing sets are selected based on their temporal order (Lyu et al., 2021). Time-based splitting ensures the model is trained on historical data and evaluated on new, unseen data. This allocation strategy facilitates model development and ensures a reliable evaluation using independent data.

I. Training Dataset: It consists of 1021 ground motion recordings of the filtered data from 2010 to 2019, which are used to develop the model.

II. Testing Dataset: It contains 230 recordings of the filtered data from 2020 to 2023, which are reserved for model evaluation.

8.4.2.3 Parameters Used for Analysis

The analytical focus of the study centred on two distinct time windows: the three-second interval immediately following the P-wave pick and the subsequent time window corresponding to the arrival of the S-wave. The selection of a 3-second time window for the P-wave phase draws from literature, emphasising the effectiveness of this choice (Y. M. Wu & Kanamori, 2005a). It balances achieving accurate S-wave amplitude estimation and providing a sufficiently wide warning window with reduced blind zone for an EEWS (Böse, Hauksson, Solanki, Kanamori, & Heaton, 2009; Caruso et al., 2017; Y. Wang et al., 2020; Y. M. Wu & Mittal, 2021).

Standard metrics such as Peak Ground Acceleration, Peak Ground Velocity, and Peak Ground Displacement can be used to represent the amplitude of seismic waves for an earthquake (Y. M. Wu & Kanamori, 2008; Y. M. Wu & Zhao, 2006). Therefore, this study computed six seismic parameters to establish relationships between P and S-wave amplitude.

For the selected P-wave window, calculations for estimating the amplitude of the P-wave include the Peak Ground Acceleration (Pa), the Peak Ground Velocity (Pv), and the Peak Ground Displacement (Pd) of the P-wave. These calculations are based on the vertical acceleration, velocity, and displacement records, as P-waves predominantly exhibit motion in the vertical direction (Y. M. Wu, 2019; H. Zhang et al., 2003).

Subsequently, for the S-wave window, key parameters to estimate the amplitude of S-waves: the Peak Ground Acceleration (PGA), the Peak Ground Velocity (PGV), and the Peak Ground Displacement (PGD) are calculated. Data from the HNE (east-west direction) and HNN (north-south direction) channels are utilised to capture these peak values, given that S-waves predominantly exhibit motion in the horizontal direction (Shearer, 2009). The PGA, PGV, and PGD values are calculated using the RotD50 method for the S-waves (Boore, 2010).

Before calculating the P-wave and S-wave parameters, the chosen ground motion recordings are filtered using a Butterworth-Bandpass filter from 0.1 to 20 Hz. This filtering step retains the earthquake signal's frequency content of interest and removes low-frequency and high-frequency ambient noise (Claerbout, 1964; Virtanen et al., 2020).

Table 8-2 summarises the parameters used in this study and their respective abbreviations.

Table 8-2: Abbreviations and descriptions of the parameters used for analysis.

Abbreviation	Description
Pa	Peak Ground Acceleration calculated for the P-wave window in ms^{-2}
Pv	Peak Ground Velocity calculated for the P-wave window in ms^{-1}
Pd	Peak Ground Displacement calculated for the P-wave window in m
PGA	Peak Ground Acceleration calculated for the S-wave window in ms^{-2}
PGV	Peak Ground Velocity calculated for the S-wave window in ms^{-1}
PGD	Peak Ground Displacement calculated for the S-wave window in m

It is important to note that this study does not focus on determining the τ_c for the P-wave window, as observed in various studies that seek to establish a relationship between τ_c and earthquake magnitude (M) (Y. Wang et al., 2020; Y. M. Wu & Kanamori, 2005b, 2005a). Instead, the primary focus is exploring relationships between P and S-wave amplitudes.

8.4.2.4 Outlier Test

Before choosing the model, it is crucial to systematically identify and remove outliers from the dataset to ensure the robustness and accuracy of the models. Outliers, which can significantly skew results, are detected using the Interquartile Range (IQR) method (Courtney Taylor, 2018; Gianluca Malato, 2021). The outlier method works as follows,

1. Calculate the dataset's first quartile (Q1) and third quartile (Q3). The first quartile is the value at the 25th percentile, and the third is at the 75th percentile.
2. Compute the IQR as the difference between Q3 and Q1 (IQR = Q3 - Q1). The IQR represents the range of the middle 50% of the data.
3. Define the lower and upper outlier thresholds using the following formulas:
    a. Lower threshold = Q1 - 1.5 * IQR
    b. Upper threshold = Q3 + 1.5 * IQR
4. Identify any data points that fall below the lower threshold or above the upper threshold. These observations are considered outliers.

This statistical approach is applied separately to the training and testing datasets to ensure the integrity of the model evaluation. This separation is critical to prevent data leakage, which could lead to overly optimistic performance estimates and compromise the model's generalisability. The outlier removal process affected approximately 0.4% to 0.5% of the training and testing datasets across all relationships.

Further, Figures I-1 to I-6 in the Appendix I illustrate the data before and after removing outliers for training and testing datasets across the nine relationships intended for construction.

8.4.2.5 Linear Regression Analysis

Linear regression is a straightforward approach used in seismology to estimate S-wave amplitudes using P-wave data. Its simplicity and ease of implementation make it an ideal choice for smaller datasets, allowing for the establishment of a reliable baseline relationship between P-wave and S-wave amplitudes. This method has been substantiated by several studies in the literature, which have demonstrated its effectiveness in accurately modelling relationships within the seismic data context (Y. M. Wu & Mittal, 2021; Yamamoto et al., 2008).

Several strategic considerations drove this study's use of a linear regression model. While machine learning models are increasingly popular due to their ability to handle complex datasets and provide accurate predictions, their application in seismology presents unique challenges (Abdalzaher et al., 2023; Hsu & Huang, 2021; J. Zhu et al., 2022a). Complex models, such as Convolutional Neural Networks (CNNs) or Recurrent Neural Networks (RNNs), require large datasets to effectively learn and generalise without overfitting (Jon Reilly, 2024; Pragati Baheti, 2021). Given the specific context of our study, where the dataset comprised MEMS-based ground motion data with a relatively limited size, there is a significant risk that a more complex model could yield unreliable predictions. This concern guided the choice towards using a simple linear regression model.

The computed parameters from the P-wave and S-wave windows served as the basis for establishing nine distinct linear regression relationships between P-wave and S-wave characteristics. To enhance the interpretability and robustness of these relationships, raw parameter values are transformed into logarithmic (log10) base values. This transformation significantly reduces the influence of extreme outliers and stabilises variance, making the data more suitable for linear modelling. Additionally, converting to logarithmic scales compresses the data range, simplifying the analysis and facilitating a more linear representation of the data. This method aids in establishing meaningful correlations and enhances the overall reliability and robustness of the empirical relationships.

The chosen linear regression equation takes the form of $\mathbf{y = ax + b}$, where x represents the independent variable (in our study, the amplitude of the P-waves, denoted as Pa, Pv, or Pd) and 'y' represents the dependent variable (the amplitude of the S-waves, represented as PGA, PGV, or PGD). The values for 'a' and 'b' in this equation are determined using the least squares method to find the best-fit linear relationship between the P-wave and S-wave amplitudes. Specifically, 'a' represents the slope of the regression line, indicating the rate of change in the S-wave amplitude concerning changes in the P-wave

amplitude, while 'b' represents the intercept, denoting the estimated S-wave amplitude when the P-wave amplitude is zero (Barbur et al., 1994; Draper & Smith, 2014).

Following the construction of the linear regression models, the residuals of each model were subjected to an error distribution analysis to evaluate the S-wave amplitude estimation. This included calculating the mean error, median error, standard deviation, and mean absolute error (MAE) for the residuals.

8.4.2.6 Evaluating the Generalisability and Suitability of Empirical Relationships

A set of metrics derived from the established linear regression models are used to evaluate generalisability and select the study's optimal empirical relationship. Further, a weighted scoring approach is employed to quantify the efficacy of each of the nine models.

Metrics

a. The Correlation Coefficient (R)

It measures the strength and direction of a linear relationship between two variables on a scatter plot (Draper & Smith, 2014). For linear regression involving two variables x (P-wave amplitude parameter) and y (S-wave amplitude parameter), R ranges from -1 to 1. A value of 1 indicates a perfect positive linear relationship, where increases in x correspond to increases in y. Conversely, a value of -1 denotes a perfect negative linear relationship, where increases in x correspond to decreases in y. A value of 0 signifies no linear correlation between the variables. R is given by the formula:

$$R = \frac{\sum_i^n \sum(x_i - \bar{x})(y_i - \bar{y})}{\sqrt{\sum_i^n \sum(x_i - \bar{x})^2 \ \sum_i^n \sum(y_i - \bar{y})^2}} \qquad (1)$$

where x_i and y_i are amplitude parameter values, and $\bar{x}$ and $\bar{y}$ are the mean values of the amplitude parameters for the P and S-waves, respectively.

b. The Coefficient of Determination (R^2)

It represents the proportion of the variance in the dependent variable that is predictable from the independent variables. It ranges from 0 to 1 where an R^2 value of 1 indicates that the regression predictions perfectly fit the data, and 0 suggests that the model does not explain any variability in the response data around its mean. The R^2 is the square value of R.

c. The Root Mean Square Error (RMSE)

It measures the standard deviation of residuals or prediction errors, providing insights into how much deviation occurs from the observed data points to the predictions made by the regression model. This is

crucial for assessing a model's accuracy, with lower RMSE values indicating a better fit to the data. RMSE is given by the formula,

$$\text{RMSE} = \sqrt{\frac{\sum_i^n \sum(y_i - \hat{y}_i)^2}{n}} \qquad (2)$$

where y_i is the observed amplitude value, $\hat{y}_i$ is the predicted amplitude value for the S-wave using the linear regression model, and n is the number of observations used.

d. 5-fold Cross Validation RMSE

It is a statistical method employed to ensure the generalisability of a constructed model. This research utilised a K-fold Cross-validation approach with K equal to 5, chosen to achieve a good balance between the model construction and validation. The training dataset (2010 to 2019) is partitioned into five equal segments. Four segments are used to train the model for each validation cycle, and the remaining segment serves as the test set. This process iterates until each fold has been used for validation exactly once. In this investigation, for each empirical relationship, the RMSE is computed across five distinct folds within the training dataset. RMSE quantifies the average magnitude of the prediction error. By assessing RMSE across all folds, the study can discern how consistently the model performs. Cross-validation is conducted on the training dataset to avoid data leakage and ensure the integrity of performance evaluations. The test dataset is reserved for the final assessment of the model, thereby preventing any bias in the model's estimated ability to generalise and ensuring an unbiased evaluation on new, unseen data.

Method for Selecting the Most Suitable Linear Regression Relationship

a. Evaluation with Testing Data

The models developed are evaluated using an independent test dataset from 2020 to 2023. This phase critically assesses each model's performance on new, unseen data, essential for verifying their robustness. The effectiveness and generalisability of the models are determined by comparing the R^2 and RMSE values from this test dataset against those from the training phase. This approach ensures that the models perform well on historical data and are reliable and accurate when applied to predict future seismic events.

b. Overfitting and Underfitting Assessment

Assessing overfitting and underfitting is crucial for ensuring the robustness of constructed models, as these phenomena can significantly affect a model's predictive accuracy on new data. Overfitting occurs when a model is overly tailored to the training data and performs well on this data but poorly generalises

to new datasets (Koehrsen, 2018; Tigran P., 2022). This often results in models that are tailored too closely to the specifics of the training data. In contrast, underfitting happens when models are too simplistic, failing to capture essential relationships within the data, leading to suboptimal performance on training and testing datasets (Koehrsen, 2018; Tigran P., 2022).

The nature of overfitting and underfitting within each constructed linear regression model is analysed using the previously introduced metrics: R^2 and RMSE for both training and testing datasets and RMSE values derived from 5-fold Cross-validation of the training data.

c. Weighted Scoring Approach

A weighted scoring framework is implemented to aggregate multiple performance metrics into a unified measure of model efficacy, which facilitates the identification of the most appropriate linear regression relationship (Griffith & Headley, 1997; Nicholas Morpus, 2024). The performance metrics considered are R^2 for the training dataset (Trained R^2), RMSE for the training dataset (Trained RMSE), the mean RMSE from 5-fold Cross-validation (Mean of 5-fold Cross-validation RMSE), R^2 for the testing dataset (Tested R^2), and RMSE for the testing dataset (Tested RMSE). These metrics are normalised to ensure comparability; higher values of R^2 are indicative of better performance, while lower values of RMSE represented lower error rates.

The following factors outline the assigned weights to various evaluation metrics employed in the model selection process and their rationale behind the chosen values.

T**he Mean of 5-fold Cross-validation RMSE** is given the highest weight (0.6) to select the most suitable relationship. This metric is crucial for accurately estimating the model's performance across diverse data subsets; prioritising a lower mean of 5-fold Cross-validation RMSE ensures that the chosen model can generalise effectively and remain reliable in real-world scenarios with potentially varying data characteristics.

Tested RMSE, weighted at 0.3, is the next most important factor. This metric directly assesses the model's performance on entirely new data, a crucial factor for the practical deployment of an EEWS. In an EEWS, encountering unseen data is the norm, emphasising the need for a model that can reliably predict earthquakes under such conditions.

Trained RMSE receives a weight of 0.2, signifying its role in indicating the model's efficacy in capturing and learning from historical data. While a lower Trained RMSE is desirable, it holds less weight than the model's generalisability and performance on unseen data.

Tested R^2 and Trained R^2 are assigned a weight of 0.1 each. While R^2 can be a valuable tool for initial exploration and assessing fit quality in linear models, it is ultimately de-emphasised in favour of RMSE for final model selection. Two factors drive this decision: RMSE possesses a clear unit (error in the original units), facilitating a more straightforward interpretation of the model's performance. Additionally, RMSE exhibits less susceptibility to overfitting compared to R^2. Table 8-3 displays the weights assigned to the chosen metrics.

Table 8-3: Assigned weights and justification for performance metrics in linear regression model selection

Metric	Weight
Trained R^2	0.1
Tested R^2	0.1
Trained RMSE	0.2
Tested RMSE	0.3
Mean of 5-fold Cross-validation RMSE	0.6

The formula for calculating the weighted score of each model integrates these normalised metrics and their respective weights to derive a composite measure of performance is expressed as:

$$\text{Weighted Score} = \left[(Normalised\ Trained\ R^2 \times 0.1) + (Normalised\ Tested\ R^2 \times 0.1) + \left(\text{Normalised Trained RMSE} \times 0.2\right) + \left(\text{Normalised Tested RMSE} \times 0.3\right) + \left(\text{Normalised Cross} - \text{Validation RMSE} \times 0.6\right)\right] \quad (3)$$

8.5 Results

8.5.1 P-wave Parameters Versus S-wave Amplitude

8.5.1.1 Pa vs. S-wave Amplitude

The initial set of relationships analysed focused on P-wave Pa values and their correlation with S-wave amplitude parameters, including PGA, PGV, and PGD (Figure 8-3).

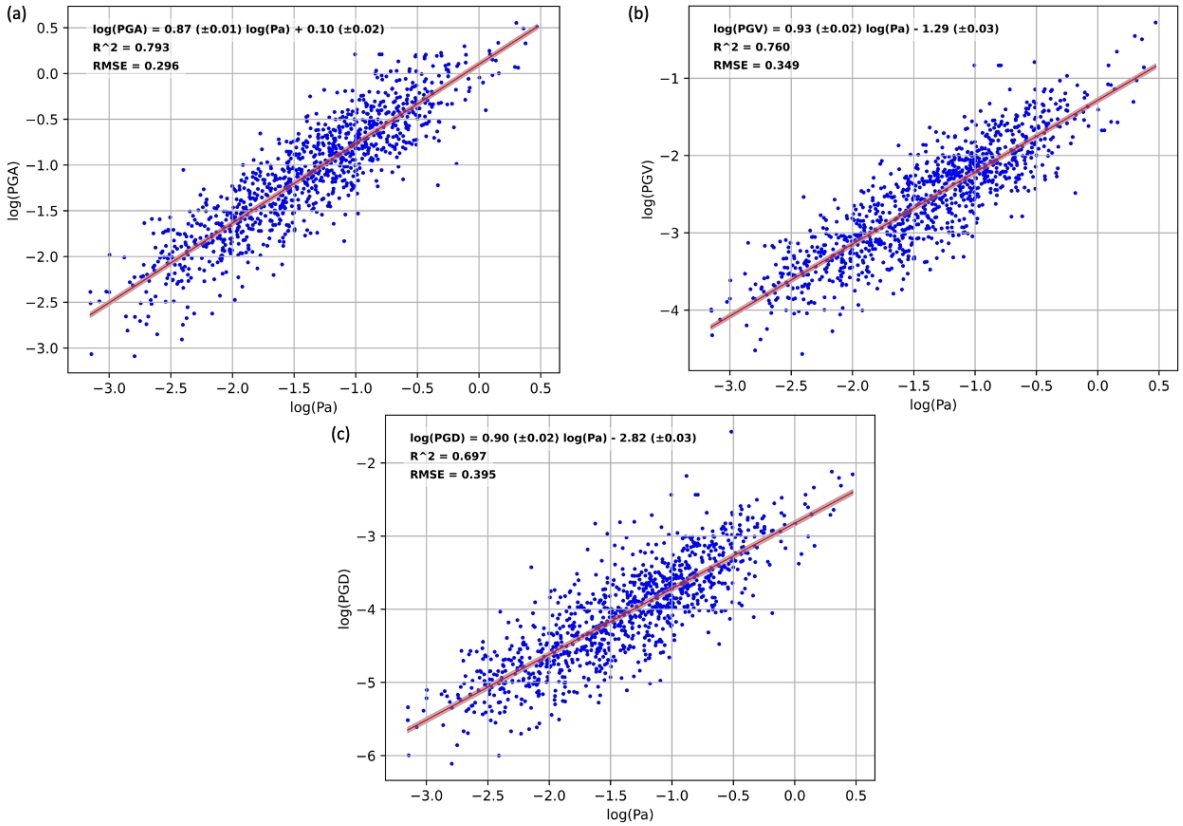

Figure 8-3. Empirical relationships between P-wave Pa and S-wave parameters for Site Class D. Panel (a) shows Pa vs PGA, (b) shows Pa vs PGV, and (c) shows Pa vs PGD. Each graph features data points in blue, a linear regression line in red, and the 95% confidence interval shaded in grey.

Table 8-4: Summary of empirical relationships, R, R2, RMSE and 5-fold Cross-validation RMSE values obtained for P-wave's Pa and S-wave amplitude parameters (PGA, PGV and PGD).

Equation	Parameters	Empirical relationship	R	R^2	RMSE	5-fold Cross-validation RMSE
1	Pa Vs PGA	log (PGA) = 0.87 (±0.01) log (Pa) + 0.10 (±0.02)	0.891	0.793	0.296	[0.384, 0.279, 0.262, 0.251, 0.36]
2	Pa Vs PGV	log (PGV) = 0.93 (±0.02) log (Pa) – 1.29 (±0.03)	0.872	0.760	0.349	[0.45, 0.321, 0.291, 0.293, 0.512]
3	Pa Vs PGD	log (PGD) = 0.90 (±0.02) log (Pa) – 2.82 (±0.03)	0.835	0.697	0.395	[0.518, 0.345, 0.319, 0.31, 0.609]

The relationship between P-wave amplitude (Pa) and S-wave amplitude measured by PGA demonstrates a strong correlation. As depicted in Figure 8-3(a), the empirical relationship (Equation 1 from Table 8-4) produced R and R^2 values of 0.891 and 0.793, indicating a robust association. This high R^2 suggests that the variability in Pa substantially explains the variance in PGA values. The RMSE of 0.296 and a 5-fold Cross-validation RMSE ranging from 0.251 to 0.384 confirm the model's accuracy and consistency.

Regarding the P-wave amplitude (Pa) compared with the S-wave's PGV, Figure 8-3(b) showcases the Pa versus PGV relationship (Equation 2 from Table 8-4), yielding R and R^2 values of 0.872 and 0.760, respectively. Although slightly lower than the Pa-PGA relationship, these figures still represent a significant correlation, indicating that Pa variations can explain a large portion of the PGV variability. The RMSE for this relationship is 0.349, with the 5-fold Cross-validation RMSE values ranging from 0.291 to 0.512, reflecting the model's reliability across different subsets of data.

Finally, the analysis of Pa against the S-wave amplitude measured by PGD is shown in Figure 8-3(c). The empirical relationship (Equation 3 from Table 8-4) resulted in R and R^2 values of 0.835 and 0.697, respectively. These values indicate a strong but less pronounced correlation compared to the earlier relationships. The RMSE of 0.395 and the 5-fold Cross-validation RMSE values between 0.310 and 0.609 suggest a slightly greater deviation from the model predictions, highlighting the challenges in predicting PGD from Pa.

8.5.1.2 Pv vs. S-wave Amplitude

The subsequent analysis explored relationships involving Pv values for P-waves and the S-wave amplitude measured as PGA, PGV, and PGD. Figure 8-4 illustrates the obtained graphs for the Pv vs PGA, Pv vs PGV, and Pv vs PGD relationships.

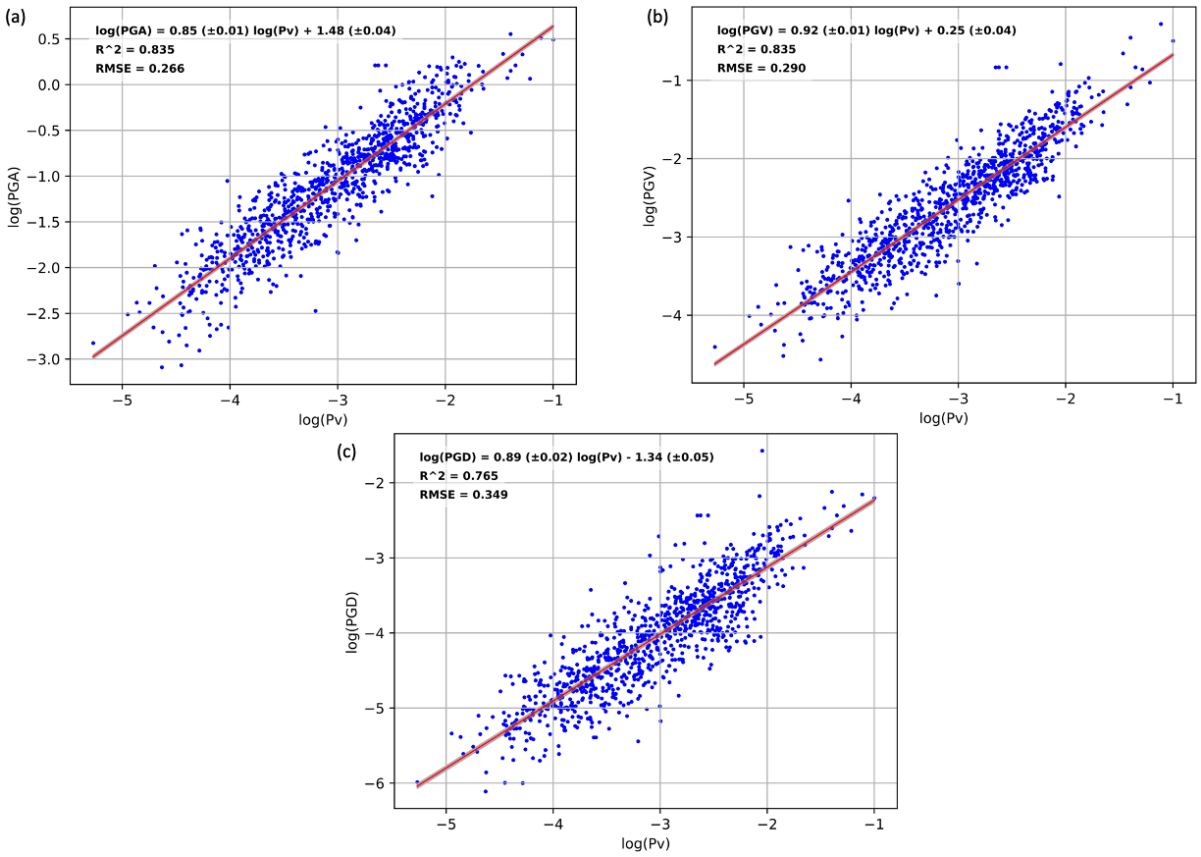

Figure 8-4. Empirical relationships between P-wave Pv and S-wave parameters for Site Class D. Panel (a) shows Pv vs PGA, (b) shows Pv vs PGV, and (c) shows Pv vs PGD. Each graph features data points in blue, a linear regression line in red, and the 95% confidence interval shaded in grey.

Table 8-5: Summary of empirical relationships, R, R2, RMSE and 5-fold Cross-validation RMSE values obtained for P-wave's Pv and S-wave amplitude parameters (PGA, PGV and PGD).

Equation	Parameters	Empirical relationship	R	R^2	RMSE	5-fold Cross-validation RMSE
4	Pv Vs PGA	log (PGA) = 0.85 (±0.01) log (Pv) + 1.48 (±0.04)	0.914	0.835	0.266	[0.33, 0.239, 0.257, 0.226, 0.297]
5	Pv Vs PGV	log (PGV) = 0.92 (±0.01) log (Pv) + 0.25 (±0.04)	0.914	0.835	0.290	[0.355, 0.263, 0.264, 0.253, 0.407]
6	Pv Vs PGD	log (PGD) = 0.89 (±0.02) log (Pv) – 1.34 (±0.05)	0.875	0.765	0.349	[0.425, 0.313, 0.31, 0.286, 0.517]

As depicted in Figure 8-4(a), the relationship between Pv and PGA (Equation 4 from Table 8-5) exhibited a robust positive correlation, with R and R^2 values of 0.914 and 0.835, respectively. These high R and R^2 values, surpassing those seen in relationships involving Pa, indicate a more consistent and robust predictive capability. The RMSE of 0.266 and the 5-fold Cross-validation RMSE ranging from 0.226 to 0.33 further underscore the model's accuracy and consistency.

The empirical analysis extended to the relationship between Pv and PGV, as illustrated in Figure 8-4(b). This relationship (Equation 5 from Table 8-5) yielded similar R and R^2 values of 0.914 and 0.835, respectively, demonstrating a robust positive correlation. This reflects the same level of consistency as the Pv versus PGA analysis despite a marginally higher RMSE of 0.290 and a 5-fold Cross-validation RMSE between 0.253 and 0.407.

Finally, Figure 8-4(c) highlights the Pv versus PGD relationship (Equation 6 from Table 8-5), which recorded R and R^2 values of 0.875 and 0.765. These values, while strong, are slightly lower than those of the previous Pv relationships. The RMSE of 0.349 and a 5-fold Cross-validation RMSE ranging from 0.286 to 0.517 suggest a more noticeable variability between observed and predicted values, reflecting the challenges in predicting PGD from Pv with the same precision as PGA or PGV.

8.5.1.3 Pd vs. S-wave Amplitude

The final set of analyses investigates the empirical relationships between P-wave amplitude, represented by Pd, and S-wave amplitudes, represented by PGA, PGV, and PGD. Figure 8-5 provides a graphical visualisation of the computed relationships, illustrating the interaction between these seismic parameters.

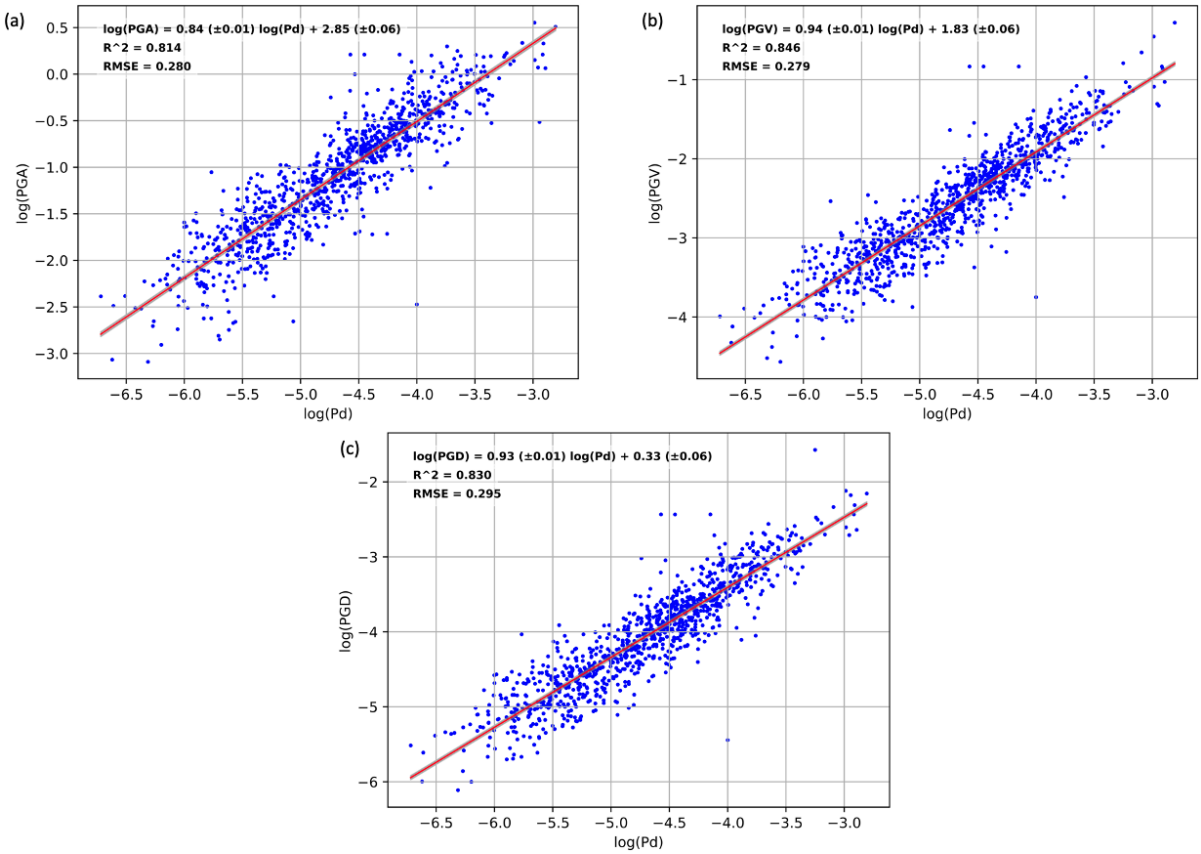

Figure 8-5. Empirical relationships between P-wave Pd and S-wave parameters for Site Class D. Panel (a) shows Pd vs PGA, (b) shows Pd vs PGV, and (c) shows Pd vs PGD. Each graph features data points in blue, a linear regression line in red, and the 95% confidence interval shaded in grey.

Table 8-6: Summary of empirical relationships, R, R2, RMSE and 5-fold Cross-validation RMSE values for P-wave's Pd and S-wave amplitude parameters (PGA, PGV and PGD).

Equation	Parameters	Empirical relationship	R	R^2	RMSE	5-fold Cross-validation RMSE
7	Pd Vs PGA	log (PGA) = 0.84 (±0.01) log (Pd) + 2.85 (±0.06)	0.902	0.814	0.280	[0.351, 0.258, 0.239, 0.239, 0.313]
8	Pd Vs PGV	log (PGV) = 0.94 (±0.01) log (Pd) + 1.83 (±0.06)	0.920	0.846	0.279	[0.33, 0.258, 0.243, 0.254, 0.349]
9	Pd Vs PGD	log (PGD) = 0.93 (±0.01) log (Pd) + 0.33 (±0.06)	0.911	0.830	0.295	[0.369, 0.266, 0.262, 0.254, 0.389]

The relationship between Pd and PGA (Equation 7 from Table 8-6) demonstrated a robust positive correlation, with R and R^2 values of 0.902 and 0.814, respectively, as shown in Figure 8-5(a). This relationship exhibited an RMSE of 0.280, with a 5-fold Cross-validation RMSE ranging between 0.239 and 0.351. These metrics suggest a firm consistency and reliability in predicting PGA from Pd.

Further, the relationship between Pd and PGV is explored and is depicted in Figure 8-5(b). This relationship (Equation 8 from Table 8-6) produced R and R^2 values of 0.920 and 0.846, respectively,

indicating an even stronger positive correlation than the Pd vs PGA relationship. The RMSE is slightly lower at 0.279, with a 5-fold Cross-validation RMSE between 0.243 and 0.349, reinforcing the model's accuracy in predicting PGV from Pd.

Lastly, Figure 8-5(c) depicts the relationship between Pd and PGD (Equation 9 from Table 8-6), yielding R and R^2 values of 0.911 and 0.830, respectively. These values suggest a substantial predictive capability, although slightly reduced compared to the Pd vs PGV relationship. The RMSE for this relationship is 0.295, with a 5-fold Cross-validation RMSE spanning from 0.254 to 0.389, indicating slightly higher variability in predictions for PGD relative to PGA and PGV.

8.5.1.4 Evaluation of Error Distribution for S-wave Amplitude Estimation

The residuals from each of the nine empirical relationships are analysed to evaluate the error distribution for the S-wave amplitude estimation. The analysis included calculating the Mean error, Median error, Standard Deviation, and Mean Absolute Error (MAE) for the residuals, in addition to the RMSE. Table 8-7 summarises the values obtained from these calculations.

Table 8-7. Summary of error distribution metrics for S-wave amplitude estimation, including mean error, median error, standard deviation, range, and MAE for each of the nine empirical relationships.

Model	Median error	Standard Deviation	MAE
Pa vs PGA	0.0121	0.296	0.234
Pa vs PGV	0.0039	0.346	0.2763
Pa vs PGD	-0.0022	0.395	0.3054
Pv vs PGA	0.0186	0.2655	0.2046
Pv vs PGV	0.0085	0.2904	0.2235
Pv vs PGD	0.0103	0.349	0.2651
Pd vs PGA	0.0109	0.2801	0.2063
Pd vs PGV	-0.0024	0.2788	0.2068
Pd vs PGD	-0.0057	0.2953	0.2213

The error distribution analysis for S-wave amplitude estimation reveals that the mean and median errors are minimal and negligible across all models, indicating that the residuals are centred around zero.

- **Standard Deviation:** The Pv vs PGA model exhibits the lowest standard deviation (0.2655), indicating greater consistency in its residuals. In contrast, the Pa vs PGD model shows the highest standard deviation (0.395), indicating higher variability.
- **MAE**: The Pv vs PGA model has the lowest MAE of 0.2046, highlighting its accuracy and reliability. Other notable performances include the Pd vs PGA model, which has an MAE of 0.2063, and the Pd vs PGV model, which has an MAE of 0.2068.

The Pv vs PGA model consistently demonstrates better performance regarding Standard Deviation, and MAE. Other models, such as Pv vs PGV and Pd vs PGA, also show strong performance, particularly the MAE, highlighting their potential effectiveness in predicting S-wave amplitudes. Further, histograms that show the frequency distribution of residuals in estimating S-wave amplitudes are plotted for each of the nine relationships and attached in the Appendix I as Figure I-7.

8.5.2 Evaluation and Generalisation of the Linear Regression Relationships with Testing Data

This section details the evaluation results of the constructed linear regression models using the testing dataset.

Table 8-8 summarises the R^2 (Tested R^2) and RMSE (Tested RMSE) values for each relationship, comparing the outcomes from the training phase and those observed with the testing phase.

Table 8-8: Comparison of Trained and Tested R^2 and RMSE Values for the Nine Linear Regression Relationships

Relationship	Trained Model		Tested Model	
	R^2	**RMSE**	**R^2**	**RMSE**
Pa vs PGA	0.793	0.296	0.639	0.343
Pa vs PGV	0.760	0.349	0.453	0.411
Pa vs PGD	0.697	0.395	0.392	0.471
Pv vs PGA	0.835	0.266	0.716	0.305
Pv vs PGV	0.835	0.290	0.618	0.343
Pv vs PGD	0.765	0.349	0.573	0.394
Pd vs PGA	0.814	0.280	0.699	0.314
Pd vs PGV	0.846	0.279	0.626	0.339
Pd vs PGD	0.830	0.295	0.632	0.366

Among the evaluated relationships, the Pv vs PGA relationship exhibited superior performance, achieving the highest R^2 of 0.716, which indicates a strong correlation and predictive capability, along with the lowest RMSE of 0.305, suggesting minimal prediction errors. In contrast, the Pa vs PGD relationship showed the least predictive accuracy, with the lowest R^2 of 0.392 and the highest RMSE of 0.471, indicating higher prediction variability.

Furthermore, relationships involving Pd in overall demonstrated commendable performance, with the Pd vs PGA relationship being notably effective, achieving an R^2 of 0.699 and an RMSE of 0.314. In contrast, relationships based on Pa generally showed poorer performance, as evidenced by lower R^2

values and higher RMSEs across the board, indicating a reduced reliability for making precise predictions.

8.5.3 Identifying Overfitting and Underfitting in Linear Regression Models

This section outlines the results concerning the analysis of overfitting and underfitting within the constructed linear regression models.

Overfitting in linear regression models is characterised by high R^2 values during training with a substantial test drop, suggesting the model memorises specifics rather than generalises. This is further indicated by low training RMSEs that increase significantly during testing and inconsistent performance across different subsets in 5-fold Cross-validation RMSE (Koehrsen, 2018; Tigran P., 2022).

Conversely, underfitting is marked by uniformly low R^2 and high RMSE across training and testing phases, reflecting the model's failure to capture essential data trends. Elevated Cross-validation RMSEs also underscore underfitting, revealing the model's inadequate performance on unseen segments of the training data (Koehrsen, 2018; Tigran P., 2022).

The analysis of the constructed relationships using the calculated metrics provides a clear indication of their varying abilities to model and predict unseen data effectively:

Relationships with Pa: The Pa vs PGA and Pa vs PGV models exhibit signs of overfitting. While their Trained R^2 values are relatively high (0.793 and 0.76, respectively), the significant drop in R^2 and increase in RMSE when moving to the test dataset (0.639 vs 0.343 for Pa vs PGA and 0.453 vs 0.411 for Pa vs PGV) suggest the models are not generalising well to unseen data. The Pa vs PGD model shows even stronger evidence of overfitting, with a very low Tested R^2 (0.392) and high Tested RMSE (0.471).

Relationships with Pv: The Pv vs PGA model demonstrates the best overall performance. Its Trained and Tested R^2 values are high (0.835 and 0.716, respectively), and the increase in Tested RMSE (0.305) is moderate. The 5-fold Cross-validation RMSE also suggests good generalisability, indicating that the model captures the underlying relationship effectively and performs well on unseen data. The Pv vs PGV and Pv vs PGD models show similar trends, although with slightly lower performance than Pv vs PGA.

Relationships with Pd: The Pd vs PGA, Pd vs PGV, and Pd vs PGD models exhibit good performance. Their Trained and Tested R^2 values are high (above 0.8 for Trained R^2 and above 0.6 for Tested R^2), and

the increases in Tested model RMSE are moderate. The 5-fold Cross Validation RMSE values also indicate good generalisability.

8.5.4 Evaluating Linear Regression Relationships Through Weighted Scoring

As outlined in the method section, the weighted scores for each constructed relationship are computed using Formula 3. The following table (Table 8-9) presents the results derived from the weighted scoring approach, quantifying the efficacy of various relationships in estimating S-wave amplitude from P-wave amplitude.

Table 8-9: Weighted scores for assessing the efficacy of linear regression relationships in estimating s-wave amplitude from P-wave amplitude.

Equation	Relationship	Weighted Score
1	Pa vs PGA	0.98
2	Pa vs PGV	0.43
3	Pa vs PGD	0
4	Pv vs PGA	1.29
5	Pv vs PGV	1
6	Pv vs PGD	0.51
7	Pd vs PGA	1.19
8	Pd vs PGV	1.12
9	Pd vs PGD	0.96

The analysis revealed a prominent relationship between Pv and PGA, evidenced by the highest weighted score of 1.29. This association stood out due to its strong correlation and consistent predictive ability, suggesting its potential value as a model within EEWSs. Conversely, relationships involving Pa displayed lower efficacy. This is reflected in their weighted scores: Pa vs PGA (0.98), Pa vs PGV (0.43), and particularly Pa vs PGD (0.0), which suggests minimal utility in employing Pa for accurate S-wave prediction. Additionally, Pd-related relationships demonstrated positive performance, with Pd vs PGA and Pd vs PGV achieving scores of 1.19 and 1.12, respectively. These scores indicate strong reliability in utilising Pd parameters for estimating S-wave amplitude, although they are surpassed by the Pv vs PGA relationship.

8.6 Discussion

This research has evaluated different P-wave parameters for estimating S-wave amplitude in EEWS, assessing their effectiveness and generalisability. The findings indicate that Pv is the most suitable parameter for estimating S-wave amplitude, especially for PGA, a crucial indicator of ground shaking.

Additionally, Pd shows robust performance, whereas Pa displays certain limitations. The subsequent section will further explore these results and discuss their broader implications.

Efficacy of Pd in Predicting S-Wave Amplitude: The correlation between P-wave amplitude and S-wave amplitude is comprehensively analysed using the metrics R, R^2, RMSE, and 5-fold Cross-validation RMSE for the nine developed models. The Pd parameter consistently demonstrated robust predictive power across its relationships with S-wave amplitudes, notably PGA, PGV, and PGD. It exhibited strong correlations, with R values exceeding 0.9 and R^2 values of 0.814, 0.846, and 0.83, respectively, indicating significant predictive capabilities (Table 8-6). Furthermore, RMSE values for these relationships remained uniformly low, below 0.3, underscoring their prediction accuracy. The 5-fold Cross-validation RMSE results further reinforced the reliability of the Pd-based models, with values ranging from 0.239 to 0.389, indicating good generalisation performance. These metrics collectively affirm Pd's efficacy as a dependable predictor of S-wave amplitude, reinforcing its value in EEWSs.

Limitations of Pa in Predicting S-Wave Amplitude: Empirical relationships utilising Pa to predict S-wave amplitudes exhibited considerably poorer fits, reflecting findings similar to those reported in studies on EEWSs employing MEMS sensors, such as the research conducted by Y. M. Wu & Kanamori (2005b). Specifically, when estimating S-wave amplitudes (PGA, PGV, and PGD) using Pa, the relationships demonstrated lower R and R^2 values and higher RMSEs, indicating a less accurate fit. The 5-fold Cross-validation RMSE values further revealed higher prediction errors across all folds for these three S-wave amplitude predictions, underscoring the models' inadequacies. Notably, the relationship between Pa and PGD is weak, recording the lowest R and R^2 values of 0.835 and 0.697, respectively, and the highest RMSE at 0.395. Cross-validation RMSEs for this relationship varied from 0.319 to 0.609, indicating substantial prediction errors and poor generalisability to new data. These results highlight the limited effectiveness of Pa as a predictor of S-wave amplitude, especially in estimating PGD.

Pv as the Optimal Predictor for S-Wave Amplitude: Despite not reaching the highest correlation levels achieved by Pd models, Pv has shown robust overall correlations as a predictor of S-wave amplitudes. The relationships involving Pv and various S-wave parameters—PGA, PGV, and PGD—demonstrate strong statistical correlations, with R values consistently above 0.85 and R^2 values exceeding 0.75. Particularly notable are the Pv versus PGA and Pv versus PGV models, which recorded R and R^2 values of 0.914 and 0.835, respectively. These high metrics signify strong linear associations between Pv and S-wave amplitudes.

The Pv vs PGA model, with its low RMSE of 0.266, stands out among the Pv relationships, indicating minimal prediction error, reflecting the model's accuracy in estimating PGA from Pv. Moreover, the 5-fold Cross-validation RMSE results further validate the reliability of the Pv-based models. The consistently low error rates across all folds highlight excellent generalisability to new, unseen data. Additionally, the error distribution analysis of S-waves indicated that the Pv vs PGA model consistently demonstrates better performance regarding Standard Deviation and MAE than other models. These findings solidify Pv's status as an effective and dependable indicator of S-wave amplitude, particularly for predicting PGA, and underscore its practical implications in real-world scenarios.

Testing Data Evaluation: Evaluating the constructed models with a test dataset spanning 2020 to 2023 is a pivotal step in assessing the generalisability and robustness of the linear regression models. As shown in Table 8-7, the Pv vs PGA relationship stands out with the highest R^2 of 0.716 for the test dataset. It underscores its strong correlation and predictive capability alongside the lowest RMSE of 0.305, indicating minimal prediction errors. However, it contrasts with the Pa vs PGD relationship, which exhibited the lowest tested R^2 of 0.392 and the highest RMSE of 0.471, highlighting considerable prediction variability. Further, relationships involving Pd overall showed commendable performance, with the Pd vs PGA relationship notably achieving an R^2 of 0.699 and an RMSE of 0.314, demonstrating its effectiveness.

Pv and Pd Avoid Overfitting and Underfitting: While the relationships with Pv and Pd demonstrated significant correlations with S-wave amplitudes, understanding their modelling characteristics regarding overfitting and underfitting is crucial (Section 8.5.3). For instance, relationships involving Pa, such as Pa vs PGA, Pa vs PGV and Pa vs PGD, exhibited overfitting with substantial drops in R^2 and increases in RMSE, suggesting poor generalisation. Conversely, the Pv vs PGA relationship showed robust performance with high R^2 values and moderate RMSE increases during testing, underscoring its effective learning and generalisation capabilities. Similarly, models involving Pd, such as Pd vs PGA, maintained high R^2 and moderate RMSE increases, indicating robust learning and predictive reliability. These insights highlight the potential of Pv and Pd parameters in providing reliable predictions in real-world settings, with the Pv vs PGA model marked as the most effective based on the measured metrics.

Rationale Behind Pa's Poor Performance and Pv and Pd's Effective Predictive Capabilities: The observed poor correlation when using Pa as the amplitude parameter for the initial motion can be attributed to its susceptibility to misinterpretations, especially in the context of nearby small seismic events. Pa may yield comparatively large values for such events, even though the resulting PGA and PGV values are relatively small. This discrepancy arises due to differences in frequency content and attenuation. Pa primarily reflects the characteristics of a very high-frequency seismic wave, which attenuates more rapidly with distance and, therefore, has a lower potential for causing significant

damage. In contrast, Pv and Pd capture lower frequency content, which attenuates less rapidly and is more indicative of the seismic energy that can cause considerable damage (Y. M. Wu & Kanamori, 2005b). Therefore, Pv and Pd correlate strongly with critical seismic amplitude indicators like PGA and PGV. Notably, Pd demonstrates a notable correlation with peak amplitude parameters, which is pivotal in assessing the seismic impact (Y. M. Wu & Kanamori, 2005b). Another critical factor is the integration process used to determine Pv and Pd. This process acts as a natural low-pass filter, smoothing out high-frequency noise and providing a more stable signal. This stability is crucial for accurate prediction models, as it reduces the likelihood of overfitting to noise and local site effects in the initial P-wave data. Therefore, using Pa as the triggering parameter in an EEW network is limited since it could lead to an increased occurrence of false alerts, undermining the effectiveness of the EEWS.

Results Comparison to Prior Research: To further contextualise the findings, a comparative analysis is conducted between the results of this study and those reported in previous research papers that have explored empirical relationships. This study compares various relationships between P-wave and S-wave amplitude parameters, enhancing the understanding of seismic predictors by detailing how different P-wave parameters correlate with S-wave amplitudes across various scenarios. In contrast, much of the literature, such as the studies by Wang et al. (2020) and Y. M. Wu & Kanamori (2005b) have focused on specific relationships like Pd vs PGV.

For instance, a study by Y.M. Wu and Kanamori (2008) in Taiwan, which used 780 records to establish a relationship between Pd and PGV, reported a standard deviation (SDV) of 0.326 but did not specify R or R^2 values; similarly, Y.M. Wu & Mittal (2021) investigated this relationship using earthquake recordings from Japan, Taiwan, and Southern California, reporting an R-value of 0.873 and an SDV of 0.326, which is slightly lower than this study's R-value of 0.920 and RMSE of 0.279 for the Pd vs PGV model. Caruso et al. (2017) built a relationship between Pd and PGV using Italian earthquake data, resulting in an R^2 of 0.760 and an SDV of 0.36, which compares to the R^2 of 0.846 reported in this study for the same relationship, although with a slightly lower RMSE of 0.279. These comparisons highlight the robustness of the empirical relationships established in the current research within the context of NZ earthquake data, underscoring the comparative performance of these models against international studies. However, direct comparisons are complicated by some studies not reporting all metrics such as R, R^2, or RMSE, which underscores the need for standardised reporting in seismic research.

Weighted Scoring Approach to Identify Optimal Model: In this study, the challenge of comparing linear regression models, particularly between Pv and Pd relationships, necessitated a method that could systematically evaluate and select the optimal model. These models often yield similar results, making it difficult to discern the most effective one for EEW applications. To address this, the weighted scoring method is introduced (Griffith & Headley, 1997). This approach allows for an objective comparison by

focusing on crucial metrics from an EEW perspective. By assigning weights to different performance metrics, such as R^2 and RMSE (see Formula 3), and evaluating them in a structured manner, this method helps prioritise models that are statistically robust and most relevant for practical implementation in seismic alert systems.

Among the assessed models (Table 8-8 provides a clear summary of these scores), the relationship between Pv and PGA stood out significantly, achieving the highest weighted score of 1.29. This score reflects its robust correlation and consistent predictive accuracy, marking it as a highly effective model within EEWSs. Conversely, models involving Pa, such as Pa vs PGV and Pa vs PGD, exhibited much lower effectiveness, with scores of 0.43 and 0, respectively, indicating their limited utility in accurate S-wave prediction. Meanwhile, Pd-related models displayed strong performance, with scores of 1.19 for Pd vs PGA and 1.12 for Pd vs PGV, demonstrating their reliability in estimating S-wave amplitude, albeit not surpassing the superior performance of the Pv vs PGA relationship.

In conclusion, the study identifies the empirical relationship between Pv and PGA as the most suitable for estimating S-wave amplitude for the Canterbury region of NZ, demonstrating superior performance across training and testing datasets. This relationship's robustness is critical for the real-time application of EEWS, providing a reliable basis for operational success. Additionally, the chosen relationship enhances the integration of the S-wave-based PLUM algorithm with the P-wave detection algorithm, effectively reducing the inherent limitations of the PLUM algorithm's warning time. As outlined in the case study below, this relationship is also crucial in establishing a P-wave amplitude threshold. By setting a critical Pv value threshold, the EEWS can trigger alerts when this value is exceeded, indicating potential significant ground shaking.

8.7 Case Study: Establishing EEW Alert Threshold for Earthquakes in Canterbury

The study presents a case study showcasing the application of the selected empirical relationship in determining the threshold for felt earthquakes. The case study aims to establish the Pv threshold that would enable the issuance of alerts for a level of shaking that would be felt in the Canterbury region of NZ. This application uses the new Ground Motion to Intensity Conversion Equations (GMICEs) (Moratalla et al., 2020) constructed for NZ to derive the Pv threshold.

8.7.1 Method

MMI Selection: The initial step involves selecting a Modified Mercalli Intensity (MMI) range suitable for EEW purposes. This range determines the ground-shaking intensity levels that necessitate issuing an alert. For this selection, the study references the MMI descriptions provided by GeoNet (Dowrick et al., 2008). This ensures alignment with the regional seismic conditions and enhances the relevance of our chosen MMI range.

S-wave Parameter Threshold Identification: To determine the threshold value for the S-wave PGA, we use Moratalla et al. (2020) study which introduced new GMICEs designed explicitly for NZ. This study established relationships between the earthquakes' MMI scale and PGA values. By plotting this relationship, the PGA value associated with perceivable ground shaking in the chosen MMI range can be identified. This value is then employed as the S-wave threshold to indicate felt ground shaking.

P-wave Parameter Threshold Derivation: Utilising the selected empirical relationship between Pv and PGA, the corresponding threshold value for the P-wave parameter (Pv) is calculated based on the identified S-wave parameter (PGA) threshold.

8.7.2 Results

According to the GeoNet MMI description (Dowrick, 1996; Dowrick et al., 2008), an MMI value of 5.0 is selected as the threshold for EEW activation. This level represents shaking generally felt outdoors, awakens most sleepers, and may alarm some individuals indoors.

PGA values corresponding to an MMI of 5.0 are calculated using the GMICEs (Formula 4 and 5) provided by Moratalla et al. (2020). Figure 8-6 graphically depicts the relationship between MMI and PGA, where the chosen MMI threshold of 5.0, relevant to EEW generation, is indicated with a green vertical line.

$$\log(PGA) = (MMI - 1.7601) / 1.992 \text{ if } MMI < 5.5277 \quad (4)$$

$$\log(PGA) = (MMI + 1.9095) / 3.9322 \text{ if } MMI \geq 5.5277 \quad (5)$$

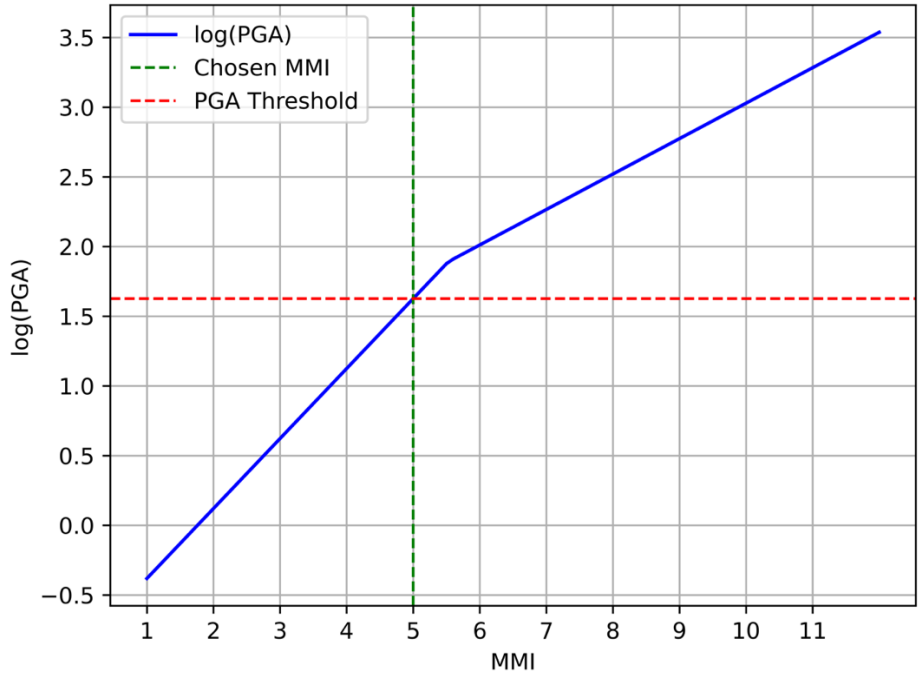

Figure 8-6. Relationship between MMI and PGA using GMICEs (1) and (2) as provided by Moratalla et al. (2020). The vertical green line represents the selected MMI value (MMI 5.0), and the horizontal red line indicates the PGA threshold for perceivable ground shaking.

PGA Threshold Identification: The corresponding log (PGA) threshold for S-waves is identified by examining the intersection point on the graph depicted in Figure 8-6. At this juncture, the log (PGA) value, determined as the threshold for S-waves, is 1.63, as indicated by the red dashed horizontal line on the graph. Upon converting this logarithmic value back to its original scale, the PGA threshold is established at 42.3 cms^{-2}.

Pv Threshold Derivation: Following the identification of the PGA threshold, this value is applied to the selected empirical relationship, defined as log (PGA) = 0.85 (±0.01) log (Pv) + 1.48 (±0.04), to derive the corresponding Pv threshold for event detection. This process established a Pv threshold ranges between 0.6 to 0.8 cms^{-1} according to the uncertainty in the linear regression coefficients. Selecting a Pv threshold of 0.6 cms^{-1} is considered most suitable, as a higher threshold may increase the risk of missed alerts, a critical concern in EEWSs.

When the Pv exceeds 0.6 cms^{-1}, the event is highly likely to be felt. Implementing a Pv threshold at 0.6 cms^{-1} would have enabled the EEWS to issue alerts for perceivable earthquake events. This threshold is applicable both in on-site EEWSs, where individual stations operate independently to issue warnings and in regional EEWSs, where data from multiple stations are aggregated to issue warnings.

This application's MMI value (5.0 or above) choice for triggering EEW alerts is grounded in GeoNet's MMI description. This approach serves as an illustrative example, showcasing the practicality of the

selected relationship for EEW purposes with a specific focus on MMIs indicative of significant seismic events. The selection of the MMI value potentially leads to debates among social and technical scientists regarding the most suitable threshold for generating alerts using the detected P-wave 3-second window. The ability to customise the threshold based on unique regional characteristics and priorities remains a valuable consideration.

8.8 Limitations and Future Work

While providing valuable insights into P and S-wave amplitude relationships for NZ based on data from the Canterbury region, the study has certain limitations and opens avenues for future research.

The study's data source primarily relies on ground motion data from the CanNet network, which utilises MEMS-based sensors. This aligns with the implementation of the CRISiSLab EEW network. Future work aims to extend the analysis by incorporating a more extensive dataset from GeoNet's strong motion sensors, providing a broader spectrum of ground motion data across NZ. Including more data will facilitate the exploration of complex machine learning-based models to construct more nuanced and accurate relationships for S-wave amplitude, thereby enhancing the precision and effectiveness of the EEWS. This expansion will also allow for a more comprehensive investigation into the P and S-wave amplitude relationships, addressing the current data source's limitations and broadening the research scope. Further, it is important to note that the results from this study are not compared with machine learning-based approaches found in the literature, as it would not be a fair comparison due to the differences in dataset sizes and complexities. Future work with a larger dataset will enable a more equitable evaluation of the performance metrics between linear regression and machine learning models.

This study's analysis considered stations installed within a single Site Class to maintain consistent soil characteristics throughout. Future research plans to expand the study to include different Site Classes within NZ. This expansion will provide a more comprehensive understanding of regional variability in P and S-wave amplitude relationships, contributing to the findings' generalisability and enhancing the EEWS's applicability across diverse geological settings.

8.9 Conclusion

This study makes a significant contribution by comparing various relationships between P-wave and S-wave amplitude parameters, distinguishing itself from prior studies that often focused on singular or

limited relationships. Among the various relationships examined, it is evident that Pv exhibited a strong and dependable correlation with PGA.

This research marks a crucial step towards establishing a robust, low-cost EEWS in NZ. Having implemented a community-engaged, low-cost EEW network in NZ (Prasanna et al., 2022), the findings will be the basis for linking detected P-waves to impending ground shaking caused by S-waves. It facilitates the integration of the S-wave-based PLUM algorithm with the P-wave detection algorithm, effectively overcoming the limited warning time inherent to the PLUM algorithm. As shown in the case study, this relationship provides a foundational element for determining the suitable threshold for EEW alerts, enhancing the system's overall responsiveness and reliability.

By choosing Pv vs PGA as the suitable relationship, we showcased its practicality by setting a threshold for the selected P-wave parameter (Pv) that triggers EEW alerts in the Canterbury region of NZ, employing an application using GMICEs. This case study approach is particularly tailored to detecting earthquakes resulting in perceivable ground shaking within the Canterbury region of NZ. However, the approach used in this study is more comprehensive than the specific use case presented; it holds the potential for application and extension to other regions in NZ or areas with similar seismic characteristics. Furthermore, employing this approach to establish empirical relationships between P and S-wave amplitudes for other regions enables the determination of thresholds for detecting ground shaking, enhancing the effectiveness of an EEWS tailored to specific geographic locations and seismic conditions.

This study has laid the foundation for establishing a relationship between P and S-wave amplitudes for EEW, contributing to improved seismic hazard mitigation in NZ. There are opportunities for future research on prioritising the expansion of the ground motion dataset and exploring complex machine learning-based techniques for predicting S-wave amplitude. The insights gained from this study provide a valuable resource for enhancing the accuracy and timeliness of EEW in NZ, ultimately safeguarding lives and property during seismic events.

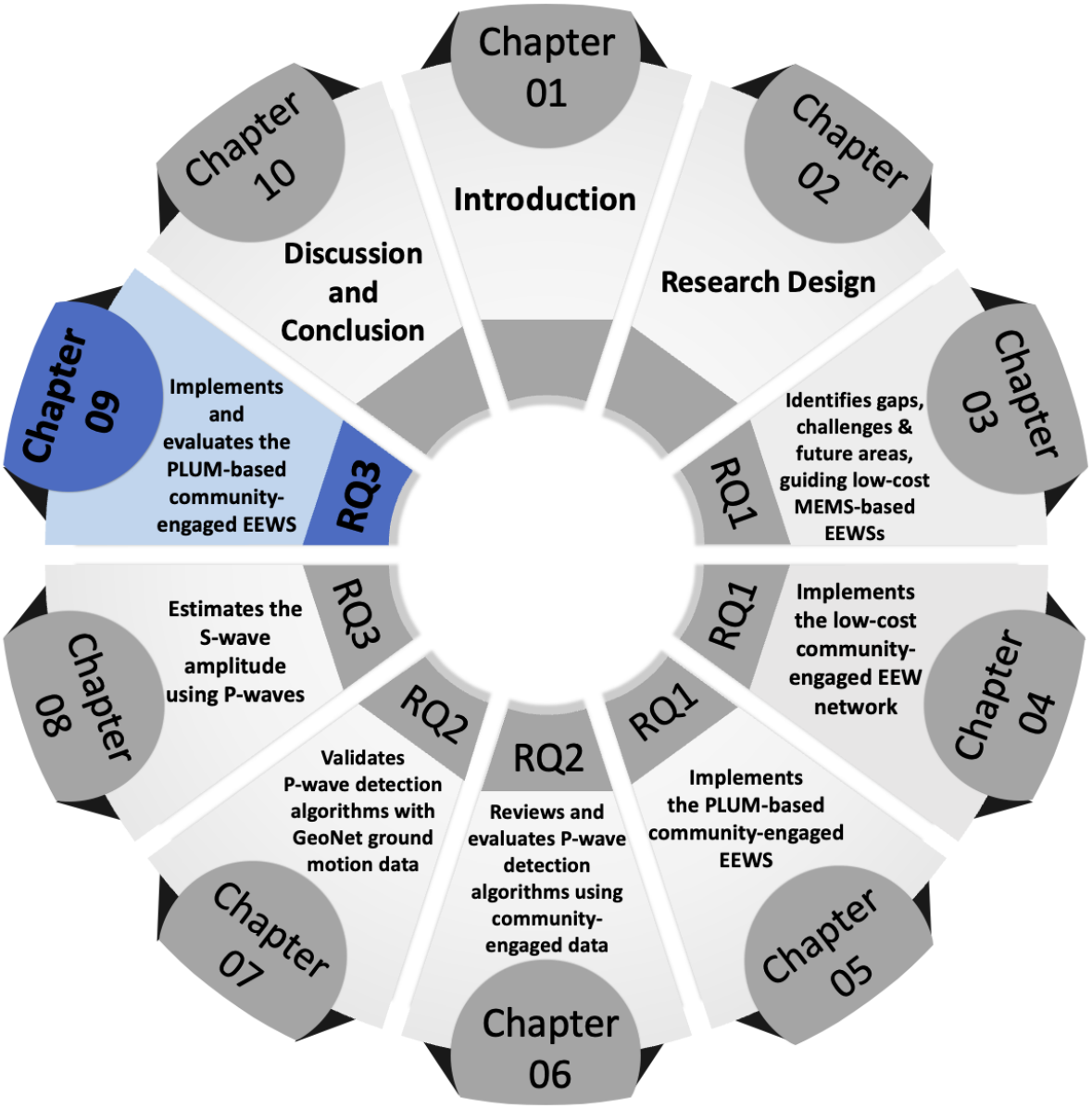
Chapter 01
Introduction
Chapter 02
Research Design
Chapter 03
RQ1
Identifies gaps, challenges & future areas, guiding low-cost MEMS-based EEWSs
Chapter 04
RQ1
Implements the low-cost community-engaged EEW network
Chapter 05
RQ1
Implements the PLUM-based community-engaged EEWS
Chapter 06
RQ2
Reviews and evaluates P-wave detection algorithms using community-engaged data
Chapter 07
RQ2
Validates P-wave detection algorithms with GeoNet ground motion data
Chapter 08
RQ3
Estimates the S-wave amplitude using P-waves
Chapter 09
RQ3
Implements and evaluates the PLUM-based community-engaged EEWS
Chapter 10
Discussion and Conclusion

MASSEY UNIVERSITY
TE KUNENGA KI PŪREHUROA
UNIVERSITY OF NEW ZEALAND

GRADUATE RESEARCH SCHOOL

STATEMENT OF CONTRIBUTION
DOCTORATE WITH PUBLICATIONS/MANUSCRIPTS

We, the candidate and the candidate's Primary Supervisor, certify that all co-authors have consented to their work being included in the thesis and they have accepted the candidate's contribution as indicated below in the *Statement of Originality*.

Name of candidate:	CHANTHUJAN CHANDRAKUMAR
Name/title of Primary Supervisor:	Aprof. Raj Prasanna
In which chapter is the manuscript /published work:	9

Please select one of the following three options:

○ The manuscript/published work is published or in press

- Please provide the full reference of the Research Output:

◉ The manuscript is currently under review for publication – please indicate:

- The name of the journal:

Seismological Research Letters

- The percentage of the manuscript/published work that was contributed by the candidate: 80.00
- Describe the contribution that the candidate has made to the manuscript/published work:

Chanthujan Chandrakumar conceptualised the article, co-constructed the methodology, and conducted the formal analysis and investigation. He also wrote the first draft of the manuscript.

○ It is intended that the manuscript will be published, but it has not yet been submitted to a journal

Candidate's Signature:	Chandrakumar Chanthujan — Digitally signed by Chandrakumar Chanthujan Date: 2024.08.14 13:48:48 +12'00'
Date:	14-Aug-2024
Primary Supervisor's Signature:	Raj Prasanna — Digitally signed by Raj Prasanna Date: 2024.08.21 11:14:46 +12'00'
Date:	21-Aug-2024

This form should appear at the end of each thesis chapter/section/appendix submitted as a manuscript/ publication or collected as an appendix at the end of the thesis.

9 Implementation of P-wave-based PLUM EEWS and Evaluation of the EEWS

This chapter presents the revised version of the seventh manuscript of this study: "A Low-Cost Earthquake Early Warning System for Aotearoa New Zealand". This study details integrating the P-wave detection algorithm into the PLUM algorithm for earthquake detection and alert generation. It also includes the performance analysis conducted on the implemented community-engaged EEWS using two versions of the PLUM algorithm: (1) the adaptation of the original PLUM to NZ, presented in Chapter 5, and (2) the P-wave detection algorithm integrated into the PLUM, presented in this chapter. The primary revisions to this chapter, compared to the original manuscript, involve the removal of content related to the adaptation of PLUM to NZ's context, as this has already been comprehensively covered in Chapter 5. Additionally, the discussion has been updated to reflect these changes. This research was conducted to meet Objective 3.3 of this thesis: To evaluate the performance of the original and the P-wave-based PLUM algorithms in the implemented EEWS.

The article presented in this chapter has been submitted to the Seismological Research Letters as:

Chandrakumar C, Tan ML, Holden C, Stephens MT, Prasanna R. 2024. Performance Evaluation of a Community Engaged Low-Cost Earthquake Early Warning System for Aotearoa New Zealand.

9.1 Introduction

Aotearoa New Zealand (NZ) faces significant seismic risks, recording an average of 15,000 earthquakes annually, including 150 strong enough to be felt (GeoNet, 2023). Efforts are underway to mitigate these risks through improved building codes, public education, and disaster response plans. However, an earthquake early warning system (EEWS) could play a crucial role in reducing earthquake impacts (Fujinawa & Noda, 2013; Nakayachi et al., 2019; Suárez et al., 2009).

EEWS can provide crucial seconds of warning before strong shaking begins, allowing people and infrastructure systems to take protective measures. Many countries have successfully implemented national EEWS, showing their effectiveness in reducing damage and improving preparedness (R. M. Allen & Melgar, 2019; Chandrakumar, Prasanna, Stephens, & Tan, 2022; Strauss & Allen, 2016).

Despite the high seismic risk, NZ does not have a national EEWS. Currently, GeoNet (GeoNet, 2017), managed by GNS Science, offers rapid post-event earthquake information through its website and mobile app (Becker, Potter, Prasanna, et al., 2020). However, there is strong public support for an EEWS, with over 90% of participants in a 2019 survey supporting EEW in NZ (Becker, Potter, Vinnell, et al., 2020). However, the high cost of establishing and maintaining a national system poses a significant challenge for a country with a population of around 5 million (Becker, Potter, Prasanna, et al., 2020). In response to this need, several EEW initiatives have emerged. Google launched an Android-based EEWS in April 2021 (R. M. Allen & Stogaitis, 2022), and several commercial providers offer localised services (Becker, Potter, Prasanna, et al., 2020).

To advance research in this space, using a novel approach to EEW, Prasanna et al., (2022) developed a low-cost community-engaged experimental EEW network in the Greater Wellington region. This network employs a decentralised processing method, contrasting the traditional centralised models employed by other EEWSs worldwide.

This study extends the Prasanna et al. (2022) network by incorporating and implementing an enhanced version of the NZ-adapted PLUM algorithm integrating P-wave detection to increase capability for earlier alerting.

While prior studies have explored individual components of this network (Chandrakumar et al., 2023; Chandrakumar, Tan, Holden, Stephens, & Prasanna, 2024), a comprehensive performance analysis of the entire system has not been conducted. This paper is the first to discuss the EEWS as a whole, providing a detailed evaluation of the enhanced experimental network. It assesses critical aspects such as ambient noise levels, false alerts, and real-time performance, using data from three recent

earthquakes. This comprehensive analysis offers new insights into the effectiveness of the network and its overall performance and provides implications for advancing EEW capabilities and implementation of low-cost EEW networks. The structure of the paper is as follows: the overall EEW approach used in this study (Section 9.2), ambient noise analysis (Section 9.3), network's performance analysis (Section 9.4), discussion (Section 9.5), and conclusion (Section 9.6).

9.2 Background on the Experimental Network

9.2.1 A Low-Cost and Citizen-Science-Led Seismic Network

The experimental network uses the affordable and versatile Raspberry Shake 4D (RS4D) (Anthony et al., 2019) seismographs equipped with Micro-Electromechanical Systems (MEMS) accelerometers. The RS4D integrates vertical geophone and accelerometers to capture comprehensive earthquake data across three axes. While the sensitivity of MEMS accelerometers may not match that of high-end sensors, they have demonstrated their potential in detecting even minor events (Anthony et al., 2019). Additionally, their affordability allows for the creation of dense sensor networks, enhancing the system's overall detection capability.

These low-cost ground motion sensors allow for citizen participation in seismology. Citizen seismology is an emerging field that fosters collaboration between professional seismologists and community volunteers who contribute valuable seismic data for EEWSs and other scientific research (K. H. Chen et al., 2020). By equipping homes and community spaces with seismic sensors, citizen seismology expands sensor networks, enhances public engagement, raises awareness about seismic risks, and potentially provides cost savings.

9.2.2 Network Status and Digital Platform

The experimental network was established in 2020-2021 through partnerships with community volunteers who hosted sensors in their homes. The initial deployment of around 20 sensors was accompanied by workshops to share knowledge and strategies, fostering a citizen-science approach (Prasanna et al., 2022; Tan et al., 2021).

The network was expanded in 2023 to increase the sensor density, resulting in a network of approximately 60 sensors, with a concentration of 45 in the lower part of North Island, NZ (Figure 9-1). Regular status checks are maintained with volunteer sensor hosts through online surveys, allowing them to provide further details about concerns, issues, and the physical status and location of the sensors.

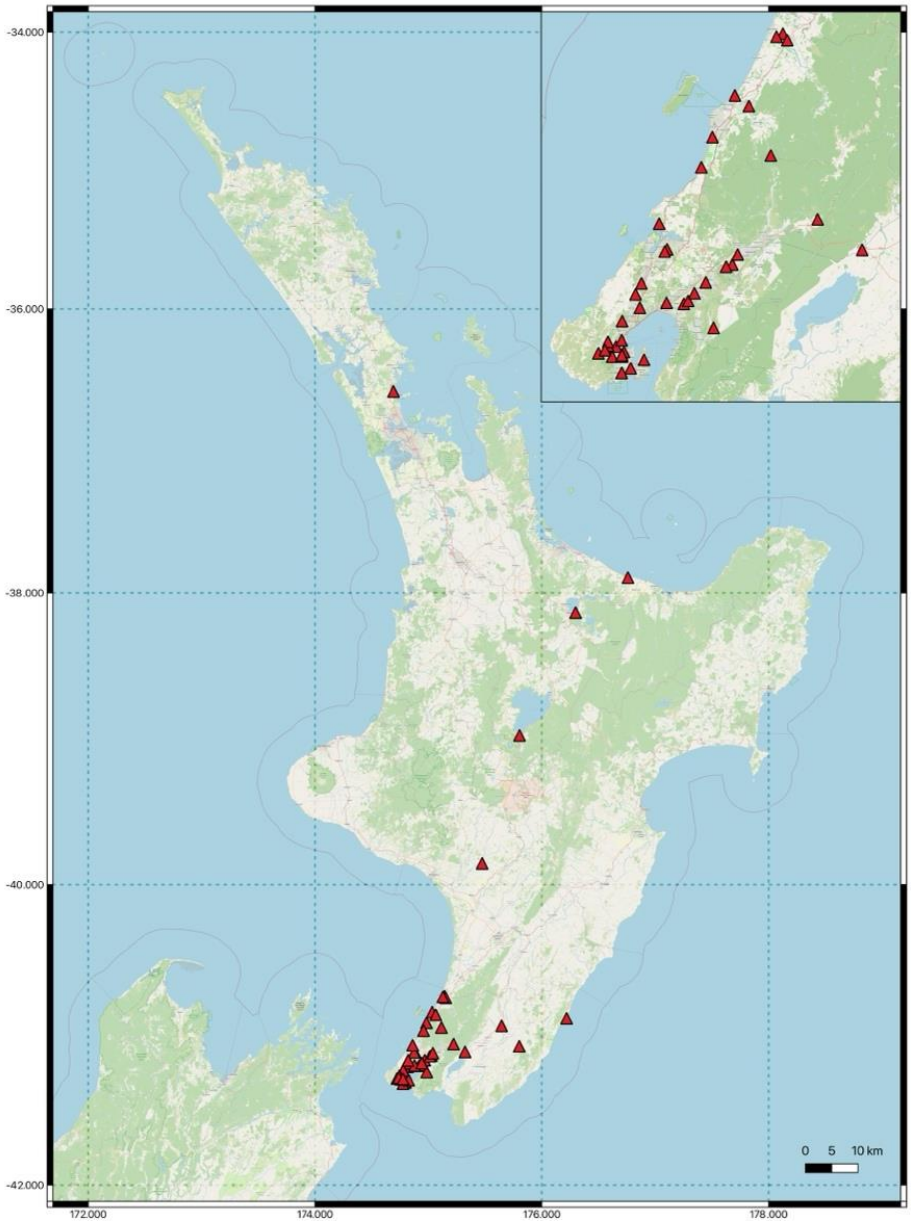

Figure 9-1. Overview of the EEW network, with red triangles indicating the RS4D stations deployed in North Island, NZ. The inset highlights the stations installed in the Greater Wellington region.

Further, a web-based digital platform was developed for real-time data observation and historical data access to facilitate network monitoring and maintenance.

9.2.3 Earthquake Detection and Alert Generation

This experimental EEW network used in this study leverages on two algorithms, both tailored specifically to the NZ context. The first algorithm, referred to as "NZ-PLUM", is an adaptation of the PLUM algorithm originally applied in Japan and proposed by Kodera et al. (2018). NZ-PLUM has been

modified to align with NZ's intensity scale as detailed in Chapter 5. The second algorithm, termed NZ-PLUM-P, builds upon NZ-PLUM by incorporating a P-wave detection component designed to enhance the capability for earlier warning. Unless specified otherwise, the terms NZ-PLUM and NZ-PLUM-P will be used throughout this paper to refer to these algorithms.

9.2.3.1 P-wave Detection Enabled NZ-PLUM (NZ-PLUM-P)

The adapted NZ-PLUM approach relies on detecting thresholds for the horizontal directions of shaking (according to the GMICEs), primarily targeting S-waves, as they are predominantly present in horizontal acceleration data (Shearer, 2009). However, relying on S-wave detection inherently limits the achievable warning times compared to source-based methods, as it delays the detection and alert process (Kodera et al., 2018). To overcome this limitation and extend the warning time, this study integrates a P-wave detection algorithm into the NZ-PLUM approach (Kodera, 2018; Kodera et al., 2018).

However, unlike high-end EEWS in Japan that utilises a Kurtosis-based P-wave detection algorithm with data from sensors installed in boreholes (Kodera, 2018), this study employs a low-cost, community-engaged EEW network. Previous research by Chandrakumar et al. (2023) compared different P-wave detection algorithms for community-engaged networks, ranking them based on their detection accuracy. The wavelet-based P-wave picker ranked highest, followed by the recursive STA/LTA algorithm. Due to challenges in optimising the wavelet-based P-wave picker for decentralised processing on the RS4D, the recursive STA/LTA algorithm is used in this implementation for integrating into the NZ-PLUM algorithm, as detailed in Section 9.5.4.

Upon real-time P-wave detection, the system calculates its amplitude using a dedicated three-second window of vertical acceleration data, as P-waves are primarily present in vertical motion (Y. M. Wu, 2019; H. Zhang et al., 2003). Subsequently, the S-wave amplitude is estimated from the detected P-wave. The system employs an established P-S wave amplitude relationship (equation 1) developed by Chandrakumar, Tan, Holden, Stephens, Punchihewa, et al. (2024) for the Canterbury region of NZ as the best proxy for the network implemented in the Wellington region. This choice is made because, apart from this relationship, no other study in the literature has explored the relationship between P and S-wave amplitudes for EEW in NZ to date. This relationship allows for estimating the S-wave amplitude (PGA) using the P-wave's Peak Ground Velocity (Pv), measured within the first three seconds. The following equation defines the relationship:

$$\log(\mathrm{PGA}) = 0.85 \log(\mathrm{Pv}) + 1.48 \qquad (1).$$

This estimated S-wave amplitude is checked against the alerting threshold (T_H = 42.3 cms^{-2}), corresponding to a P-wave Pv value of 0.6 cms^{-1}, as derived from the P-S wave amplitude relationship.

9.2.3.2 Architecture for Running Both algorithms to Predict Intensity

The NZ-PLUM and NZ-PLUM-P algorithms are integrated into the EEW sensor network, running continuously in real time. These algorithms work in parallel, detecting P-waves and S-waves as they occur and estimating seismic intensity at each prediction point. Figure 9-2 illustrates the workflow for earthquake detection with the use of NZ-PLUM and NZ-PLUM-P algorithms for a single observation station over a three-second time window.

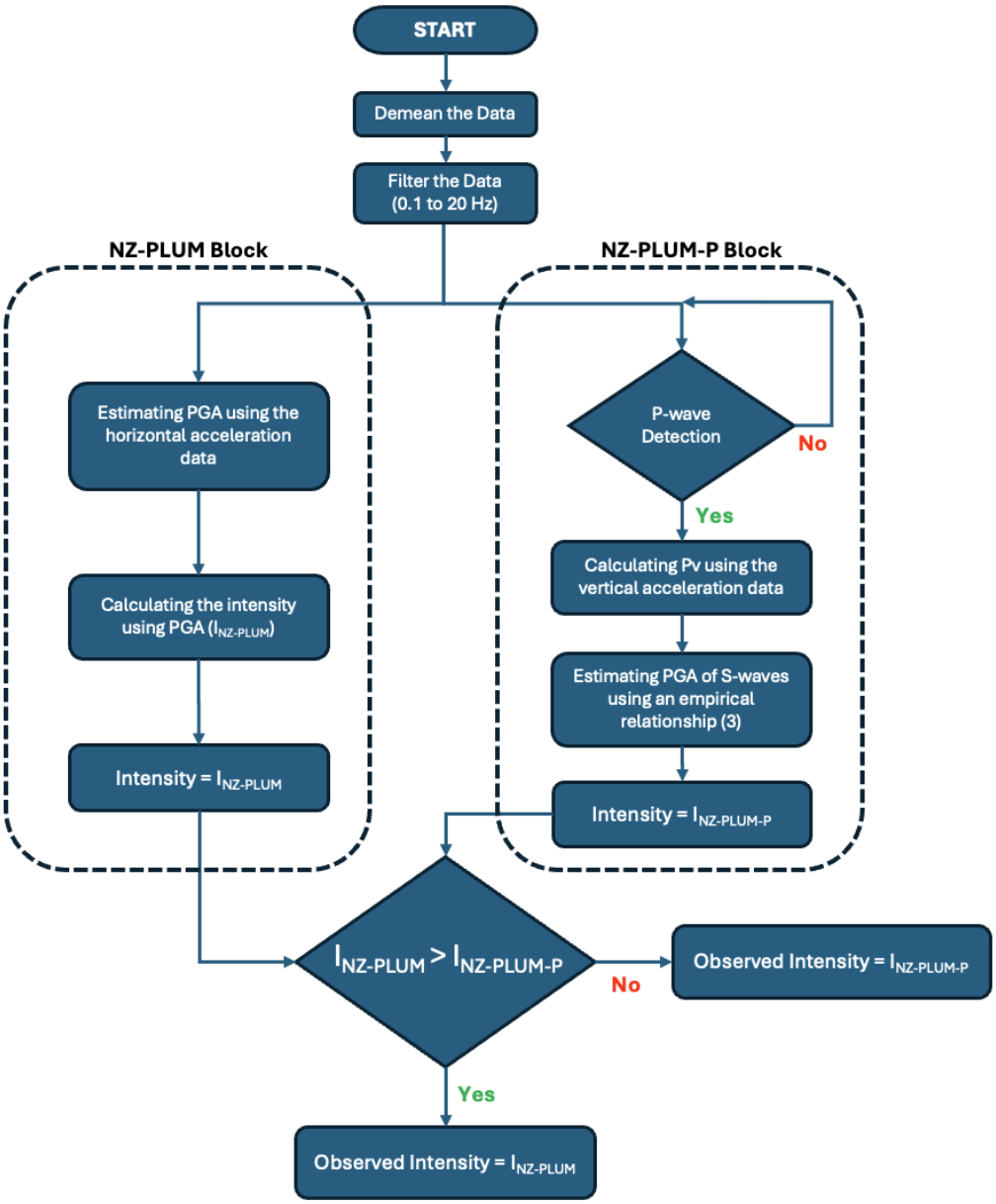

Figure 9-2. Flowchart of the NZ-PLUM and NZ-PLUM-P algorithms' operational architecture for a single observation station during a three-second time window.

If a P-wave is successfully detected, the NZ-PLUM-P algorithm is employed. When a P-wave pick is identified, the higher intensity value from either method (NZ-PLUM or NZ-PLUM-P) is chosen as the observed intensity for that observation station. If P-wave detection fails, the observed intensity is determined using the NZ-PLUM algorithm. Utilising the observed intensities from all observation stations, the system assigns the maximum observed intensity to the prediction point.

9.2.3.3 The Processing Architecture and Alert Generation

When a station's observed intensity surpasses the T_H, the system initiates an event to decide whether to send an EEW alert to a prediction point. In this study, prediction points are designate as the RS4D sensors themselves. This approach differs from Kodera et al.'s (2018) system, which selects prediction points based on regional seismic activity to optimally disseminate alerts to affected areas. This modification is tailored for a community-engaged network, where alerts are delivered to sensor hosts, ensuring alignment with the network's community-focused design.

The implemented EEWS employs a decentralised processing architecture (Chandrakumar, Tan, Holden, Stephens, & Prasanna, 2024), allowing seismic data to be analysed and alerts to be issued directly at the data collection point, without a centralised server. Both the NZ-PLUM and NZ-PLUM-P algorithms are processed within the sensors. Unlike the PLUM algorithm (Kodera et al., 2018), which requires real-time intensity updates from all observation stations to a centralised unit each second, our system employs a dual-tiered structure of RS4D sensors —Primary and Secondary—within this decentralised framework.

Within each prediction radius, one RS4D sensor is designated as the Primary sensor, tasked with two key functionalities: (1) intensity prediction and (2) alert generation for its prediction site. Surrounding sensors within the same radius serve as Secondary sensors responsible for transmitting real-time observed intensity data to the Primary sensor for analysis. A single sensor, therefore, may function as a Primary sensor for one prediction point and as a Secondary sensor for another; particularly in areas where prediction radii overlap. The selection of a Primary sensor is strategically based on its processing load, favouring sensors with minimal existing commitments to other prediction points.

Secondary sensors forward intensity updates to the Primary sensor only when the observed intensity exceeds an internal threshold set to MMI 3.0 (equivalent to a PGA of 4 cms^{-2}). This internal threshold helps maintain optimal performance of the Primary sensor by minimising the influx of data packets during PLUM operation. Additionally, it ensures that only critical intensity information is shared, protecting the privacy of sensor hosts. In a community-engaged EEW network, sending all data to a

Primary station could potentially expose sensitive information to hackers, such as a family's daily habits or private conversations (Bassetti & Panizzi, 2022).

Upon receiving the intensity estimation from a Secondary sensor, the Primary sensor predicts the intensity at the prediction points by taking the maximum observed intensity, including its own estimation. If a station's observed intensity exceeds the T_H, the system opens a 5-second time window to await confirmation for another threshold exceedance from any Secondary sensor within a 30-km radius. If the predicted intensity at the prediction point is greater than MMI 5.0 ($PGA > T_H$) from two or more observational stations, then the Primary station generates an alert to the prediction point; otherwise, the event is dismissed.

9.3 Ambient Noise Analysis

In the community-engaged EEW network context, ambient noise within the sensor array is a significant concern as sensors are not often placed in optimal locations where environmental noise can be minimised. Hosts, who are volunteers, typically prefer to avoid significant alterations to their living spaces, such as drilling or digging, which are necessary for optimal sensor installation (Paul et al., 2023). As a result, the presence of ambient noise within the network can impact the accuracy and reliability of the early warning system. To address this issue, ambient noise levels were analysed using data from 32 ground motion sensors in the network.

9.3.1 Data Selection

Data were initially extracted from 32 ground motion sensors from the network. For this specific ambient noise test, data from one month, June 1st to June 30th, 2024, were selected to capture typical ambient noise levels. The first step involved verifying the completeness of the downloaded data and selecting only those stations with data availability exceeding 90%. This approach ensures a comprehensive assessment based on reliable and sufficient data coverage for the initial evaluation of ambient noise across the network.

Of the 32 stations, 27 had data availability between 90% and 93% and were selected for this test. Five stations fell below the 90% threshold. Discontinuities in the recordings, leading to less than 100% data availability, were often due to interruptions in power supply or internet connectivity.

9.3.2 Method

To evaluate ambient noise at each station, the noise's power spectral density (PSD) was calculated across a critical frequency range of 0.1 to 30 Hz, essential for seismic data analysis. The data preprocessing stage included filtering the seismic signals using the Obspy bandpass filter (Krischer et al., 2015), focusing on the velocimetric vertical component of the RS4D stations (Paul et al., 2023).

The ambient noise levels at each station were determined by generating probability density function (PDF) curves following the methodology outlined by McNamara & Buland (2004). The detailed steps and functions used for processing the PDFs can be referenced in the Obspy documentation (Krischer et al., 2015). This Python-based library implements the McNamara and Buland method for PSD and ambient noise analysis.

Along with the ambient noise measurements from the stations, high- and low-noise models that define the average limits of ambient noise—obtained from a worldwide network of seismograph stations (New Low Noise Model (NLNM) and New High Noise Model (NHLM)) (Peterson, 1993) are plotted for comparison.

9.3.3 Results

In this study, the 27 stations are classified based on their PSD into three categories of ambient noise: low-noise, medium-noise, and high-noise stations (Figure 9-3). This classification is determined through visual inspection of the PSD curves, assessing how closely these curves align with the ambient noise ranges defined by the NLNM and NHLM.

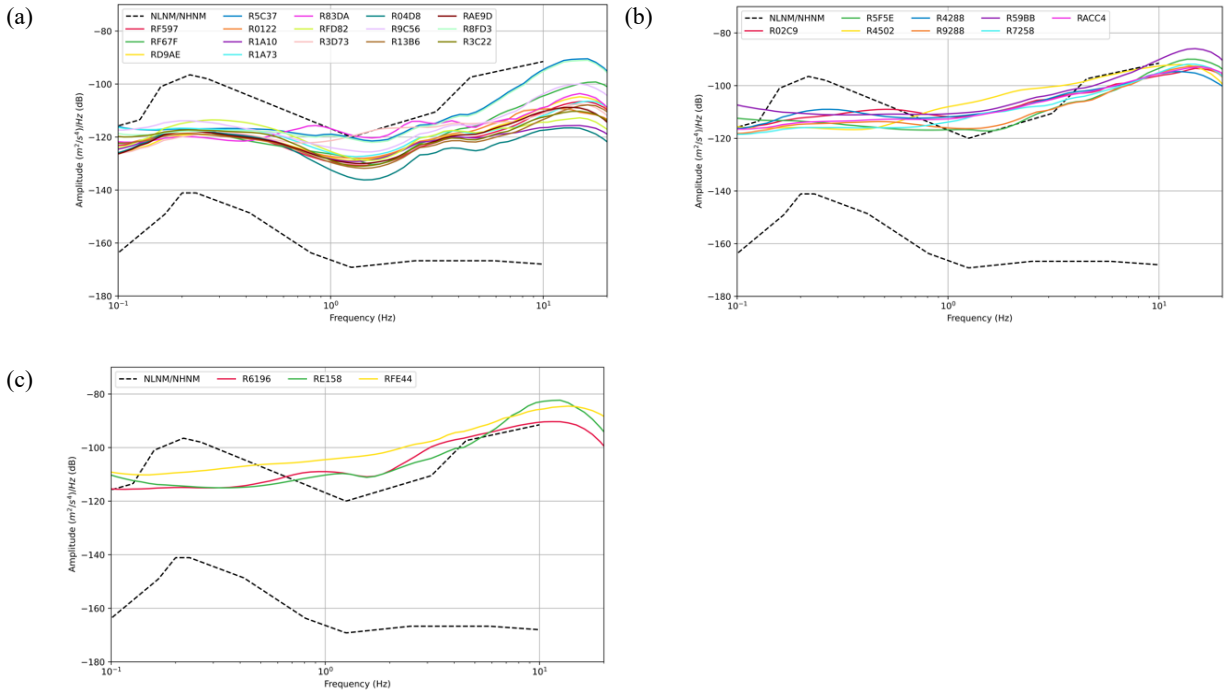

Figure 9-3. Power Spectral Density (PSD) analysis. (a) Low-noise stations, (b) Medium-noise stations, and (c) High-noise stations.

Among the 27 stations, 16 sensors exhibit low noise levels, eight display medium noise levels, and three register high noise levels. Analysis of the sensor locations alongside the ambient noise recorded reveals that the low-noise sensors are typically installed in environments modified to reduce interference, such as isolated ground areas, specifically the sensors RD9AE, R04D8, RFD82, R9C56, RAE9D and R0122—are installed on concrete floors within storerooms, indicating minimal human activity influenced these readings.

Conversely, the sensors classified as medium-noise are primarily located in living rooms, where higher human activity can contribute to increased noise levels. However, these locations are strategically selected to ensure adequate coverage for the network. The three high-noise sensors (Figure 3-c) are positioned in areas with significant human foot traffic and near noise-generating appliances such as washing machines and dishwashers. Additionally, their placement in frequently used corridors further contributes to the elevated noise levels observed.

The PSD analysis for stations classified as low noise, illustrated in Figure 3-a, shows that the PSD values fall within the ambient noise ranges defined by the NLNM and NHNM. This alignment indicates proper sensor installation and the potential for effective seismic event recording within the dominant frequency range of 0.1 to 10 Hz (Tajima & Hayashida, 2018).

In Figure 3-b, the medium-noise stations demonstrate PSD values that remain within the NLNM and NHNM ranges between 0.1 and 0.5 Hz, indicating their suitability for detecting large teleseismic earthquakes, which typically occur within this frequency band. However, at frequencies above 0.5 Hz, the PSD values begin to approach the NHNM, significantly exceeding it beyond 1 Hz. This elevated noise level at higher frequencies could impair the stations' ability to detect weaker, high-frequency seismic signals, often associated with smaller or distant earthquakes (Paul et al., 2023). The increased ambient noise in this frequency range reduces the sensors' sensitivity to these crucial signals, potentially limiting the effectiveness of the EEWS in detecting more subtle seismic activities. The high-noise stations exhibit a similar trend to the medium-noise stations, though with even greater deviations from the NHNM, particularly in the case of station RFE44.

9.4 Network Performance Analysis

The evaluation of the system's performance began with its full operation on April 1, 2024. Since its implementation, the network has recorded 12 earthquake events. A GeoNet search for the Wellington and Marlborough region identified 30 earthquake events, seven of which had over 1,000 felt reports. Of these, the network successfully detected six events, missing only one. In addition to these six events, the network recorded six more events with epicentres outside the Wellington and Marlborough region, with magnitudes ranging from 3.6 to 4.5 (refer to Table J-1 in the Appendix J for the list of 12 recorded earthquakes).

The performance analysis presented in this study focused on the three most recent earthquake events, each with more than 1,000 felt reports, that caused noticeable shaking in the Wellington region (see Figure 9-4).

The first event (EQ1) was a magnitude 3.9 earthquake (GeoNet, 2024a) with the following details:

- Location: 5 km northwest of Porirua
- Depth: 25 km
- Time: May 23, 2024, at 01:36:32 NZ time.

The second event (EQ2) was a magnitude 4.1 earthquake (GeoNet, 2024b):

- Location: 10 km northwest of Porirua
- Depth: 20 km
- Time: June 3, 2024, at 22:05:58 NZ time.

The third event (EQ3) was a magnitude 4.0 earthquake (GeoNet, 2024c):

- Location: 40 km east of Seddon
- Depth: 20 km
- Time: July 6, 2024, at 01:17:15 NZ time.

Further, only five prediction points (P1, P2, P3, P4 and P5) were selected among the sensors to evaluate the decentralised approach's performance, as shown in Figure 9-4. P1 was chosen to encompass the maximum number of stations within its prediction radius, while the remaining four prediction points were randomly selected. The selected five prediction points and their corresponding Primary and Secondary stations within the 30 km prediction radius are shown in Figure J-1 in Appendix J.

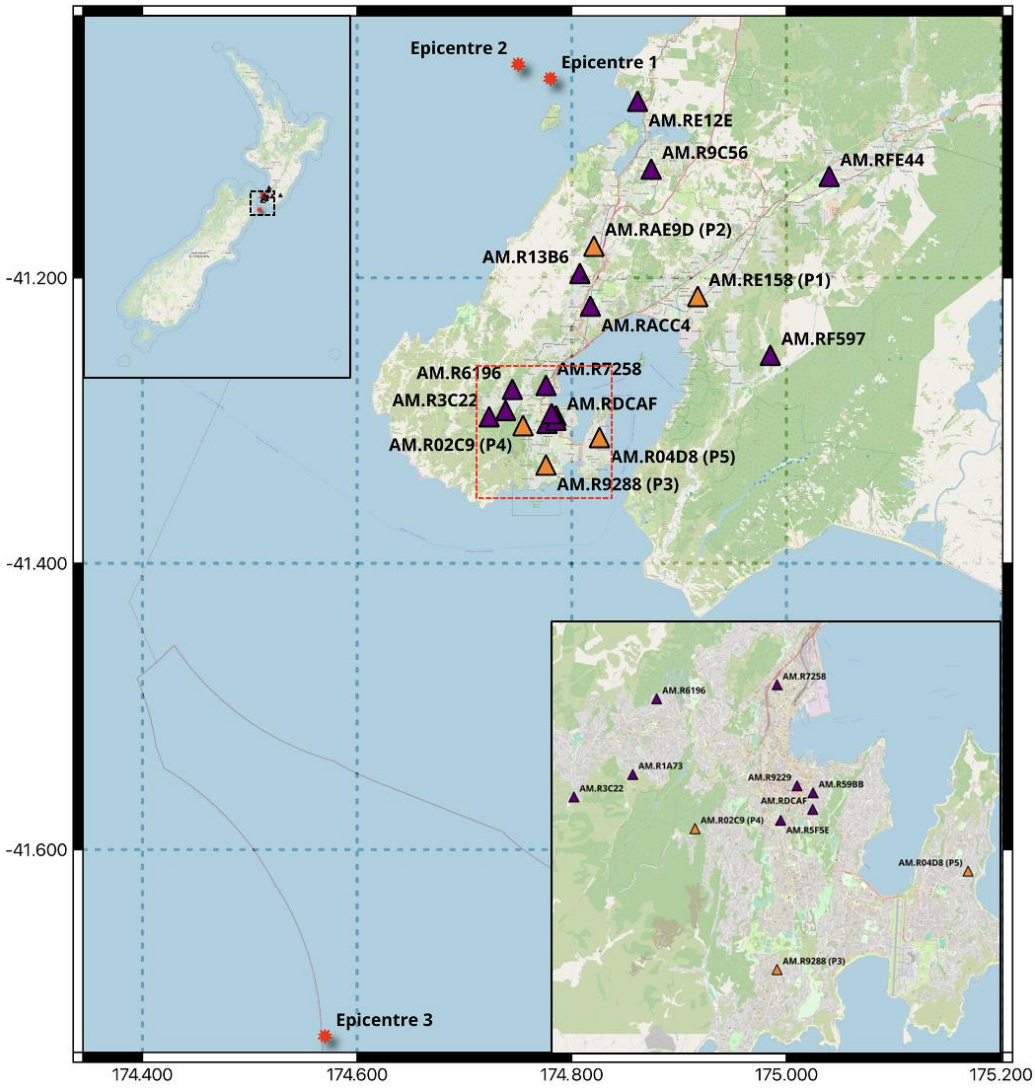

Figure 9-4. Map illustrating the epicentre locations of the recorded earthquakes, with points marked as Epicentre 1, Epicentre 2, and Epicentre 3 corresponding to the first, second, and third events, respectively. Sensor locations are depicted with triangle icons, where purple triangles represent general sensors and orange triangles indicate prediction.

The performance analysis of the implemented EEWS focuses on two critical areas: 1) the system's latency and maximum achievable warning time with the current setup, and 2) the frequency of false alerts from installation to the study's completion.

9.4.1 Assessment of System Latency and Maximum Warning Time

For the implemented system, the alerting intensity is lowered to MMI 3.0, corresponding to $T_H = 4$ cms^{-2}, to measure the system's preliminary performance during an earthquake. This lower threshold increases the likelihood of capturing an earthquake event, as it is more probable than the actual threshold of MMI 5.0, given the infrequency of higher-intensity earthquakes. The selected threshold allows for assessing the network's performance, specifically in calculating system latency for generating alerts and the achievable warning times. Hereafter, T_H refers to the lowered value of 4 cms^{-2} in the subsequent sections unless specified otherwise. It is important to note that the threshold value used was solely for testing purposes and will not be used to issue real-life alerts.

9.4.1.1 Data Selection

The data used in this assessment were drawn from the three most recent earthquakes (EQ1, EQ2 and EQ3) that resulted in felt levels of shaking in the Greater Wellington region, recorded with the lowered threshold of MMI 3.0. The selected events provided a basis for examining system latency and maximum warning times using the NZ-PLUM and NZ-PLUM-P algorithms for the five prediction points.

9.4.1.2 Method

The system's performance was evaluated using two key metrics: system latency and warning time for the NZ-PLUM and NZ-PLUM-P algorithms.

- **Detection Delay:** The time interval between the detections of shaking by the first two stations during an earthquake, primarily influenced by the distance separating these stations.

- **System Latency:** This is the time between the first station detecting shaking within the prediction radius and the target point receiving the alert. It influences the size of the late alert zone—the area near the earthquake's epicentre that receives no warning. Minimising latency is crucial for timely warnings in regions with the highest shaking intensity and potential damage.

- **Warning Time:** Defined as the interval between receiving an alert and the arrival of the more damaging S-waves at the target points. The S-wave arrival time is determined using the recursive STA/LTA algorithm applied to the ground motion data recorded at the target point and is manually cross-checked.

In addition to the actual S-wave pick times reported by the recursive STA/LTA algorithm, the "felt shaking time" was determined by calculating the horizontal PGA exceeding T_H, corresponding to an MMI 3.0 intensity. This intensity is assumed to be the threshold at which shaking becomes noticeable. If the PGA at a prediction point does not surpass T_H, the felt shaking time is not reported and remains blank in the subsequent tables.

9.4.1.3 Results

This section summarises the key findings on system latency and warning times from the three case studies, highlighting the main observations and comparisons between the NZ-PLUM and NZ-PLUM-P algorithms. For a comprehensive view, including detailed picking timestamps and waveform figures reported by the triggered stations and prediction points, refer to Appendix K.

9.4.1.3.1 Case Study 1: Earthquake on May 23, 2024

Figure 9-5-a shows the stations in red triangles, which were the first to be triggered during the earthquake for the NZ-PLUM algorithm. For prediction points P1, P2, and P5, the stations AM.R9C56 and AM.RFE44 were the first to exceed the threshold, however, for prediction points P3 and P4, AM.RFE44 is outside the 30 km radius, so only AM.R9C56 and AM.RAE9D exceeded the threshold initially. In contrast, the NZ-PLUM-P algorithm triggered stations AMRE12E and AM.R9C56 are the first for all five prediction points within the 30 km radius, as shown in Figure 9-5-b.

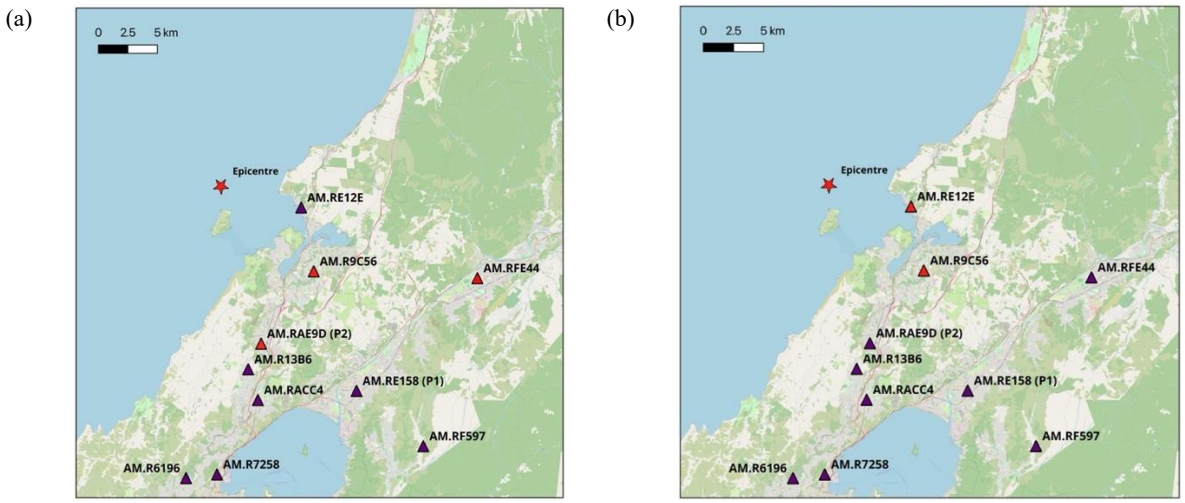

Figure 9-5. Stations first triggered (shown as red triangles) during the first earthquake: (a) using the NZ-PLUM algorithm and (b) using the NZ-PLUM-P algorithm.

An analysis of the detection times and ground motion recordings revealed that, although the NZ-PLUM approach primarily relies on S-waves and horizontal thresholds, in this instance, stations AM.R9C56 and AM.RFE44 were triggered by P-waves, as summarised in Table 9-1. Being closer to the epicentre, these stations detected significant horizontal shaking from the P-waves. However, station AM.RAE9D exceeded the threshold with the S-waves. Despite its proximity to the epicentre, station AM.RE12E did not exceed the detection threshold (Figure 9-5-a), recording a maximum PGA of 2.2 cms^{-2}, likely due to site-specific characteristics. The three-dimensional ground motion data from AM.RE12E is provided in Figure J-2 in the Appendix J. In contrast, the NZ-PLUM-P algorithm detected P-waves at the first two stations closer to the epicentre, enabling earlier earthquake detection (Table 9-1).

Table 9-1. Summary of the wave phases that triggered the first and second stations, detection delays, system latencies, warning times, and felt shaking times for each prediction point using the NZ-PLUM and NZ-PLUM-P algorithms for EQ1.

Prediction point	Triggered wave phase for the first station		Triggered wave phase for the second station		Detection delay		System latency		Warning time		Felt shaking time
	NZ-PLUM	NZ-PLUM-P	NZ-PLUM	NZ-PLUM-P	NZ-PLUM	NZ-PLUM-P	NZ-PLUM	NZ-PLUM-P	NZ-PLUM	NZ-PLUM-P	
P1	P	P	P	P	1.946	0.321	2.624	1.275	1.812	4.312	-
P2	P	P	P	P	1.946	0.321	2.677	1.328	1.430	3.430	01:36:44
P3	P	P	S	P	4.427	0.321	5.236	1.137	0.860	5.61	01:36:48
P4	P	P	S	P	4.427	0.321	5.236	1.137	1.30	3.050	-
P5	P	P	P	P	1.946	0.321	2.497	1.148	3.9	5.900	-

P and **S** denote the waves used to trigger alerts. **P** indicates using P-waves (Primary waves), while **S** indicates S-waves (Secondary waves).

System latency: As shown in Table 9-1, the system latency of NZ-PLUM for earthquake warnings ranged from 2.5 to 5.2 seconds across the five prediction points. P1, P2, and P5 have shorter system latency than P3 and P4; this is affected by the detection delay (1.9 to 4.4 seconds) that depends on earthquake direction and sensor distribution. Excluding wave propagation, the system required just 0.678 to 0.809 seconds to detect shaking, generate an alert, transmit, and log the event. For NZ-PLUM-P, system latency ranged from 1.1 to 1.3 seconds, primarily due to a minimal detection delay of just 0.3 seconds between the first two stations.

Warning time: According to the prediction point locations (Figure 9-4), P3, P4, and P5 should receive longer warning times for EQ1, while P1 and P2 should have shorter times. For NZ-PLUM, P5 had the longest warning time at 3.9 seconds, while P3 had the shortest at 0.86 seconds. P5's longer warning time is expected, given its greater distance from the epicentre (Table 9-1). However, P3 and P4, despite their distance from the epicentre, experienced reduced warning times due to delays in confirming the second station. Although the first station for P3 and P4 triggered with P-waves, subsequent stations did not, causing the second station to be triggered by S-waves. This threshold-based approach in NZ-PLUM increased detection delays and reduced warning times, even when the first station was triggered with P-waves.

In contrast, the NZ-PLUM-P algorithm significantly improved warning times for all five prediction points due to earlier alerts from P-wave detection. P5 saw the most significant benefit, with a warning time of 5.9 seconds (a two-second improvement), while P3's warning time increased substantially to 5.6 seconds from the 0.8 seconds provided by NZ-PLUM (Table 9-1).

Felt shaking: Felt shaking was recorded only at P2 and P3, but warnings were generated for all prediction points, as shown in Table 9-1.

9.4.1.3.2 Case Study 2: Earthquake on June 3, 2024

Similar to the first, the second case study involved an earthquake with an epicentre north of Wellington and yielded comparable results.

This case presented an interesting observation: both the NZ-PLUM and NZ-PLUM-P algorithms used P-waves for alert generation (Table 9-2), but NZ-PLUM showed longer detection times than NZ-PLUM-P. In NZ-PLUM, stations AM.R9C56 and AM.R7258 were the first to exceed the threshold for all prediction points despite closer stations like AM.RE12E and others (AM.RAE9D, AM.R13B6, and AM.RACC4) near the epicentre (Figure 9-6-a) did not surpass the threshold with P-waves; S-waves triggered them. Consequently, AM.R9C56 and AM.R7258 became the first stations to trigger with P-

waves. In contrast, for NZ-PLUM-P, stations AM.RE12E and AM.R9C56 detected the shaking first (Figure 9-6-b), benefiting from earlier P-wave detection at AM.RE12E, closer to the epicentre.

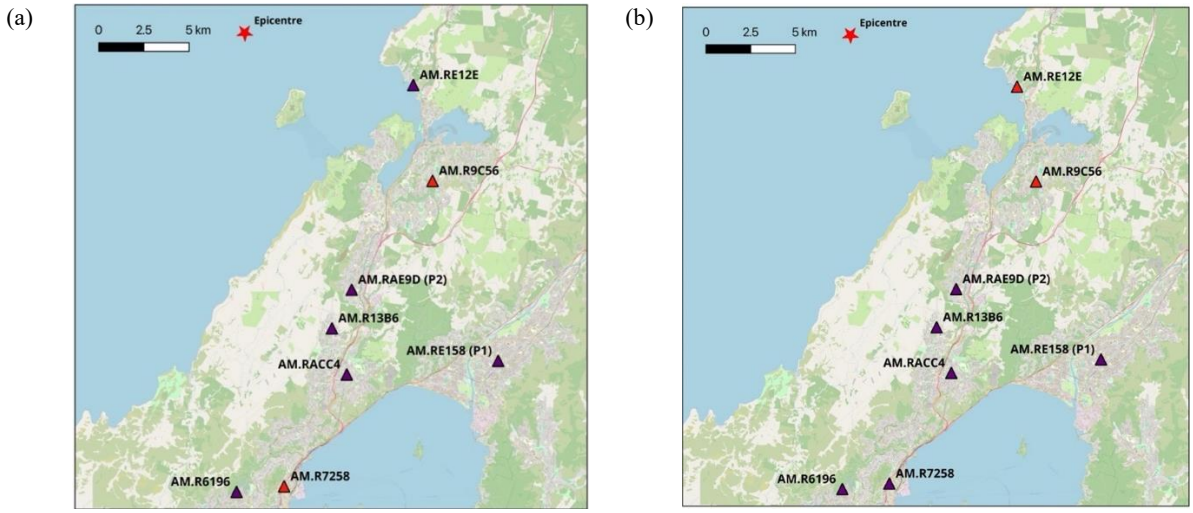

Figure 9-6. Stations first triggered (shown as red triangles) during the first earthquake: (a) using the NZ-PLUM algorithm and (b) using the NZ-PLUM-P algorithm.

System latency: NZ-PLUM-P reported shorter system latency, ranging from 1 to 1.2 seconds, compared to NZ-PLUM's 1.7 to 1.9 seconds (Table 9-2). The detection delay played a crucial role in the system latency, where for NZ-PLUM, the detection delay was ~ 1 second, and for NZ-PLUM-P, it was around ~ 0.3 seconds. Excluding wave propagation time, the estimated latency for processing and transmission for both NZ-PLUM (0.6-0.8 seconds) and NZ-PLUM-P (0.7 to 0.9 seconds) are similar to case study 1, indicating consistent processing times within the systems.

Table 9-2. Summary of the wave phases that triggered the first and second stations, detection delays, system latencies, warning times, and felt shaking times for each prediction point using the NZ-PLUM and NZ-PLUM-P algorithms for EQ2.

Prediction point	Triggered wave phase for the first station		Triggered wave phase for the second station		Detection delay		System latency		Warning time		Felt shaking time
	NZ-PLUM	NZ-PLUM-P	NZ-PLUM	NZ-PLUM-P	NZ-PLUM	NZ-PLUM-P	NZ-PLUM	NZ-PLUM-P	NZ-PLUM	NZ-PLUM-P	
P1	P	P	P	P	1.085	0.261	1.794	1.105	3.380	4.63	22:06:05
P2	P	P	P	P	1.085	0.261	1.707	1.018	2.45	3.7	22:06:03
P3	P	P	P	P	1.085	0.261	1.886	1.197	4.49	5.74	22:06:07
P4	P	P	P	P	1.085	0.261	1.656	0.967	4.42	5.67	-
P5	P	P	P	P	1.085	0.261	1.850	1.161	4.47	5.72	-

P and **S** denote the waves used to trigger alerts. **P** indicates using P-waves (Primary waves), while **S** indicates S-waves (Secondary waves).

Warning time: Both algorithms generated alerts using P-waves, so the warning times were not drastically different. However, if NZ-PLUM had relied on S-waves, it would have caused a delay of about 4 seconds, resulting in no warning for P1 and P2 due to their proximity to the epicentre. NZ-PLUM-P's earlier P-wave detection provided a wider warning window, with an average increase of 1.25 seconds in warning time across all prediction points (Table 9-2). This is particularly beneficial for areas near the earthquake's source, like P2, which received a 3.7-second warning— unattainable with NZ-PLUM upon S-wave detection. This highlights NZ-PLUM-P's effectiveness in reducing the blind zone during the EEW generation.

Felt shake: Residents at P4 and P5 likely would not feel the shaking (MMI less than 3.0), yet they would still receive a warning with both algorithms (Table 9-2).

9.4.1.3.3 Case Study 3: Earthquake on July 6, 2024

This case study evaluates the NZ-PLUM approach when S-waves are the primary trigger for earthquake detection (Table 9-3). The M4.0 earthquake east of Seddon, due to the distance between the epicentre and the sensor network, did not generate significant horizontal shaking with P-waves. As a result, none of the initial triggering stations were activated by P-waves. Figure 9-7-a shows the stations first triggered (red triangles). For prediction points P1, P2, P4, and P5, stations AM.R9288 and AM.R770A were the first to exceed the threshold. However, for P3, the alert relied on stations AM.R770A and AM.R02C9 exceeding the threshold. In the NZ-PLUM-P approach (Figure 9-7-b), the first two stations detecting shaking for P1, P2, P4, and P5 are the same as in NZ-PLUM. For P3, the alert leveraged stations AM.R770A and AM.R5C37, differing from NZ-PLUM, which used AM.R770A and AM.RFE44.

(a)

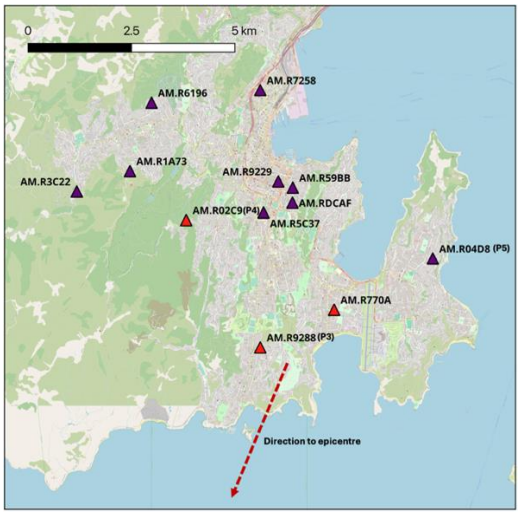

(b)

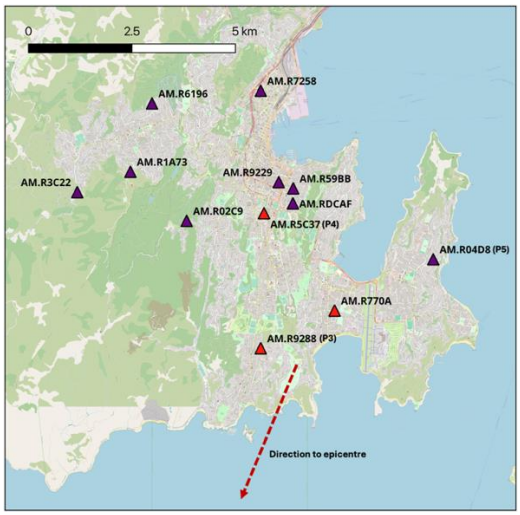

Figure 9-7. Stations first triggered (shown as red triangles) during the first earthquake: (a) using the NZ-PLUM algorithm and (b) using the NZ-PLUM-P algorithm.

System latency: For NZ-PLUM, system latency varied from 0.75 to 1.3 seconds, with intrinsic latency (excluding detection delay) ranging from 0.5 to 0.8 seconds. For NZ-PLUM-P, system latency ranged from 0.75 to 1.15 seconds, with intrinsic latency between 0.35 and 0.75 seconds (Table 9-3).

Table 9-3. Summary of the wave phases that triggered the first and second stations, detection delays, system latencies, warning times, and felt shaking times for each prediction point using the NZ-PLUM and NZ-PLUM-P algorithms for EQ3.

Prediction point	Triggered wave phase for the first station		Triggered wave phase for the second station		Detection delay		System latency		Warning time		Felt shaking time
	NZ-PLUM	NZ-PLUM-P	NZ-PLUM	NZ-PLUM-P	NZ-PLUM	NZ-PLUM-P	NZ-PLUM	NZ-PLUM-P	NZ-PLUM	NZ-PLUM-P	
P1	S	P	S	P	0.504	0.004	1.302	0.962	2.250	10	-
P2	S	P	S	P	0.504	0.004	1.148	1.167	2.450	9.841	01:17:27
P3	S	P	S	P	0.009	0.393	0.746	0.756	No Warning	5.990	01:17:23
P4	S	P	S	P	0.504	0.004	1.280	0.940	No Warning	6.5	01:17:24
P5	S	P	S	P	0.504	0.004	1.071	0.981	No Warning	6.37	-

P and **S** denote the waves used to trigger alerts. **P** indicates using P-waves (Primary waves), while **S** indicates S-waves (Secondary waves).

Warning time: For NZ-PLUM, despite a minimal detection delay between the first two stations, crucial for enhancing warning time, detecting earthquakes upon S-wave arrival significantly reduces the warning time. As shown in Table 9-3, the warning times for prediction points P1 and P2, which are farther from the epicentre, were only 2.25 and 2.45 seconds, respectively. Prediction points P3 and P4, positioned on the frontline of first detection, received no warning since the NZ-PLUM approach detected the shaking upon the arrival of the S-waves at these stations, resulting in late warnings. Similarly, P5, which falls within the blind zone, also received a late alert.

In contrast, NZ-PLUM-P provided substantial improvements in warning times. For P1 and P2, the warning times were extended to 10 and 9.8 seconds, respectively, compared to just 2.25 and 2.45 seconds with NZ-PLUM. Similarly, P3 and P5 saw warning times of 5.99 and 6.37 seconds, while P4, which initially fell within a blind zone under NZ-PLUM, received 6.5 seconds of warning (Table 9-3). These enhanced warning times are primarily due to the earthquake's occurrence approximately 47 kilometres from the first detected stations, resulting in a significant delay between the arrival of P-waves and S-waves at the sensor network in the Greater Wellington region. This time gap allowed the detection of P-waves to trigger early alerts for households near the first detected stations well before

the arrival of the more destructive S-waves. Therefore NZ-PLUM-P algorithm is particularly advantageous for areas closer to the epicentre of distant earthquakes.

Felt shake: Residents at P2, P3, and P4 felt the shaking according to MMI 3.0 threshold analysis. While NZ-PLUM provided a warning only for P2, NZ-PLUM-P successfully issued warnings for all three points (see Table 9-3).

9.4.2 False Alert Assessment

In a community-engaged EEWS, ambient noise from the environment and human activities can cause false detections at individual stations, potentially leading to false alerts if more than two stations are triggered within a five-second time window. This section investigates the number of alerts triggered by the Primary stations for the five prediction points, evaluating the system's reliability in generating accurate alerts since implementation.

For this assessment, the NZ-PLUM and NZ-PLUM-P algorithms were first evaluated using the actual alerting threshold of MMI 5.0. The results indicated neither algorithm triggered any alerts, effectively avoiding false alarms. Although the NZ-PLUM-P algorithm successfully detected P-waves in numerous times, it did not exceed the Pv threshold of 0.6 cms^{-1} within the initial 3-second window required for alert generation by two stations within the designated time frame. Similarly, no stations exceeded the T_H for NZ-PLUM.

To further analyse false alerts, the false alerts recorded with MMI 3.0 are analysed, corresponding to a T_H of 4 cms^{-2} for NZ-PLUM and a Pv of 0.04 cms^{-1} for NZ-PLUM-P. This helps assess the system's sensitivity and understand its behaviour under less stringent conditions. Testing one prediction point (P1) with the lowered threshold resulted in NZ-PLUM reporting 16 alerts, with three correctly identifying actual earthquake events and 13 false alerts. At the same threshold, NZ-PLUM-P generated 115 alerts, correctly identifying 12 actual earthquake events but producing 103 false alerts, as summarised in Table 9-4.

Table 9-4. Summary of Alerts Generated by NZ-PLUM-P Algorithm for Prediction Point P1 at MMI 3.0 Threshold with different number of Triggering Stations

Triggering Stations for Alert	Number of Alerts Generated	Actual Earthquakes Detected	False Alerts
2	115	12	103
3	42	12	30
4	13	12	1

While the number of alerts generated for NZ-PLUM-P alerts seems high, it is essential to note that lowering the alerting threshold to MMI 3.0 is impractical for real-world use, as it corresponds to

minimal shaking levels. However, further testing highlights that false alerts can be mitigated by increasing the number of triggering stations for NZ-PLUM-P. In further testing, increasing the number of triggering stations for NZ-PLUM-P reduced false alerts: with three triggering stations, false alerts dropped to 30, and with four triggering stations, they decreased to just one (See Table 9-4). This indicates that using a quadruple station requirement for alert generation significantly reduces false alerts, even with an alerting intensity of MMI 3.0. However, this comes at the cost of increased system latency due to the additional detection time required.

A similar analysis with the NZ-PLUM algorithm showed that when three and four stations were required to trigger, only three alerts were generated in each case, all corresponded to actual earthquakes, resulting in zero false alerts.

9.5 Discussion

9.5.1 Insights From the Design and Deployment of a Community-Engaged Network

The design and deployment of a community-engaged EEW network using low-cost RS4D sensors provide valuable insights into leveraging citizen participation in seismic monitoring. The collaboration between scientists and community volunteers fosters a sense of ownership and engagement, enhancing the overall effectiveness of the network. This approach broadens the geographic coverage of sensor networks and promotes public awareness and education about seismic risks. The total of 60 sensors, mainly concentrated in the lower part of North Island, NZ, demonstrates the scalability and adaptability of the network. While challenges such as optimal sensor installation methods and data quality arose, the overall positive response from the community underscored the potential for such initiatives. Using a digital platform for real-time data observation and historical data access further supports network maintenance and monitoring, ensuring timely and accurate seismic data collection.

9.5.2 Significance of the Adaptation and Modification of PLUM Using Decentralised Processing

Integration of a P-wave detection algorithm into the modified PLUM (NZ-PLUM-P) significantly enhances the system's capability to provide early warnings. By detecting the less destructive P-waves before the arrival of the more damaging S-waves, the NZ-PLUM-P approach extends the warning window. This extended warning time is crucial, allowing individuals and organisations to take protective actions, potentially saving lives and reducing economic losses. The modifications also

address the limitations of the NZ-PLUM approach, which primarily relies on S-wave detection and may not provide adequate warnings in regions close to the earthquake epicentre.

Moreover, the adoption of decentralised processing is instrumental in optimising the performance and reliability of the EEWS. By distributing computational tasks across the sensor network, this approach eliminates the vulnerability of a centralised system to single points of failure (Chandrakumar, Tan, Holden, Stephens, & Prasanna, 2024). Consequently, data processing and alert generation occur locally, accelerating response times and minimising system latency. This decentralised architecture also reinforces the system's robustness, as the failure of individual sensors or sensor clusters does not compromise overall functionality. Further, compared to centralised processing, a decentralised architecture is more cost-effective because it leverages the growing affordability and increasing processing power of MEMS-based sensors, which handle computations directly on-site, reducing the need for extensive centralised infrastructure (Prasanna et al., 2022).

Finally, decentralised processing facilitates the network's scalability and adaptability. The seamless integration of additional sensors and the system's expansion without extensive infrastructure modifications are advantageous for the implemented community-engaged network. This approach enhances the system's technical performance, contributing to its long-term sustainability and the community's overall resilience.

9.5.3 Implications From Network's Performance

9.5.3.1 Ambient Noise Analysis

The noise analysis revealed a varied noise environment across the community-engaged sensor network. The classification into low-noise, medium-noise, and high-noise categories shows that most sensors (14 out of 21) have low noise levels, indicating successful installations in relatively quiet areas. These low-noise sensors, particularly those in isolated ground areas or storerooms, are vital for reliably detecting significant teleseismic events. Their proximity to the sensor's self-noise level at low frequencies (0.1 to 0.5 Hz) is particularly advantageous for capturing these events.

However, sensors in living rooms or near kitchens experience higher ambient noise levels due to human activity and appliances, potentially hindering the detection of weaker seismic signals. While the current noise levels are generally acceptable for detecting significant seismic events, further optimising sensor placement is needed. Encouraging hosts to install sensors in low-noise environments, such as basements or isolated areas, could improve network performance. Education and support from the EEWS administrators can help volunteers understand the importance of optimal sensor placement.

Balancing practical installation considerations with technical requirements for low-noise environments is crucial. Overall, tolerating higher noise levels in a community-engaged EEWS requires careful consideration of the trade-offs between network density, data quality, and desired system performance.

9.5.3.2 Real-Time Analysis

The case studies provided valuable insights into the comparative performance of the NZ-PLUM and NZ-PLUM-P approaches, particularly regarding their ability to generate timely and accurate alerts. The key implications observed from the three case studies are as follows:

- **Effectiveness of P-Wave Detection:** The NZ-PLUM-P algorithm consistently outperformed the NZ-PLUM approach by leveraging P-wave detection to trigger alerts at both detection stations across all three case studies. This capability significantly reduced system latency and increased warning times, particularly for regions near the epicentre, where early detection can mitigate earthquake impacts. In contrast, the NZ-PLUM approach, relying on S-wave detection and horizontal thresholds, faced notable limitations. In Case Study 3, where the earthquake was farther from the sensor network, it failed to trigger early warnings at several target points due to its reliance on S-waves. The threshold-based approach in NZ-PLUM often missed the earliest waveforms at the closest stations, especially when site characteristics caused the threshold to be exceeded only at certain locations.
- **Improved Warning Times with NZ-PLUM-P:** NZ-PLUM-P provided considerably longer warning times across all case studies. The approach's ability to detect P-waves earlier at stations closer to the epicentre significantly reduced detection delay and system latency. This led to increased warning times, particularly in scenarios where the earthquake's epicentre was distant from the sensor network, as seen in Case Study 3. The improved warning times are critical for reducing the blind zone and enhancing the overall effectiveness of the EEW system.

Overall, the case studies reinforce the importance of P-wave detection for EEW and suggest that incorporating NZ-PLUM-P into EEW systems can lead to more effective and reliable alerts, particularly in regions vulnerable to seismic activity. However, the extent of these improvements depends on the delay between P-wave and S-wave arrivals, influenced by the distance between the epicentre and the

sensor network. Greater epicentral distances result in longer delays and extended warning times, while closer earthquakes yield minimal warning time differences between the two approaches.

Despite the strengths and limitations of both approaches, their simultaneous use offers significant benefits. The NZ-PLUM-P approach activates for distant earthquakes, while either approach can handle closer earthquakes, depending on which detects the shaking first. This dual approach maximises the potential of the PLUM approach in a decentralised, community-engaged EEWS.

The analysis of target points that did not exceed the alerting threshold of MMI 3.0, where shaking was not felt, highlights instances where warnings were issued despite the absence of significant ground shaking. Such false positives, often referred to as "Precautionary Alerts," are currently considered acceptable according to the literature; however, public opinion may evolve over time as experience with the system increases. Studies, such as Cochran et al. (2019), indicate that the public does not typically perceive an alert as false if no shaking is felt, but rather if no earthquake occurred, such as in cases of technical malfunctions or non-earthquake noise.

This phenomenon, known as "over-alerting," is an inherent limitation of the PLUM algorithm, where predicted ground motions exceed the threshold, but the actual shaking does not (Cochran et al., 2019). To address this, the alerting threshold for PLUM must be optimised to balance missed, correct, and precautionary alerts according to user requirements. For instance, some users may prefer more precautionary alerts to ensure timely warnings, even at the cost of occasional unnecessary actions. Others might prioritise fewer alerts to avoid frequent interruptions or precautionary measures.

This trade-off can be quantified using a cost-ratio (CR) analysis as proposed by Minson et al., (2019). CR considers the relative costs of missed, correct, and precautionary alerts, as well as the cost of potential damage versus the cost of taking protective action. Integrating this analysis into the PLUM algorithm could enable the system to determine optimal alerting thresholds tailored to the needs of target sites and their users, maximising the benefit of early warnings.

9.5.3.3 False Alert Analysis

The false alert analysis highlights the reliability of the community-engaged EEWS in generating accurate alerts, especially with the threshold set at MMI 5.0. Since the system's launch, the NZ-PLUM and NZ-PLUM-P algorithms have reported zero alerts, indicating no earthquakes producing shaking above MMI 5.0.

When the threshold was lowered to MMI 3.0 for further analysis, NZ-PLUM, with three triggering stations, generated alerts only for actual earthquakes (3) that caused felt shaking, demonstrating its

reliability even at lower thresholds. Similarly, the NZ-PLUM-P algorithm, with four triggering stations, reliably detected actual earthquakes (12), including distant events, with just one false alert. This indicates that the low-cost, community-engaged network can remain reliable at lower thresholds if the number of triggering stations is increased.

However, it is important to note that increasing the number of required triggering stations comes at the cost of extended detection times, which may compromise the warning time. Therefore, while the system can effectively detect smaller earthquakes with a lower threshold, careful consideration must be given to balancing detection accuracy with the need for timely alerts.

Overall, the NZ-PLUM-P approach significantly enhances warning times compared to the NZ-PLUM approach by reducing detection delays and providing timely alerts, even for areas near the epicentre. The integration of both PLUM approaches ensures the system can effectively handle earthquakes of varying magnitudes and distances, offering a robust early warning mechanism. These results confirm that a community-engaged, low-cost EEWS with decentralised processing, incorporating both NZ-PLUM and NZ-PLUM-P approaches, is a viable solution for increasing warning times and reducing the blind zone, thus enhancing earthquake preparedness and safety.

9.5.4 Future Works and Limitations

1. **Network Expansion and Region-wise Alerting:** The algorithms will be rolled out to the entire network, enabling each sensor to function as a target point, thereby improving coverage and functionality. Additionally, adopting region-wise alerting, similar to Japan's PLUM approach, will be explored. Generating alerts for predefined regions rather than individual target points is expected to improve the warning capabilities by extending the warning coverage and increasing the warning time.
2. **Site Amplification Factors:** Future studies will incorporate site-specific soil amplification factors to improve intensity predictions at target points according to the original PLUM approach, addressing a current limitation in the system.
3. **Playback with historical earthquakes:** Future research will evaluate the performance of both PLUM-based approaches by conducting playbacks of historical earthquakes recorded by the

implemented EEWS. This analysis will provide insights into the system's effectiveness across a broader range of seismic events.

4. **Empirical Relationship for S-wave Amplitude:** The current empirical relationship for estimating S-wave amplitude, derived from Canterbury region earthquakes (2010–2023) (Chandrakumar, Tan, Holden, Stephens, Punchihewa, et al., 2024), is applied to the Wellington-based network in this study due to the lack of a region-specific relationship for Wellington. While this provides a starting point, it may affect prediction accuracy given regional geological differences. Future work will focus on developing a Wellington-specific relationship using local GeoNet data to improve the accuracy of S-wave amplitude estimations for the region.
5. **Phase Overlap Challenge in S- and P-Wave Discrimination:** A potential limitation occurs when P- and S-waves overlap within the same rolling three-second window during S-wave amplitude estimation, potentially leading to overestimated amplitudes and false alerts. Future work should focus on improving phase discrimination using advanced P-wave detection algorithms and machine learning to better distinguish between P- and S-waves.
6. **Noise Reduction Strategies:** Efforts will be made to work with sensor hosts to explore noise reduction strategies, balancing optimal sensor placement with volunteer engagement to ensure the network's continued effectiveness.

9.6 Conclusion

This study successfully demonstrates the feasibility and effectiveness of a low-cost EEWS in NZ, achieved through a community-engaged sensor network. The network, its digital platform, and the use of both NZ-PLUM and NZ-PLUM-P algorithms have been successfully implemented and evaluated.

A noise analysis reveals that most sensors recorded low ambient noise levels, with only one sensor exhibiting high noise. This generally favourable noise environment supports accurate seismic detection. The system's reliability is further confirmed by the minimal number of false alerts generated since the system's implementation, indicating the network's robustness.

The analysis of three detected earthquakes shows that the NZ-PLUM-P approach significantly enhances warning times compared to the NZ-PLUM approach, particularly for areas closer to the epicentre of distant earthquakes. This improvement is crucial for timely alerts and increasing the system's effectiveness in mitigating earthquake-related risks.

Future work includes:

- Expanding the algorithm across the entire network
- Optimising the wavelet-based P-wave picker for decentralised processing
- Incorporating site amplification factors to improve intensity predictions
- Engaging with hosts of medium and high-noise sensors to explore possible noise reduction strategies

This study establishes the practicality of a low-cost, community-engaged EEWS and identifies future enhancements to improve system performance and coverage. The findings demonstrate the potential for such systems to contribute to EEW in seismically vulnerable nations at a low cost.


Chapter 01
Introduction
Chapter 02
Research Design
RQ1
Identifies gaps, challenges & future areas, guiding low-cost MEMS-based EEWSs
Chapter 03
RQ1
Implements the low-cost community-engaged EEW network
Chapter 04
RQ1
Implements the PLUM-based community-engaged EEWS
Chapter 05
RQ2
Reviews and evaluates P-wave detection algorithms using community-engaged data
Chapter 06
RQ2
Validates P-wave detection algorithms with GeoNet ground motion data
Chapter 07
RQ3
Estimates the S-wave amplitude using P-waves
Chapter 08
RQ3
Implements and evaluates the PLUM-based community-engaged EEWS
Chapter 09
Chapter 10
Discussion and Conclusion

10 Discussion and Conclusion

This chapter brings together the components presented in the thesis, including discussions on their research questions, and key outcomes, followed by a synthesis of contributions to research and practice. The chapter concludes by summarising limitations, highlighting potential extensions, and shedding light on future research directions.

10.1 Addressing the Research Questions

This study is motivated by the potential of recent advancements in low-cost MEMS-based ground motion sensors and innovative algorithms to provide a feasible alternative. These technologies offer a promising solution for developing a community-engaged, low-cost EEWS capable of providing timely and accurate warnings without the prohibitive costs associated with traditional systems (Brooks et al., 2021; Paul et al., 2023; Prasanna et al., 2022). However, significant challenges remain, particularly in decentralised processing and alert generation using ground motion-based algorithms to enhance warning capabilities (Chandrakumar, Prasanna, Stephens, & Tan, 2022). Thus, this doctoral research set out to answer three questions:

1. How can a community-engaged, low-cost MEMS-based EEW network run the PLUM algorithm using decentralised processing be implemented?
2. How can P-waves be optimally detected in a community-engaged EEW network?
3. How can a P-wave detection algorithm be integrated into the PLUM algorithm to extend the warning window?

This section summarises how research questions were answered through the accomplishment of the research objectives.

10.1.1 Research Question 1: How can a Community-Engaged, Low-Cost MEMS-based EEW Network Run the PLUM Algorithm Using Decentralised Processing Be Implemented?

This study pursued three primary objectives to address the first research question,

1. Conduct a comprehensive review of global EEW approaches and analyse their methodologies.
2. Develop an experimental community-engaged EEW network by installing low-cost MEMS-based ground motion sensors in households within the Greater Wellington region.
3. Adapt and implement the PLUM algorithm using decentralised processing within the experimental EEW network.

The systematic literature review, detailed in Chapter 3, accomplished the first objective. This review examined 59 peer-reviewed research articles on low-cost MEMS-based EEWSs globally, comprehensively understanding how these systems are implemented. The key findings include the limited use of ground motion-based or wavefield-based algorithms for earthquake detection and alert generation, along with underexplored areas such as network security, decentralised processing, and the use of smartphones for EEW when mobile (Chandrakumar, Prasanna, Stephens, & Tan, 2022).

Implementing a low-cost MEMS-based EEWS, as described in Chapter 4, achieved the second objective. This was accomplished through two phases of sensor installation, with this PhD study primarily focusing on the second phase. Community engagement with the public in the Wellington region was integral to this process, involving the generation of two questionnaires to gather detailed information on sensor installation locations and their environmental conditions. Additionally, a methodology for selecting sensor locations, a comprehensive installation guide, and a technical note comparing the performance of different installation methods for RS4D sensors were developed, contributing to the successful implementation of the network.

The second objective was fulfilled by implementing a low-cost MEMS-based EEWS, as described in Chapter 4. This was accomplished through two phases of sensor installation where this PhD study focused on primarily the second phase. Through community-engagement with the public of Wellington region, two questionnaires were generated to gather information on the sensor installation locations and their environmental conditions. Further, a methodology for choosing the sensor locations, a comprehensive installation guide and a technical note on comparing performance of different installation method for RS4D sensors helped achieving the objective.

The adaptation and implementation of the PLUM algorithm using decentralised processing, as presented in Chapter 5, accomplished the third objective. This adaptation involved modifying the original PLUM to NZ-PLUM algorithm align with the NZ MMI scale and implementing it with a decentralised processing approach. A Primary-Secondary two-tier sensor architecture was created to distribute the processing load of the EEW algorithm across resource-constrained sensors within the community-engaged network.

10.1.2 Research Question 2: How can P-waves Be Optimally Detected in a Community-Engaged EEW Network?

To address the second research question, which aims to identify the most appropriate P-wave detection algorithm for a community-engaged EEW network, the study outlines three research objectives.

1. Review the literature on P-wave detection algorithms implemented globally.
2. Compare the performance of various existing P-wave detection algorithms suitable for decentralised processing using ground motion data captured from the experimental community-engaged EEW network in the Greater Wellington Region.
3. Validate the results obtained from objective 2.2 using a more extensive ground motion dataset.

The literature review on global P-wave detection algorithms, presented in Chapter 6, accomplished the first objective. This review traced the evolution of P-wave detection methodologies, highlighting a progression from traditional statistical approaches to advanced machine learning techniques. It provided an in-depth overview of how P-wave detection algorithms have developed, moving towards more complex and accurate methods for improving earthquake early warning systems (Chandrakumar, Prasanna, Stephens, Tan, et al., 2022).

The comparative analysis of four identified P-wave detection algorithms achieved the second objective to select the most suitable algorithm for decentralised processing using ground motion data from the experimental community-engaged EEW network (as detailed in Chapter 6). The algorithms were selected based on the findings of the literature review. The analysis focused on the accuracy of detection, particularly the rates of false and missed detections during a specific earthquake event. The evaluation concluded that the wavelet-based P-wave picker algorithm was the most effective, demonstrating minimal false and missed detections (Chandrakumar et al., 2023).

The validation of the wavelet-based P-wave picker algorithm using a more extensive dataset from the GeoNet sensor network, as discussed in Chapter 7, accomplished the third objective. This validation applied statistical measures to assess the robustness and reliability of the algorithms' P-wave picks over

a broader dataset. The results reinforced the suitability of the wavelet-based P-wave picker for implementation in a community-engaged EEW network.

In summary, this PhD project analysed existing P-wave algorithms and selected and validated the wavelet-based P-wave picker as the most suitable for the low-cost, community-engaged network. Through this process, it was demonstrated that P-waves can be optimally detected in a community-engaged EEW network. Moreover, this algorithm can be implemented using decentralised processing and has shown a high accuracy rate with minimal false and missed detections.

10.1.3 Research Question 3: How can a P-wave Detection Algorithm Be Integrated into the PLUM Algorithm to Extend the Warning Window?

The study outlined three specific objectives to address the third research question, which explores how a P-wave detection algorithm can be integrated into the NZ-PLUM algorithm to extend the warning window:

1. Establish a relationship between the amplitude of P-waves and S-waves in NZ.
2. Implement the P-wave-based NZ-PLUM algorithm (NZ-PLUM-P) with decentralised processing in the experimental EEW network.
3. Evaluate the performance of the NZ-PLUM and NZ-PLUM-P algorithms in the implemented EEWS.

Literature on the PLUM algorithm indicated that integrating a P-wave detection algorithm requires constructing a relationship between the amplitudes of P-waves and S-waves (Kodera, 2018). To establish a correlation between the amplitudes of P-waves and S-waves, a linear regression method was employed using ground motion data from the GeoNet network (Chandrakumar, Tan, Holden, Stephens, Punchihewa, et al., 2024). As detailed in Chapter 8, the most robust relationship was selected through statistical analysis from nine different linear relationships. This work fulfilled the first objective.

The selected P-wave detection algorithm was then integrated into the NZ-PLUM algorithm, resulting in the development of the NZ-PLUM-P algorithm. This new algorithm was subsequently adapted for decentralised processing within the community-engaged EEWS, as described in Chapter 9, thereby accomplishing the second objective.

Finally, the performance of the NZ-PLUM algorithm and the newly integrated NZ-PLUM-P algorithm within the implemented EEWS was evaluated. This evaluation, presented in Chapter 9, focused on system noise levels, the frequency of false alerts, and the overall effectiveness in terms of warning time and system latency. This assessment met the third objective.

In summary, this PhD project successfully integrated a P-wave detection algorithm into the NZ-PLUM-based EEWS, implemented with decentralised processing, and ran it alongside the NZ-PLUM algorithm. Then, the implementation was tested, and an extended warning window was demonstrated, enhancing the overall effectiveness of the EEWS.

10.1.4 Contributions of the Study

This research has made significant contributions to both the theoretical and practical aspects of EEWS. By implementing a design science-led low-cost, community-engaged EEWS, this study provides valuable insights and advancements for academic and practitioner communities. One of the key contributions of this study is the comprehensive review of existing EEWS implementation approaches, culminating in a step-by-step guide for establishing a community-engaged, low-cost MEMS-based EEWS using the PLUM algorithm. This guide fills a crucial gap in EEW research by offering well-defined methods for setting up robust, cost-effective systems, selecting appropriate detection algorithms, and determining suitable processing architectures. It also provides detailed insights into implementing the PLUM algorithm with decentralised processing and strategies for enhancing the warning window. These contributions are especially valuable for researchers and practitioners, addressing common challenges in understanding and deploying community-engaged EEWSs. The specific contributions to research are detailed in the following sections.

10.1.4.1 System Literature Review

The literature extensively discusses the implementation of low-cost EEWSs using MEMS-based sensors. However, a focused review specifically on EEWSs implemented with MEMS-based sensors has not been thoroughly explored in the research domain. While several studies have reviewed EEW research, such as R. M. Allen & Melgar (2019), Cremen & Galasso (2020), McBride et al. (2022), Tan et al. (2022), Velazquez et al. (2020), they primarily cover the seismological, engineering, social, and organisational aspects and general state-of-the-art approaches to EEW. None comprehensively reviews existing low-cost EEWSs worldwide, focusing on technical aspects. Such a technical review is timely and invaluable for identifying the strengths and weaknesses of various approaches, thereby informing future research directions in low-cost EEW. This thesis addresses this gap through a systematic literature review in Chapter 3 (Chandrakumar, Prasanna, Stephens, & Tan, 2022), marking the first comprehensive exploration of low-cost EEWSs with MEMS-based sensors.

The systematic review provides three significant contributions to the research community:

1. It presented a comprehensive classification framework for EEWSs, categorised based on the number of sensors and the characteristics of the algorithms. While previous classifications exist, such as those based on the number of sensors used for alert generation (Picozzi, Emolo, et al., 2015) and the type of EEW algorithm (R. M. Allen & Melgar, 2019), this framework offers a standardised method for classifying any EEWS globally. It considers both the type of warning issued and the specific EEW algorithm employed, providing a more holistic view of EEWS configurations and their operational methodologies.
2. The review analysed various global MEMS-based EEWS implementations, detailing their earthquake detection and alert generation methodologies. It distinguished between on-site and regional alert generation methods and categorises EEW algorithms as source- or ground-motion-based.
3. The review identified limitations and future research areas for low-cost EEWSs. Future areas of potential research include ground motion-based algorithms, network security, decentralised processing, and smartphones for mobile EEW.

The findings of this literature review are published in the journal "Frontiers in Sensors," providing a valuable resource for future research and development in low-cost EEWSs (Chandrakumar, Prasanna, Stephens, & Tan, 2022).

10.1.4.2 Implementation of a Community-Engaged EEW network

Implementing the community-engaged EEW network is a pivotal aspect of this study, as detailed in Chapter 4. In this phase, ground motion sensors were distributed to selected sensor hosts, who were asked to install them in their households. This project can be distinguished as the first of its kind, where community members hosted and installed the network, fully embracing a citizen science approach. This model granted more authority and responsibility to the volunteers, fostering greater community involvement and engagement, potentially increasing earthquake preparedness through raising awareness and understanding of EEW systems among participants.

The questionnaire developed during this phase can be a starting point for aiding information gathering before sensor distribution for future community-engaged EEW networks. The questions can be adapted and modified to the context of other networks. Additionally, the installation guide created for this study can be easily adapted and used to support future research to assist citizen seismologists in installing low-cost ground motion sensors in their homes. The guide shows an example of how to help guide

participants on best practices for sensor installations in their homes, which is critical for accurate data collection.

While previous studies have compared ground motion sensor performances (Anthony et al., 2019; Fu et al., 2019; Holland, 2003), this study makes a significant contribution by being the first to explore and discuss the impact of different sensor installation methods on a commonly used floor type within a community-engaged EEW network, using shake table experiments (See Appendix B). This adaptable and extendable testing method provides a robust standard for testing various sensor installation methods for ground motion recording across different floor types. This practical insight not only fills a critical gap in the existing literature but also provides valuable guidance for optimising sensor placement in real-world settings, ultimately enhancing the effectiveness of community-engaged EEWS.

The technical note has been submitted to the Bulletin of the New Zealand Society for Earthquake Engineering.

10.1.4.3 Adapting PLUM for NZ

Initially developed in Japan, the PLUM algorithm was designed to calculate real-time pseudo-seismic intensity using the Ir parameter derived from three-dimensional acceleration data (Kodera et al., 2018). This calculation aligned with Japan's JMA instrumental seismic intensity (Iinst). Similarly, the algorithm had been adapted to the MMI scale for the ShakeAlert network on the West Coast of the USA (Cochran et al., 2019). However, PLUM had not yet been adapted to the NZ MMI scale. This study presented an approach for adapting the PLUM algorithm to the NZ MMI scale, using GMICEs constructed by Moratalla et al. (2020), as detailed in Chapter 9. Although this contribution is specific to NZ, it provides a foundational approach for implementing the PLUM algorithm in other settings. Other countries can adapt this approach to align with their own MMI GMICEs, making it broadly applicable to various seismic warning systems.

This study has been submitted to the journal Seismological Research Letters.

10.1.4.4 Method for Selecting P-wave Picker

P-wave detection algorithms are critical for identifying P-waves during earthquake events, an essential function of EEWS (Hafez et al., 2020). However, in the literature, selecting a specific P-wave detection algorithm is often justified by citing its accuracy without providing a comparative analysis with other existing algorithms. This study has addressed this gap by proposing a method for comparing the performance of four different P-wave detection algorithms, using metrics such as false and missed

detections at a station level instead of analysing false and missed alerts at a system level (Chandrakumar et al., 2023).

Additionally, the study introduced a statistical approach to evaluate the timing accuracy of these algorithms relative to manual picks. A manual P-wave picking tool was developed and made available to researchers to facilitate this process, providing a practical resource for manual P-wave detection.

This method allows researchers to systematically compare the performance of different P-wave detection algorithms and select the most suitable one based on their ground motion data quality.

The comparative analysis of the algorithms, using data from a community-engaged ground motion network, is published as a journal article in the New Zealand Journal of Geology and Geophysics (Chandrakumar et al., 2023). Further statistical analysis, utilising a larger ground motion dataset, has been submitted to the Springer Earth Science Informatics Journal.

The manual P-wave picking tool is available on GitHub as an open-access tool and can be accessed at a GitHub repository[13].

10.1.4.5 P-wave Detection Algorithm for a Community-Engaged EEW Network

Detecting P-waves in a community-engaged EEW network presents unique challenges, because ground motion sensors are installed by community members rather than researchers or EEW organizations (Chandrakumar et al., 2023). In professional settings, sensors are typically placed in optimal locations with minimal noise interference. However, in community-engaged networks, the sensors may experience higher noise levels despite instructions for firm installation in quiet areas. As a result, standard P-wave detection algorithms, like the widely used standard STA/LTA or the Kurtosis-based P-wave picker, may not perform effectively in these environments (Chandrakumar et al., 2023).

This study demonstrates that the wavelet-based P-wave picker is the most effective algorithm for detecting P-waves with minimal false and missed detections in community-engaged and GeoNet MEMS-based ground motion data. These findings indicate that the standard STA/LTA algorithm is less suitable for data with high noise levels, as is often the case in community-engaged settings. The study recommends using the wavelet-based P-wave picker to provide a reliable option for P-wave detection

[13] https://github.com/Chanthujan/Manual_P_wave_Pick_Tool

in noisy environments. This finding will greatly benefit the research community, especially those engaged in low-cost EEW solutions.

These results are published in the New Zealand Journal of Geology and Geophysics (Chandrakumar et al., 2023).

10.1.4.6 P to S-wave Amplitude Relationship

Estimating S-wave amplitude from the P-wave window upon P-wave detection is crucial for providing essential information about impending ground shaking, which is vital for triggering EEW alerts (Y. Wang et al., 2020; Y. M. Wu & Mittal, 2021; Yamamoto et al., 2008). This study made a significant contribution by comparing various relationships between P-wave and S-wave amplitude parameters, offering a comprehensive method for selecting the most appropriate relationship in the context of EEW (Chandrakumar, Tan, Holden, Stephens, Punchihewa, et al., 2024). This approach distinguishes itself from previous studies that often focused on limited or singular relationships for estimating S-wave amplitudes (Böse, Hauksson, Solanki, Kanamori, & Heaton, 2009; Caruso et al., 2017; Y. Wang et al., 2020; Zollo et al., 2014).

The findings underscore that the correlation between Peak Ground Velocity of P-waves and the Peak Ground Acceleration of S-waves is both robust and reliable, representing a crucial advancement in the development of a robust EEWS in NZ. This established relationship serves as a foundational element in determining suitable thresholds for EEW alerts, thereby enhancing the system's overall responsiveness and reliability (Chandrakumar, Tan, Holden, Stephens, Punchihewa, et al., 2024). While the study is based in NZ ground motion data, the method—utilising a 3-second P-wave to estimate S-wave amplituteds and selecting the most appropriate relationship—holds potential for adaptation in other regions, enabling researchers to refine their EEW systems with their optimal relationship for improved accuracy and effectiveness. This study is published in Earth Science Informatics (Chandrakumar, Tan, Holden, Stephens, Punchihewa, et al., 2024).

Additionally, the study introduced a visual inspection tool to verify the accuracy of P-wave and S-wave picks against the ground motion data, ensuring the validity of input data before constructing the relationship. The visual inspection tool is available through a GitHub Repository[14].

[14] https://github.com/Chanthujan/Visual_Inspection_Tool

10.1.4.7 Decentralised Processing Adaptation for NZ-PLUM and NZ-PLUM-P Algorithms

Traditionally, most EEWSs utilise a centralised processing approach, transmitting data from ground motion sensors to a central computer for earthquake detection and alert generation (Prasanna et al., 2022). However, recent studies have demonstrated that decentralised processing can enhance system latency, improve redundancy, and reduce implementation costs (Bassetti & Panizzi, 2022; Fleming et al., 2009; Prasanna et al., 2022).

This research introduced a Primary-Secondary two-tier decentralised architecture (Chandrakumar, Tan, Holden, Stephens, & Prasanna, 2024), effectively adapting both the NZ-PLUM and NZ-PLUM-P algorithms. This approach makes a significant contribution to the field by demonstrating how decentralised processing can be implemented using resource-constrained sensor nodes, thereby eliminating the dependency on centralised processing units. Moreover, decentralised processing can enhance the network's efficiency and resilience, making it more cost-effective and robust against failures.

This decentralised approach for running the original PLUM algorithm is detailed in a conference proceeding published in the Proceedings of the 21st ISCRAM Conference, Münster, Germany, May 2024 (Chandrakumar, Tan, Holden, Stephens, & Prasanna, 2024).

10.1.4.8 Performance Analysis with Real-World Case Studies

This study offers a significant theoretical and practical contribution by implementing and evaluating a real-world community-engaged EEW network. The performance evaluation case studies of the three recorded earthquakes are detailed in Chapter 9. Unlike previous research that relies on simulation environments using existing ground motion data (Cochran et al., 2019; Prasanna et al., 2022), this study's approach involved live, community-engaged network comprising over 40 ground motion sensors installed with community participation. Monitoring actual seismic events provides robust data and insights into the EEWS's effectiveness, serving as valuable benchmarks for other regions considering similar implementations.

This study's findings not only validate theoretical algorithms and architectures, but also demonstrates the practical viability of engaging communities in the development and operation of EEW systems. Further, it provides provide potential opportunity for public education for earthquake resilience, as it can be a means to communicate about the importance of EEWSs, their operational mechanics, and the benefits they provide. The study also highlighted the potential of the NZ-PLUM-P algorithm to enhance warning times and reduce the blind zone during an earthquake compared to the NZ-PLUM algorithm. These insights are crucial for guiding similar initiatives in implementing low-cost EEW networks,

emphasizing the value of the original PLUM and the P-wave detection-enabled PLUM for their potential advantages.

The performance analysis of the implemented EEWS has been submitted to the Journal Seismological Research Letters.

10.2 Research Outputs

This research has been presented on several research platforms including five journal publications and two conference publications. The author received the following awards during this research on communicating the research to the broader audience.

- "Best Student Paper Award" award for the conference publication titled "Adapting PLUM: Earthquake Early Warning with Node-Level Processing in New Zealand" at the Proceedings of the 21st ISCRAM Global Conference, Münster, Germany, May 2024.
- Third place at the QuakeCoRE Wellington Chapter 5 min Lightning talk in 2022 and 2023.
- People's Choice Award at the Massey 3-min lightning talk event 2023.
- First place at the QuakeCoRE Wellington Chapter 5 min Lightning talk in 2024.

Apart from the above achievements, the research was presented as posters, abstracts, and lightning talks in the following forums.

- 2021 – RNC STARR TALKS (3MT style presentation)
  Title: An Ecosystem of Low-cost Sensors for Earthquake Early Warning with Extended Warning Time.
- 2022 - Disastrous Doctorate (3MT style presentation)
- 2022 - RNC STARR TALKS (10MT style presentation)
  Title: An Ecosystem of Low-cost Sensors toward Earthquake Early Warning
- 2022 – CRISiSLab Webinar (Presentation)
  Title: Saving Precious Seconds: A decentralised Architecture for Earthquake Early Warning
- 2022 - QuakeCoRE Annual Meeting (Poster presentation)
  Title: An ecosystem of low-cost sensors toward earthquake early warning: An earthquake early warning system with multi-sensor capability.
- 2022 - QuakeCoRE Annual Meeting (Poster presentation)
  Title: Saving precious seconds: A low-cost earthquake early warning system for Aotearoa, New Zealand

- 2022 – ISCRAM Asia Pacific Doctoral Colloquium (Poster Presentation)
  Title: An Ecosystem of Low-cost Sensors toward Earthquake Early Warning: An Earthquake Early Warning System with multi-sensor capability
- 2022 – ISCRAM Asia Pacific Conference (Presentation)
  Title: Literature review on earthquake early warning algorithms for detecting P-waves and earthquake magnitude estimation: Initial literature review findings.
- 2023 - Disastrous Doctorate (3MT style presentation)
  Title: An Ecosystem of low-cost sensors toward Earthquake Early Warning Network
- 2023 - Seismological Society of America Annual Meeting; Puerto Rico, USA. (Presentation)
  Title: False and missed alerts: A performance analysis of a community-engaged earthquake early warning system. Session: Earthquake early warning optimization and efficacy.
- 2023 - RNC Symposium (Poster presentation)
  Title: A community-engaged earthquake early warning system (EEWS) with extended warning time and multi-sensor capability.
- 2023 - QuakeCoRE Annual Meeting (Poster presentation)
  Title: Extended warning window: A P-wave-based community-engaged earthquake early warning system.
- 2023 – Geoscience conference, Wellington, New Zealand (Presentation)
  Title: Implementation of an experimental MEMS-based EEW sensor network supported by decentralised peer-to-peer mesh networking architecture.
- 2024 - RNC Symposium (Poster presentation)
  Title: "A Decentralised Approach" - Implementing the PLUM Algorithm at Node-Level in a Community-Engaged EEW Network in New Zealand.
- 2024 - ISCRAM Global Conference, Münster, Germany (Presentation)
  Title: Adapting PLUM: Earthquake Early Warning with Node-Level Processing in New Zealand.
- 2024 – RNC STARR TALKS (5MT style presentation)
  Title: Shake It Up: How Communities and Low-Cost Tech Can Beat Earthquakes!

10.3 Research Implications

As discussed, NZ lacks an official EEWS to alert the public and authorities during seismic events despite the country's high seismic activity. A primary barrier to a national EEWS is the substantial costs of developing and maintaining a high-end system. This study has demonstrated how a low-cost EEWS can be implemented using MEMS-based sensors and a community-engaged approach.

Unlike previous research that tested systems in controlled environments, this study implemented a real-world network of over 40 ground motion sensors actively operating for earthquake detection and alert generation. This network uses a robust EEW algorithm with decentralised processing in the lower part of the North Island, NZ. The fully decentralised EEWS model presented here can be scaled into a real-time system across New Zealand or adapted for use in other countries seeking to implement an EEWS at a lower cost.

The step-by-step guide for implementing a community-engaged EEWS is a significant contribution, providing a versatile framework that can be applied to various MEMS-based ground motion sensors with limited processing power. The methodologies developed for selecting P-wave detection algorithms, constructing P-S wave amplitude relationships, selecting the most suitable P-S wave amplitude relationship, and evaluating EEW network performance can be applied to low-cost and high-end sensor networks.

Another crucial implication of this study is its potential to serve as a secondary support system for national-level high-end EEWSs. While the network can function independently to generate EEW alerts, it can also enhance the performance of existing high-end EEWSs by increasing sensor density and enhancing warnings capabilities, especially in blind zones of source-based systems. The PLUM approach in this network offers immediate warnings, complementing traditional source-based approaches.

If NZ were to implement a high-end EEWS using the existing GeoNet sensors, this community-engaged, low-cost network could still serve as a cost-effective solution to increase sensor density nationwide. Installing high-end sensors across the entire country would be prohibitively expensive, potentially costing hundreds of millions of dollars, making this network a feasible alternative.

Further, the decentralised PLUM approach proposed in this study, including the adaptation of the original PLUM for NZ (NZ-PLUM) and the integration of the P-wave detection-enabled PLUM (NZ-PLUM-P), could be implemented in the GeoNet's high-end sensor network. This would significantly enhance the capability to provide effective EEW alerts across NZ, ensuring a more robust and comprehensive EEWS.

10.4 Limitations and Future work

Despite the significant contributions of this doctoral research, several limitations must be acknowledged, which also pave the way for future work.

First, the study does not incorporate site amplification factors in the PLUM algorithm, which is typically used to account for amplification effects due to geographical location when predicting intensity. Future research should focus on integrating these amplification factors to enhance the accuracy of intensity predictions, particularly in diverse geographic settings.

Second, the study utilised a P-S wave amplitude relationship developed for the Canterbury region as the best available proxy for the EEW network implemented in the Wellington region. This decision was made due to the absence of other studies exploring P-S wave relationships for earthquake early warning in NZ. However, this reliance on a region-specific relationship highlights the need for future research to develop and validate P-S wave relationships tailored to different regions within NZ. Such region-specific calibrations would enhance the robustness and accuracy of EEWS implementations across the country.

Third, the performance analysis of the implemented community-engaged EEWS was limited to only five prediction points for alert dissemination. This limitation arose due to time constraints and the defined scope of this PhD research. Evaluating more prediction points would have required a significantly longer time frame to thoroughly analyse the performance and troubleshoot any issues within the network. As a result, the study focused on a smaller subset of prediction points to provide a baseline comparison and demonstrate the system's functionality. Future work should expand the performance analysis to include all possible prediction points within the network to ensure a comprehensive assessment of the EEWS's effectiveness and reliability.

Further, while the study primarily focused on enhancing the technical aspects of the EEWS, such as improving sensor placement and data accuracy, it is crucial to consider the broader impact of community engagement on the system's overall effectiveness. Future research should explore how participation in the EEWS influences individuals' knowledge and perceptions of earthquakes, their response to EEW alerts, and their overall preparedness for seismic events. Understanding these social impacts is vital for developing a more comprehensive and resilient EEWS. Conducting follow-up studies with participants, including interviews and focus group discussions, could provide deeper insights into how community involvement influences public awareness and preparedness. This approach would inform strategies for enhancing community resilience and improving EEWS implementations' effectiveness.

Lastly, the study uses the recursive STA/LTA algorithm instead of the wavelet-based P-wave picker for integration with the NZ-PLUM algorithm. Although the wavelet-based picker showed higher accuracy, it increased processing time when integrated with the NZ-PLUM algorithm, making the recursive STA/LTA a more viable choice for the current decentralised processing setup. Future research should

focus on further optimising and exploring the integration of the wavelet-based picker to enhance the system's accuracy without compromising processing efficiency.

These limitations highlight several areas for further investigation, which are crucial for advancing the development and implementation of low-cost, community-engaged EEWS. Detailed discussions on these limitations and potential future work are presented in the seven manuscripts that form the core of this PhD research.

10.5 Conclusion

This thesis explored the implementation of a community-engaged, low-cost MEMS-based EEWS using decentralised processing, addressing gaps in current EEWS implementations, particularly for resource-limited regions with frequent seismic activity. The study found that low-cost MEMS-based sensors deployed within a community-engaged framework can function effectively in a decentralised setup, providing timely and reliable earthquake alerts. By adapting the PLUM algorithm to the NZ MMI scale and integrating P-wave detection, the system showed potential improvements in warning time. The study has made available detailed methodologies, developed software tools, and a real-life ground motion network, demonstrating the practical applicability of the EEW approaches through an artefact developed based on the DSR methodology. The contributions of this thesis are significant for both academic research and practical EEWS implementations, providing a comprehensive guide for setting up a low-cost, community-engaged EEWS and emphasising the importance of PLUM algorithm, P-wave detection and decentralised processing. The findings also highlight areas for further investigation, particularly in rolling out the EEW algorithm to all the sensors in the implemented network and expanding the system's geographic coverage.

References

Abdalzaher, M. S., Sami Soliman, M., El-Hady, S. M., Benslimane, A., & Elwekeil, M. (2022). A Deep Learning Model for Earthquake Parameters Observation in IoT System-Based Earthquake Early Warning. IEEE Internet of Things Journal, 9(11). https://doi.org/10.1109/JIOT.2021.3114420

Abdalzaher, M. S., Soliman, M. S., & El-Hady, S. M. (2023). Seismic Intensity Estimation for Earthquake Early Warning Using Optimized Machine Learning Model. IEEE Transactions on Geoscience and Remote Sensing, 61. https://doi.org/10.1109/TGRS.2023.3296520

Adhikari, M., Paton, D., Johnston, D., Prasanna, R., & McColl, S. T. (2018). Modelling predictors of earthquake hazard preparedness in Nepal. Procedia Engineering, 212, 910–917. https://doi.org/10.1016/j.proeng.2018.01.117

Aizu, I. (2011). The role of ICT during the disaster – A story of how Internet and other information and communication services could or could not help relief operations at the Great East Japan Earthquake. Global Information Society Watch Report 2011, 1–7.

Algiriyage, N., Prasanna, R., Stock, K., Doyle, E. E. H., & Johnston, D. (2022). Multi-source Multimodal Data and Deep Learning for Disaster Response: A Systematic Review. SN Computer Science, 3(1). https://doi.org/10.1007/s42979-021-00971-4

Allen, R. M., & Kanamori, H. (2003). The potential for earthquake early warning in Southern California. Science, 300(5620), 786–789. https://doi.org/10.1126/science.1080912

Allen, R. M., Kong, Q., & Martin-Short, R. (2020). The MyShake Platform: A Global Vision for Earthquake Early Warning. Pure and Applied Geophysics, 177(4), 1699–1712. https://doi.org/10.1007/s00024-019-02337-7

Allen, R. M., & Melgar, D. (2019). Earthquake early warning: Advances, scientific challenges, and societal needs. Annual Review of Earth and Planetary Sciences, 47, 361–388. https://doi.org/10.1146/annurev-earth-053018-060457

Allen, R. M., & Stogaitis, M. (2022). Global growth of earthquake early warning. In Science (Vol. 375, Issue 6582, pp. 717–718). American Association for the Advancement of Science. https://doi.org/10.1126/science.abl5435

Allen, R. V. (1978). Automatic earthquake recognition and timing from single traces. Bulletin of the Seismological Society of America, 68(5). https://doi.org/10.1785/bssa0680051521

Anderson, H., & Webb, T. (1994). New Zealand seismicity: Patterns revealed by the upgraded National Seismograph Network. New Zealand Journal of Geology and Geophysics, 37(4). https://doi.org/10.1080/00288306.1994.9514633

Anthony, R. E., Ringler, A. T., Wilson, D. C., & Wolin, E. (2019). Do low-cost seismographs perform well enough for your network? An overview of laboratory tests and field observations of the OSOP raspberry shake 4D. In Seismological Research Letters (Vol. 90, Issue 1). https://doi.org/10.1785/0220180251

Atefi, S., Heidari, R., Mirzaei, N., & Siahkoohi, H. R. (2017). Rapid estimation of earthquake magnitude by a new wavelet-based proxy. Seismological Research Letters, 88(6). https://doi.org/10.1785/0220170146

Avery, H. R., Berrill, J. B., Coursey, P. F., Deam, B. L., Dewe, M. B., François, C. C., Pettinga, J. R., & Yetton, M. D. (2004). The Canterbury university strong-motion recording project. 13th World Conference on Earthquake Engineering, 1335.

Baillard, C., Crawford, W. C., Ballu, V., Hibert, C., & Mangeney, A. (2014). An automatic kurtosis-based P-and S-phase picker designed for local seismic networks. Bulletin of the Seismological Society of America, 104(1), 394–409. https://doi.org/10.1785/0120120347

Barbur, V. A., Montgomery, D. C., & Peck, E. A. (1994). Introduction to Linear Regression Analysis. The Statistician, 43(2). https://doi.org/10.2307/2348362

Bassetti, E., & Panizzi, E. (2022). Earthquake Detection at the Edge: IoT Crowdsensing Network. Information (Switzerland), 13(4). https://doi.org/10.3390/info13040195

Becker, J. S., Potter, S. H., Prasanna, R., Tan, M. L., Payne, B. A., Holden, C., Horspool, N., Smith, R., & Johnston, D. M. (2020). Scoping the potential for earthquake early warning in Aotearoa New Zealand: A sectoral analysis of perceived benefits and challenges. International Journal of Disaster Risk Reduction, 51. https://doi.org/10.1016/j.ijdrr.2020.101765

Becker, J. S., Potter, S. H., Vinnell, L. J., Nakayachi, K., McBride, S. K., & Johnston, D. M. (2020). Earthquake early warning in Aotearoa New Zealand: a survey of public perspectives to guide warning system development. Humanities and Social Sciences Communications, 7(1). https://doi.org/10.1057/s41599-020-00613-9

Berkeley University. (2022). PEER Ground Motion Database - PEER Center. NGA-West2.

Berrill, J., Avery, H., Dewe, M., Chanerley, A., Alexander, N. N., Dyer, C., Holden, C., & Fry, B. (2011). The Canterbury Accelerograph Network (CanNet) and some Results from the September 2010, M7.1 Darfield Earthquake.

Bhardwaj, R., Kumar, A., & Sharma, M. L. (2013). Root sum of squares cumulative velocity: An attribute for earthquake early warning. Disaster Advances, 6(3).

Bindi, D., Boxberger, T., Orunbaev, S., Pilz, M., Stankiewicz, J., Pittore, M., Iervolino, I., Ellguth, E., & Parolai, S. (2015). On-site early-warning system for Bishkek (Kyrgyzstan). Annals of Geophysics, 58(1). https://doi.org/10.4401/ag-6664

Bogiatzis, P., & Ishii, M. (2015). Continuouswavelet decomposition algorithms for automatic detection of compressional- and shear-wave arrival times. Bulletin of the Seismological Society of America, 105(3). https://doi.org/10.1785/0120140267

Boon, D., Perrin, N. D., Dellow, G. D., Van Dissen, R., & Lukovic, & B. (2011). Site Subsoil Classification of Lower Hutt. Proceedings of the Ninth Pacific Conference on Earthquake Engineering Building an Earthquake-Resilient Society.

Boore, D. M. (2010). Orientation-independent, nongeometric-mean measures of seismic intensity from two horizontal components of motion. In Bulletin of the Seismological Society of America (Vol. 100, Issue 4). https://doi.org/10.1785/0120090400

Böse, M., Hauksson, E., Solanki, K., Kanamori, H., & Heaton, T. H. (2009). Real-time testing of the on-site warning algorithm in southern California and its performance during the July 29 2008 Mw5.4 Chino Hills earthquake. Geophysical Research Letters, 36(5). https://doi.org/10.1029/2008GL036366

Böse, M., Hauksson, E., Solanki, K., Kanamori, H., Wu, Y. M., & Heaton, T. H. (2009). A new trigger criterion for improved real-time performance of onsite earthquake early warning in Southern California. Bulletin of the Seismological Society of America, 99(2 A). https://doi.org/10.1785/0120080034

Bose, S., De, A., & Chakrabarti, I. (2020). Framework for Automated Earthquake Event Detection Based on Denoising by Adaptive Filter. IEEE Transactions on Circuits and Systems I: Regular Papers, 67(9), 3070–3083. https://doi.org/10.1109/TCSI.2020.2984960

Bossu, R., Finazzi, F., Steed, R., Fallou, L., & Bondár, I. (2021). " Shaking in 5 seconds!" A Voluntary Smartphone-based Earthquake Early Warning System. ArXiv Preprint ArXiv:2102.06739.

Boxberger, T., Fleming, K., Pittore, M., Parolai, S., Pilz, M., & Mikulla, S. (2017). The multi-parameter wireless sensing system (MPwise): Its description and application to earthquake risk mitigation. Sensors (Switzerland), 17(10). https://doi.org/10.3390/s17102400

Brocke, J., Hevner, A., & Maedche, A. (2020). Introduction to Design Science Research. https://doi.org/10.1007/978-3-030-46781-4_1

Brooks, B. A., Protti, M., Ericksen, T., Bunn, J., Vega, F., Cochran, E. S., Duncan, C., Avery, J., Minson, S. E., & Chaves, E. (2021). Robust earthquake early warning at a fraction of the cost: ASTUTI Costa Rica. AGU Advances, 2(3), e2021AV000407.

Caruso, A., Colombelli, S., Elia, L., Picozzi, M., & Zollo, A. (2017). An on-site alert level early warning system for Italy. Journal of Geophysical Research: Solid Earth, 122(3). https://doi.org/10.1002/2016JB013403

Cascone, V., Boaga, J., & Cassiani, G. (2021). Small Local Earthquake Detection Using Low-Cost MEMS Accelerometers: Examples in Northern and Central Italy. The Seismic Record, 1(1), 20–26.

Castilla, M.-J., Huenupan, F., Curilem, M., Fustos, I., Martin, C. S., & Franco-Marin, L. (2023). P and S wave detection for the Nevados de Chillan Volcanic Complex (Chile), based on spectro-temporal features. Journal of Volcanology and Geothermal Research, 107756. https://doi.org/10.1016/j.jvolgeores.2023.107756

Chamoli, B. P., Kumar, A., Chen, D. Y., Gairola, A., Jakka, R. S., Pandey, B., Kumar, P., & Rathore, G. (2021). A Prototype Earthquake Early Warning System for Northern India. In Journal of Earthquake Engineering (Vol. 25, Issue 12, pp. 2455–2473). Taylor and Francis Ltd. https://doi.org/10.1080/13632469.2019.1625828

Chandrakumar, C., Prasanna, R., Stephens, M. T., & Tan, M. L. (2022). Earthquake early warning systems based on low-cost ground motion sensors: A systematic literature review. Frontiers in Sensors, 3. https://doi.org/10.3389/fsens.2022.1020202

Chandrakumar, C., Prasanna, R., Stephens, M. T., Tan, M. L., Holden, C., Punchihewa, A., Becker, J. S., Jeong, S., & Ravishan, D. (2022). Literature review on Earthquake Early Warning Algorithms Algorithms for Detecting P-Waves and Earthquake Magnitude Estimation: Initial Literature

Review Findings. In H. Thomas & L. Vincent (Eds.), Building Disaster Resilience, ISCRAM Asia Pacific Conference (pp. 138–155). ISCRAM ASIA PACIFIC 2022.

Chandrakumar, C., Tan, M. L., Holden, C., Stephens, M. T., & Prasanna, R. (2023). Performance analysis of P-wave detection algorithms for a community-engaged earthquake early warning system–a case study of the 2022 M5.8 Cook Strait earthquake. New Zealand Journal of Geology and Geophysics. https://doi.org/10.1080/00288306.2023.2284276

Chandrakumar, C., Tan, M. L., Holden, C., Stephens, M. T., & Prasanna, R. (2024). Adapting PLUM: Earthquake Early Warning with Node-Level Processing in New Zealand.

Chandrakumar, C., Tan, M. L., Holden, C., Stephens, M. T., Punchihewa, A., & Prasanna, R. (2024). Estimating S-wave amplitude for earthquake early warning in New Zealand: Leveraging the first 3 seconds of P-Wave. Earth Science Informatics. https://doi.org/10.1007/s12145-024-01403-6

Chen, D. Y., Hsiao, N. C., & Wu, Y. M. (2015). The earthworm based earthquake alarm reporting system in Taiwan. Bulletin of the Seismological Society of America, 105(2), 568–579. https://doi.org/10.1785/0120140147

Chen, D. Y., Wu, Y. M., & Chin, T. L. (2015). Incorporating Low-Cost Seismometers into the Central Weather Bureau Seismic Network for Earthquake Early Warning in Taiwan. Terrestrial, Atmospheric & Oceanic Sciences, 26(5).

Chen, D. Y., Wu, Y. M., & Chin, T. L. (2017). An empirical evolutionary magnitude estimation for early warning of earthquakes. Journal of Asian Earth Sciences, 135. https://doi.org/10.1016/j.jseaes.2016.12.028

Chen, K. H., Bossu, R., & Liang, W. T. (2020). Editorial: The Power of Citizen Seismology: Science and Social Impacts. In Frontiers in Earth Science (Vol. 8). https://doi.org/10.3389/feart.2020.610813

Chung, A. I., Henson, I., & Allen, R. M. (2019). Optimizing earthquake early warning performance: ElarmS-3. Seismological Research Letters, 90(2 A). https://doi.org/10.1785/0220180192

Claerbout, J. F. (1964). Detection of P-waves from weak sources at great distances. Geophysics, 29(2), 197–211. https://doi.org/10.1190/1.1439350

Clayton, R. W., Heaton, T., Kohler, M., Chandy, M., Guy, R., & Bunn, J. (2015). Community seismic network: A dense array to sense earthquake strong motion. Seismological Research Letters, 86(5), 1354–1363. https://doi.org/10.1785/0220150094

Clinton, J., Zollo, A., Marmureanu, A., Zulfikar, C., & Parolai, S. (2016). State-of-the art and future of earthquake early warning in the European region. Bulletin of Earthquake Engineering, 14(9). https://doi.org/10.1007/s10518-016-9922-7

Cochran, E. S., Bunn, J., Minson, S. E., Baltay, A. S., Kilb, D. L., Kodera, Y., & Hoshiba, M. (2019). Event detection performance of the PLUM earthquake early warning algorithm in southern California. Bulletin of the Seismological Society of America, 109(4), 1524–1541. https://doi.org/10.1785/0120180326

Cochran, E. S., Lawrence, J. F., Christensen, C., & Jakka, R. S. (2009). The quake-catcher network: Citizen science expanding seismic horizons. Seismological Research Letters, 80(1), 26–30. https://doi.org/10.1785/gssrl.80.1.26

Colombelli, S., Caruso, A., Zollo, A., Festa, G., & Kanamori, H. (2015). A P wave-based, on-site method for earthquake early warning. Geophysical Research Letters, 42(5). https://doi.org/10.1002/2014GL063002

Coppola, D. P. (2007). Introduction to international disaster management. Butterworth Heinemann.

Courtney Taylor. (2018, April 26). What Is the Interquartile Range Rule? https://www.thoughtco.com/what-is-the-interquartile-range-rule-3126244

Cremen, G., & Galasso, C. (2020). Earthquake early warning: Recent advances and perspectives. In Earth-Science Reviews (Vol. 205). Elsevier B.V. https://doi.org/10.1016/j.earscirev.2020.103184

Creswell, J. W. (2014a). Research design: qualitative, quantitative, and mixed methods approaches. In Research Design.

Creswell, J. W. (2014b). The Selection of a Research Approach. In Research Design. https://doi.org/45593:01

Cuéllar, A., Suárez, G., & Espinosa-Aranda, J. M. (2018). An earthquake early warning algorithm based on the P-wave energy released in the ts–tp interval. Bulletin of the Seismological Society of America, 108(1). https://doi.org/10.1785/0120170115

D'Alessandro, A., D'anna, R., Greco, L., Passafiume, G., Scudero, S., Speciale, S., & Vitale, G. (2018). Monitoring Earthquake through MEMS Sensors (MEMS project) in the town of Acireale (Italy). 5th IEEE International Symposium on Inertial Sensors and Systems, INERTIAL 2018 - Proceedings, 1–4. https://doi.org/10.1109/ISISS.2018.8358143

D'Alessandro, A., Luzio, D., & D'Anna, G. (2014). Urban MEMS based seismic network for post-earthquakes rapid disaster assessment. Advances in Geosciences, 40, 1–9. https://doi.org/10.5194/adgeo-40-1-2014

D'Alessandro, A., Scudero, S., Vitale, G., Di Benedetto, A., & Bosco, G. Lo. (2020). Optimization of low-cost monitoring systems for on-site earthquake early-warning of critical infrastructures. International Conference on Computational Science and Its Applications, 963–975.

D'Angelo, N., Di Benedetto, A., Adelfio, G., D'Alessandro, A., & Chiodi, M. (2022). A new picking algorithm based on the variance piecewise constant models. Stochastic Environmental Research and Risk Assessment. https://doi.org/10.1007/s00477-022-02218-x

Ding, W., Liao, C., & Wang, H. (2017). MEMS-based seismic intensity instrument for earthquake early warning. International Journal of Computational Science and Engineering, 15(1–2), 41–48. https://doi.org/10.1504/IJCSE.2017.085978

Dobry, R., Borcherdt, R. D., Crouse, C. B., Idriss, I. M., Joyner, W. B., Martin, G. R., Power, M. S., Rinne, E. E., & Seed, R. B. (2000). New Site Coefficients and Site Classification System Used in Recent Building Seismic Code Provisions. Earthquake Spectra, 16(1). https://doi.org/10.1193/1.1586082

Dokht, R. M. H., Kao, H., Visser, R., & Smith, B. (2019). Seismic event and phase detection using time-frequency representation and convolutional neural networks. Seismological Research Letters, 90(2 A). https://doi.org/10.1785/0220180308

Dowrick, D. J. (1996). The Modified Mercalli earthquake intensity scale-revisions arising from recent studies of New Zealand earthquakes. Bulletin of the New Zealand National Society for Earthquake Engineering, 29(2).

Dowrick, D. J., Hancox, G. T., Perrin, N. D., & Dellow, G. D. (2008). The modified mercalli intensity scale - Revisions arising from New Zealand experience. Bulletin of the New Zealand Society for Earthquake Engineering, 41(3). https://doi.org/10.5459/bnzsee.41.3.193-205

Draper, N. R., & Smith, H. (2014). Applied regression analysis. In Applied Regression Analysis. https://doi.org/10.1002/9781118625590

DzIewonski, A. M. (2021). The FDSN: history and objectives. Annals of Geophysics, 37(5). https://doi.org/10.4401/ag-4191

Faulkner, M., Olson, M., Chandy, R., Krause, J., Chandy, K. M., & Krause, A. (2011). Demo abstract, the next big one: Detecting earthquakes and other rare events from community-based sensors. Proceedings of the 10th ACM/IEEE International Conference on Information Processing in Sensor Networks, IPSN'11, 121–122.

Finazzi, F. (2016). The earthquake network project: Toward a crowdsourced smartphone-based earthquake early warning system. Bulletin of the Seismological Society of America, 106(3), 1088–1099.

Finazzi, F. (2020). The Earthquake Network Project: A Platform for Earthquake Early Warning, Rapid Impact Assessment, and Search and Rescue. Frontiers in Earth Science, 8. https://doi.org/10.3389/feart.2020.00243

Finazzi, F., & Fassò, A. (2017). A statistical approach to crowdsourced smartphone-based earthquake early warning systems. Stochastic Environmental Research and Risk Assessment, 31(7), 1649–1658. https://doi.org/10.1007/s00477-016-1240-8

Fischer, J., Redlich, J.-P., Zschau, J., Milkereit, C., Picozzi, M., Fleming, K., Brumbulli, M., Lichtblau, B., & Eveslage, I. (2012). A wireless mesh sensing network for early warning. Journal of Network and Computer Applications, 35(2), 538–547. http://10.0.3.248/j.jnca.2011.07.016

Fleming, K., Picozzi, M., Milkereit, C., Kühnlenz, F., Lichtblau, B., Fischer, J., Zulfikar, C., Özel, O., Zschau, J., Milkereit, C., Picozzi, M., Fleming, K., Veit, I., Jäckel, K. H., Hönig, M., Nachtigall, J., Woith, H., Fischer, J., Redlich, J. P., … Kafadar, N. (2009). The self-organizing seismic early warning information network (SOSEWIN). Seismological Research Letters, 80(5), 755–771. https://doi.org/10.1785/gssrl.80.5.755

Flick, U. (2007). Analyzing Qualitative Data. In Designing Qualitative Research (pp. 100–108). SAGE Publications, Ltd. https://doi.org/10.4135/9781849208826.n10

Flick, U. (2018). The SAGE Handbook of Qualitative Data Collection. In The SAGE Handbook of Qualitative Data Collection. https://doi.org/10.4135/9781526416070

Franchi, F., Marotta, A., Rinaldi, C., Graziosi, F., & D'Errico, L. (2019). IoT-based Disaster Management System on 5G uRLLC Network. 6th International Conference on Information and Communication Technologies for Disaster Management, ICT-DM 2019. https://doi.org/10.1109/ICT-DM47966.2019.9032897

Fu, J., Li, Z., Meng, H., Wang, J., & Shan, X. (2019). Performance Evaluation of Low-Cost Seismic Sensors for Dense Earthquake Early Warning: 2018–2019 Field Testing in Southwest China. Sensors, 19(9), 1999. https://doi.org/10.3390/s19091999

Fujinawa, Y., & Noda, Y. (2013). Japan's earthquake early warning system on 11 March 2011: Performance, shortcomings, and changes. In Earthquake Spectra (Vol. 29, Issue SUPPL.1). https://doi.org/10.1193/1.4000127

GeoNet. (2017). GeoNet Home. https://www.geonet.org.nz/

GeoNet. (2022a). Geonet M5.8 Earthquake-22nd September 2022. https://doi.org/https://doi.org/10.21420/0S8P-TZ38

GeoNet. (2022b). GeoNet M5.8 Earthquake-22nd September 2022 intensity data. https://doi.org/https://doi.org/10.21420/0S8P-TZ38

GeoNet. (2023). GeoNet statistics. https://www.geonet.org.nz/earthquake/statistics_long

GeoNet. (2024a). Magnitude 3.9, Thu May 23 2024 1:36 AM. https://www.geonet.org.nz/earthquake/2024p385316

GeoNet. (2024b). Magnitude 4.0, Sat Jul 6 2024 1:17 AM. https://www.geonet.org.nz/earthquake/2024p504198

GeoNet. (2024c). Magnitude 4.1, Mon Jun 3 2024 10:05 PM. https://www.geonet.org.nz/earthquake/2024p417352

Gianluca Malato. (2021, November 1). Outlier identification using Interquartile Range. Towards Data Science. https://towardsdatascience.com/outlier-identification-using-interquartile-range-74f5de12932a

Given, D. D., Allen, R. M., Baltay, A. S., Bodin, P., Cochran, E. S., Creager, K., Groot, R. M. de, Gee, L. S., Hauksson, E., Heaton, T. H., Hellweg, M., Murray, J. R., Thomas, V. I., Toomey, D., & Yelin, T. S. (2018). Revised technical implementation plan for the ShakeAlert system—An

earthquake early warning system for the West Coast of the United States. In Open-File Report. https://doi.org/10.3133/ofr20181155

GNS Science. (2022). GeoNet Aotearoa New Zealand Strong Motion Data Products. https://data.gns.cri.nz/metadata/srv/eng/catalog.search#/metadata/25c52e65-dbf9-4687-8343-3ca0b60961c1

GNS Science. (2023, August 28). Earthquake Early Warning in New Zealand. GNS Science. https://www.gns.cri.nz/news/earthquake-early-warning-in-new-zealand/

Goldkuhl, G. (2004). Meanings of Pragmatism : Ways to conduct information systems research. International Business.

Griffith, A., & Headley, J. D. (1997). Using a weighted score model as an aid to selecting procurement methods for small building works. Construction Management and Economics, 15(4), 341–348. https://doi.org/10.1080/014461997372890

Hafez, A. G., Abdel Azim, A., Soliman, M. S., & Yayama, H. (2020). Real-time P-wave picking for earthquake early warning system using discrete wavelet transform. NRIAG Journal of Astronomy and Geophysics, 9(1), 1–6. https://doi.org/10.1080/20909977.2019.1698144

Hafez, A. G., Khan, M. T. A., & Kohda, T. (2010). Clear P-wave arrival of weak events and automatic onset determination using wavelet filter banks. Digital Signal Processing: A Review Journal, 20(3). https://doi.org/10.1016/j.dsp.2009.10.002

Hafez, A. G., Rabie, M., & Kohda, T. (2013). Seismic noise study for accurate P-wave arrival detection via MODWT. Computers and Geosciences, 54, 148–159. https://doi.org/10.1016/j.cageo.2012.12.002

Heidari, R., Shomali, Z. H., & Ghayamghamian, M. R. (2013). Magnitude-scaling relations using period parameters τc and τpmax,for tehran region, Iran. Geophysical Journal International, 192(1). https://doi.org/10.1093/gji/ggs012

Hernon, P. (2004). The Sage Encyclopedia of Social Science Research Methods. Library & Information Science Research, 26(3). https://doi.org/10.1016/j.lisr.2004.02.002

Hevner, A. (2007). A Three Cycle View of Design Science Research. https://www.researchgate.net/publication/254804390

Hevner, A., March, S. T., Park, J., & Ram, S. (2004). DESIGN SCIENCE IN INFORMATION SYSTEMS RESEARCH 1. In Design Science in IS Research MIS Quarterly (Vol. 28, Issue 1).

Hloupis, G., & Vallianatos, F. (2013). Wavelet-based rapid estimation of earthquake magnitude oriented to early warning. IEEE Geoscience and Remote Sensing Letters, 10(1). https://doi.org/10.1109/LGRS.2012.2191932

Hloupis, G., & Vallianatos, F. (2015). Wavelet-Based Methods for Rapid Calculations of Magnitude and Epicentral Distance: An Application to Earthquake Early Warning System. Pure and Applied Geophysics, 172(9). https://doi.org/10.1007/s00024-015-1081-2

Holland, A. (2003). Earthquake data recorded by the MEMS accelerometer: Field testing in Idaho. Seismological Research Letters, 74(1). https://doi.org/10.1785/gssrl.74.1.20

Hong, H., Ni, L., & Sun, H. (2021). Application and Prospect of MEMS Technology to Geophysics. Proceedings of the 16th Annual IEEE International Conference on Nano/Micro Engineered and Molecular Systems, NEMS 2021, 1863–1866. https://doi.org/10.1109/NEMS51815.2021.9451455

Hoshiba, M. (2013). Real-time prediction of ground motion by Kirchhoff-Fresnel boundary integral equation method: Extended front detection method for Earthquake Early Warning. J. Geophys. Res. Solid Earth, 118, 1038–1050. https://doi.org/10.1002/jgrb.50119

Hoshiba, M. (2021). Real-Time Prediction of Impending Ground Shaking: Review of Wavefield-Based (Ground-Motion-Based) Method for Earthquake Early Warning. In Frontiers in Earth Science (Vol. 9). Frontiers Media S.A. https://doi.org/10.3389/feart.2021.722784

Hoshiba, M., & Aoki, S. (2015). Numerical shake prediction for earthquake early warning: Data assimilation, real-time shake mapping, and simulation of wave propagation. Bulletin of the Seismological Society of America, 105(3), 1324–1338. https://doi.org/10.1785/0120140280

Hoshiba, M., & Iwakiri, K. (2011). Initial 30 seconds of the 2011 off the pacific coast of tohoku earthquake (Mw9.0)-amplitude and τc for magnitude estimation for earthquake early Warning. Earth, Planets and Space, 63(7), 553–557. https://doi.org/10.5047/eps.2011.06.015

Hoshiba, M., Iwakiri, K., Hayashimoto, N., Shimoyama, T., Hirano, K., Yamada, Y., Ishigaki, Y., & Kikuta, H. (2011). Outline of the 2011 off the pacific coast of tohoku earthquake (M w 9.0) - earthquake early warning and observed seismic intensity. Earth, Planets and Space, 63(7), 547–551. https://doi.org/10.5047/eps.2011.05.031

Hsu, T. Y., & Huang, C.-W. (2021). Onsite Early Prediction of PGA Using CNN With Multi-Scale and Multi-Domain P-Waves as Input. Frontiers in Earth Science, 9. https://doi.org/10.3389/feart.2021.626908

Hsu, T. Y., & Nieh, C. P. (2020). On-site earthquake early warning using smartphones. Sensors (Switzerland), 20(10). https://doi.org/10.3390/s20102928

Hsu, T. Y., Wu, Y. M., & Chien, C. C. (2018). How well can we evaluate post-earthquake building safety using low-cost MEMS seismometers. Proceedings of the 7th Asia-Pacific Workshop on Structural Health Monitoring, APWSHM 2018, 866–877. https://www.scopus.com/inward/record.uri?eid=2-s2.0-85064651814&partnerID=40&md5=757b316b29165982ab11be41fe24f27d

Hsu, T. Y., Yin, R. C., & Wu, Y.-M. (2018). Evaluating post-earthquake building safety using economical MEMS seismometers. Sensors (Switzerland), 18(5). https://doi.org/10.3390/s18051437

Hu, X.-X., Wang, X.-Z., Chen, B., Li, C.-H., Tang, Y.-X., Shen, X.-Y., Zhong, Y., Chen, Z.-L., & Teng, Y.-T. (2021). Improved Resolution and Cost Performance of Low-Cost MEMS Seismic Sensor through Parallel Acquisition. Sensors, 21(7970), 7970. https://doi.org/10.3390/s21237970

Huang, X., Lee, J., Kwon, Y.-W., & Lee, C.-H. (2020). CrowdQuake: A Networked System of Low-Cost Sensors for Earthquake Detection via Deep Learning. Proceedings of the ACM SIGKDD International Conference on Knowledge Discovery and Data Mining, 3261–3271. https://doi.org/10.1145/3394486.3403378

Information Systems (IS). (2023, May). TechTarget. https://www.techtarget.com/whatis/definition/IS-information-system-or-information-services#:~:text=What%20is%20an%20information%20system,raw%20data%20into%20useful%20information.

Jan, J. C., Huang, H.-H., Wu, Y.-M., Chen, C.-C., & Lin, C.-H. (2018). Near-Real-Time Estimates on Earthquake Rupture Directivity Using Near-Field Ground Motion Data From a Dense Low-Cost Seismic Network. GEOPHYSICAL RESEARCH LETTERS, 45(15), 7496–7503. https://doi.org/10.1029/2018GL078262

Johnson, R. B., & Onwuegbuzie, A. J. (2004). Mixed Methods Research: A Research Paradigm Whose Time Has Come. Educational Researcher, 33(7). https://doi.org/10.3102/0013189X033007014

Jon Reilly. (2024, November 24). Overfitting and Underfitting in Machine Learning. https://www.akkio.com/post/overfitting-and-underfitting-in-machine-learning

Kanamori, H. (2005). Real-time seismology and earthquake damage mitigation. Annual Review of Earth and Planetary Sciences, 33. https://doi.org/10.1146/annurev.earth.33.092203.122626

Kanamori, H., Hauksson, E., & Heaton, T. (1997). Real-time seismology and earthquake hazard mitigation. Nature, 390(6659), 461–464. https://doi.org/10.1038/37280

Kaushik, V., & Walsh, C. A. (2019). Pragmatism as a research paradigm and its implications for Social Work research. Social Sciences, 8(9). https://doi.org/10.3390/socsci8090255

Kelemen, M., & Rumens, N. (2008). An Introduction to Critical Management Research: 8 Critical Perspectives on Qualitative Research. In An Introduction to Critical Management Research.

Khalqillah, A., Isa, M., & Muksin, U. (2018). A GUI based automatic detection of seismic P-wave arrivals by using Short Term Average/Long Term Average (STA/LTA) method. Journal of Physics: Conference Series, 1116(3). https://doi.org/10.1088/1742-6596/1116/3/032014

Khan, I. (2020). Collaborative Earthquake Detection and Response Using Smart Devices. Proceedings of the IEEE/ACM 7th International Conference on Mobile Software Engineering and Systems, 36–37. https://doi.org/10.1145/3387905.3388602

Khan, I., & Kwon, Y. W. (2022). P-Detector: Real-Time P-Wave Detection in a Seismic Waveform Recorded on a Low-Cost MEMS Accelerometer Using Deep Learning. IEEE Geoscience and Remote Sensing Letters, 19. https://doi.org/10.1109/LGRS.2022.3161017

Kilani, M. Al, & Kobziev, V. (2016). An Overview of Research Methodology in Information System (IS). OALib, 03(11). https://doi.org/10.4236/oalib.1103126

Kilb, D., Bunn, J. J., Saunders, J. K., Cochran, E. S., Minson, S. E., Baltay, A., O'Rourke, C. T., Hoshiba, M., & Kodera, Y. (2021). The PLUM Earthquake Early Warning Algorithm: A Retrospective Case Study of West Coast, USA, Data. Journal of Geophysical Research: Solid Earth, 126(7). https://doi.org/10.1029/2020JB021053

Klein, H. K., & Myers, M. D. (1999). A SET OF PRINCIPLES FOR CONDUCTING AND EVALUATING INTERPRETIVE FIELD STUDIES IN INFORMATION SYSTEMS 1.

Kobayashi, M. (2014). Experience of infrastructure damage caused by the Great East Japan Earthquake and countermeasures against future disasters. IEEE Communications Magazine, 52(3), 23–29. https://doi.org/10.1109/MCOM.2014.6766080

Kodera, Y. (2018). Real-Time Detection of Rupture Development: Earthquake Early Warning Using P Waves From Growing Ruptures. Geophysical Research Letters, 45(1), 156–165. https://doi.org/10.1002/2017GL076118

Kodera, Y., Saitou, J., Hayashimoto, N., Adachi, S., Morimoto, M., Nishimae, Y., & Hoshiba, M. (2016). Earthquake early warning for the 2016 Kumamoto earthquake: Performance evaluation of the current system and the next-generation methods of the Japan Meteorological Agency 2016 Kumamoto earthquake sequence and its impact on earthquake science and hazard assessment Manabu Hashimoto, Martha Savage, Takuya Nishimura and Haruo Horikawa 4.Seismology. Earth, Planets and Space, 68(1). https://doi.org/10.1186/s40623-016-0567-1

Kodera, Y., Yamada, Y., Hirano, K., Tamaribuchi, K., Adachi, S., Hayashimoto, N., Morimoto, M., Nakamura, M., & Hoshiba, M. (2018). The propagation of local undamped motion (PLUM) method: A simple and robust seismic wavefield estimation approach for earthquake early warning. Bulletin of the Seismological Society of America, 108(2), 983–1003. https://doi.org/10.1785/0120170085

Koehrsen, W. (2018, January 29). Overfitting vs. Underfitting: A Complete Example. Towards Data Science. https://towardsdatascience.com/overfitting-vs-underfitting-a-complete-example-d05dd7e19765

Kohler, M. D., Cochran, E. S., Given, D., Guiwits, S., Neuhauser, D., Henson, I., Hartog, R., Bodin, P., Kress, V., Thompson, S., Felizardo, C., Brody, J., Bhadha, R., & Schwarz, S. (2018). Earthquake early warning shakealert system: West coast wide production prototype. Seismological Research Letters, 89(1), 99–107. https://doi.org/10.1785/0220170140

Kohler, M. D., Smith, D. E., Andrews, J., Chung, A. I., Hartog, R., Henson, I., Given, D. D., de Groot, R., & Guiwits, S. (2020). Earthquake early warning Shakealert 2.0: Public rollout. Seismological Research Letters, 91(3). https://doi.org/10.1785/0220190245

Kong, Q., Allen, R. M., & Schreier, L. (2016). MyShake: Initial observations from a global smartphone seismic network. Geophysical Research Letters, 43(18), 9588–9594. https://doi.org/10.1002/2016GL070955

Kong, Q., Inbal, A., Allen, R. M., Lv, Q., & Puder, A. (2019). Machine learning aspects of the myshake global smartphone seismic network. Seismological Research Letters, 90(2 A), 546–552. https://doi.org/10.1785/0220180309

Kong, Q., Kwon, Y.-W., Schreierz, L., Allen, S., Allen, R., & Strauss, J. (2015). Smartphone-based networks for earthquake detection. 2015 15th International Conference on Innovations for Community Services (I4CS), 1–8.

Kong, Q., Lv, Q., & Allen, R. M. (2019). Earthquake early warning and beyond: Systems challenges in smartphone-based seismic network. Proceedings of the 20th International Workshop on Mobile Computing Systems and Applications, 57–62.

Kong, Q., Martin-Short, R., & Allen, R. M. (2020). Toward global earthquake early warning with the myshake smartphone seismic network, part 1: Simulation platform and detection algorithm. Seismological Research Letters, 91(4), 2206–2217. https://doi.org/10.1785/0220190177

Krischer, L., Megies, T., Barsch, R., Beyreuther, M., Lecocq, T., Caudron, C., & Wassermann, J. (2015). ObsPy: A bridge for seismology into the scientific Python ecosystem. Computational Science and Discovery, 8(1). https://doi.org/10.1088/1749-4699/8/1/014003

Küperkoch, L., Meier, T., Lee, J., & Friederich, W. (2010). Automated determination of P-phase arrival times at regional and local distances using higher order statistics. Geophysical Journal International, 181(2). https://doi.org/10.1111/j.1365-246X.2010.04570.x

Kuyuk, H. S., & Allen, R. M. (2013). A global approach to provide magnitude estimates for earthquake early warning alerts. Geophysical Research Letters, 40(24), 6329–6333. https://doi.org/10.1002/2013GL058580

Kuyuk, H. S., Allen, R. M., Brown, H., Hellweg, M., Henson, I., & Neuhauser, D. (2014). Designing a network-based earthquake early warning algorithm for California: ElarmS-2. Bulletin of the Seismological Society of America, 104(1), 162–173. https://doi.org/10.1785/0120130146

Kwon, J., Heo, T., Kim, J. K., & Oh, H. S. (2018). A new P-Wave detector via moving empirical cumulative distribution function. Bulletin of the Seismological Society of America, 108(4), 2080–2089. https://doi.org/10.1785/0120170307

Kwon, Y. W., Ahn, J. K., Lee, J., & Lee, C. H. (2020). Earthquake Early Warning Using Low-Cost MEMS Sensors. International Geoscience and Remote Sensing Symposium (IGARSS), 6635–6637. https://doi.org/10.1109/IGARSS39084.2020.9323438

Lancieri, M., & Zollo, A. (2008). A Bayesian approach to the real-time estimation of magnitude from the early P and S wave displacement peaks. Journal of Geophysical Research: Solid Earth, 113(12). https://doi.org/10.1029/2007JB005386

Lapins, S., Goitom, B., Kendall, J. M., Werner, M. J., Cashman, K. V., & Hammond, J. O. S. (2021). A Little Data Goes a Long Way: Automating Seismic Phase Arrival Picking at Nabro Volcano With Transfer Learning. Journal of Geophysical Research: Solid Earth, 126(7). https://doi.org/10.1029/2021JB021910

Lee, J., Khan, I., Choi, S., & Kwon, Y.-W. (2019). A Smart IoT Device for Detecting and Responding to Earthquakes. Electronics (2079-9292), 8(12), 1546. http://ezproxy.massey.ac.nz/login?url=https://search.ebscohost.com/login.aspx?direct=true&AuthType=ip,cookie,url,uid&db=edb&AN=140942345&site=eds-live&scope=site&authtype=sso&custid=s3027306

Lee, J., Kim, J. S., Choi, S., & Kwon, Y. W. (2019). A Smart Device Using Low-Cost Sensors to Detect Earthquakes. 2019 IEEE International Conference on Big Data and Smart Computing, BigComp 2019 - Proceedings, 1–4. https://doi.org/10.1109/BIGCOMP.2019.8679190

Li, J., Jin, X., Wei, Y., & Zhang, H. (2013). Continuous estimates on the earthquake early warning magnitude by use of the near-field acceleration records. Earthquake Science, 26(5). https://doi.org/10.1007/s11589-013-0040-1

Li, Z., Meier, M. A., Hauksson, E., Zhan, Z., & Andrews, J. (2018). Machine Learning Seismic Wave Discrimination: Application to Earthquake Early Warning. Geophysical Research Letters, 45(10). https://doi.org/10.1029/2018GL077870

Lin, T., Wu, Y., & Chin, T. (2012). Apply low-cost acceleration sensors to the Earthquake Early Warning Systems in Taiwan. AGU Fall Meeting Abstracts, 2012, S53B-2499.

Liu, H., Li, S., & Song, J. (2022). Discrimination between Earthquake P Waves and Microtremors via a Generative Adversarial Network. Bulletin of the Seismological Society of America, 112(2). https://doi.org/10.1785/0120210231

Liu, H., Song, J., & Li, S. (2022). Seismic Event Identification Based on a Generative Adversarial Network and Support Vector Machine. Frontiers in Earth Science, 10. https://doi.org/10.3389/feart.2022.814655

Lizurek, G., Marmureanu, A., & Wiszniowski, J. (2017). Fast Moment Magnitude Determination from P-wave Trains for Bucharest Rapid Early Warning System (BREWS). Pure and Applied Geophysics, 174(3). https://doi.org/10.1007/s00024-017-1480-7

Lyu, Y., Li, H., Sayagh, M., Jiang, Z. M., & Hassan, A. E. (2021). An Empirical Study of the Impact of Data Splitting Decisions on the Performance of AIOps Solutions. ACM Transactions on Software Engineering and Methodology, 30(4). https://doi.org/10.1145/3447876

Massey University. (2024). Code of ethical conduct for research, teaching, and evaluations involving human participants. https://www.massey.ac.nz/research/ethics/human-ethics/#Usingparticipantsinresearch

McBride, S. K., Smith, H., Morgoch, M., Sumy, D., Jenkins, M., Peek, L., Bostrom, A., Baldwin, D., Reddy, E., De Groot, R., Becker, J., Johnston, D., & Wood, M. (2022). Evidence-based guidelines for protective actions and earthquake early warning systems. In Geophysics (Vol. 87, Issue 1). https://doi.org/10.1190/geo2021-0222.1

McNamara, D. E., & Buland, R. P. (2004). Ambiente noise levels in the continental United States. Bulletin of the Seismological Society of America, 94(4), 1517–1527. https://doi.org/10.1785/012003001

Mehrazarin, S., Tang, B., Leyba, K., Han, J., & Beheshti, M. (2016). A MacBook based earthquake early warning system. Proceedings - IEEE INFOCOM, 2016-Septe, 1029–1030. https://doi.org/10.1109/INFCOMW.2016.7562237

Meier, M. A., Heaton, T., & Clinton, J. (2015). The Gutenberg algorithm: Evolutionary Bayesian magnitude estimates for earthquake early warning with a filter bank. Bulletin of the Seismological Society of America, 105(5). https://doi.org/10.1785/0120150098

Mertens, D. M. (2015). Research and Evaluation in Education and Psychology: Integrating Diversity with Quantitative, Qualitative, and Mixed Methods. Second Edition, SAGE Publications (CA), 2004-Aug-10. In SAGE Publications.

Minson, S. E., Baltay, A. S., Cochran, E. S., Hanks, T. C., Page, M. T., McBride, S. K., Milner, K. R., & Meier, M. A. (2019). The Limits of Earthquake Early Warning Accuracy and Best Alerting Strategy. Scientific Reports, 9(1). https://doi.org/10.1038/s41598-019-39384-y

Minson, S. E., Brooks, B. A., Glennie, C. L., Murray, J. R., Langbein, J. O., Owen, S. E., Heaton, T. H., Iannucci, R. A., & Hauser, D. L. (2015). Crowdsourced earthquake early warning. Science Advances, 1(3), 1–8. https://doi.org/10.1126/sciadv.1500036

Mittal, H., Wu, Y. M., Sharma, M. L., Yang, B. M., & Gupta, S. (2019). Testing the performance of earthquake early warning system in northern India. Acta Geophysica, 67(1), 59. https://doi.org/10.1007/s11600-018-0210-6

Moratalla, J. M., Goded, T., Rhoades, D. A., Canessa, S., & Gerstenberger, M. C. (2020). New ground motion to intensity conversion equations (GMICEs) for New Zealand. Seismological Research Letters, 92(1). https://doi.org/10.1785/0220200156

Morgan, D. L. (2007). Paradigms Lost and Pragmatism Regained: Methodological Implications of Combining Qualitative and Quantitative Methods. Journal of Mixed Methods Research, 1(1). https://doi.org/10.1177/2345678906292462

Mousavi, S. M., Ellsworth, W. L., Zhu, W., Chuang, L. Y., & Beroza, G. C. (2020). Earthquake transformer—an attentive deep-learning model for simultaneous earthquake detection and phase picking. Nature Communications, 11(1). https://doi.org/10.1038/s41467-020-17591-w

Myers, M. D. (2008). Prepared for U.S. Geological Survey and the Advanced National Seismic System National Implementation Committee Instrumentation Guidelines for the Advanced National Seismic System Open-File Report 2008-1262.

Nadin, E. (2020). How good is earthquake early warning? Temblor. https://doi.org/10.32858/temblor.071

Nakamura, Y. (2004). UrEDAS, urgent earthquake detection and alarm system, now and future. 13th World Conference on Earthquake Engineering, 908.

Nakayachi, K., Becker, J. S., Potter, S. H., & Dixon, M. (2019). Residents' Reactions to Earthquake Early Warnings in Japan. Risk Analysis, 39(8), 1723–1740. https://doi.org/10.1111/risa.13306

Nicholas Morpus. (2024, April 22). A Step-by-Step Guide for Using a Weighted Scoring Model. The Ascent.

Noda, S., & Ellsworth, W. L. (2017). Determination of earthquake magnitude for early warning from the time dependence of P-wave amplitudes. Bulletin of the Seismological Society of America, 107(4). https://doi.org/10.1785/0120170048

Noda, S., Yamamoto, S., & Ellsworth, W. L. (2016). Rapid estimation of earthquake magnitude from the arrival time of the peak high-frequency amplitude. Bulletin of the Seismological Society of America, 106(1). https://doi.org/10.1785/0120150108

Nof, R. N., Chung, A. I., Rademacher, H., Dengler, L., & Allen, R. M. (2019). MEMS accelerometer mini-array (MAMA): A low-cost implementation for earthquake early warning enhancement. Earthquake Spectra, 55(1), 21–38. https://doi.org/10.1193/021218EQS036M

Nogeste, K. (2007). Research Strategy Development for Dummies : Define a Framework of Research Options and then Use It.

Ochoa, L. H., Niño, L. F., & Vargas, C. A. (2018). Fast magnitude determination using a single seismological station record implementing machine learning techniques. Geodesy and Geodynamics, 9(1). https://doi.org/10.1016/j.geog.2017.03.010

Odaka, T., Ashiya, K., Tsukada, S., Sato, S., Ohtake, K., & Nozaka, D. (2003). A new method of quickly estimating epicentral distance and magnitude from a single seismic record. Bulletin of the Seismological Society of America, 93(1). https://doi.org/10.1785/0120020008

Olson, E. L., & Allen, R. M. (2005). The deterministic nature of earthquake rupture. Nature, 438(7065), 212–215. https://doi.org/10.1038/nature04214

Orlikowski, W. J., & Baroudi, J. J. (1991). Studying Information Technology in Organizations: Research Approaches and Assumptions. In Research (Vol. 2, Issue 1). https://www.jstor.org/stable/23010611

Paul, S., Monfret, T., Courboulex, F., Chèze, J., Calais, E., Symithe, S. J., Deschamps, A., Peix, F., Ambrois, D., Martin, X., Fleur, S. S., & Boisson, D. (2023). Monitoring of Local Earthquakes in Haiti Using Low-Cost, Citizen-Hosted Seismometers and Regional Broadband Stations. Seismological Research Letters, 94(6), 2725–2739. https://doi.org/10.1785/0220230059

Peng, C., Chen, Y., Chen, Q., Yang, J., Wang, H., Zhu, X., Xu, Z., & Zheng, Y. (2017). A new type of tri-axial accelerometers with high dynamic range MEMS for earthquake early warning. Computers and Geosciences, 100, 179–187. http://10.0.3.248/j.cageo.2017.01.001

Peng, C., Jiang, P., Chen, Q., Ma, Q., & Yang, J. (2019). Performance evaluation of a dense MEMS-based seismic sensor array deployed in the Sichuan-Yunnan border region for earthquake early warning. Micromachines, 10(11). https://doi.org/10.3390/mi10110735

Peng, C., Jiang, P., Ma, Q., Wu, P., Su, J., Zheng, Y., & Yang, J. (2021). Performance Evaluation of an Earthquake Early Warning System in the 2019–2020 M6.0 Changning, Sichuan, China, Seismic Sequence. Frontiers in Earth Science, 9. https://doi.org/10.3389/feart.2021.699941

Peng, C., Ma, Q., Jiang, P., Huang, W., Yang, D., Peng, H., Chen, L., & Yang, J. (2020). Performance of a hybrid demonstration earthquake early warning system in the sichuan-yunnan border region. Seismological Research Letters, 91(2A), 835–846. https://doi.org/10.1785/0220190101

Peng, C., Yang, J., Xue, B., Zhu, X., & Chen, Y. (2014). Exploring the feasibility of earthquake early warning using records of the 2008 Wenchuan earthquake and its aftershocks. Soil Dynamics and Earthquake Engineering, 57. https://doi.org/10.1016/j.soildyn.2013.11.005

Peng, C., Zhu, X., Yang, J., Xue, B., & Chen, Y. (2013). Development of an integrated onsite earthquake early warning system and test deployment in Zhaotong, China. Computers and Geosciences, 56, 170–177. https://doi.org/10.1016/j.cageo.2013.03.018

Peterson, J. (1993). Observations and modelling of seismic background noise. Open-File Report 93-322. In Seismological Research Letters (Vol. 79, Issue 2).

Picozzi, M., Colombelli, S., Zollo, A., Carranza, M., & Buforn, E. (2015). A Threshold-Based Earthquake Early-Warning System for Offshore Events in Southern Iberia. Pure and Applied Geophysics, 172(9). https://doi.org/10.1007/s00024-014-1009-2

Picozzi, M., Emolo, A., Martino, C., Zollo, A., Miranda, N., Verderame, G., Boxberger, T., Elia, L., Del Gaudio, S., Colombelli, S., Amoroso, O., Brondi, P., De Risi, M. T., Parolai, S., Bindi, D., Boxberger, T., Miranda, N., Buonaiuto, L., & Amelia, A. (2015). Earthquake early warning system for schools: A feasibility study in southern Italy. Seismological Research Letters, 86(2A), 398–412. https://doi.org/10.1785/0220140194

Potter, S. H., Becker, J. S., Johnston, D. M., & Rossiter, K. P. (2015). An overview of the impacts of the 2010-2011 Canterbury earthquakes. International Journal of Disaster Risk Reduction, 14. https://doi.org/10.1016/j.ijdrr.2015.01.014

Pragati Baheti. (2021, December 1). What is Overfitting in Deep Learning [+10 Ways to Avoid It]. https://www.v7labs.com/blog/overfitting

Prasanna, R., Chandrakumar, C., Nandana, R., Holden, C., Punchihewa, A., Becker, J. S., Jeong, S., Liyanage, N., Ravishan, D., Sampath, R., & Tan, M. L. (2022). “Saving Precious Seconds”—A Novel Approach to Implementing a Low-Cost Earthquake Early Warning System with Node-

Level Detection and Alert Generation. Informatics, 9(1), 25. https://doi.org/10.3390/informatics9010025

Prasanna, R., Yang, L., King, M., & Huggins, T. J. (2017). Information Systems for Supporting Fire Emergency Response. Journal of Enterp, 80(4), 605–624. https://doi.org/10.1108/JEIM-12-2015-0120

Qingkai, K., & Ming, Z. (2012). Evaluation of earthquake signal characteristics for early warning. Journal of Earthquake Engineering and Engineering Vibration, 11(3), 435–443. https://doi.org/10.1007/s11803-012-0133-1

Raspberry Shake, S. A. (2017). Raspberry Shake Data Center. https://doi.org/https://doi.org/10.7914/SN/AM.

Reddy, R., & Nair, R. R. (2013). The efficacy of support vector machines (SVM) in robust determination of earthquake early warning magnitudes in central Japan. Journal of Earth System Science, 122(5). https://doi.org/10.1007/s12040-013-0346-3

Ringler, A. T., & Evans, J. R. (2015). A quick SEED tutorial. Seismological Research Letters, 86(6). https://doi.org/10.1785/0220150043

Rydelek, P., & Horiuchi, S. (2006). Earth science: Is earthquake rupture deterministic? Nature, 442(7100). https://doi.org/10.1038/nature04963

Saad, O. M., & Chen, Y. (2021). Earthquake Detection and P-Wave Arrival Time Picking Using Capsule Neural Network. IEEE Transactions on Geoscience and Remote Sensing, 59(7). https://doi.org/10.1109/TGRS.2020.3019520

Santamaria, A. F., Raimondo, P., Tropea, M., De Rango, F., & Aiello, C. (2019). An IoT surveillance system based on a decentralised architecture. Sensors (Switzerland), 19(6). https://doi.org/10.3390/s19061469

Satriano, C., Elia, L., Martino, C., Lancieri, M., Zollo, A., & Iannaccone, G. (2011). PRESTo, the earthquake early warning system for Southern Italy: Concepts, capabilities and future perspectives. Soil Dynamics and Earthquake Engineering, 31(2), 137–153. https://doi.org/10.1016/j.soildyn.2010.06.008

Saunders, J. K., Minson, S. E., Baltay, A. S., Bunn, J. J., Cochran, E. S., Kilb, D. L., O'Rourke, C. T., Hoshiba, M., & Kodera, Y. (2022). Real-Time Earthquake Detection and Alerting Behavior of

PLUM Ground-Motion-Based Early Warning in the United States. Bulletin of the Seismological Society of America. https://doi.org/10.1785/0120220022

Scotland, J. (2012). Exploring the philosophical underpinnings of research: Relating ontology and epistemology to the methodology and methods of the scientific, interpretive, and critical research paradigms. English Language Teaching, 5(9). https://doi.org/10.5539/elt.v5n9p9

Semmens, S., Perrin, N. D., Dellow, G., & Van Dissen, & R. (2011). site subsoil classification of Wellington City (Vol. 5). http://pet.gns.cri.nz

Shearer, P. M. (2009). Introduction to seismology, second edition. Cambridge University Press, 4(3).

Simons, F. J., Dando, B. D. E., & Allen, R. M. (2006). Automatic detection and rapid determination of earthquake magnitude by wavelet multiscale analysis of the primary arrival. Earth and Planetary Science Letters, 250(1–2). https://doi.org/10.1016/j.epsl.2006.07.039

Sokolov, V., Wenzel, F., Wen, K. L., & Jean, W. Y. (2012). On the influence of site conditions and earthquake magnitude on ground-motion within-earthquake correlation: Analysis of PGA data from TSMIP (Taiwan) network. Bulletin of Earthquake Engineering, 10(5), 1401–1429. https://doi.org/10.1007/s10518-012-9368-5

Stevenson, J. R., Becker, J., Cradock-Henry, N., Johal, S., Johnston, D., Orchiston, C., & Seville, E. (2017). Economic and social reconnaissance: Kaikōura earthquake 2016. Bulletin of the New Zealand Society for Earthquake Engineering, 50(2). https://doi.org/10.5459/bnzsee.50.2.343-351

Stevenson, J. R., Kachali, H., Whitman, Z., Seville, E., Vargo, J., & Wilson, T. (2011). Preliminary observations of the impacts the 22 February Christchurch earthquake had on organisations and the economy: A report from the field (22 February - 22 March 2011). Bulletin of the New Zealand Society for Earthquake Engineering, 44(2). https://doi.org/10.5459/bnzsee.44.2.65-76

Strauss, J. A., & Allen, R. M. (2016). Benefits and costs of earthquake early warning. Seismological Research Letters, 87(3), 765–772. https://doi.org/10.1785/0220150149

Strauss, J. A., Kong, Q., Pothan, S., Thompson, S., Mejia, R. F., Allen, S., Patel, S., & Allen, R. M. (2020). MyShake Citizen Seismologists Help Launch Dual-Use Seismic Network in California. Frontiers in Communication, 5. https://doi.org/10.3389/fcomm.2020.00032

Suárez, G., Espinosa-Aranda, J. M., Cuéllar, A., Ibarrola, G., García, A., Zavala, M., Maldonado, S., & Islas, R. (2018). A dedicated seismic early warning network: The mexican seismic alert system

(SASMEX). Seismological Research Letters, 89(2A), 382–391. https://doi.org/10.1785/0220170184

Suárez, G., Novelo, D., & Mansilla, E. (2009). Performance evaluation of the seismic alert system (SAS) in Mexico City: A seismological and a social perspective. Seismological Research Letters, 80(5). https://doi.org/10.1785/gssrl.80.5.707

Subedi, S., Hetényi, G., Denton, P., & Sauron, A. (2020). Seismology at School in Nepal: A Program for Educational and Citizen Seismology Through a Low-Cost Seismic Network. Frontiers in Earth Science, 8. https://doi.org/10.3389/feart.2020.00073

Sugondo, R. A., & Machbub, C. (2021). P-Wave detection using deep learning in time and frequency domain for imbalanced dataset. Heliyon, 7(12). https://doi.org/10.1016/j.heliyon.2021.e08605

Taale, A., Ventura, C. E., & Marti, J. (2021). On the feasibility of IoT-based smart meters for earthquake early warning. Earthquake Spectra, 37(3), 2066–2083. https://doi.org/10.1177/8755293020981964

Tajima, F., & Hayashida, T. (2018). Earthquake early warning: what does "seconds before a strong hit" mean? In Progress in Earth and Planetary Science (Vol. 5, Issue 1). https://doi.org/10.1186/s40645-018-0221-6

Tan, M. L., Becker, J. S., Stock, K., Prasanna, R., Brown, A., Kenney, C., Cui, A., & Lambie, E. (2022). Understanding the social aspects of earthquake early warning: A literature review. Frontiers in Communication, 7. https://www.frontiersin.org/articles/10.3389/fcomm.2022.939242

Tan, M. L., Brown, A., Stock, K., Becker, J. S., Kenney, C., Lambie, E., Cui, A., & Prasanna, R. (2023). 'Balancing human needs with technology' 1 —a design-led approach for exploring an earthquake early warning system in Aotearoa New Zealand. In Design for Emergency Management (pp. 124–140). Routledge. https://doi.org/10.4324/9781003306771-9

Tan, M. L., Prasanna, R., Becker, J. S., Brown, A., Lambie, E., Johnston, D. M., Stock, K., & De Alwis, D. (2021). Outlook for earthquake early warning for Aotearoa New Zealand: Insights from initiating a community-of-practice. 2021 Technical Conference for the New Zealand Society for Earthquake Engineering, 1–8.

Tigran P. (2022, October 17). Overfitting and underfitting in machine learning. SuperAnnotate. https://www.superannotate.com/blog/overfitting-and-underfitting-in-machine-learning

Tous, R., Alvarado, L., Otero, B., Cruz, L., & Rojas, O. (2020). Deep neural networks for earthquake detection and source region estimation in north-central venezuela. Bulletin of the Seismological Society of America, 110(5). https://doi.org/10.1785/0120190172

Trnkoczy. (2012). Understanding and parameter setting of STA/LTA trigger algorithm (Bormann P., Ed.). IASPEI New Manual of Seismological Observatory Practice 2 (NMSOP-2), IASPEI.

Tsuno, S. (2021). Applicability of On-Site P-Wave Earthquake Early Warning to Seismic Data Observed During the 2011 Off the Pacific Coast of Tohoku Earthquake, Japan. Frontiers in Earth Science, 9. https://doi.org/10.3389/feart.2021.681199

TurnKey Earthquake Early Warning. (2020). https://earthquake-turnkey.eu/the-project/

Tusa, G., Musumeci, C., & Patanè, D. (2017). Estimation of earthquake early warning parameters for eastern sicily. Bulletin of the Seismological Society of America, 107(3). https://doi.org/10.1785/0120160247

Uga, T., Nagaosa, T., & Kawashima, D. (2012). An emergency earthquake warning system using mobile terminals with a built-in accelerometer. 2012 12th International Conference on ITS Telecommunications, 837–842.

Usage of Wool Carpet in New Zealand. (n.d.). Retrieved March 26, 2024, from https://www.waimakariri.govt.nz/council/news-and-information/2023/09/new-zealand-wool-carpet-set-for-council-owned-facilities.

Vallianatos, F., Karakonstantis, A., & Sakelariou, N. (2021). Estimation of earthquake early warning parameters for eastern gulf of corinth and western attica region (Greece). first results. Sensors, 21(15). https://doi.org/10.3390/s21155084

Velazquez, O., Pescaroli, G., Cremen, G., & Galasso, C. (2020). A Review of the Technical and Socio-Organizational Components of Earthquake Early Warning Systems. Frontiers in Earth Science, 8. https://doi.org/10.3389/feart.2020.533498

Virtanen, P., Gommers, R., Oliphant, T. E., Haberland, M., Reddy, T., Cournapeau, D., Burovski, E., Peterson, P., Weckesser, W., Bright, J., van der Walt, S. J., Brett, M., Wilson, J., Millman, K. J., Mayorov, N., Nelson, A. R. J., Jones, E., Kern, R., Larson, E., … Vázquez-Baeza, Y. (2020). SciPy 1.0: fundamental algorithms for scientific computing in Python. Nature Methods, 17(3). https://doi.org/10.1038/s41592-019-0686-2

Walter, J. I., Ogwari, P., Thiel, A., Ferrer, F., & Woelfel, I. (2020). easyQuake: Putting machine learning to work for your regional seismic network or local earthquake study. Seismological Research Letters, 92(1). https://doi.org/10.1785/0220200226

Wang, C. Y., Huang, T. C., & Wu, Y. M. (2022). Using LSTM Neural Networks for Onsite Earthquake Early Warning. Seismological Research Letters, 93(2A), 814–826. https://doi.org/10.1785/0220210197

Wang, K. S., Mittal, H., Wu, Y.-M., & Chao, W.-A. (2018). Building effects on the p-alert-based real-time shaking map determination. Seismological Research Letters, 89(6), 2314–2321. https://doi.org/10.1785/0220170252

Wang, Y., Li, S., & Song, J. (2020). Threshold-based evolutionary magnitude estimation for an earthquake early warning system in the Sichuan–Yunnan region, China. Scientific Reports, 10(1), 1–12. https://doi.org/10.1038/s41598-020-78046-2

Wang, Z., & Zhao, B. (2017). Automatic event detection and picking of P, S seismic phases for earthquake early warning and application for the 2008 Wenchuan earthquake. Soil Dynamics and Earthquake Engineering, 97. https://doi.org/10.1016/j.soildyn.2017.03.017

Wang, Z., & Zhao, B. (2018). A new Mw estimation parameter for use in earthquake early warning systems. Journal of Seismology, 22(1). https://doi.org/10.1007/s10950-017-9708-7

Wellington City Council. (2022). Soil Classifications Wellington. https://data-wcc.opendata.arcgis.com/datasets/WCC::soilclassifications/about

Wells, D. L., & Coppersmith, K. J. (1994). New empirical relationships among magnitude, rupture length, rupture width, rupture area, and surface displacement. Bulletin - Seismological Society of America, 84(4).

Wibowo, A., Pratama, C., Sahara, D. P., Heliani, L. S., Rasyid, S., Akbar, Z., Muttaqy, F., & Sudrajat, A. (2022). Earthquake Early Warning System Using Ncheck and Hard-Shared Orthogonal Multitarget Regression on Deep Learning. IEEE Geoscience and Remote Sensing Letters, 19. https://doi.org/10.1109/LGRS.2021.3066346

Withers, M., Aster, R., Young, C., Beiriger, J., Harris, M., Moore, S., & Trujillo, J. (1998). A comparison of select trigger algorithms for automated global seismic phase and event detection. Bulletin of the Seismological Society of America, 88(1), 95–106.

Won, J., Park, J., Park, J.-W., & Kim, I. (2020). Bleseis: Low-cost iot sensor for smart earthquake detection and notification. Sensors (Switzerland), 20(10). https://doi.org/10.3390/s20102963

Wu, A., Lee, J., Khan, I., & Kwon, Y. W. (2021). CrowdQuake+: Data-driven Earthquake Early Warning via IoT and Deep Learning. Proceedings - 2021 IEEE International Conference on Big Data, Big Data 2021, 2068–2075. https://doi.org/10.1109/BigData52589.2021.9671971

Wu, B. R., Hsiao, N.-C., Lin, P.-Y., Hsu, T.-Y., Chen, C.-Y., Huang, S.-K., & Chiang, H.-W. (2017). An integrated earthquake early warning system and its performance at schools in Taiwan. Journal of Seismology, 21(1), 165–180. https://doi.org/10.1007/s10950-016-9595-3

Wu, Y. M. (2019). Performance of a Low-Cost Earthquake Early Warning System (P-Alert) and shake map production during the 2018 Mw 6.4 Hualien (Taiwan) Earthquake. Geophysical Research Abstracts, 21, 1.

Wu, Y. M., Chen, D. Y., Lin, T. L., Hsieh, C. Y., Chin, T. L., Chang, W. Y., Li, W. Sen, & Ker, S. H. (2013). A high-density seismic network for earthquake early warning in Taiwan based on low cost sensors. Seismological Research Letters, 84(6), 1048–1054. https://doi.org/10.1785/0220130085

Wu, Y. M., & Kanamori, H. (2005a). Experiment on an onsite early warning method for the Taiwan early warning system. Bulletin of the Seismological Society of America, 95(1), 347–353. https://doi.org/10.1785/0120040097

Wu, Y. M., & Kanamori, H. (2005b). Rapid assessment of damage potential of earthquakes in Taiwan from the Beginning of P waves. Bulletin of the Seismological Society of America, 95(3), 1181–1185. https://doi.org/10.1785/0120040193

Wu, Y. M., & Kanamori, H. (2008). Development of an earthquake early warning system using real-time strong motion signals. Sensors, 8(1), 1–9. https://doi.org/10.3390/s8010001

Wu, Y. M., Kanamori, H., Allen, R. M., & Hauksson, E. (2007). Determination of earthquake early warning parameters, τc and Pd, for southern California. Geophysical Journal International, 170(2), 711–717. https://doi.org/10.1111/j.1365-246X.2007.03430.x

Wu, Y. M., & Mittal, H. (2021). A Review on the Development of Earthquake Warning System Using Low-Cost Sensors in Taiwan. Sensors (Basel, Switzerland), 21(22). https://doi.org/10.3390/s21227649

Wu, Y. M., & Zhao, L. (2006). Magnitude estimation using the first three seconds P-wave amplitude in earthquake early warning. Geophysical Research Letters, 33(16), 4–7. https://doi.org/10.1029/2006GL026871

Xi, Z. (2020). The comparison of decentralized and centralized structure of network communication in different application fields.

Xu, Y., Wang, J. P., Wu, Y. M., & Kuo-Chen, H. (2017). Reliability assessment on earthquake early warning: A case study from Taiwan. Soil Dynamics and Earthquake Engineering, 92. https://doi.org/10.1016/j.soildyn.2016.10.015

Yamada, M., & Mori, J. (2022). P-wave picking for earthquake early warning: Refinement of a Tpdmethod. Geophysical Journal International, 228(1). https://doi.org/10.1093/gji/ggab349

Yamamoto, S., Rydelek, P., Horiuchi, S., Wu, C., & Nakamura, H. (2008). On the estimation of seismic intensity in earthquake early warning systems. Geophysical Research Letters, 35(7). https://doi.org/10.1029/2007GL033034

Yang, B. M., Huang, T.-C., & Wu, Y.-M. (2018). Shakingalarm: A nontraditional regional earthquake early warning system based on time-dependent anisotropic peak ground-motion attenuation relationships. Bulletin of the Seismological Society of America, 108(3), 1219–1230. https://doi.org/10.1785/0120170105

Yang, B. M., Mittal, H., & Wu, Y.-M. (2021). Real-Time Production of PGA, PGV, Intensity, and Sa Shakemaps Using Dense MEMS-Based Sensors in Taiwan. Sensors (14248220), 21(3), 943. http://10.0.13.62/s21030943

Yang, Y., & Motosaka, M. (2015). Ground motion estimation using front sitewave form data based on RVM for earthquake earlywarning. Journal of Disaster Research, 10(4). https://doi.org/10.20965/jdr.2015.p0667

Yanwei, W., Xiaojun, L., Zifa, W., Jianping, S., & Enhe, B. (2021). Deep learning for P-wave arrival picking in earthquake early warning. Earthquake Engineering and Engineering Vibration, 20(2). https://doi.org/10.1007/s11803-021-2027-6

Yin, R. C., Wu, Y.-M., & Hsu, T.-Y. (2016). Application of the low-cost MEMS-type seismometer for structural health monitoring: A pre-study. Conference Record - IEEE Instrumentation and Measurement Technology Conference, 2016-July. https://doi.org/10.1109/I2MTC.2016.7520389

Zambrano, A. M., Perez, I., Palau, C., & Esteve, M. (2014). Quake detection system using smartphone-based wireless sensor network for early warning. In 2014 IEEE International Conference on Pervasive Computing and Communication Workshops (PERCOM WORKSHOPS), Pervasive Computing and Communications Workshops (PERCOM Workshops), 2014 IEEE International Conference on (pp. 297–302). IEEE. https://doi.org/10.1109/PerComW.2014.6815221

Zambrano, A. M., Perez, I., Palau, C., & Esteve, M. (2015). Distributed Sensor System for Earthquake Early Warning Based on the Massive Use of Low Cost Accelerometers. IEEE Latin America Transactions, Latin America Transactions, IEEE (Revista IEEE America Latina), IEEE Latin Am. Trans., 13(1), 291–298. https://doi.org/10.1109/TLA.2015.7040661

Zambrano, A. M., Perez, I., Palau, C., & Esteve, M. (2017). Technologies of Internet of Things applied to an Earthquake Early Warning System. Future Generation Computer Systems, 75, 206–215. https://doi.org/10.1016/J.FUTURE.2016.10.009

Zhang, H., Thurber, C., & Rowe, C. (2003). Automatic P-wave arrival detection and picking with multiscale wavelet analysis for single-component recordings. Bulletin of the Seismological Society of America, 93(5), 1904–1912. https://doi.org/10.1785/0120020241

Zhang, X., Zhang, M., & Tian, X. (2021). Real-Time Earthquake Early Warning With Deep Learning: Application to the 2016 M 6.0 Central Apennines, Italy Earthquake. Geophysical Research Letters, 48(5). https://doi.org/10.1029/2020GL089394

Zhao, Y., Deng, P., Liu, J., Wang, M., & Wan, J. (2021). LCANet: Lightweight Context-Aware Attention Networks for Earthquake Detection and Phase-Picking on IoT Edge Devices. IEEE Systems Journal. https://doi.org/10.1109/JSYST.2021.3114689

Zhu, J., Li, S., & Song, J. (2022a). Hybrid Deep-Learning Network for Rapid On-Site Peak Ground Velocity Prediction. IEEE Transactions on Geoscience and Remote Sensing, 60. https://doi.org/10.1109/TGRS.2022.3230829

Zhu, J., Li, S., & Song, J. (2022b). Magnitude Estimation for Earthquake Early Warning with Multiple Parameter Inputs and a Support Vector Machine. Seismological Research Letters, 93(1). https://doi.org/10.1785/0220210144

Zhu, J., Li, S., Song, J., & Wang, Y. (2021). Magnitude Estimation for Earthquake Early Warning Using a Deep Convolutional Neural Network. Frontiers in Earth Science, 9. https://doi.org/10.3389/feart.2021.653226

Zhu, W., & Beroza, G. C. (2019). PhaseNet: A deep-neural-network-based seismic arrival-time picking method. Geophysical Journal International, 216(1). https://doi.org/10.1093/gji/ggy423

Zhu, W., Biondi, E., Li, J., Yin, J., Ross, Z. E., & Zhan, Z. (2023). Seismic arrival-time picking on distributed acoustic sensing data using semi-supervised learning. Nature Communications, 14(1). https://doi.org/10.1038/s41467-023-43355-3

Zhu, W., Tai, K. S., Mousavi, S. M., Bailis, P., & Beroza, G. C. (2022). An End-To-End Earthquake Detection Method for Joint Phase Picking and Association Using Deep Learning. Journal of Geophysical Research: Solid Earth, 127(3). https://doi.org/10.1029/2021JB023283

Zollo, A., Amoroso, O., Lancieri, M., Wu, Y. M., & Kanamori, H. (2010). A threshold-based earthquake early warning using dense accelerometer networks. Geophysical Journal International, 183(2). https://doi.org/10.1111/j.1365-246X.2010.04765.x

Zollo, A., Colombelli, S., Elia, L., Emolo, A., Festa, G., Iannaccone, G., Martino, C., & Gasparini, P. (2014). An Integrated Regional and On-Site Earthquake Early Warning System for Southern Italy: Concepts, Methodologies and Performances. March, 117–137. https://doi.org/10.1007/978-3-642-12233-0_7

Zollo, A., Lancieri, M., & Nielsen, S. (2006). Earthquake magnitude estimation from peak amplitudes of very early seismic signals on strong motion records. Geophysical Research Letters, 33(23), 2–7. https://doi.org/10.1029/2006GL027795

Zou, Z.-X., Zhang, M., He, X.-D., Lin, S.-F., Dong, Z.-Y., & Sun, K. (2019). Seismic monitoring network based on mems sensors. Earthquake Science, 32(3–4), 179–185. https://doi.org/10.29382/eqs-2019-0179-08

Appendix A

Human Ethics Notification

MASSEY UNIVERSITY
TE KUNENGA KI PŪREHUROA
UNIVERSITY OF NEW ZEALAND

27/04/2023

Dear: Chanthujan Chandrakumar

Re: Low Risk Notification - 4000027269 - An Evaluation of Data Quality and Network Performance for a Low-cost Community-engaged Earthquake Early Warning System

Thank you for submitting a low risk notification for your research/teaching/evaluation.

This email is to acknowledge receipt of the low risk notification and to inform you that the details of your project have been recorded in our database for inclusion in the annual reports to the Health Research Council Ethics Committee (HRCEC) and the Massey University Research Committee (URC).

You may proceed with your research, though it is advisable to provide a couple of weeks before commencing, as all low risk notifications are checked for completeness and clarity by a Research Ethics Advisor. You may be contacted if your application is incomplete and/or further clarification is required.

The low risk notification for this project is valid for a maximum of three years.

Please notify me if situations subsequently occur which cause you to reconsider your initial ethical analysis.

If a sponsoring organisation, funding authority (e.g., the Health Research Council) or a journal require evidence of ethical approval from a Human Ethics Committee (with an approval number), you need to complete a full Massey University Human Ethics application to be reviewed and approved by one of our Human Ethics Committees. Applications must be submitted and approved prior to the commencement of the research.

Please note that travel undertaken by students must be approved by the supervisor and the relevant Pro Vice-Chancellor and be in accordance with the Policy and Procedures for Course-Related Student Travel Overseas. In addition, the supervisor must advise the University's Insurance Officer.

If you have any concerns about the conduct of this research that you want to raise with someone other than the researcher(s), please contact the Research Ethics Office, email humanethics@massey.ac.nz. "

Please include the following statement on all public documents (e.g., information sheet, consent form) related to your project:

> ***This project has been evaluated by peer review and judged to be low risk. Consequently, it has not been reviewed by one of the University's Human Ethics Committees. The researcher(s) named above are responsible for the ethical conduct of this research.***
>
> ***If you have any concerns about the ethical conduct of this research that you want to raise with someone other than the researcher(s), please contact Massey University Human Ethics by email: humanethics@massey.ac.nz.***

I wish you all the best in your research, teaching or evaluation activities and appreciate your thoughtful consideration of ethics principles and practices.

Ngā mihi nui,

Professor Tracy Riley
Acting Chair, Research Ethics Chair's Committee

Research Ethics Office, Research and Enterprise
Massey University, Private Bag 11 222, Palmerston North, 4442, New Zealand T 06 951 6841; 06 951 6840
E humanethics@massey.ac.nz; animalethics@massey.ac.nz; gtc@massey.ac.nz

MASSEY UNIVERSITY
TE KUNENGA KI PŪREHUROA
UNIVERSITY OF NEW ZEALAND

13/09/2023

Dear: Chanthujan Chandrakumar

Re: Low Risk Notification - 4000028144 - Increasing Sensor Density for a Low-cost Community-Engaged Earthquake Early Warning System through Sensor Installation

Thank you for submitting a low risk notification for your research/teaching/evaluation.

This email is to acknowledge receipt of the low risk notification and to inform you that the details of your project have been recorded in our database for inclusion in the annual reports to the Health Research Council Ethics Committee (HRCEC) and the Massey University Research Committee (URC).

You may proceed with your research, though it is advisable to provide a couple of weeks before commencing, as all low risk notifications are checked for completeness and clarity by a Research Ethics Advisor. You may be contacted if your application is incomplete and/or further clarification is required.

The low risk notification for this project is valid for a maximum of three years.

Please notify me if situations subsequently occur which cause you to reconsider your initial ethical analysis.

If a sponsoring organisation, funding authority (e.g., the Health Research Council) or a journal require evidence of ethical approval from a Human Ethics Committee (with an approval number), you need to complete a full Massey University Human Ethics application to be reviewed and approved by one of our Human Ethics Committees. Applications must be submitted and approved prior to the commencement of the research.

Please note that travel undertaken by students must be approved by the supervisor and the relevant Pro Vice-Chancellor and be in accordance with the Policy and Procedures for Course-Related Student Travel Overseas. In addition, the supervisor must advise the University's Insurance Officer.

If you have any concerns about the conduct of this research that you want to raise with someone other than the researcher(s), please contact the Research Ethics Office, email humanethics@massey.ac.nz. "

Please include the following statement on all public documents (e.g., information sheet, consent form) related to your project:

> ***This project has been evaluated by peer review and judged to be low risk. Consequently, it has not been reviewed by one of the University's Human Ethics Committees. The researcher(s) named above are responsible for the ethical conduct of this research.***
>
> ***If you have any concerns about the ethical conduct of this research that you want to raise with someone other than the researcher(s), please contact Massey University Human Ethics by email: humanethics@massey.ac.nz.***

I wish you all the best in your research, teaching or evaluation activities and appreciate your thoughtful consideration of ethics principles and practices.

Ngā mihi nui,

Professor Tracy Riley
Acting Chair, Research Ethics Chair's Committee

Research Ethics Office, Research and Enterprise
Massey University, Private Bag 11 222, Palmerston North, 4442, New Zealand T 06 951 6841; 06 951 6840
E humanethics@massey.ac.nz; animalethics@massey.ac.nz; gtc@massey.ac.nz

Appendix B

Technical Note

Technical Note: Installation Methods for Ground Motion Sensors in Community-engaged Earthquake Early Warning System

Abstract

This research investigates installation methods for ground motion accelerometers within a community-engaged Earthquake Early Warning (EEW) network, where untrained volunteers install sensors in their homes. Four installation methods were evaluated on plush wool-type carpets using a shake table with sinusoidal waveforms within the expected frequency range of earthquake ground motions and real-world earthquake acceleration data from historical events. The performance of these methods in accurately capturing key characteristics of ground motions was assessed through statistical and frequency analysis relative to a reference accelerometer fixed to the shake table. The findings indicate that both the loosely placed sensor and the anti-slip sticker method provide effective solutions, with the loosely placed sensor offering optimal accuracy and ease of installation and the anti-slip sticker method providing greater stability. The study highlights the need for future research to explore additional installation methods and floor types using three-dimensional shake tables to enhance broader applicability.

Introduction

New Zealand (NZ), prone to frequent seismic activity due to its geographical position, currently needs a comprehensive national Earthquake Early Warning System (EEWS). Although the GeoNet program provides valuable seismic data, it does not offer real-time earthquake warning capabilities. In response, the CRISiSLab research group at Massey University has launched a pioneering project to develop a community-engaged EEWS utilising low-cost Raspberry Shake 4D (RS4D) ground motion sensors equipped with MEMS-based accelerometers (Prasanna et al., 2022). These sensors represent an innovative step towards enhancing seismic preparedness through a decentralised, community-driven strategy. This technical note focuses on a series of shake table tests to evaluate various installation methods for RS4D sensors. The aim is to identify a balance between accurate seismic data collection and practical installation by untrained volunteers in residential settings, which is crucial for successfully deploying a community-engaged EEWS.

Shake Table Tests

Test Setup

The experimental setup was designed to replicate residential conditions closely, focusing on plush wool carpet flooring due to its prevalence in NZ homes (Usage of Wool Carpet in New Zealand, n.d.). The evaluation considered five distinct installation methods for the RS4D sensors, with a comprehensive test plan developed to assess each method's impact on data accuracy and sensor stability.

Figure B.1-1 illustrates the shake table implementation for the plush wool carpet floor type. Five sensors were installed on the shake table, with each sensor employing a different installation method including one reference sensor fixed directly to the shake table, and four sensors installed using 'simple' methods:

1. Reference Sensor: Served as a control, directly screwed onto the shake table to ensure maximum fidelity in recorded seismic data.
2. Loosely Placed Sensor: Positioned freely on the plush wool carpet to assess performance without any securing mechanism.
3. Loosely Placed Sensor with Anti-Slip Sticker: Employed an anti-slip sticker to gauge the effect of minimal stabilisation on data accuracy.
4. Sensor with Steel Base: A steel plate was attached to the sensor's base, adding weight and stability to examine if increased inertia benefits data integrity.
5. Sensor Fixed with Tape: Utilised double-sided tape for attachment.

Ground Motion Series

The tests were carried out in two phases to provide a range of performance data. First, the sensors were subjected to sinusoidal waves across selected frequencies (0.1 Hz to 20 Hz), reflecting typical seismic activity ranges. This phase of the work aimed to assess sensor responses to a spectrum of the inputs, using frequencies of 0.5, 1, 5, 10, and 15 Hz for a targeted examination of sensor performance in varying seismic scenarios (frequencies summarised in Table B.1-1).

Next, the study expanded its focus to evaluate the performance of seismic sensor installation methods using recorded data from three historically significant earthquakes: the 1992 Cape Mendocino earthquake (EQ1), the 1940 El Centro earthquake (EQ2), and the 1994 Northridge earthquake (EQ3). These events were chosen for their notable impacts on seismic research, providing a spectrum of data for realistic sensor performance assessment. Factors influencing selection included each earthquake's area intensity, duration spread (D5-95), and spectral acceleration at approximately 0.1 seconds. EQ1's

high intensity and broad duration spread are ideal for assessing sensors in intense seismic conditions. EQ2 offers a range of motion intensities for understanding sensor behaviour in variable conditions. Lastly, EQ3, with its moderate intensity and significant spectral acceleration, is apt for testing sensor accuracy in intermediate yet significant seismic events. As summarised in Table B.1-2, the characteristics of these earthquakes are instrumental in evaluating the effectiveness of different sensor installation methods.

Sinusoidal Motion Results

The study utilised Fourier Spectral Analysis (FSA) to examine ground motion data from sensors compared to a reference sensor (Table B.1-1), with the Root Mean Square Error (RMSE) serving as the quantifiable metric for accuracy in seismic signal capture. Results from Table B.1-3 show that the loosely placed sensor installation method consistently yielded the lowest RMSE values across a wide range of frequencies. For instance, at 0.1 Hz, the RMSE was just 0.00008, and even at higher frequencies like 20 Hz, the value increased only to 0.02707. The anti-slip sticker installation method also performed well, showing minor deviations compared to the loosely placed sensor, with an RMSE of 0.00009 at 0.1 Hz and 0.02887 at 20 Hz. In contrast, other methods, such as sticking to the floor and steel plate installations, exhibited higher RMSE values, indicating a more significant deviation from the reference sensor data. These findings highlight the loosely placed sensor as the most accurate, followed closely by the anti-slip sticker method.

Earthquake Ground Motion Results

The study conducted shake table simulations (Figure B.1-2) of three significant earthquakes to evaluate how various RS4D sensor installation methods on plush wool carpet flooring capture seismic data. The comparative analysis, which included visual and statistical evaluations of waveform data, revealed significant deviations for sensors installed using a steel plate method compared to a reference sensor's recordings. In contrast, the loosely placed sensor on the plush wool carpet demonstrated a closer match to the reference sensor, indicating high accuracy in ground motion detection. RMSE values from Table B.1-4 further support this, with the loosely placed method consistently showing the lowest deviations across all earthquake scenarios. For instance, during EQ1, the RMSE for the loosely placed sensor was 0.0027, while the anti-slip sticker method, which performed second best, had an RMSE of 0.0046. Sticking to the floor and using a steel plate showed higher RMSE values across the three earthquakes, indicating notable deviations from the reference sensor. This pattern persisted across EQ2 and EQ3, confirming the precision of the loosely placed method, followed by the anti-slip sticker method's reliability in accurately capturing seismic signals.

The Acceleration Response Spectrum (ARS) analysis aligned with these results, showing that the loosely placed sensors' acceleration spectra closely tracked the reference sensor in all three simulations, particularly in the mid-period range, as depicted in Figure B.1-3. RMSE values from Table B.1-5, such as 0.0017 for EQ1, underscore the method's reliability. The anti-slip sticker-based sensor installation method showed the second-best performance, closely following the loosely placed sensor with minimal deviations.

Peak Ground Acceleration (PGA) analysis provided additional insights into installation method performance, highlighting the loosely placed method's consistency with the reference sensor (Table B.1-6). Notably, the loosely placed sensors deviated by just 2.7% for EQ1, far less than the deviations for other methods. For EQ2 and EQ3, deviations of 22.18% and 3.42% were observed. The anti-slip sticker-based sensor installation method showed the second-best performance compared to the reference sensor, with deviations of 22.41% for EQ1, 34.26% for EQ2, and 15.16% for EQ3.

A Comment about Vertical Acceleration

The shake table's limitation to only horizontal movements required an assessment of sensor installation slip without explicitly applying vertical acceleration. The potential for slip was evaluated by comparing the horizontal shear force applied by the earthquake to the static frictional force at the sensor installation interface, with a frictional force greater than the seismic shear force indicating that no slip would occur.

Vertical ground motion data from the PEER Ground Motion Database (Berkeley University, 2022) were used to analyse the vertical ground reaction force applied to sensors during three earthquake scenarios for each installation method. The ratio of seismic shear force to frictional force was plotted over the time series for each earthquake, establishing a no-slip threshold at a ratio value of 1 (Figure B.1-4). Results indicated that installations with anti-slip stickers had the least potential for slip, followed by steel-plated installations. The loosely placed sensor exhibited the highest probability of slip among the methods tested.

Despite the lower stability of the loosely placed sensor, it demonstrated the highest accuracy in seismic signal replication, as evidenced by consistently lower RMSE values across a broad frequency range. This accuracy, combined with the simplicity of the installation process and the absence of a need for additional securing mechanisms, highlights the effectiveness of the loosely placed method for RS4D sensor installation on plush wool carpeting. On the other hand, the anti-slip sticker method also showed strong performance, with minimal deviations compared to the loosely placed sensor and greater stability against slip. Given these findings, this study recommends both the loosely placed and anti-slip sticker installation methods, acknowledging that each has advantages and disadvantages.

Additional research using a three-dimensional shake table is required to further identify the most suitable installation method. This will enable a more comprehensive sensor performance evaluation under realistic seismic conditions, providing deeper insights into the optimal installation techniques.

Conclusion

This research comprehensively evaluated four RS4D sensor installation methods on plush wool carpets in NZ homes. It identified both the loosely placed and anti-slip sticker methods as effective, with the loosely placed method demonstrating high accuracy in seismic data replication and the anti-slip sticker method providing greater stability against slip. Despite the shake table's limitation to simulating only horizontal ground motion, the developed methodology is adaptable and robust, suitable for advanced, three-dimensional shake tables and applicable for broader testing across various flooring types. Future studies will expand this research to include a broader range of flooring materials in residential and commercial settings. They aim to develop guidelines for optimal sensor installation using three-dimensional shake tables to analyse vertical movements closely. This work significantly enhances the effectiveness of community-engaged EEW networks by recommending the most suitable sensor installation methods for community households.

Appendix B.1

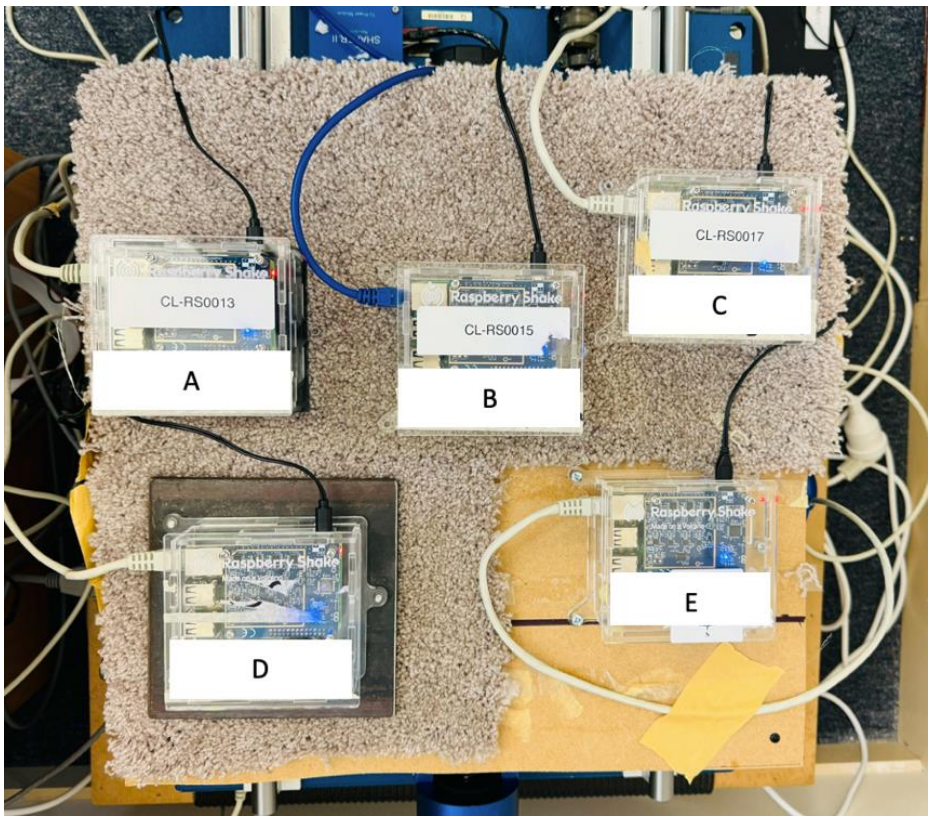

Figure B.1-1: Shake table test setup for plush wool carpet flooring with the four different installation methods along with the reference sensor: (a) a sensor with an anti-slip sticker, (b) a sensor stuck to the floor, (c) a sensor placed loosely, (d) a sensor with a steel plate, and (e) a sensor screwed to the shake table (reference sensor).

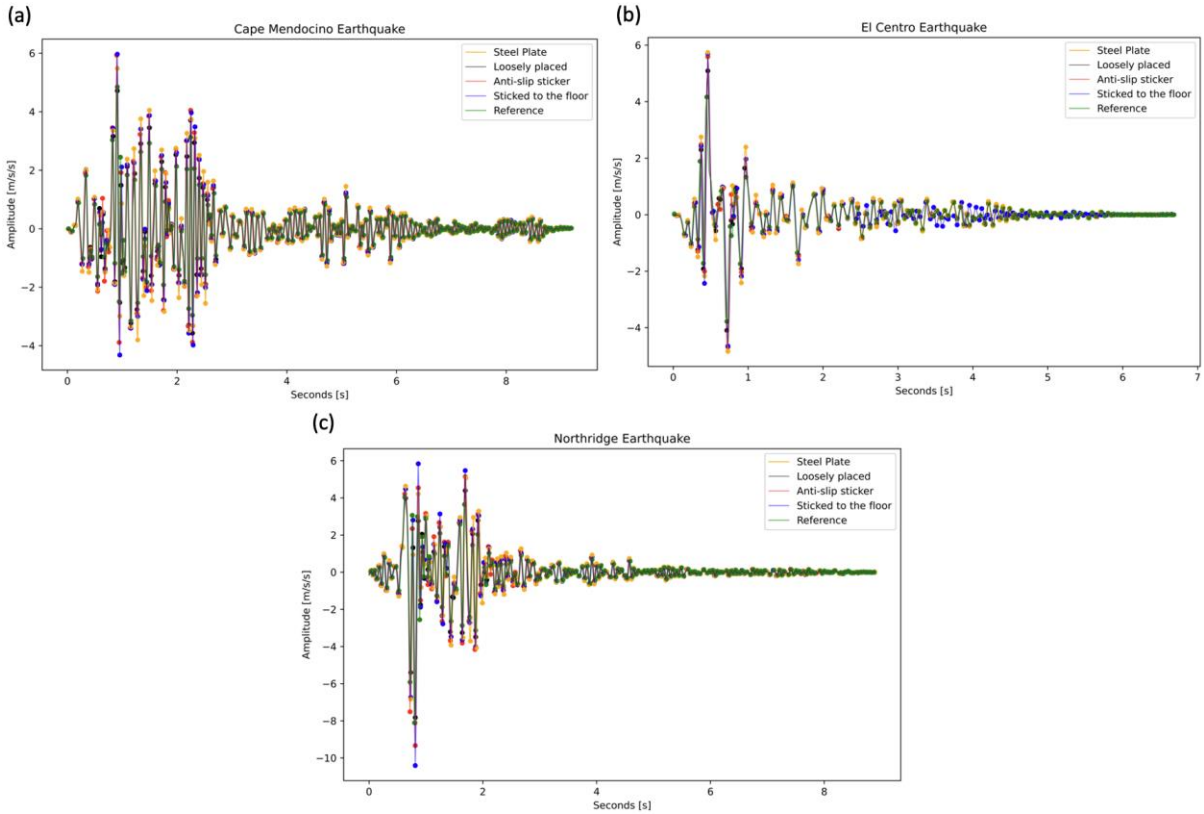

Figure B.1-2: Displays the 3-second waveforms captured for the chosen three earthquakes using the four sensor installation methods mentioned above alongside the reference sensor.

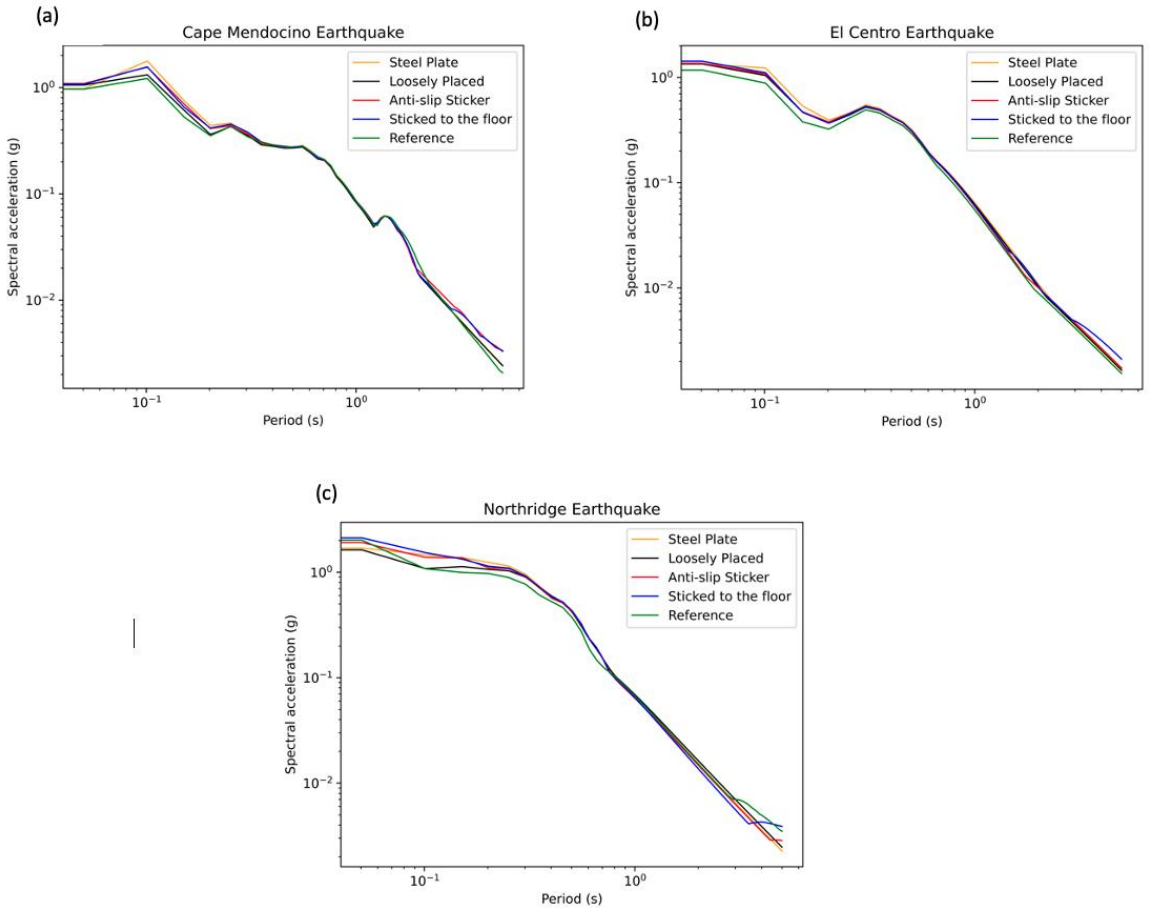

Figure B.1-3: Displays spectral acceleration comparison captured for the chosen three earthquakes using the mentioned four sensor installation methods alongside with the reference sensor.

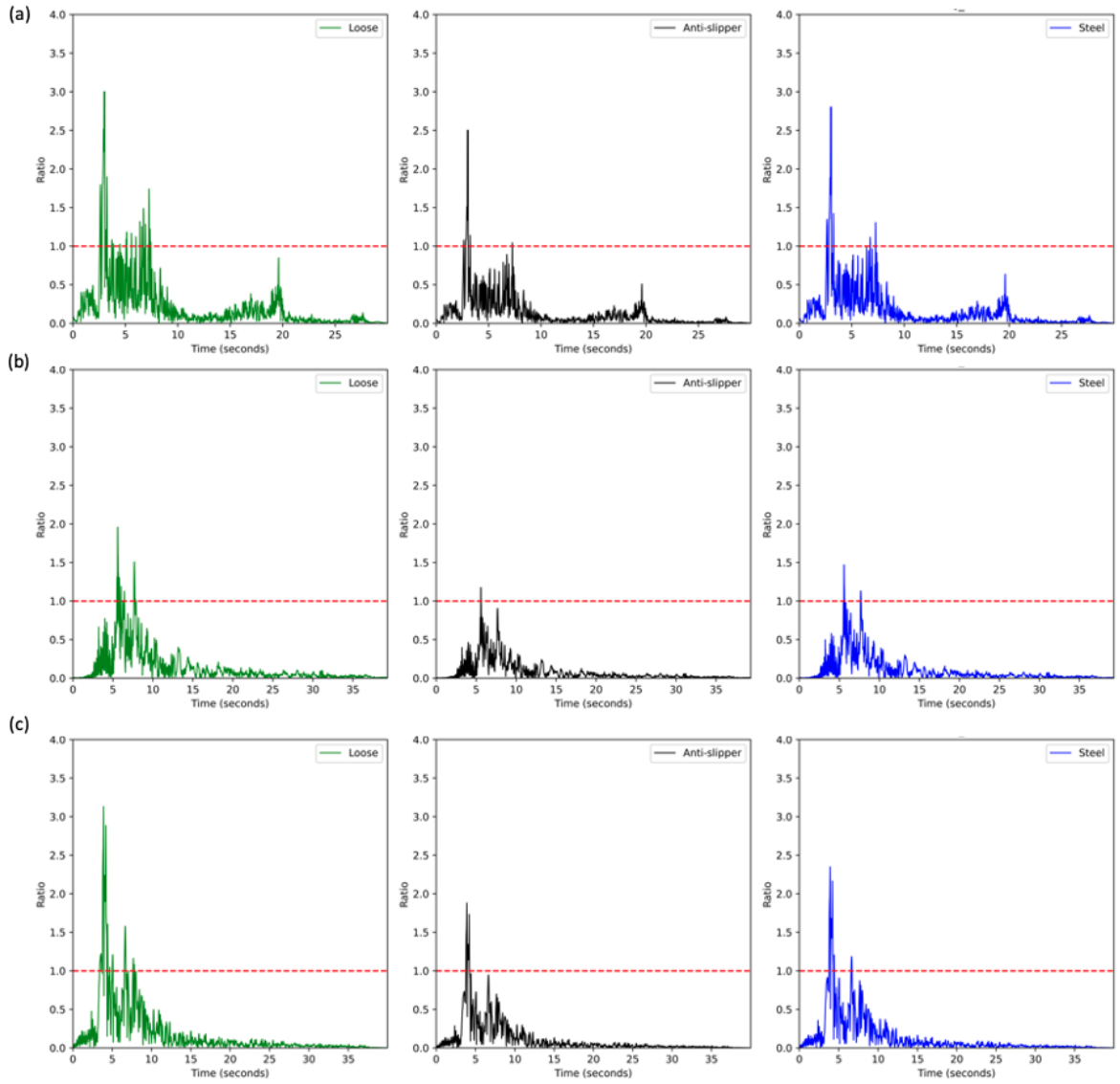

Figure B.1-4: (a), (b) and (C) Show the Ratio of Horizontal Force to Frictional Force at the Wool Carpet Interface for EQ1, EQ2 and EQ3, respectively, along with their Installation Methods (loosely placed, anti-slippery stickered and steel plated). The red horizontal line represents the stability threshold ratio value of 1.

Table B.1-1: Ground Motion Recordings and Fourier Spectra for Five Sensors Across Selected Frequencies (0.1 to 20 Hz).

Frequency	Ground motion recordings	Fourier Spectrum
0.5 Hz	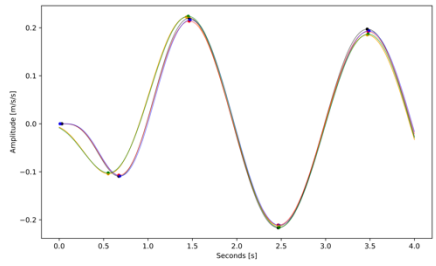	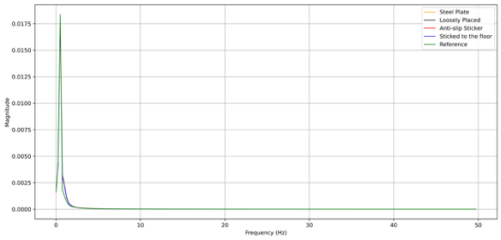
1 Hz	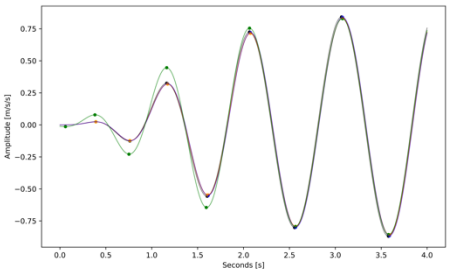	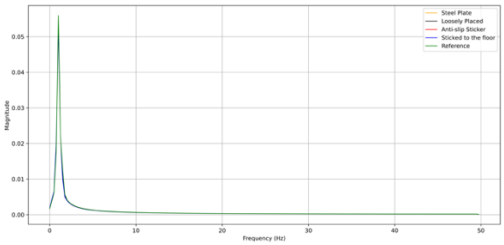
5Hz	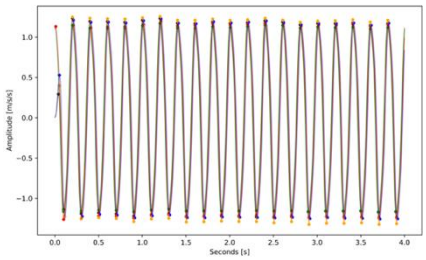	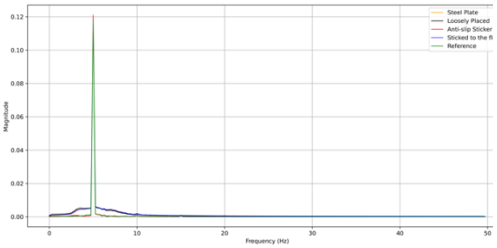
10Hz	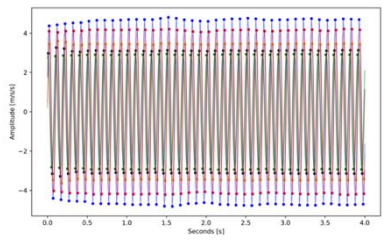	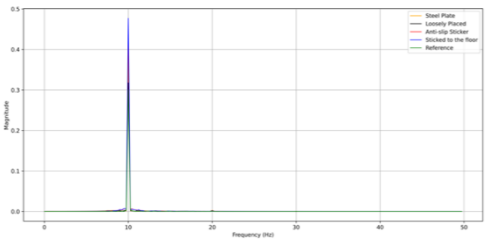

Frequency	Ground motion recordings	Fourier Spectrum
15Hz	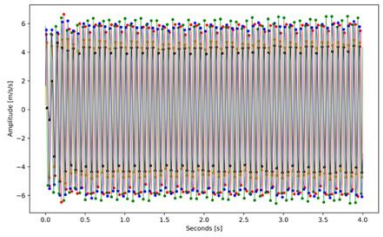	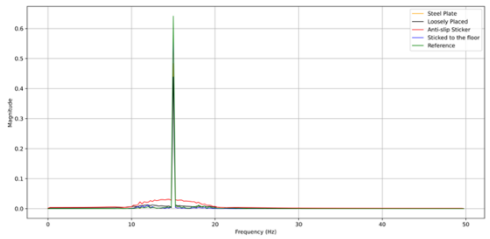

Table B.1-2: Area intensity, duration spread (D5-95), and spectral acceleration at approximately 0.1 seconds for the chosen earthquakes in the North-South direction.

EQs	Areas Intensity (m/s)	Duration Spread (s)	Exact spectral acceleration at ~0.1s (ms^{-2})
EQ1	5.96	6.2	15.47
EQ2	1.69	8.3	9.57
EQ3	2.60	6.8	13.1

Table B.1-3: RMSE Values for FS Across Different Installation Types Compared to the Reference Sensor.

Installation Method	0.1 Hz	0.3 Hz	0.5 Hz	1 Hz	3 Hz	5 Hz	7 Hz	10Hz	13 Hz	15 Hz	17 Hz	20 Hz
Loosely placed	0.00008	0.00015	0.00023	0.00057	0.00029	0.00064	0.00307	0.00368	0.00546	0.01315	0.00544	0.02707
Anti-slip Sticker	0.00009	0.0001	0.00024	0.0006	0.0003	0.00099	0.00432	0.01063	0.00497	0.02049	0.0045	0.02887
Sticked to the floor	0.00012	0.00012	0.00028	0.00068	0.00031	0.00087	0.0043	0.0106	0.00544	0.0056	0.0034	0.02413
Steel plate	0.00015	0.00018	0.00027	0.0008	0.00046	0.00144	0.00803	0.00829	0.00852	0.01128	0.0053	0.02658

Table B.1-4: RMSE Values in Comparison to the Reference Sensor

Earthquake	Loosely placed	Anti-slip Sticker	Sticked to the floor	Steel plate
EQ1	0.0027	0.0046	0.0048	0.0051

Earthquake	Loosely placed	Anti-slip Sticker	Sticked to the floor	Steel plate
EQ2	0.003	0.0041	0.0051	0.0047
EQ3	0.004	0.0048	0.0061	0.0077

Table B.1-5: RMSE Values for Acceleration Response Spectrum Analysis

Earthquake	Loosely placed	Anti-slip Sticker	Sticked to the floor	Steel plate
EQ1	0.0017	0.0043	0.0062	0.0042
EQ2	0.0029	0.0034	0.0048	0.004
EQ3	0.005	0.006	0.0079	0.0073

Table B.1-6: Displays PGA percentage difference with reference to the reference sensor computed for the chosen three earthquakes using the mentioned four sensor installation methods.

Earthquake	Loosely placed (%)	Anti-slip Sticker (%)	Sticked to the floor (%)	Steel plate (%)
EQ1	2.7	22.41	23.14	23.09
EQ2	22.18	34.26	36.85	37.89
EQ3	3.42	15.16	28.46	15

Appendix C

Information Sheet

An Evaluation of Data Quality and Network Performance for a Low-cost Community-engaged Earthquake Early Warning System

INFORMATION SHEET

Dear Participant,

I invite you to participate in my study entitled "An Evaluation of Data Quality and Network Performance for a Low-cost Community-engaged Earthquake Early Warning System". Below are details which may help you decide whether to participate in this survey.

About the Researcher

I am Chanthujan Chandrakumar, a PhD candidate at the Joint Centre for Disaster Research, Massey University, New Zealand. The purpose of this survey is to collect data as part of my doctoral project, which is being supervised by a panel of experts including Dr Raj Prasanna (main supervisor, Massey University), Dr Max T. Stephens (co-supervisor, University of Auckland), Dr Marion Tan (co-supervisor, Massey University), and Dr Caroline Holden (Seismocity).

About the Project

My study looks at the installation and location of Raspberry Shake 4D ground motion sensors in homes. Through this survey, I aim to gather valuable information on how and where the Raspberry Shake 4D sensors were installed in homes. I expect to use the results of this survey to improve the quality and performance of the community-engaged Earthquake Early Warning network in Aotearoa New Zealand, by enhancing the installation method and location of the sensors.

Participant Selection

Participation in this survey is open to community members who have installed the Raspberry Shake 4D ground motion sensors in their households. To participate in this survey, you must be at least 18 years old. The purpose of this survey is to gather information on the installation and location of the sensors.

Participating in the Study

Taking part will involve completing an online questionnaire which will take up to 10 to 15 minutes of your time.

Your rights as a participant

You are under no obligation to accept this invitation. Completion of the questionnaire implies consent. If you decide to participate, you have the right to:

- decline to answer any particular question;
- withdraw from the study by not answering the questions;
- ask any questions about the study at any time during participation;
- provide information on the understanding that your name will not be used unless you give permission to the researcher;
- be given access to a summary of the project findings when it is concluded.

Data Management

Your responses will be used only for this study. Only the researcher and the supervision panel will have access to your survey responses. Your responses will be combined with all other participants' data for analysis. A coding system is designed to make sure that there are no duplications of responses, but you will not be identified by your responses. Questionnaires will be properly disposed of after encoding. Results of the study may also be used in academic publication, but your anonymity will be maintained.

Should you have any concerns, issues or questions, please contact me at +64 [redacted] or email me at cchandra2@massey.ac.nz.

This project (Application ID: 4000027269) has been evaluated by peer review and judged to be low risk. Consequently, it has not been reviewed by one of the University's Human Ethics Committees. The researcher(s) named in this document are responsible for the ethical conduct of this research. If you

have any concerns about the conduct of this research that you want to raise with someone other than the researcher(s), please contact Professor Craig Johnson, Director (Research Ethics), email humanethics@massey.ac.nz.

Sincerely,

Chanthujan Chandrakumar
Joint Centre for Disaster Research
School of Psychology
Wellington Campus
Massey University
Phone: [redacted]
Email: cchandra2@massey.ac.nz

Appendix D

Questionnaire – Data Quality Analysis

An Evaluation of Data Quality and Network Performance for a Low-cost Community-engaged Earthquake Early Warning System

Thank you for taking the time to participate in this survey!

This survey is conducted by CRISiSLab regarding the installation and location of Raspberry Shake 4D ground motion sensors in your homes. As an active member of the CRISiSLab Community-engaged Earthquake Early Warning network, your input is valuable to us.

Data from your sensor provide valuable data for earthquake research. Our team has started analysing the data captured in the past and we are planning to improve the quality of the network and data. However, in order to properly interpret this data, we need to know more about how and where you installed your sensor. Therefore, we request your participation in this survey, which will take approximately 10 minutes to complete. Thank you in advance for your participation in this important endeavour.

Your participation is voluntary. By agreeing to participate in this survey, you are providing your consent for the data collected to be used for research. Data will only be published at an aggregate level; individual responses will be kept confidential. You have the right to withdraw from the survey at any time.

"This project (Application ID: 4000027269) has been evaluated by peer review andjudged to be low risk Consequently, it has not been reviewed by one of the University's Human Ethics Committees. The researcher(s) named in this document are responsible for the ethical conduct of this research. If you have any concems about the conduct of this research that you want to raise with someone other than the researcher(s), please contact Professor Craig Johnson, Director (Research Ethics), email humanethics@massey.ac.nz."

1. Please provide the address of where the sensor is located. For all succeeding questions please think about this address.

2. Is your place in a multi-storey flat/apartment or a separate house?
   - ○ In a multi-storey flat/apartment
   - ○ A separate house

3. Where in your house is the sensor installed?
   - ○ Garage
   - ○ In the house, ground level.
   - ○ In the house, first floor
   - ○ In the house, second floor
   - ○ Others, please specify.

4. To the best of your knowledge, what is the ground type of your place? Select all that applies.
   - ○ On solid rock
   - ○ On weathered rock
   - ○ On soft soil
   - ○ On sand
   - ○ Other:
   - ○ Unsure

5. Please select the best description about your place:
   - ○ On a hillside
   - ○ At the bottom of a hill
   - ○ On flat surface
   - ○ Ona dune

6. Is your place near a body of water (less than 2kms)?
   - ○ Yes, by a river (how close in meters?)
   - ○ Yes, by the sea (how close in meters?)
   - ○ Yes, by a lake (how close in meters?)

7. How busy is your neighbourhood? Select all that applies.
   - ○ In a busy neighbourhood
   - ○ In a quiet neighbourhood
   - ○ Near other houses/buildings
   - ○ Near a busy road

8. Is your sensor on the floor?
   - ○ Yes, on the floor.
   - ○ No, please specify (e.g. on the table, windowsill, etc.)

9. What is the type of floor that the sensor is installed?
   - ○ Wooden floor
   - ○ Stone floor
   - ○ Tiled floor
   - ○ Concrete floor
   - ○ Carpeted floor
   - ○ Others, please specify.

10. Is the sensor securely fixed in its installed location, or can it be moved or easily dislodged?
   - ○ Fixed: The sensor is securely attached and cannot be moved or shifted around.
   - ○ Loose: The sensor not securely attached and can be moved or easily dislodged.

11. Type of broadband connection used at your location.
   - ○ Fibre
   - ○ Cable
   - ○ VDSL
   - ○ Wireless
   - ○ ADSL
   - ○ Please specify the area if none of the above suits you

12. Does the sensor affect your internet connectivity? If there is an impact, please specify the nature and extent of the impact.
   - ○ No, the sensor does not affect my internet.
   - ○ Yes, the sensor affects internet connectivity. Please specify.
   - ○ I don't know. Can you describe any disturbances in your area since the sensor installation that may have affected the quality of data collected (e.g., nearby construction, heavy traffic, etc.)?

13. How often do you check if the sensor is working?
   - ○ Never
   - ○ Rarely (once in a month)
   - ○ Occasionally (more than one in a month)
   - ○ Frequently (once in a week)
   - ○ Always (daily)

14. Have you experienced technical difficulties while operating the sensor?
    - ○ No
    - ○ Yes, please specify:

15. Please take a photo of your sensor and upload the image.

We thank you for your time spent taking this survey. Your response has been recorded.

Appendix E

Phase 1 - Sensor Installation Images

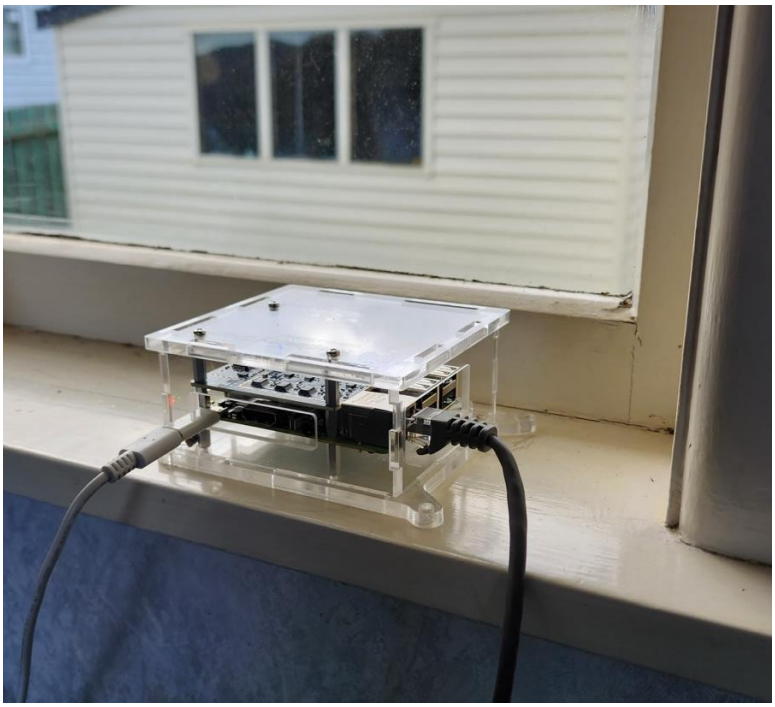

Figure E-1. Sensor installed on a windowsill without any attachments.

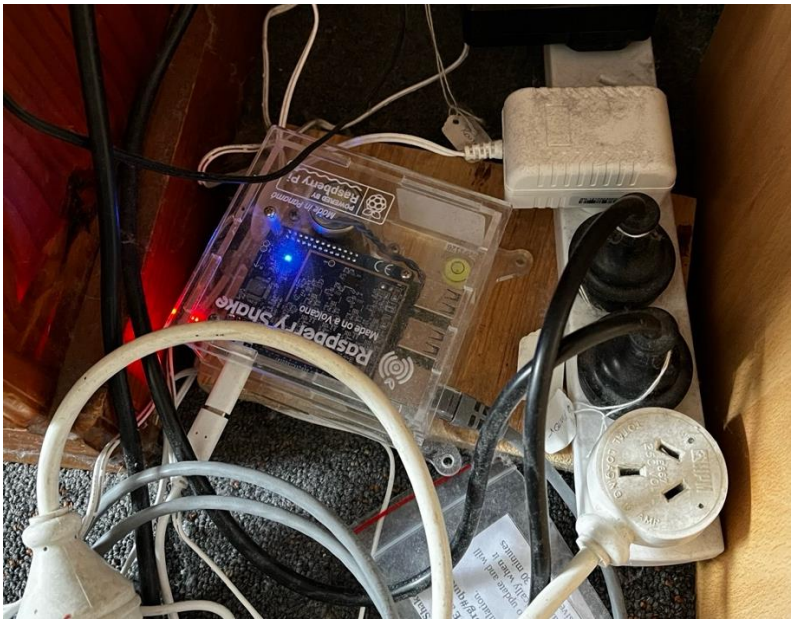

Figure E-2. Sensor partially placed on a wooden plank near electronic devices.

Figure E-3. Sensor positioned on the edge of a cabinet.

Figure E-4. Sensor placed on the floor but not levelled horizontally.

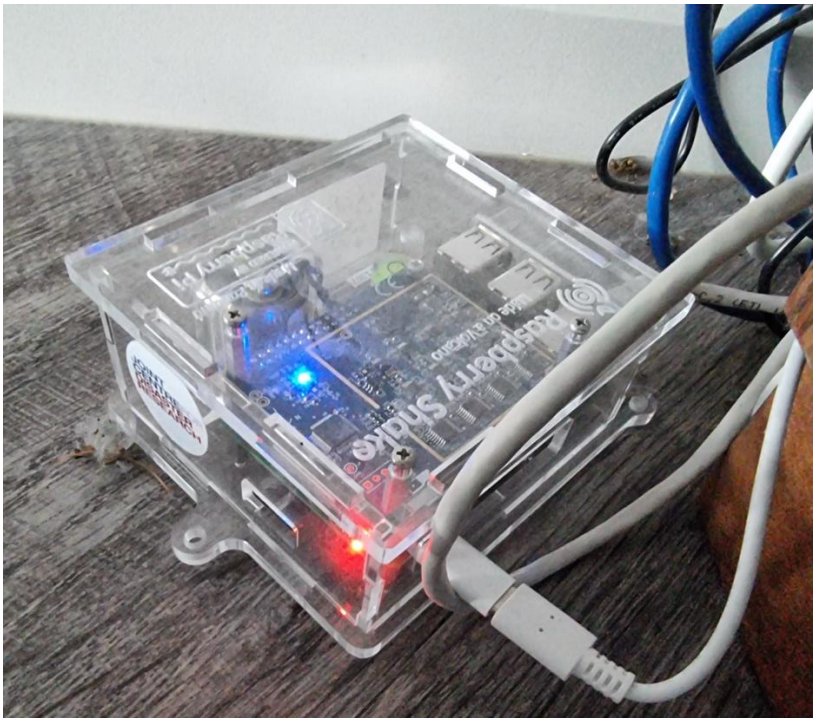

Figure E-5. Sensor placed on the floor without proper alignment to true north.

Figure E-6. Sensor firmly placed on the floor and aligned to true north.

Appendix F

Sensor Installation Guide

Installation Guide for RS4D Sensor – CRISiSLab Experimental Earthquake Early Warning (EEW) Network

1. Introduction

Welcome to the Raspberry Shake (RS) 4D Installation Guide for Sensor Hosts! We appreciate your participation in the Community-Engaged Earthquake Early Warning (EEW) Network, powered by the RS 4D ground motion detection sensors. Your involvement is pivotal in advancing earthquake monitoring within our community.

This guide has been meticulously crafted to provide detailed, step-by-step instructions to ensure a seamless setup process for your RS 4D sensor. Whether you are an experienced tech enthusiast or new to sensor installation, this guide will walk you through each stage, from unpacking to successful configuration.

Within these pages, you will find essential information about the RS 4D sensor, system requirements, safety precautions, and detailed installation steps. We have included guidance on sensor placement for optimal performance, network configuration for Ethernet connection, and sensor installation procedures.

Should you encounter any questions or challenges during the installation process, please do not hesitate to ask for assistance. Contact us at xxx. Your success with the RS 4D installation is paramount to us, and our team is readily available to provide guidance.

Thank you for being so committed to this innovative EEW network. Together, we aim to contribute to the safety and well-being of our community by enhancing earthquake monitoring capabilities. Let's get started on this exciting journey towards a safer future.

2. Package Contents

I. **The Sensor:** The RS 4D sensor.
II. **Power Cable:** A power cable connects the sensor to a power source.
III. **Ethernet Cable (Internet should be provided only via Ethernet):** To facilitate a stable and reliable Internet connection, we provide an Ethernet cable.

IV. **Additional Materials (if requested):** In some cases, additional materials may be provided upon request to assist in securing the sensor to a stable surface within your household.

Please take a moment to inspect the contents of the package to ensure that all items are present and in good condition before proceeding with the installation process. If you have any concerns about the package contents, do not hesitate to contact our support team for assistance.

3. System Requirements

I. **Continuous Power:** The RS 4D sensor requires a continuous power source via a standard power outlet. Ensure that the sensor remains plugged-in to an electricity source to maintain uninterrupted data collection.

II. **Internet Connection via Ethernet cable:** To ensure a stable and reliable Internet connection for the sensor, it must be connected to a dedicated Ethernet port. Ethernet ensures consistent data transmission and is critical to the sensor's functionality.

Please verify that your installation location meets these system requirements before proceeding with the sensor setup. These requirements will help guarantee the sensor's effectiveness and reliability in capturing ground motion data.

4. Safety Precautions

Your safety and the proper functioning of the RS 4D sensor are of utmost importance. Please take note of the following safety precautions:

- **Indoor Installation Only:** The RS 4D sensor is not designed for outdoor use and is not water-resistant. It should only be installed indoors, away from rain, moisture, or extreme humidity exposure. Keep the sensor in a dry and sheltered location within your household.
- **Stable Placement:** Ensure the sensor is placed on a stable and level surface. This stability is crucial to prevent any accidental falls or disruptions to data collection.
- **Proper Cable Management:** Safely route and secure all cables to prevent tripping hazards and potential damage to the sensor or other equipment. Avoid pinching or bending cables excessively.
- **No Direct Sunlight:** Avoid exposing the sensor to direct sunlight, as extreme heat can affect its performance. Place the sensor away from windows or sources of direct sunlight.
- **Handling Precautions:** When handling the sensor, do not force or exert excessive pressure on any part. Treat it with care to avoid damage.

By adhering to these safety precautions, you can help ensure the longevity and effectiveness of the RS 4D sensor while maintaining a safe environment within your household.

5. Installation Steps

Follow these step-by-step instructions to ensure a successful installation of the RS 4D sensor:

I. Choose the Installation Location:

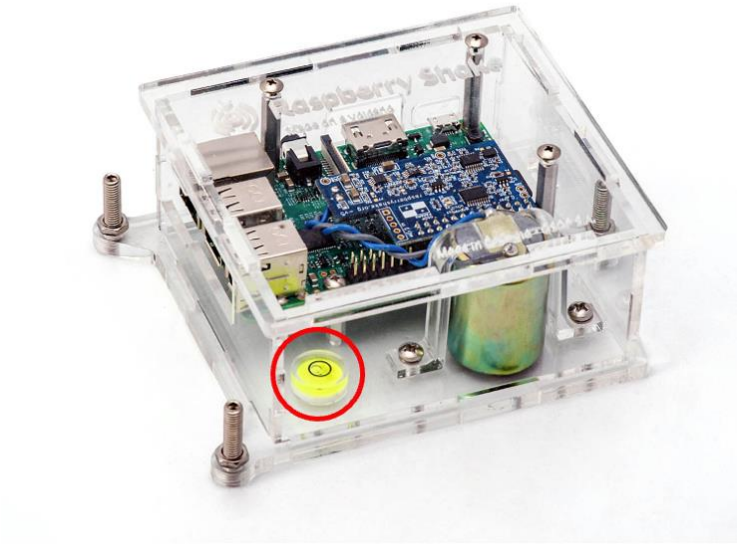

Figure F-1: the levelling air bubble is indicated by the red circle in RS 4D ground motion sensor.

Select a stable surface on the lowest floor of your building for the sensor installation. This location should minimise exposure to excessive vibrations or movements, such as those caused by appliances like washing machines or dryers. Ensuring a stable surface is crucial for accurate data collection. To check the sensor's levelling, use the air bubble indicator on the sensor, which shows whether it's horizontal (as indicated in figure F-1 by a red circle).

Additionally, consider minimising potential electromagnetic interference by positioning the sensor away from devices like televisions, heaters, or other sources of electromagnetic interference. While not mandatory, this can enhance the sensor's performance.

Endeavour to securely fix the sensor in place, while its not mandatory, placing the sensor stable as much as possible, avoiding loose placement, can enhance data quality and overall performance.

II. Align the Sensor Toward True North:

To ensure precise alignment of your Raspberry Shake sensor with true geographic north, please follow these instructions:

- **iOS (Apple) Users:** You can use the built-in compass app if you have an iOS device (Apple). To set it to true north, follow these steps:
    - Visit this link for a step-by-step guide: Set the iPhone Compass to Use True North.
    - Alternatively, you can watch a video tutorial on YouTube: YouTube Tutorial.
- **Android Users:** For Android users, you can download the "Compass Steel 3D" application from the Google Play Appstore. Be sure to enable the "True" mode within the app to activate the true north direction.
- **Compass Device:** If you have a separate compass device, you can use it to align the sensor with true north. Follow the standard procedures for using your compass device to determine true north.

The Raspberry Shake sensor is equipped with a North Arrow indicator that will assist you in achieving the correct alignment.

Remember that this alignment should be based on true north, not magnetic north, for accurate data collection. Proper alignment is a mandatory step to ensure the reliability and precision of your seismic data.

III. Power Connection:

Connect the RS 4D sensor to a nearby power outlet using the provided power cable. Ensure that the sensor receives continuous power to operate effectively.

IV. Ethernet Connection:

Connect the sensor to your home network via Ethernet. Use the supplied Ethernet cable to establish a reliable and uninterrupted internet connection. Ensure the Ethernet cable is connected securely to the sensor and your network router.

By following these installation steps in the specified order, you can optimise the performance of the RS 4D sensor, ensuring accurate and reliable ground motion data collection for the Community-Engaged EEW Network.

6. Verifying Sensor Operation

After successfully installing the RS 4D sensor, it will automatically power on. Please take note of the following steps to ensure that your sensor is installed and functioning correctly:

1) **Initial Software Update:** When your RS 4D is powered on for the first time, it will automatically update the software. The duration of this update may vary depending on your available bandwidth and the time elapsed since the sensor's manufacturing. It could take anywhere from a few seconds to several minutes to complete.
2) **Checking Sensor Operation:** To verify that the sensor is installed correctly and operational, follow these steps:
    a. **Prepare a computer:** Ensure you have access to a computer connected to the same network as the RS 4D sensor (it is preferred to connect the computer to the same network using ethernet).
    b. **Open a Web Browser:** Launch a web browser on your computer. We recommend using Google Chrome as your web browser, which actively supports web elements. While other browsers may work, Internet Explorer is not preferred.
    c. **Access the Interface:** In the web browser's address bar, type the URL: http://rs.local/. This web address provides access to the interface for communicating with your RS 4D sensor.
3) **Verification:** Upon accessing the web interface, the RS 4D sensor is functioning correctly if you see a display resembling Figure F-2 with your sensor information.
4) **Confirmation Email:** To confirm the successful installation of your sensor, please send us an email (cchandra2@massey.ac.nz) stating that the sensor has been installed successfully. Additionally, include an image of the installed sensor in your email. Our research team will handle the sensor configuration from this point forward.

This verification process ensures that your RS 4D sensor is operational and ready for data collection. If you encounter any issues during this process or have questions, please do not hesitate to contact our support team for assistance (Chanthujan Chandrakumar – email: cchandra2@massey.ac.nz).

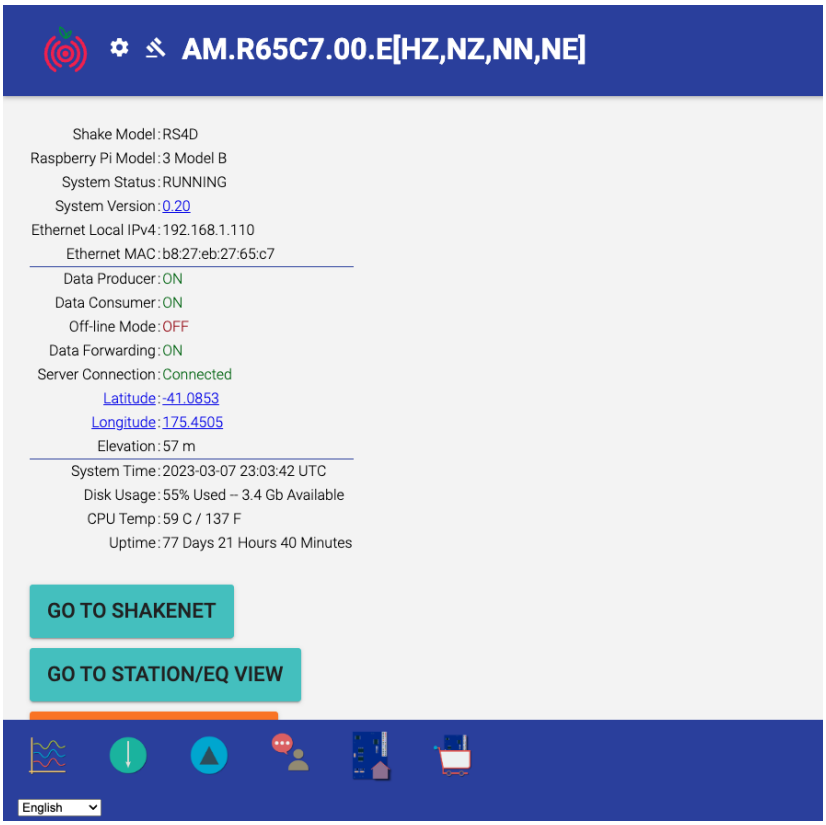

Figure F-2: the web interface of the RS 4D sensor

7. Proper Shutdown Procedure for Your Sensor (Do not just unplug!)

If you intend to move the RS 4D (RS) seismometer to another location or wish to stop recording seismic data, following the proper shutdown procedure is crucial. It is acceptable to manipulate the Ethernet connection of the RS while the power remains connected. But, unplugging the power cable can damage the memory card (SD card) in most cases. To ensure the safe and correct shutdown of the RS seismometer, please follow these steps:

1) **Computer Connection:** Ensure you have a computer or laptop connected to the same network, similar to the installation process.
2) **Access the RS Interface:**
    a. Open your web browser on the connected computer. In the web browser's address bar, enter the URL: http://rs.local/. Navigate to the "ACTIONS" tab within the RS interface as shown in the screenshot below (Figure F-3).
3) **Shutdown Process:**
    a. In the "ACTIONS" tab, locate and click the "SHUTDOWN" button. A confirmation pop-up window will appear. Click "OK" to confirm the shutdown.

Figure F-3: the sample web interface of the RS 4D sensor which indicates the tab and button to shut down the sensor properly

4) **Wait for Confirmation:**
   a. Wait until you see the message "RS 4D is down." This indicates that the RS seismometer has been successfully shut down.
5) **Disconnecting:**
   a. Once you are confident that the RS is shut down, you can safely disconnect all cables and components.

Following this proper shutdown procedure, you can safeguard your RS seismometer and prevent potential damage to the memory card. This ensures the longevity and reliability of your seismic data recording equipment.

8. Conclusion

Congratulations on successfully setting up your RS 4D seismometer as part of the Community-Engaged Earthquake Early Warning (EEW) Network. Your participation is invaluable in advancing earthquake monitoring within our community.

In this comprehensive installation guide, we have covered essential steps to ensure the optimal performance of your sensor, including selecting an appropriate installation location, precise alignment with True North, secure power and Ethernet connections, and proper shutdown procedures.

Remember that your RS 4D sensor will automatically update its software upon initial start-up, which may take a few moments to complete. After installation, verify the sensor's operation by accessing the web interface via http://rs.local/. If the interface resembles Figure 2, your sensor is functioning correctly.

To confirm your successful installation, please send us an email (cchandra2@massey.ac.nz) stating that the sensor has been installed successfully, along with an image of the installed sensor. Our research team will handle the sensor configuration from this point forward.

Thank you for being part of this innovative EEW network. Together, we are contributing to the safety and well-being of our community by enhancing earthquake monitoring capabilities. If you have any questions or require further assistance, do not hesitate to contact our support team. Your commitment to this project is greatly appreciated, and we look forward to the valuable data contributions from your RS 4D seismometer.

Appendix G

Questionnaire - Sensor Installation Information

CRISiSlab Sensor Installation Information

The purpose of this questionnaire is to gather essential information related to your participation as a Raspberry Shake (RS) ground motion detection sensor host within our community-engaged Earthquake Early Warning (EEW) project. Your responses will aid in the proper configuration and placement of the sensor at your residence, ultimately contributing to the success of this research endeavour.

Your cooperation in filling out this questionnaire is greatly appreciated, as it assists us in achieving our research goals and enhancing earthquake early warning capabilities in New Zealand. Thank you for your participation in this significant research endeavour.

1. What is your name?
2. What is the address of your location you are planning to install the sensor?
3. Where do you plan to install the sensor within your property? (e.g., backyard, garage, living room)
4. What type of flooring is present at the sensor installation location? Please select the most applicable option.
   - ○ Concrete
   - ○ Wooden
   - ○ Tile
   - ○ Carpet
   - ○ Other:
5. Is the sensor installation location near any equipment or machinery that may generate vibrations during operation? Please select the most applicable option:
   - ○ No, there are no vibrating equipment nearby.
   - ○ Yes, there are vibrating equipment nearby.
6. If answered "yes" to the previous question, please specify the type of equipment and approximate distance from the sensor location.
7. Are you willing to adhere or affix the sensor to the floor for optimal performance? Please select the most applicable option:
   - ○ Yes, I am willing to adhere the sensor to the floor.
   - ○ No, I prefer not to adhere the sensor to the floor.

8. Please specify any additional materials you require for the installation process. If you need a longer ethernet cable or power cable than what we provide (3 meters of ethernet cable and a 1.5-meter-long power cable), kindly indicate your requirements here.
9. Are you available and comfortable with the proposed installation dates for the sensor, which are scheduled from 2 October 2023 to 15 October 2023? Please share any concerns or alternative suggestions if these dates do not align with your availability or preferences.
10. Regarding the delivery of the sensor, what would be the most convenient option for you? Would you prefer to collect the sensor from Massey University, or would you like us to arrange for the sensor to be delivered to your location? Your input will help us ensure a smooth process for sensor distribution.
11. Would you be able to provide a clear picture of the location where you plan to install the sensor? A photo will help us assess the suitability of the installation site and the sensor installation method.

We thank you for your time spent taking this survey. Your response has been recorded.

Appendix H

Phase 2 - Sensor Installation Images

Figure H-1. Sensor installed on the floor using double-sided tape, aligned to true north.

Figure H-2. Sensor installed on wool carpet using an anti-slip sticker, aligned to true north.

Figure H-3. Sensor installed on wool carpet using an anti-slip sticker, aligned to true north.

Figure H-4. Sensor installed on a concrete floor in a storeroom, aligned to true north, and secured with wooden planks to avoid disturbances.

Figure H-5. Sensor installed on a concrete floor in a storeroom, aligned to true north, and secured with a wooden box to avoid disturbances.

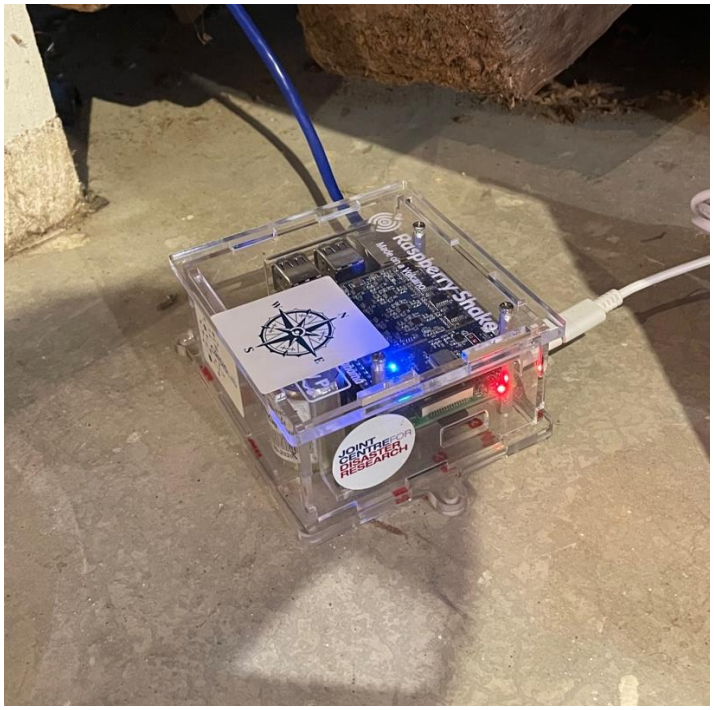

Figure H-6. Sensor installed on a concrete floor and aligned to true north.

Figure H-7. Sensor installed on wool carpet using an anti-slip sticker and aligned to true north.

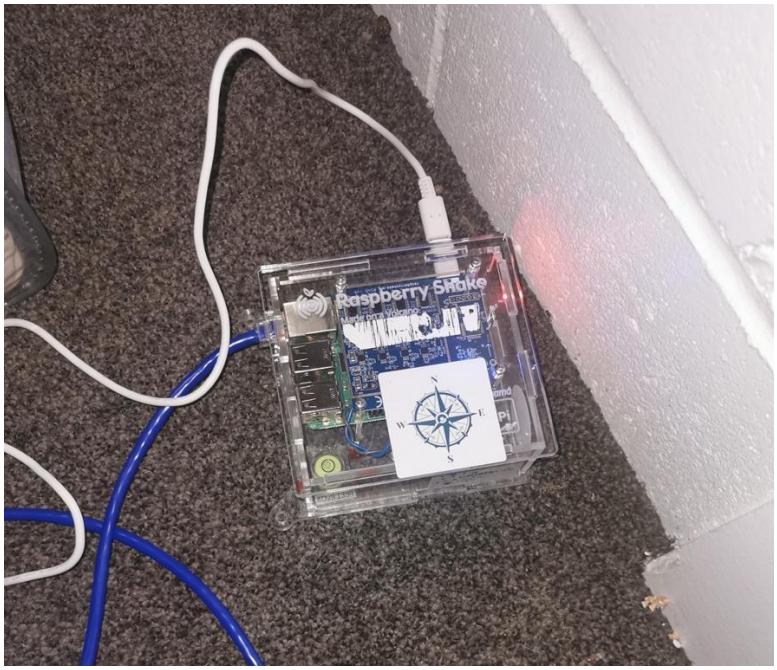

Figure H-8. Sensor installed on wool carpet using an anti-slip sticker and aligned to true north.

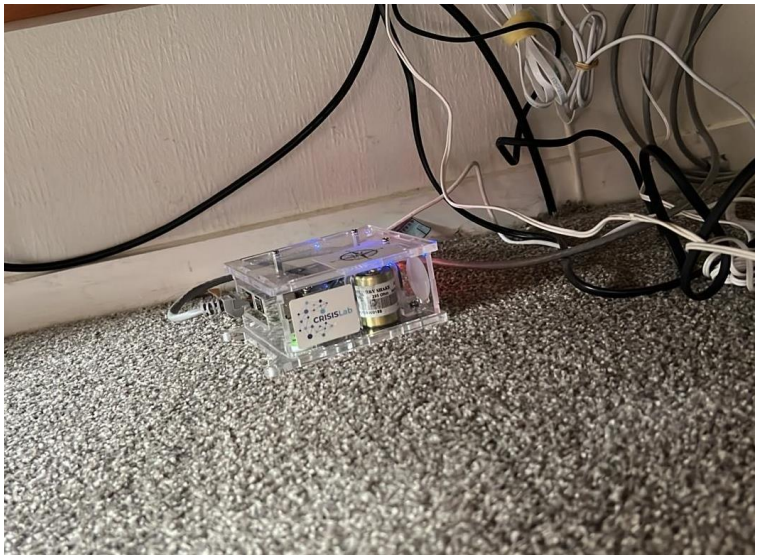

Figure H-9. Sensor installed on wool carpet using an anti-slip sticker and aligned to true north.

Appendix I

Estimation of S-wave Amplitude Leveraging the Initial P-waves

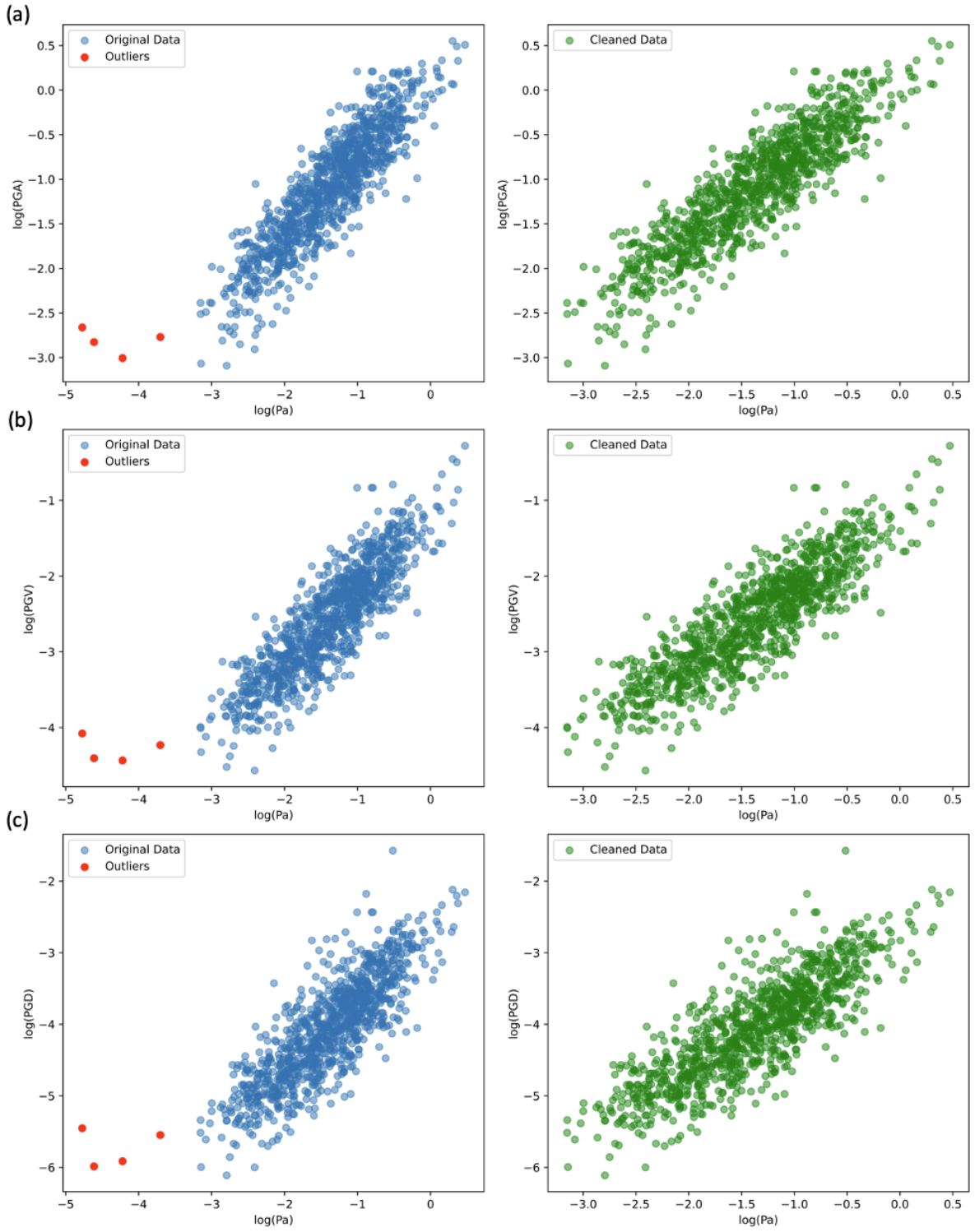

Figure I-1: It shows the original and cleaned training data for relationships using Pa as the input parameter. Panel (a) displays Pa vs. PGA, panel (b) shows Pa vs. PGV, and panel (c) depicts Pa vs. PGD, with each panel comparing original data (left) and data post-outlier removal (right).

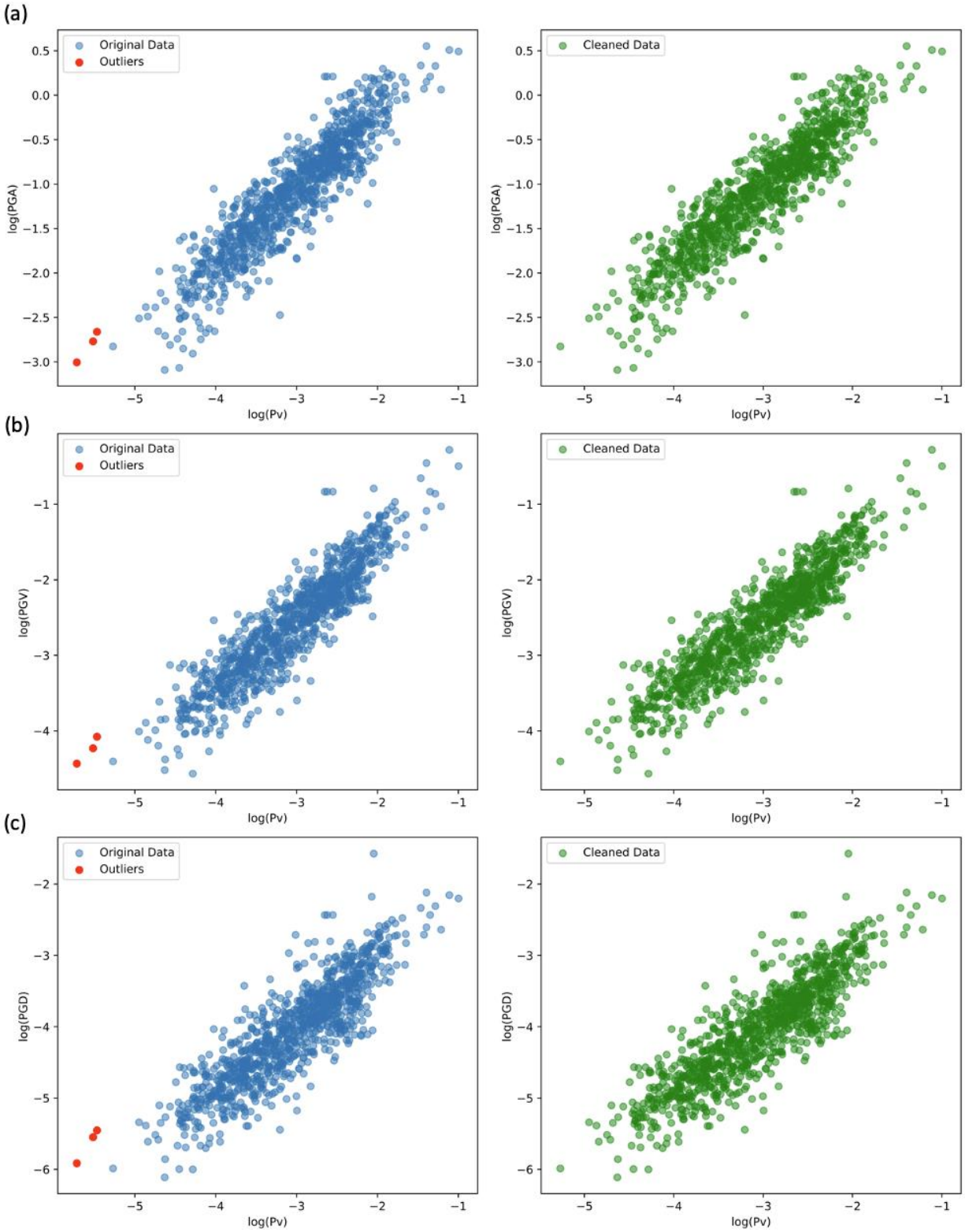

Figure I-2: It shows the original and cleaned training data for relationships using Pv as the input parameter. Panel (a) displays Pv vs. PGA, panel (b) shows Pv vs. PGV, and panel (c) depicts Pv vs. PGD, with each panel comparing original data (left) and data post-outlier removal (right).

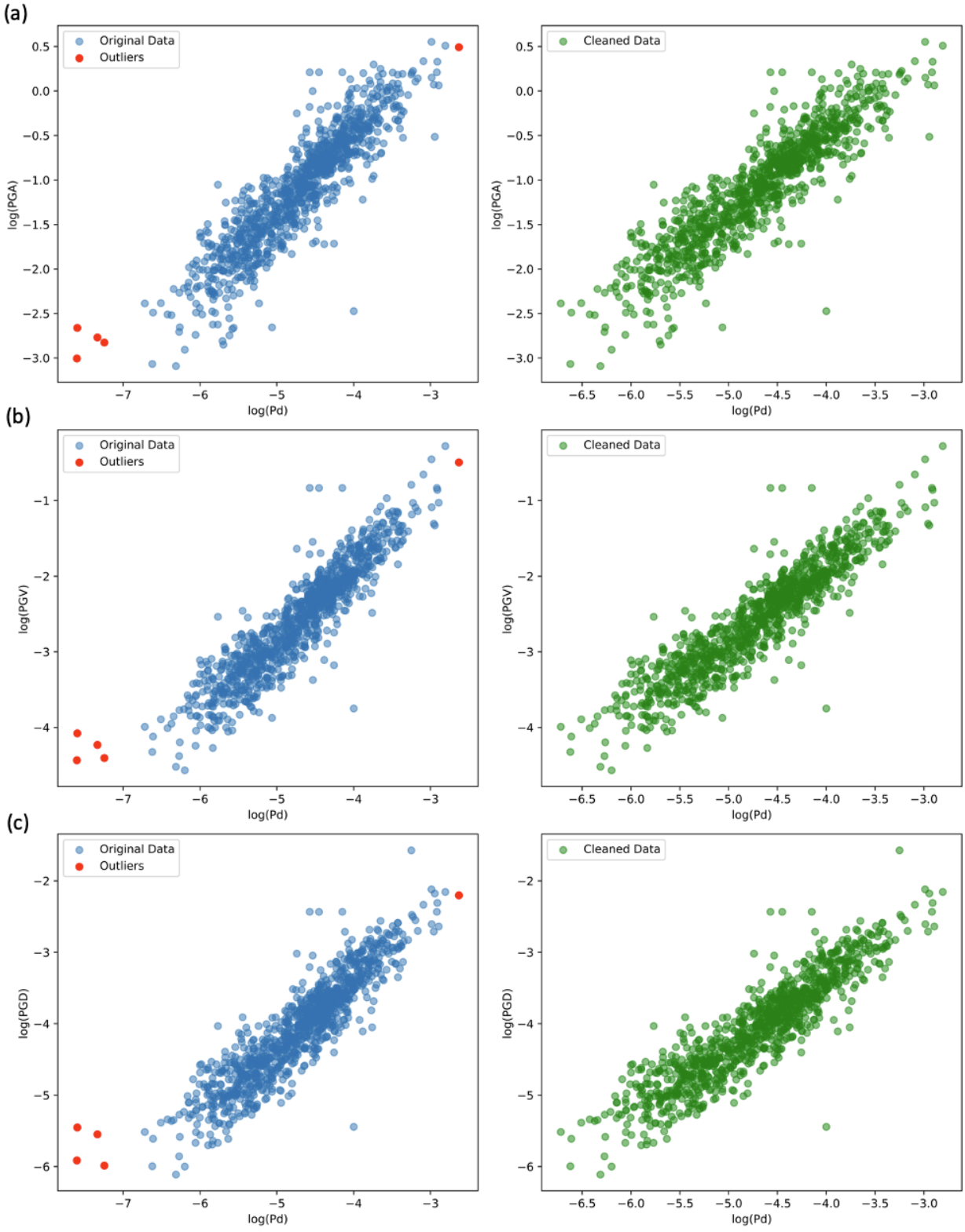

Figure I-3: It shows the original and cleaned training data for relationships using Pd as the input parameter. Panel (a) displays Pd vs. PGA, panel (b) shows Pd vs. PGV, and panel (c) depicts Pd vs. PGD, with each panel comparing original data (left) and data post-outlier removal (right).

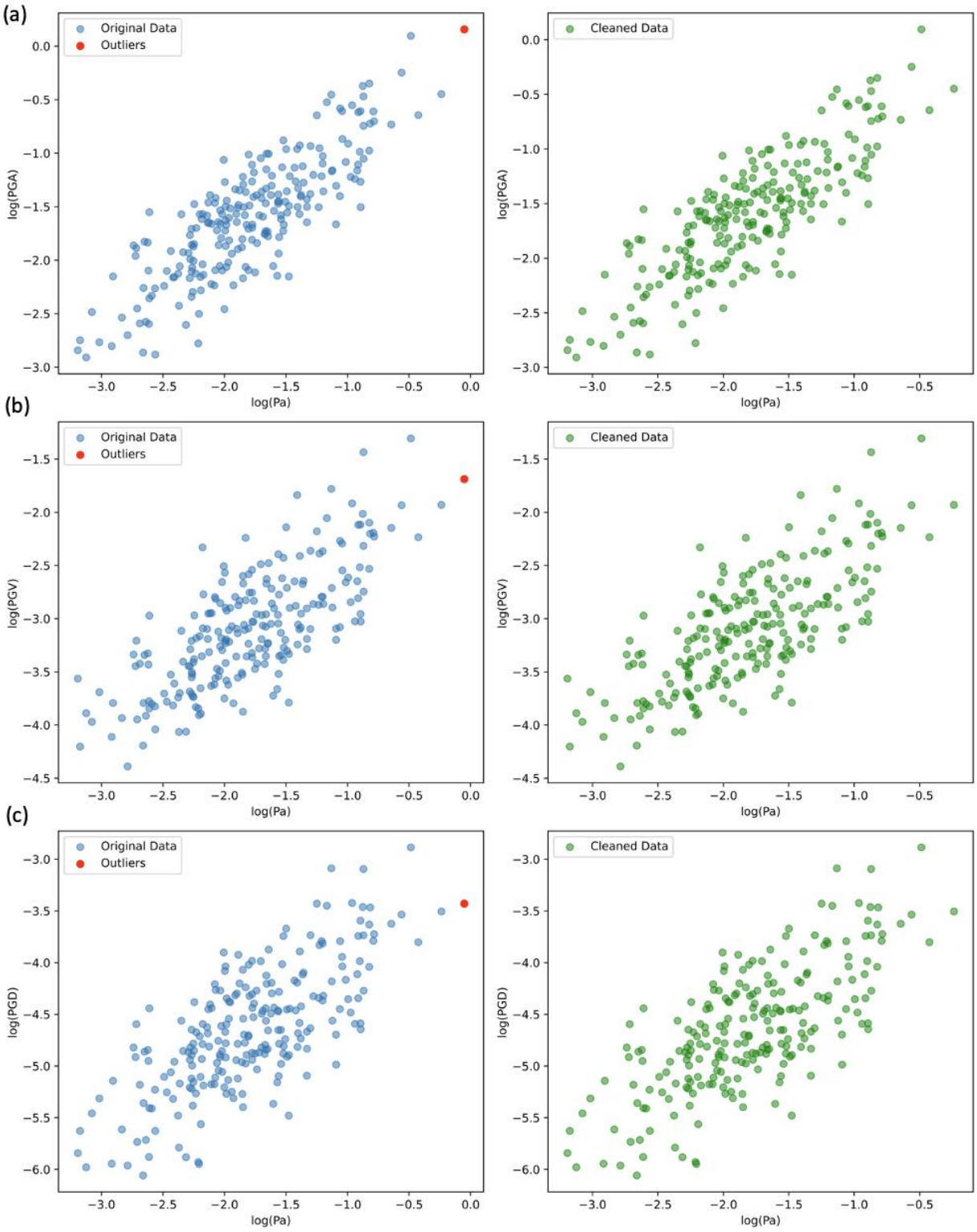

Figure I-4: It shows the original and cleaned testing data for relationships using Pa as the input parameter. Panel (a) displays Pa vs. PGA, panel (b) shows Pa vs. PGV, and panel (c) depicts Pa vs. PGD, with each panel comparing original data (left) and data post-outlier removal (right).

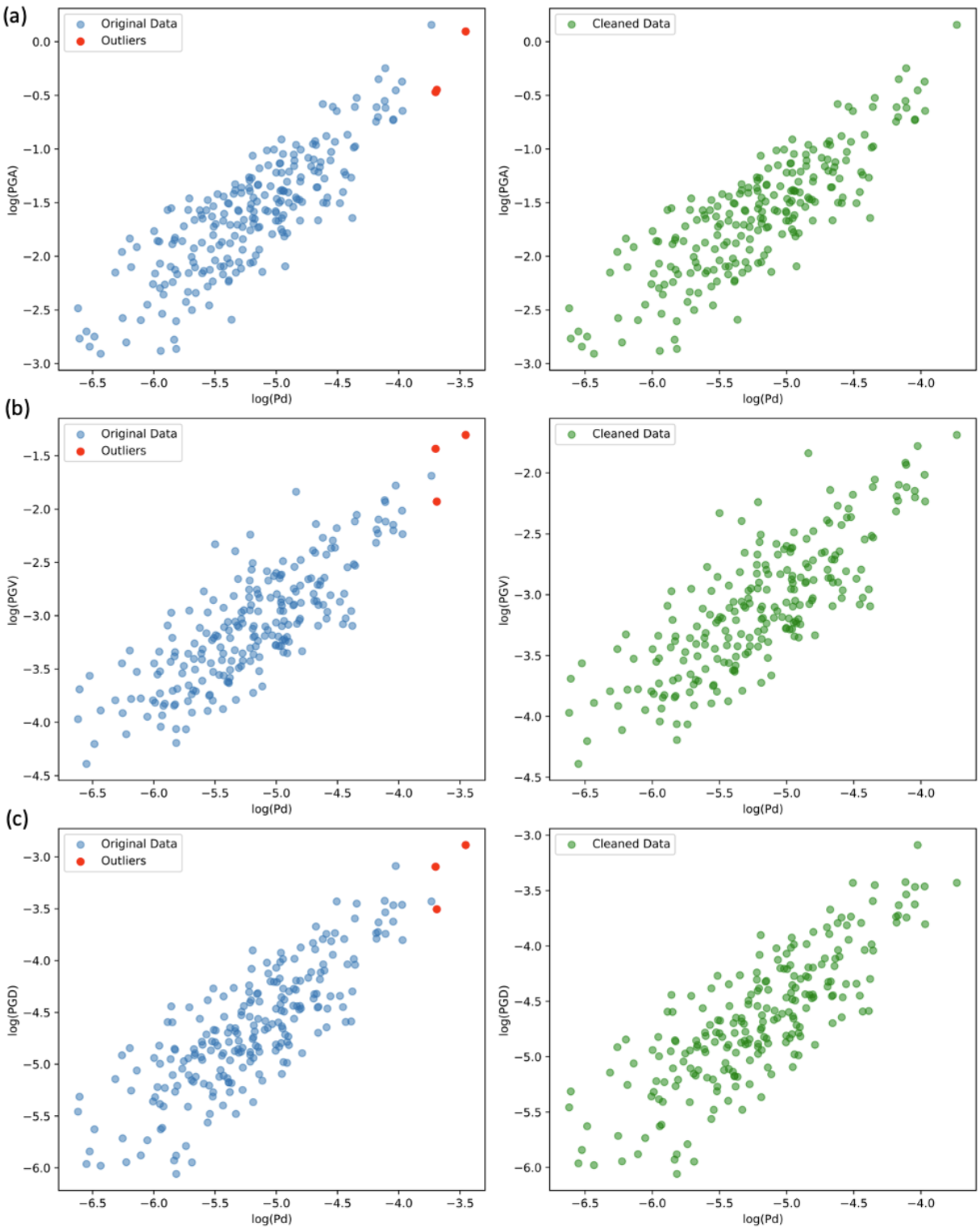

Figure I-5: It shows the original and cleaned testing data for relationships using Pv as the input parameter. Panel (a) displays Pv vs. PGA, panel (b) shows Pv vs. PGV, and panel (c) depicts Pv vs. PGD, with each panel comparing original data (left) and data post-outlier removal (right).

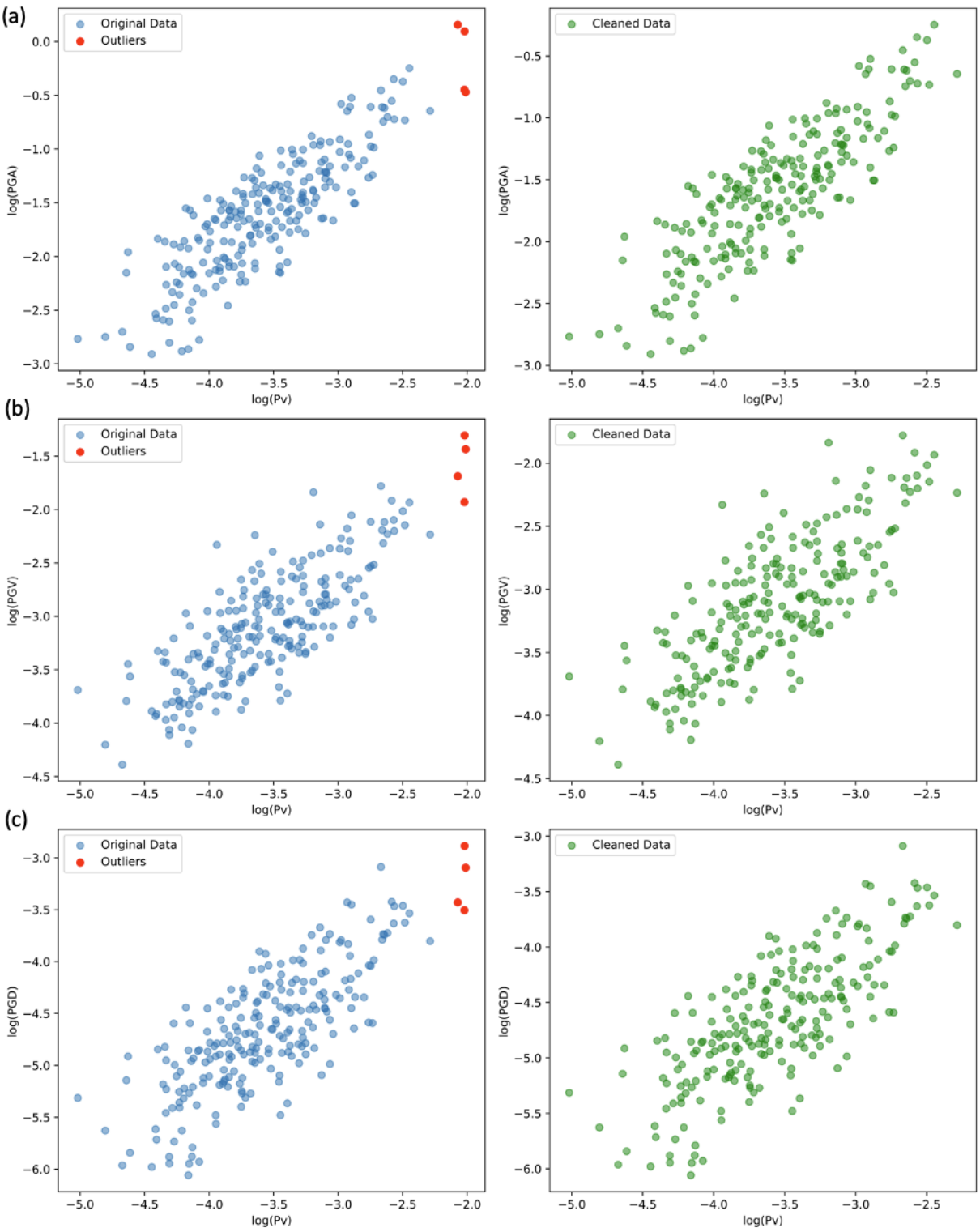

Figure I-6: It shows the original and cleaned testing data for relationships using Pv as the input parameter. Panel (a) displays Pv vs. PGA, panel (b) shows Pv vs. PGV, and panel (c) depicts Pv vs. PGD, with each panel comparing original data (left) and data post-outlier removal (right).

(a)

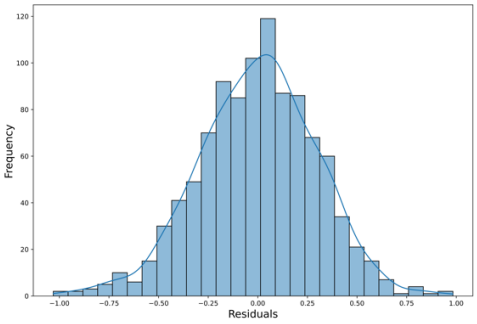
Frequency
Residuals

(b)

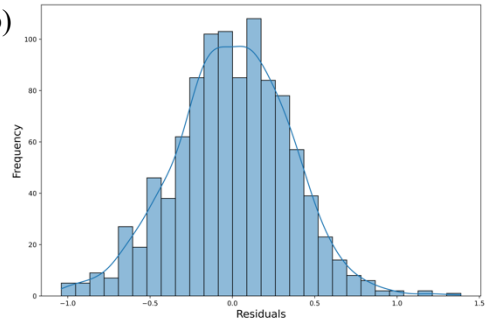
Frequency
Residuals

(c)

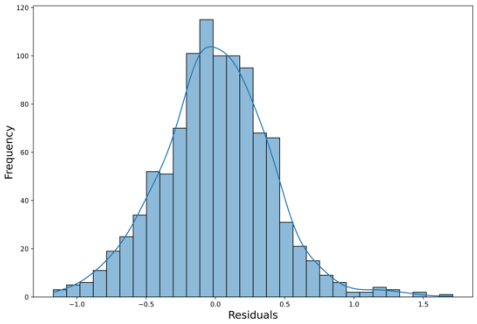
Frequency
Residuals

(d)

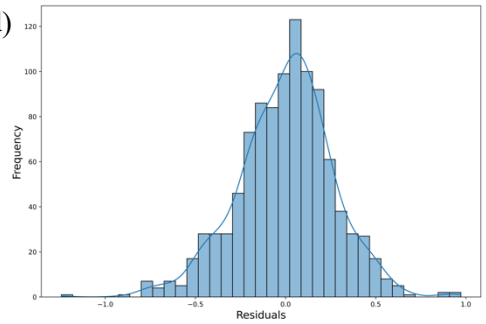
Frequency
Residuals

(e)

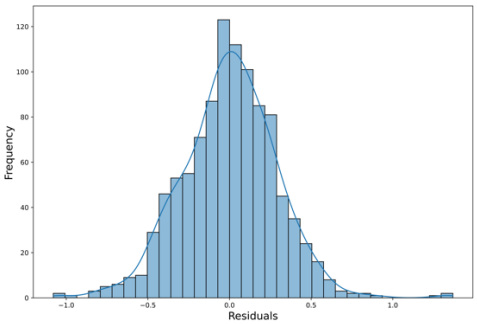
Frequency
Residuals

(f)

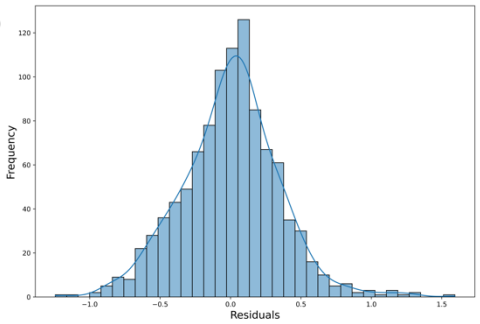
Frequency
Residuals

(g)

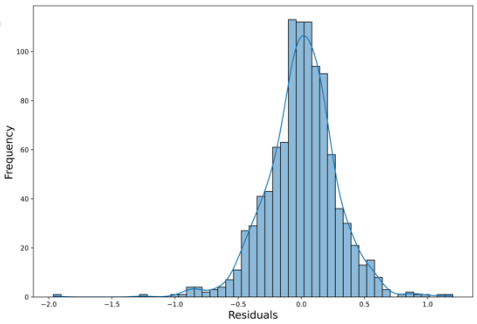
Frequency
Residuals

(h)

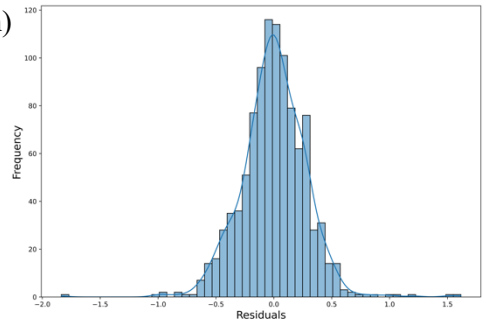
Frequency
Residuals

(i)

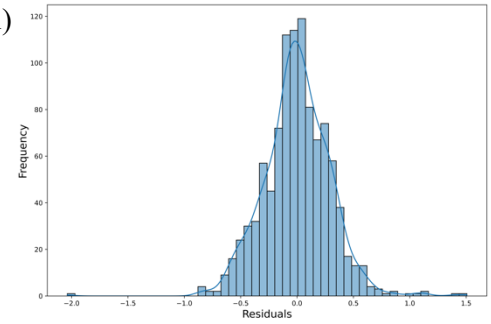

Figure I-7: it shows the histograms that show the frequency distribution of residuals in estimating S-wave amplitudes where plot (a) shows the histogram for Pa vs PGA, (b) Pa vs PGV, (c) Pa vs PGD, (d) Pv vs PGA, (e) Pv vs PGV, (f) Pv vs PGD, (g) Pd vs PGA, (h) Pd vs PGV and (i) Pd vs PGD

Appendix J

Implementation of P-wave-based PLUM EEWS and Evaluation of the EEWS.

Table J-1. List of earthquake events detected by the network from April 1 to July 14, 2024, including geonet event id, origin time, magnitude and number of felt reports. Rows highlighted in yellow are the events recorded having the epicentre in the Wellington & Marlborough region according to GeoNet quake search.

Date	GeoNet event ID	Origin time	Magnitude	Number of felt reports
Apr-26	2024p314478	Fri Apr 26, 2024, 8:34 PM	4.5	2895
Apr-27	2024p317184	Sat Apr 27, 2024, 8:36 PM	4.2	3951
Apr-30	2024p323992	Tue Apr 30, 2024, 9:02 AM	4.2	82
Apr-30	2024p325156	Tue Apr 30, 2024, 7:23 PM	4.8	12964
May-17	2024p371291	Fri May 17, 2024, 9:04 PM	3.8	3706
May-23	2024p385316	Thu May 23, 2024, 1:36 AM	3.9	3350
May-29	2024p403633	Wed May 29, 2024, 8:15 PM	3.6	0
Jun-03	2024p417352	Mon Jun 3, 2024, 10:05 PM	4.1	16690
Jun-06	2024p423234	Thu Jun 6, 2024, 2:19 AM	5.1	2231
Jun-11	2024p437264	Tue Jun 11, 2024, 6:54 AM	3.8	56
Jul-07	2024p504198	Sat Jul 6, 2024, 1:17 AM	4	2128
Jul-07	2024p507659	Sun Jul 7, 2024, 8:01 AM	4	8

(a)

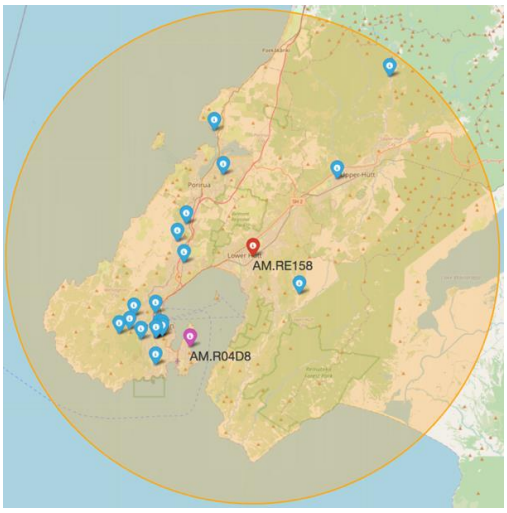

(b)

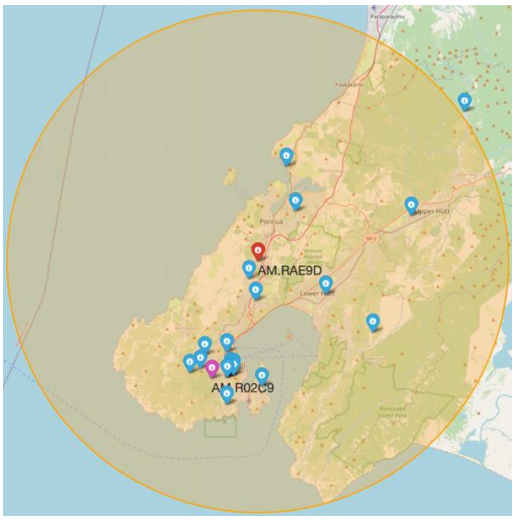

(b)

(d)

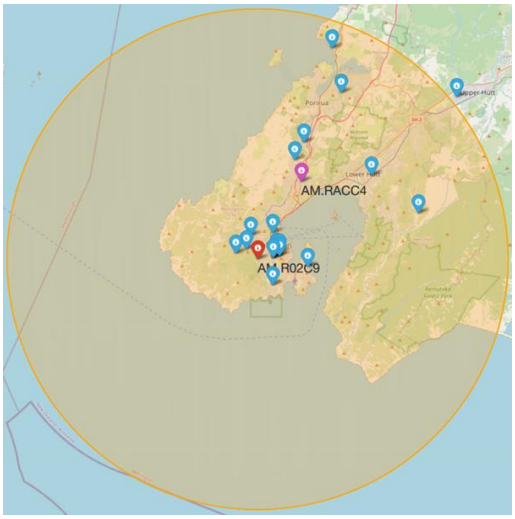

(c)

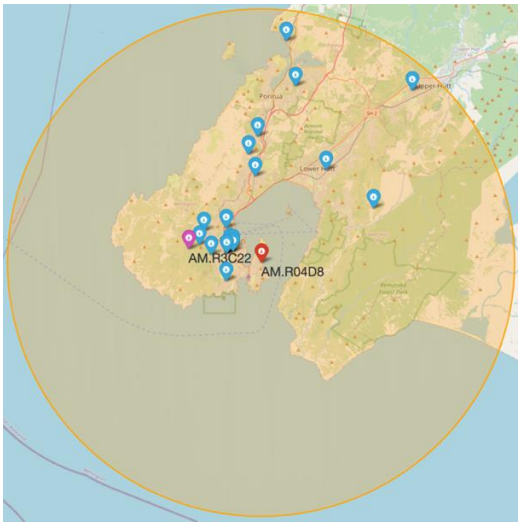

Figure J-1. Selected prediction points (red), Primary stations (purple), and Secondary stations (blue) within a 30 km prediction radius for the PLUM-based EEWS in the Greater Wellington region.

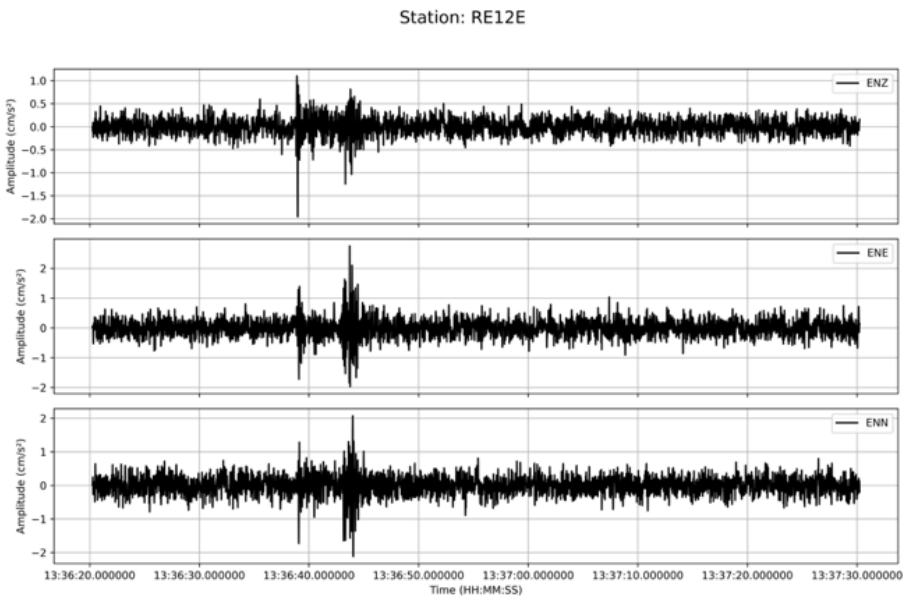

Figure J-2: Ground motion data captured by the station AM.RE12E in three dimensions.

Appendix K

Supplementary File on Case Studies

1. Case Study 1: Earthquake on May 23, 2024

1.1. NZ-PLUM algorithm

The table summarises (Table K-1) the first two stations exceeding the alerting threshold MMI 3.0 within a 30 km radius for each prediction point. It also includes the detection delay between the first two detection stations, alert generated time at the Primary station, alert received time at the prediction point, and system latency for the entire alert generation process.

Table K-1. The detection times and system latency for each prediction point, including alert generation and detection delays.

Prediction point	**Time 1st Station Exceeds Threshold**	**Time 2nd Station Exceeds Threshold**	**Detection Delay**	**Alert Generated time**	**Alert received time**	**System Latency**
P1	01:36:39.564	01:36:41.51	1.946	01:36:41.811	01:36:42.188	2.624
P2	01:36:39.564	01:36:41.51	1.946	01:36:41.8	01:36:42.241	2.677
P3	01:36:39.564	01:36:43.991	4.427	01:36:44.41	01:36:44.8	5.236
P4	01:36:39.564	01:36:43.991	4.427	01:36:44.415	01:36:44.8	5.236
P5	01:36:39.564	01:36:41.51	1.946	01:36:41.783	01:36:42.061	2.497

Figure K-1-a, K-1-b and K-1-c display three dimensional waveforms from the stations that first detected the shaking. The red vertical line indicates that the time T_H is exceeded in the horizontal acceleration data.

(a)

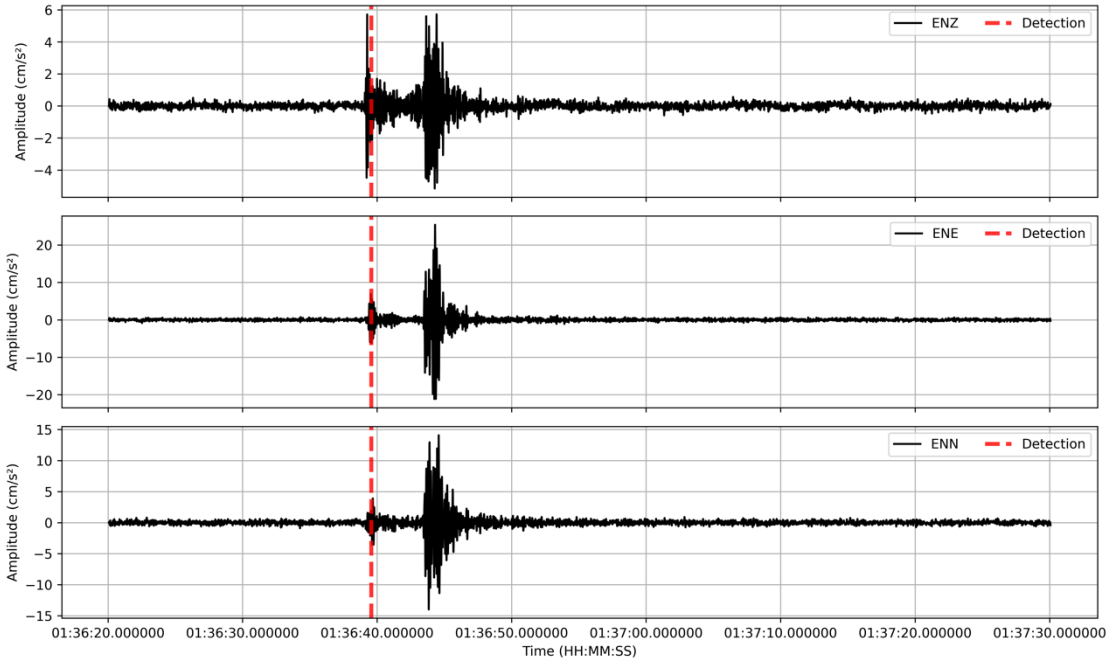
ENZ
Detection
Amplitude (cm/s²)
ENE
Detection
Amplitude (cm/s²)
ENN
Detection
Amplitude (cm/s²)
01:36:20.000000
01:36:30.000000
01:36:40.000000
01:36:50.000000
01:37:00.000000
01:37:10.000000
01:37:20.000000
01:37:30.000000
Time (HH:MM:SS)

(b)

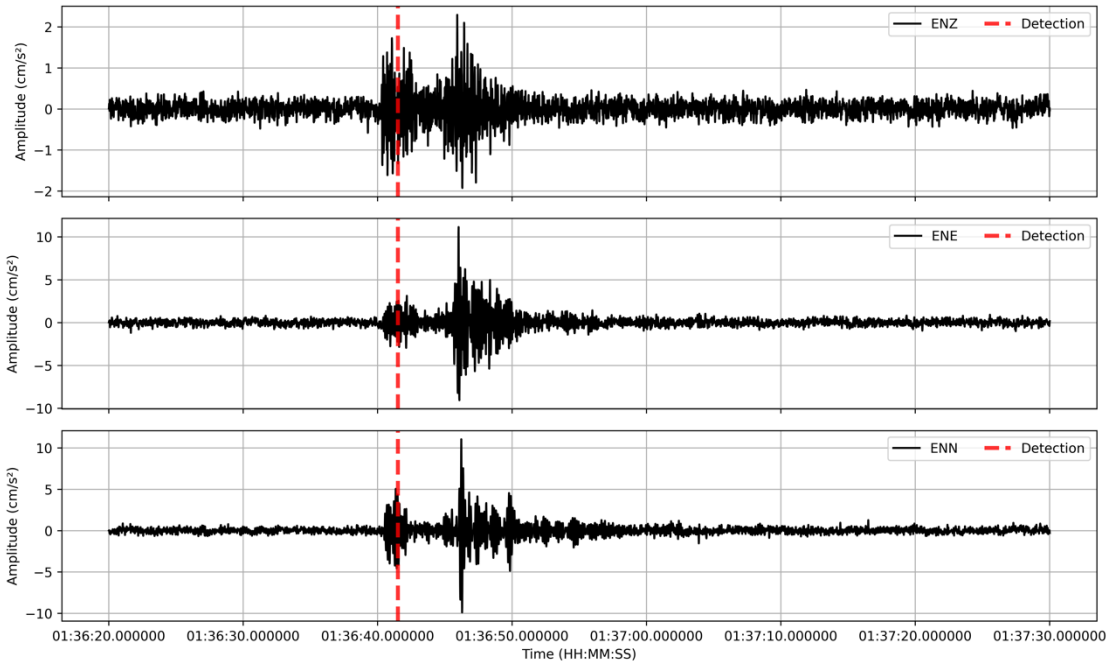
ENZ
Detection
Amplitude (cm/s²)
ENE
Detection
Amplitude (cm/s²)
ENN
Detection
Amplitude (cm/s²)
01:36:20.000000
01:36:30.000000
01:36:40.000000
01:36:50.000000
01:37:00.000000
01:37:10.000000
01:37:20.000000
01:37:30.000000
Time (HH:MM:SS)

(c)

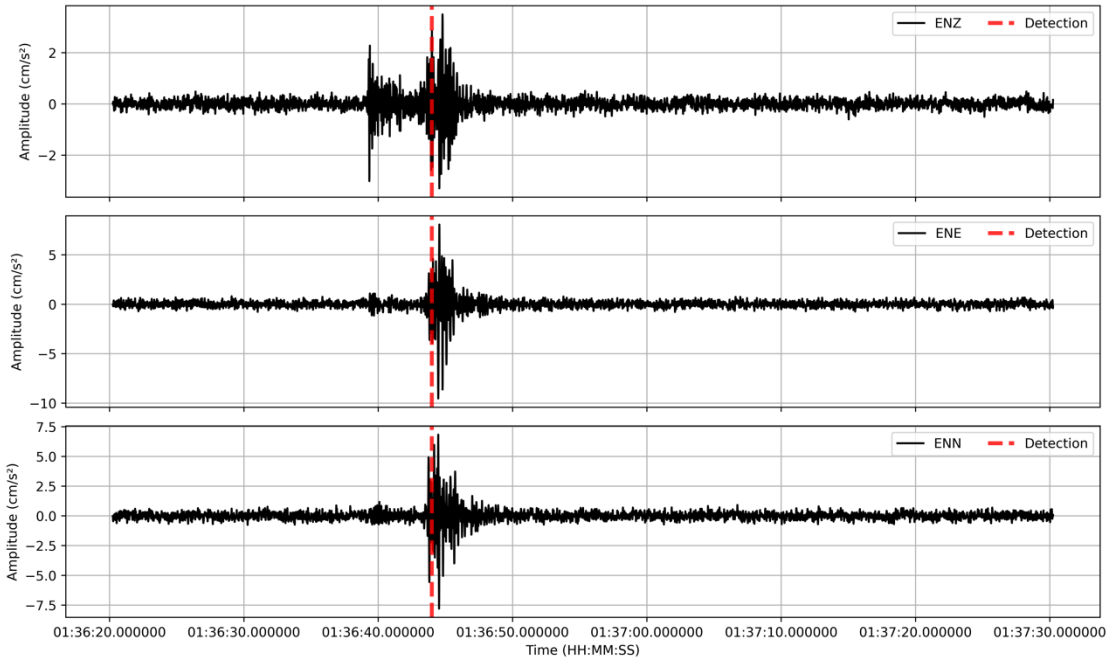

Figure K-1. Waveforms captured by the stations that detected the shaking first. The red vertical line indicates the time alerting threshold exceeded four cms^{-2} in the horizontal acceleration data. (a) Station AM.R9C56, (b) Station AM.RFE44, (c) Station AM.RAE9D.

The table K-2 summarises the achieved warning times for each prediction point. It includes the alert logged time, theoretical S-wave arrival time, and felt shaking time (if applicable).

Table K-2. Summary of warning times for each prediction point. The table includes the time the alert is logged, the theoretical S-wave arrival time, the felt shaking time, and the calculated warning time.

Prediction point	**Time Alert Logged**	**Felt shaking time (S-PGA)**	**Theoretical S-wave arrival time (S-Pick)**	**Warning time (Seconds)**
P1	01:36:42.188	-	01:36:44.000	1.812
P2	01:36:42.241	01:36:43.991	01:36:43.671	1.430
P3	01:36:44.8	01:36:47.800	01:36:45.660	0.860
P4	01:36:44.8	-	01:36:46.100	1.30
P5	01:36:42.061	-	01:36:45.961	3.9

Figure K-2 shows the ground motion data from the prediction points, with vertical lines indicating the alert logged time (red), actual S-wave arrival time (blue), and felt shaking time (green).

(a) Station: RE158

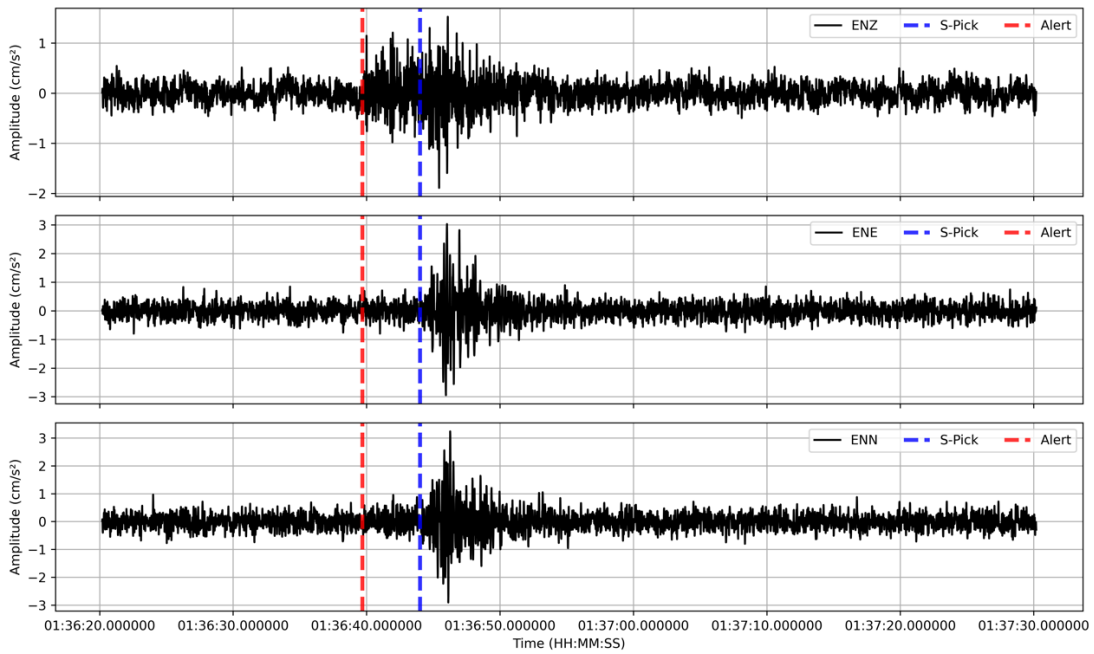

(b) Station: RAE9D

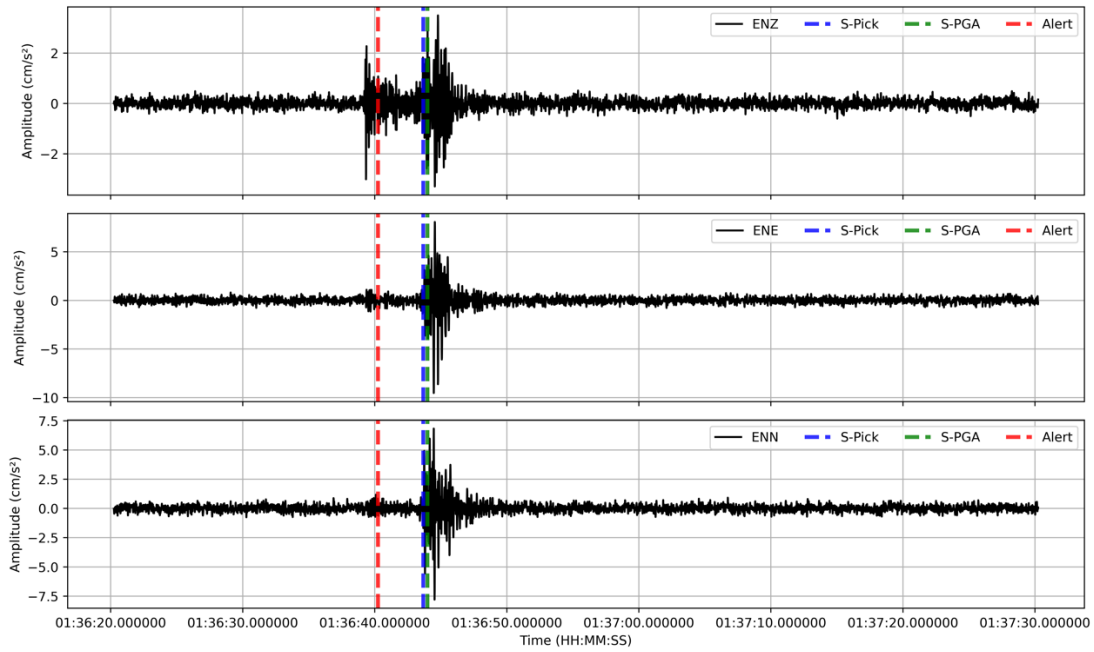

(c) Station: R9288

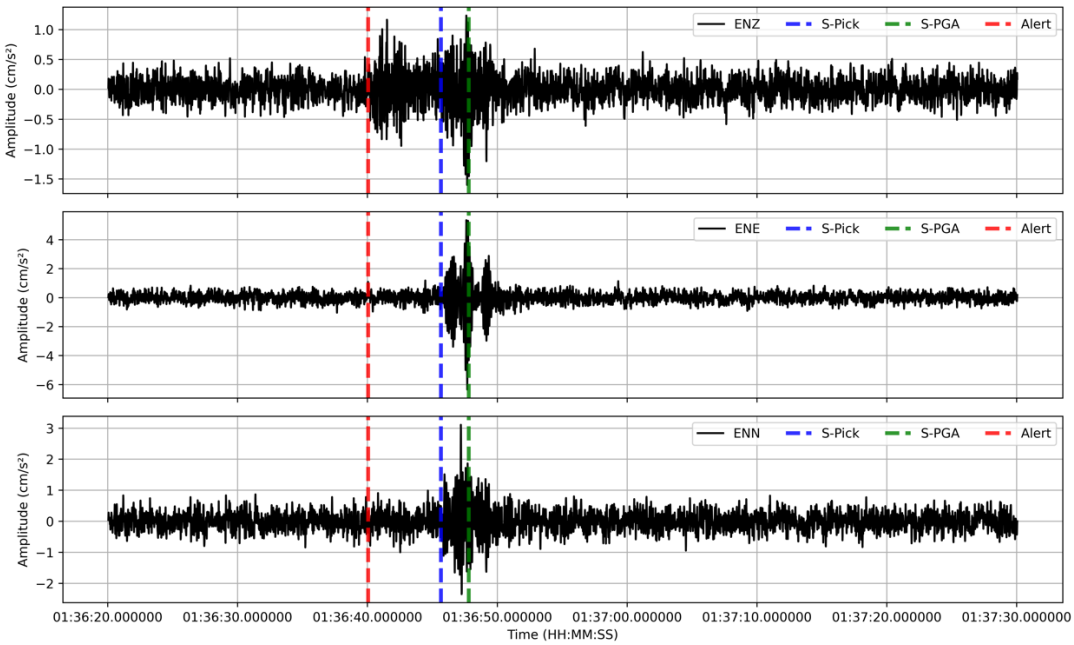

(d) Station: R02C9

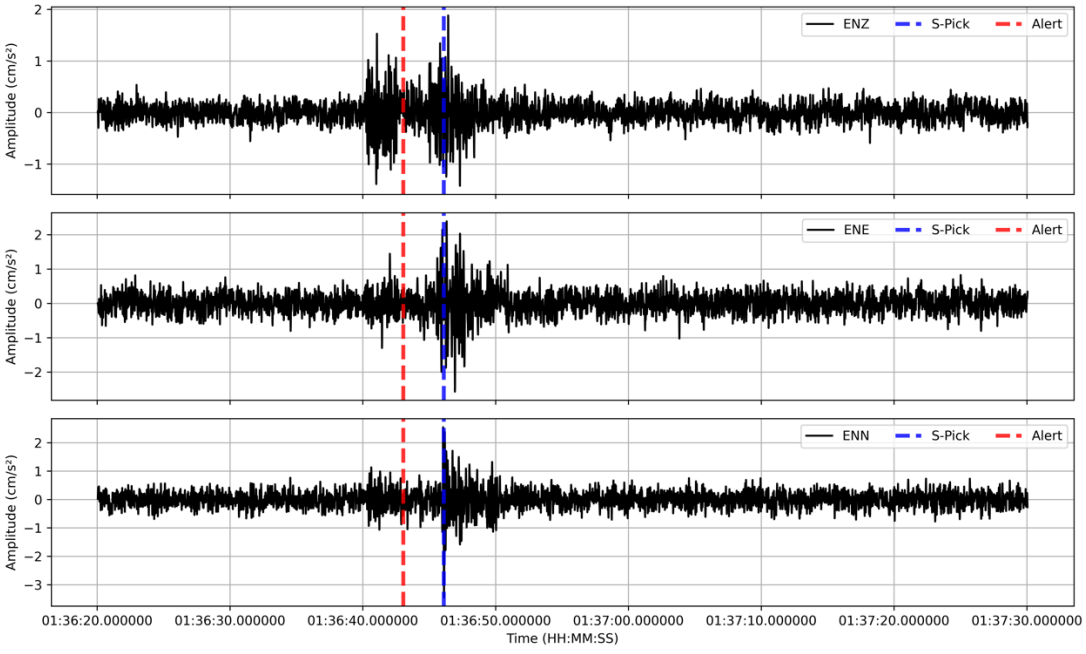

(e)

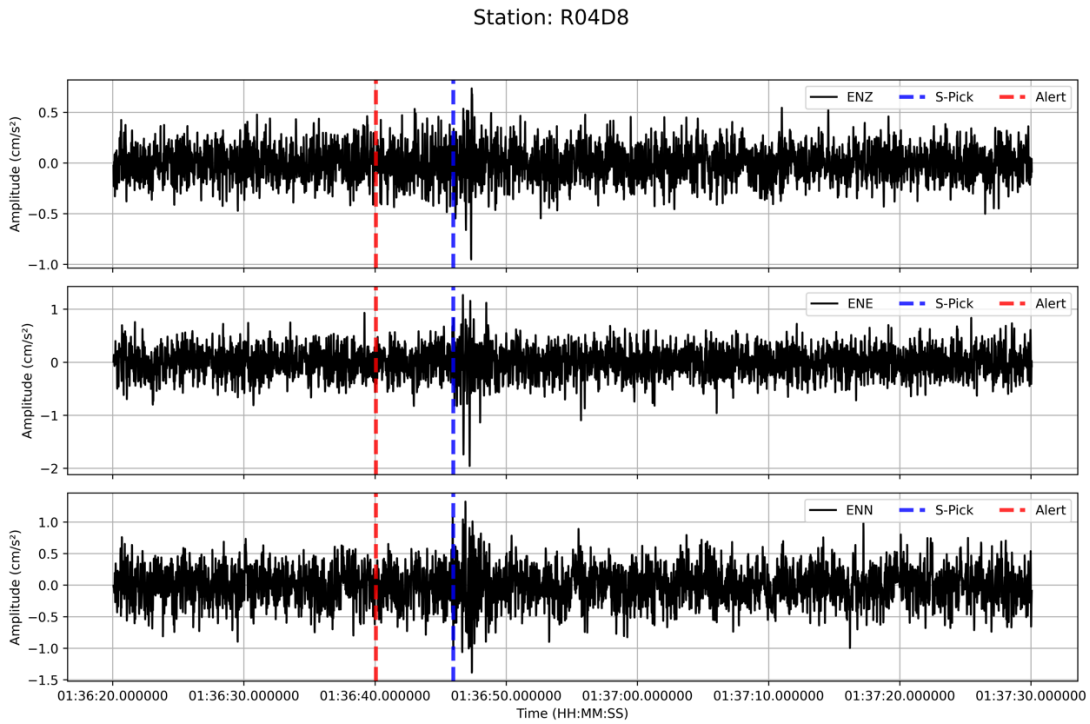

Figure K-2. Ground motion data from the prediction points, with vertical lines indicating the alert logged time (red), actual S-wave arrival time (blue), and felt shaking time (green). (a) P1, (b) P2, (c) P3, (d) P4, and (e) P5.

1.2. NZ-PLUM-P algorithm

The figures and tables follow the same order as the NZ-PLUM algorithm.

The table below (Table K-3) summarises the detection times, alert receipt times at each prediction point, and the overall system latency for generating alerts.

Table K-3. The detection times and system latency for each prediction point, including alert generation and detection delays.

Prediction point	**Time 1st Station Exceeds Threshold**	**Time 2nd Station Exceeds Threshold**	**Detection Delay**	**Alert Generated time**	**Alert received time**	**System Latency**
P1	01:36:38.913	01:36:39.174	0.321	01:36:39.811	01:36:40.188	1.275
P2	01:36:38.913	01:36:39.174	0.321	01:36:39.8	01:36:40.241	1.328
P3	01:36:38.913	01:36:39.174	0.321	01:36:39.66	01:36:40.050	1.137
P4	01:36:38.913	01:36:39.174	0.321	01:36:39.665	01:36:40.050	1.137
P5	01:36:38.913	01:36:39.314	0.321	01:36:39.783	01:36:40.061	1.148

Figure **K-**3-a and K-3-b display the waveforms from the stations that first detected shaking.

(a)

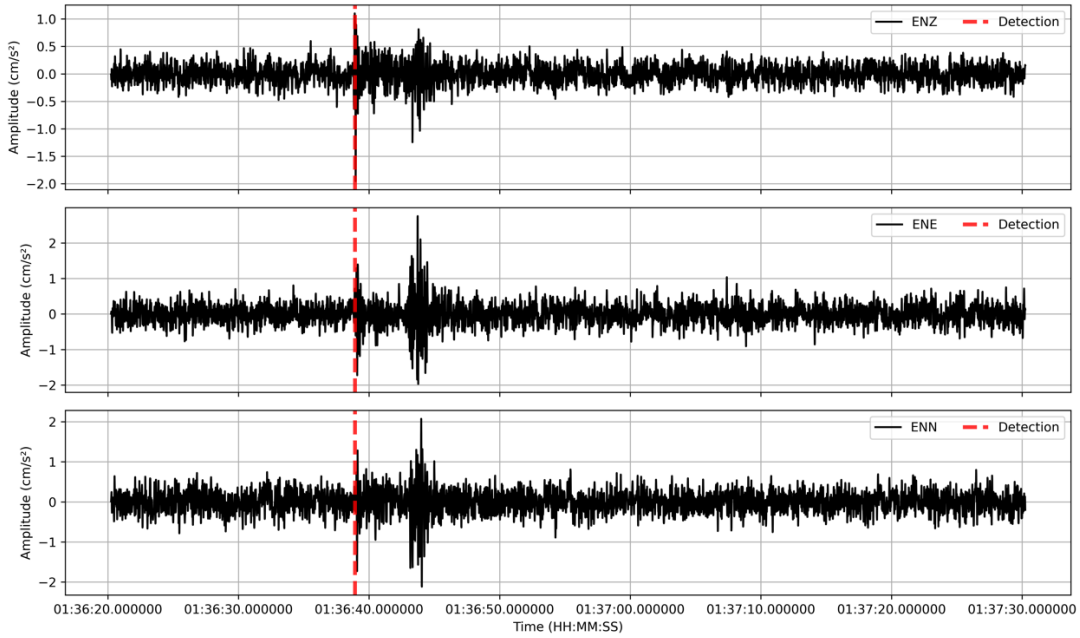

(b)

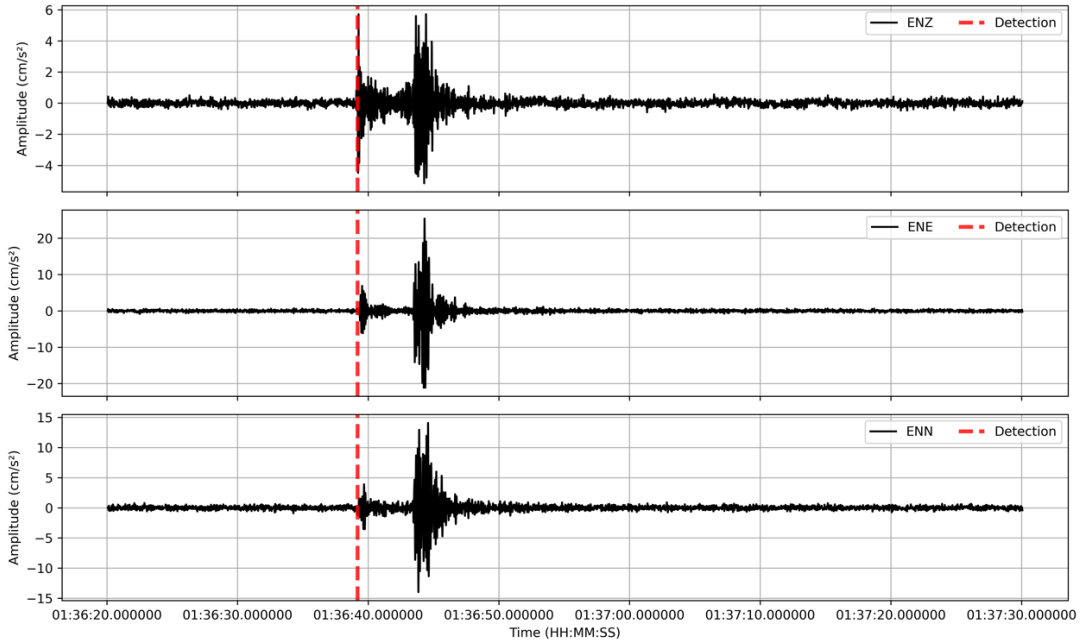

Figure K-3. Waveforms from the stations that first detected shaking where the red vertical line indicates the P-wave detection time for each station. (a) Station AM.RE12E, (b) Station AM.R9C56..

The following table (Table K-4) summarises the warning times for each prediction point using the NZ-PLUM-P approach, highlighting the increase in warning time compared to NZ-PLUM.

Table k-4. Comparison of Warning Times Using the NZ-PLUM-P Approach and the NZ-PLUM Approach

Prediction point	**Time Alert Logged**	**Felt shaking time (S-PGA)**	**Theoretical S-wave arrival time (S-Pick)**	**Warning time (Seconds)**	**Increase in Warning time compared to NZ-PLUM**
P1	01:36:39.688	-	01:36:44.000	4.312	2.5
P2	01:36:40.241	01:36:43.991	01:36:43.671	3.430	2
P3	01:36:40.050	01:36:47.800	01:36:45.660	5.61	4.75
P4	01:36:43.050	-	01:36:46.100	3.050	1.75
P5	01:36:40.061	-	01:36:45.961	5.900	2.0

The following figures (Figure K-4) show the ground motion data from the prediction points, with vertical lines indicating the alert logged time (red), actual S-wave arrival time (blue), and felt shaking time (green).

(a)

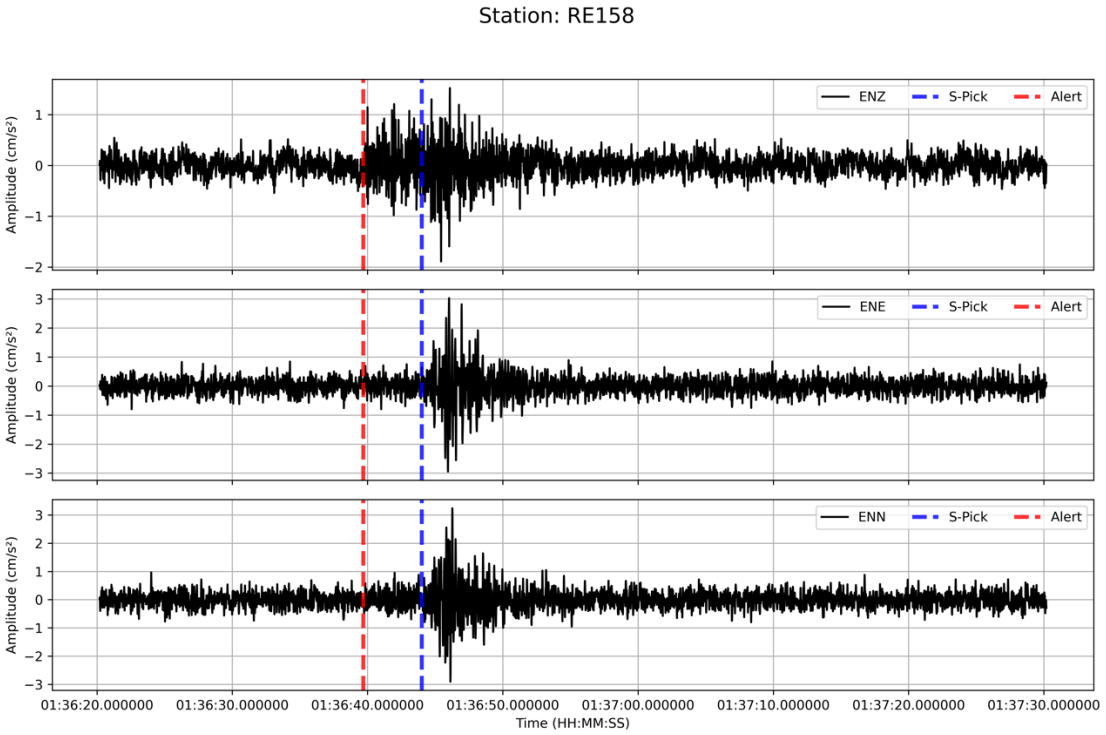
Station: RE158
ENZ
S-Pick
Alert
ENE
S-Pick
Alert
ENN
S-Pick
Alert
Amplitude (cm/s²)
01:36:20.000000
01:36:30.000000
01:36:40.000000
01:36:50.000000
01:37:00.000000
01:37:10.000000
01:37:20.000000
01:37:30.000000
Time (HH:MM:SS)

(b)

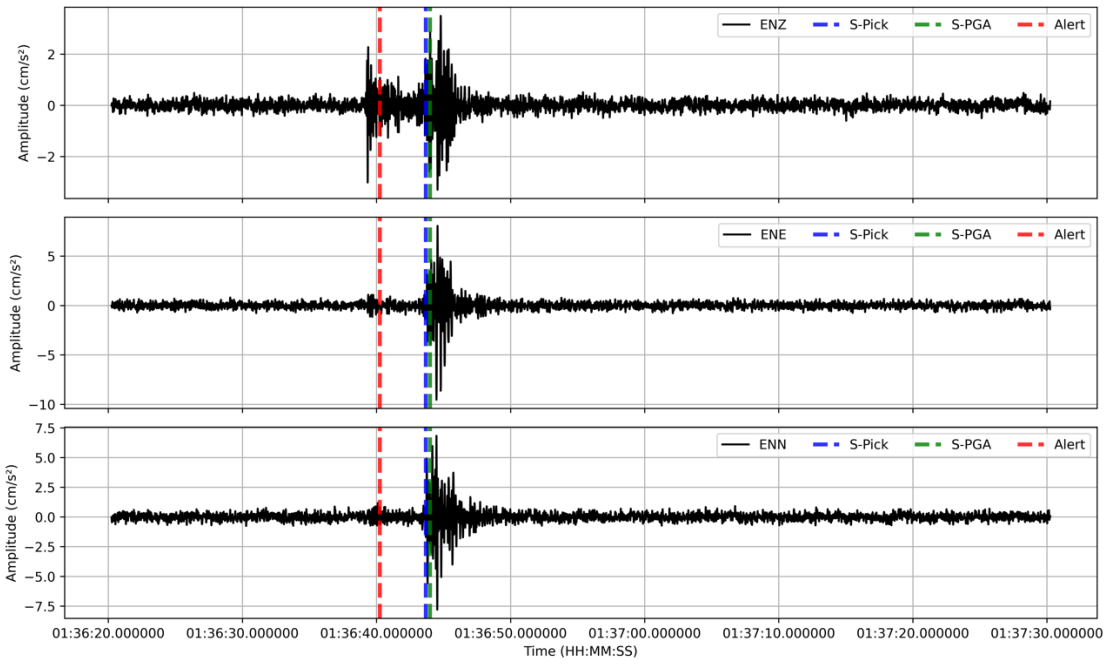
Station: RAE9D
ENZ
S-Pick
S-PGA
Alert
ENE
S-Pick
S-PGA
Alert
ENN
S-Pick
S-PGA
Alert
Amplitude (cm/s²)
01:36:20.000000
01:36:30.000000
01:36:40.000000
01:36:50.000000
01:37:00.000000
01:37:10.000000
01:37:20.000000
01:37:30.000000
Time (HH:MM:SS)

(c) Station: R9288

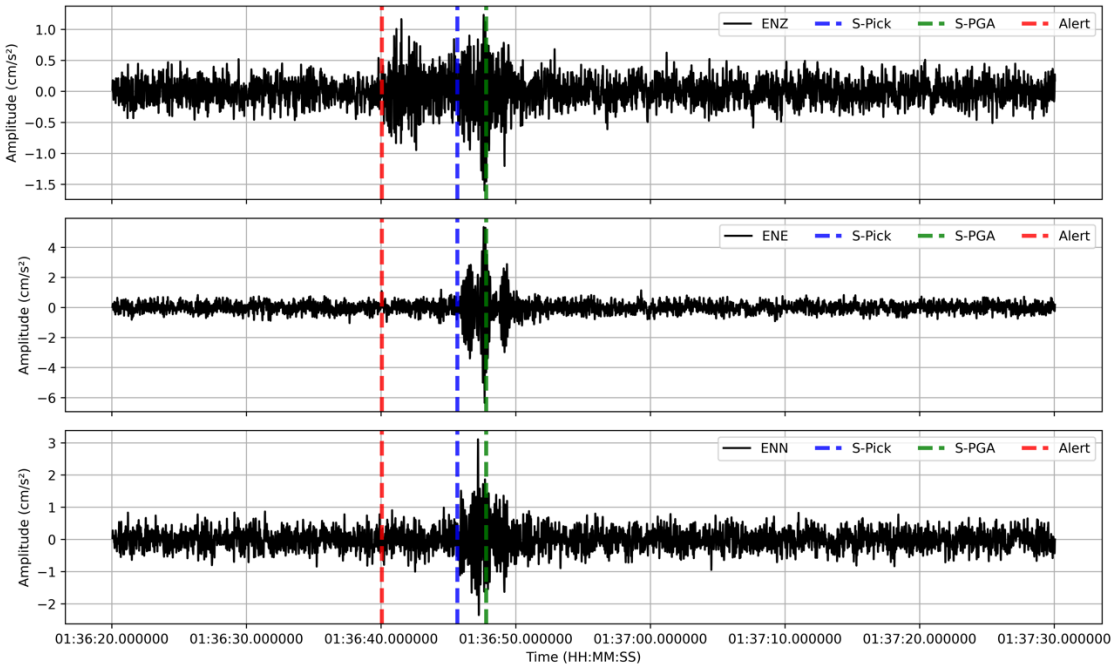

(d) Station: R02C9

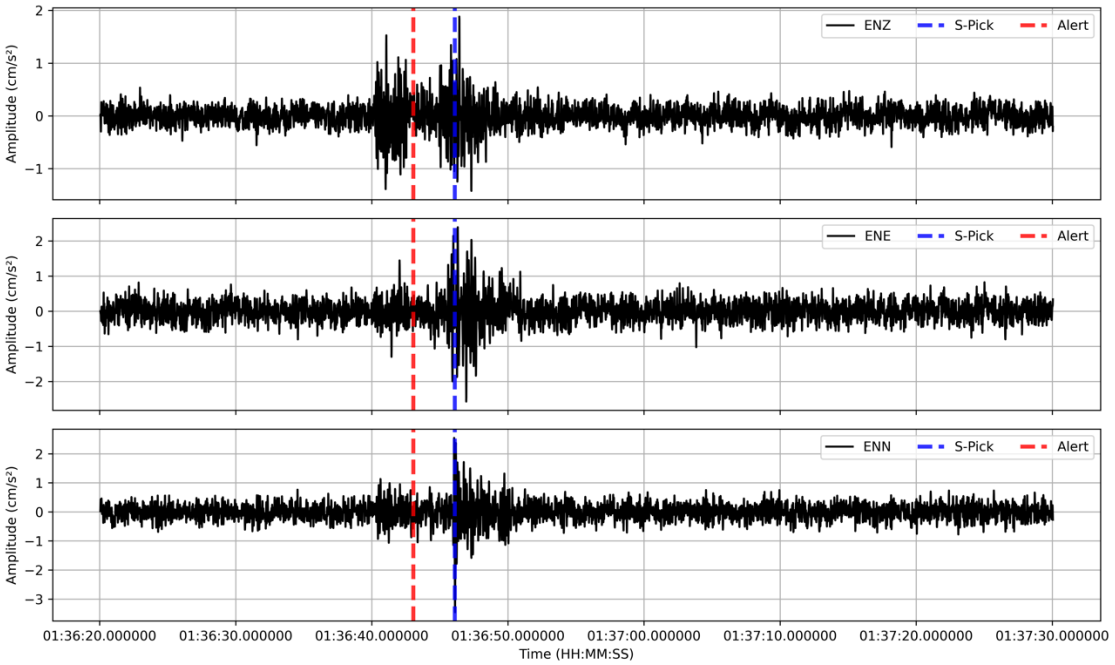

(e)

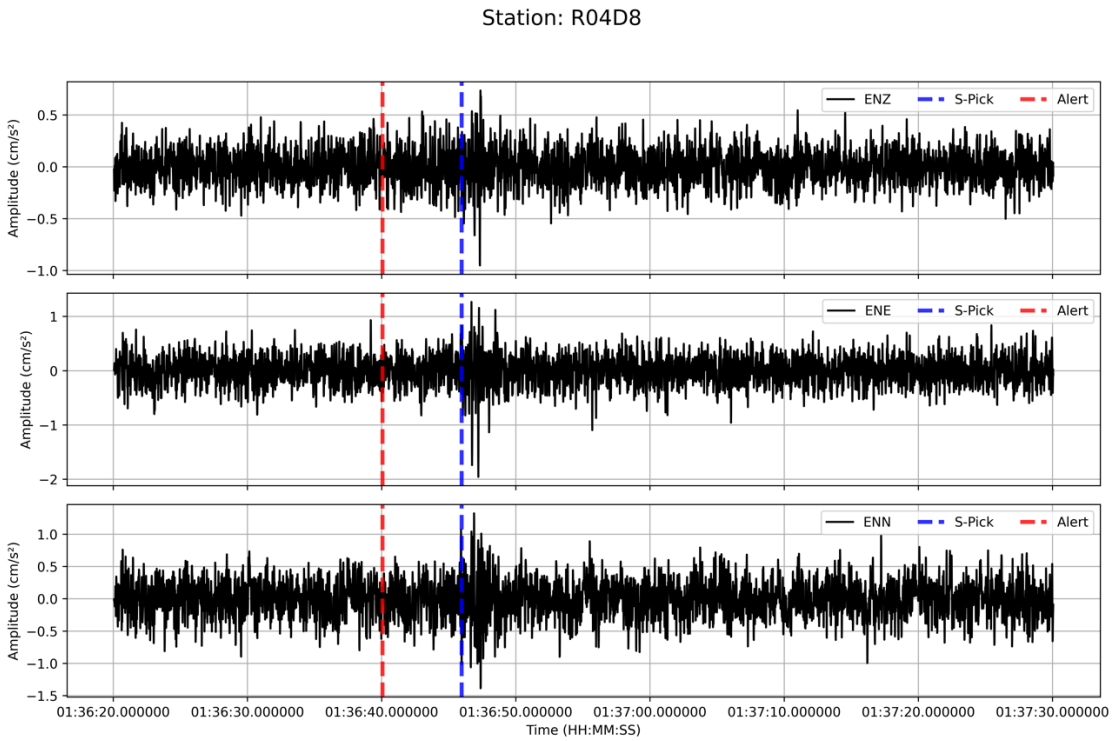

Figure K-4. Ground motion data from the prediction points, with vertical lines indicating the alert logged time (red), actual S-wave arrival time (blue), and felt shaking time (green). (a) P1, (b) P2, (c) P3, (d) P4, and (e) P5.

2. Case Study 2: Earthquake on June 3, 2024

2.1. NZ-PLUM algorithm

The table below (Table K-5) summarises the detection times, alert generation times, and system latency for each prediction point.

Table K-5. The detection times and system latency for each prediction point, including alert generation and detection delays.

Prediction point	Time 1st Station Exceeds Threshold	Time 2nd Station Exceeds Threshold	Detection Delay	Alert Generated time	Alert received time	System Latency
P1	22:05:58.814	22:05:59.899	1.085	22:06:00.164	22:06:00.608	1.794
P2	22:05:58.814	22:05:59.899	1.085	22:06:00.22	22:06:00.521	1.707
P3	22:05:58.814	22:05:59.899	1.085	22:06:00.27	22:06:00.7	1.886
P4	22:05:58.814	22:05:59.899	1.085	22:06:00.175	22:06:00.47	1.656
P5	22:05:58.814	22:05:59.899	1.085	22:06:00.244	22:06:00.664	1.850

The following figures show the timestamps during the detection of shaking by the first two stations, indicated by a vertical red line, along with their obtained data (Figure K-5).

(a)

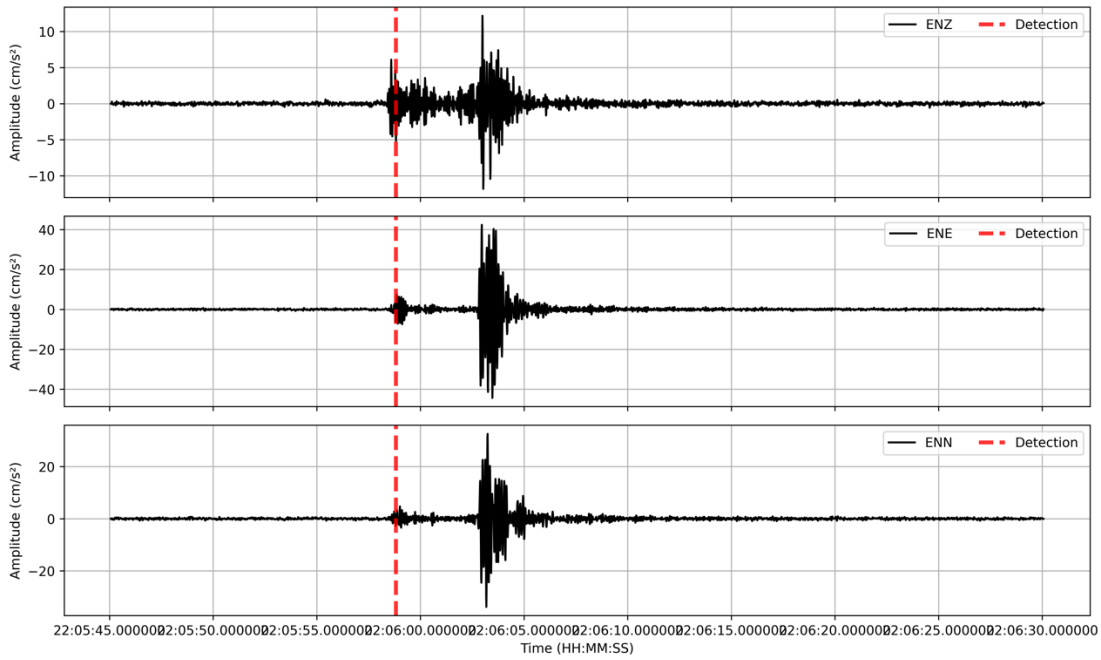

(b)

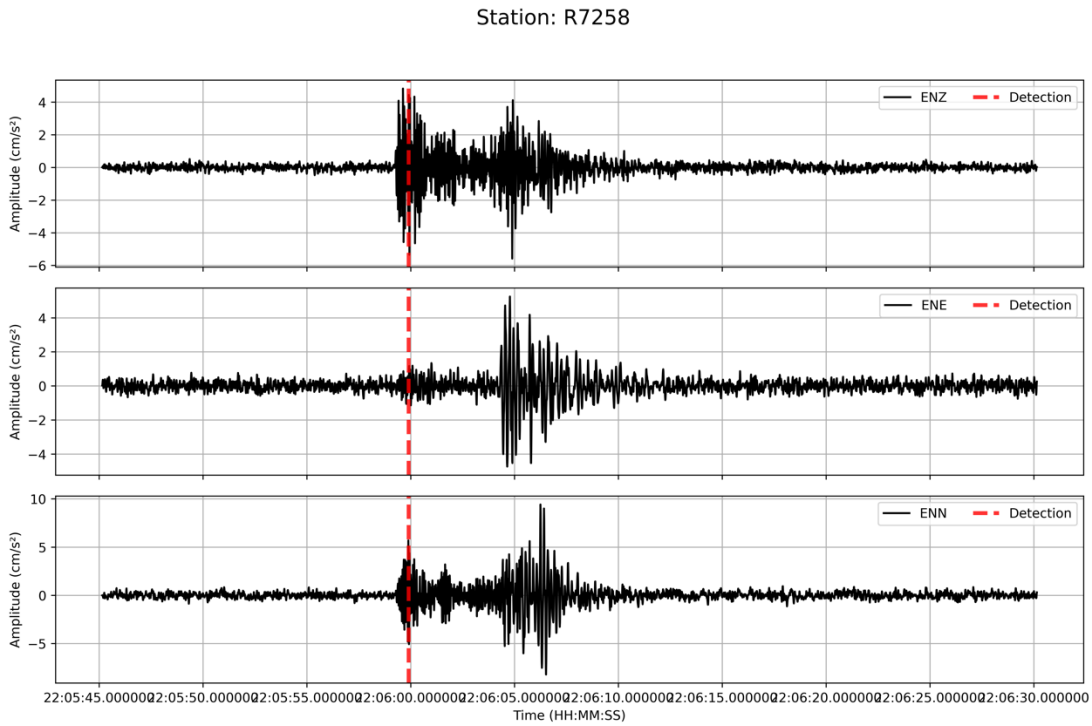

Figure K-5. Waveforms captured by the stations that detected the shaking first. The red vertical line indicates the time alerting threshold exceeded four cms^{-2} in the horizontal acceleration data. (a) Station AM.R9C56, (b) Station AM.R7258.

The following table (Table K-6) summarises the warning times achieved for each prediction point with the NZ-PLUM approach.

Table K-6. Summary of warning times for each prediction point. The table includes the time the alert is logged, the theoretical S-wave arrival time, the felt shaking time, and the calculated warning time.

Prediction point	Time Alert Logged	Felt shaking time (S-PGA)	Theoretical S-wave arrival time (S-Pick)	Warning time (Seconds)
P1	22:06:00.608	22:06:04.608	22:06:03.988	3.380
P2	22:06:00.521	22:06:03.271	22:06:02.971	2.45
P3	22:06:00.7	22:06:06.950	22:06:05.190	4.49
P4	22:06:00.47	-	22:06:04.890	4.42
P5	22:06:00.664	-	22:06:05.134	4.47

The following figures (Figure K-6) show the ground motion data from the prediction points, with vertical lines indicating the alert logged time (red), actual S-wave arrival time (blue), and felt shaking time (green).

(a)

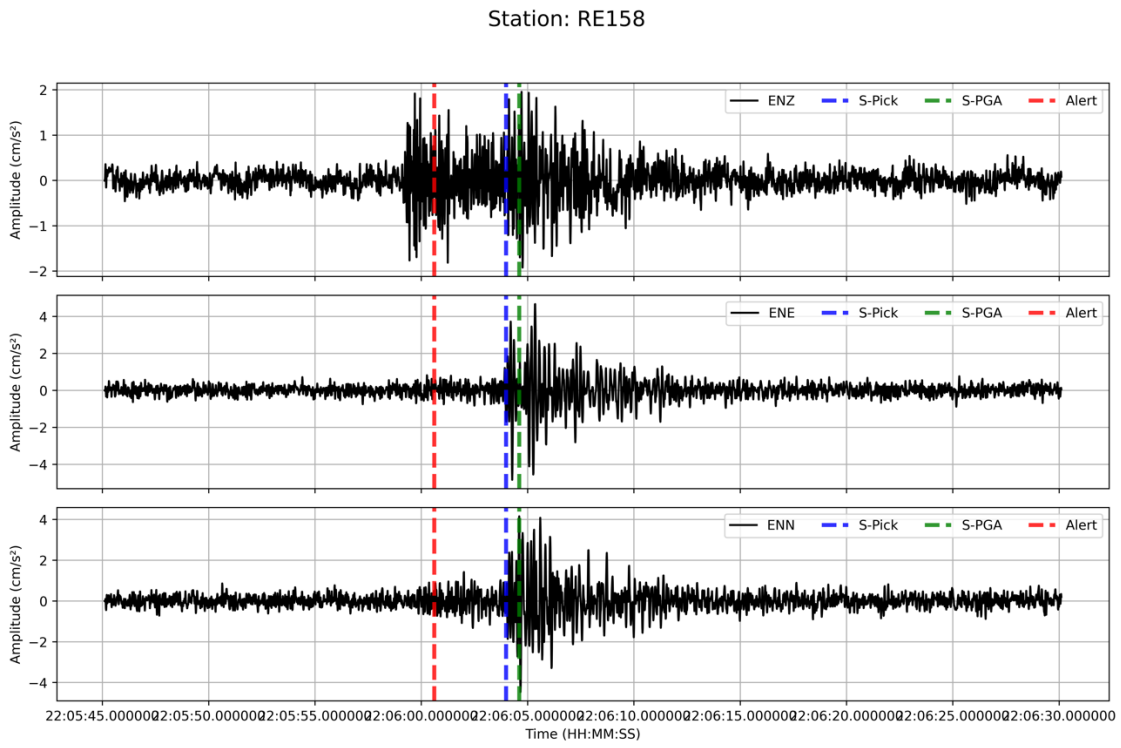

(b) Station: RAE9D

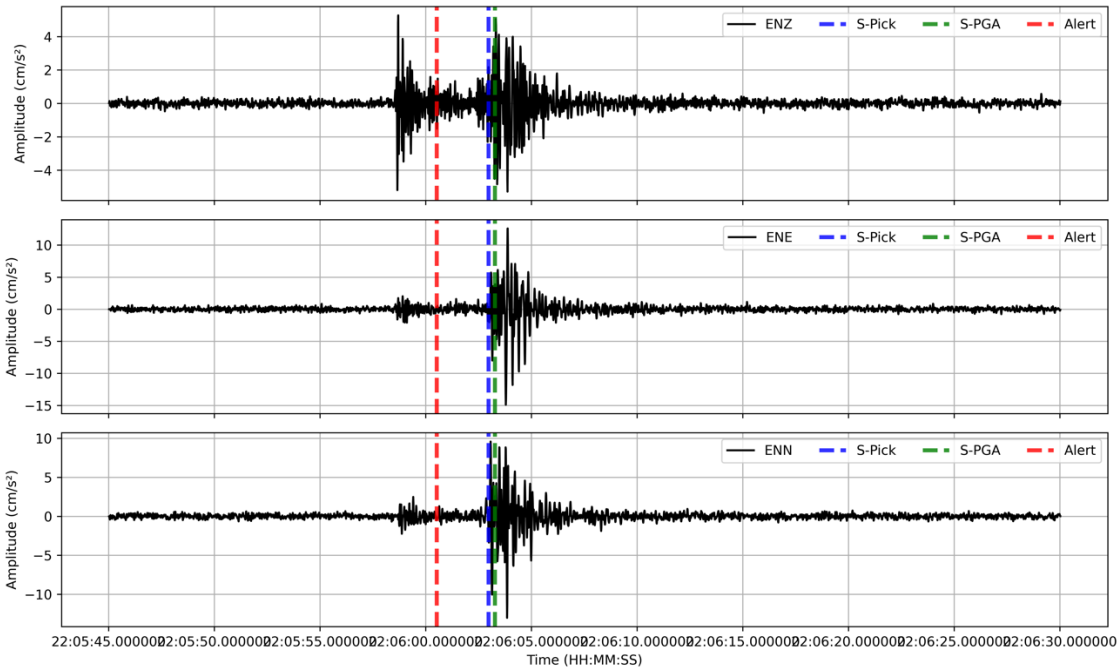

(c) Station: R9288

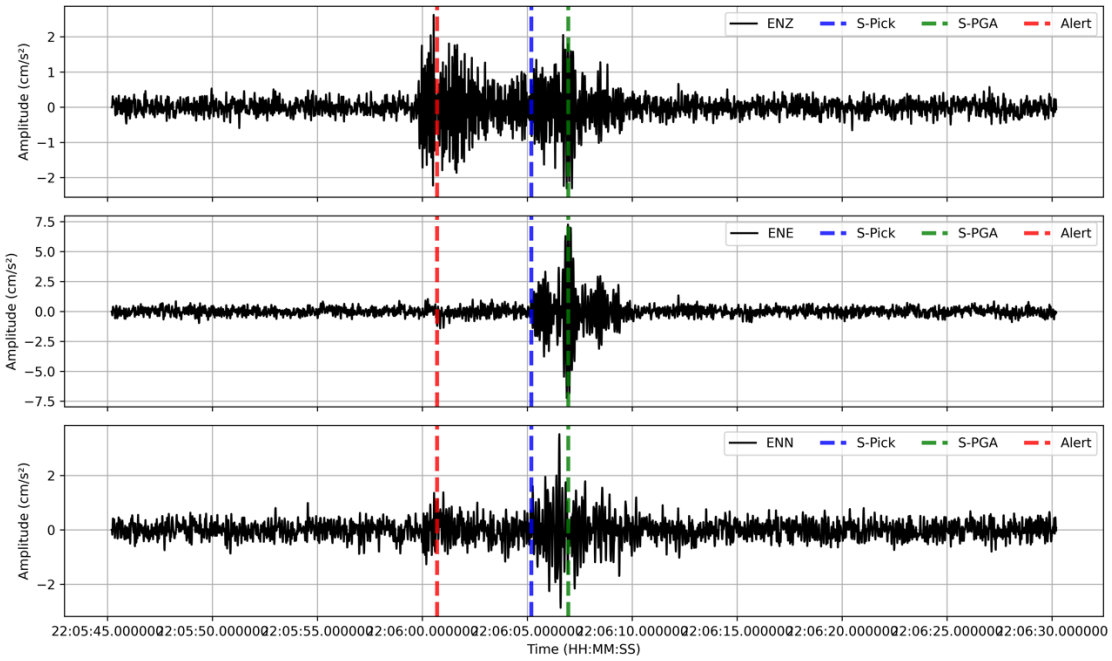

(d)

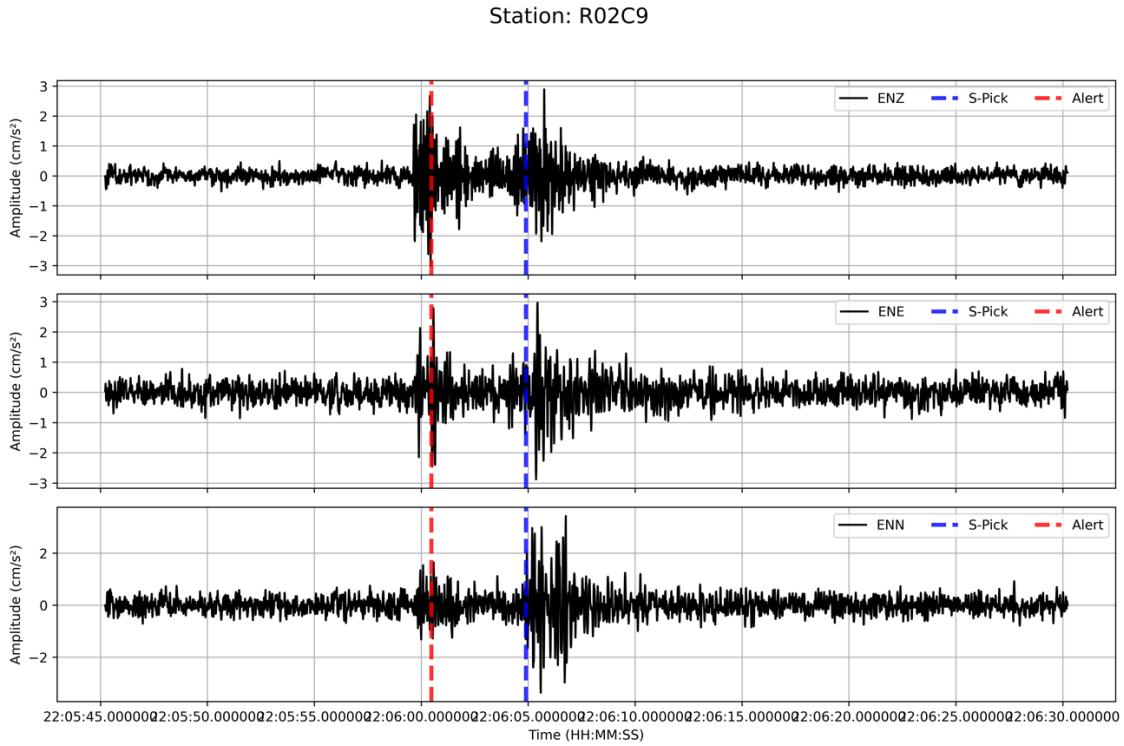

(e)

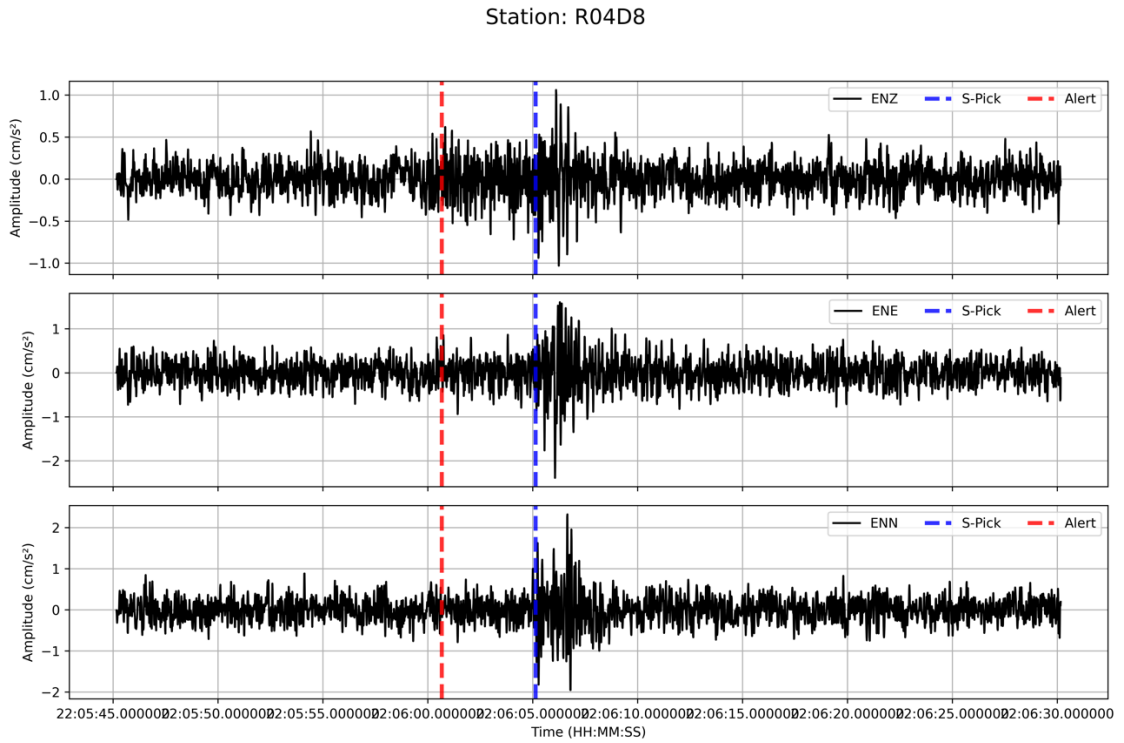

Figure K-6. Ground motion data from the prediction points, with vertical lines indicating the alert logged time (red), actual S-wave arrival time (blue), and felt shaking time (green). (a) P1, (b) P2, (c) P3, (d) P4, and (e) P5.

2.2. NZ-PLUM-P algorithm

Table K-7 summarises the detection times, alert generation, and system latency for each point.

Table K-7. The detection times and system latency for each prediction point, including alert generation and detection delays.

Prediction point	Time 1st Station Exceeds Threshold	Time 2nd Station Exceeds Threshold	Detection Delay	Alert Generated time	Alert received time	System Latency
P1	22:05:58.253	22:05:58.434	0.261	22:05:58.914	22:05:59.358	1.105
P2	22:05:58.253	22:05:58.434	0.261	22:05:58.97	22:05:59.271	1.018
P3	22:05:58.253	22:05:58.434	0.261	22:05:59.02	22:05:59.45	1.197
P4	22:05:58.253	22:05:58.434	0.261	22:05:58.925	22:05:59.22	0.967
P5	22:05:58.253	22:05:58.434	0.261	22:05:58.994	22:05:59.414	1.161

Figure K-7 shows the timestamps during the detection of shaking by the first two stations, indicated by a vertical red line, along with their obtained data.

(a)

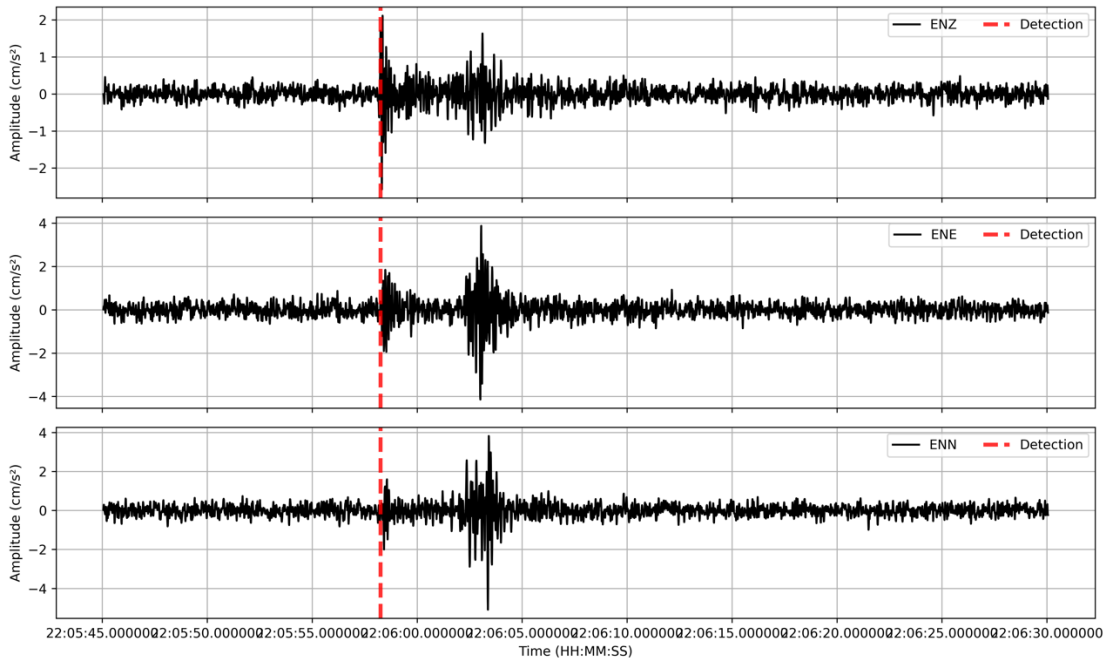

(b)

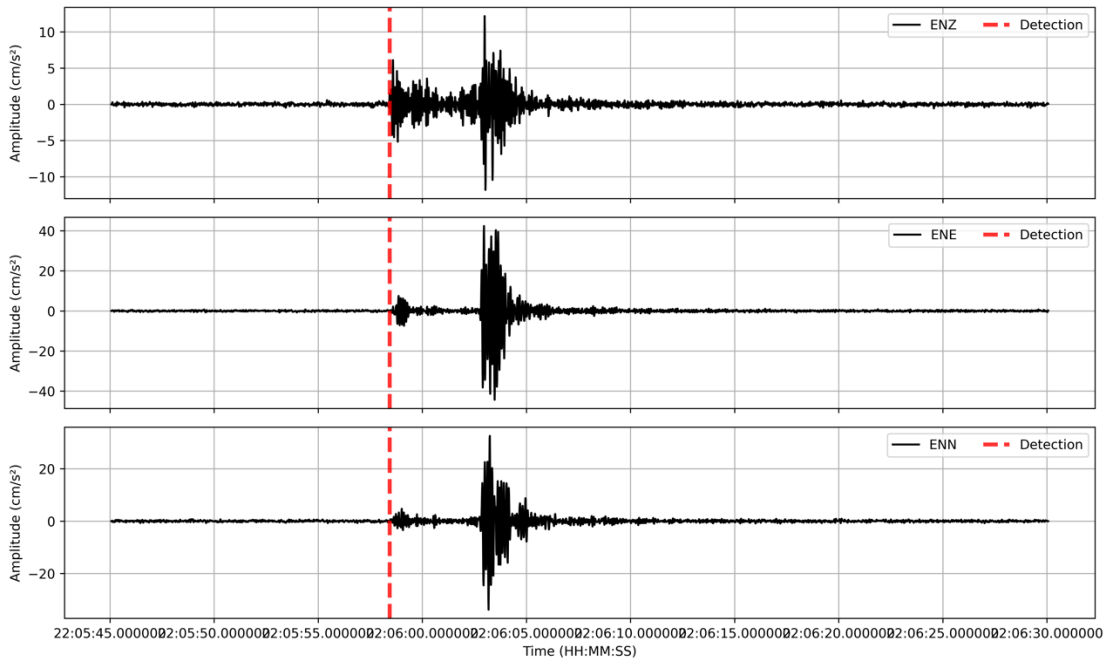

Figure K-7. Waveforms from the stations that first detected shaking where the red vertical line indicates the P-wave detection time for each station. (a) Station AM.RE12E, (b) Station AM.R9C56.

Table K-8 summarises the achieved warning times for each prediction point and compares them to the NZ-PLUM approach.

Table K-8. Comparison of Warning Times Using the NZ-PLUM-P Approach and the NZ-PLUM Approach

Prediction point	**Time Alert Logged**	**Felt shaking time (S-PGA)**	**Theoretical S-wave arrival time (S-Pick)**	**Warning time (Seconds)**	**Increase in Warning time compared to NZ-PLUM**
P1	22:05:59.358	22:06:04.608	22:06:03.988	4.63	1.25
P2	22:05:59.271	22:06:03.271	22:06:02.971	3.7	1.25
P3	22:05:59.45	22:06:06.950	22:06:05.190	5.74	1.25
P4	22:05:59.22	-	22:06:04.890	5.67	1.25
P5	22:05:59.414	-	22:06:05.134	5.72	1.25

Figure K-8 illustrates the ground motion data from the prediction points, with vertical lines representing the alert logged time (red), actual S-wave arrival time (blue), and felt shaking time (green).

(a) Station: RE158

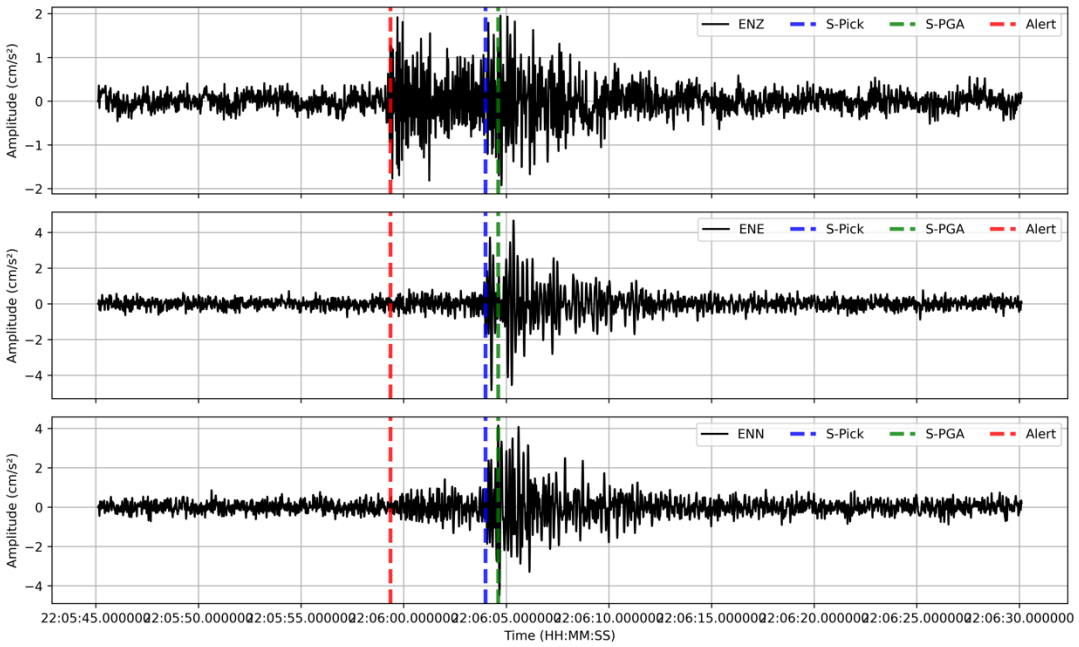

(b) Station: RAE9D

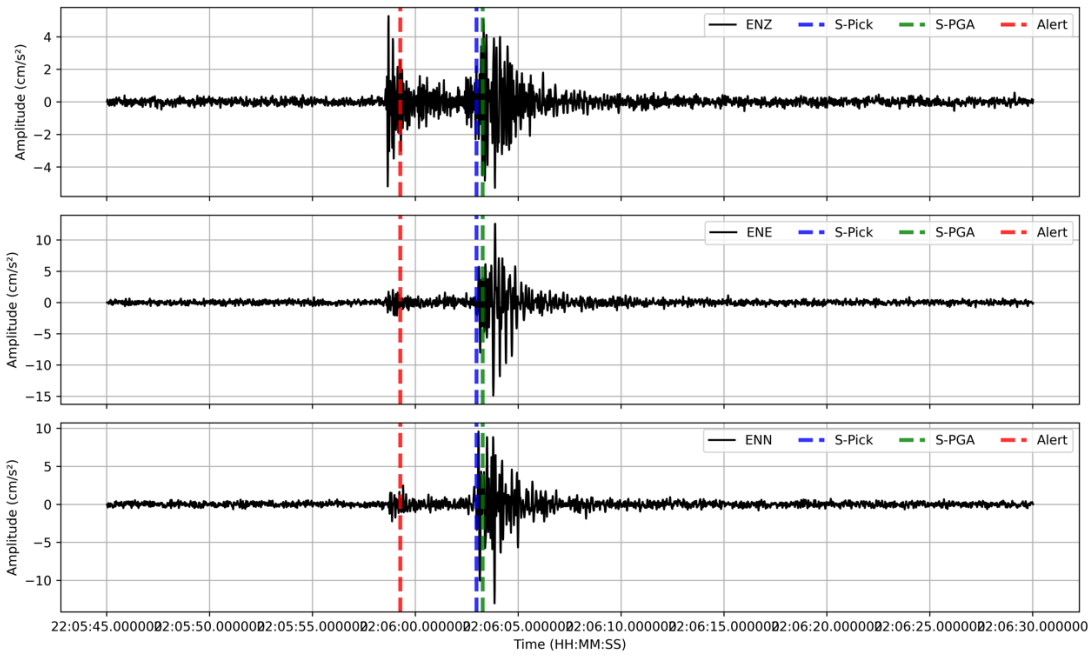

(c) Station: R9288

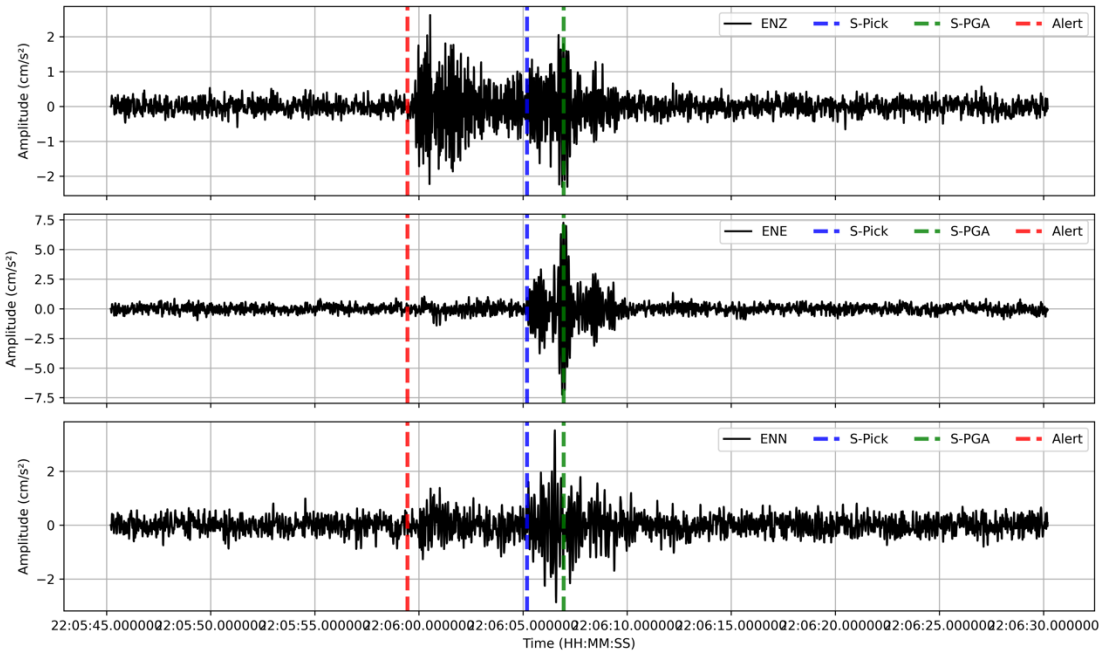

(d) Station: R02C9

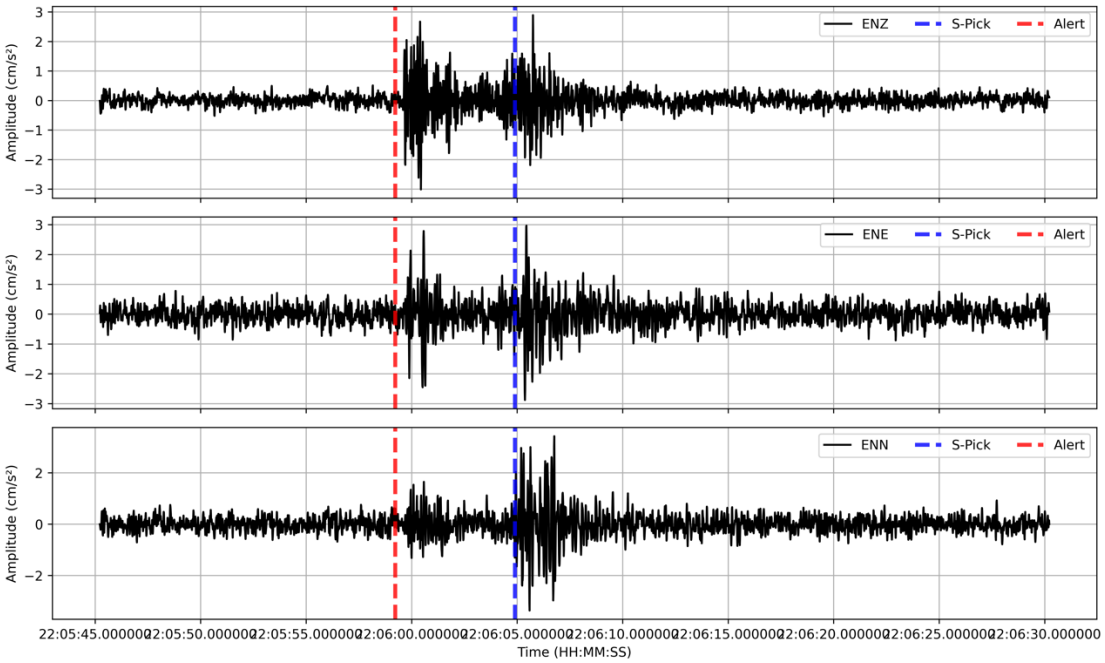

(e)

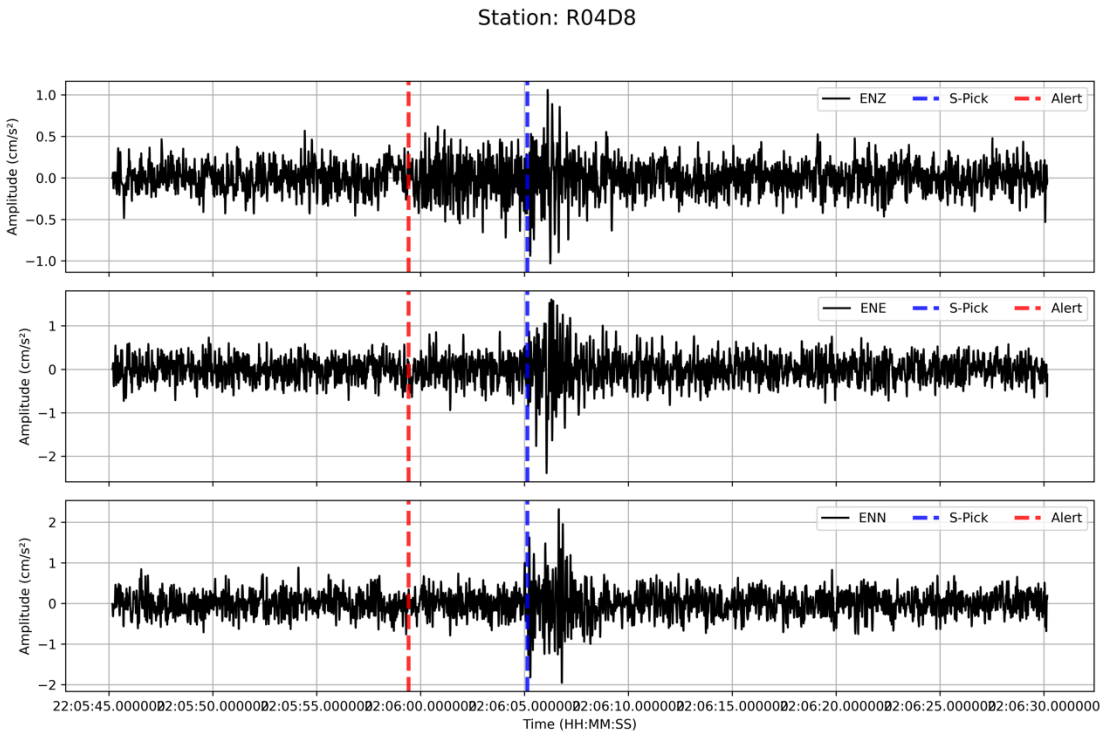

Figure K-8. Ground motion data from the prediction points, with vertical lines indicating the alert logged time (red), actual S-wave arrival time (blue), and felt shaking time (green). (a) P1, (b) P2, (c) P3, (d) P4, and (e) P5.

3. Case Study 3: Earthquake on July 6, 2024

3.1. NZ-PLUM algorithm

Table K-9 summarises each prediction point's detection times, alert generation, and system latency.

Table K-9. The detection times and system latency for each prediction point, including alert generation and detection delays.

Prediction point	Time 1st Station Exceeds Threshold	Time 2nd Station Exceeds Threshold	Detection Delay	Alert Generated time	Alert received time	System Latency
P1	01:17:22.753	01:17:23.257	0.504	01:17:23.574	01:17:24.055	1.302
P2	01:17:22.753	01:17:23.257	0.504	01:17:23.533	01:17:23.901	1.148
P3	01:17:23.257	01:17:23.266	0.009	01:17:23.65	01:17:24.003	0.746
P4	01:17:22.753	01:17:23.257	0.504	01:17:23.621	01:17:24.033	1.280
P5	01:17:22.753	01:17:23.257	0.504	01:17:23.370	01:17:23.824	1.071

Figure K-9 shows the timestamps during detection by the first two stations (marked by red lines), along with their corresponding data.

(a)

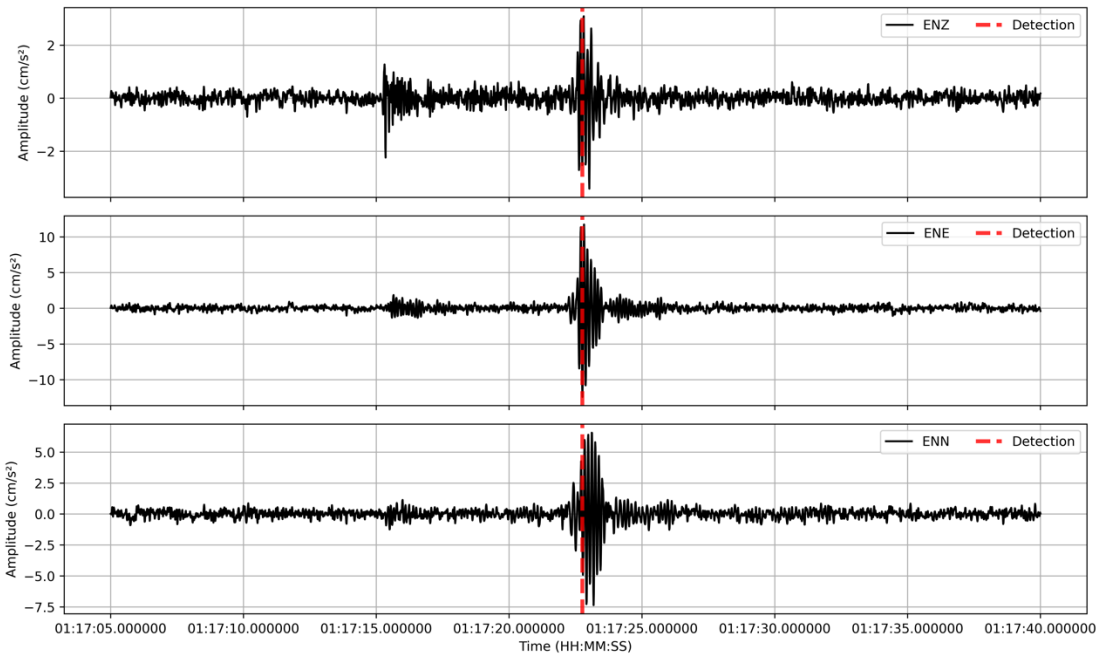
ENZ
Detection
Amplitude (cm/s²)
ENE
Detection
Amplitude (cm/s²)
ENN
Detection
Amplitude (cm/s²)
01:17:05.000000
01:17:10.000000
01:17:15.000000
01:17:20.000000
01:17:25.000000
01:17:30.000000
01:17:35.000000
01:17:40.000000
Time (HH:MM:SS)

(b)

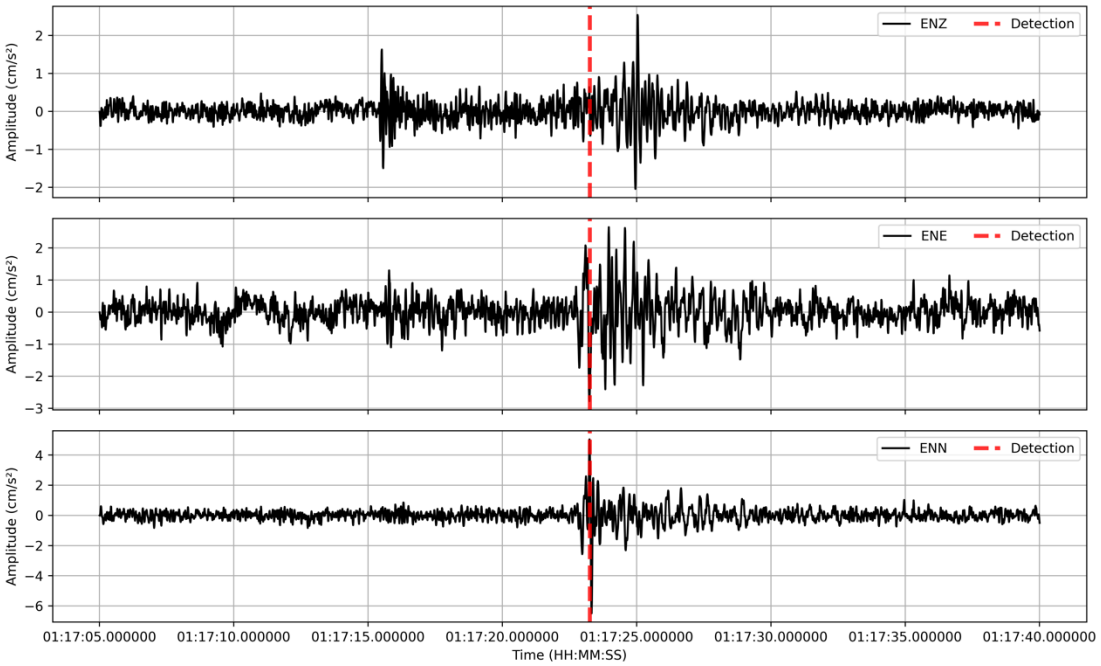
ENZ
Detection
Amplitude (cm/s²)
ENE
Detection
Amplitude (cm/s²)
ENN
Detection
Amplitude (cm/s²)
01:17:05.000000
01:17:10.000000
01:17:15.000000
01:17:20.000000
01:17:25.000000
01:17:30.000000
01:17:35.000000
01:17:40.000000
Time (HH:MM:SS)

(c)

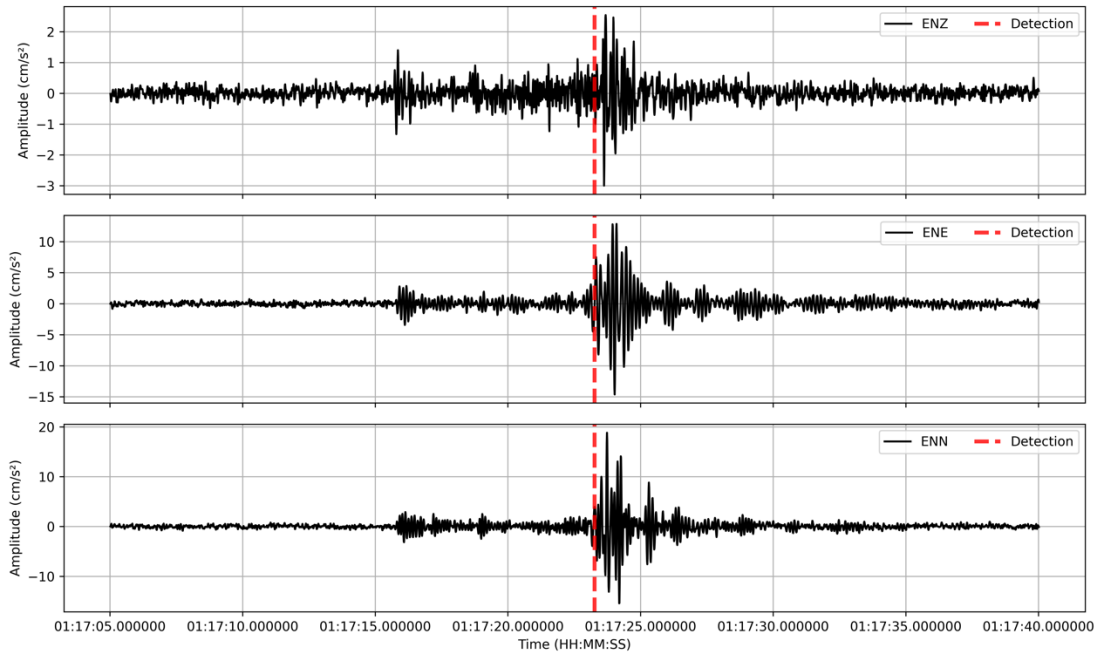

Figure K-9. Waveforms captured by the stations that detected the shaking first. The red vertical line indicates the time alerting threshold exceeded four cms^{-2} in the horizontal acceleration data. (a) Station AM.R9288, (b) Station AM.R770A, (c) Station AM. R02C9.

Table K-10 summarises the warning times achieved for each prediction point upon detection with horizontal acceleration data.

Table K-10. Warning times, S-wave arrival times, and felt shaking times for each prediction point (P1-P5) using the NZ-PLUM approach.

Prediction point	**Time Alert Logged**	**Felt shaking time (S-PGA)**	**Theoretical S-wave arrival time (S-Pick)**	**Warning time (Seconds)**
P1	01:17:24.055	-	01:17:26.305	2.250
P2	01:17:23.901	01:17:27.151000	01:17:26.351	2.450
P3	01:17:24.003	01:17:22.753	01:17:22.243	No Warning
P4	01:17:24.033	01:17:23.783	01:17:22.783	No Warning
P5	01:17:23.824	-	01:17:22.694	No Warning

The following figures show the ground motion data from the prediction points, with vertical lines indicating the alert logged time (red), actual S-wave arrival time (blue), and felt shaking time (green) (Figure K-10).

(a)

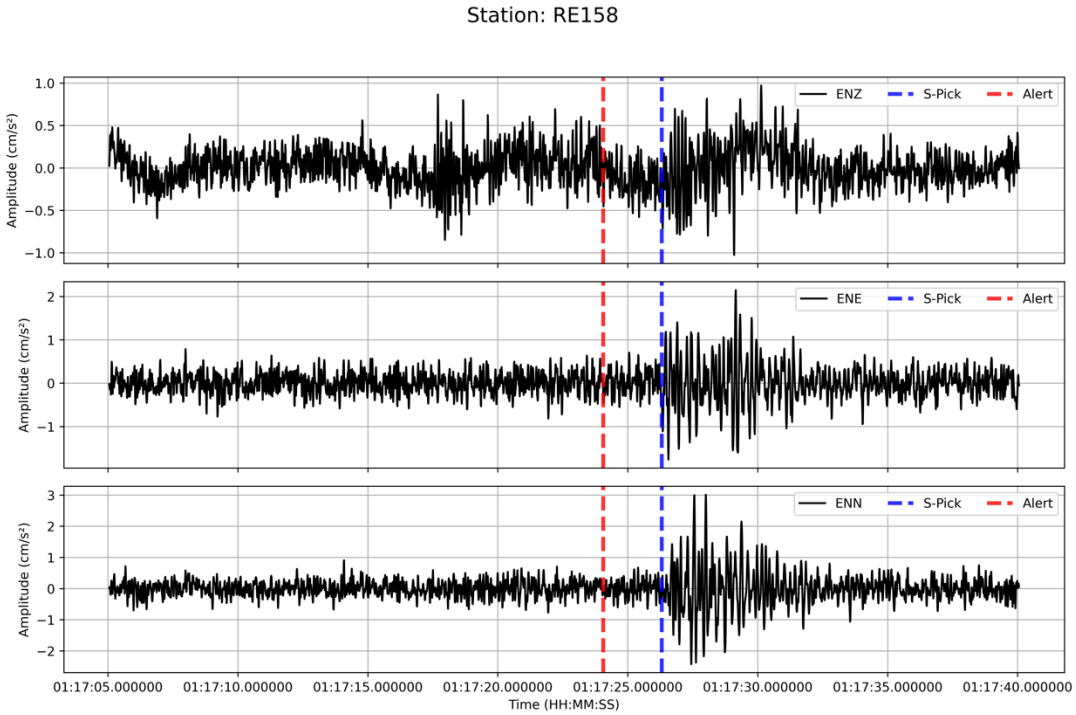
Station: RE158
ENZ
S-Pick
Alert
ENE
S-Pick
Alert
ENN
S-Pick
Alert
Amplitude (cm/s²)
Time (HH:MM:SS)
01:17:05.000000
01:17:10.000000
01:17:15.000000
01:17:20.000000
01:17:25.000000
01:17:30.000000
01:17:35.000000
01:17:40.000000

(b)

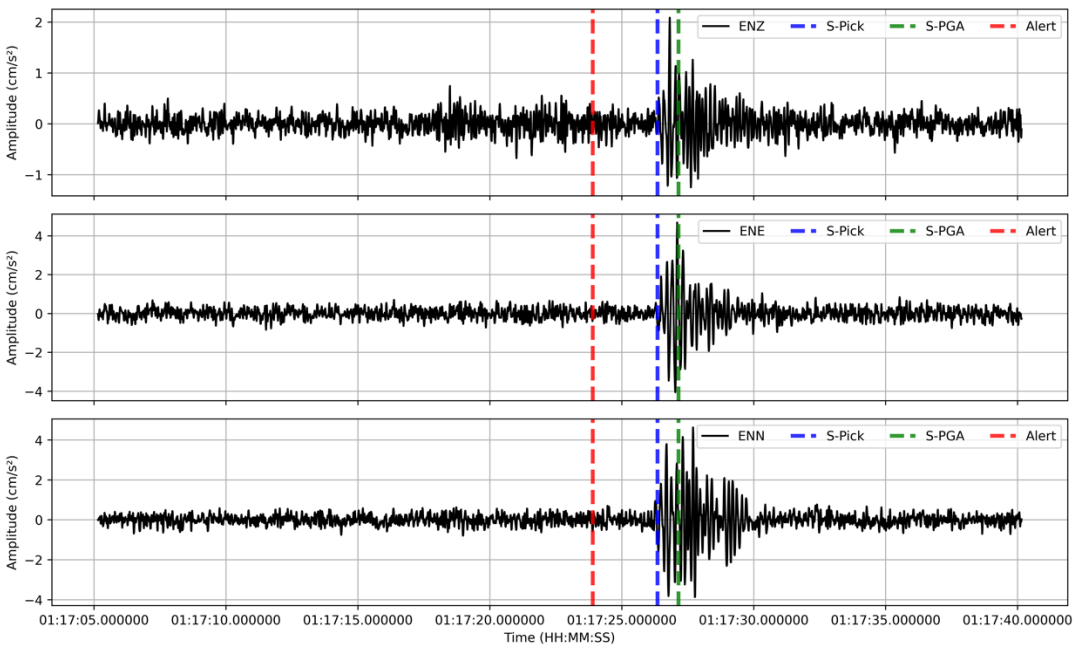
Station: RAE9D
ENZ
S-Pick
S-PGA
Alert
ENE
S-Pick
S-PGA
Alert
ENN
S-Pick
S-PGA
Alert
Amplitude (cm/s²)
Time (HH:MM:SS)
01:17:05.000000
01:17:10.000000
01:17:15.000000
01:17:20.000000
01:17:25.000000
01:17:30.000000
01:17:35.000000
01:17:40.000000

(c)

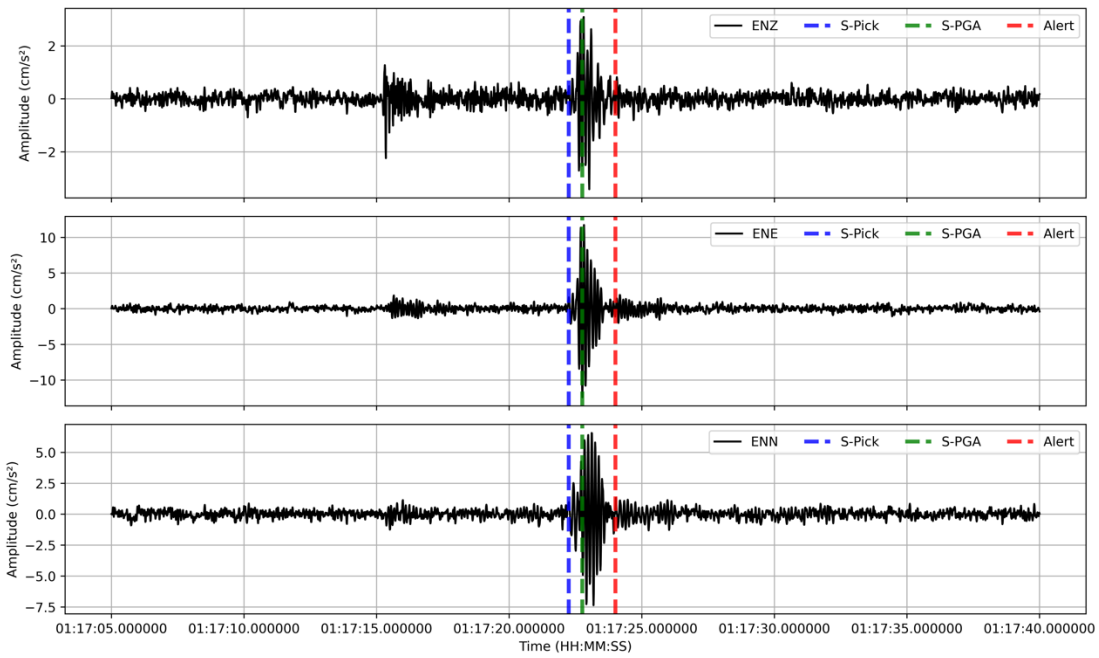
Station: R9288
ENZ
S-Pick
S-PGA
Alert
ENE
ENN
Amplitude (cm/s²)
Time (HH:MM:SS)
01:17:05.000000
01:17:10.000000
01:17:15.000000
01:17:20.000000
01:17:25.000000
01:17:30.000000
01:17:35.000000
01:17:40.000000

(d)

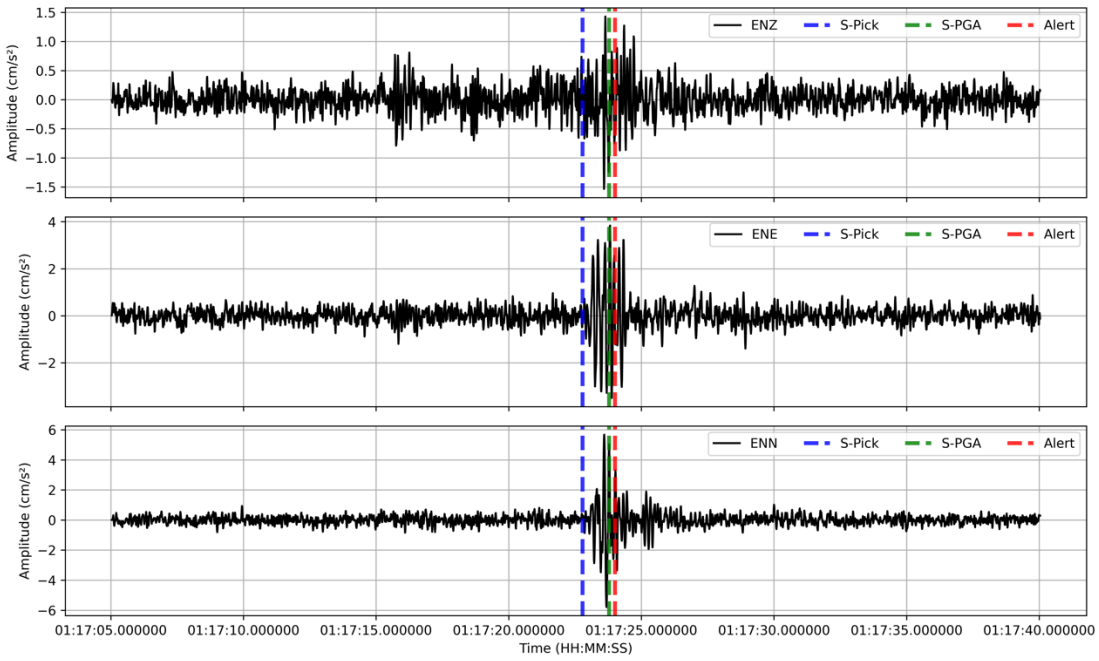
Station: R02C9
ENZ
S-Pick
S-PGA
Alert
ENE
ENN
Amplitude (cm/s²)
Time (HH:MM:SS)
01:17:05.000000
01:17:10.000000
01:17:15.000000
01:17:20.000000
01:17:25.000000
01:17:30.000000
01:17:35.000000
01:17:40.000000

(e)

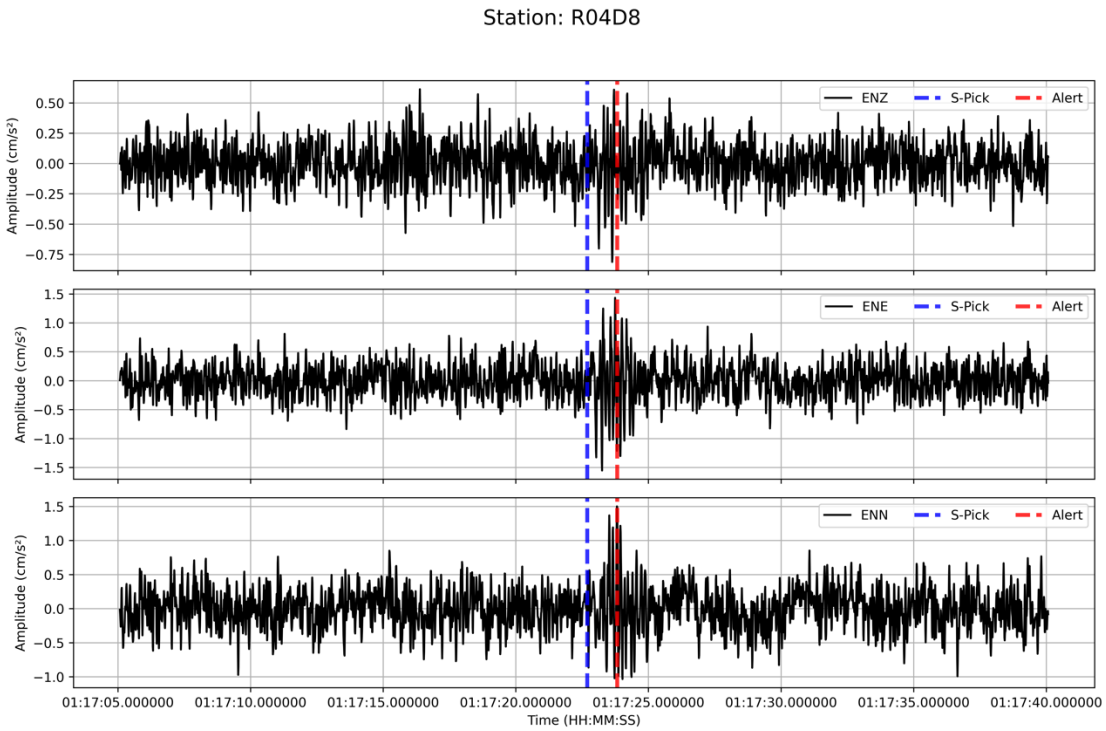

Figure K-10. Ground motion data from the prediction points, with vertical lines indicating the alert logged time (red), actual S-wave arrival time (blue), and felt shaking time (green). (a) P1, (b) P2, (c) P3, (d) P4, and (e) P5.

3.2. NZ-PLUM-P algorithm

Table K-11 summarises the reported detection times for the first two stations, the alert received time at the prediction point, and the system latency for the total alert generation process.

Table K-11. The detection times and system latency for each prediction point, including alert generation and detection delays.

Prediction point	Time 1st Station Exceeds Threshold	Time 2nd Station Exceeds Threshold	Detection Delay	Alert Generated time	Alert received time	System Latency
P1	01:17:15.343	01:17:15.497	0.004	01:17:15.824	01:17:16.305	0.962
P2	01:17:15.343	01:17:15.497	0.004	01:17:15.783	01:17:16.51	1.167
P3	01:17:15.497	01:17:15.760	0.393	01:17:15.900	01:17:16.253	0.756
P4	01:17:15.343	01:17:15.497	0.004	01:17:15.871	01:17:16.283	0.940
P5	01:17:15.343	01:17:15.497	0.004	01:17:15.87	01:17:16.324	0.981

The following figures show the timestamps during the detection of shaking by the first two stations, indicated by a vertical red line, along with their obtained data (Figure K-11).

(a)

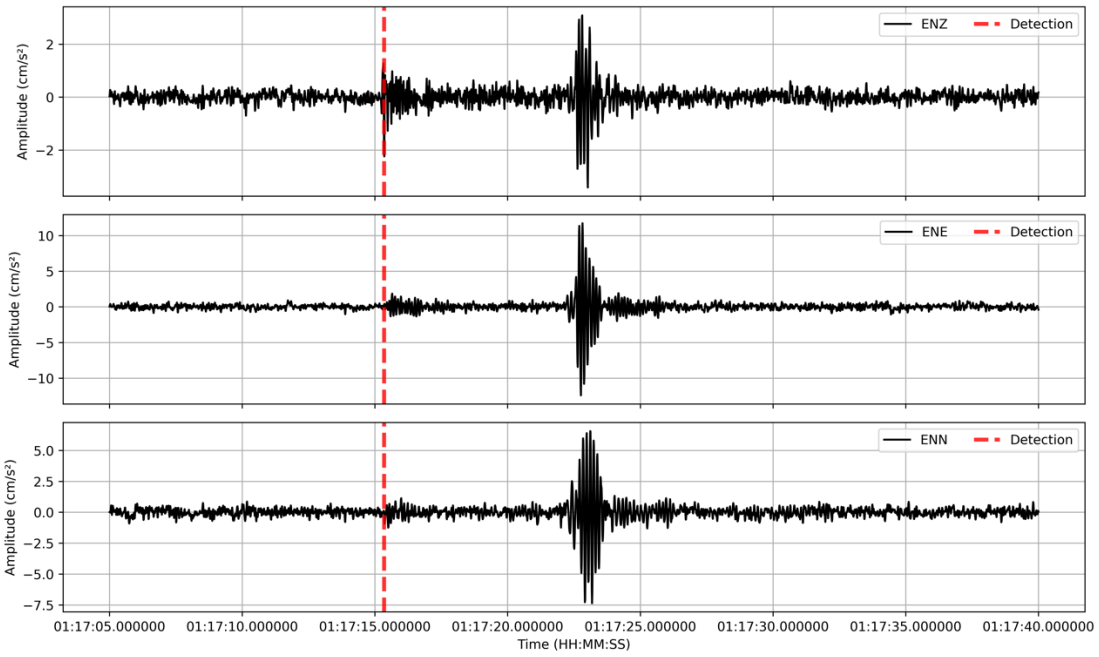
ENZ
Detection
Amplitude (cm/s²)
ENE
Detection
Amplitude (cm/s²)
ENN
Detection
Amplitude (cm/s²)
01:17:05.000000
01:17:10.000000
01:17:15.000000
01:17:20.000000
01:17:25.000000
01:17:30.000000
01:17:35.000000
01:17:40.000000
Time (HH:MM:SS)

(b)

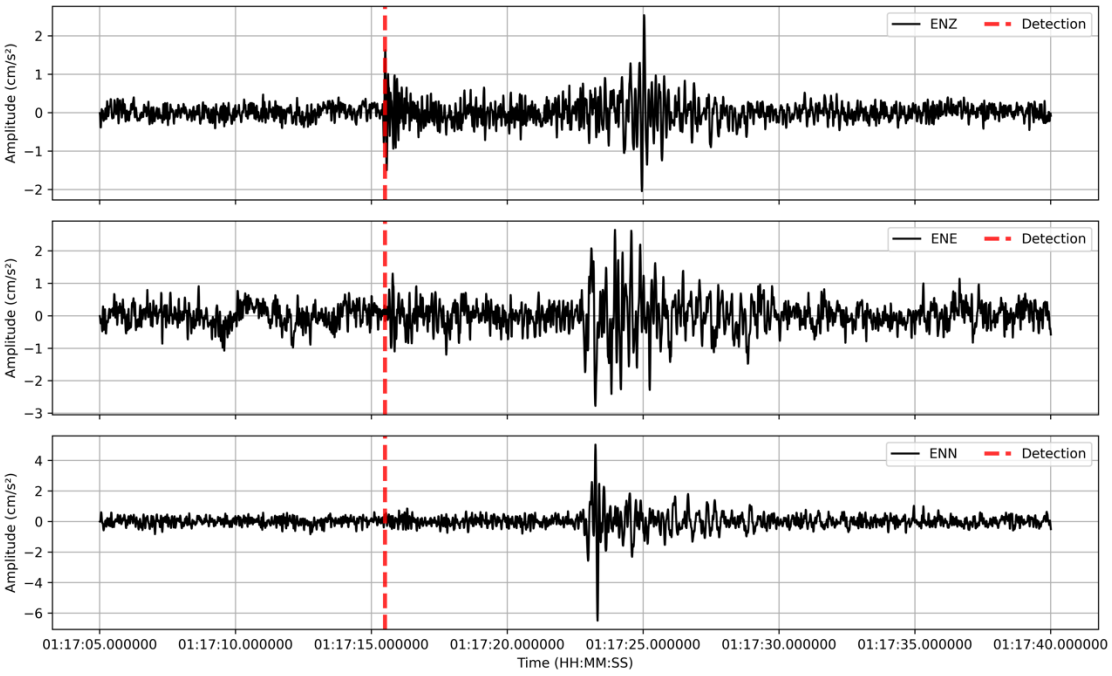
ENZ
Detection
Amplitude (cm/s²)
ENE
Detection
Amplitude (cm/s²)
ENN
Detection
Amplitude (cm/s²)
01:17:05.000000
01:17:10.000000
01:17:15.000000
01:17:20.000000
01:17:25.000000
01:17:30.000000
01:17:35.000000
01:17:40.000000
Time (HH:MM:SS)

(c)

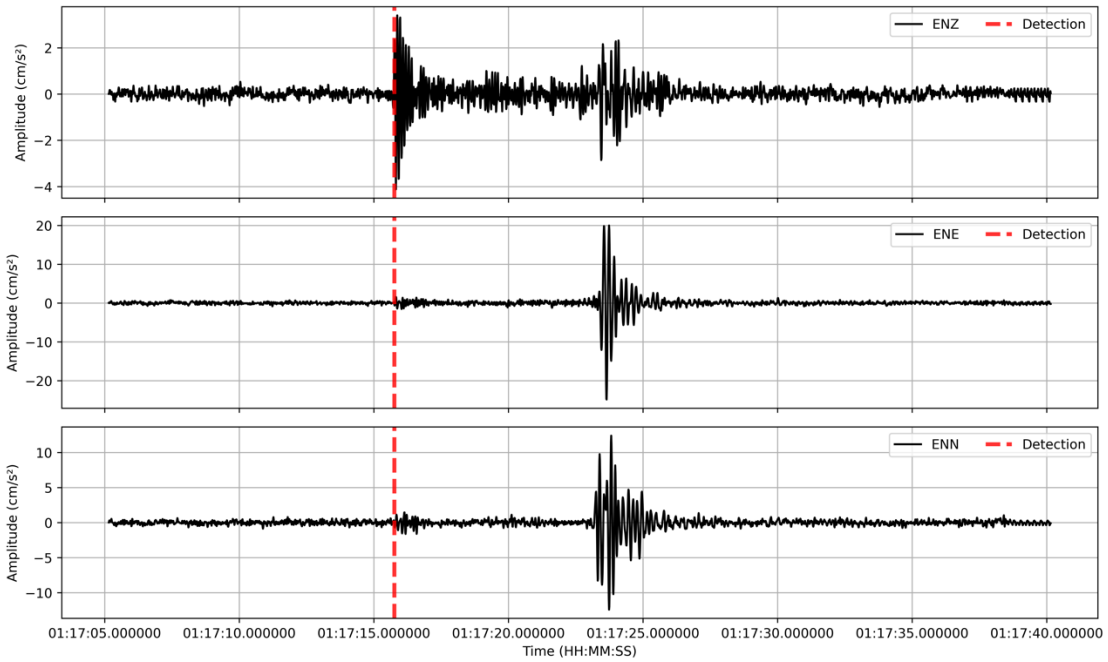

Figure K-11. Waveforms from the stations that first detected shaking where the red vertical line indicates the P-wave detection time for each station. (a) Station AM.R9288, (b) Station AM.R770A, (c) AM.R5C37.

Table K-12 summarises the warning times achieved for each prediction point with the NZ-PLUM approach upon detection using horizontal acceleration data.

Table K-12. Comparison of Warning Times Using the NZ-PLUM-P Approach and the NZ-PLUM Approach

Prediction point	**Time Alert Logged**	**Felt shaking time (S-PGA)**	**Theoretical S-wave arrival time (S-Pick)**	**Warning time (Seconds)**	**Increase in Warning time compared to NZ-PLUM**
P1	01:17:16.305	-	01:17:26.305	10	7.75
P2	01:17:16.51	01:17:27.151	01:17:26.351	9.841	7.391
P3	01:17:16.253	01:17:22.753	01:17:22.243	5.990	7.75
P4	01:17:16.283	01:17:23.783	01:17:22.783	6.5	7.75
P5	01:17:16.324	-	01:17:22.694	6.37	7.5

The following figures show the ground motion data from the prediction points, with vertical lines indicating the alert logged time (red), actual S-wave arrival time (blue), and felt shaking time (green) (Figure K-12).

(a)

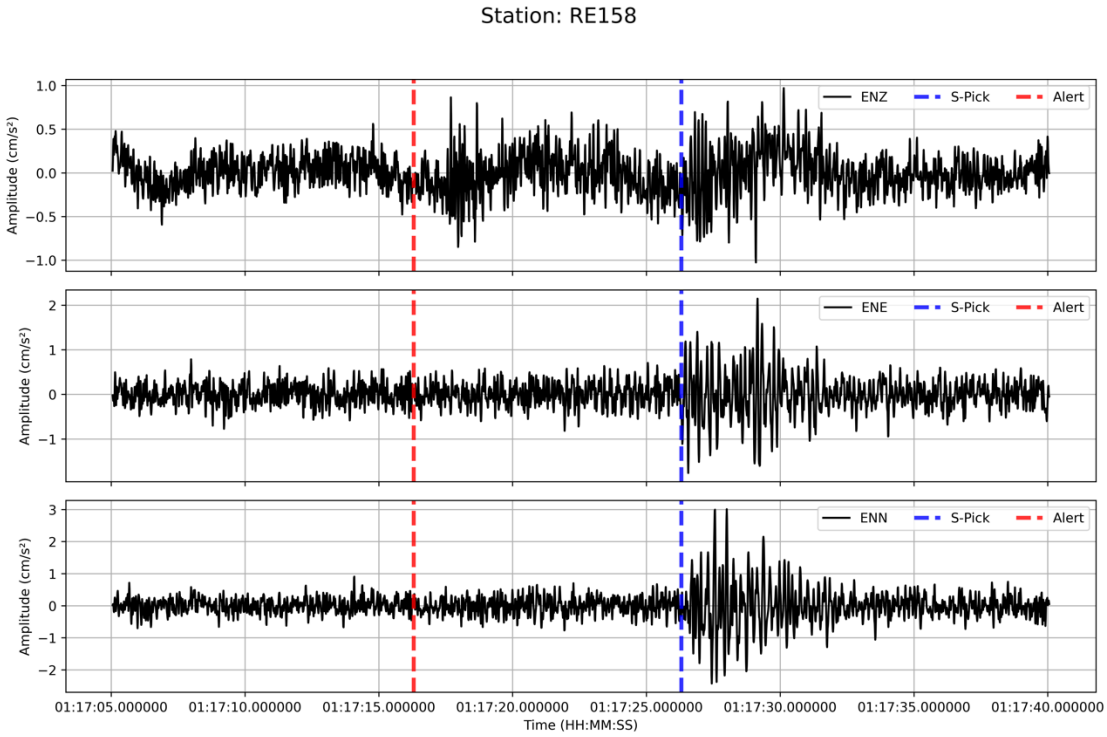
Station: RE158
ENZ
S-Pick
Alert
ENE
S-Pick
Alert
ENN
S-Pick
Alert
Amplitude (cm/s²)
01:17:05.000000
01:17:10.000000
01:17:15.000000
01:17:20.000000
01:17:25.000000
01:17:30.000000
01:17:35.000000
01:17:40.000000
Time (HH:MM:SS)

(b)

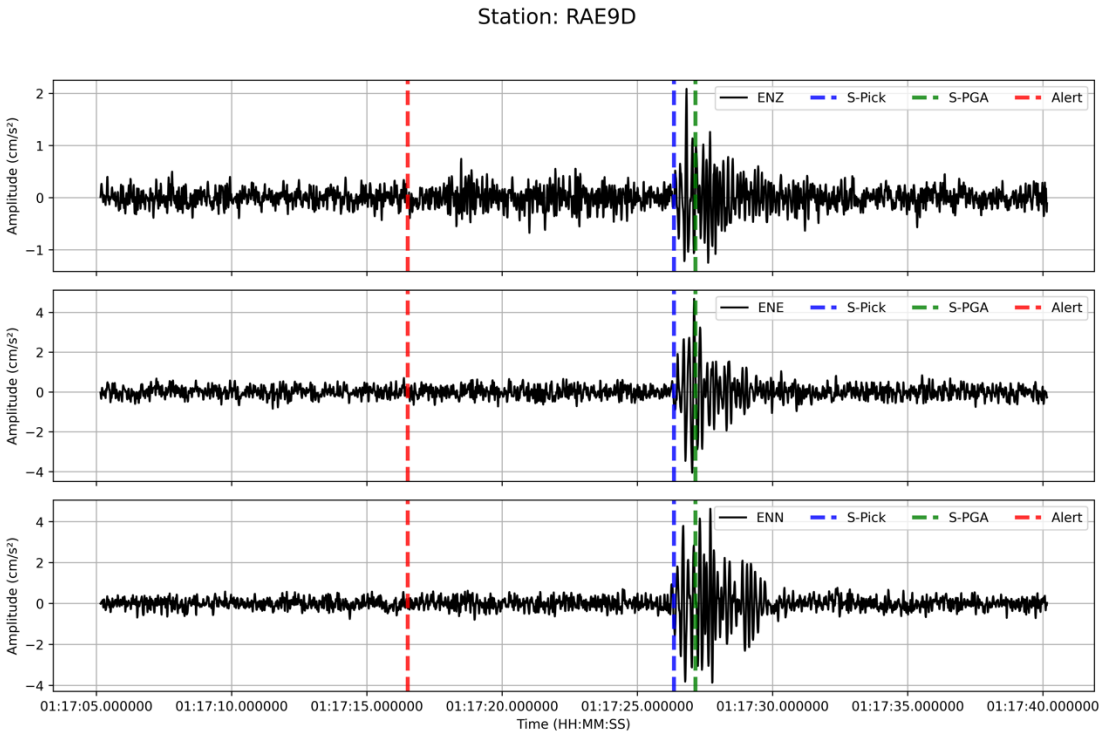
Station: RAE9D
ENZ
S-Pick
S-PGA
Alert
ENE
S-Pick
S-PGA
Alert
ENN
S-Pick
S-PGA
Alert
Amplitude (cm/s²)
01:17:05.000000
01:17:10.000000
01:17:15.000000
01:17:20.000000
01:17:25.000000
01:17:30.000000
01:17:35.000000
01:17:40.000000
Time (HH:MM:SS)

(c)

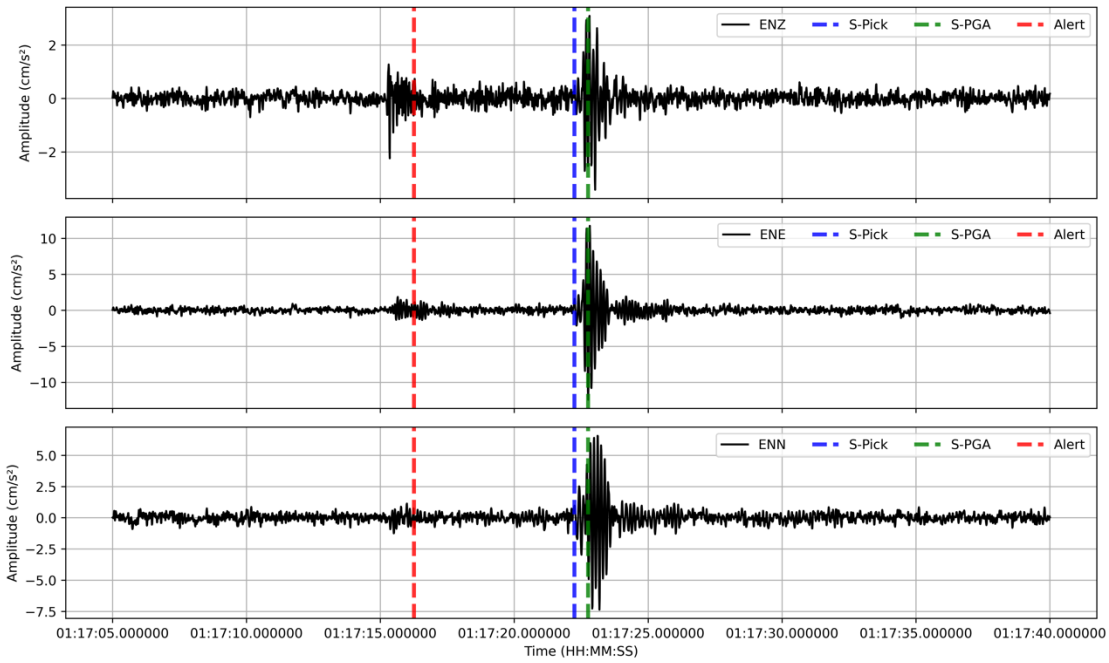
Station: R9288
ENZ
S-Pick
S-PGA
Alert
ENE
ENN
Amplitude (cm/s²)
01:17:05.000000
01:17:10.000000
01:17:15.000000
01:17:20.000000
01:17:25.000000
01:17:30.000000
01:17:35.000000
01:17:40.000000
Time (HH:MM:SS)

(d)

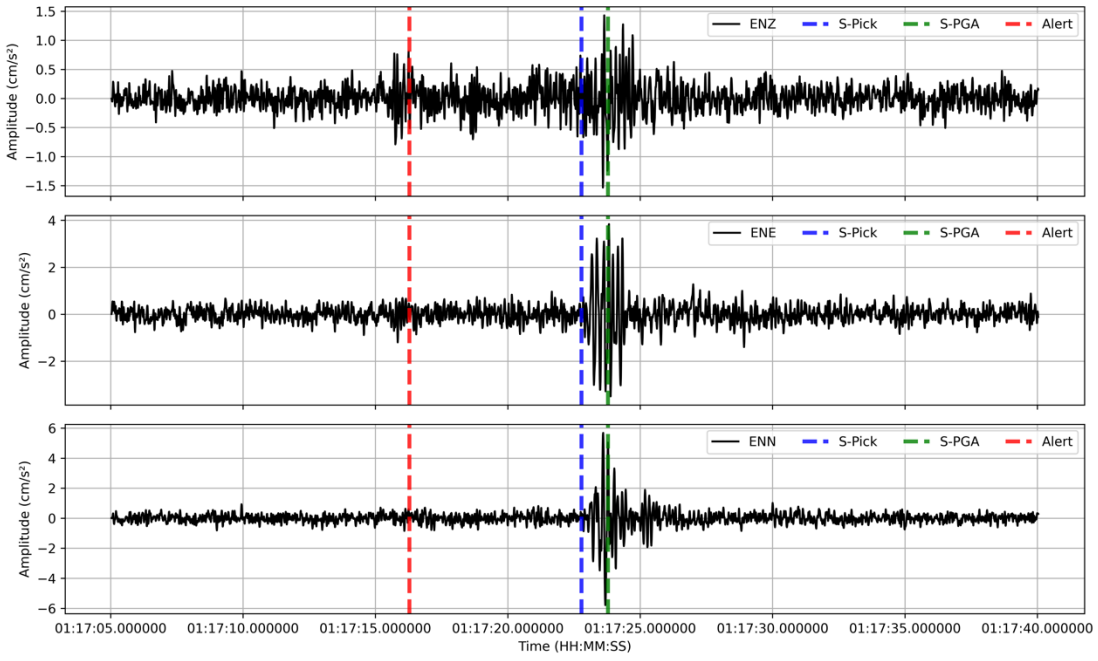
Station: R02C9
ENZ
S-Pick
S-PGA
Alert
ENE
ENN
Amplitude (cm/s²)
01:17:05.000000
01:17:10.000000
01:17:15.000000
01:17:20.000000
01:17:25.000000
01:17:30.000000
01:17:35.000000
01:17:40.000000
Time (HH:MM:SS)

(e)

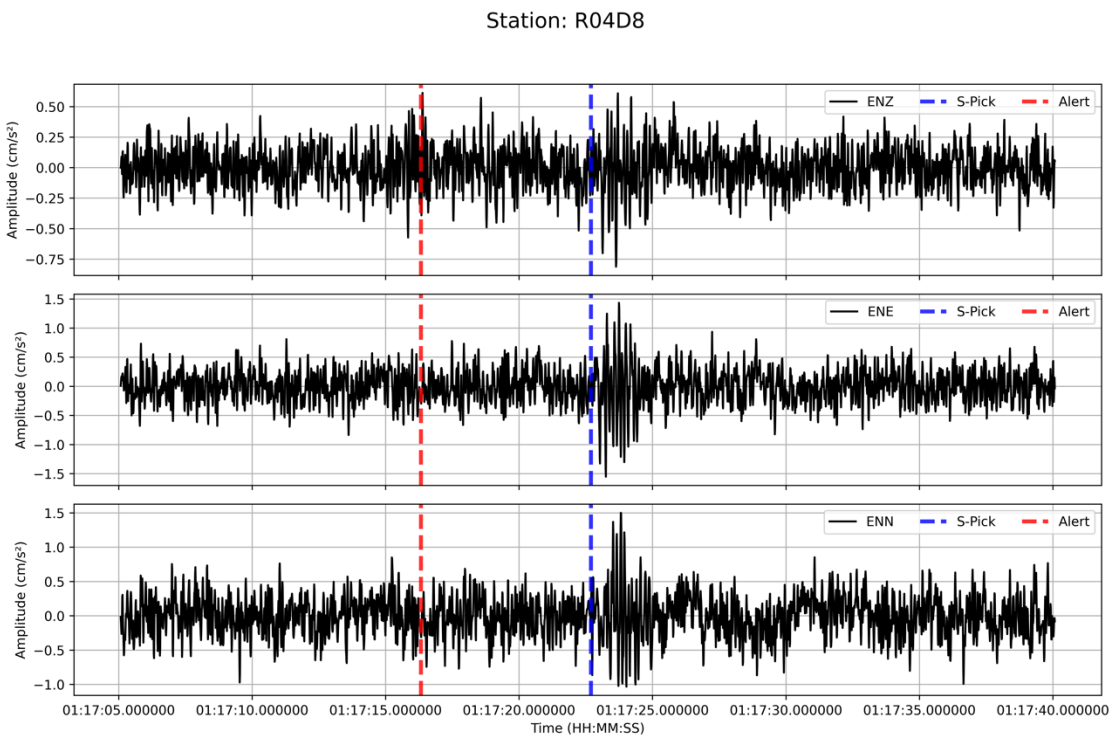

Figure K-12. Ground motion data from the prediction points, with vertical lines indicating the alert logged time (red), actual S-wave arrival time (blue), and felt shaking time (green). (a) P1, (b) P2, (c) P3, (d) P4, and (e) P5.